

APPLICATION OF MESHLESS ELEMENT FREE GALERKIN METHOD IN HEAT TRANSFER PROBLEMS

THESIS

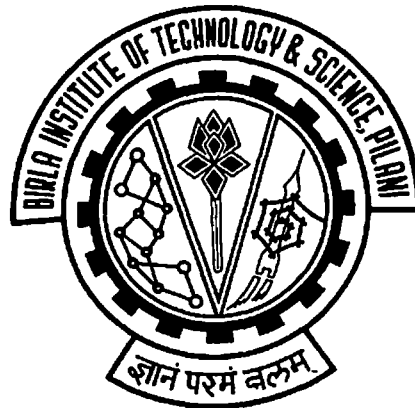
Submitted in partial fulfillment
of the requirements for the degree of
DOCTOR OF PHILOSOPHY

By

Indra Vir Singh

Under the Supervision of

Prof. Ravi Prakash



**BIRLA INSTITUTE OF TECHNOLOGY AND SCIENCE
PILANI (RAJASTHAN) INDIA**

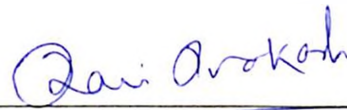
2004

DEDICATED TO MY FAMILY

**BIRLA INSTITUTE OF TECHNOLOGY & SCIENCE
PILANI (RAJASTHAN)**

CERTIFICATE

This is to certify that the thesis entitled “**Application of Meshless Element Free Galerkin Method in Heat Transfer Problems**” and submitted by **Indra Vir Singh** ID No. **2000PHXF014** for award of Ph.D. Degree of the Institute, embodies original work done by him under my supervision.



Signature in full of the Supervisor

4/2/04

Name in capital block letters: RAVI PRAKASH

Designation: Professor of Mechanical Engineering &
Dean, Research & Consultancy Division

ACKNOWLEDGEMENTS

I wish to express deep sense of gratitude and sincere thanks to my thesis supervisor Prof. Ravi Prakash, Dean, Research and Consultancy Division for his able guidance, encouragement and suggestions throughout the period of this research work. It has been a privilege for me to work under his guidance.

Much appreciation is expressed to Prof. Sandeep Kumar, Sungai Petani, Malaysia for his valuable suggestions, moral support and assistance.

Gratitude is also accorded to BITS, Pilani for providing all the necessary facilities to complete the research work. My special thanks go to Prof. S. Venkateswaran, Vice Chancellor, B.I.T.S. for giving me an opportunity to do research at the Institute. I also thank Prof. L. K. Maheshwari, Director for his encouragement and guidance. I take this opportunity to thank Prof. K. E. Raman Deputy Director (Administration), Prof. V. S. Rao, Deputy Director (Off-Campus) and Prof. A. K. Sarkar, Dean, Instruction Division, for providing the necessary infrastructure and other facilities.

I also express my gratitude for the kind encouragement and appreciation for my work by Mr. Sanjay Vashishtha and Mr. Sanjay D. Pohekar, Research and Consultancy Division and my colleagues.

Special thanks to Prof. Rajiv Gupta, Dean Educational Hardware Division for his guidance and invaluable assistance throughout my research work.

Finally a very special expression of appreciation is extended to my family members. Without their encouragement, patience, and understanding, this endeavor would not have been possible. I would like to record my special affection and thanks to my wife Anjali whose constant persuasion and moral support has been a source of inspiration to me.

ABSTRACT

This thesis deals with the numerical solution of heat transfer problems using meshless element free Galerkin (EFG) method and the parallel implementation of the EFG code developed. The EFG method utilizes moving least square (MLS) approximants to approximate the unknown function of temperature. These MLS approximants are constructed by using a weight function, a basis function and a set of non-constants coefficients. The essential boundary conditions are enforced using Lagrange multiplier technique. Variational method has been utilized to obtain discrete equations. Software has been developed to obtain the numerical solution. Four new weight functions namely hyperbolic, exponential, rational and cosine have been proposed. Numerical results (temperature values) have been obtained using existing (cubicspline, quarticspline, Gaussian and quadratic) and proposed (hyperbolic, exponential, rational and cosine) EFG weight functions in one-dimensional (1-D), two-dimensional (2-D) and three-dimensional (3-D) domains (four cases in each domain). A comparison has been made amongst the results obtained using proposed EFG weight functions, existing EFG weight functions and finite element method (FEM). The results obtained by EFG method are found in good agreement with those obtained by FEM. The effect of scaling parameter (d_{\max}) on EFG results has also been discussed in detail and it gives acceptable results in the range of $1 < d_{\max} < 1.5$ for cubicspline, quarticspline, Gaussian, exponential and rational weight functions. It is also observed that the EFG results obtained by proposed exponential weight functions are the most reliable in this range of scaling parameter. A new parallel algorithm has been developed for the EFG method to reduce its computational cost. The codes have been written in FORTRAN language using MPI (Message Passing Interface) library and executed on a MIMD (Multiple Instruction Multiple Data) type supercomputer, PARAM 10000. Three model heat transfer problems have been solved (one each in 1-D, 2-D and 3-D domains) to validate the proposed parallel algorithm. For 8 processors, the speedup and efficiency are obtained to be 2.22 & 27.78% respectively for 1100 nodes in 1-D, 5.44 & 67.95% respectively for 1200 nodes in 2-D and 4.66 & 58.22% respectively for 1320 nodes in 3-D. It is evident from the analysis that the increase in data size (i.e. number of nodes) results in improved speedup and efficiency.

TABLE OF CONTENTS

ACKNOWLEDGEMENT	i
ABSTRACT	ii
TABLE OF CONTENTS	iii
LIST OF TABLES	vii
LIST OF FIGURES	xxv
LIST OF SYMBOLS	xxxii
CHAPTER-1: INTRODUCTION	1
CHAPTER-2: LITERATURE REVIEW	5
CHAPTER-3: THE ELEMENT FREE GALERKIN METHOD	
3.1 Introduction	19
3.2 Moving Least Square Approximants	19
3.3 Efficient Shape Function Calculation	24
3.4 Weight Function Description	25
3.5 Enforcement of Essential Boundary Conditions	28
CHAPTER-4: 1-D HEAT TRANSFER ANALYSIS	
4.1 INTRODUCTION	31
<i>CASE-I</i>	31
4.2 DISCRETIZATION OF THE GOVERNING EQUATION	31
4.3 NUMERICAL RESULTS AND DISCUSSION	33
4.3.1 <i>Steady State Analysis</i>	33
4.3.2 <i>Transient Analysis</i>	44
<i>CASE-II</i>	54
4.4 DISCRETIZATION OF THE GOVERNING EQUATION	54
4.5 NUMERICAL RESULTS AND DISCUSSION	56

4.5.1 <i>Steady State Analysis</i>	56
4.5.2 <i>Transient Analysis</i>	67
CASE-III	76
4.6 DISCRETIZATION OF THE GOVERNING EQUATION	76
4.7 NUMERICAL RESULTS AND DISCUSSION	78
4.7.1 <i>Steady State Analysis</i>	78
4.7.2 <i>Transient Analysis</i>	89
CASE-IV	98
4.8 DISCRETIZATION OF THE GOVERNING EQUATION	98
4.9 NUMERICAL RESULTS AND DISCUSSION	100
4.9.1 <i>Steady State Analysis</i>	100
4.9.2 <i>Transient Analysis</i>	111
4.10 CONCLUSION	120
CHAPTER-5: 2-D HEAT TRANSFER ANALYSIS	
5.1 INTRODUCTION	121
CASE-I	121
5.2 DISCRETIZATION OF THE GOVERNING EQUATION	121
5.3 NUMERICAL RESULTS AND DISCUSSION	123
5.3.1 <i>Steady State Analysis</i>	124
5.3.2 <i>Transient Analysis</i>	135
CASE-II	145
5.4 DISCRETIZATION OF THE GOVERNING EQUATION	145
5.5 NUMERICAL RESULTS AND DISCUSSION	147
5.5.1 <i>Steady State Analysis</i>	147
5.5.2 <i>Transient Analysis</i>	158

<i>CASE-III</i>	167
5.6 DISCRETIZATION OF THE GOVERNING EQUATION	167
5.7 NUMERICAL RESULTS AND DISCUSSION	169
5.7.1 <i>Steady State Analysis</i>	169
5.7.2 <i>Transient Analysis</i>	181
<i>CASE-IV</i>	190
5.8 DISCRETIZATION OF THE GOVERNING EQUATION	190
5.9 NUMERICAL RESULTS AND DISCUSSION	192
5.9.1 <i>Steady State Analysis</i>	193
5.9.2 <i>Transient Analysis</i>	205
5.10 CONCLUSION	214
CHAPTER-6: 3-D HEAT TRANSFER ANALYSIS	
6.1 INTRODUCTION	215
<i>CASE-I</i>	215
6.2 DISCRETIZATION OF THE GOVERNING EQUATION	215
6.3 NUMERICAL RESULTS AND DISCUSSION	218
6.3.1 <i>Steady State Analysis</i>	218
6.3.2 <i>Transient Analysis</i>	229
<i>CASE-II</i>	239
6.4 DISCRETIZATION OF THE GOVERNING EQUATION	239
6.5 NUMERICAL RESULTS AND DISCUSSION	244
6.5.1 <i>Steady State Analysis</i>	244
6.5.2 <i>Transient Analysis</i>	256
<i>CASE-III</i>	265
6.6 DISCRETIZATION OF THE GOVERNING EQUATION	265

6.7 NUMERICAL RESULTS AND DISCUSSION	268
6.7.1 <i>Steady State Analysis</i>	269
6.7.2 <i>Transient Analysis</i>	281
CASE-IV	290
6.8 DISCRETIZATION OF THE GOVERNING EQUATION	290
6.9 NUMERICAL RESULTS AND DISCUSSION	293
6.9.1 <i>Steady State Analysis</i>	294
6.9.2 <i>Transient Analysis</i>	303
6.10 CONCLUSION	310
CHAPTER-7: PARALLEL COMPUTING SOLUTION	
7.1 INTRODUCTION	311
7.2 PARALLEL CODE DEVELOPMENT	312
7.2.1 <i>Parallel Algorithm for the Solution of Linear Equations</i>	316
7.2.2 <i>Hardware and Software Employed</i>	318
7.3 NUMERICAL RESULTS AND DISCUSSION	318
7.3.1 <i>One-Dimensional Model Problem</i>	318
7.3.2 <i>Two-Dimensional Model Problem</i>	326
7.3.3 <i>Three-Dimensional Model Problem</i>	333
7.4 CONCLUSION	340
CHAPTER-8: CONCLUSION AND FUTURE SCOPE OF WORK	
REFERENCES	343
APPENDIX	353
LIST OF PUBLICATIONS	354

LIST OF TABLES

Table No.	Title	Page No.
4.1	Data for the 1-D model shown in Fig. 4.1	35
4.2	Comparison of EFG results obtained using 11 nodes with FEM and analytical results at the location ($x = 0.2\text{ m}$) of the 1-D model shown in Fig. 4.1	36
4.3	Comparison of EFG results obtained using 21 nodes with FEM and analytical results at the location ($x = 0.2\text{ m}$) of the 1-D model shown in Fig. 4.1	37
4.4	Comparison of EFG results obtained using 11 nodes with FEM and analytical results at the location ($x = 0.4\text{ m}$) of the 1-D model shown in Fig. 4.1	37
4.5	Comparison of EFG results obtained using 21 nodes with FEM and analytical results at the location ($x = 0.4\text{ m}$) of the 1-D model shown in Fig. 4.1	37
4.6	Comparison of EFG results obtained using 11 nodes with FEM and analytical results at the location ($x = 0.6\text{ m}$) of the 1-D model shown in Fig. 4.1	38
4.7	Comparison of EFG results obtained using 21 nodes with FEM and analytical results at the location ($x = 0.6\text{ m}$) of the 1-D model shown in Fig. 4.1	38
4.8	Comparison of EFG results obtained using 11 nodes with FEM and analytical results at the location ($x = 0.8\text{ m}$) of the 1-D model shown in Fig. 4.1	39
4.9	Comparison of EFG results obtained using 21 nodes with FEM and analytical results at the location ($x = 0.8\text{ m}$) of the 1-D model shown in Fig. 4.1	39
4.10	Effect of scaling parameter on EFG results obtained using 11 nodes at the location ($x = 0.4\text{ m}$) of the 1-D model shown in Fig. 4.1	40
4.11	Effect of scaling parameter on EFG results obtained using 21 nodes at the location ($x = 0.4\text{ m}$) of the 1-D model shown in Fig. 4.1	40
4.12	Effect of scaling parameter on EFG results obtained using 11 nodes at the location ($x = 0.8\text{ m}$) of the 1-D model shown in Fig. 4.1	41
4.13	Effect of scaling parameter on EFG results obtained using 21 nodes at the location ($x = 0.8\text{ m}$) of the 1-D model shown in Fig. 4.1	41
4.14	Convergence analysis of EFG results obtained using different time step at the location ($x = 0.4\text{ m}$) of the 1-D model shown in Fig. 4.1	45
4.15	Comparison of EFG results obtained using 11 nodes with FEM at the location	46

	($x = 0.2\text{ m}$) of the 1-D model shown in Fig. 4.1 for $d_{\max} = 1.01$	
4.16	Comparison of EFG results obtained using 11 nodes with FEM at the location ($x = 0.2\text{ m}$) of the 1-D model shown in Fig. 4.1 for $d_{\max} = 1.51$	46
4.17	Comparison of EFG results obtained using 21 nodes with FEM at the location ($x = 0.2\text{ m}$) of the 1-D model shown in Fig. 4.1 for $d_{\max} = 1.01$	47
4.18	Comparison of EFG results obtained using 21 nodes with FEM at the location ($x = 0.2\text{ m}$) of the 1-D model shown in Fig. 4.1 for $d_{\max} = 1.51$	47
4.19	Comparison of EFG results obtained using 11 nodes with FEM at the location ($x = 0.6\text{ m}$) of the 1-D model shown in Fig. 4.1 for $d_{\max} = 1.01$	48
4.20	Comparison of EFG results obtained using 11 nodes with FEM at the location ($x = 0.6\text{ m}$) of the 1-D model shown in Fig. 4.1 for $d_{\max} = 1.51$	48
4.21	Comparison of EFG results obtained using 21 nodes with FEM at the location ($x = 0.6\text{ m}$) of the 1-D model shown in Fig. 4.1 for $d_{\max} = 1.01$	49
4.22	Comparison of EFG results obtained using 21 nodes with FEM at the location ($x = 0.6\text{ m}$) of the 1-D model shown in Fig. 4.1 for $d_{\max} = 1.51$	49
4.23	Data for the 1-D model shown in Fig. 4.9	58
4.24	Comparison of EFG results obtained using 11 nodes with FEM results at the location ($x = 0.4\text{ m}$) of the 1-D model shown in Fig. 4.9	59
4.25	Comparison of EFG results obtained using 21 nodes with FEM results at the location ($x = 0.4\text{ m}$) of the 1-D model shown in Fig. 4.9	59
4.26	Comparison of EFG results obtained using 11 nodes with FEM results at the location ($x = 0.6\text{ m}$) of the 1-D model shown in Fig. 4.9	60
4.27	Comparison of EFG results obtained using 21 nodes with FEM results at the location ($x = 0.6\text{ m}$) of the 1-D model shown in Fig. 4.9	60
4.28	Comparison of EFG results obtained using 11 nodes with FEM results at the location ($x = 0.8\text{ m}$) of the 1-D model shown in Fig. 4.9	61
4.29	Comparison of EFG results obtained using 21 nodes with FEM results at the location ($x = 0.8\text{ m}$) of the 1-D model shown in Fig. 4.9	61
4.30	Comparison of EFG results obtained using 11 nodes with FEM results at the location ($x = 1\text{ m}$) of the 1-D model shown in Fig. 4.9	62
4.31	Comparison of EFG results obtained using 21 nodes with FEM results at the	62

	location ($x = 1\text{ m}$) of the 1-D model shown in Fig. 4.9	
4.32	Effect of scaling parameter on EFG results obtained using 11 nodes at the location ($x = 0.8\text{ m}$) of the 1-D model shown in Fig. 4.9	63
3.33	Effect of scaling parameter on EFG results obtained using 21 nodes at the location ($x = 0.8\text{ m}$) of the 1-D model shown in Fig. 4.9	63
4.34	Effect of scaling parameter on EFG results obtained using 11 nodes at the location ($x = 1\text{ m}$) of the 1-D model shown in Fig. 4.9	64
4.35	Effect of scaling parameter on EFG results obtained using 21 nodes at the location ($x = 1\text{ m}$) of the 1-D model shown in Fig. 4.9	64
4.36	Comparison of EFG results obtained using 11 nodes with FEM at the location ($x = 0.2\text{ m}$) of the 1-D model shown in Fig. 4.9 for $d_{\max} = 1.01$	68
4.37	Comparison of EFG results obtained using 11 nodes with FEM at the location ($x = 0.2\text{ m}$) of the 1-D model shown in Fig. 4.9 for $d_{\max} = 1.51$	68
4.38	Comparison of EFG results obtained using 21 nodes with FEM at the location ($x = 0.2\text{ m}$) of the 1-D model shown in Fig. 4.9 for $d_{\max} = 1.01$	69
4.39	Comparison of EFG results obtained using 21 nodes with FEM at the location ($x = 0.2\text{ m}$) of the 1-D model shown in Fig. 4.9 for $d_{\max} = 1.51$	69
4.40	Comparison of EFG results obtained using 11 nodes with FEM at the location ($x = 0.6\text{ m}$) for $d_{\max} = 1.01$	70
4.41	Comparison of EFG results obtained using 11 nodes with FEM at the location ($x = 0.6\text{ m}$) of the 1-D model shown in Fig. 4.9 for $d_{\max} = 1.51$	70
4.42	Comparison of EFG results obtained using 21 nodes with FEM at the location ($x = 0.6\text{ m}$) of the 1-D model shown in Fig. 4.9 for $d_{\max} = 1.01$	71
4.43	Comparison of EFG results obtained using 21 nodes with FEM at the location ($x = 0.6\text{ m}$) of the 1-D model shown in Fig. 4.9 for $d_{\max} = 1.51$	71
4.44	Data for the 1-D model shown in Fig.4.16	80
4.45	Comparison of EFG results obtained using 11 nodes with FEM results at the location ($x = 0.02\text{ m}$) of the 1-D model shown in Fig.4.16	81
4.46	Comparison of EFG results obtained using 21 nodes with FEM results at the location ($x = 0.02\text{ m}$) of the 1-D model shown in Fig.4.16	81
4.47	Comparison of EFG results obtained using 11 nodes with FEM results at the	82

	location ($x = 0.04$ m) of the 1-D model shown in Fig.4.16	
4.48	Comparison of EFG results obtained using 21 nodes with FEM results at the location ($x = 0.04$ m) of the 1-D model shown in Fig.4.16	82
4.49	Comparison of EFG results obtained using 11 nodes with FEM results at the location ($x = 0.06$ m) of the 1-D model shown in Fig.4.16	83
4.50	Comparison of EFG results obtained using 21 nodes with FEM results at the location ($x = 0.06$ m) of the 1-D model shown in Fig.4.16	83
4.51	Comparison of EFG results obtained using 11 nodes with FEM results at the location ($x = 0.08$ m)	84
4.52	Comparison of EFG results obtained using 21 nodes with FEM results at the location ($x = 0.08$ m) of the 1-D model shown in Fig.4.16	84
4.53	Effect of scaling parameter on EFG results obtained using 11 nodes at the location ($x = 0.02$ m) of the 1-D model shown in Fig.4.16	85
4.54	Effect of scaling parameter on EFG results obtained using 21 nodes at the location ($x = 0.02$ m) of the 1-D model shown in Fig.4.16	85
4.55	Effect of scaling parameter on EFG results obtained using 11 nodes at the location ($x = 0.06$ m) of the 1-D model shown in Fig.4.16	86
4.56	Effect of scaling parameter on EFG results obtained using 21 nodes at the location ($x = 0.06$ m) of the 1-D model shown in Fig.4.16	86
4.57	Comparison of EFG results obtained using 11 nodes with FEM at the location ($x = 0.02$ m) of the 1-D model shown in Fig.4.16 for $d_{\max} = 1.01$	90
4.58	Comparison of EFG results obtained using 11 nodes with FEM at the location ($x = 0.02$ m) of the 1-D model shown in Fig.4.16 for $d_{\max} = 1.51$	90
4.59	Comparison of EFG results obtained using 21 nodes with FEM at the location ($x = 0.02$ m) of the 1-D model shown in Fig.4.16 for $d_{\max} = 1.01$	91
4.60	Comparison of EFG results obtained using 21 nodes with FEM at the location ($x = 0.02$ m) of the 1-D model shown in Fig.4.16 for $d_{\max} = 1.51$	91
4.61	Comparison of EFG results obtained using 11 nodes with FEM at the location ($x = 0.06$ m) of the 1-D model shown in Fig.4.16 for $d_{\max} = 1.01$	92
4.62	Comparison of EFG results obtained using 11 nodes with FEM at the location ($x = 0.06$ m) of the 1-D model shown in Fig.4.16 for $d_{\max} = 1.51$	92

4.63	Comparison of EFG results obtained using 21 nodes with FEM at the location ($x = 0.06$ m) of the 1-D model shown in Fig.4.16 for $d_{\max} = 1.01$	93
4.64	Comparison of EFG results obtained using 21 nodes with FEM at the location ($x = 0.06$ m) of the 1-D model shown in Fig.4.16 for $d_{\max} = 1.51$	93
4.65	Data for 1-D model shown in Fig. 4.23	102
4.66	Comparison of EFG results obtained using 11 nodes with FEM results at the location ($r = 0$) of 1-D model shown in Fig. 4.23	103
4.67	Comparison of EFG results obtained using 21 nodes with FEM results at the location ($r = 0$) of 1-D model shown in Fig. 4.23	103
4.68	Comparison of EFG results obtained using 11 nodes with FEM results at the location ($r = 0.2$ m) of 1-D model shown in Fig. 4.23	104
4.69	Comparison of EFG results obtained using 21 nodes with FEM results at the location ($r = 0.2$ m) of 1-D model shown in Fig. 4.23	104
4.70	Comparison of EFG results obtained using 11 nodes with FEM results at the location ($r = 0.4$ m) of 1-D model shown in Fig. 4.23	105
4.71	Comparison of EFG results obtained using 21 nodes with FEM results at the location ($r = 0.4$ m) of 1-D model shown in Fig. 4.23	105
4.72	Comparison of EFG results obtained using 11 nodes with FEM results at the location ($r = 0.6$ m) of 1-D model shown in Fig. 4.23	106
4.73	Comparison of EFG results obtained using 21 nodes with FEM results at the location ($r = 0.6$ m) of 1-D model shown in Fig. 4.23	106
4.74	Effect of scaling parameter on EFG results obtained using 11 nodes at the location ($r = 0.2$ m) of 1-D model shown in Fig. 4.23	107
4.75	Effect of scaling parameter on EFG results obtained using 21 nodes at the location ($r = 0.2$ m) of 1-D model shown in Fig. 4.23	107
4.76	Effect of scaling parameter on EFG results obtained using 11 nodes at the location ($r = 0.6$ m) of 1-D model shown in Fig. 4.23	108
4.77	Effect of scaling parameter on EFG results obtained using 21 nodes at the location ($r = 0.6$ m) of 1-D model shown in Fig. 4.23	108
4.78	Comparison of EFG results obtained using 11 nodes with FEM at the location ($r = 0.2$ m) of 1-D model shown in Fig. 4.23 for $d_{\max} = 1.01$	112

4.79	Comparison of Temperature value obtained using 11 nodes with FEM at the location ($r = 0.2$ m) of 1-D model shown in Fig. 4.23 for $d_{\max} = 1.51$	112
4.80	Table 4.79 Comparison of EFG results obtained using 21 nodes with FEM at the location ($r = 0.2$ m) of 1-D model shown in Fig. 4.23 for $d_{\max} = 1.01$	113
4.81	Comparison of Temperature value obtained using 21 nodes with FEM at the location ($r = 0.2$ m) of 1-D model shown in Fig. 4.23 for $d_{\max} = 1.51$	113
4.82	Comparison of EFG results obtained using 11 nodes with FEM at the location ($r = 0.6$ m) of 1-D model shown in Fig. 4.23 for $d_{\max} = 1.01$	114
4.83	Comparison of Temperature value obtained using 11 nodes with FEM at the location ($r = 0.6$ m) for $d_{\max} = 1.51$	114
4.84	Comparison of EFG results obtained using 21 nodes with FEM at the location ($r = 0.6$ m) of 1-D model shown in Fig. 4.23 for $d_{\max} = 1.01$	115
485	Comparison of Temperature value obtained using 21 nodes with FEM at the location ($r = 0.6$ m) of 1-D model shown in Fig. 4.23 for $d_{\max} = 1.51$	115
5.1	Data for the 2-D model shown in Fig. 5.1	126
5.2	Comparison of EFG results obtained using 25 nodes with FEM and analytical results at the location ($x = 0.5$ m, $y = 1$ m) of the 2-D model shown in Fig. 5.1	127
5.3	Comparison of EFG results obtained using 81 nodes with FEM and analytical results at the location ($x = 0.5$ m, $y = 1$ m) of the 2-D model shown in Fig. 5.1	127
5.4	Comparison of EFG results obtained using 25 nodes with FEM and analytical results at the location ($x = 0.5$ m, $y = 0.5$ m) of the 2-D model shown in Fig. 5.1	128
5.5	Comparison of EFG results obtained using 81 nodes with FEM and analytical results at the location ($x = 0.5$ m, $y = 0.5$ m) of the 2-D model shown in Fig. 5.1	128
5.6	Comparison of EFG results obtained using 25 nodes with FEM and analytical results at the location ($x = 1$ m, $y = 1$ m) of the 2-D model shown in Fig. 5.1	129
5.7	Comparison of EFG results obtained using 81 nodes with FEM and analytical results at the location ($x = 1$ m, $y = 1$ m) of the 2-D model shown in Fig. 5.1	129
5.8	Comparison of EFG results obtained using 25 nodes with FEM and analytical results at the location ($x = 1$ m, $y = 0.5$ m) of the 2-D model shown in Fig. 5.1	130
5.9	Comparison of EFG results obtained using 81 nodes with FEM and analytical results at the location ($x = 1$ m, $y = 0.5$ m) of the 2-D model shown in Fig. 5.1	130

5.10	Effect of scaling parameter on EFG results obtained using 25 nodes at the location ($x = 0.5$ m, $y = 0.5$ m) of the 2-D model shown in Fig. 5.1	131
5.11	Effect of scaling parameter on EFG results obtained using 81 nodes at the location ($x = 0.5$ m, $y = 0.5$ m) of the 2-D model shown in Fig. 5.1	131
5.12	Effect of scaling parameter on EFG results obtained using 25 nodes at the location ($x = 1$ m, $y = 0.5$ m) of the 2-D model shown in Fig. 5.1	132
5.13	Effect of scaling parameter on EFG results obtained using 81 nodes at the location ($x = 1$ m, $y = 0.5$ m) of the 2-D model shown in Fig. 5.1	132
5.14	Convergence analysis of EFG results obtained using different time step at the location ($x = 1$ m, $y = 1$ m) of the 2-D model shown in Fig. 5.1	136
5.15	Comparison of EFG results obtained using 25 nodes with FEM at the location ($x = 0.5$ m, $y = 0.5$ m) of the 2-D model shown in Fig. 5.1 for $d_{\max} = 1.01$	137
5.16	Comparison of EFG results obtained using 25 nodes with FEM at the location ($x = 0.5$ m, $y = 0.5$ m) of the 2-D model shown in Fig. 5.1 for $d_{\max} = 1.51$	137
5.17	Comparison of EFG results obtained using 81 nodes with FEM at the location ($x = 0.5$ m, $y = 0.5$ m) of the 2-D model shown in Fig. 5.1 for $d_{\max} = 1.01$	138
5.18	Comparison of EFG results obtained using 81 nodes with FEM at the location ($x = 0.5$ m, $y = 0.5$ m) of the 2-D model shown in Fig. 5.1 for $d_{\max} = 1.51$	138
5.19	Comparison of EFG results obtained using 25 nodes with FEM at the location ($x = 1$ m, $y = 0.5$ m) of the 2-D model shown in Fig. 5.1 for $d_{\max} = 1.01$	139
5.20	Comparison of EFG results obtained using 25 nodes with FEM at the location ($x = 1$ m, $y = 0.5$ m) of the 2-D model shown in Fig. 5.1 for $d_{\max} = 1.51$	139
5.21	Comparison of EFG results obtained using 81 nodes with FEM at the location ($x = 1$ m, $y = 0.5$ m) of the 2-D model shown in Fig. 5.1 for $d_{\max} = 1.01$	140
5.22	Comparison of EFG results obtained using 81 nodes with FEM at the location ($x = 1$ m, $y = 0.5$ m) of the 2-D model shown in Fig. 5.1 for $d_{\max} = 1.51$	140
5.23	Data for the 2-D model shown in Fig. 5.9	149
5.24	Comparison of EFG results obtained using 25 nodes with FEM results at the location ($x = 0.025$ m, $y = 0$ m) of the 2-D model shown in Fig. 5.9	150
5.25	Comparison of EFG results obtained using 81 nodes with FEM results at the location ($x = 0.025$ m, $y = 0$ m) of the 2-D model shown in Fig. 5.9	150

5.26	Comparison of EFG results obtained using 25 nodes with FEM results at the location ($x = 0.05$ m, $y = 0$ m) of the 2-D model shown in Fig. 5.9	151
5.27	Comparison of EFG results obtained using 81 nodes with FEM results at the location ($x = 0.05$ m, $y = 0$ m) of the 2-D model shown in Fig. 5.9	151
5.28	Comparison of EFG results obtained using 25 nodes with FEM results at the location ($x = 0.075$ m, $y = 0$ m) of the 2-D model shown in Fig. 5.9	152
5.29	Comparison of EFG results obtained using 81 nodes with FEM results at the location ($x = 0.075$ m, $y = 0$ m) of the 2-D model shown in Fig. 5.9	152
5.30	Comparison of EFG results obtained using 25 nodes with FEM results at the location ($x = 0.1$ m, $y = 0$ m) of the 2-D model shown in Fig. 5.9	153
5.31	Comparison of EFG results obtained using 81 nodes with FEM results at the location ($x = 0.1$ m, $y = 0$ m) of the 2-D model shown in Fig. 5.9	153
5.32	Effect of scaling parameter on EFG results obtained using 25 nodes at the location ($x = 0.025$ m, $y = 0$ m) of the 2-D model shown in Fig. 5.9	154
5.33	Effect of scaling parameter on EFG results obtained using 81 nodes at the location ($x = 0.025$ m, $y = 0$ m) of the 2-D model shown in Fig. 5.9	154
5.34	Effect of scaling parameter on EFG results obtained using 25 nodes at the location ($x = 0.075$ m, $y = 0.0$ m) of the 2-D model shown in Fig. 5.9	155
5.35	Effect of scaling parameter on EFG results obtained using 81 nodes at the location ($x = 0.075$ m, $y = 0.0$ m) of the 2-D model shown in Fig. 5.9	155
5.36	Comparison of EFG results obtained using 25 nodes with FEM at the location ($x = 0.025$ m, $y = 0$ m) of the 2-D model shown in Fig. 5.9 for $d_{\max} = 1.01$	159
5.37	Comparison of EFG results obtained using 25 nodes with FEM at the location ($x = 0.025$ m, $y = 0$ m) of the 2-D model shown in Fig. 5.9 for $d_{\max} = 1.51$	159
5.38	Comparison of EFG results obtained using 81 nodes with FEM at the location ($x = 0.025$ m, $y = 0$ m) of the 2-D model shown in Fig. 5.9 for $d_{\max} = 1.01$	160
5.39	Comparison of EFG results obtained using 81 nodes with FEM at the location ($x = 0.025$ m, $y = 0$ m) of the 2-D model shown in Fig. 5.9 for $d_{\max} = 1.51$	160
5.40	Comparison of EFG results obtained using 25 nodes with FEM at the location ($x = 0.075$ m, $y = 0$ m) of the 2-D model shown in Fig. 5.9 for $d_{\max} = 1.01$	161
5.41	Comparison of EFG results obtained using 81 nodes with FEM at the location	161

	($x = 0.075$ m, $y = 0$ m) of the 2-D model shown in Fig. 5.9 for $d_{\max} = 1.51$	
5.42	Comparison of EFG results obtained using 81 nodes with FEM at the location ($x = 0.075$ m, $y = 0$ m) of the 2-D model shown in Fig. 5.9 for $d_{\max} = 1.01$	162
5.43	Comparison of EFG results obtained using 81 nodes with FEM at the location ($x = 0.075$ m, $y = 0$ m) of the 2-D model shown in Fig. 5.9 for $d_{\max} = 1.51$	162
5.44	Data for the 2-D model shown in Fig. 5.16	172
5.45	Comparison of EFG results obtained using 65 nodes with FEM results at the location ($x = 0.2$ m, $y = 0.4$ m) of the 2-D model shown in Fig. 5.16	173
5.46	Comparison of EFG results obtained using 225 nodes with FEM results at the location ($x = 0.2$ m, $y = 0.4$ m) of the 2-D model shown in Fig. 5.16	173
5.47	Comparison of EFG results obtained using 65 nodes with FEM results at the location ($x = 0.2$ m, $y = 0$ m) of the 2-D model shown in Fig. 5.16	174
5.48	Comparison of EFG results obtained using 225 nodes with FEM results at the location ($x = 0.2$ m, $y = 0$ m) of the 2-D model shown in Fig. 5.16	174
5.49	Comparison of EFG results obtained using 65 nodes with FEM results at the location ($x = 0.4$ m, $y = 0.4$ m) of the 2-D model shown in Fig. 5.16	175
5.50	Comparison of EFG results obtained using 225 nodes with FEM results at the location ($x = 0.4$ m, $y = 0.4$ m) of the 2-D model shown in Fig. 5.16	175
5.51	Comparison of EFG results obtained using 65 nodes with FEM results at the location ($x = 0.4$ m, $y = 0$ m) of the 2-D model shown in Fig. 5.16	176
5.52	Comparison of EFG results obtained using 225 nodes with FEM results at the location ($x = 0.4$ m, $y = 0$ m) of the 2-D model shown in Fig. 5.16	176
5.53	Effect of scaling parameter on EFG results obtained using 65 nodes at the location ($x = 0.2$ m, $y = 0$ m) of the 2-D model shown in Fig. 5.16	177
5.54	Effect of scaling parameter on EFG results obtained using 225 nodes at the location ($x = 0.2$ m, $y = 0$ m) of the 2-D model shown in Fig. 5.16	177
5.55	Effect of scaling parameter on EFG results obtained using 65 nodes at the location ($x = 0.4$ m, $y = 0$ m) of the 2-D model shown in Fig. 5.16	178
5.56	Effect of scaling parameter on EFG results obtained using 225 nodes at the location ($x = 0.4$ m, $y = 0$ m) of the 2-D model shown in Fig. 5.16	178
5.57	Comparison of EFG results obtained using 65 nodes with FEM at the location	182

	($x = 0.2 \text{ m}$, $y = 0 \text{ m}$) of the 2-D model shown in Fig. 5.16 for $d_{\max} = 1.01$	
5.58	Comparison of EFG results obtained using 65 nodes with FEM at the location ($x = 0.2 \text{ m}$, $y = 0 \text{ m}$) of the 2-D model shown in Fig. 5.16 for $d_{\max} = 1.51$	182
5.59	Comparison of EFG results obtained using 225 nodes with FEM at the location ($x = 0.2 \text{ m}$, $y = 0 \text{ m}$) of the 2-D model shown in Fig. 5.16 for $d_{\max} = 1.01$	183
5.60	Comparison of EFG results obtained using 225 nodes with FEM at the location ($x = 0.2 \text{ m}$, $y = 0 \text{ m}$) of the 2-D model shown in Fig. 5.16 for $d_{\max} = 1.51$	183
5.61	Comparison of EFG results obtained using 65 nodes with FEM at the location ($x = 0.4 \text{ m}$, $y = 0.4 \text{ m}$) of the 2-D model shown in Fig. 5.16 for $d_{\max} = 1.01$	184
5.62	Comparison of EFG results obtained using 65 nodes with FEM at the location ($x = 0.4 \text{ m}$, $y = 0.4 \text{ m}$) of the 2-D model shown in Fig. 5.16 for $d_{\max} = 1.51$	184
5.63	Comparison of EFG results obtained using 225 nodes with FEM at the location ($x = 0.4 \text{ m}$, $y = 0.4 \text{ m}$) for $d_{\max} = 1.01$	185
5.64	Comparison of EFG results obtained using 225 nodes with FEM at the location ($x = 0.4 \text{ m}$, $y = 0.4 \text{ m}$) of the 2-D model shown in Fig. 5.16 for $d_{\max} = 1.51$	185
5.65	Data for 2-D model shown in Fig 5.23	196
5.66	Comparison of EFG results obtained using 25 nodes with FEM results at the location ($r = 0.5 \text{ m}$ & $z = 1 \text{ m}$) of 2-D model shown in Fig 5.23	197
5.67	Comparison of EFG results obtained using 81 nodes with FEM results at the location ($r = 0.5 \text{ m}$ & $z = 1 \text{ m}$) of 2-D model shown in Fig 5.23	197
5.68	Comparison of EFG results obtained using 25 nodes with FEM results at the location ($r = 0.5 \text{ m}$ & $z = 0.75 \text{ m}$) of 2-D model shown in Fig 5.23	198
5.69	Comparison of EFG results obtained using 81 nodes with FEM results at the location ($r = 0.5 \text{ m}$ & $z = 0.75 \text{ m}$) of 2-D model shown in Fig 5.23	198
5.70	Comparison of EFG results obtained using 25 nodes with FEM results at the location ($r = 0.5 \text{ m}$ & $z = 0.5 \text{ m}$) of 2-D model shown in Fig 5.23	199
5.71	Comparison of EFG results obtained using 81 nodes with FEM results at the location ($r = 0.5 \text{ m}$ & $z = 0.5 \text{ m}$) of 2-D model shown in Fig 5.23	199
5.72	Comparison of EFG results obtained using 25 nodes with FEM results at the location ($r = 0.5 \text{ m}$ & $z = 0.25 \text{ m}$) of 2-D model shown in Fig 5.23	200
5.73	Comparison of EFG results obtained using 81 nodes with FEM results at the	200

	location ($r = 0.5 \text{ m}$ & $z = 0.25 \text{ m}$) of 2-D model shown in Fig 5.23	
5.74	Effect of scaling parameter on EFG results obtained using 25 nodes at the location ($r = 0.5 \text{ m}$ & $z = 1 \text{ m}$) of 2-D model shown in Fig 5.23	201
5.75	Effect of scaling parameter on EFG results obtained using 81 nodes at the location ($r = 0.5 \text{ m}$ & $z = 1 \text{ m}$) of 2-D model shown in Fig 5.23	201
5.76	Effect of scaling parameter on EFG results obtained using 25 nodes at the location ($r = 0.5 \text{ m}$ & $z = 0.5 \text{ m}$) of 2-D model shown in Fig 5.23	202
5.77	Effect of scaling parameter on EFG results obtained using 81 nodes at the location ($r = 0.5 \text{ m}$ & $z = 0.5 \text{ m}$) of 2-D model shown in Fig 5.23	202
5.78	Comparison of EFG results obtained using 25 nodes with FEM at the location ($r = 0.5 \text{ m}$ & $z = 1 \text{ m}$) of 2-D model shown in Fig 5.23 for $d_{\max} = 1.01$	206
5.79	Comparison of EFG results obtained using 25 nodes with FEM at the location ($r = 0.5 \text{ m}$ & $z = 1 \text{ m}$) of 2-D model shown in Fig 5.23 for $d_{\max} = 1.51$	206
5.80	Comparison of EFG results obtained using 81 nodes with FEM at the location ($r = 0.5 \text{ m}$ & $z = 1 \text{ m}$) of 2-D model shown in Fig 5.23 for $d_{\max} = 1.01$	207
5.81	Comparison of EFG results obtained using 81 nodes with FEM at the location ($r = 0.5 \text{ m}$ & $z = 1 \text{ m}$) of 2-D model shown in Fig 5.23 for $d_{\max} = 1.51$	207
5.82	Comparison of EFG results obtained using 25 nodes with FEM at the location ($r = 0.5 \text{ m}$ & $z = 0.5 \text{ m}$) of 2-D model shown in Fig 5.23 for $d_{\max} = 1.01$	208
5.83	Comparison of EFG results obtained using 25 nodes with FEM at the location ($r = 0.5 \text{ m}$ & $z = 0.5 \text{ m}$) of 2-D model shown in Fig 5.23 for $d_{\max} = 1.51$	208
5.84	Comparison of EFG results obtained using 81 nodes with FEM at the location ($r = 0.5 \text{ m}$ & $z = 0.5 \text{ m}$) of 2-D model shown in Fig 5.23 for $d_{\max} = 1.01$	209
5.85	Comparison of EFG results obtained using 81 nodes with FEM at the location ($r = 0.5 \text{ m}$ & $z = 0.5 \text{ m}$) of 2-D model shown in Fig 5.23 for $d_{\max} = 1.51$	209
6.1	Data for the 3-D model shown in Fig. 6.1	220
6.2	Comparison of EFG results obtained using 27 nodes with FEM and analytical results at the location ($x = 0.5 \text{ m}$, $y = 1 \text{ m}$ & $z = 1 \text{ m}$) of the 3-D model shown in Fig. 6.1	221
6.3	Comparison of EFG results obtained using 125 nodes with FEM and analytical results at the location ($x = 0.5 \text{ m}$, $y = 1 \text{ m}$ & $z = 1 \text{ m}$) of the 3-D model shown	221

	in Fig. 6.1	
6.4	Comparison of EFG results obtained using 27 nodes with FEM and analytical results at the location ($x = 0.5$ m, $y = 1$ m & $z = 0.5$ m) of the 3-D model shown in Fig. 6.1	222
6.5	Comparison of EFG results obtained using 125 nodes with FEM and analytical results at the location ($x = 0.5$ m, $y = 1$ m & $z = 0.5$ m) of the 3-D model shown in Fig. 6.1	222
6.6	Comparison of EFG results obtained using 27 nodes with FEM and analytical results at the location ($x = 1$ m, $y = 1$ m & $z = 1$ m) of the 3-D model shown in Fig. 6.1	223
6.7	Comparison of EFG results obtained using 125 nodes with FEM and analytical results at the location ($x = 1$ m, $y = 1$ m & $z = 1$ m) of the 3-D model shown in Fig. 6.1	223
6.8	Comparison of EFG results obtained using 27 nodes with FEM and analytical results at the location ($x = 1$ m, $y = 1$ m & $z = 0.5$ m) of the 3-D model shown in Fig. 6.1	224
6.9	Comparison of EFG results obtained using 125 nodes with FEM and analytical results at the location ($x = 1$ m, $y = 1$ m & $z = 0.5$ m) of the 3-D model shown in Fig. 6.1	224
6.10	Effect of scaling parameter on EFG results obtained using 27 nodes at the location ($x = 0.5$ m, $y = 1$ m & $z = 0.5$ m) of the 3-D model shown in Fig. 6.1	225
6.11	Effect of scaling parameter on EFG results obtained using 125 nodes at the location ($x = 0.5$ m, $y = 1$ m & $z = 0.5$ m) of the 3-D model shown in Fig. 6.1	225
6.12	Effect of scaling parameter on EFG results obtained using 27 nodes at the location ($x = 1$ m, $y = 1$ m & $z = 0.5$ m) of the 3-D model shown in Fig. 6.1	226
6.13	Effect of scaling parameter on EFG results obtained using 125 nodes at the location ($x = 1$ m, $y = 1$ m & $z = 0.5$ m) of the 3-D model shown in Fig. 6.1	226
6.14	Convergence study of EFG results (temperature values) obtained using different time step at the location ($x = 1$ m, $y = 1$ m & $z = 1$ m) of the 3-D model shown in Fig. 6.1	230
6.15	Comparison of EFG results obtained using 27 nodes with FEM at the location	231

	($x = 0.5 \text{ m}$, $y = 1 \text{ m}$ & $z = 0.5 \text{ m}$) of the 3-D model shown in Fig. 6.1 for $d_{\max} = 1.01$	
6.16	Comparison of EFG results obtained using 27 nodes with FEM at the location ($x = 0.5 \text{ m}$, $y = 1 \text{ m}$ & $z = 0.5 \text{ m}$) of the 3-D model shown in Fig. 6.1 for $d_{\max} = 1.51$	231
6.17	Comparison of EFG results obtained using 125 nodes with FEM at the location ($x = 0.5 \text{ m}$, $y = 1 \text{ m}$ & $z = 0.5 \text{ m}$) of the 3-D model shown in Fig. 6.1 for $d_{\max} = 1.01$	232
6.18	Comparison of EFG results obtained using 125 nodes with FEM at the location ($x = 0.5 \text{ m}$, $y = 1 \text{ m}$ & $z = 0.5 \text{ m}$) of the 3-D model shown in Fig. 6.1 for $d_{\max} = 1.51$	232
6.19	Comparison of EFG results obtained using 27 nodes with FEM at the location ($x = 1 \text{ m}$, $y = 1 \text{ m}$ & $z = 0.5 \text{ m}$) of the 3-D model shown in Fig. 6.1 for $d_{\max} = 1.01$	233
6.20	Comparison of EFG results obtained using 27 nodes with FEM at the location ($x = 1 \text{ m}$, $y = 1 \text{ m}$ & $z = 0.5 \text{ m}$) of the 3-D model shown in Fig. 6.1 for $d_{\max} = 1.51$	233
6.21	Comparison of EFG results obtained using 125 nodes with FEM at the location ($x = 1 \text{ m}$, $y = 1 \text{ m}$ & $z = 0.5 \text{ m}$) of the 3-D model shown in Fig. 6.1 for $d_{\max} = 1.01$	234
6.22	Comparison of EFG results obtained using 125 nodes with FEM at the location ($x = 1 \text{ m}$, $y = 1 \text{ m}$ & $z = 0.5 \text{ m}$) of the 3-D model shown in Fig. 6.1 for $d_{\max} = 1.51$	234
6.23	Data for 3-D model shown in Fig 6.9	247
6.24	Comparison of EFG results obtained using 96 nodes with FEM results at the location ($x = 0.2 \text{ m}$, $y = 0 \text{ m}$ & $z = 0.2 \text{ m}$) of the 3-D model shown in Fig 6.9	248
6.25	Comparison of EFG results obtained using 144 nodes with FEM results at the location ($x = 0.2 \text{ m}$, $y = 0 \text{ m}$ & $z = 0.2 \text{ m}$) of the 3-D model shown in Fig 6.9	248
6.26	Comparison of EFG results obtained using 96 nodes with FEM results at the location ($x = 0.4 \text{ m}$, $y = 0 \text{ m}$ & $z = 0.3 \text{ m}$) of the 3-D model shown in Fig 6.9	249
6.27	Comparison of EFG results obtained using 144 nodes with FEM results at the	249

	location ($x = 0.4 \text{ m}$, $y = 0 \text{ m}$ & $z = 0.3 \text{ m}$) of the 3-D model shown in Fig 6.9	
6.28	Comparison of EFG results obtained using 96 nodes with FEM results at the location ($x = 0.5 \text{ m}$, $y = 0 \text{ m}$ & $z = 0.1 \text{ m}$) of the 3-D model shown in Fig 6.9	250
6.29	Comparison of EFG results obtained using 144 nodes with FEM results at the location ($x = 0.5 \text{ m}$, $y = 0 \text{ m}$ & $z = 0.1 \text{ m}$) of the 3-D model shown in Fig 6.9	250
6.30	Comparison of EFG results obtained using 96 nodes with FEM results at the location ($x = 0.6 \text{ m}$, $y = 0 \text{ m}$ & $z = 0.3 \text{ m}$) of the 3-D model shown in Fig 6.9	251
6.31	Comparison of EFG results obtained using 144 nodes with FEM results at the location ($x = 0.6 \text{ m}$, $y = 0 \text{ m}$ & $z = 0.3 \text{ m}$) of the 3-D model shown in Fig 6.9	251
6.32	Effect of scaling parameter on EFG results obtained using 96 nodes at the location ($x = 0.2 \text{ m}$, $y = 0 \text{ m}$ & $z = 0.2 \text{ m}$) of the 3-D model shown in Fig 6.9	252
6.33	Effect of scaling parameter on EFG results obtained using 144 nodes at the location ($x = 0.2 \text{ m}$, $y = 0 \text{ m}$ & $z = 0.2 \text{ m}$) of the 3-D model shown in Fig 6.9	252
6.34	Effect of scaling parameter on EFG results obtained using 96 nodes at the location ($x = 0.5 \text{ m}$, $y = 0 \text{ m}$ & $z = 0.1 \text{ m}$) of the 3-D model shown in Fig 6.9	253
6.35	Effect of scaling parameter on EFG results obtained using 144 nodes at the location ($x = 0.5 \text{ m}$, $y = 0 \text{ m}$ & $z = 0.1 \text{ m}$) of the 3-D model shown in Fig 6.9	253
6.36	Comparison of EFG results obtained using 96 nodes with FEM at the location ($x = 0.4 \text{ m}$, $y = 0 \text{ m}$ & $z = 0.2 \text{ m}$) of the 3-D model shown in Fig 6.9 for $d_{\max} = 1.01$	257
6.37	Comparison of Temperature value obtained using 96 nodes with FEM at the location ($x = 0.4 \text{ m}$, $y = 0 \text{ m}$ & $z = 0.2 \text{ m}$) of the 3-D model shown in Fig 6.9 for $d_{\max} = 1.51$	257
6.38	Comparison of Temperature value obtained using 144 nodes with FEM at the location ($x = 0.4 \text{ m}$, $y = 0 \text{ m}$ & $z = 0.2 \text{ m}$) of the 3-D model shown in Fig 6.9 for $d_{\max} = 1.01$	258
6.39	Comparison of Temperature value obtained using 144 nodes with FEM at the location ($x = 0.4 \text{ m}$, $y = 0 \text{ m}$ & $z = 0.2 \text{ m}$) of the 3-D model shown in Fig 6.9 for $d_{\max} = 1.51$	258
6.40	Comparison of Temperature value obtained using 96 nodes with FEM at the location ($x = 0.5 \text{ m}$, $y = 0 \text{ m}$ & $z = 0.1 \text{ m}$) of the 3-D model shown in Fig 6.9	259

	for $d_{\max} = 1.01$	
6.41	Comparison of Temperature value obtained using 96 nodes with FEM at the location ($x = 0.5$ m, $y = 0$ m & $z = 0.1$ m) of the 3-D model shown in Fig 6.9 for $d_{\max} = 1.51$	259
6.42	Comparison of Temperature value obtained using 144 nodes with FEM at the location ($x = 0.5$ m, $y = 0$ m & $z = 0.1$ m) of the 3-D model shown in Fig 6.9 for $d_{\max} = 1.01$	260
6.43	Comparison of Temperature value obtained using 144 nodes with FEM at the location ($x = 0.5$ m, $y = 0$ m & $z = 0.1$ m) of the 3-D model shown in Fig 6.9 for $d_{\max} = 1.51$	260
6.44	Data for the 3-D model shown in Fig. 6.16	272
6.45	Comparison of EFG results obtained using 63 nodes with FEM results at the location ($x = 0.2$ m, $y = 0.4$ m & $z = 0.4$ m) of the 3-D model shown in Fig. 6.16	273
6.46	Comparison of EFG results obtained using 325 nodes with FEM results at the location ($x = 0.2$ m, $y = 0.4$ m & $z = 0.4$ m) of the 3-D model shown in Fig. 6.16	273
6.47	Comparison of EFG results obtained using 63 nodes with FEM results at the location ($x = 0.2$ m, $y = 0.4$ m & $z = 0$ m) of the 3-D model shown in Fig. 6.16	274
6.48	Comparison of EFG results obtained using 325 nodes with FEM results at the location ($x = 0.2$ m, $y = 0.4$ m & $z = 0$ m) of the 3-D model shown in Fig. 6.16	274
6.49	Comparison of EFG results obtained using 63 nodes with FEM results at the location ($x = 0.4$ m, $y = 0.4$ m & $z = 0.4$ m) of the 3-D model shown in Fig. 6.16	275
6.50	Comparison of EFG results obtained using 325 nodes with FEM results at the location ($x = 0.4$ m, $y = 0.4$ m & $z = 0.4$ m) of the 3-D model shown in Fig. 6.16	275
6.51	Comparison of EFG results obtained using 63 nodes with FEM results at the location ($x = 0.4$ m, $y = 0.2$ m & $z = 0.2$ m) of the 3-D model shown in Fig. 6.16	276
6.52	Comparison of EFG results obtained using 325 nodes with FEM results at the	276

	location ($x = 0.4 \text{ m}$, $y = 0.2 \text{ m}$ & $z = 0.2 \text{ m}$) of the 3-D model shown in Fig. 6.16	
6.53	Effect of scaling parameter on EFG results obtained using 63 nodes at the location ($x = 0.2 \text{ m}$, $y = 0.4 \text{ m}$ & $z = 0.4 \text{ m}$) of the 3-D model shown in Fig. 6.16	277
6.54	Effect of scaling parameter on EFG results obtained using 325 nodes at the location ($x = 0.2 \text{ m}$, $y = 0.4 \text{ m}$ & $z = 0.4 \text{ m}$) of the 3-D model shown in Fig. 6.16	277
6.55	Effect of scaling parameter on EFG results obtained using 63 nodes at the location ($x = 0.4 \text{ m}$, $y = 0.2 \text{ m}$ & $z = 0.2 \text{ m}$) of the 3-D model shown in Fig. 6.16	278
6.56	Effect of scaling parameter on EFG results obtained using 325 nodes at the location ($x = 0.4 \text{ m}$, $y = 0.2 \text{ m}$ & $z = 0.2 \text{ m}$) of the 3-D model shown in Fig. 6.16	278
6.57	Comparison of EFG results obtained using 63 nodes with FEM at the location ($x = 0.4 \text{ m}$, $y = 0.4 \text{ m}$ & $z = 0 \text{ m}$) of the 3-D model shown in Fig. 6.16 for $d_{\max} = 1.01$	282
6.58	Comparison of Temperature value obtained using 63 nodes with FEM at the location ($x = 0.4 \text{ m}$, $y = 0.4 \text{ m}$ & $z = 0 \text{ m}$) of the 3-D model shown in Fig. 6.16 for $d_{\max} = 1.51$	282
6.59	Comparison of EFG results obtained using 325 nodes with FEM at the location ($x = 0.4 \text{ m}$, $y = 0.4 \text{ m}$ & $z = 0 \text{ m}$) of the 3-D model shown in Fig. 6.16 for $d_{\max} = 1.01$	283
6.60	Comparison of Temperature value obtained using 325 nodes with FEM at the location ($x = 0.4 \text{ m}$, $y = 0.4 \text{ m}$ & $z = 0 \text{ m}$) of the 3-D model shown in Fig. 6.16 for $d_{\max} = 1.51$	283
6.61	Comparison of EFG results obtained using 63 nodes with FEM at the location ($x = 0.4 \text{ m}$, $y = 0.2 \text{ m}$ & $z = 0.2 \text{ m}$) of the 3-D model shown in Fig. 6.16 for $d_{\max} = 1.01$	284
6.62	Comparison of Temperature value obtained using 63 nodes with FEM at the location ($x = 0.4 \text{ m}$, $y = 0.2 \text{ m}$ & $z = 0.2 \text{ m}$) of the 3-D model shown in Fig.	284

	6.16 for $d_{\max} = 1.51$	
6.63	Comparison of EFG results obtained using 325 nodes with FEM at the location ($x = 0.4$ m, $y = 0.2$ m & $z = 0.2$ m) of the 3-D model shown in Fig. 6.16 for $d_{\max} = 1.01$	285
6.64	Comparison of Temperature value obtained using 325 nodes with FEM at the location ($x = 0.4$ m, $y = 0.2$ m & $z = 0.2$ m) of the 3-D model shown in Fig. 6.16 for $d_{\max} = 1.51$	285
6.65	Data for the 3-D model shown in Fig. 6.23	296
6.66	Comparison of EFG results obtained using 72 nodes with FEM results at the location ($r = 0.5$ m, $\theta = 0$ m & $z = 0$ m) of the 3-D model shown in Fig. 6.23	297
6.67	Comparison of EFG results obtained using 216 nodes with FEM results at the location ($r = 0.5$ m, $\theta = 0$ m & $z = 0$ m) of the 3-D model shown in Fig. 6.23	297
6.68	Comparison of EFG results obtained using 72 nodes with FEM results at the location ($r = 0.5$ m, $\theta = 0$ m & $z = 0.25$ m) of the 3-D model shown in Fig. 6.23	298
6.69	Comparison of EFG results obtained using 216 nodes with FEM results at the location ($r = 0.5$ m, $\theta = 0$ m & $z = 0.25$ m) of the 3-D model shown in Fig. 6.23	298
6.70	Comparison of EFG results obtained using 72 nodes with FEM results at the location ($r = 0.5$ m, $\theta = 0$ m & $z = 0.5$ m) of the 3-D model shown in Fig. 6.23	299
6.71	Comparison of EFG results obtained using 216 nodes with FEM results at the location ($r = 0.5$ m, $\theta = 0$ m & $z = 0.5$ m) of the 3-D model shown in Fig. 6.23	299
6.72	Effect of scaling parameter on EFG results obtained using 72 nodes at the location ($r = 0.5$ m, $\theta = 0$ m & $z = 0.25$ m) of the 3-D model shown in Fig. 6.23	300
6.73	Effect of scaling parameter on EFG results obtained using 216 nodes at the location ($r = 0.5$ m, $\theta = 0$ m & $z = 0.25$ m) of the 3-D model shown in Fig. 6.23	300
6.74	Comparison of EFG results obtained using 72 nodes with FEM at the location ($r = 0.5$ m, $\theta = 0$ m & $z = 0.25$ m) of the 3-D model shown in Fig. 6.23 for $d_{\max} = 1.01$	304
6.75	Comparison of Temperature value obtained using 72 nodes with FEM at the location ($r = 0.5$ m, $\theta = 0$ m & $z = 0.25$ m) of the 3-D model shown in Fig. 6.23 for $d_{\max} = 1.51$	304
6.76	Comparison of EFG results obtained using 216 nodes with FEM at the	305

	location ($r = 0.5$ m, $\theta = 0$ m & $z = 0.25$ m) of the 3-D model shown in Fig. 6.23 for $d_{\max} = 1.01$	
6.77	Comparison of Temperature value obtained using 216 nodes with FEM at the location ($r = 0.5$ m, $\theta = 0$ m & $z = 0.25$ m) of the 3-D model shown in Fig. 6.23 for $d_{\max} = 1.51$	305
7.1	Variation of total time & solution (inversion) time with data size (no. of nodes) for 1-D problem (Chapter 4: Case-III)	313
7.2	Variation of total time & solution (inversion) time with data size (no. of nodes) for 2-D problem (Chapter 5: Case-I)	314
7.3	Variation of total time & solution (inversion) time with data size (no. of nodes) for 3-D problem (Chapter 6: Case-I)	315
7.4	Variation of total time, communication time, speedup and efficiency with number of processors for 700 nodes	320
7.5	Variation of total time, communication time, speedup and efficiency with number of processors for 951 nodes	322
7.6	Variation of total time, communication time, speedup and efficiency with number of processors for 1100 nodes	324
7.7	Variation of total time, communication time, speedup and efficiency with number of processors for 676 nodes	327
7.8	Variation of total time, communication time, speedup and efficiency with number of processors for 961 nodes	329
7.9	Variation of total time, communication time, speedup and efficiency with number of processors for 1200 nodes	331
7.10	Variation of total time, communication time, speedup and efficiency with number of processors for 729 nodes	334
7.11	Variation of total time, communication time, speedup and efficiency with number of processors for 1000 nodes	336
7.12	Variation of total time, communication time, speedup and efficiency with number of processors for 1320 nodes	338

LIST OF FIGURES

Figure No.	Title	Page No.
4.1	One-dimensional model	35
4.2	Effect of scaling parameter on EFG results at the location ($x = 0.2\text{ m}$) of the 1-D model shown in Fig. 4.1	42
4.3	Effect of scaling parameter on EFG results at the location ($x = 0.6\text{ m}$) of the 1-D model shown in Fig. 4.1	43
4.4	Convergence analysis of EFG results obtained using different time step at the location ($x = 0.2\text{ m}$) of the 1-D model shown in Fig. 4.1	45
4.5	Comparison of EFG results obtained using 11 nodes with FEM at the location ($x = 0.4\text{ m}$) of the 1-D model shown in Fig. 4.1	50
4.6	Comparison of EFG results obtained using 21 nodes with FEM at the location ($x = 0.4\text{ m}$) of the 1-D model shown in Fig. 4.1	51
4.7	Comparison of EFG results obtained using 11 nodes with FEM at the location ($x = 0.8\text{ m}$) of the 1-D model shown in Fig. 4.1	52
4.8	Comparison of EFG results obtained using 21 nodes with FEM at the location ($x = 0.8\text{ m}$) of the 1-D model shown in Fig. 4.1	53
4.9	One-dimensional model	58
4.10	Effect of scaling parameter on EFG results at the location ($x = 0.2\text{ m}$) of the 1-D model shown in Fig. 4.9	65
4.11	Effect of scaling parameter on EFG results at the location ($x = 0.6\text{ m}$) of the 1-D model shown in Fig. 4.9	66
4.12	Comparison of EFG results obtained using 11 nodes with FEM at the location ($x = 0.8\text{ m}$) of the 1-D model shown in Fig. 4.9	72
4.13	Comparison of EFG results obtained using 21 nodes with FEM at the location ($x = 0.8\text{ m}$) of the 1-D model shown in Fig. 4.9	73
4.14	Comparison of EFG results obtained using 11 nodes with FEM at the location ($x = 1\text{ m}$) of the 1-D model shown in Fig. 4.9	74
4.15	Comparison of EFG results obtained using 21 nodes with FEM at the location ($x = 1\text{ m}$) of the 1-D model shown in Fig. 4.9	75

4.16	One-dimensional model	80
4.17	Effect of scaling parameter on EFG results at the location ($x = 0.04$ m) of the 1-D model shown in Fig.4.16	87
4.18	Effect of scaling parameter on EFG results at the location ($x = 0.08$ m) of the 1-D model shown in Fig.4.16	88
4.19	Comparison of EFG results obtained using 11 nodes with FEM at the location ($x = 0.04$ m) of the 1-D model shown in Fig.4.16	94
4.20	Comparison of EFG results obtained using 21 nodes with FEM at the location ($x = 0.04$ m) of the 1-D model shown in Fig.4.16	95
4.21	Comparison of EFG results obtained using 11 nodes with FEM at the location ($x = 0.10$ m) of the 1-D model shown in Fig.4.16	96
4.22	Comparison of EFG results obtained using 21 nodes with FEM at the location ($x = 0.10$ m) of the 1-D model shown in Fig.4.16	97
4.23	One-dimensional model	102
4.24	Effect of scaling parameter on EFG results at the location ($r = 0$) of the 1-D model shown in Fig. 4.23	109
4.25	Effect of scaling parameter on EFG results at the location ($r = 0.4$ m) of the 1-D model shown in Fig. 4.23	110
4.26	Comparison of EFG results obtained using 11 nodes with FEM at the location ($r = 0$) of the 1-D model shown in Fig. 4.23	116
4.27	Comparison of EFG results obtained using 21 nodes with FEM at the location ($r = 0$) of the 1-D model shown in Fig. 4.23	117
4.28	Comparison of EFG results obtained using 11 nodes with FEM at the location ($r = 0.4$ m) of the 1-D model shown in Fig. 4.23	118
4.29	Comparison of EFG results obtained using 21 nodes with FEM at the location ($r = 0.4$ m) of the 1-D model shown in Fig. 4.23	119
5.1	Two-dimensional model	126
5.2	Effect of scaling parameter on EFG results at the location ($x = 0.5$ m, $y = 1$ m) of the 2-D model shown in Fig. 5.1	133
5.3	Effect of scaling parameter on EFG results at the location ($x = 1$ m, $y = 1$ m) of the 2-D model shown in Fig. 5.1	134

5.4	Convergence analysis of EFG results obtained using different time step at the location ($x = 0.5$ m, $y = 1$ m) of the 2-D model shown in Fig. 5.1	136
5.5	Comparison of EFG results obtained using 25 nodes with FEM at the location ($x = 0.5$ m, $y = 1$ m) of the 2-D model shown in Fig. 5.1	141
5.6	Comparison of EFG results obtained using 81 nodes with FEM at the location ($x = 0.5$ m, $y = 1$ m) of the 2-D model shown in Fig. 5.1	142
5.7	Comparison of EFG results obtained using 25 nodes with FEM at the location ($x = 1$ m, $y = 1$ m) of the 2-D model shown in Fig. 5.1	143
5.8	Comparison of EFG results obtained using 81 nodes with FEM at the location ($x = 1$ m, $y = 1$ m) of the 2-D model shown in Fig. 5.1	144
5.9	Two-dimensional fin model	149
5.10	Effect of scaling parameter on EFG results at the location ($x = 0.05$ m, $y = 0$ m) of the 2-D model shown in Fig. 5.9	156
5.11	Effect of scaling parameter on EFG results at the location ($x = 0.1$ m, $y = 0$ m) of the 2-D model shown in Fig. 5.9	157
5.12	Comparison of EFG results obtained using 25 nodes with FEM at the location ($x = 0.05$ m, $y = 0$ m) of the 2-D model shown in Fig. 5.9	163
5.13	Comparison of EFG results obtained using 81 nodes with FEM at the location ($x = 0.05$ m, $y = 0$ m) of the 2-D model shown in Fig. 5.9	164
5.14	Comparison of EFG results obtained using 25 nodes with FEM at the location ($x = 0.1$ m, $y = 0$ m) of the 2-D model shown in Fig. 5.9	165
5.15	Comparison of EFG results obtained using 81 nodes with FEM at the location ($x = 0.1$ m, $y = 0$ m) of the 2-D model shown in Fig. 5.9	166
5.16	Two-dimensional model of composite slabs	171
5.17	Effect of scaling parameter on EFG results at the location ($x = 0.2$ m, $y = 0.4$ m) of the 2-D model shown in Fig. 5.16	179
5.18	Effect of scaling parameter on EFG results at the location ($x = 0.4$ m, $y = 0.4$ m) of the 2-D model shown in Fig. 5.16	180
5.19	Comparison of EFG results obtained using 65 nodes with FEM at the location ($x = 0.4$ m, $y = 0.2$ m) of the 2-D model shown in Fig. 5.16	186
5.20	Comparison of EFG results obtained using 225 nodes with FEM at the	187

	location ($x = 0.4$ m, $y = 0.2$ m) of the 2-D model shown in Fig. 5.16	
5.21	Comparison of EFG results obtained using 65 nodes with FEM at the location ($x = 0.4$ m, $y = 0$ m) of the 2-D model shown in Fig. 5.16	188
5.22	Comparison of EFG results obtained using 225 nodes with FEM at the location ($x = 0.4$ m, $y = 0$ m) of the 2-D model shown in Fig. 5.16	189
5.23	Two-dimensional model	195
5.24	Effect of scaling parameter on EFG results at the location ($r = 0.5$ m & $z = 0.75$ m) of 2-D model shown in Fig 5.23	203
5.25	Effect of scaling parameter on EFG results at the location ($r = 0.5$ m & $z = 0.25$ m) of 2-D model shown in Fig 5.23	204
5.26	Comparison of EFG results obtained using 25 nodes with FEM at the location ($r = 0.5$ m & $z = 0.75$ m) of 2-D model shown in Fig 5.23	210
5.27	Comparison of EFG results obtained using 81 nodes with FEM at the location ($r = 0.5$ m & $z = 0.75$ m) of 2-D model shown in Fig 5.23	211
5.28	Comparison of EFG results obtained using 25 nodes with FEM at the location ($r = 0.5$ m & $z = 0.25$ m) of 2-D model shown in Fig 5.23	212
5.29	Comparison of EFG results obtained using 81 nodes with FEM at the location ($r = 0.5$ m & $z = 0.25$ m) of 2-D model shown in Fig 5.23	213
6.1	Three-dimensional model	220
6.2	Effect of scaling parameter on EFG results at the location ($x = 0.5$ m, $y = 1$ m & $z = 1$ m) of the 3-D model shown in Fig. 6.1	227
6.3	Effect of scaling parameter on EFG results at the location ($x = 1$ m, $y = 1$ m & $z = 1$ m) of the 3-D model shown in Fig. 6.1	228
6.4	Convergence analysis of EFG results obtained using different time step at the location ($x = 0.5$ m, $y = 1$ m & $z = 1$ m) of the 3-D model shown in Fig. 6.1	230
6.5	Comparison of EFG results obtained using 27 nodes with FEM at the location ($x = 0.5$ m, $y = 0.5$ m & $z = 1$ m) of the 3-D model shown in Fig. 6.1	235
6.6	Comparison of EFG results obtained using 125 nodes with FEM at the location ($x = 0.5$ m, $y = 0.5$ m & $z = 1$ m) of the 3-D model shown in Fig. 6.1	236
6.7	Comparison of EFG results obtained using 27 nodes with FEM at the location ($x = 1$ m, $y = 1$ m & $z = 1$ m) of the 3-D model shown in Fig. 6.1	237

6.8	Comparison of EFG results obtained using 125 nodes with FEM at the location ($x = 1\text{ m}$, $y = 1\text{ m}$ & $z = 1\text{ m}$) of the 3-D model shown in Fig. 6.1	238
6.9	Three-dimensional model of composites	246
6.10	Effect of scaling parameter on EFG results at the location ($x = 0.4\text{ m}$, $y = 0\text{ m}$ & $z = 0.3\text{ m}$) of the 3-D model shown in Fig 6.9	254
6.11	Effect of scaling parameter on EFG results at the location ($x = 0.6\text{ m}$, $y = 0\text{ m}$ & $z = 0.3\text{ m}$) of the 3-D model shown in Fig 6.9	255
6.12	Comparison of EFG results obtained using 96 nodes with FEM at the location ($x = 0.6\text{ m}$, $y = 0\text{ m}$ & $z = 0.2\text{ m}$) of the 3-D model shown in Fig 6.9	261
6.13	Comparison of EFG results obtained using 144 nodes with FEM at the location ($x = 0.6\text{ m}$, $y = 0\text{ m}$ & $z = 0.2\text{ m}$) of the 3-D model shown in Fig 6.9	262
6.14	Comparison of EFG results obtained using 96 nodes with FEM at the location ($x = 0.6\text{ m}$, $y = 0\text{ m}$ & $z = 0.3\text{ m}$) of the 3-D model shown in Fig 6.9	263
6.15	Comparison of EFG results obtained using 144 nodes with FEM at the location ($x = 0.6\text{ m}$, $y = 0\text{ m}$ & $z = 0.3\text{ m}$) of the 3-D model shown in Fig 6.9	264
6.16	Three-dimensional model of composite slabs	271
6.17	Effect of scaling parameter on EFG results at the location ($x = 0.2\text{ m}$, $y = 0.4\text{ m}$ & $z = 0\text{ m}$) of the 3-D model shown in Fig. 6.16	279
6.18	Effect of scaling parameter on EFG results at the location ($x = 0.4\text{ m}$, $y = 0.4\text{ m}$ & $z = 0\text{ m}$) of the 3-D model shown in Fig. 6.16	280
6.19	Comparison of EFG results obtained using 63 nodes with FEM at the location ($x = 0.2\text{ m}$, $y = 0.4\text{ m}$ & $z = 0\text{ m}$) of the 3-D model shown in Fig. 6.16	286
6.20	Comparison of EFG results obtained using 325 nodes with FEM at the location ($x = 0.2\text{ m}$, $y = 0.4\text{ m}$ & $z = 0\text{ m}$) of the 3-D model shown in Fig. 6.16	287
6.21	Comparison of EFG results obtained using 63 nodes with FEM at the location ($x = 0.4\text{ m}$, $y = 0.4\text{ m}$ & $z = 0.4\text{ m}$) of the 3-D model shown in Fig. 6.16	288
6.22	Comparison of EFG results obtained using 325 nodes with FEM at the location ($x = 0.4\text{ m}$, $y = 0.4\text{ m}$ & $z = 0.4\text{ m}$) of the 3-D model shown in Fig. 6.16	289
6.23	Three-dimensional model of composite cylinder	295
6.24	Effect of scaling parameter on EFG results at the location ($r = 0.5\text{ m}$, $\theta = 0\text{ m}$ & $z = 0\text{ m}$) of the 3-D model shown in Fig. 6.23	301

7.16	Variation of total time and communication time with number of processors for 961 nodes	329
7.17	Variation of speedup with number of processors for 961 nodes	330
7.18	Variation of efficiency with number of processors for 961 nodes	330
7.19	Variation of total time and communication time with number of processors for 1200 nodes	331
7.20	Variation of speedup with number of processors for 1200 nodes	332
7.21	Variation of efficiency with number of processors for 1200 nodes	332
7.22	Variation of total time and communication time with number of processors for 729 nodes	334
7.23	Variation of speedup with number of processors for 729 nodes	335
7.24	Variation of efficiency with number of processors for 729 nodes	335
7.25	Variation of total time and communication time with number of processors for 1000 nodes	336
7.26	Variation of speedup with number of processors for 1000 nodes	337
7.27	Variation of efficiency with number of processors for 1000 nodes	337
7.28	Variation of total time and communication time with number of processors for 1320 nodes	338
7.29	Variation of efficiency with number of processors for 1320 nodes	339
730	Variation of efficiency with number of processors for 1320 nodes	339

LIST OF SYMBOLS

$\mathbf{a}(\mathbf{x})$	vector of non-constant coefficients
$\mathbf{a}^T(\mathbf{x})$	transpose of vector $\mathbf{a}(\mathbf{x})$
A_c	area of cross section of fin model, m^2
c	specific heat of the material, kJ/kg-K
c_{xj}, c_{yj}, c_{zj}	distances to the nearest neighbors in x, y and z directions
$\cos(\bar{n}, x)$	cosine of angle between \bar{n} and x -axis
$\cos(\bar{n}, y)$	cosine of angle between \bar{n} and y -axis
$\cos(\bar{n}, z)$	cosine of angle between \bar{n} and z -axis
C.S.	cubicspline
d_{\max}	scaling parameter
h	convective heat transfer coefficient, $\text{W/m}^2\text{-K}$
k	thermal conductivity of the material, W/m-K
k_x, k_y, k_z	thermal conductivity of the material in x, y and z -directions, W/m-K
k_r, k_θ	thermal conductivity of the material in r and θ -directions, W/m-K
k'	degree of the polynomial
m	number of terms in the basis
M	$h\left(\frac{P_r}{A_c}\right)T_\infty$
n	number of nodes in the domain of influence of \mathbf{x}
N	number of iterations
\bar{N}	number of equations
\bar{n}	outward normal to the surface
N_K	Lagrange interpolant

$\mathbf{p}(\mathbf{x})$	vector of basis functions
$\mathbf{p}^T(\mathbf{x})$	transpose of vector $\mathbf{p}(\mathbf{x})$
P_r	perimeter of the cross section of fin model, m
Q.S.	quarticspline
\dot{Q}	rate of internal heat generation per unit volume, W/m^3
$\bar{r}_x, \bar{r}_y, \bar{r}_z$	normalized radii along x, y and z directions
S_i	surfaces of three dimensional models
t	time, sec
$T(\mathbf{x})$	Actual function (i.e. temperature)
$T^h(\mathbf{x})$	moving least square approximant
\dot{T}	$\frac{\partial T}{\partial t}$
T_i	nodal parameter
T_s	surface temperature, $^{\circ}\text{C}$
T_{∞}	surrounding fluid temperature, $^{\circ}\text{C}$
$T_{,x}$	$\frac{\partial T}{\partial x}$
$T_{,y}$	$\frac{\partial T}{\partial y}$
$T_{,z}$	$\frac{\partial T}{\partial z}$
V	three dimensional domain ($V_1 \cup V_2$)
$w(\mathbf{x} - \mathbf{x}_i)$	weight function
$w_{,x}$	$\frac{\partial w}{\partial x}$

$$w_{,y} \quad \frac{\partial w}{\partial y}$$

$$w_{,z} \quad \frac{\partial w}{\partial z}$$

x Gauss points

x_I nodal point

x_I, y_I, z_I coordinates of the I^{th} node

Greek Symbols

δ variational parameter

λ and λ' Lagrangian multipliers

$\Phi_I(\mathbf{x})$ shape function

ρ density of the material, kg/m^3

CHAPTER 1

INTRODUCTION

1.1 INTRODUCTION

Heat transfer problems can be solved by different numerical techniques. These include finite difference method (FDM), finite volume method (FVM), boundary element method (BEM) and finite element method (FEM). Among all these techniques, FEM is a well established and powerful numerical technique to solve the heat transfer problems. Although FEM is quite successful but the discretization of complex three-dimensional geometry and re-meshing of the domain changing with time, is very rigorous, time-consuming and burdensome task in comparison of assembly and solution of the finite element equations. In spite of its numerous advantages and unparalleled success, it is not well suited for certain classes of problems, such as crack propagation and moving discontinuities, plate bending, solution of higher order partial differential equations, phase transformation, moving phase boundaries, modeling of multi-scale phenomena, dynamic impact problems and thermal analysis of turbine blades. To avoid these problems, recently a class of new methods has been developed, known as meshless method. This class of methods includes smooth particle hydrodynamics (SPH) (Monaghan, 1988), diffuse element method (DEM) (Nayroles et al., 1992), element free Galerkin (EFG) method (Belytschko et al., 1994), reproducing kernel particle method (RKPM) (Liu et al., 1995a), finite point method (FPM) (Onate et al., 2001), partition of unity method (PUM) (Melenk and Babuska, 1996), *H-p* cloud method (Durate and Oden, 1996), free mesh method (FMM) (Yagawa and Yamada, 1996), boundary node method (BNM) (Mukherjee and Mukherjee, 1997), natural element method (NEM) (Sukumar et al., 1998b), local boundary integral equation (LBIE) method (Zhu et al., 1998a), meshless local Petrov-Galerkin (MLPG) method (Atluri and Zhu, 1998), the method of finite spheres (De and Bathe, 2000), regular hybrid boundary node method (RHBNM) (Zhang et al., 2003), local

point interpolation method (LPIM) (Liu and Gu, 2001a) and local radial point interpolation method (LRPIM) (Liu and Gu, 2001b).

The results obtained by most of these meshless methods are found competitive with those obtained by FEM in different areas of engineering and sciences. The only big hurdle with the wide implementation of these meshless methods is their high computational cost. To reduce their computational cost, few researchers have parallelized free mesh method (FMM), smooth particle hydrodynamics (SPH), reproducing kernel particle method (RKPM) and partition of unity method (PUM).

Among all the meshless methods developed so far, the EFG method is being successfully used to solve various problems in different areas such as fracture mechanics, static and dynamic fracture, wave and crack propagation, vibration analysis, viscoelasticity, plates and shells, non-destructive testing (NDT), electromagnetic field, contact problems in metal forming. The results obtained by this method are more accurate (Lu et al., 1994) as compared to FEM. The only big hurdle remains with the wide implementation of this method is its computational cost which is quite large in comparison to FEM (Belytschko et al., 1996b,c; Dolbow and Belytschko, 1998; Singh et al., 2003a). Even though it has been identified by the researchers (Belytschko et al., 1994) that the EFG method can also be applied in the area of heat transfer, significant work has not been carried out in this area. Therefore, present research work mainly concentrates on the applicability of the meshless EFG method in the area of heat transfer. Since the accuracy of results obtained by EFG method is largely dependent on weight function, four new weight functions are also proposed and studied in this thesis work. In view of the currently felt need for parallel programming version for most of meshless methods, a parallel algorithm for the EFG method is developed and the results obtained by this parallel code are also presented.

1.2 OBJECTIVE OF THE RESEARCH

The purpose of this research work is to apply the meshless element free Galerkin (EFG) method in the area of heat transfer and to develop a parallel algorithm. The objectives of the present work are:

- To apply the EFG method in the area of heat transfer.
- To develop new weight functions.
- To find the most appropriate weight function for heat transfer applications.
- To find the range of scaling parameter for heat transfer problems.
- To develop a parallel algorithm to reduce the computational cost.

1.3 SCOPE OF THE RESEARCH

The EFG method has been successfully used in some areas like fracture mechanics, plates and shells, wave and crack propagation, electromagnetic field, non-destructive testing (NDT), vibration analysis and viscoelasticity, etc. So far, this method has not been applied to solve higher order partial differential equation, phase transformation, moving phase boundaries, thermal analysis of turbine blades and complex fluid flow problems. Therefore, the present work describes the applicability of EFG method in the area of heat transfer and its parallel implementation. Moreover, the present analysis not only checks the applicability of EFG method in the area of heat transfer and its parallel implementation, but also gives certain fruitful results (e.g. the range of scaling parameter and most appropriate weight function for heat transfer applications).

1.4 ORGANIZATION OF THE RESEARCH

Chapter 1 introduces to heat transfer problems and the various aspects considered in the present work. The objective and scope of the present analysis have also been emphasized along with the organization of the work.

Chapter 2 deals with the literature review of the various meshless methods including EFG method, which are used in the areas of engineering and sciences. The parallelization of the meshless methods has also been discussed in this chapter.

In Chapter 3, the EFG method has been discussed in detail. Initially the introduction of the EFG method has been presented. A discussion on moving least square (MLS) approximants is given. The technique for efficiently calculating the shape functions and their derivatives is presented. Also the description of the weight function and imposition of essential (Dirichlet) boundary conditions has been demonstrated.

Chapter 4 gives the discretization, formulation and results for 1-D heat transfer problems. Four cases have been discussed in detail. It also gives an emphasis on the effect of weight function and scaling parameter on EFG results (temperature values) in one-dimensional heat transfer problems.

Chapter 5 presents discretization, formulation and solution of 2-D heat transfer problems. Four different cases have been fully analyzed. It also presents the effect of weight function and scaling parameter on EFG results (temperature values) in two-dimensional heat transfer problems.

The discretization, formulation and solution of 3-D heat transfer problems are given in Chapter 6. Four cases have been chosen to check the applicability of the EFG method. Moreover, the effect of weight functions and scaling parameter on the EFG results (temperature values) has also been discussed.

In Chapter 7, a new parallel algorithm has been proposed for the EFG method. The parallel code has been written in FORTRAN language using MPI message passing library and executed on a MIMD type 'PARAM 10000' supercomputer. The proposed algorithm has been validated by solving three model heat transfer problems one each in 1-D, 2-D and 3-D domains.

Conclusions are summarized in Chapter 8 and few suggestions for future scope of work are also mentioned.

CHAPTER 2

LITERATURE REVIEW

For more than 30 years, finite element method (FEM) has been a well-established and popular numerical technique, not only to solve the problems of heat transfer but also to solve various problems in the areas of engineering and science. Although FEM is quite successful, the discretization of three-dimensional complex geometries and re-meshing of the domain changing with time is a very tedious and time-consuming process. Assembly and solution of the finite element equations also often lead to numerical errors. Despite its numerous advantages, it is not well suited for certain classes of problems, such as crack propagation and moving discontinuities, moving phase boundaries, phase transformation, plate bending, large deformations, solution of higher order partial differential equations, modeling of multi-scale phenomena, thermal analysis of turbine blades and dynamic impact problems. Therefore, it has become a necessity to find a method that may be somewhat more expensive from the viewpoint of computational time but requires less time in the preparation of data. To avoid these problems, recently a class of new methods has been developed, known as meshless (meshfree) method.

In meshless (meshfree) methods, interpolants (strictly speaking approximants) are constructed solely on the basis of a set of scattered nodes whereas in case of finite element method, interpolants are constructed by using a number of small elements known as finite elements. There is a small difference between the interpolants used in FEM and meshless methods. In case of FEM, the variation of unknown variable is approximated using interpolating polynomials and nodal values of the variable on each element, while it is not the case with meshless methods. This is the key feature that distinguishes FEM from meshless methods.

A number of meshless methods have been developed so far including smooth particle hydrodynamics (SPH) (Monaghan, 1988; Monaghan, 1992), diffuse element method (DEM) (Nayroles et al., 1992, 1994; Marechal et. al., 1993), element-free Galerkin (EFG) method (Belytschko et al., 1994; Lu et al., 1994), reproducing kernel particle method (RKPM) (Liu et al., 1995a,b,1996; Chen et al., 1997; Jun et al., 1998; Aluru, 1998), finite point method (FPM) (Onate et al., 2001), partition of unity method (PUM) (Melenk and Babuska, 1996; Babuska and Melenk, 1997), *H-p* cloud method (Durate and Oden, 1996), free mesh method (FMM) (Yagawa and Yamada, 1996; Yagawa and Furukawa, 2000), boundary node method (BNM) (Mukherjee and Mukherjee, 1997), natural element method (NEM) (Sukumar, 1998a,b), local boundary integral equation (LBIE) method (Zhu et al., 1998a,b; Atluri et al., 2000; Long and Zhang, 2002), meshless local Petrov-Galerkin (MLPG) method (Atluri and Zhu, 1998; Cho and Atluri, 2001; Atluri and Shen, 2002; Xiao and McCarthy, 2003), the method of finite spheres (De and Bathe, 2000,2001a,b), regular hybrid boundary node method (RHBNM) (Zhang et al., 2003; Zhang and Yao, 2003), local point interpolation method (LPIM) (Liu and Gu, 2001a; Gu and Liu, 2001) and local radial point interpolation method (LRPIM) (Liu and Gu, 2001b).

All these meshless methods have a common feature that only nodal data is required to describe the interpolation of field variables. Although, in most of meshless methods, Galerkin formulation is utilized to develop the discrete equations but the major difference among these methods lies in the interpolation (approximation) techniques. Generally, three different interpolation (approximation) techniques have been used in meshless methods, kernel approximation, moving least square (MLS) approximation and partition of unity.

Lucy (1977) developed the first meshless method that is known as smooth particle hydrodynamic (SPH) method (Lucy, 1977; Gingold and Monaghan, 1977). Even though SPH is not a Galerkin based meshless method, its particle nature renders it to be a meshless

method. The applications of SPH have primarily been focused in the area of hydrodynamics and in the simulation of astrophysical phenomena.

A parallel but distinctively different path was taken by Nayroles and his co-workers to develop diffuse element method (DEM) in which they first used the MLS approximations (Lancaster and Salkauskas, 1981) to develop Galerkin equations (Nayroles et al., 1992,1994).

The diffuse element method (DEM) was then further refined and modified by Belytschko and his co-workers (Belytschko et al., 1994; Lu et al., 1994) and they called their method, element free Galerkin (EFG) method. For example, a higher-order quadrature rule based on a background mesh of cells was used for numerical integration and certain terms in the derivatives of the interpolants (approximants), which were omitted in the DEM, were included in the EFG method. These improvements were found to be necessary for achieving good accuracy and convergence. This class of methods are more consistent and stable but more expensive from the computational time point of view. The details of the EFG method are given in next chapter of this thesis.

Liu et al. (1995a) proposed a meshless reproducing kernel particle method (RKPM) with an approximation based on a convolution integral (continuous kernel). They introduced a correction function in the continuous kernel (convolution integral) which corrects the consistency near the boundaries as well as at nonuniform nodal spacing. Adding this correction function in the continuous kernel enhances the accuracy of the solution as compared to SPH method. In contrast to SPH, RKPM satisfies consistency because the reproducing conditions were used to construct the method, whereas SPH lacks constant consistency for nonuniform nodal spacing and on the boundaries. Therefore, RKPM can be considered as SPH with a correction function that restores consistency. Another difference with SPH is that SPH uses collocation methods to develop the discrete equations whereas RKPM as well as most of the other meshless methods use Galerkin method to develop

discrete equations. Belytschko et al. (1996c) showed that the discrete form of the convolution integral yields the approximants which are identical to EFG approximants. In other words, there is no distinction between EFG and RKPM since the approximants are identical. The difference, if any, originates from algorithm and implementational issues that are adopted in two methods. The primary focus of RKPM has been in solving computational fluid mechanics problems governed by the compressible Navier-Stokes equations whereas EFG method was mostly applied to solve the problems of solid and fracture mechanics.

Oñate et al. (2001) applied to elasticity problems, a new and truly meshless method, known as finite point method (FPM) which they originally invented in 1995. It is a truly meshless method since it does not require the background cells either for the interpolation of field variables or for the numerical integration. The approximation around each point is obtained by using a MLS approximation scheme in conjunction with point collocation to solve fluid and solid mechanics problems.

Melenk and Babuska (1996) recognized that meshless methods based on MLS approximations are specific instances of partition of unity method (PUM). The soul of PUM lies in the fact that a conforming space is easily constructed by using any system of local approximation spaces without any loss in approximation properties. It is well known that the creation of conforming finite element spaces is a difficult task, and in the light of this, PUM provides greater flexibility in the choice of local nodal basis functions.

H - p cloud method which was developed by Durate and Oden (1996) uses MLS approximations as a partition of unity to locally enhance the polynomial order of the approximation. In H - p cloud method, the local approximation is constructed by multiplying a partition of unity by polynomials or other classes of functions. The simplicity of p -adaptivity is particularly attractive and very promising attribute of the H - p cloud method.

Yagawa and Yamada (1996) developed a virtually meshless method, called free-mesh method (FMM). Few developments in FMM were made by Yagawa and Furukawa (2000). FMM has good features of local meshing and equation construction process at each node. The local meshing process avoids the difficulty of global meshing over the entire domain and this local process of mesh generation starts node-by-node independently therefore the whole process of mesh generation can be parallelized easily. Since FMM has same number of equations as FEM, which ensures same accuracy as obtained by FEM.

Boundary node method (BNM) developed by Mukherjee and Mukherjee (1997) combines the MLS interpolants with the boundary integral equation (BIE) to solve the boundary value problems. The BNM has the capability of dimension reduction due to the presence of boundary integral equation and also to deal with complicated boundaries such as moving boundaries. In the absence of delta property of MLS approximation, this method could not satisfy the essential (Dirichlet) boundary conditions exactly. This method also requires background cells for numerical integration.

Natural element method (NEM) (Sukumar, 1998a) utilizes the natural neighbor (n-n) coordinates (Sibson, 1980) for the construction of interpolation functions. Natural neighbor interpolation (Sukumar et al., 1998b) relies on concepts such as Voronoi diagrams and Delaunay tessellations in computational geometry to construct the interpolation functions. Despite its fairly simple and appealing structure, sound theoretical basis for construction, and desirable smoothness properties, n-n interpolation has received little attention in the area of multivariate data interpolation, in comparison with other schemes such as moving least square (MLS) approximants (Lancaster and Salkauskas, 1981), radial basis functions (Sukumar, 1998a) and Shepard's interpolant (Krongauz, 1996a).

Zhu et al. (1998a,b) developed a meshless local boundary integral equation (LBIE) method which involves only local boundary integration centered at a node. They called their

method as a truly meshless method since it does not require the background cells either for the interpolation of field variables or for the integration of the weak formulation. It utilizes a local unsymmetric weak form (LUWF) and shape functions from MLS approximation scheme.

Atluri and Zhu (1998) also presented a truly meshless local Petrov Galerkin (MLPG) method which is based on a local symmetric weak form (LSWF) in conjunction with the MLS approximations. All integrals in this method are carried out over a regularly shaped domains using Gauss quadrature, thereby eliminating the need for background cells. Both MLPG and LBIE methods are truly meshless methods. Only difference between them is that MLPG method utilizes a local symmetric weak form (LSWF) whereas LBIE method uses a local unsymmetric weak form (LUWF) for obtaining the discrete equations. Moreover, in LBIE method, few singular integrals appear in the local boundary integral equation therefore a special attention has to be paid during integration of the weak form.

Few more developments in these meshless methods using MLPG approach were done by De and Bathe (2000) to obtain a powerful solution technique. They proposed a new truly meshless method known as the method of finite spheres. This method can be viewed as a special case of the general formulation of MLPG method. The method of finite spheres (De and Bathe, 2001a,b) uses rational (non-polynomial) approximation functions and integration domains are spheres, spherical shells and general sectors. Therefore, in this method, the concept of MLPG method has been used with a specific choice of geometric sub-domains, test and trial functions, numerical integration techniques and a procedure for imposing the essential boundary conditions.

The regular hybrid boundary node method (RHBNM) (Zhang et al., 2003; Zhang and Yao, 2003) was developed in 2001. In contrast to BNM, it does not require background cells for the numerical integration. Therefore it also comes in the category of truly meshless

methods. This method does not involve any singular integrals in the solution therefore very high accuracy can be achieved with a small number of boundary nodes.

A new meshless local point interpolation method (LPIM) (Liu and Gu, 2001a; Gu and Liu, 2001) utilizes the polynomial basis functions which are having delta property. A local weak form is developed using weighted residual method based on the idea of MLPG method. This method is a truly meshless method and its computational cost is much lower because of the simple approximation functions. Liu and Gu (2001b) replaced the polynomial basis functions by radial basis functions and called their method a local radial point interpolation method (LRPIM).

It is widely reported in the literature that the results obtained by most of these meshless methods are quite competitive with those obtained by FEM in different areas of engineering and sciences. The only big hurdle with the wide implementation of these meshless methods is their high computational cost. To overcome this situation, few researchers have parallelized some of these meshless methods.

Shirazaki and Yagawa (1999) parallelized the FMM method and applied it to solve large scale viscous incompressible flow problems. They achieved the parallel efficiencies 68.39% and 93.82% using 32 processors and 50.08% and 59.75% using 64 processors for 645370 and 904340 node models, respectively. They found out that parallel efficiency increases with the increase in data size. Yagawa and Furukawa (2000) put a further improvement in parallel FMM and solved the large scale heat conduction, fluid and fracture problems on MIMD-type parallel computer (HITACHI SR2201). For the heat conduction problems, they obtained the parallel efficiency nearly 90% using 64 processors and found that parallel efficiency does not decrease with the increase in the number of processors. They obtained the efficiencies of 68.39% and 93.82% for 645370 and 904340 node models, respectively using 32 processors in fluid flow problems.

Medina and Chen (2000) parallelized the SPH to solve the problems of damage in composite structures. Goozee and Jacobs (2003) used distributed and shared memory parallelism to further improve the parallel SPH code.

Günther et al. (2000) developed a parallel RKPM code to solve viscous compressible Navier Stokes equations. The code was written to handle the boundary conditions in parallel and implemented on a distributed memory IBM SP supercomputer.

Griebel and Schweitzer (2002) presented a parallel code for PUM. This code is based on data decomposition approach which utilizes a key-based tree implementation and a weighted space filling curve ordering scheme for load balancing. They applied this code to solve the elliptic partial differential equation.

So far, among all these meshless methods, the EFG method has been successfully used to solve a large variety of problems in different areas of engineering and sciences. The EFG method, developed by Belytschko et al. (1994) was first used to solve elasticity problems. They used Lagrange multiplier method to enforce essential boundary conditions. This method was further refined by Lu et al. (1994) to solve partial differential equations. They used modified variational principle to enforce essential boundary conditions. In this technique, Lagrange multipliers were replaced by their physical meaning.

Lu et al. (1995) used the orthogonal basis functions in MLS approximation to apply the EFG method for wave propagation and dynamic fracture problems. The weak form of the kinematic (essential) boundary conditions was used to enforce the essential boundary conditions. Through this analysis, it was concluded that the weak form of the essential boundary condition is identical to the method of Lagrange multipliers if the same shape functions are used for Lagrange multipliers, test and trial functions.

Belytschko and Tabbara (1996) used the EFG method to solve the problems on dynamic crack propagation. The essential boundary conditions were imposed by collocation method

and the discrete equations were obtained by Hamilton's principle. They tested and applied this method to solve elasto-dynamic non-linear crack growth problems.

Belytschko et al. (2000) further used this method to study the mixed mode dynamic crack propagation in concrete. The essential boundary conditions were imposed by explicit time integration scheme and coupling with finite elements. The discrete equations were obtained using variational method. Fracture process zone (FPZ) model was used to replicate the salient features of dynamic crack growth with arbitrary path.

In 1996, Krysl and Belytschko used the EFG method for the analysis of thin (Kirchhoff) plates (Krysl and Belytschko, 1996a) and thin shells (Krysl and Belytschko, 1996b) using C^1 continuous interpolation functions. They used Lagrange multiplier technique to enforce the essential boundary conditions.

Fleming et al. (1997) proposed two ways to enrich the EFG formulation. The first one is enriched trial function formulation and other one is enriched basis function formulation. In these formulations, modified variational principle technique (Lu et al., 1994) was used to impose the essential boundary conditions. They applied these EFG formulations to solve crack tip field problems.

In 1997, Sukumar and his co-workers applied the EFG method to solve fracture mechanics problems (Sukumar et al., 1997). Enriched basis functions were used in EFG formulation and the essential boundary conditions were imposed by coupling EFG method with finite elements (Belytschko et al., 1996a) along with the essential boundaries.

Cingoski et al. (1998) applied the EFG method for electromagnetic field computations. They obtained the results for 1-D model and compared with those obtained by exact method.

The EFG method was used by Bouillard and Suleau (1998) to acoustic wave propagation addressed by Helmholtz equation. They analyzed the effect of dispersion and pollution

phenomena on EFG solution. The essential (Dirichlet) boundary conditions were imposed by Lagrange multiplier method. Variational method was used to obtain the discrete equations.

Iura and Kanaizuka (2000) applied the EFG method to analyze a flexible translational joint. The original shape functions were modified to impose the essential boundary conditions by the same way as that of FEM. The discrete equations were obtained using Hamilton's principle.

Du (2000) used the EFG method for the simulation of stationary two-dimensional shallow water flows in rivers. The essential boundary conditions were imposed by two methods, direct method and penalty method. The direct method does not satisfy the delta property. Even then for this particular application, it was found that the direct imposition of essential of boundary conditions give better results in comparison to penalty method.

Xuan et al. (2001) used this method in eddy current non-destructive testing (NDT) applications. The essential (Dirichlet) boundary conditions were imposed by Lagrange multiplier method.

Rao and Rahman (2000) put a significant contribution to the EFG method. They proposed a new full transformation method to implement the essential boundary conditions exactly and a new weight function based on *students's t-distribution*. They applied the EFG method to analyze the five different cases of linear-elastic cracked structures subject to single and mixed mode loading conditions. In 2001, they used the EFG method for reliability analysis of linear-elastic structures with spatially varying random material properties (Rahman and Rao, 2001). A random field representing material properties was discretized into a set of random variables with statistical properties. They used full transformation method to impose the essential boundary conditions. In 2002, they used this method in probabilistic fracture mechanics (Rao and Rahman, 2002; Rahman and Rao, 2002) and in 2003, they further used this method for

calculating stress intensity factors (SIFs) for a stationary crack in two-dimensional functionally graded materials of arbitrary geometry (Rao and Rahman, 2003).

Li and Belytschko (2001) applied the EFG method for contact problems in metal forming analysis. The numerical results show that the EFG method is very effective in solving the problems with extremely large deformations and large material distortions such as upsetting, rolling and extrusion processes.

Ventura et al. (2002) proposed a new vector level set method for modeling of propagating cracks in EFG method. They found that this vector level set method is also applicable to other meshless methods such finite cloud method and RKPM.

In 2002, Liu and his co-workers applied the EFG method for the buckling analysis of isotropic and symmetrically laminated composite plates using classical lamination theory (Liu et al., 2002b). The essential boundary conditions were imposed by Lagrange multiplier and orthogonal transformation techniques. They concluded that the EFG method performs much better than FEM results in terms of CPU time to obtain the results of same accuracy,

Xiao and Dhanasekar coupled the EFG method with FE method using collocation approach to implement the essential (Dirichlet) boundary conditions exactly (Xiao and Dhanasekar, 2002). They applied this method to evaluate the displacements of a beam in pure bending and to evaluate the stress intensity factors of a single edge cracked specimen under tension.

Liu et al. (2002a) used the EFG method for static and free vibration analysis of spatial thin shell structures. For static load analysis, the essential boundary conditions were enforced using penalty and Lagrange multiplier methods while for frequency analysis, the essential boundary conditions were imposed through a weak form using orthogonal transformation technique.

Ren et al. (2002) applied the EFG method to simulate the superelastic behaviour of shape memory alloys (SMA). The incremental displacement-based EFG formulation for large deformation is developed by employing the continuum tangent stiffness tensor in the weak form of the equilibrium equations. An effective approach of imposing the essential boundary conditions was developed by eliminating the unknown constrained nodal variables from the discrete equations.

Karim and his-coworkers analyzed the transient response of a saturated porous elastic soil layer under wave-induced loading using two dimensional numerical procedure based on EFG method (Karim et al., 2002). The essential and periodic boundary conditions were implemented using Lagrange multiplier method. Crank-Nicolson technique was used for time domain approximation. A one-dimensional example was solved for temporal periodic conditions and a two-dimensional example for both temporal and spatial periodic conditions.

Li et al. (2003) applied the EFG method for the free surface seepage analysis of uniform earth dam. Steady and transient seepage were analyzed in uniform earth dam.

In 2003, Liew and his co-workers presented the numerical simulation of the pseudoelastic behavior of a shape memory alloy (SMA) beam using the element free Galerkin method (Liew et al., 2003). They proposed a new method to impose the essential boundary conditions. In this method, the unknown nodal variables of constrained nodes were replaced by known displacements and other nodal variables of the unconstrained nodes, and rearranged the discrete equations to explicitly provide the prescribed displacements in a vector of nodal variables.

Kamitani and his co-workers (Kamitani et al., 2003) developed a numerical code for calculating the shielding current density in the high temperature superconductor (HTS) plate using EFG method. The essential boundary conditions were directly incorporated in the weak form of the formulation.

Haitian and Yan (2003) combined the EFG method with precise algorithm in time domain to solve viscoelasticity problems. The essential boundary conditions were imposed by coupling FE-EFG technique with precise algorithm. By this technique, they analyzed two 1-D viscoelastic problems.

In 2003, Chen and his co-workers (Chen et al., 2003) applied the EFG method to obtain the natural frequencies of composite laminates of complicated shapes in free vibration analysis. The essential boundary conditions were imposed by Lagrange multiplier method and orthogonal transformation technique was employed to implement the essential boundary conditions in the eigenvalue equation.

Xiong et al. (2004) applied the EFG method for the analysis of plane strain rolling in slightly compressible rigid-plastic materials. In their work, special emphasis was placed on the construction of shape functions and their derivatives and the treatment of frictional effects along the contact interface between the work piece and the roll. Two alternative numerical techniques were put forwards to treat the velocity discontinuity near the corner of the roll entry. The effectiveness of the proposed approach was discussed by comparing theoretical predictions with experimental data found in the literature.

Lee and Yoon (2004) proposed an enhanced EFG method with enhancement functions to improve the solution accuracy for linear elastic fracture problem. The enhancement functions were added to the conventional EFG approximation for the implicit description of near-tip field. The discontinuity of crack surface was efficiently modeled by introducing a discontinuity function. Essential boundary conditions were enforced with the penalty method and a coupling with finite element. Crack growth was modeled implicitly without node operation so that the initial node arrangement was not modified until the end of analysis. The robustness of the enhanced EFG method was shown by examining the stress intensity factor and errors for various crack problems.

Although, the meshless EFG method has been successfully used to solve various types of problems in different areas and the results obtained by this method are more accurate (Lu et al., 1994; Belytschko et al., 1996a; Bouillard and Suleau, 1998; Dolbow and Belytschko, 1998) as compared to FEM, lack of wide implementation of this method is due to computational cost which is quite large in comparison to FEM (Belytschko et al., 1996b,c; Dolbow and Belytschko, 1998; Singh et al., 2003a). Even though it has been identified by the researchers (Belytschko et al., 1994) that the EFG method can also be applied in the area of heat transfer, much of the work has not been carried out. Therefore, in the present work, the EFG method was applied in the area of heat transfer. Since the accuracy of results obtained by EFG method is largely dependent on weight function, new weight functions is also proposed and studied in this thesis work. In view of the currently felt need for parallel programming version for many meshless numerical methods, a parallel algorithm for the EFG method is developed. The results obtained by this parallel code are also presented.

CHAPTER 3

THE ELEMENT FREE GALERKIN METHOD

3.1 INTRODUCTION

In principle, meshless element free Galerkin (EFG) method is almost identical to finite element method. The main difference lies in the character of approximants (i.e. interpolants in FEM). The EFG method utilizes moving least square (MLS) approximants, which are constructed in terms of nodes only. Therefore, there is no need of element and element connectivity data like FEM. In EFG method, an unknown function $T(\mathbf{x})$ is approximated by $T^h(\mathbf{x})$, where $T(\mathbf{x})$ is the actual function and $T^h(\mathbf{x})$ is its approximation. The MLS approximation consists of three components: a basis function usually a polynomial, a weight function associated with each node and a set of coefficients that depends on node position (Karim et al., 2002). The weight function is non-zero over a small sub-domain around the node. This non-zero domain is called compact support or domain of influence.

MLS approximants contains one attractive property that their continuity is related to the continuity of the weight function therefore, a low order polynomial basis (linear basis) can be used to generate highly continuous approximations by choosing an appropriate weight function (Dolbow and Belytschko, 1998).

3.2 MOVING LEAST SQUARE (MLS) APPROXIMANTS

In the present work, the moving least square (MLS) approximation scheme has been used to develop mesh-free shape functions. The unknown function $T(\mathbf{x})$ is approximated by moving least square (MLS) (Lancaster and Salkaukas, 1981) approximants $T^h(\mathbf{x})$ over the computational domain (Belytschko et al., 1994; Singh et al., 2002). The local approximation is given as:

$$T^h(\mathbf{x}) = \sum_{j=1}^m p_j(\mathbf{x}) a_j(\mathbf{x}) \equiv \mathbf{p}^T(\mathbf{x}) \mathbf{a}(\mathbf{x}) \quad (3.1)$$

where

$\mathbf{p}(\mathbf{x})$ is a vector of complete basis functions (usually polynomial) is given as:

$$\mathbf{p}^T(\mathbf{x}) = [1, x, y, z, xy, yz, zx, \dots, x^{k'}, y^{k'}, z^{k'}] \quad (3.2)$$

and $\mathbf{a}(\mathbf{x})$ is a vector of unknown coefficients

$$\mathbf{a}^T(\mathbf{x}) = [a_1(\mathbf{x}), a_2(\mathbf{x}), a_3(\mathbf{x}), \dots, a_m(\mathbf{x})] \quad (3.3)$$

where $\mathbf{x}^T = [x \ y \ z]$, k' is degree of the polynomial and m is the number of terms in the basis.

Some complete polynomial basis functions and corresponding coefficient vectors are given as

1-D: Linear basis

$$\mathbf{p}^T(\mathbf{x}) = [1, x], \quad (m = 2, \text{ linear}) \quad (3.4)$$

$$\mathbf{a}^T(\mathbf{x}) = [a_1(x), a_2(x)] \quad (3.5)$$

Quadratic basis

$$\mathbf{p}^T(\mathbf{x}) = [1, x, x^2], \quad (m = 3, \text{ quadratic}) \quad (3.6)$$

$$\mathbf{a}^T(\mathbf{x}) = [a_1(x), a_2(x), a_3(x)] \quad (3.7)$$

2-D: Linear basis

$$\mathbf{p}^T(\mathbf{x}) = [1, x, y] \quad (m = 3, \text{ linear}) \quad (3.8)$$

$$\mathbf{a}^T(\mathbf{x}) = [a_1(\mathbf{x}), a_2(\mathbf{x}), a_3(\mathbf{x})] \quad (3.9)$$

Quadratic basis

$$\mathbf{p}^T(\mathbf{x}) = [1, x, y, xy, x^2, y^2], \quad (m = 6, \text{ quadratic}) \quad (3.10)$$

$$\mathbf{a}^T(\mathbf{x}) = [a_1(\mathbf{x}), a_2(\mathbf{x}), a_3(\mathbf{x}), a_4(\mathbf{x}), a_5(\mathbf{x}), a_6(\mathbf{x})] \quad (3.11)$$

3-D: Linear basis

$$\mathbf{p}^T(\mathbf{x}) = [1 \ x \ y \ z] \quad (m = 4, \text{ linear}) \quad (3.12)$$

$$\mathbf{a}^T(\mathbf{x}) = [a_1(\mathbf{x}), a_2(\mathbf{x}), a_3(\mathbf{x}), a_4(\mathbf{x})] \quad (3.13)$$

Quadratic basis

$$\mathbf{p}^T(\mathbf{x}) = [1, x, y, z, xy, yz, zx, x^2, y^2, z^2] \quad (m = 10, \text{quadratic}) \quad (3.14)$$

$$\mathbf{a}^T(\mathbf{x}) = [a_1(\mathbf{x}), a_2(\mathbf{x}), a_3(\mathbf{x}), a_4(\mathbf{x}), a_5(\mathbf{x}), a_6(\mathbf{x}), a_7(\mathbf{x}), a_8(\mathbf{x}), a_9(\mathbf{x}), a_{10}(\mathbf{x})] \quad (3.15)$$

The unknown coefficients $\mathbf{a}(\mathbf{x})$ in Eq. (3.1) are the functions of \mathbf{x} and coefficients $\mathbf{a}(\mathbf{x})$ at any given point \mathbf{x} are determined by minimizing the weighted least square sum J (i.e. weighted least square sum of difference between local approximation at that point and nodal parameter T_I).

$$J = \sum_{I=1}^n w(\mathbf{x} - \mathbf{x}_I) [\mathbf{p}^T(\mathbf{x})\mathbf{a}(\mathbf{x}) - T_I]^2 \quad (3.16)$$

where T_I is the nodal parameter at $\mathbf{x} = \mathbf{x}_I$, but these are not nodal values of $T^h(\mathbf{x} = \mathbf{x}_I)$ because $T^h(\mathbf{x})$ is an approximant not an interpolant; $w(\mathbf{x} - \mathbf{x}_I)$ is a non zero weight function of node I at \mathbf{x} and n is the number of nodes in the domain of influence of \mathbf{x} for which $w(\mathbf{x} - \mathbf{x}_I) \neq 0$. The stationary value of J in Eq. (3.16) with respect to $\mathbf{a}(\mathbf{x})$ leads the following set of linear equations:

$$\mathbf{A}(\mathbf{x})\mathbf{a}(\mathbf{x}) = \mathbf{B}(\mathbf{x})\mathbf{T} \quad (3.17)$$

or

$$\mathbf{a}(\mathbf{x}) = \mathbf{A}^{-1}(\mathbf{x})\mathbf{B}(\mathbf{x})\mathbf{T} \quad (3.18)$$

where \mathbf{A} and \mathbf{B} are given as:

In 1-D

$$\mathbf{A}(x) = \sum_{I=1}^n w(x - x_I) \mathbf{p}(x_I) \mathbf{p}^T(x_I) = w(x - x_1) \begin{bmatrix} 1 & x_1 \\ x_1 & x_1^2 \end{bmatrix} + \dots + w(x - x_n) \begin{bmatrix} 1 & x_n \\ x_n & x_n^2 \end{bmatrix} \quad (3.19)$$

$$\mathbf{B}(x) = [w(x - x_1)\mathbf{p}(x_1), \dots, w(x - x_n)\mathbf{p}(x_n)] = \left\{ w(x - x_1) \begin{bmatrix} 1 \\ x_1 \end{bmatrix}, \dots, w(x - x_n) \begin{bmatrix} 1 \\ x_n \end{bmatrix} \right\} \quad (3.20)$$

In 2-D

$$\begin{aligned}
\mathbf{A} &= \sum_{l=1}^n w(\mathbf{x} - \mathbf{x}_l) \mathbf{p}(\mathbf{x}_l) \mathbf{p}^T(\mathbf{x}_l) \\
&= w(\mathbf{x} - \mathbf{x}_1) \begin{bmatrix} 1 & x_1 & y_1 \\ x_1 & x_1^2 & x_1 y_1 \\ y_1 & x_1 y_1 & y_1^2 \end{bmatrix} + w(\mathbf{x} - \mathbf{x}_2) \begin{bmatrix} 1 & x_2 & y_2 \\ x_2 & x_2^2 & x_2 y_2 \\ y_2 & x_2 y_2 & y_2^2 \end{bmatrix} + \dots \\
&+ w(\mathbf{x} - \mathbf{x}_n) \begin{bmatrix} 1 & x_n & y_n \\ x_n & x_n^2 & x_n y_n \\ y_n & x_n y_n & y_n^2 \end{bmatrix}
\end{aligned} \tag{3.21}$$

$$\begin{aligned}
\mathbf{B}(\mathbf{x}) &= \{w(\mathbf{x} - \mathbf{x}_1) \mathbf{p}(\mathbf{x}_1), w(\mathbf{x} - \mathbf{x}_2) \mathbf{p}(\mathbf{x}_2), \dots, w(\mathbf{x} - \mathbf{x}_n) \mathbf{p}(\mathbf{x}_n)\} \\
&= \left\{ w(\mathbf{x} - \mathbf{x}_1) \begin{bmatrix} 1 \\ x_1 \\ y_1 \end{bmatrix}, w(\mathbf{x} - \mathbf{x}_2) \begin{bmatrix} 1 \\ x_2 \\ y_2 \end{bmatrix}, \dots, w(\mathbf{x} - \mathbf{x}_n) \begin{bmatrix} 1 \\ x_n \\ y_n \end{bmatrix} \right\}
\end{aligned} \tag{3.22}$$

In 3-D

$$\begin{aligned}
\mathbf{A}(\mathbf{x}) &= \sum_{l=1}^n w(\mathbf{x} - \mathbf{x}_l) \mathbf{p}(\mathbf{x}_l) \mathbf{p}^T(\mathbf{x}_l) \\
&= w(\mathbf{x} - \mathbf{x}_1) \begin{bmatrix} 1 & x_1 & y_1 & z_1 \\ x_1 & x_1^2 & x_1 y_1 & x_1 z_1 \\ y_1 & x_1 y_1 & y_1^2 & y_1 z_1 \\ z_1 & x_1 z_1 & y_1 z_1 & z_1^2 \end{bmatrix} + w(\mathbf{x} - \mathbf{x}_2) \begin{bmatrix} 1 & x_2 & y_2 & z_2 \\ x_2 & x_2^2 & x_2 y_2 & x_2 z_2 \\ y_2 & x_2 y_2 & y_2^2 & y_2 z_2 \\ z_2 & x_2 z_2 & y_2 z_2 & z_2^2 \end{bmatrix} + \dots \\
&+ w(\mathbf{x} - \mathbf{x}_n) \begin{bmatrix} 1 & x_n & y_n & z_n \\ x_n & x_n^2 & x_n y_n & x_n z_n \\ y_n & x_n y_n & y_n^2 & y_n z_n \\ z_n & x_n z_n & y_n z_n & z_n^2 \end{bmatrix}
\end{aligned} \tag{3.23}$$

$$\begin{aligned}
\mathbf{B}(\mathbf{x}) &= \{w(\mathbf{x} - \mathbf{x}_1) \mathbf{p}(\mathbf{x}_1), w(\mathbf{x} - \mathbf{x}_2) \mathbf{p}(\mathbf{x}_2), \dots, w(\mathbf{x} - \mathbf{x}_n) \mathbf{p}(\mathbf{x}_n)\} \\
&= \left\{ w(\mathbf{x} - \mathbf{x}_1) \begin{bmatrix} 1 \\ x_1 \\ y_1 \\ z_1 \end{bmatrix}, w(\mathbf{x} - \mathbf{x}_2) \begin{bmatrix} 1 \\ x_2 \\ y_2 \\ z_2 \end{bmatrix}, \dots, w(\mathbf{x} - \mathbf{x}_n) \begin{bmatrix} 1 \\ x_n \\ y_n \\ z_n \end{bmatrix} \right\}
\end{aligned} \tag{3.24}$$

By substituting Eq. (3.18) in Eq. (3.1), the MLS approximant is obtained as:

$$T^h(\mathbf{x}) = \sum_{l=1}^n \Phi_l(\mathbf{x}) T_l = \Phi^T(\mathbf{x}) \mathbf{T} \tag{3.25}$$

where

$$\Phi^T(\mathbf{x}) = \{\Phi_1(\mathbf{x}), \Phi_2(\mathbf{x}), \Phi_3(\mathbf{x}), \dots, \Phi_n(\mathbf{x})\} \quad (3.26)$$

$$\mathbf{T}^T = [T_1, T_2, T_3 \dots T_n] \quad (3.27)$$

The mesh free shape function $\Phi_I(\mathbf{x})$ is defined as:

$$\Phi_I(\mathbf{x}) = \sum_{j=0}^m p_j(\mathbf{x}) (\mathbf{A}^{-1}(\mathbf{x}) \mathbf{B}(\mathbf{x}))_{jI} = \mathbf{p}^T \mathbf{A}^{-1} \mathbf{B}_I \quad (3.28)$$

The linear consistency requirements for the shape function $\Phi_I(\mathbf{x})$ (Belytschko et al., 1996b) are given as:

$$\sum_{I=1}^n \Phi_I(\mathbf{x}) = 1 \quad (3.29a)$$

$$\sum_{I=1}^n \Phi_I(\mathbf{x}) x_I = x \quad (3.29b)$$

$$\sum_{I=1}^n \Phi_I(\mathbf{x}) y_I = y \quad (3.29c)$$

$$\sum_{I=1}^n \Phi_I(\mathbf{x}) z_I = z \quad (3.29d)$$

The derivative of the shape function is calculated as:

$$\Phi_{I,x}(\mathbf{x}) = (\mathbf{p}^T \mathbf{A}^{-1} \mathbf{B}_I)_{,x} = \mathbf{p}^T_{,x} \mathbf{A}^{-1} \mathbf{B}_I + \mathbf{p}^T (\mathbf{A}^{-1})_{,x} \mathbf{B}_I + \mathbf{p}^T \mathbf{A}^{-1} \mathbf{B}_{I,x} \quad (3.30)$$

where

$$\mathbf{B}_{I,x}(\mathbf{x}) = \frac{dw}{dx} (\mathbf{x} - \mathbf{x}_I) \mathbf{p}(\mathbf{x}_I) \quad (3.31)$$

and $\mathbf{A}^{-1}_{,x}$ is computed as:

$$\mathbf{A}^{-1}_{,x} = -\mathbf{A}^{-1} \mathbf{A}_{,x} \mathbf{A}^{-1} \quad (3.32)$$

where

$$\mathbf{A}_{,x} = \sum_{I=1}^n \frac{dw}{dx} (\mathbf{x} - \mathbf{x}_I) \mathbf{p}(\mathbf{x}_I) \mathbf{p}^T(\mathbf{x}_I) \quad (3.33)$$

3.3 EFFICIENT SHAPE FUNCTION CALCULATION

To compute the mesh free shape functions Φ_I , it is necessary to calculate A^{-1} . In 1-D problems, this operation of inverting the matrix is not very difficult but in 2-D and 3-D problems, this exercise becomes very much expensive from computational time point of view. To overcome this situation, Dolbow and Belytschko (1998) proposed a computationally inexpensive alternative approach. This approach (Liu et al., 2002a) involves the LU decomposition of the A matrix. The shape function is given as:

$$\Phi_I(\mathbf{x}) = \mathbf{p}^T(\mathbf{x})\mathbf{A}^{-1}(\mathbf{x})\mathbf{B}_I(\mathbf{x}) = \gamma^T(\mathbf{x})\mathbf{B}_I(\mathbf{x}) \quad (3.34)$$

where

$$\gamma^T(\mathbf{x}) = \mathbf{p}^T(\mathbf{x})\mathbf{A}^{-1}(\mathbf{x}). \quad (3.35)$$

This leads to the relationship

$$\mathbf{A}(\mathbf{x})\gamma(\mathbf{x}) = \mathbf{p}(\mathbf{x}) \quad (3.36)$$

The vector $\gamma(\mathbf{x})$ is to be calculated using LU decomposition of the matrix A followed by back substitution.

The partial derivatives of $\gamma(\mathbf{x})$ can be recursively calculated as:

$$\mathbf{A}(\mathbf{x})\gamma_{,x}(\mathbf{x}) = \mathbf{p}_{,x}(\mathbf{x}) - \mathbf{A}_{,x}(\mathbf{x})\gamma(\mathbf{x}) \quad (3.37)$$

$$\mathbf{A}(\mathbf{x})\gamma_{,y}(\mathbf{x}) = \mathbf{p}_{,y}(\mathbf{x}) - \mathbf{A}_{,y}(\mathbf{x})\gamma(\mathbf{x}) \quad (3.38)$$

$$\mathbf{A}(\mathbf{x})\gamma_{,z}(\mathbf{x}) = \mathbf{p}_{,z}(\mathbf{x}) - \mathbf{A}_{,z}(\mathbf{x})\gamma(\mathbf{x}) \quad (3.39)$$

$$\mathbf{A}(\mathbf{x})\gamma_{,xx}(\mathbf{x}) = \mathbf{p}_{,xx}(\mathbf{x}) - \mathbf{A}_{,xx}(\mathbf{x})\gamma(\mathbf{x}) - 2\mathbf{A}_{,x}(\mathbf{x})\gamma_{,x}(\mathbf{x}) \quad (3.40)$$

$$\mathbf{A}(\mathbf{x})\gamma_{,yy}(\mathbf{x}) = \mathbf{p}_{,yy}(\mathbf{x}) - \mathbf{A}_{,yy}(\mathbf{x})\gamma(\mathbf{x}) - 2\mathbf{A}_{,y}(\mathbf{x})\gamma_{,y}(\mathbf{x}) \quad (3.41)$$

$$\mathbf{A}(\mathbf{x})\gamma_{,zz}(\mathbf{x}) = \mathbf{p}_{,zz}(\mathbf{x}) - \mathbf{A}_{,zz}(\mathbf{x})\gamma(\mathbf{x}) - 2\mathbf{A}_{,z}(\mathbf{x})\gamma_{,z}(\mathbf{x}) \quad (3.42)$$

$$\mathbf{A}(\mathbf{x})\gamma_{,xy}(\mathbf{x}) = \mathbf{p}_{,xy}(\mathbf{x}) - \mathbf{A}_{,xy}(\mathbf{x})\gamma(\mathbf{x}) - \mathbf{A}_{,x}(\mathbf{x})\gamma_{,y}(\mathbf{x}) - \mathbf{A}_{,y}(\mathbf{x})\gamma_{,x}(\mathbf{x}) \quad (3.43)$$

$$\mathbf{A}(\mathbf{x})\gamma_{,yz}(\mathbf{x}) = \mathbf{p}_{,yz}(\mathbf{x}) - \mathbf{A}_{,yz}(\mathbf{x})\gamma(\mathbf{x}) - \mathbf{A}_{,y}(\mathbf{x})\gamma_{,z}(\mathbf{x}) - \mathbf{A}_{,z}(\mathbf{x})\gamma_{,y}(\mathbf{x}) \quad (3.44)$$

$$\mathbf{A}(\mathbf{x})\gamma_{,zz}(\mathbf{x}) = \mathbf{p}_{,zz}(\mathbf{x}) - \mathbf{A}_{,zz}(\mathbf{x})\gamma(\mathbf{x}) - \mathbf{A}_{,z}(\mathbf{x})\gamma_{,z}(\mathbf{x}) - \mathbf{A}_{,z}(\mathbf{x})\gamma_{,z}(\mathbf{x}) \quad (3.45)$$

The derivatives of shape function are given as:

$$\Phi_{I,x}(\mathbf{x}) = \gamma^T_{,x}(\mathbf{x})\mathbf{B}_I(\mathbf{x}) + \gamma^T(\mathbf{x})\mathbf{B}_{I,x}(\mathbf{x}) \quad (3.46)$$

$$\Phi_{I,y}(\mathbf{x}) = \gamma^T_{,y}(\mathbf{x})\mathbf{B}_I(\mathbf{x}) + \gamma^T(\mathbf{x})\mathbf{B}_{I,y}(\mathbf{x}) \quad (3.47)$$

$$\Phi_{I,z}(\mathbf{x}) = \gamma^T_{,z}(\mathbf{x})\mathbf{B}_I(\mathbf{x}) + \gamma^T(\mathbf{x})\mathbf{B}_{I,z}(\mathbf{x}) \quad (3.48)$$

$$\Phi_{I,xx}(\mathbf{x}) = \gamma^T_{,xx}(\mathbf{x})\mathbf{B}_I(\mathbf{x}) + 2\gamma^T_{,x}(\mathbf{x})\mathbf{B}_{I,x}(\mathbf{x}) + \gamma^T(\mathbf{x})\mathbf{B}_{I,xx}(\mathbf{x}) \quad (3.49)$$

$$\Phi_{I,yy}(\mathbf{x}) = \gamma^T_{,yy}(\mathbf{x})\mathbf{B}_I(\mathbf{x}) + 2\gamma^T_{,y}(\mathbf{x})\mathbf{B}_{I,y}(\mathbf{x}) + \gamma^T(\mathbf{x})\mathbf{B}_{I,yy}(\mathbf{x}) \quad (3.50)$$

$$\Phi_{I,zz}(\mathbf{x}) = \gamma^T_{,zz}(\mathbf{x})\mathbf{B}_I(\mathbf{x}) + 2\gamma^T_{,z}(\mathbf{x})\mathbf{B}_{I,z}(\mathbf{x}) + \gamma^T(\mathbf{x})\mathbf{B}_{I,zz}(\mathbf{x}) \quad (3.51)$$

$$\Phi_{I,xy}(\mathbf{x}) = \gamma^T_{,x}(\mathbf{x})\mathbf{B}_{I,y}(\mathbf{x}) + \gamma^T_{,y}(\mathbf{x})\mathbf{B}_{I,x}(\mathbf{x}) + \gamma^T(\mathbf{x})\mathbf{B}_{I,xy}(\mathbf{x}) + \gamma^T_{,y}(\mathbf{x})\mathbf{B}_{I,x}(\mathbf{x}) \quad (3.52)$$

$$\Phi_{I,xz}(\mathbf{x}) = \gamma^T_{,x}(\mathbf{x})\mathbf{B}_{I,z}(\mathbf{x}) + \gamma^T_{,z}(\mathbf{x})\mathbf{B}_{I,x}(\mathbf{x}) + \gamma^T(\mathbf{x})\mathbf{B}_{I,xz}(\mathbf{x}) + \gamma^T_{,z}(\mathbf{x})\mathbf{B}_{I,x}(\mathbf{x}) \quad (3.53)$$

$$\Phi_{I,zx}(\mathbf{x}) = \gamma^T_{,z}(\mathbf{x})\mathbf{B}_{I,x}(\mathbf{x}) + \gamma^T_{,x}(\mathbf{x})\mathbf{B}_{I,z}(\mathbf{x}) + \gamma^T(\mathbf{x})\mathbf{B}_{I,zx}(\mathbf{x}) + \gamma^T_{,x}(\mathbf{x})\mathbf{B}_{I,z}(\mathbf{x}) \quad (3.54)$$

3.4 WEIGHT FUNCTION DESCRIPTION

The choice of weight function $w(\mathbf{x} - \mathbf{x}_I)$ affects the resulting approximation $T^h(\mathbf{x}_I)$ in EFG and other meshless methods. The weight function is non-zero over a small neighborhood of a node \mathbf{x}_I , called the support or domain of influence of node I . The smoothness and continuity of the shape function Φ_I depends on the smoothness and continuity of the weight function $w(\mathbf{x} - \mathbf{x}_I)$. If weight function is C^1 continuous then shape function will also have C^1 continuity. Therefore, the selection of appropriate weight function is essential in EFG and other meshless methods.

The weight function must satisfy the following requirements (Li et al., 2003; Singh and Prakash, 2003):

- (i) It should have a compact support to preserve the local character of MLS approximation.
- (ii) It must be positive, continuous and differentiable in the domain of influence.
- (iii) It should be zero outside the domain of influence.
- (iv) It should decrease in magnitude as the distance from \mathbf{x} to \mathbf{x}_j increases.
- (v) It should have a relatively larger value for a node, which is closer to the evaluation point than those of far nodes.
- (vi) The nodes in the domain of influence should not be collinear (except 1-D) and the number of nodes must be larger than the number of terms in the basis ($n > m$).

The different weight functions used in present analysis are written as a function of normalized radius \bar{r} as:

The cubicspline (C.S.) weight function (Belytschko et al., 1996c)

$$w(\mathbf{x} - \mathbf{x}_j) = w(\bar{r}) = \begin{cases} \frac{2}{3} - 4\bar{r}^2 + 4\bar{r}^3 & \bar{r} \leq \frac{1}{2} \\ \frac{4}{3} - 4\bar{r} + 4\bar{r}^2 - \frac{4}{3}\bar{r}^3 & \frac{1}{2} < \bar{r} \leq 1 \\ 0 & \bar{r} > 1 \end{cases} \quad (3.55a)$$

The quarticspline (Q.S.) weight function (Belytschko et al., 1996c)

$$w(\mathbf{x} - \mathbf{x}_j) = w(\bar{r}) = \begin{cases} 1 - 6\bar{r}^2 + 8\bar{r}^3 - 3\bar{r}^4 & 0 \leq \bar{r} \leq 1 \\ 0 & \bar{r} > 1 \end{cases} \quad (3.55b)$$

Gaussian weight function (Belytschko et al., 1996c)

$$w(\mathbf{x} - \mathbf{x}_j) = w(\bar{r}) = \begin{cases} e^{-(2.5\bar{r})^2} & 0 \leq \bar{r} \leq 1 \\ 0 & \bar{r} > 1 \end{cases} \quad (3.55c)$$

The quadratic weight function (Krysl and Belytschko, 2001)

$$w(\mathbf{x} - \mathbf{x}_j) = w(\bar{r}) = \begin{cases} 1 - \bar{r}^2 & 0 \leq \bar{r} \leq 1 \\ 0 & \bar{r} > 1 \end{cases} \quad (3.55d)$$

The hyperbolic weight function (Singh et al., 2002)

$$w(\mathbf{x} - \mathbf{x}_I) = w(\bar{r}) = \begin{cases} \operatorname{sech}(\bar{r} + 3) & 0 \leq \bar{r} \leq 1 \\ 0 & \bar{r} > 1 \end{cases} \quad (3.55e)$$

The exponential weight function

$$w(\mathbf{x} - \mathbf{x}_I) = w(\bar{r}) = \begin{cases} 100^{-\bar{r}} & 0 \leq \bar{r} \leq 1 \\ 0 & \bar{r} > 1 \end{cases} \quad (3.55f)$$

The rational weight function (Singh et al., 2003b)

$$w(\mathbf{x} - \mathbf{x}_I) = w(\bar{r}) = \begin{cases} \frac{1}{\bar{r}^2 + 0.1} & 0 \leq \bar{r} \leq 1 \\ 0 & \bar{r} > 1 \end{cases} \quad (3.55g)$$

The cosine weight function

$$w(\mathbf{x} - \mathbf{x}_I) = w(\bar{r}) = \begin{cases} \cos\left(\frac{\pi \bar{r}}{2}\right) & 0 \leq \bar{r} \leq 1 \\ 0 & \bar{r} > 1 \end{cases} \quad (3.55h)$$

$$\text{where } (\bar{r}) = \frac{\|\mathbf{x} - \mathbf{x}_I\|}{d_{mI}}$$

$\|\mathbf{x} - \mathbf{x}_I\|$ is the distance from a sampling point \mathbf{x} to a node \mathbf{x}_I and d_{mI} is the domain of influence of node I .

In 3-D

$$(\bar{r}_x) = \frac{\|\mathbf{x} - \mathbf{x}_I\|}{d_{mxI}} \quad (3.56a)$$

$$(\bar{r}_y) = \frac{\|\mathbf{x} - \mathbf{x}_I\|}{d_{myI}} \quad (3.56b)$$

$$(\bar{r}_z) = \frac{\|\mathbf{x} - \mathbf{x}_I\|}{d_{mzI}} \quad (3.56c)$$

and

$$d_{mxI} = d_{\max} c_{xI} \quad (3.57a)$$

$$d_{mxl} = d_{\max} c_{xl} \quad (3.57b)$$

$$d_{mzl} = d_{\max} c_{zl} \quad (5.57c)$$

d_{\max} = scaling parameter which defines size of the domain of influence and c_{xl} , c_{yl} & c_{zl} at node l are the distances to the nearest neighbors. d_{mxl} , d_{myl} and d_{mzl} are chosen such that the matrix is non-singular at every point in the domain.

The weight function at any given point is obtained as:

$$w(\mathbf{x} - \mathbf{x}_l) = w(\bar{r}_x) w(\bar{r}_y) w(\bar{r}_z) = w_x w_y w_z \quad (5.58)$$

where $w(\bar{r}_x)$, $w(\bar{r}_y)$ and $w(\bar{r}_z)$ can be calculated by replacing \bar{r} by \bar{r}_x , \bar{r}_y and \bar{r}_z in the expression of $w(\bar{r})$.

The derivatives of the weight functions are calculated as:

$$w_{,x} = \frac{dw_x}{dx} w_y w_z \quad (3.59a)$$

$$w_{,y} = \frac{dw_y}{dy} w_x w_z \quad (3.59b)$$

$$w_{,z} = \frac{dw_z}{dz} w_x w_y \quad (3.59c)$$

3.5 ENFORCEMENT OF ESSENTIAL BOUNDARY CONDITIONS

The EFG shape functions do not satisfy the Kronecker delta property: $\Phi_l(\mathbf{x}_j) \neq \delta_{lj}$ which means that the EFG approximants are not equal to the true function at nodes unless the weight function is singular i.e. the nodal parameters T_j are not the nodal values of $T^h(\mathbf{x}_j)$.

In other word, the approximation at the I^{th} node depends not only on the nodal parameter but also on the number of nodes with in the domain of influence of node l . The lacking of Kronecker delta property in EFG shape functions Φ_l poses some difficulty in the imposition of essential boundary conditions as compared to finite element method. For that different numerical techniques have been proposed to enforce the essential boundary conditions in

EFG method such as Lagrange multiplier method (Belytschko et al., 1994; Bouillard and Suleau, 1998; Karim et al., 2002), modified variational principle approach (Lu et al., 1994; Fleming et al., 1997), coupling with finite element method (Beytschko et al., 1996a; Krongauz and Belytschko, 1996b; Sukumar et al., 1997), penalty approach (Gavete et al., 2000; Du, 2000; Liu et al., 2002b) and full transformation technique (Rao and Rahman, 2000; Rahman and Rao, 2001), etc.

Lu et al., (1994) proposed modified variational principle approach. in this approach Lagrange multipliers were replaced by their physical meaning. Although this leads to banded set of equations, the results are not as accurate when compared with those by Lagrange multipliers approach. Another approach coupling with finite elements) proposed by Krongauz and Belytschko (1996b) is to necklace the EFG domain with FEM domain and apply the boundary conditions to the finite elements nodes. This coupling technique dramatically simplifies the enforcement of essential boundary conditions but compromises the salient features of EFG method and makes the numerical integration an even more burdensome task. Penalty approach (Liu et al., 2002a) is easy to enforce the essential boundary conditions and give the discrete equations in simple form similar of the FEM. This approach not only preserves symmetry and positive definite property of the matrix but also have the bandedness property of matrix. However the improper selection of penalty parameter can lead to wrong results. Rao and Rahman (2000) presented an efficient full transformation technique to enforce the essential boundary conditions. This approach removes some of the shortcomings of Lagrange multiplier method but it is not easy to implement. Although. Lagrange multiplier method (Belytschko et al., 1994) does not have positive definite and bandedness properties of the system matrix still it has been used in the present work due to its accuracy.

In 2-D, Lagrange multiplier λ is expressed as:

$$\lambda(\mathbf{x}) = N_I(s) \lambda_I, \quad \mathbf{x} \in \Gamma \quad (3.60a)$$

$$\delta \lambda(\mathbf{x}) = N_i(s) \delta \lambda_i, \quad \mathbf{x} \in \Gamma \quad (3.60b)$$

where $N_i(s)$ is a Lagrange interpolant and s is the length along the essential boundary conditions.

In 3-D, Lagrange multiplier λ is expressed as:

$$\lambda(\mathbf{x}) = N_i(a) \lambda_i, \quad \mathbf{x} \in S \quad (3.61a)$$

$$\delta \lambda(\mathbf{x}) = N_i(a) \delta \lambda_i, \quad \mathbf{x} \in S \quad (3.61b)$$

where $N_i(a)$ is a Lagrange interpolant and a is the area for the essential boundary conditions.

CHAPTER 4

1-D HEAT TRANSFER ANALYSIS

4.1 INTRODUCTION

This chapter describes the application of EFG method in one-dimensional (1-D) heat transfer problems. Four different cases have been chosen to check the applicability of this method in 1-D heat transfer problems. The steady-state and transient analysis of different model problems have been carried out. The effect of scaling parameter on EFG results has also been discussed in detail.

➤ CASE-I

4.2 DISCRETIZATION OF THE GOVERNING EQUATION

The general form of energy equation for one-dimensional heat transfer with thermal properties independent of temperature is given as:

$$k \frac{\partial^2 T}{\partial x^2} + \dot{Q} = \rho c \left(\frac{\partial T}{\partial t} \right) \quad (4.1a)$$

The essential boundary conditions are:

$$\text{at } x = 0, \quad T = T_L \quad (4.1b)$$

$$\text{at } x = L, \quad T = T_R \quad (4.1c)$$

The weighted integral form of Eq. (4.1a) is given as:

$$\int_0^L w \left\{ k \frac{\partial^2 T}{\partial x^2} + \dot{Q} - \rho c \frac{\partial T}{\partial t} \right\} dx = 0 \quad (4.2)$$

The weak form of Eq. (4.2) will be

$$\int_0^L \left[-k \frac{\partial w}{\partial x} \frac{\partial T}{\partial x} \right] dx - \int_0^L \rho c w \dot{T} dx + \int_0^L \dot{Q} w dx + \left[w k \frac{\partial T}{\partial x} \right]_0^L = 0 \quad (4.3)$$

The functional $I(T)$ is obtained as:

$$I(T) = \frac{1}{2} \int_0^L \left[k \left(\frac{\partial T}{\partial x} \right)^2 \right] dx + \int_0^L \rho c \dot{T} T dx - \int_0^L \dot{Q} T dx \quad (4.4)$$

Using Lagrange multiplier technique to enforce essential boundary conditions, the functional $I^*(T)$ is obtained as

$$I^*(T) = \frac{1}{2} \int_0^L \left[k \left(\frac{\partial T}{\partial x} \right)^2 \right] dx + \int_0^L \rho c \dot{T} T dx - \int_0^L \dot{Q} T dx + \lambda (T - T_L) \Big|_{x=0} + \lambda' (T - T_R) \Big|_{x=L} \quad (4.5)$$

Using Variational method, Eq. (4.5) reduces to

$$\begin{aligned} \delta I^*(T) = & \int_0^L \left[k \frac{\partial T}{\partial x} \delta \frac{\partial T}{\partial x} \right] dx + \int_0^L \rho c \dot{T} \delta T dx - \int_0^L \dot{Q} \delta T dx + \\ & \lambda \delta T \Big|_{x=0} + \delta \lambda (T - T_L) \Big|_{x=0} - \lambda' \delta T \Big|_{x=L} + \delta \lambda' (T - T_R) \Big|_{x=L} \end{aligned} \quad (4.6)$$

Since δT , $\delta \lambda$ and $\delta \lambda'$ are arbitrary in preceding equation, the following relations are obtained by using Eq. (3.25) and Eq. (4.6)

$$[\mathbf{K}]\{\mathbf{T}\} + [\mathbf{C}]\{\dot{\mathbf{T}}\} + [\mathbf{G}]\{\lambda\} + [\mathbf{G}']\{\lambda'\} = \{\mathbf{f}\} \quad (4.7a)$$

$$[\mathbf{G}']\{\mathbf{T}\} = \{T_L\} \quad (4.7b)$$

$$[\mathbf{G}']\{\mathbf{T}\} = \{T_R\} \quad (4.7c)$$

where

$$K_{IJ} = \int_0^L [k \Phi_{I,x}^T \Phi_{J,x}] dx \quad (4.8a)$$

$$C_{IJ} = \int_0^L \rho c \Phi_I^T \Phi_J dx \quad (4.8b)$$

$$f_I = \int_0^L \dot{Q} \Phi_I dx \quad (4.8c)$$

$$G_{IK} = \Phi_K \Big|_{x=0} \quad (4.8d)$$

$$G'_{IK} = \Phi_K \Big|_{x=L} \quad (4.8e)$$

Using Crank-Nicolson technique for time approximation, the Eq. (4.7) can be written as:

$$\begin{bmatrix} \mathbf{K}^* + \mathbf{C} & \mathbf{G} & \mathbf{G}' \\ \mathbf{G}^T & 0 & 0 \\ \mathbf{G}'^T & 0 & 0 \end{bmatrix} \begin{bmatrix} \mathbf{T}_N \\ \lambda \\ \lambda' \end{bmatrix} = \begin{bmatrix} \mathbf{R}_N \\ T_L \\ T_R \end{bmatrix} \quad (4.9)$$

where

$$\mathbf{R}_N = ([\mathbf{C}] - (1 - \alpha)\Delta t [\mathbf{K}])\{\mathbf{T}\}_{N-1} + \alpha\Delta t\{\mathbf{f}\}_N + (1 - \alpha)\Delta t\{\mathbf{f}\}_{N-1} \quad (4.10a)$$

$$\mathbf{K}^* = \alpha\Delta t [\mathbf{K}] \quad (4.10b)$$

4.3 NUMERICAL RESULTS AND DISCUSSION

The different parameters used for steady-state and transient analysis of one-dimensional model shown in Fig. 4.1 are tabulated in Table 4.1. The EFG results are obtained using different weight functions for two sets of nodes and the FEM results are obtained using linear bar element for same sets of nodes. The EFG results have been compared with those obtained by finite element and analytical (Holman, 1989) methods. A comparative study is carried out to evaluate the performance of different weight functions.

4.3.1 Steady-state analysis

The results (temperature values) presented in Table 4.2 are obtained using different EFG weight functions for two values of scaling parameter (i.e. $d_{\max} = 1.01$ & $d_{\max} = 1.51$) and it shows a comparison of temperature values obtained using 11 nodes with those obtained by FEM and analytical methods at the location ($x = 0.2\text{m}$). Table 4.3 shows a comparison of temperature values obtained by EFG method using different weight functions for two values of scaling parameter with those obtained by FEM and analytical methods at the same location i.e. ($x = 0.2\text{m}$) for 21 nodes. A comparison of temperature values obtained using different EFG weight functions with FEM and analytical methods for 11 and 21 nodes, is presented in Table 4.4 and Table 4.5 respectively at the location ($x = 0.4\text{m}$). Similar type of comparisons

of temperature values are shown in Table 4.6 for 11 nodes at the location ($x = 0.6\text{m}$), in Table 4.7 for 21 nodes at the location ($x = 0.6\text{m}$), in Table 4.8 for 11 nodes at the location ($x = 0.8\text{m}$) and in Table 4.9 for 21 nodes at the location ($x = 0.8\text{m}$). From the results presented in Table 4.2 to Table 4.9, it is observed that EFG results obtained using different weight functions are similar for $d_{\max} = 1.01$. However for $d_{\max} = 1.51$, only cubicspline, quarticspline, Gaussian, exponential and rational weight functions give acceptable results. It is also observed that the EFG results obtained using different weight functions are in good agreement with those obtained by FEM and analytical methods. Moreover with the increase in number of nodes EFG results starts converging.

The effect of scaling parameter (d_{\max}) on EFG results obtained using different weight functions is presented in Table 4.10 for 11 nodes and Table 4.11 for 21 nodes respectively at the location ($x = 0.4\text{m}$). Similar effect of scaling parameter on EFG results is shown in Table 4.12 for 11 nodes and Table 4.13 for 21 nodes at the location ($x = 0.8\text{m}$). Fig. 4.2 shows the effect of scaling parameter on EFG results obtained using 11 and 21 nodes at the location ($x = 0.2\text{m}$). Similar effect of scaling parameter on EFG results is observed in Fig. 4.3 at the location ($x = 0.6\text{m}$). From tables and figures, it is clear that only cubicspline, quarticspline, Gaussian, exponential and rational weight functions give acceptable results in the range $1.0 < d_{\max} < 2.0$ whereas the results obtained using quadratic, hyperbolic and cosine weight functions are varying in abrupt manner with scaling parameter. Therefore EFG results obtained using quadratic, hyperbolic and cosine weight functions are not acceptable in the range $1.0 < d_{\max} < 2.0$. It is also observed that there is minimum variation in EFG results with scaling parameter for exponential weight function.

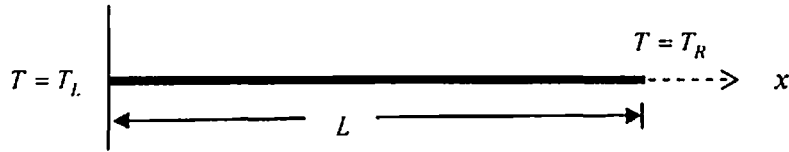


Fig. 4.1 One-dimensional model

Table 4.1 Data for the 1-D model shown in Fig. 4.1

Parameters	Value of the parameter
Length (L)	1 m
Thermal conductivity (k)	400 W/m-K
Density of the material (ρ)	10000 kg/m ³
Specific heat (c)	400 kJ/kg-K
Rate of internal heat generation (\dot{Q})	8000 W/m ³
Surrounding fluid temperature (T_∞)	20 °C
Initial temperature (T_m)	0 °C
Time step size (Δt)	100 sec
Temperature at $x = 0$	100 °C
Temperature at $x = L$	0 °C

Table 4.2 Comparison of EFG results obtained using 11 nodes with FEM and analytical results at the location ($x = 0.2$ m) of the 1-D model shown in Fig. 4.1

Weight function	EFG				FEM		Analytical
	$d_{max} = 1.01$		$d_{max} = 1.51$		T (°C)	% error	
	T (°C)	% error	T (°C)	% error			
C. S.	81.6000	0.0000	81.6001	0.0001	81.6000	0.0000	81.6000
Q. S.	81.6000	0.0000	81.6001	0.0001			
Gaussian	81.6000	0.0000	81.6041	0.0050			
Quadratic	81.6000	0.0000	82.3222	0.8850			
Hyperbolic	81.6000	0.0000	90.5004	10.9073			
Exponential	81.6000	0.0000	81.5890	-0.0135			
Rational	81.6000	0.0000	81.5605	-0.0484			
Cosine	81.6000	0.0000	81.9930	0.4816			

Table 4.3 Comparison of EFG results obtained using 21 nodes with FEM and analytical results at the location ($x = 0.2$ m) of the 1-D model shown in Fig. 4.1

Weight function	EFG				FEM		Analytical
	$d_{max} = 1.01$		$d_{max} = 1.51$		T (°C)	% error	
	T (°C)	% error	T (°C)	% error			
C. S.	81.6000	0.0000	81.6000	0.0000	81.6000	0.0000	81.6000
Q. S.	81.6000	0.0000	81.6000	0.0000			
Gaussian	81.6000	0.0000	81.6010	0.0012			
Quadratic	81.6000	0.0000	81.4294	-0.2091			
Hyperbolic	81.6000	0.0000	85.1920	4.4020			
Exponential	81.6000	0.0000	81.5971	-0.0035			
Rational	81.6000	0.0000	81.5957	-0.0053			
Cosine	81.6000	0.0000	81.0791	-0.6384			

Table 4.4 Comparison of EFG results obtained using 11 nodes with FEM and analytical results at the location ($x = 0.4$ m) of the 1-D model shown in Fig. 4.1

Weight function	EFG				FEM		Analytical
	$d_{\max} = 1.01$		$d_{\max} = 1.51$		T (°C)	% error	
	T (°C)	% error	T (°C)	% error			T (°C)
C. S.	62.4000	0.0000	62.4001	0.0002	62.4000	0.0000	62.4000
Q. S.	62.4000	0.0000	62.4001	0.0002			
Gaussian	62.4000	0.0000	62.4040	0.0064			
Quadratic	62.4000	0.0000	62.3026	-0.1561			
Hyperbolic	62.4000	0.0000	65.3112	4.6654			
Exponential	62.4000	0.0000	62.3902	-0.0157			
Rational	62.4000	0.0000	62.3884	-0.0186			
Cosine	62.4000	0.0000	62.5539	0.2466			

Table 4.5 Comparison of EFG results obtained using 21 nodes with FEM and analytical results at the location ($x = 0.4$ m) of the 1-D model shown in Fig. 4.1

Weight function	EFG				FEM		Analytical
	$d_{\max} = 1.01$		$d_{\max} = 1.51$		T (°C)	% error	
	T (°C)	% error	T (°C)	% error			T (°C)
C. S.	62.4000	0.0000	62.4000	0.0000	62.4000	0.0000	62.4000
Q. S.	62.4000	0.0000	62.4000	0.0000			
Gaussian	62.4000	0.0000	62.4010	0.0016			
Quadratic	62.4000	0.0000	62.3120	-0.1410			
Hyperbolic	62.4000	0.0000	63.1198	1.1535			
Exponential	62.4000	0.0000	62.3975	-0.0040			
Rational	62.4000	0.0000	62.3970	-0.0048			
Cosine	62.4000	0.0000	61.5816	-1.3115			

Table 4.6 Comparison of EFG results obtained using 11 nodes with FEM and analytical results at the location ($x = 0.6$ m) of the 1-D model shown in Fig. 4.1

Weight function	EFG				FEM		Analytical
	$d_{\max} = 1.01$		$d_{\max} = 1.51$		T (°C)	% error	T (°C)
	T (°C)	% error	T (°C)	% error			
C. S.	42.4000	0.0000	42.4001	0.0002	42.4000	0.0000	42.4000
Q. S.	42.4000	0.0000	42.4001	0.0002			
Gaussian	42.4000	0.0000	42.4040	0.0094			
Quadratic	42.4000	0.0000	42.7607	0.8507			
Hyperbolic	42.4000	0.0000	37.1552	-12.3698			
Exponential	42.4000	0.0000	42.3908	-0.0217			
Rational	42.4000	0.0000	42.3914	-0.0203			
Cosine	42.4000	0.0000	42.5603	0.3781			

Table 4.7 Comparison of EFG results obtained using 21 nodes with FEM and analytical results at the location ($x = 0.6$ m) of the 1-D model shown in Fig. 4.1

Weight function	EFG				FEM		Analytical
	$d_{\max} = 1.01$		$d_{\max} = 1.51$		T (°C)	% error	T (°C)
	T (°C)	% error	T (°C)	% error			
C. S.	42.4000	0.0000	42.4000	0.0000	42.4000	0.0000	42.4000
Q. S.	42.4000	0.0000	42.4000	0.000			
Gaussian	42.4000	0.0000	42.4010	0.0024			
Quadratic	42.4000	0.0000	42.3813	-0.0441			
Hyperbolic	42.4000	0.0000	41.8186	-1.3712			
Exponential	42.4000	0.0000	42.3978	-0.0052			
Rational	42.4000	0.0000	42.3982	-0.0042			
Cosine	42.4000	0.0000	41.5825	-1.9281			

Table 4.8 Comparison of EFG results obtained using 11 nodes with FEM and analytical results at the location ($x = 0.8\text{ m}$) of the 1-D model shown in Fig. 4.1

Weight function	EFG				FEM		Analytical
	$d_{\max} = 1.01$		$d_{\max} = 1.51$		T (°C)	% error	
	T (°C)	% error	T (°C)	% error			
C. S.	21.6000	0.0000	21.6001	0.0005	21.6000	0.0000	21.6000
Q. S.	21.6000	0.0000	21.6001	0.0005			
Gaussian	21.6000	0.0000	21.6040	0.0185			
Quadratic	21.6000	0.0000	22.0367	2.0218			
Hyperbolic	21.6000	0.0000	9.9703	-53.8412			
Exponential	21.6000	0.0000	21.5921	-0.0366			
Rational	21.6000	0.0000	21.6224	0.1037			
Cosine	21.6000	0.0000	21.9888	1.8000			

Table 4.9 Comparison of EFG results obtained using 21 nodes with FEM and analytical results at the location ($x = 0.8\text{ m}$) of the 1-D model shown in Fig. 4.1

Weight function	EFG				FEM		Analytical
	$d_{\max} = 1.01$		$d_{\max} = 1.51$		T (°C)	% error	
	T (°C)	% error	T (°C)	% error			
C. S.	21.6000	0.0000	21.6000	0.0000	21.6000	0.0000	21.6000
Q. S.	21.6000	0.0000	21.6000	0.0000			
Gaussian	21.6000	0.0000	21.6010	0.0046			
Quadratic	21.6000	0.0000	21.5453	-0.2532			
Hyperbolic	21.6000	0.0000	17.3587	-19.6356			
Exponential	21.6000	0.0000	21.5982	-0.0083			
Rational	21.6000	0.0000	21.5996	-0.0018			
Cosine	21.6000	0.0000	21.0807	-2.4042			

Table 4.10 Effect of scaling parameter on EFG results obtained using 11 nodes at the location ($x = 0.4$ m) of the 1-D model shown in Fig. 4.1

Scaling Parameter	Temperature ($^{\circ}$ C)							
	C. S.	Q. S	Gaussian	Quadratic	Hyperbolic	Exponential	Rational	Cosine
1.01	62.4000	62.4000	62.4000	62.4000	62.4000	62.4000	62.4000	62.4000
1.21	62.4000	62.4000	62.4000	62.4000	62.4000	62.4000	62.4000	62.4000
1.41	62.4000	62.4000	62.4000	62.4000	62.4000	62.4000	62.4000	62.4000
1.61	62.4055	62.4100	62.4075	22.4216	65.9703	62.3913	62.3935	0.3163
1.81	62.4257	62.4404	62.4186	234.9653	61.5955	62.3945	62.4035	111.1831
2.01	62.4441	62.4694	62.4343	158.8394	-326.9098	62.3944	62.3788	95.7380
2.21	62.4705	62.5721	62.4633	196.4522	-131.7198	62.3962	62.3855	129.3561
2.41	62.5376	62.6328	62.5541	213.9497	85.3274	62.3976	62.3941	151.1536
2.61	62.5642	61.0790	62.8141	235.2454	-20.1869	62.4031	62.4816	204.0527
2.81	61.4922	54.0303	63.4037	290.5388	-57.4471	62.4115	62.4416	239.3163
3.01	49.0687	45.2470	64.2749	353.2578	-114.4655	62.1297	61.1012	281.4844

Table 4.11 Effect of scaling parameter on EFG results obtained using 21 nodes at the location ($x = 0.4$ m) of the 1-D model shown in Fig. 4.1

Scaling Parameter	Temperature ($^{\circ}$ C)							
	C. S.	Q. S	Gaussian	Quadratic	Hyperbolic	Exponential	Rational	Cosine
1.01	62.4000	62.4000	62.4000	62.4000	62.4000	62.4000	62.4000	62.4000
1.21	62.4000	62.4000	62.4000	62.4000	62.4000	62.4000	62.4000	62.4000
1.41	62.4000	62.4000	62.4000	62.4000	62.4000	62.4000	62.4000	62.4000
1.61	62.4014	62.4025	62.4019	54.9645	64.1165	62.3978	62.3984	54.0570
1.81	62.4064	62.4101	62.4046	257.9605	69.2547	62.3986	62.4009	104.4035
2.01	62.4108	62.4143	62.4084	96.7492	21.3547	62.3978	62.3927	129.6589
2.21	62.4141	62.4221	62.4138	94.9982	190.4654	62.3980	62.3998	134.1992
2.41	62.4257	62.4959	62.4281	95.1441	364.7052	62.3982	62.4125	104.3666
2.61	62.4915	62.7785	62.4831	3.0291	-9.9129	62.3991	62.4608	-51.8707
2.81	62.7822	63.3720	62.6472	-68.2054	-178.6431	62.4016	62.4986	-63.2660
3.01	63.0621	65.3978	62.9915	-69.2963	-76.7663	61.9495	60.3640	-25.7713

Table 4.12 Effect of scaling parameter on EFG results obtained using 11 nodes at the location ($x = 0.8\text{ m}$) of the 1-D model shown in Fig. 4.1

Scaling Parameter	Temperature ($^{\circ}\text{C}$)							
	C. S.	Q. S	Gaussian	Quadratic	Hyperbolic	Exponential	Rational	Cosine
1.01	21.6000	21.6000	21.6000	21.6000	21.6000	21.6000	21.6000	21.6000
1.21	21.6000	21.6000	21.6000	21.6000	21.6000	21.6000	21.6000	21.6000
1.41	21.6000	21.6000	21.6000	21.6000	21.6000	21.6000	21.6000	21.6000
1.61	21.6055	21.6099	21.6072	-0.5770	5.2842	21.5959	21.6223	-14.4645
1.81	21.6247	21.6328	21.6119	-127.4838	-12.1280	21.6061	21.6008	-35.2355
2.01	21.6170	21.5222	21.5802	-50.7077	-222.2715	21.6159	21.5291	-25.2990
2.21	21.4613	20.8773	21.4089	59.6425	-138.9054	21.6233	21.4028	-37.3191
2.41	20.8545	18.8683	20.8916	55.8988	-86.3957	21.6236	21.1811	-39.4913
2.61	18.9719	12.9638	19.6621	61.9579	25.3318	21.5157	21.8063	-74.9529
2.81	12.7695	3.3939	16.9444	-108.6863	35.7859	21.5078	21.7894	-139.602
3.01	-9.4972	-31.0873	11.3089	-199.2055	67.5297	21.4016	21.2338	-220.514

Table 4.13 Effect of scaling parameter on EFG results obtained using 21 nodes at the location ($x = 0.8\text{ m}$) of the 1-D model shown in Fig. 4.1

Scaling Parameter	Temperature ($^{\circ}\text{C}$)							
	C. S.	Q. S	Gaussian	Quadratic	Hyperbolic	Exponential	Rational	Cosine
1.01	21.6000	21.6000	21.6000	21.6000	21.6000	21.6000	21.6000	21.6000
1.21	21.6000	21.6000	21.6000	21.6000	21.6000	21.6000	21.6000	21.6000
1.41	21.6000	21.6000	21.6000	21.6000	21.6000	21.6000	21.6000	21.6000
1.61	21.6014	21.6025	21.6019	35.1594	13.6184	21.5987	21.5998	36.2229
1.81	21.6064	21.6099	21.6048	201.8041	-11.4111	21.5998	21.6009	61.6561
2.01	21.6102	21.6052	21.6098	69.6704	-194.2075	21.6003	21.5993	169.5690
2.21	21.6023	21.5048	21.6183	100.1086	-142.6333	21.6008	21.6023	279.6172
2.41	21.5200	20.9352	21.6183	110.0123	-198.6662	21.6011	21.6024	197.7131
2.61	21.0434	18.2316	21.6199	-84.2119	146.8000	21.6033	21.8429	42.3328
2.81	18.5550	9.0833	21.4010	81.1018	343.4000	21.6063	22.0550	111.3497
3.01	4.5641	-5.0492	20.4346	128.7914	590.0000	21.4602	21.6411	130.6299

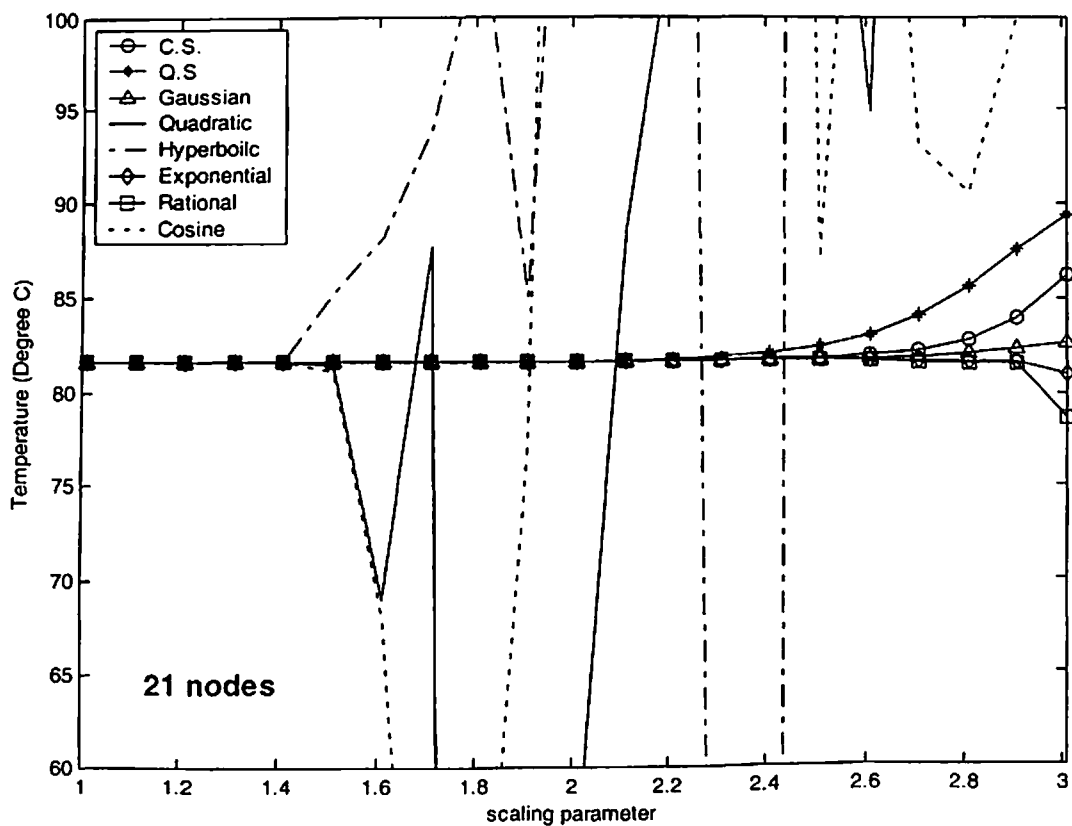
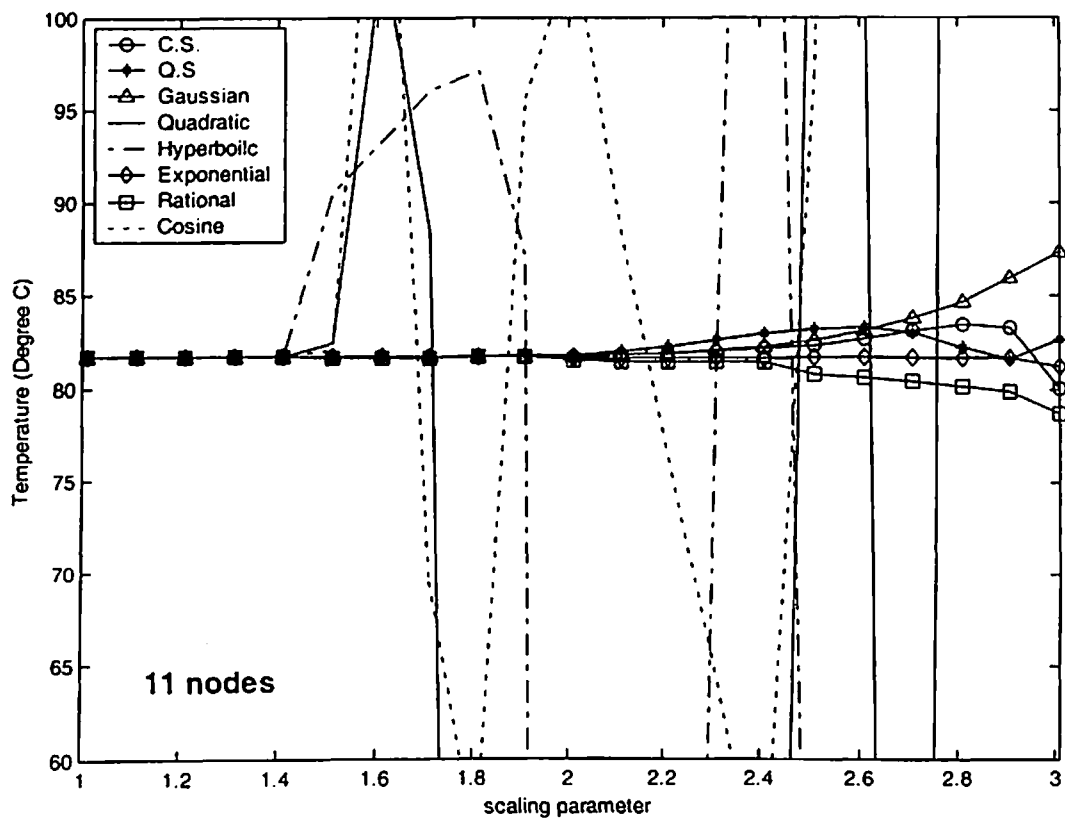


Fig. 4.2 Effect of scaling parameter on EFG results at the location ($x = 0.2$ m) of the 1-D model shown in Fig. 4.1

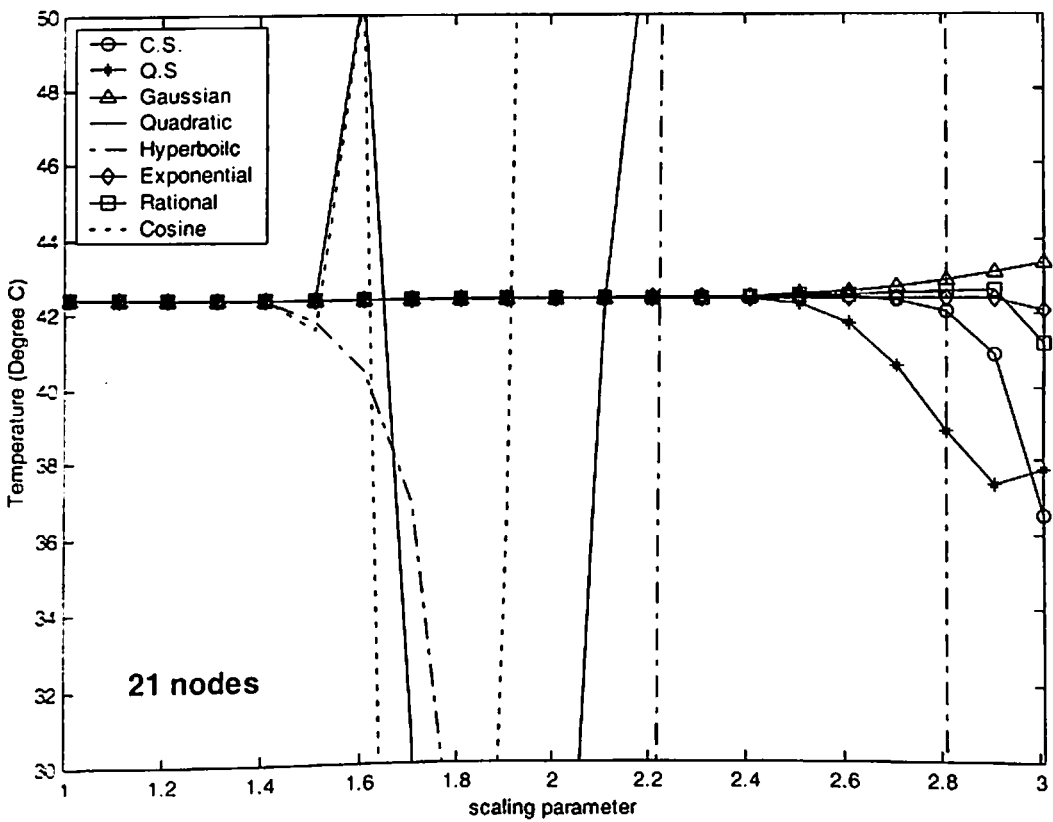
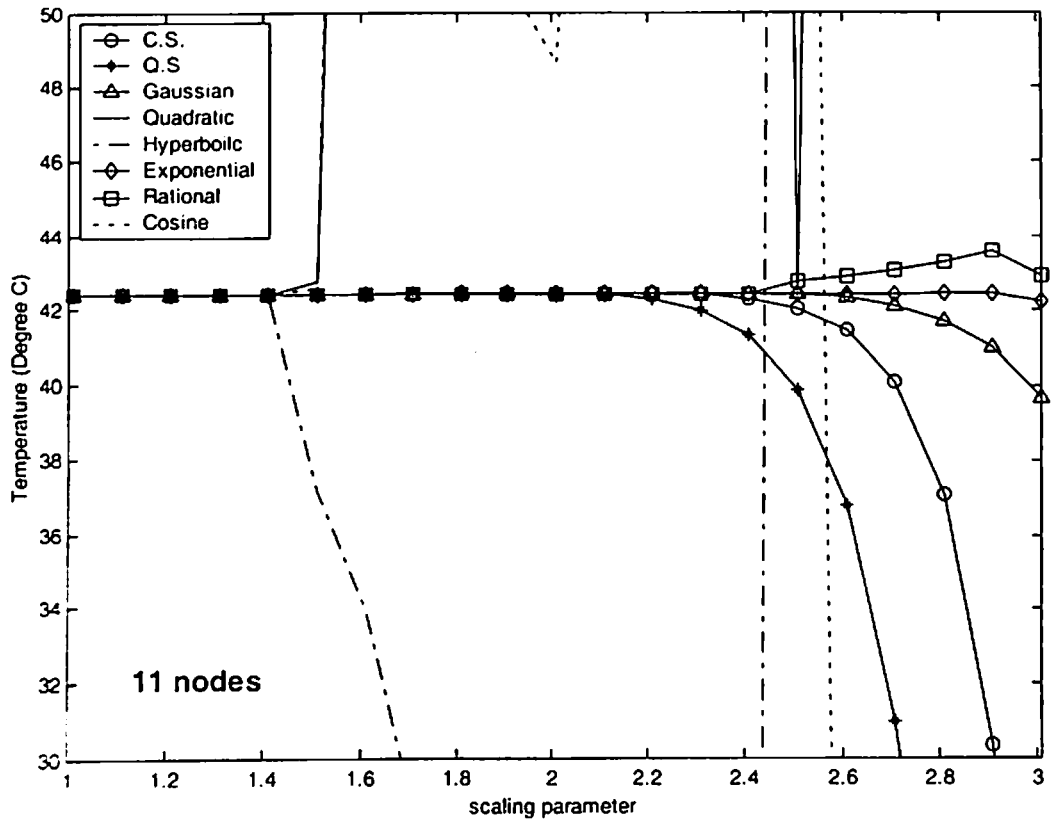


Fig. 4.3 Effect of scaling parameter on EFG results at the location ($x = 0.6$ m) of the 1-D model shown in Fig. 4.1

4.3.2 Transient analysis

The transient analysis of 1-D model shown in Fig. 4.1 has been carried out using different EFG weight functions. Table 4.14 and Fig. 4.4 show the convergence analysis using different time steps at two different locations. The solution with 1000 sec time step continues to oscillate with decreasing amplitude until it converges at 15000 sec. This time step (1000 sec) is nearly 20% of the total time required to achieve steady state condition in first two time steps (i.e. 100 sec and 500 sec). For time steps up to 500 sec, the EFG results are well converged and this time step is approximately 10% of the total time required for achieving steady state. In the present analysis, time step of 100 sec has been taken which is nearly 2% of the total time required to achieve steady state condition.

Table 4.15 and Table 4.16 show the comparison of EFG results (temperature values) obtained using 11 nodes with FEM results at the location ($x=0.2\text{m}$) for $d_{\max}=1.01$ and $d_{\max}=1.51$ respectively. Similar comparison of temperature values obtained using 21 nodes is presented in Table 4.17 and Table 4.18 for $d_{\max}=1.01$ and $d_{\max}=1.51$ respectively at the same location i.e. ($x=0.2\text{m}$). Table 4.19 and Table 4.20 shows the comparison of temperature values obtained using 11 nodes with FEM results at the different location ($x=0.6\text{m}$) for $d_{\max}=1.01$ and $d_{\max}=1.51$ respectively. Similar comparison of temperature values obtained using 21 nodes with FEM results is also presented in Table 4.21 and Table 4.22 for $d_{\max}=1.01$ and $d_{\max}=1.51$ respectively at the location i.e. ($x=0.6\text{m}$). Fig 4.5 shows the comparison of temperature values obtained using 11 nodes with FEM for $d_{\max}=1.01$ and $d_{\max}=1.51$ at the location ($x=0.4\text{m}$). Similar comparison of temperature values obtained using 21 nodes with FEM is shown in Fig. 4.6 at the same location i.e. ($x=0.4\text{m}$). Fig 4.7 shows the comparison of temperature values obtained using 11 nodes with FEM for $d_{\max}=1.01$ and $d_{\max}=1.51$ at the location ($x=0.8\text{m}$). Similar comparison of temperature values obtained using 21 nodes with FEM is shown in Fig. 4.8 at the same

location i.e. ($x = 0.8\text{m}$). From the results presented in tables and figures, it is clear that the EFG results obtained using different weight functions are similar for $d_{\max} = 1.01$ but for $d_{\max} = 1.51$ only cubicspline (C.S.), quarticspline (Q.S), Gaussian, exponential and rational weight functions give acceptable results. It has also been observed that the EFG results are in good agreement with those obtained by FEM.

Table 4.14 Convergence analysis of EFG results obtained using different time step at the location ($x = 0.4\text{ m}$) of the 1-D model shown in Fig. 4.1

Time (sec) $\times 10^2$	Time Step Size		
	100 sec	500 sec	1000 sec
0	0.0000	0.0000	0.0000
10	37.3692	29.5071	18.0546
20	53.2527	50.9520	48.1850
30	59.0122	58.4164	58.5522
40	61.1463	61.0381	59.9812
50	61.9324	61.9507	62.4932
60	62.2181	62.2593	61.7792

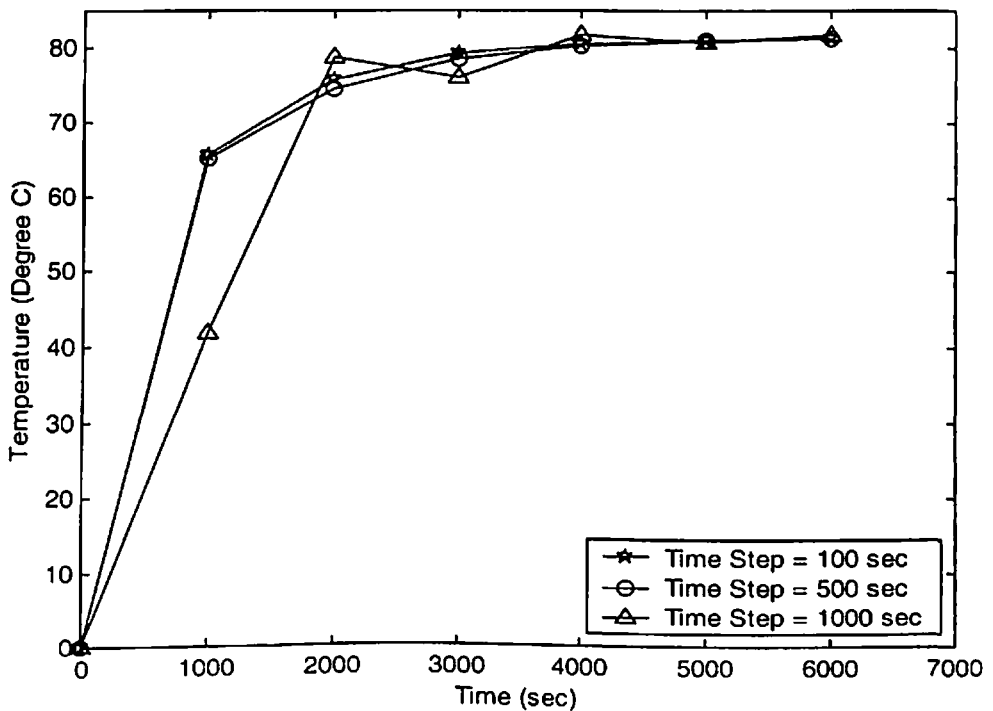


Fig. 4.4 Convergence analysis of EFG results obtained using different time step at the location ($x = 0.2\text{ m}$) of the 1-D model shown in Fig. 4.1

Table 4.15 Comparison of EFG results obtained using 11 nodes with FEM at the location ($x = 0.2$ m) of the 1-D model shown in Fig. 4.1 for $d_{max} = 1.01$

Time (sec) $\times 10^2$	Temperature ($^{\circ}$ C)								
	$d_{max} = 1.01$								FEM
	C. S.	Q. S	Gaussian	Quadratic	Hyperbolic	Exponential	Rational	Cosine	
0	0.0000	0.0000	0.0000	0.0000	0.0000	0.0000	0.0000	0.0000	0.0000
6	53.3887	53.3887	53.3887	53.3887	53.3887	53.3887	53.3887	53.3887	58.3264
12	67.8810	67.8810	67.8810	67.8810	67.8810	67.8810	67.8810	67.8810	69.7341
16	74.1548	74.1548	74.1548	74.1548	74.1548	74.1548	74.1548	74.1548	75.1533
24	77.4525	77.4525	77.4525	77.4525	77.4525	77.4525	77.4525	77.4525	78.0601
30	79.2523	79.2523	79.2523	79.2523	79.2523	79.2523	79.2523	79.2523	79.6531
36	80.2456	80.2456	80.2456	80.2456	80.2456	80.2456	80.2456	80.2456	80.5289
42	80.7982	80.7982	80.7982	80.7982	80.7982	80.7982	80.7982	80.7982	81.0108
48	81.1089	81.1089	81.1089	81.1089	81.1089	81.1089	81.1089	81.1089	81.2758
54	81.2861	81.2861	81.2861	81.2861	81.2861	81.2861	81.2861	81.2861	81.4217
60	81.3893	81.3893	81.3893	81.3893	81.3893	81.3893	81.3893	81.3893	81.5019

Table 4.16 Comparison of EFG results obtained using 11 nodes with FEM at the location ($x = 0.2$ m) of the 1-D model shown in Fig. 4.1 for $d_{max} = 1.51$

Time (sec) $\times 10^2$	Temperature ($^{\circ}$ C)								
	$d_{max} = 1.51$								FEM
	C. S.	Q. S	Gaussian	Quadratic	Hyperbolic	Exponential	Rational	Cosine	
0	0.0000	0.0000	0.0000	0.0000	0.0000	0.0000	0.0000	0.0000	0.0000
6	53.3871	53.3857	53.2599	27.6949	84.5846	53.3796	52.6504	37.3217	58.3264
12	67.8806	67.8803	67.8419	51.4845	87.4115	67.7830	67.3114	61.4446	69.7341
16	74.1547	74.1545	74.1356	61.6015	88.7517	74.0811	73.7709	71.1078	75.1533
24	77.4524	77.4524	77.4421	66.7551	89.5186	77.3945	77.1692	75.8761	78.0601
30	79.2523	79.2523	79.2475	69.7629	89.9707	79.1997	79.0180	78.4583	79.6531
36	80.2456	80.2457	80.2446	71.6954	90.2334	80.1946	80.0376	79.9095	80.5289
42	80.7983	80.7984	80.7999	73.0316	90.3821	80.7481	80.6075	80.7390	81.0108
48	81.1090	81.1091	81.1124	74.0150	90.4632	81.0596	80.9316	81.2181	81.2758
54	81.2862	81.2863	81.2910	74.7802	90.5049	81.2377	81.1203	81.4977	81.4217
60	81.3895	81.3896	81.3952	75.4047	90.5242	81.3419	81.2334	81.6629	81.5019

Table 4.17 Comparison of EFG results obtained using 21 nodes with FEM at the location ($x = 0.2\text{ m}$) of the 1-D model shown in Fig. 4.1 for $d_{\max} = 1.01$

Time (sec) $\times 10^2$	Temperature ($^{\circ}\text{C}$)								
	$d_{\max} = 1.01$								FEM
	C. S.	Q. S	Gaussian	Quadratic	Hyperbolic	Exponential	Rational	Cosine	
0	0.0000	0.0000	0.0000	0.0000	0.0000	0.0000	0.0000	0.0000	0.0000
6	55.6972	55.6972	55.6972	55.6972	55.6972	55.6972	55.6972	55.6972	56.5998
12	68.9420	68.9420	68.9420	68.9420	68.9420	68.9420	68.9420	68.9420	69.5324
16	74.6310	74.6310	74.6310	74.6310	74.6310	74.6310	74.6310	74.6310	75.2534
24	77.6537	77.6537	77.6537	77.6537	77.6537	77.6537	77.6537	77.6537	78.1741
30	79.3204	79.3204	79.3204	79.3204	79.3204	79.3204	79.3204	79.3204	79.7327
36	80.2464	80.2464	80.2464	80.2464	80.2464	80.2464	80.2464	80.2464	80.5777
42	80.7635	80.7635	80.7635	80.7635	80.7635	80.7635	80.7635	80.7635	81.0389
48	81.0543	81.0543	81.0543	81.0543	81.0543	81.0543	81.0543	81.0543	81.2917
54	81.2199	81.2199	81.2199	81.2199	81.2199	81.2199	81.2199	81.2199	81.4305
60	81.3160	81.3160	81.3160	81.3160	81.3160	81.3160	81.3160	81.3160	81.5067

Table 4.18 Comparison of EFG results obtained using 21 nodes with FEM at the location ($x = 0.2\text{ m}$) of the 1-D model shown in Fig. 4.1 for $d_{\max} = 1.51$

Time (sec) $\times 10^2$	Temperature ($^{\circ}\text{C}$)								
	$d_{\max} = 1.51$								FEM
	C. S.	Q. S	Gaussian	Quadratic	Hyperbolic	Exponential	Rational	Cosine	
0	0.0000	0.0000	0.0000	0.0000	0.0000	0.0000	0.0000	0.0000	0.0000
6	55.6970	55.6969	55.6873	64.9893	64.3463	55.7171	55.6947	59.9144	56.5998
12	68.9414	68.9410	68.9123	74.8300	74.9890	69.0726	69.2735	71.7314	69.5324
16	74.6305	74.6300	74.6002	78.9527	79.6253	74.7585	74.9787	76.7576	75.2534
24	77.6532	77.6529	77.6271	80.9240	82.1437	77.7548	77.9460	79.2396	78.1741
30	79.3200	79.3197	79.2988	81.8185	83.5679	79.3944	79.5478	80.4718	79.7327
36	80.2462	80.2459	80.2292	82.1558	84.3756	80.2979	80.4163	81.0508	80.5777
42	80.7633	80.7631	80.7498	82.2164	84.8306	80.7974	80.8865	81.2907	81.0389
48	81.0542	81.0540	81.0434	82.1513	85.0837	81.0750	81.1403	81.3604	81.2917
54	81.2198	81.2197	81.2111	82.0387	85.2215	81.2307	81.2769	81.3500	81.4305
60	81.3159	81.3158	81.3089	81.9177	85.2938	81.3193	81.3503	81.3066	81.5067

Table 4.19 Comparison of EFG results obtained using 11 nodes with FEM at the location ($x = 0.6$ m) of the 1-D model shown in Fig. 4.1 for $d_{\max} = 1.01$

Time (sec) $\times 10^2$	Temperature ($^{\circ}$ C)								
	$d_{\max} = 1.01$								FEM
	C. S.	Q. S	Gaussian	Quadratic	Hyperbolic	Exponential	Rational	Cosine	
0	0.0000	0.0000	0.0000	0.0000	0.0000	0.0000	0.0000	0.0000	0.0000
6	7.6401	7.6401	7.6401	7.6401	7.6401	7.6401	7.6401	7.6401	9.5396
12	22.2129	22.2129	22.2129	22.2129	22.2129	22.2129	22.2129	22.2129	23.6177
16	31.0674	31.0674	31.0674	31.0674	31.0674	31.0674	31.0674	31.0674	32.0047
24	36.0265	36.0265	36.0265	36.0265	36.0265	36.0265	36.0265	36.0265	36.6754
30	38.7741	38.7741	38.7741	38.7741	38.7741	38.7741	38.7741	38.7741	39.2501
36	40.2990	40.2990	40.2990	40.2990	40.2990	40.2990	40.2990	40.2990	40.6670
42	41.1505	41.1505	41.1505	41.1505	41.1505	41.1505	41.1505	41.1505	41.4466
48	41.6306	41.6306	41.6306	41.6306	41.6306	41.6306	41.6306	41.6306	41.8755
54	41.9055	41.9055	41.9055	41.9055	41.9055	41.9055	41.9055	41.9055	42.1114
60	42.0663	42.0663	42.0663	42.0663	42.0663	42.0663	42.0663	42.0663	42.2412

Table 4.20 Comparison of EFG results obtained using 11 nodes with FEM at the location ($x = 0.6$ m) of the 1-D model shown in Fig. 4.1 for $d_{\max} = 1.51$

Time (sec) $\times 10^2$	Temperature ($^{\circ}$ C)								
	$d_{\max} = 1.51$								FEM
	C. S.	Q. S	Gaussian	Quadratic	Hyperbolic	Exponential	Rational	Cosine	
0	0.0000	0.0000	0.0000	0.0000	0.0000	0.0000	0.0000	0.0000	0.0000
6	7.6399	7.6398	7.6199	-5.6255	16.9914	7.5375	7.0829	0.3676	9.5396
12	22.2116	22.2105	22.1335	4.0141	23.3921	22.4759	22.7860	15.5795	23.6177
16	31.0663	31.0654	31.0012	12.6787	28.3122	31.3104	31.7381	26.5753	32.0047
24	36.0257	36.0250	35.9801	18.8643	31.5155	36.1955	36.5630	33.2317	36.6754
30	38.7736	38.7732	38.7443	23.0664	33.5559	38.8759	39.1570	37.0972	39.2501
36	40.2988	40.2985	40.2817	25.9456	34.8484	40.3487	40.5515	39.3220	40.6670
42	41.1504	41.1503	41.1422	27.9882	35.6673	41.1621	41.3009	40.6043	41.4466
48	41.6307	41.6307	41.6286	29.5075	36.1878	41.6157	41.7035	41.3475	41.8755
54	41.9056	41.9057	41.9077	30.6961	36.5203	41.8726	41.9204	41.7821	42.1114
60	42.0664	42.0665	42.0713	31.6705	36.7342	42.0218	42.0381	42.0394	42.2412

Table 4.21 Comparison of EFG results obtained using 21 nodes with FEM at the location ($x = 0.6$ m) of the 1-D model shown in Fig. 4.1 for $d_{max} = 1.01$

Time (sec) $\times 10^2$	Temperature ($^{\circ}$ C)								
	$d_{max} = 1.01$								FEM
	C. S.	Q. S	Gaussian	Quadratic	Hyperbolic	Exponential	Rational	Cosine	
0	0.0000	0.0000	0.0000	0.0000	0.0000	0.0000	0.0000	0.0000	0.0000
6	7.9090	7.9090	7.9090	7.9090	7.9090	7.9090	7.9090	7.9090	9.3695
12	22.3785	22.3785	22.3785	22.3785	22.3785	22.3785	22.3785	22.3785	23.3749
16	31.2744	31.2744	31.2744	31.2744	31.2744	31.2744	31.2744	31.2744	31.8273
24	36.2567	36.2567	36.2567	36.2567	36.2567	36.2567	36.2567	36.2567	36.5559
30	39.0114	39.0114	39.0114	39.0114	39.0114	39.0114	39.0114	39.0114	39.1724
36	40.5312	40.5312	40.5312	40.5312	40.5312	40.5312	40.5312	40.5312	40.6177
42	41.3693	41.3693	41.3693	41.3693	41.3693	41.3693	41.3693	41.3693	41.4159
48	41.8315	41.8315	41.8315	41.8315	41.8315	41.8315	41.8315	41.8315	41.8566
54	42.0865	42.0865	42.0865	42.0865	42.0865	42.0865	42.0865	42.0865	42.0999
60	42.2271	42.2271	42.2271	42.2271	42.2271	42.2271	42.2271	42.2271	42.2343

Table 4.22 Comparison of EFG results obtained using 21 nodes with FEM at the location ($x = 0.6$ m) of the 1-D model shown in Fig. 4.1 for $d_{max} = 1.51$

Time (sec) $\times 10^2$	Temperature ($^{\circ}$ C)								
	$d_{max} = 1.51$								FEM
	C. S.	Q. S	Gaussian	Quadratic	Hyperbolic	Exponential	Rational	Cosine	
0	0.0000	0.0000	0.0000	0.0000	0.0000	0.0000	0.0000	0.0000	0.0000
6	7.9090	7.9090	7.9067	5.4256	6.2731	7.8824	7.8111	15.1033	9.3695
12	22.3784	22.3783	22.3696	18.6320	20.0247	22.4002	22.4013	27.5930	23.3749
16	31.2743	31.2742	31.2667	27.9285	29.0035	31.3031	31.3291	35.0084	31.8273
24	36.2566	36.2566	36.2515	33.6046	34.3112	36.2794	36.3038	38.9452	36.5559
30	39.0114	39.0113	39.0082	36.9862	37.4074	39.0272	39.0448	40.9210	39.1724
36	40.5312	40.5311	40.5294	39.0029	39.2115	40.5415	40.5537	41.8439	40.6177
42	41.3693	41.3693	41.3685	40.2186	40.2641	41.3755	41.3845	42.2181	41.4159
48	41.8315	41.8315	41.8314	40.9632	40.8796	41.8347	41.8418	42.3174	41.8566
54	42.0865	42.0865	42.0868	41.4284	41.2407	42.0875	42.0934	42.2879	42.0999
60	42.2272	42.2272	42.2278	41.7256	41.4535	42.2267	42.2316	42.2055	42.2343

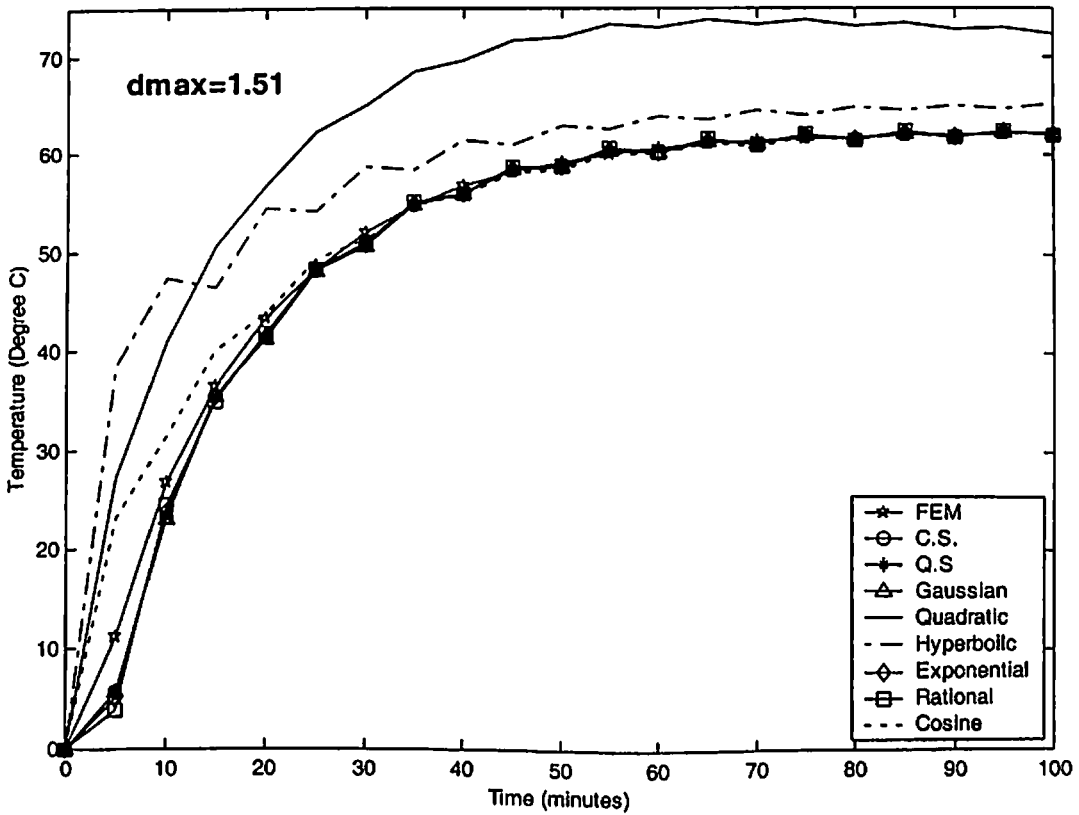
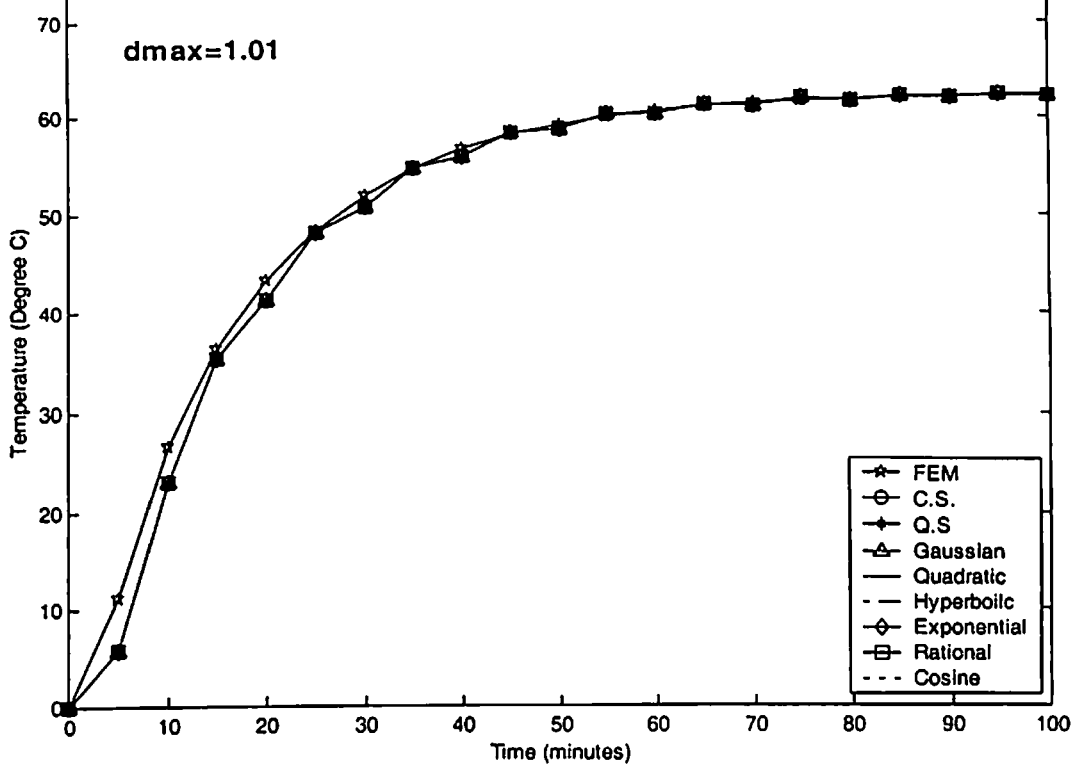
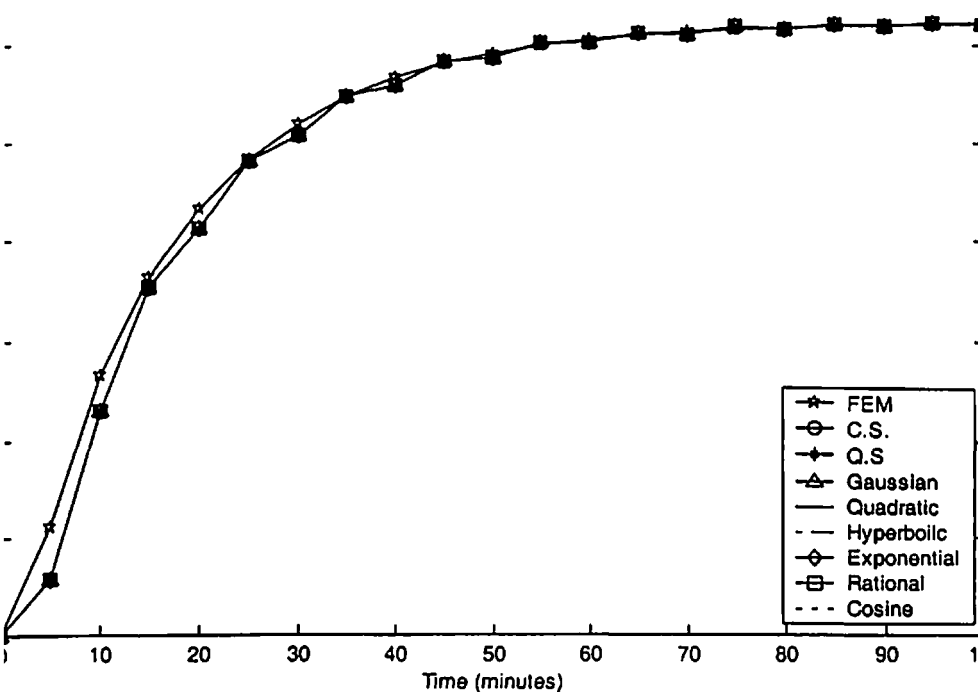
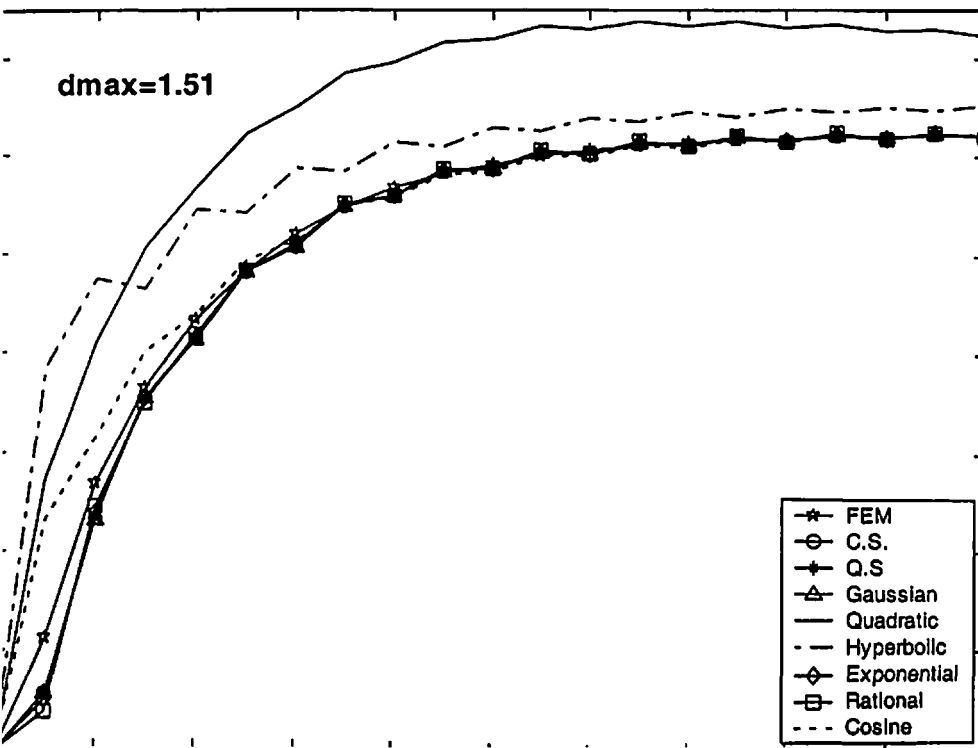


Fig. 4.5 Comparison of EFG results obtained using 11 nodes with FEM at the location ($x = 0.4$ m) of the 1-D model shown in Fig. 4.1

dmax=1.01



dmax=1.51



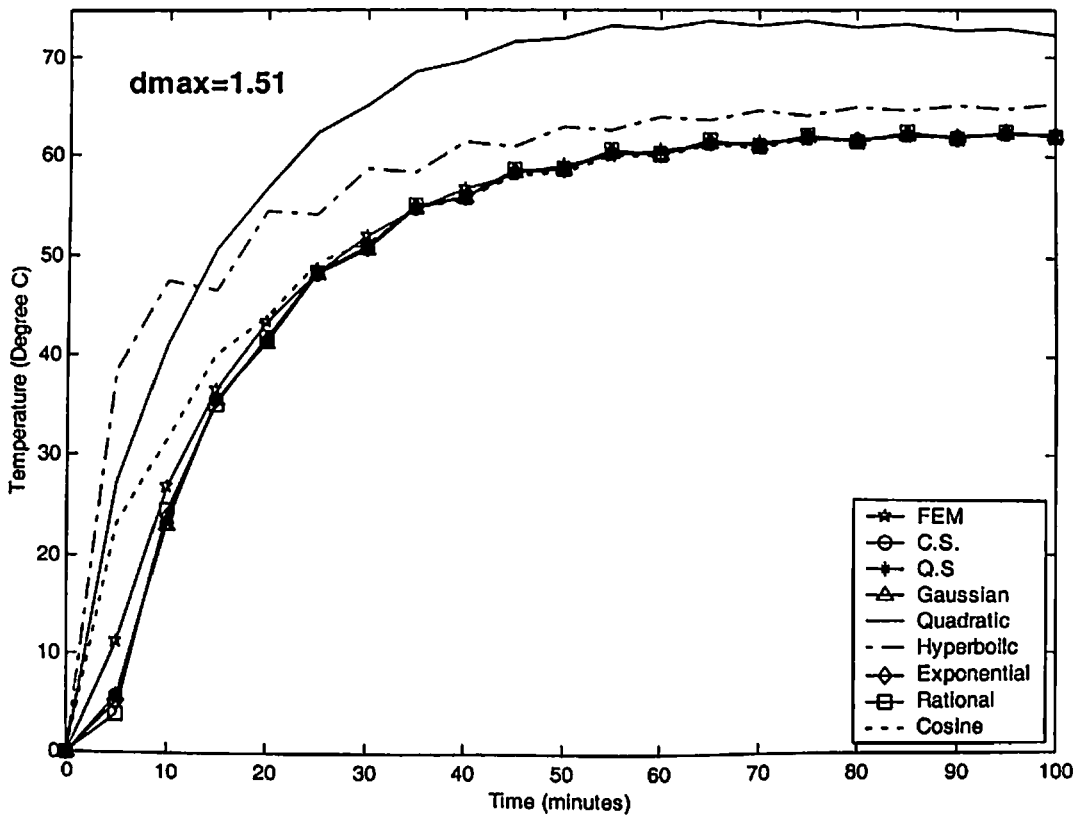
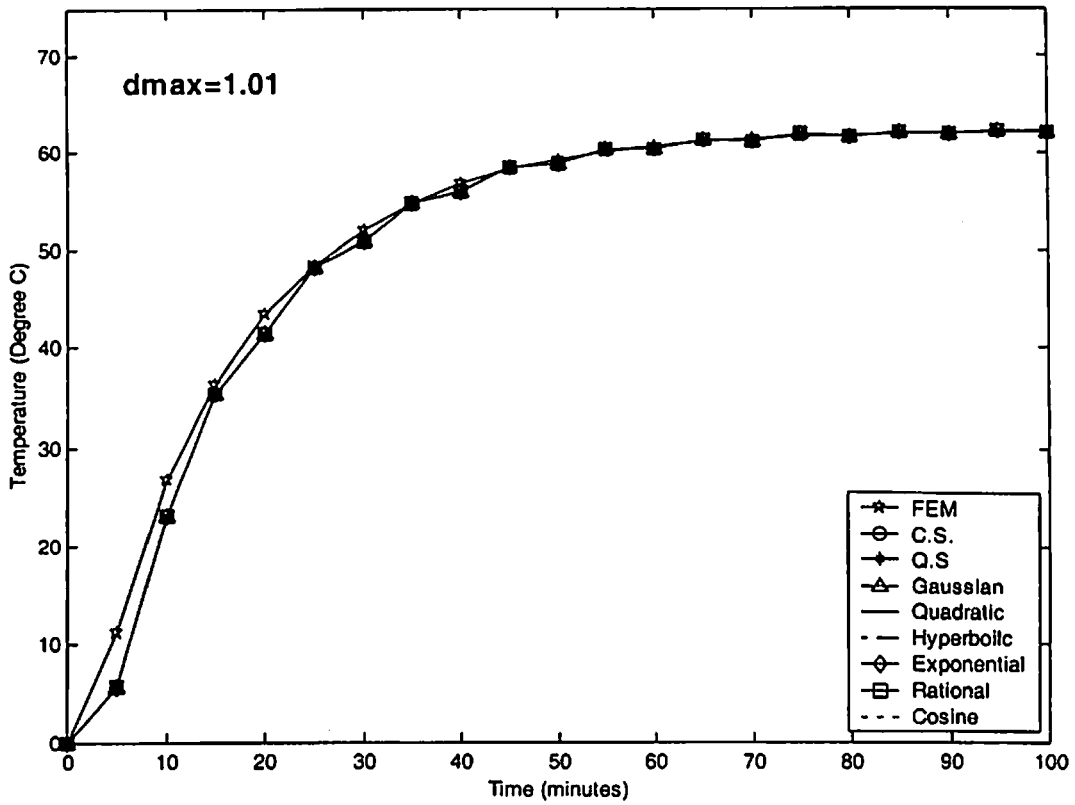


Fig. 4.5 Comparison of EFG results obtained using 11 nodes with FEM at the location ($x = 0.4$ m) of the 1-D model shown in Fig. 4.1

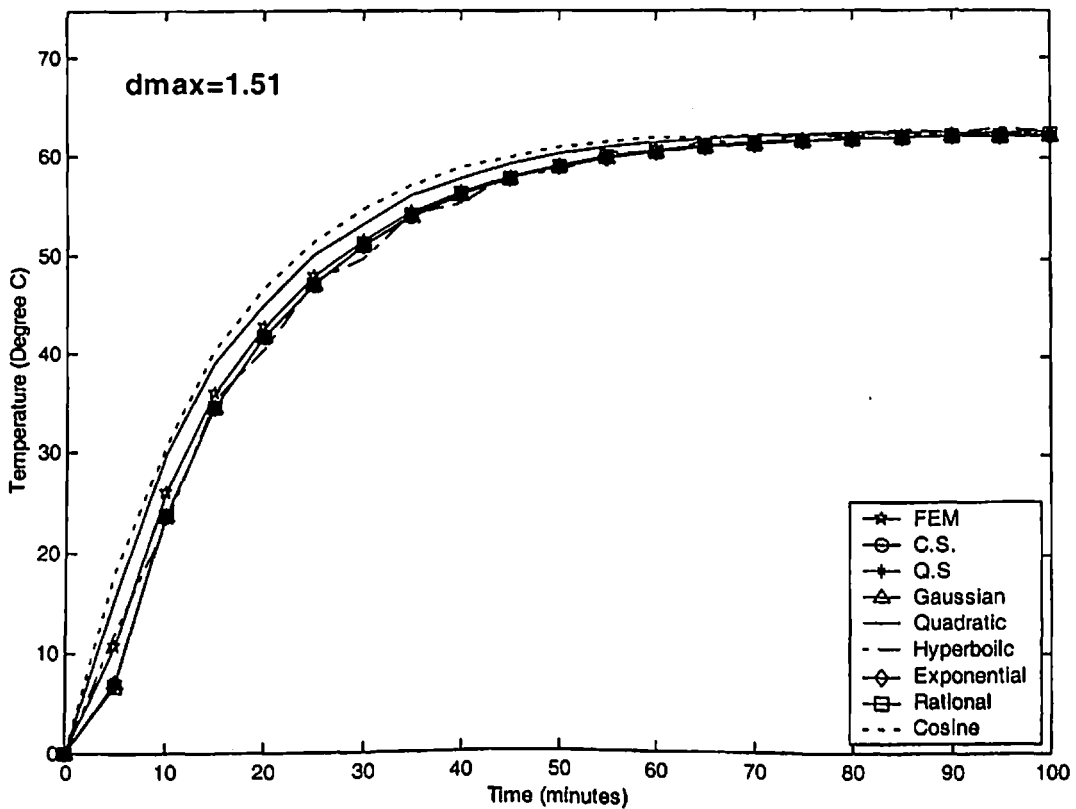
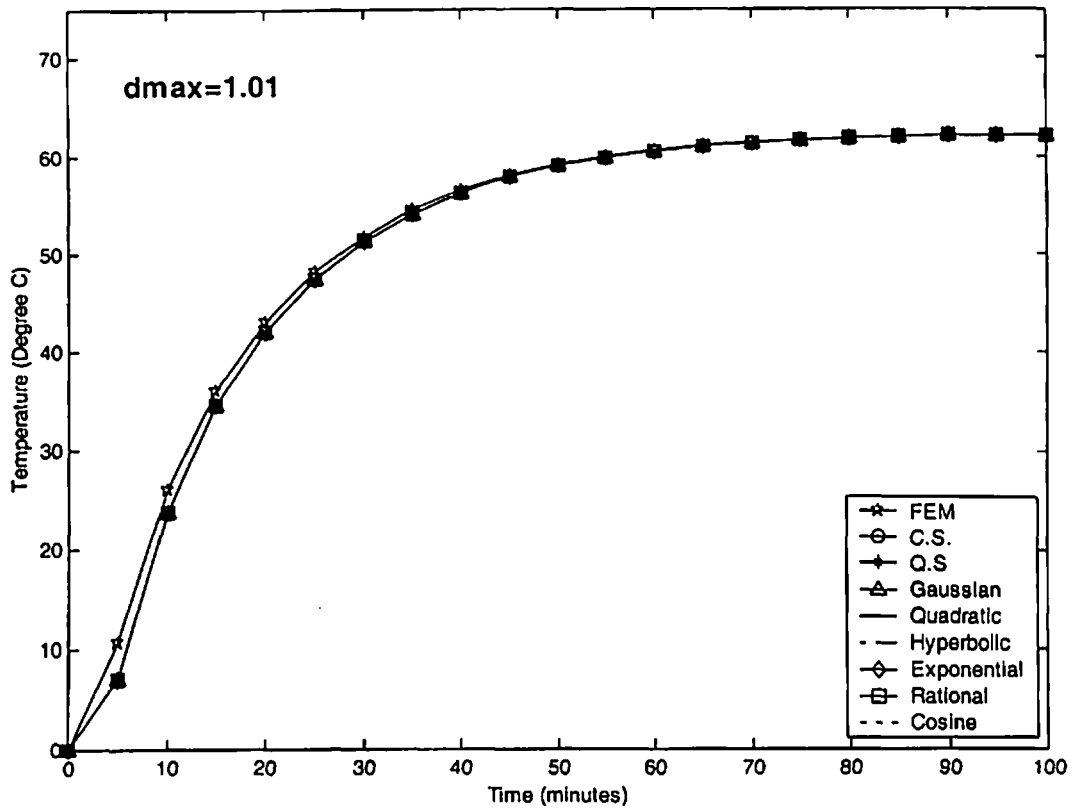


Fig. 4.6 Comparison of EFG results obtained using 21 nodes with FEM at the location ($x = 0.4$ m) of the 1-D model shown in Fig. 4.1

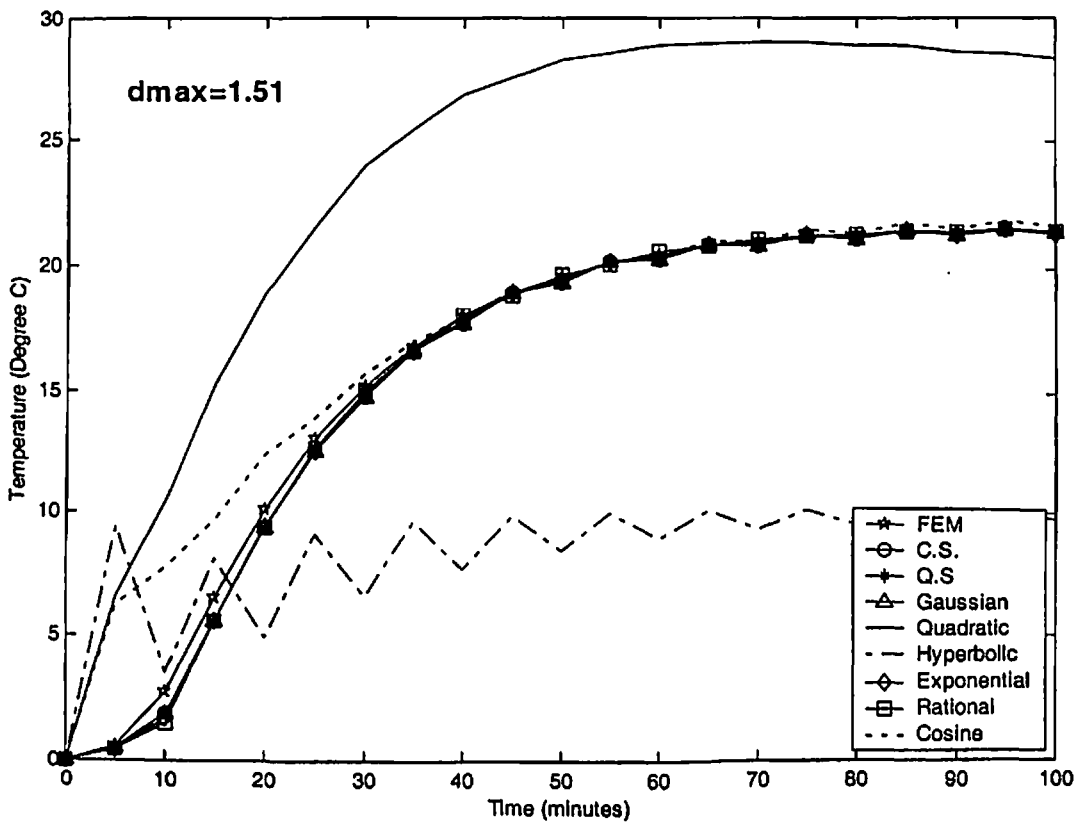
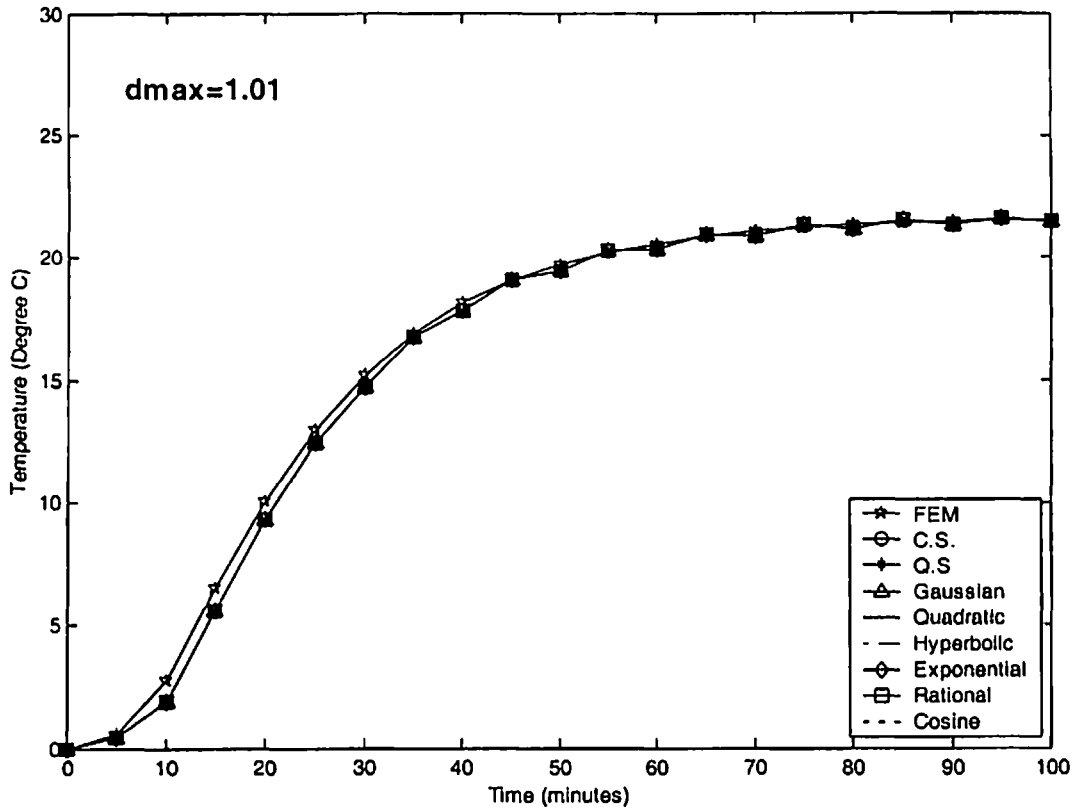


Fig. 4.7 Comparison of EFG results obtained using 11 nodes with FEM at the location ($x = 0.8\text{m}$) of the 1-D model shown in Fig. 4.1

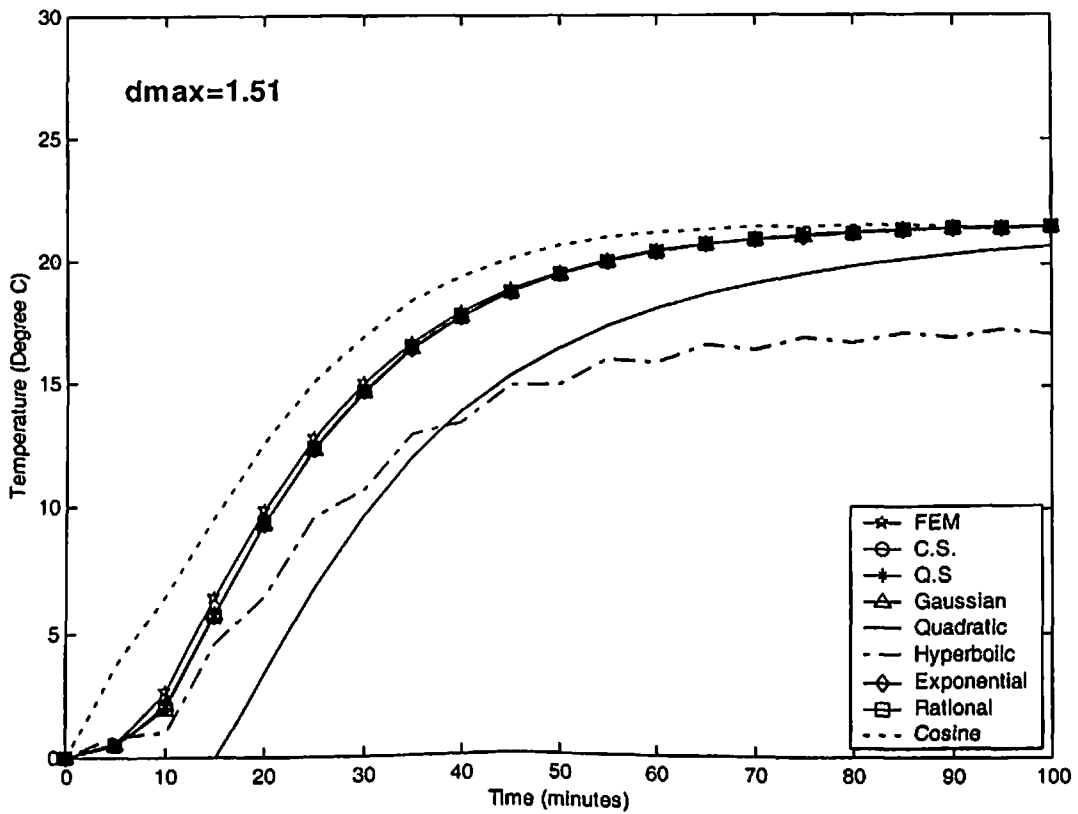
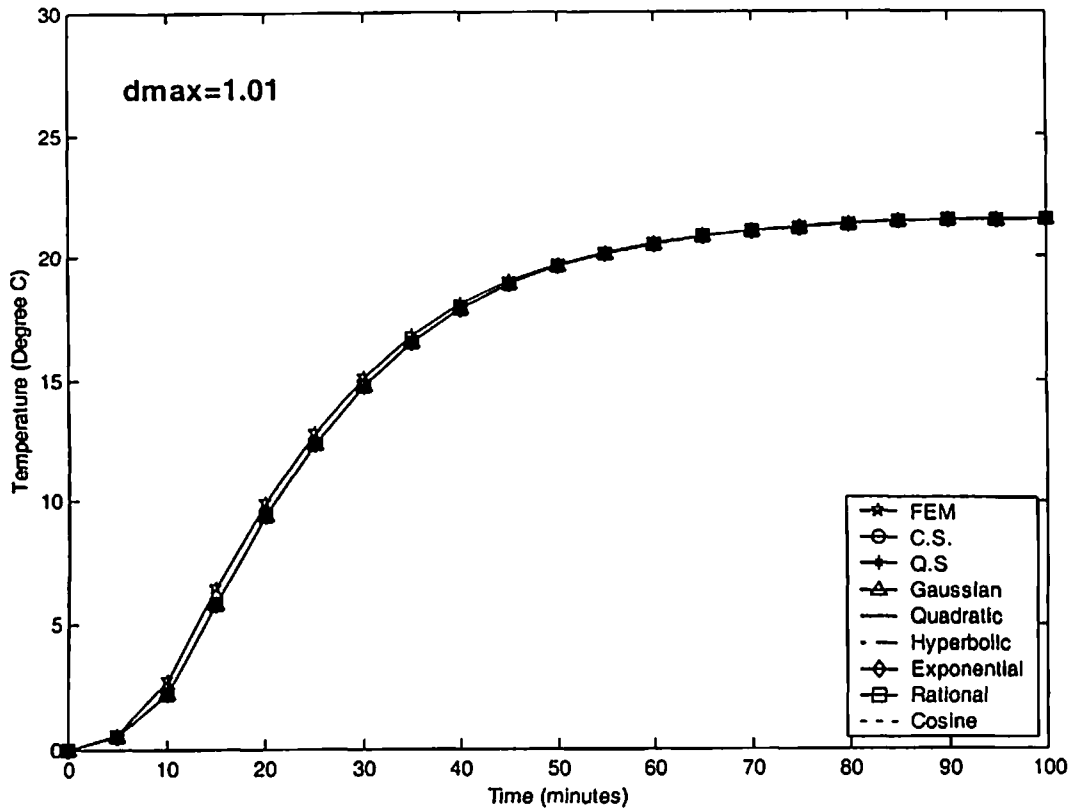


Fig. 4.8 Comparison of EFG results obtained using 21 nodes with FEM at the location ($x = 0.8\text{m}$) of the 1-D model shown in Fig. 4.1

➤ **CASE-II**

4.4 DISCRETIZATION OF THE GOVERNING EQUATION

The general form of energy equation for one-dimensional heat transfer in composite slabs with thermal properties independent of temperature is given as:

$$k \frac{\partial^2 T}{\partial x^2} + \dot{Q} = \rho c \left(\frac{\partial T}{\partial t} \right) \quad (4.11a)$$

The boundary conditions are:

$$\text{at } x = 0 \quad T = T_l \quad (4.11b)$$

$$\text{at } x = L_1 + L_2 \text{ or } (L) \quad -k \frac{\partial T}{\partial x} = h(T - T_\infty) \quad (4.11c)$$

The compatibility requirement at the interface is given as:

$$-k_1 \frac{\partial T}{\partial x} \Big|_{x=L_1} = -k_2 \frac{\partial T}{\partial x} \Big|_{x=L_1} \quad (4.11d)$$

The weighted integral form of Eq. (4.11a) is given as:

$$\int_0^L w \left\{ k \frac{\partial^2 T}{\partial x^2} + \dot{Q} - \rho c \frac{\partial T}{\partial t} \right\} dx = 0 \quad (4.12)$$

The weak form of Eq. (4.12) will be

$$\begin{aligned} & \int_0^{L_1} \left[-k_1 \frac{\partial w}{\partial x} \frac{\partial T}{\partial x} \right] dx + \int_{L_1}^L \left[-k_2 \frac{\partial w}{\partial x} \frac{\partial T}{\partial x} \right] dx - \int_0^{L_1} \rho_1 c_1 w \dot{T} dx - \\ & \int_{L_1}^L \rho_2 c_2 w \dot{T} dx + \int_0^{L_1} \dot{Q}_1 w dx + \int_{L_1}^L \dot{Q}_2 w dx + \left[w k \frac{\partial T}{\partial x} \right]_0^L = 0 \end{aligned} \quad (4.13)$$

The functional $I(T)$ is obtained as:

$$\begin{aligned} I(T) = & \frac{1}{2} \int_0^{L_1} \left[k_1 \left(\frac{\partial T}{\partial x} \right)^2 \right] dx + \frac{1}{2} \int_{L_1}^L \left[k_2 \left(\frac{\partial T}{\partial x} \right)^2 \right] dx + \int_0^{L_1} \rho_1 c_1 \dot{T} T dx + \\ & \int_{L_1}^L \rho_2 c_2 \dot{T} T dx - \int_0^{L_1} \dot{Q}_1 T dx - \int_{L_1}^L \dot{Q}_2 T dx + \frac{hT^2}{2} \Big|_{x=L} - hT_\infty T \Big|_{x=L} \end{aligned} \quad (4.14)$$

Using Lagrange multiplier technique to enforce essential boundary conditions, the functional

$I^*(T)$ is obtained as:

$$I^*(T) = \frac{1}{2} \int_0^{L_1} \left[k_1 \left(\frac{\partial T}{\partial x} \right)^2 \right] dx + \frac{1}{2} \int_{L_1}^L \left[k_2 \left(\frac{\partial T}{\partial x} \right)^2 \right] dx + \int_0^{L_1} \rho_1 c_1 \dot{T} T dx + \int_{L_1}^L \rho_2 c_2 \dot{T} T dx - \int_0^{L_1} \dot{Q}_1 T dx - \int_{L_1}^L \dot{Q}_2 T dx + \left. \frac{hT^2}{2} \right|_{x=L} - hT_\infty T \Big|_{x=L} + \lambda(T - T_L) \Big|_{x=0} \quad (4.15)$$

Using Variational method, Eq. (4.15) changes to

$$\delta I^*(T) = \int_0^{L_1} \left[k_1 \frac{\partial T}{\partial x} \delta \frac{\partial T}{\partial x} \right] dx + \int_{L_1}^L \left[k_2 \frac{\partial T}{\partial x} \delta \frac{\partial T}{\partial x} \right] dx + \int_0^{L_1} \rho_1 c_1 \dot{T} \delta T dx + \int_{L_1}^L \rho_2 c_2 \dot{T} \delta T dx - \int_0^{L_1} \dot{Q}_1 \delta T dx - \int_{L_1}^L \dot{Q}_2 \delta T dx + hT \delta T \Big|_{x=L} - hT_\infty \delta T \Big|_{x=L} + \lambda \delta T \Big|_{x=0} + \delta \lambda (T - T_L) \Big|_{x=0} \quad (4.16)$$

Since δT and $\delta \lambda$ are arbitrary in preceding equation, the following relations are obtained by

using Eq. (3.25) and Eq. (4.16)

$$[\mathbf{K}]\{\mathbf{T}\} + [\mathbf{C}]\{\dot{\mathbf{T}}\} + [\mathbf{G}]\{\lambda\} = \{\mathbf{f}\} \quad (4.17a)$$

$$[\mathbf{G}^T]\{\mathbf{T}\} = \{T_L\} \quad (4.17b)$$

where

$$K_{IJ} = \int_0^{L_1} [k_1 \Phi_{I,x}^T \Phi_{J,x}] dx + \int_{L_1}^L [k_2 \Phi_{I,x}^T \Phi_{J,x}] dx + h \Phi_I^T \Phi_J \Big|_{x=L} \quad (4.18a)$$

$$C_{IJ} = \int_0^{L_1} \rho_1 c_1 \Phi_I^T \Phi_J dx + \int_{L_1}^L \rho_2 c_2 \Phi_I^T \Phi_J dx \quad (4.18b)$$

$$f_I = \int_0^{L_1} \dot{Q}_1 \Phi_I dx + \int_{L_1}^L \dot{Q}_2 \Phi_I dx + hT_\infty \Phi_I \Big|_{x=L} \quad (4.18c)$$

$$G_{IK} = \Phi_K \Big|_{x=0} \quad (4.18d)$$

Using Crank-Nicolson technique for time approximation, the Eq. (4.17) can be written as:

$$\begin{bmatrix} \mathbf{K}^* + \mathbf{C} & \mathbf{G} \\ \mathbf{G}^T & 0 \end{bmatrix} \begin{bmatrix} \mathbf{T}_N \\ \lambda \end{bmatrix} = \begin{bmatrix} \mathbf{R}_N \\ T_l \end{bmatrix} \quad (4.19)$$

where

$$\mathbf{R}_N = ([\mathbf{C}] - (1 - \alpha)\Delta t [\mathbf{K}]) \{\mathbf{T}\}_{N-1} + \alpha \Delta t \{\mathbf{f}\}_N + (1 - \alpha)\Delta t \{\mathbf{f}\}_{N-1} \quad (4.20a)$$

$$\mathbf{K}^* = \alpha \Delta t [\mathbf{K}] \quad (4.20b)$$

4.5 NUMERICAL RESULTS AND DISCUSSION

The different parameters used for steady-state and transient analysis of one-dimensional composite model shown in Fig. 4.9 are tabulated in Table 4.23. The EFG results are obtained using different weight functions for two sets of nodes and the FEM results are obtained using linear bar element for same sets of nodes. A comparison is made among the results obtained using different EFG weight functions.

4.5.1 Steady-state analysis

The results presented in Table 4.24 are obtained by EFG method using different weight functions for two values of scaling parameter (i.e. $d_{\max} = 1.01$ & $d_{\max} = 1.51$) and it shows a comparison of temperature values obtained using 11 nodes with those obtained by FEM at the location ($x = 0.4$ m). Table 4.25 shows a comparison of temperature values obtained by EFG method using different weight functions for two values of scaling parameter with those obtained by FEM at the same location i.e. ($x = 0.4$ m) for 21 nodes. A comparison of temperature values obtained using different EFG weight functions with FEM for 11 and 21 nodes, is presented in Table 4.26 and Table 4.27 respectively at the location ($x = 0.6$ m). Similar type of comparisons of temperature values are shown in Table 4.28 for 11 nodes at the location ($x = 0.8$ m), in Table 4.29 for 21 nodes at the location ($x = 0.8$ m), in Table 4.30 for 11 nodes at the location ($x = 1$ m) and in Table 4.31 for 21 nodes at the location ($x = 1$ m). From the results presented in Table 4.24 to Table 4.31, it is observed that EFG results

obtained using different weight functions are similar for $d_{\max} = 1.01$. However for $d_{\max} = 1.51$, only cubicspline, quarticspline, Gaussian, exponential and rational weight functions give acceptable results. It is also observed that EFG results obtained using different weight functions are in good agreement with those obtained by FEM. Moreover with increase in number of nodes, the EFG results start converging.

The effect of scaling parameter (d_{\max}) on EFG results obtained using different weight functions is presented in Table 4.32 for 11 nodes and Table 4.33 for 21 nodes respectively at the location ($x = 0.8$ m). Similar effect of scaling parameter on EFG results is shown in Table 4.34 for 11 nodes and Table 4.35 for 21 nodes at the location ($x = 1$ m). Fig. 4.10 shows the effect of scaling parameter on EFG results obtained using 11 and 21 nodes at the location ($x = 0.2$ m). Similar effect of scaling parameter on EFG results is observed in Fig. 4.11 at the location ($x = 0.6$ m). From tables and figures, it is clear that only cubicspline, quarticspline, Gaussian, exponential and rational weight functions give acceptable results in the range $1.0 < d_{\max} < 2.4$ whereas the results obtained using quadratic, hyperbolic and cosine weight functions are varying in abrupt manner with scaling parameter. Therefore EFG results obtained using quadratic, hyperbolic and cosine weight functions are not acceptable in the range $1.0 < d_{\max} < 2.4$. It is also observed that there is minimum variation in EFG results with scaling parameter for exponential weight function.

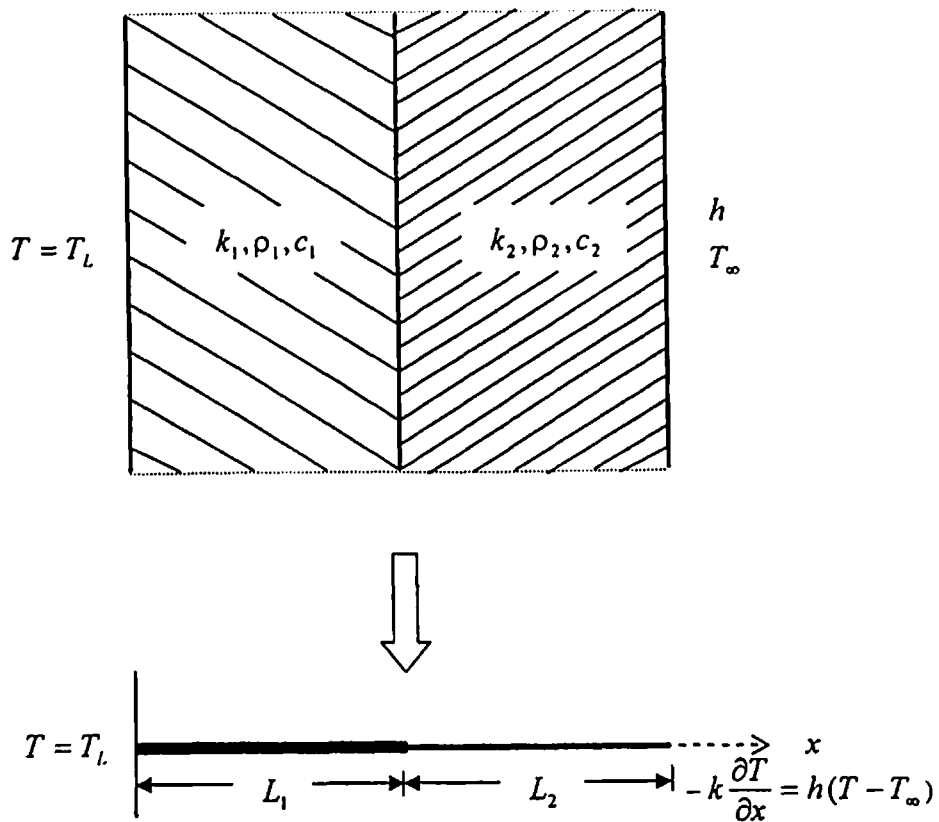


Fig. 4.9 One-dimensional model

Table 4.23 Data for the 1-D model shown in Fig. 4.9

Parameters	Value of the parameter
Length (L_1)	0.5 m
Length (L_2)	0.5 m
Thermal conductivity of material 1 (k_1)	400 W/m-K
Thermal conductivity of material 2 (k_2)	100 W/m-K
Density of the material 1 (ρ_1)	10000 kg/m ³
Density of the material 2 (ρ_2)	8000 kg/m ³
Specific heat of material 1 (c_1)	400 kJ/kg-K
Specific heat of material 2 (c_2)	300 kJ/kg-K
Rate of internal heat generation (\dot{Q})	0 W/m ³
Surrounding fluid temperature (T_∞)	20 °C
Initial temperature (T_{in})	100 °C
Time step size (Δt)	100 sec
Temperature at end $x = 0$ (T_L)	100 °C

Table 4.24 Comparison of EFG results obtained using 11 nodes with FEM results at the location ($x = 0.4$ m) of the 1-D model shown in Fig. 4.9

Weight function	EFG				FEM T (°C)
	$d_{\max} = 1.01$		$d_{\max} = 1.51$		
	T (°C)	% diff with FEM	T (°C)	% diff with FEM	
C. S.	92.3810	-0.5468	92.3810	-0.5468	92.8889
Q. S.	92.3810	-0.5468	92.3811	-0.5467	
Gaussian	92.3810	-0.5468	92.3830	-0.5446	
Quadratic	92.3810	-0.5468	58.3964	-37.1331	
Hyperbolic	92.3810	-0.5468	91.3675	-1.6379	
Exponential	92.3810	-0.5468	92.3714	-0.5571	
Rational	92.3810	-0.5468	92.3424	-0.5883	
Cosine	92.3810	-0.5468	96.6060	4.0017	

Table 4.25 Comparison of EFG results obtained using 21 nodes with FEM results at the location ($x = 0.4$ m) of the 1-D model shown in Fig. 4.9

Weight function	EFG				FEM T (°C)
	$d_{\max} = 1.01$		$d_{\max} = 1.51$		
	T (°C)	% diff with FEM	T (°C)	% diff with FEM	
C. S.	92.6437	-0.2640	92.6437	-0.2640	92.8889
Q. S.	92.6437	-0.2640	92.6437	-0.2640	
Gaussian	92.6437	-0.2640	92.6450	-0.2640	
Quadratic	92.6437	-0.2640	87.7250	-5.5592	
Hyperbolic	92.6437	-0.2640	93.4782	0.6344	
Exponential	92.6437	-0.2640	92.6393	-0.2687	
Rational	92.6437	-0.2640	92.6402	-0.2677	
Cosine	92.6437	-0.2640	102.8820	10.7581	

Table 4.26 Comparison of EFG results obtained using 11 nodes with FEM results at the location ($x = 0.6$ m) of the 1-D model shown in Fig. 4.9

Weight function	EFG				FEM
	$d_{\max} = 1.01$		$d_{\max} = 1.51$		
	T (°C)	% diff with FEM	T (°C)	% diff with FEM	T (°C)
C. S.	82.8571	-1.3606	82.8573	-1.3604	84.0000
Q. S.	82.8571	-1.3606	82.8574	-1.3604	
Gaussian	82.8571	-1.3606	82.8628	-1.3538	
Quadratic	82.8571	-1.3606	131.8180	56.9262	
Hyperbolic	82.8571	-1.3606	82.2172	-2.1224	
Exponential	82.8571	-1.3606	82.8362	-1.3855	
Rational	82.8571	-1.3606	82.8080	-1.4191	
Cosine	82.8571	-1.3606	85.8611	2.2156	

Table 4.27 Comparison of EFG results obtained using 21 nodes with FEM results at the location ($x = 0.6$ m) of the 1-D model shown in Fig. 4.9

Weight function	EFG				FEM
	$d_{\max} = 1.01$		$d_{\max} = 1.51$		
	T (°C)	% diff with FEM	T (°C)	% diff with FEM	T (°C)
C. S.	83.4483	-0.6568	83.4483	-0.6568	84.0000
Q. S.	83.4483	-0.6568	83.4484	-0.6568	
Gaussian	83.4483	-0.6568	83.4513	-0.6532	
Quadratic	83.4483	-0.6568	91.3608	8.7629	
Hyperbolic	83.4483	-0.6568	84.1876	0.2233	
Exponential	83.4483	-0.6568	83.4385	-0.6685	
Rational	83.4483	-0.6568	83.4398	-0.6669	
Cosine	83.4483	-0.6568	99.7836	18.7900	

Table 4.28 Comparison of EFG results obtained using 11 nodes with FEM results at the location ($x = 0.8\text{m}$) of the 1-D model shown in Fig. 4.9

Weight function	EFG				FEM
	$d_{\max} = 1.01$		$d_{\max} = 1.51$		
	$T (^{\circ}\text{C})$	% diff with FEM	$T (^{\circ}\text{C})$	% diff with FEM	$T (^{\circ}\text{C})$
C. S.	67.6190	-3.0938	67.6193	-3.0934	69.7778
Q. S.	67.6190	-3.0938	67.6195	-3.0931	
Gaussian	67.6190	-3.0938	67.6328	-3.0740	
Quadratic	67.6190	-3.0938	44.8242	-35.7615	
Hyperbolic	67.6190	-3.0938	69.2876	-0.7025	
Exponential	67.6190	-3.0938	67.5792	-3.1509	
Rational	67.6190	-3.0938	67.5855	-3.1418	
Cosine	67.6190	-3.0938	66.7390	-4.3550	

Table 4.29 Comparison of EFG results obtained using 21 nodes with FEM results at the location ($x = 0.8\text{m}$) of the 1-D model shown in Fig. 4.9

Weight function	EFG				FEM
	$d_{\max} = 1.01$		$d_{\max} = 1.51$		
	$T (^{\circ}\text{C})$	% diff with FEM	$T (^{\circ}\text{C})$	% diff with FEM	$T (^{\circ}\text{C})$
C. S.	68.7356	-1.4936	68.7357	-1.4935	69.7778
Q. S.	68.7356	-1.4936	68.7358	-1.4933	
Gaussian	68.7356	-1.4936	68.7414	-1.4853	
Quadratic	68.7356	-1.4936	87.6381	25.5960	
Hyperbolic	68.7356	-1.4936	68.9638	-1.1666	
Exponential	68.7356	-1.4936	68.7173	-1.5198	
Rational	68.7356	-1.4936	68.7183	-1.5184	
Cosine	68.7356	-1.4936	84.4254	20.9918	

Table 4.30 Comparison of EFG results obtained using 11 nodes with FEM results at the location ($x = 1$ m) of the 1-D model shown in Fig. 4.9

Weight function	EFG				FEM
	$d_{\max} = 1.01$		$d_{\max} = 1.51$		
	T (°C)	% diff with FEM	T (°C)	% diff with FEM	T (°C)
C. S.	56.1905	1.1428	56.1908	1.1433	55.5556
Q. S.	56.1905	1.1428	56.1911	1.1439	
Gaussian	56.1905	1.1428	56.2079	1.1741	
Quadratic	56.1905	1.1428	68.0085	22.4152	
Hyperbolic	56.1905	1.1428	57.1774	2.9192	
Exponential	56.1905	1.1428	56.1040	0.9871	
Rational	56.1905	1.1428	56.0800	0.9439	
Cosine	56.1905	1.1428	61.1209	10.0175	

Table 4.31 Comparison of EFG results obtained using 21 nodes with FEM results at the location ($x = 1$ m) of the 1-D model shown in Fig. 4.9

Weight function	EFG				FEM
	$d_{\max} = 1.01$		$d_{\max} = 1.51$		
	T (°C)	% diff with FEM	T (°C)	% diff with FEM	T (°C)
C. S.	55.8621	0.5517	55.8622	0.5519	55.5556
Q. S.	55.8621	0.5517	55.8624	0.5522	
Gaussian	55.8621	0.5517	55.8706	0.5670	
Quadratic	55.8621	0.5517	60.5147	8.9264	
Hyperbolic	55.8621	0.5517	56.2420	1.2355	
Exponential	55.8621	0.5517	55.8201	0.4761	
Rational	55.8621	0.5517	55.8086	0.4554	
Cosine	55.8621	0.5517	61.9574	11.5232	

Table 4.32 Effect of scaling parameter on EFG results obtained using 11 nodes at the location ($x = 0.8\text{m}$) of the 1-D model shown in Fig. 4.9

Scaling Parameter	Temperature ($^{\circ}\text{C}$)							
	C. S.	Q. S	Gaussian	Quadratic	Hyperbolic	Exponential	Rational	Cosine
1.01	67.6190	67.6190	67.6190	67.6190	67.6190	67.6190	67.6190	67.6190
1.21	67.6190	67.6190	67.6190	67.6190	67.6190	67.6190	67.6190	67.6190
1.41	67.6190	67.6190	67.6190	67.6190	67.6190	67.6190	67.6190	67.6190
1.61	67.6426	67.6674	67.6472	101.3645	70.3955	67.5824	67.6062	124.1289
1.81	67.8071	68.0826	67.7096	204.8154	82.6078	67.5944	67.6616	159.8405
2.01	68.1777	68.9506	67.8424	129.3796	100.5336	67.6135	67.7329	88.5109
2.21	68.7815	70.0870	68.0665	110.1179	95.8187	67.6404	67.8312	84.9284
2.41	69.6760	71.5764	68.3843	106.4776	64.9861	67.6743	67.9527	85.3516
2.61	71.0981	74.0683	68.7519	22.7000	55.7435	67.6037	67.9363	-248.5062
2.81	73.8205	77.6991	69.2324	-1325.40	19.4382	67.6176	68.1840	-481.8810
3.01	80.9423	79.9077	69.8670	466.5000	126.3568	67.6353	68.5026	298.7535

Table 4.33 Effect of scaling parameter on EFG results obtained using 21 nodes at the location ($x = 0.8\text{m}$) of the 1-D model shown in Fig. 4.9

Scaling Parameter	Temperature ($^{\circ}\text{C}$)							
	C. S.	Q. S	Gaussian	Quadratic	Hyperbolic	Exponential	Rational	Cosine
1.01	68.7356	68.7356	68.7356	68.7356	68.7356	68.7356	68.7356	68.7356
1.21	68.7356	68.7356	68.7356	68.7356	68.7356	68.7356	68.7356	68.7356
1.41	68.7356	68.7356	68.7356	68.7356	68.7356	68.7356	68.7356	68.7356
1.61	68.7455	68.7543	68.7465	54.9546	69.0610	68.7193	68.7227	49.5543
1.81	68.7879	68.8362	68.7622	510.2401	72.9895	68.7243	68.7313	69.0347
2.01	68.8444	68.9699	68.7825	66.2578	54.3091	68.7296	68.7381	23.0901
2.21	68.9334	69.2410	68.8054	65.1579	35.8072	68.7350	68.7485	-28.6265
2.41	69.1296	69.8539	68.8390	67.2968	253.4473	68.7401	68.7622	30.3862
2.61	69.6337	71.3570	68.8762	-224.1299	38.2441	68.7522	68.6924	14.8047
2.81	70.9508	73.3940	68.9685	46.9192	-76.5491	68.7562	68.6531	49.9786
3.01	75.5215	73.5534	69.1565	33.0628	-66.9493	68.7578	68.6061	6.9884

Table 4.34 Effect of scaling parameter on EFG results obtained using 11 nodes at the location ($x = 1\text{ m}$) of the 1-D model shown in Fig. 4.9

Scaling Parameter	Temperature ($^{\circ}\text{C}$)							
	C. S.	Q. S	Gaussian	Quadratic	Hyperbolic	Exponential	Rational	Cosine
1.01	56.1905	56.1905	56.1905	56.1905	56.1905	56.1905	56.1905	56.1905
1.21	56.1905	56.1905	56.1905	56.1905	56.1905	56.1905	56.1905	56.1905
1.41	56.1905	56.1905	56.1905	56.1905	56.1905	56.1905	56.1905	56.1905
1.61	56.2191	56.2446	56.2244	69.7143	57.4322	56.1043	56.1101	78.7127
1.81	56.3418	56.4739	56.2855	91.3621	60.0905	56.1118	56.1771	78.2962
2.01	56.5003	56.7389	56.3942	78.1890	66.7970	56.1267	56.2503	62.8495
2.21	56.6983	57.0453	56.5577	78.4848	65.0892	56.1486	56.3376	65.1943
2.41	56.9747	57.4771	56.7778	79.7363	55.1690	56.1760	56.4360	66.9468
2.61	57.4083	58.1996	57.0925	35.4011	48.5391	56.2117	56.7803	-108.4905
2.81	58.2008	59.3245	57.4516	-499.4653	25.7560	56.2634	56.9725	-155.3312
3.01	60.0115	60.3310	57.8818	260.0808	120.2633	56.3202	57.1890	155.9815

Table 4.35 Effect of scaling parameter on EFG results obtained using 21 nodes at the location ($x = 1\text{ m}$) of the 1-D model shown in Fig. 4.9

Scaling Parameter	Temperature ($^{\circ}\text{C}$)							
	C. S.	Q. S	Gaussian	Quadratic	Hyperbolic	Exponential	Rational	Cosine
1.01	55.8621	55.8621	55.8621	55.8621	55.8621	55.8621	55.8621	55.8621
1.21	55.8621	55.8621	55.8621	55.8621	55.8621	55.8621	55.8621	55.8621
1.41	55.8621	55.8621	55.8621	55.8621	55.8621	55.8621	55.8621	55.8621
1.61	55.8760	55.8884	55.8786	61.8934	56.1992	55.8203	55.8232	63.2532
1.81	55.9358	56.0004	55.9083	-326.6920	56.0960	55.8240	55.8556	58.2360
2.01	56.0132	56.1303	55.9611	56.4249	52.6438	55.8312	55.8911	91.2827
2.21	56.1101	56.2812	56.0405	62.4137	49.3719	55.8418	55.9336	173.3159
2.41	56.2464	56.4991	56.1476	59.0345	126.6772	55.8551	55.9818	107.4870
2.61	56.4656	56.8806	56.3013	-71.7237	60.3824	55.8725	56.1450	-37.5618
2.81	56.8780	57.4626	56.4793	16.6236	68.4764	55.8975	56.2359	-18.2257
3.01	57.8374	57.9494	56.6946	122.9053	46.7861	55.9251	56.3441	62.2759

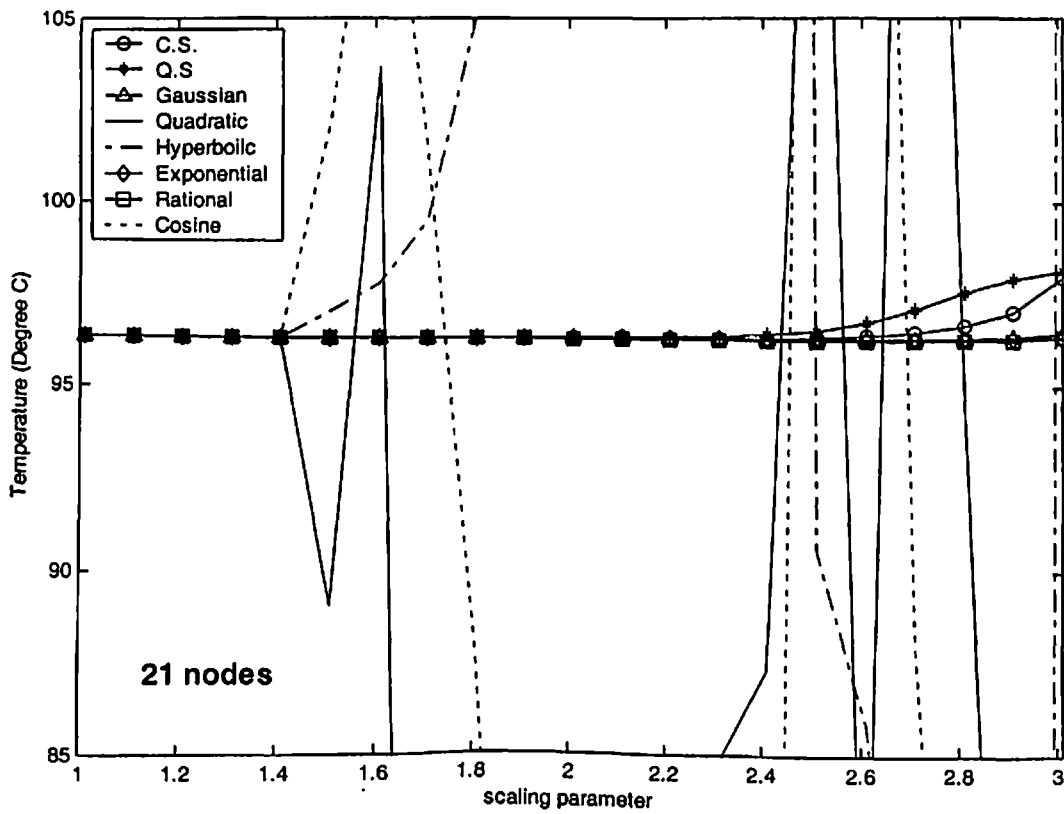
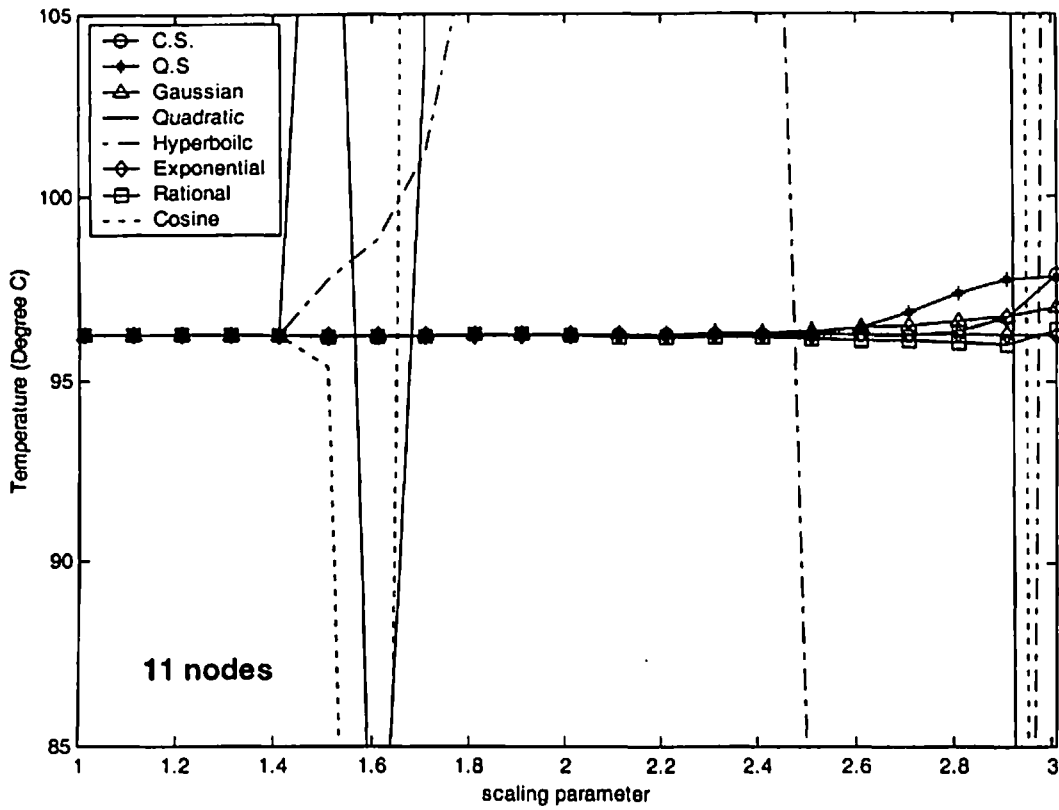


Fig. 4.10 Effect of scaling parameter on EFG results at the location ($x = 0.2$ m) of the 1-D model shown in Fig. 4.9

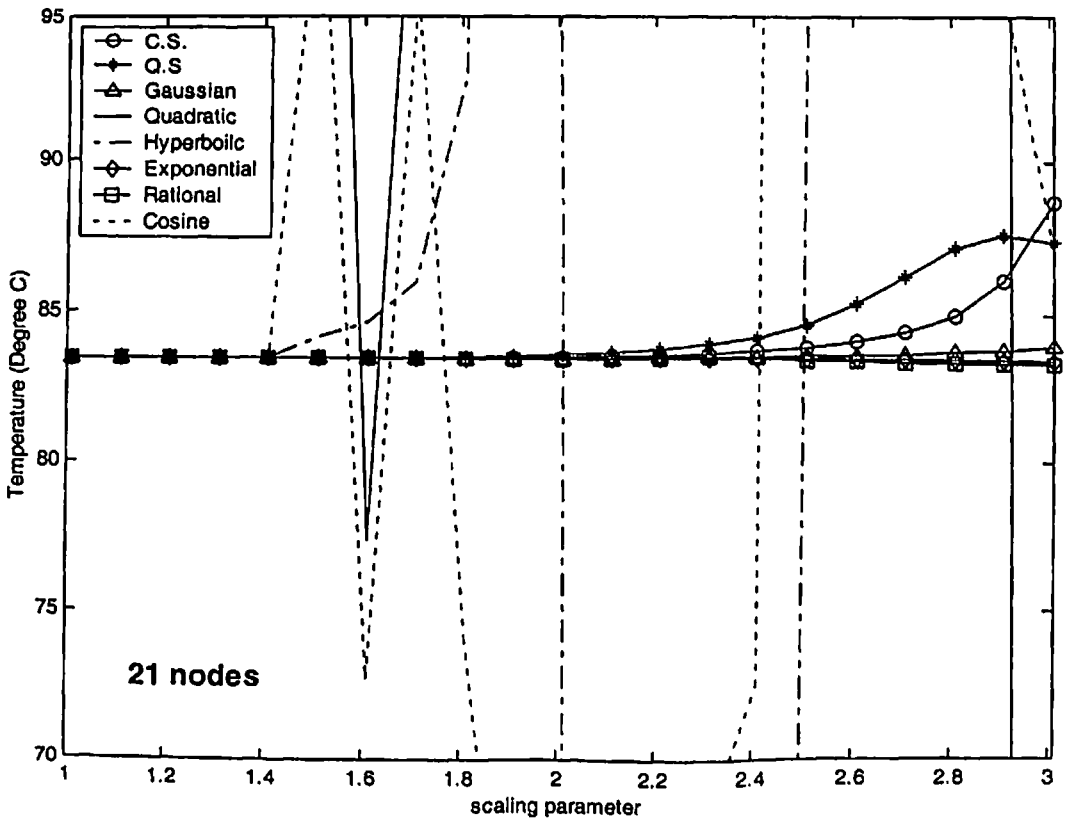
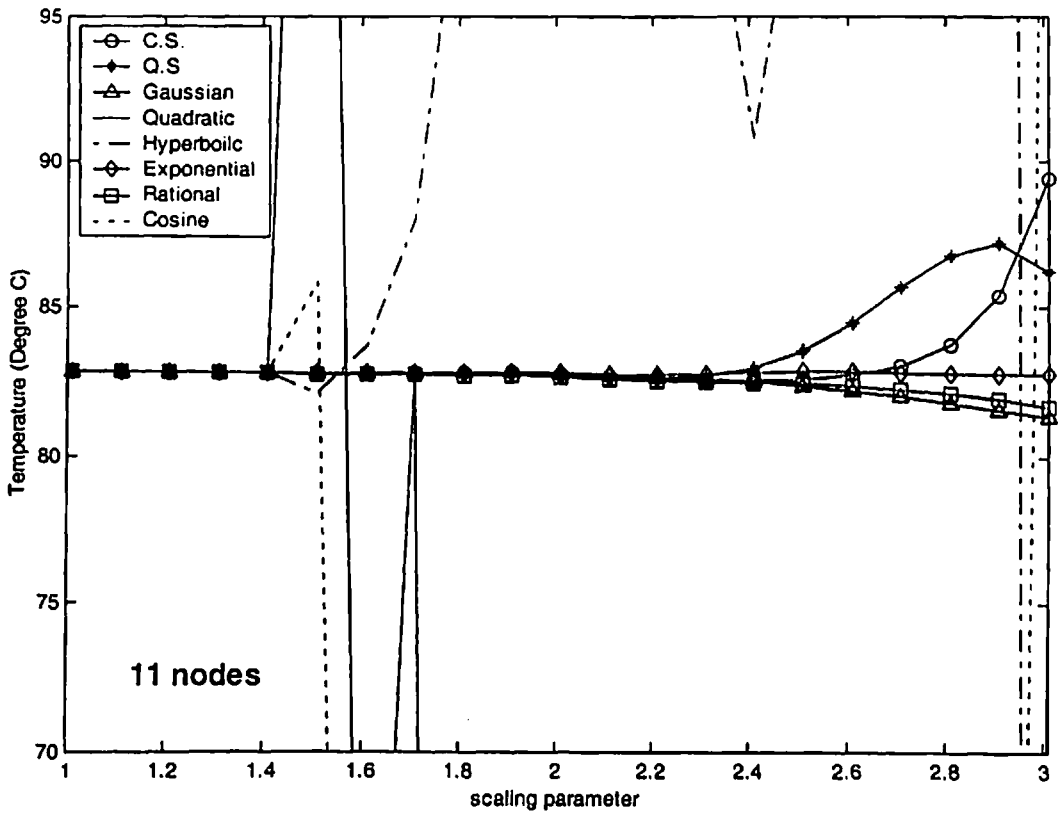


Fig. 4.11 Effect of scaling parameter on EFG results at the location ($x = 0.6$ m) of the 1-D model shown in Fig. 4.9

4.5.2 Transient analysis

The transient analysis of 1-D composite model is carried out using different EFG weight functions. Table 4.36 and Table 4.37 show the comparison of temperature values obtained using 11 nodes with FEM results at the location ($x = 0.2\text{ m}$) for $d_{\max} = 1.01$ and $d_{\max} = 1.51$ respectively. Similar comparison of temperature values obtained using 21 nodes with FEM results is presented in Table 4.38 and Table 4.39 for $d_{\max} = 1.01$ and $d_{\max} = 1.51$ respectively at the same location i.e. ($x = 0.2\text{ m}$). For this case (i.e. CASE-II) of 1-D transient analysis, time step of 100 sec has been taken which is nearly 1% of the total time required to achieve steady state condition. Table 4.40 and Table 4.41 shows the comparison of temperature values obtained using 11 nodes with FEM results at the different location ($x = 0.6\text{ m}$) for $d_{\max} = 1.01$ and $d_{\max} = 1.51$ respectively. Similar comparison of temperature values obtained using 21 nodes with FEM results is also presented in Table 4.42 and Table 4.43 for $d_{\max} = 1.01$ and $d_{\max} = 1.51$ respectively at the location ($x = 0.6\text{ m}$). Fig 4.12 shows the comparison of temperature values obtained using 11 nodes with FEM for $d_{\max} = 1.01$ and $d_{\max} = 1.51$ at the location ($x = 0.8\text{ m}$). Similar comparison of temperature values obtained using 21 nodes with FEM is shown in Fig. 4.13 at the same location i.e. ($x = 0.8\text{ m}$). Fig 4.14 shows the comparison of temperature values obtained using 11 nodes with FEM for $d_{\max} = 1.01$ and $d_{\max} = 1.51$ at the location ($x = 1\text{ m}$). Similar comparison of temperature values obtained using 21 nodes with FEM is shown in Fig. 4.15 at the same location i.e. ($x = 1\text{ m}$). From the results presented in tables and figures, it is clear that the EFG results obtained using different weight functions are similar for $d_{\max} = 1.01$ but for $d_{\max} = 1.51$ only cubicspline (C.S.), quarticspline (Q.S), Gaussian, exponential and rational weight functions give acceptable results. It has also been observed that the EFG results are in good agreement with those obtained by FEM.

Table 4.36 Comparison of EFG results obtained using 11 nodes with FEM at the location ($x = 0.2$ m) of the 1-D model shown in Fig. 4.9 for $d_{max} = 1.01$

Time (sec) $\times 10^2$	Temperature ($^{\circ}$ C)								
	$d_{max} = 1.01$								FEM
	C. S.	Q. S	Gaussian	Quadratic	Hyperbolic	Exponential	Rational	Cosine	
0	100.000	100.000	100.000	100.000	100.000	100.000	100.000	100.000	100.000
10	99.8928	99.8928	99.8928	99.8928	99.8928	99.8928	99.8928	99.8928	99.9101
20	99.0701	99.0701	99.0701	99.0701	99.0701	99.0701	99.0701	99.0701	99.1898
30	98.1799	98.1799	98.1799	98.1799	98.1799	98.1799	98.1799	98.1799	98.3729
40	97.5117	97.5117	97.5117	97.5117	97.5117	97.5117	97.5117	97.5117	97.7451
50	97.0557	97.0557	97.0557	97.0557	97.0557	97.0557	97.0557	97.0557	97.3089
60	96.7542	96.7542	96.7542	96.7542	96.7542	96.7542	96.7542	96.7542	97.0159
70	96.5570	96.5570	96.5570	96.5570	96.5570	96.5570	96.5570	96.5570	96.8215
80	96.4286	96.4286	96.4286	96.4286	96.4286	96.4286	96.4286	96.4286	96.6930
90	96.3452	96.3452	96.3452	96.3452	96.3452	96.3452	96.3452	96.3452	96.6082
100	96.2910	96.2910	96.2910	96.2910	96.2910	96.2910	96.2910	96.2910	96.5524

Table 4.37 Comparison of EFG results obtained using 11 nodes with FEM at the location ($x = 0.2$ m) of the 1-D model shown in Fig. 4.9 for $d_{max} = 1.51$

Time (sec) $\times 10^2$	Temperature ($^{\circ}$ C)								
	$d_{max} = 1.51$								FEM
	C. S.	Q. S	Gaussian	Quadratic	Hyperbolic	Exponential	Rational	Cosine	
0	100.000	100.000	100.000	100.000	100.000	100.000	100.000	100.000	100.000
10	99.8927	99.8926	99.8898	100.3458	99.7459	99.9126	99.9468	99.9017	99.9101
20	99.0701	99.0701	99.0704	100.8600	99.1759	99.0761	99.0954	99.4084	99.1898
30	98.1799	98.1800	98.1820	101.4282	98.7149	98.1758	98.1784	98.5354	98.3729
40	97.5118	97.5118	97.5143	102.1348	98.3895	97.5041	97.4991	97.7209	97.7451
50	97.0558	97.0558	97.0582	102.9531	98.1687	97.0474	97.0396	97.0793	97.3089
60	96.7542	96.7542	96.7564	103.8363	98.0211	96.7461	96.7377	96.6054	97.0159
70	96.5570	96.5571	96.5591	104.7437	97.9229	96.5496	96.5412	96.2646	96.8215
80	96.4287	96.4287	96.4306	105.6459	97.8577	96.4218	96.4138	96.0218	96.6930
90	96.3452	96.3453	96.3470	106.5233	97.8144	96.3388	96.3313	95.8491	96.6082
100	96.2910	96.2911	96.2927	107.3641	97.7857	96.2850	96.2779	95.7258	96.5524

Table 4.38 Comparison of EFG results obtained using 21 nodes with FEM at the location ($x = 0.2$ m) of the 1-D model shown in Fig. 4.9 for $d_{max} = 1.01$

Time (sec) $\times 10^2$	Temperature ($^{\circ}$ C)								
	$d_{max} = 1.01$								FEM
	C. S.	Q. S.	Gaussian	Quadratic	Hyperbolic	Exponential	Rational	Cosine	
0	100.000	100.000	100.000	100.000	100.000	100.000	100.000	100.000	100.0009
10	99.8862	99.8862	99.8862	99.8862	99.8862	99.8862	99.8862	99.8862	9.8936
20	99.1268	99.1268	99.1268	99.1268	99.1268	99.1268	99.1268	99.1268	99.1787
30	98.2819	98.2819	98.2819	98.2819	98.2819	98.2819	98.2819	98.2819	98.3712
40	97.6366	97.6366	97.6366	97.6366	97.6366	97.6366	97.6366	97.6366	97.7479
50	97.1907	97.1907	97.1907	97.1907	97.1907	97.1907	97.1907	97.1907	97.3131
60	96.8928	96.8928	96.8928	96.8928	96.8928	96.8928	96.8928	96.8928	97.0202
70	96.6963	96.6963	96.6963	96.6963	96.6963	96.6963	96.6963	96.6963	96.8252
80	96.5672	96.5672	96.5672	96.5672	96.5672	96.5672	96.5672	96.5672	96.6960
90	96.4825	96.4825	96.4825	96.4825	96.4825	96.4825	96.4825	96.4825	96.6106
100	96.4271	96.4271	96.4271	96.4271	96.4271	96.4271	96.4271	96.4271	96.5542

Table 4.39 Comparison of EFG results obtained using 21 nodes with FEM at the location ($x = 0.2$ m) of the 1-D model shown in Fig. 4.9 for $d_{max} = 1.51$

Time (sec) $\times 10^2$	Temperature ($^{\circ}$ C)								
	$d_{max} = 1.51$								FEM
	C. S.	Q. S.	Gaussian	Quadratic	Hyperbolic	Exponential	Rational	Cosine	
0	100.000	100.000	100.000	100.000	100.000	100.000	100.000	100.000	100.0009
10	99.8862	99.8862	99.8856	99.4071	99.9638	99.8908	99.8984	100.7783	9.8936
20	99.1268	99.1268	99.1268	97.3256	99.3871	99.1287	99.1344	101.3990	99.1787
30	98.2819	98.2819	98.2826	95.2884	98.7143	98.2808	98.2826	101.5806	98.3712
40	97.6366	97.6366	97.6375	93.6883	98.1880	97.6341	97.6340	101.6440	97.7479
50	97.1907	97.1908	97.1916	92.5052	97.8175	97.1877	97.1870	101.6901	97.3131
60	96.8929	96.8929	96.8937	91.6433	97.5661	96.8898	96.8889	101.7388	97.0202
70	96.6963	96.6963	96.6971	91.0149	97.3977	96.6933	96.6924	101.7901	96.8252
80	96.5672	96.5672	96.5680	90.5535	97.2855	96.5643	96.5635	101.8406	96.6960
90	96.4825	96.4826	96.4833	90.2118	97.2108	96.4798	96.4791	101.8878	96.6106
100	96.4271	96.4271	96.4278	89.9563	97.1611	96.4245	96.4239	101.9305	96.5542

Table 4.40 Comparison of EFG results obtained using 11 nodes with FEM at the location ($x = 0.6$ m) of the 1-D model shown in Fig. 4.9 for $d_{max} = 1.01$

Time (sec) $\times 10^2$	Temperature ($^{\circ}$ C)								
	$d_{max} = 1.01$								FEM
	C. S.	Q. S	Gaussian	Quadratic	Hyperbolic	Exponential	Rational	Cosine	
0	100.000	100.000	100.000	100.000	100.000	100.000	100.000	100.000	100.000
10	97.0086	97.0086	97.0086	97.0086	97.0086	97.0086	97.0086	97.0086	97.5036
20	92.3814	92.3814	92.3814	92.3814	92.3814	92.3814	92.3814	92.3814	93.2377
30	89.1171	89.1171	89.1171	89.1171	89.1171	89.1171	89.1171	89.1171	90.1629
40	86.9402	86.9402	86.9402	86.9402	86.9402	86.9402	86.9402	86.9402	88.0797
50	85.5129	85.5129	85.5129	85.5129	85.5129	85.5129	85.5129	85.5129	86.6929
60	84.5828	84.5828	84.5828	84.5828	84.5828	84.5828	84.5828	84.5828	85.7755
70	83.9780	83.9780	83.9780	83.9780	83.9780	83.9780	83.9780	83.9780	85.1702
80	83.5851	83.5851	83.5851	83.5851	83.5851	83.5851	83.5851	83.5851	84.7711
90	83.3300	83.3300	83.3300	83.3300	83.3300	83.3300	83.3300	83.3300	84.5081
100	83.1643	83.1643	83.1643	83.1643	83.1643	83.1643	83.1643	83.1643	84.3348

Table 4.41 Comparison of EFG results obtained using 11 nodes with FEM at the location ($x = 0.6$ m) of the 1-D model shown in Fig. 4.9 for $d_{max} = 1.51$

Time (sec) $\times 10^2$	Temperature ($^{\circ}$ C)								
	$d_{max} = 1.51$								FEM
	C. S.	Q. S	Gaussian	Quadratic	Hyperbolic	Exponential	Rational	Cosine	
0	100.000	100.000	100.000	100.000	100.000	100.000	100.000	100.000	100.000
10	97.0088	97.0090	97.0240	99.5907	97.1258	97.0167	97.1030	98.6668	97.5036
20	92.3817	92.3819	92.3978	99.8760	91.9765	92.3662	92.4075	96.3769	93.2377
30	89.1173	89.1175	89.1317	100.5139	88.6294	89.0912	89.0990	93.7819	90.1629
40	86.9405	86.9407	86.9529	101.5511	86.4478	86.9105	86.8990	91.6349	88.0797
50	85.5131	85.5133	85.5238	102.8885	85.0133	85.4828	85.4612	90.0205	86.6929
60	84.5830	84.5831	84.5923	104.4092	84.0664	84.5537	84.5271	88.8516	85.7755
70	83.9782	83.9783	83.9864	106.0173	83.4403	83.9505	83.9217	88.0177	85.1702
80	83.5853	83.5854	83.5928	107.6440	83.0260	83.5590	83.5295	87.4249	84.7711
90	83.3301	83.3303	83.3370	109.2435	82.7519	83.3052	83.2755	87.0028	84.5081
100	83.1644	83.1645	83.1709	110.7873	82.5704	83.1405	83.1110	86.7007	84.3348

Table 4.42 Comparison of EFG results obtained using 21 nodes with FEM at the location ($x = 0.6$ m) of the 1-D model shown in Fig. 4.9 for $d_{max} = 1.01$

Time (sec) $\times 10^2$	Temperature ($^{\circ}$ C)								
	$d_{max} = 1.01$								FEM
	C. S.	Q. S	Gaussian	Quadratic	Hyperbolic	Exponential	Rational	Cosine	
0	100.000	100.000	100.000	100.000	100.000	100.000	100.000	100.000	100.000
10	97.2413	97.2413	97.2413	97.2413	97.2413	97.2413	97.2413	97.2413	97.4361
20	92.8313	92.8313	92.8313	92.8313	92.8313	92.8313	92.8313	92.8313	93.2243
30	89.6697	89.6697	89.6697	89.6697	89.6697	89.6697	89.6697	89.6697	90.1708
40	87.5413	87.5413	87.5413	87.5413	87.5413	87.5413	87.5413	87.5413	88.0953
50	86.1332	86.1332	86.1332	86.1332	86.1332	86.1332	86.1332	86.1332	86.7097
60	85.2075	85.2075	85.2075	85.2075	85.2075	85.2075	85.2075	85.2075	85.7908
70	84.6005	84.6005	84.6005	84.6005	84.6005	84.6005	84.6005	84.6005	85.1830
80	84.2028	84.2028	84.2028	84.2028	84.2028	84.2028	84.2028	84.2028	84.7814
90	83.9424	83.9424	83.9424	83.9424	83.9424	83.9424	83.9424	83.9424	84.5161
100	83.7718	83.7718	83.7718	83.7718	83.7718	83.7718	83.7718	83.7718	84.3408

Table 4.43 Comparison of EFG results obtained using 21 nodes with FEM at the location ($x = 0.6$ m) of the 1-D model shown in Fig. 4.9 for $d_{max} = 1.51$

Time (sec) $\times 10^2$	Temperature ($^{\circ}$ C)								
	$d_{max} = 1.51$								FEM
	C. S.	Q. S	Gaussian	Quadratic	Hyperbolic	Exponential	Rational	Cosine	
0	100.000	100.000	100.000	100.000	100.000	100.000	100.000	100.000	100.000
10	97.2413	97.2414	97.2446	100.6190	97.5745	97.2460	97.2734	101.9326	97.4361
20	92.8314	92.8314	92.8357	98.0153	93.4077	92.8271	92.8438	101.4027	93.2243
30	89.6698	89.6699	89.6744	95.7094	90.3871	89.6607	89.6720	100.5492	90.1708
40	87.5414	87.5414	87.5459	94.0842	88.3205	87.5295	87.5363	99.9377	88.0953
50	86.1332	86.1333	86.1376	93.0130	86.9332	86.1204	86.1240	99.5737	86.7097
60	85.2076	85.2077	85.2117	92.3281	86.0091	85.1946	85.1963	99.3846	85.7908
70	84.6006	84.6007	84.6045	91.8990	85.3953	84.5879	84.5884	99.3063	85.1830
80	84.2029	84.2030	84.2066	91.6355	84.9882	84.1906	84.1905	99.2936	84.7814
90	83.9425	83.9425	83.9460	91.4775	84.7182	83.9306	83.9301	99.3174	84.5161
100	83.7719	83.7720	83.7753	91.3860	84.5391	83.7604	83.7598	99.3595	84.3408

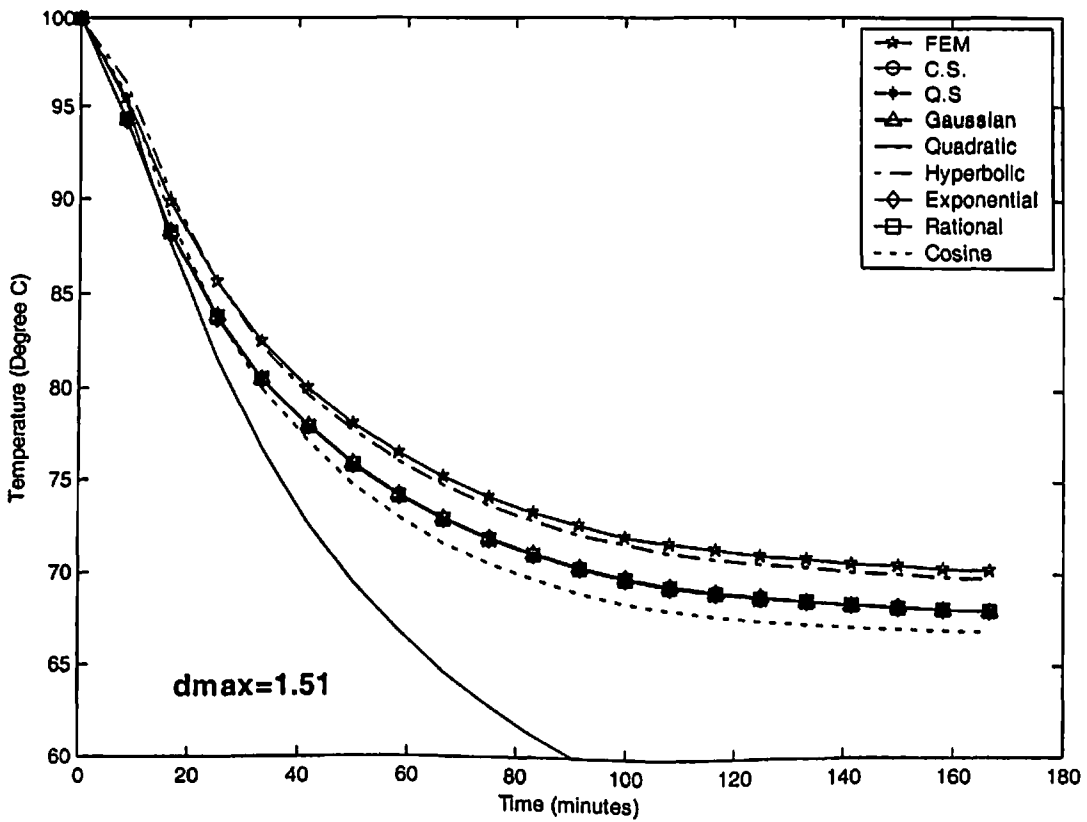
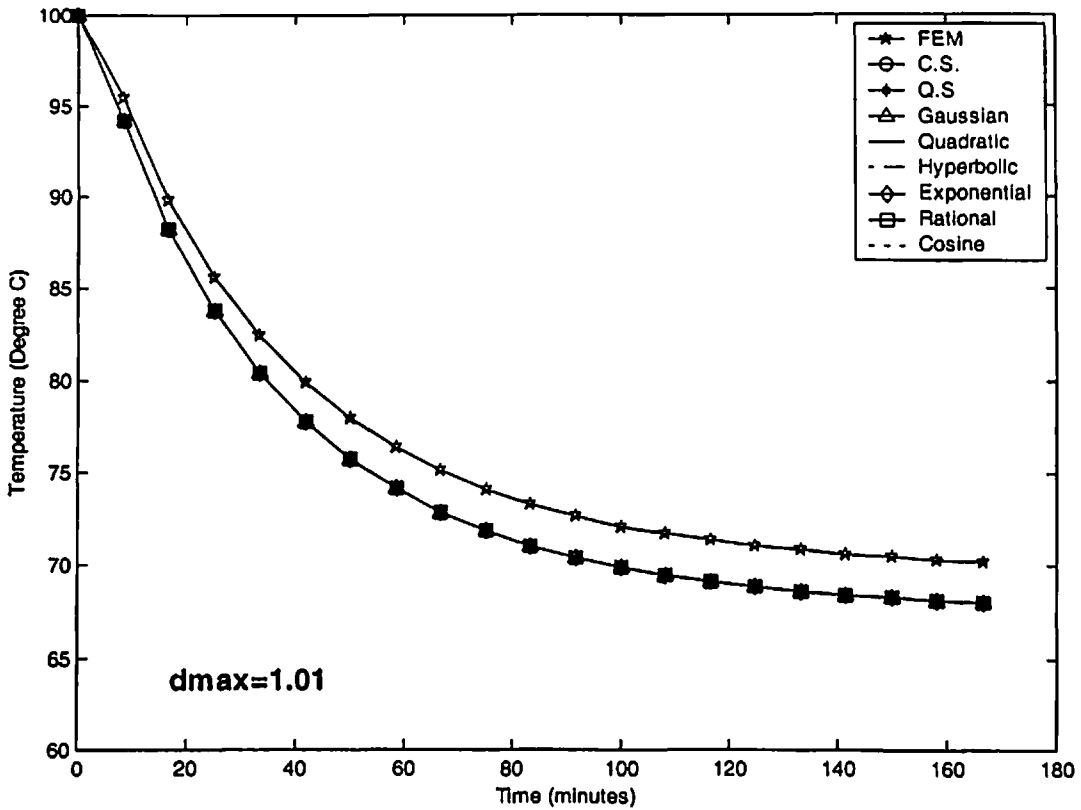


Fig. 4.12 Comparison of EFG results obtained using 11 nodes with FEM at the location ($x = 0.8$ m) of the 1-D model shown in Fig. 4.9

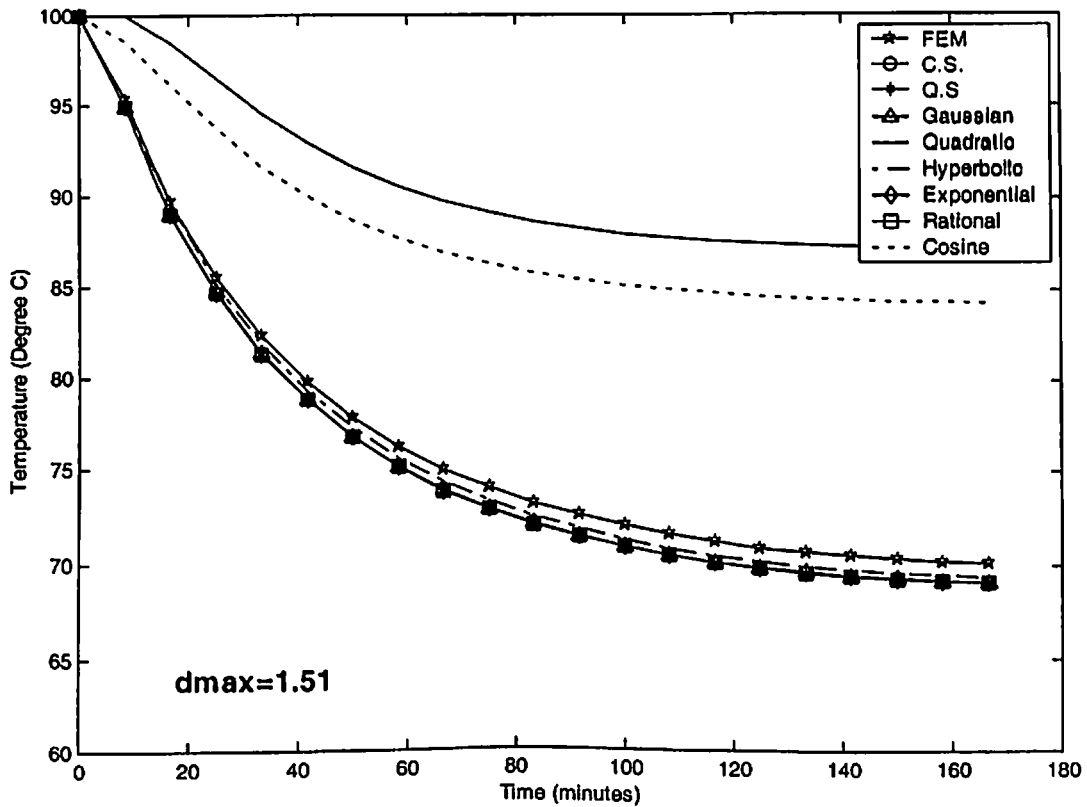
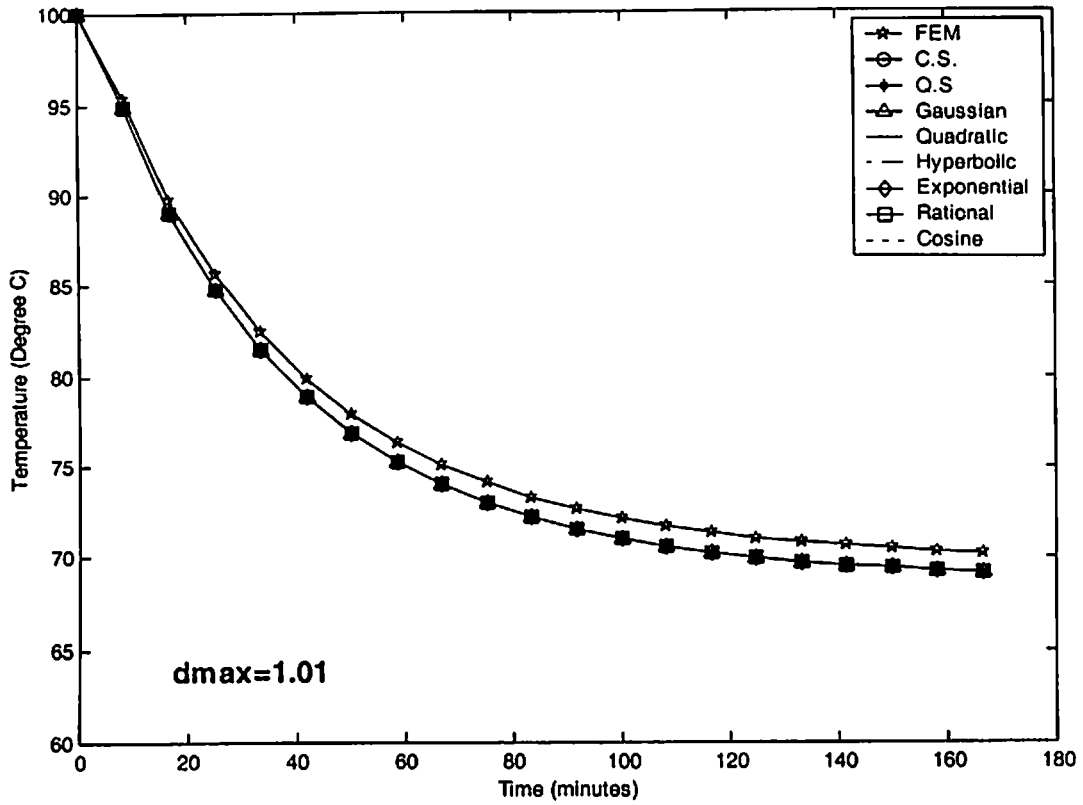


Fig. 4.13 Comparison of EFG results obtained using 21 nodes with FEM at the location ($x = 0.8$ m) of the 1-D model shown in Fig. 4.9

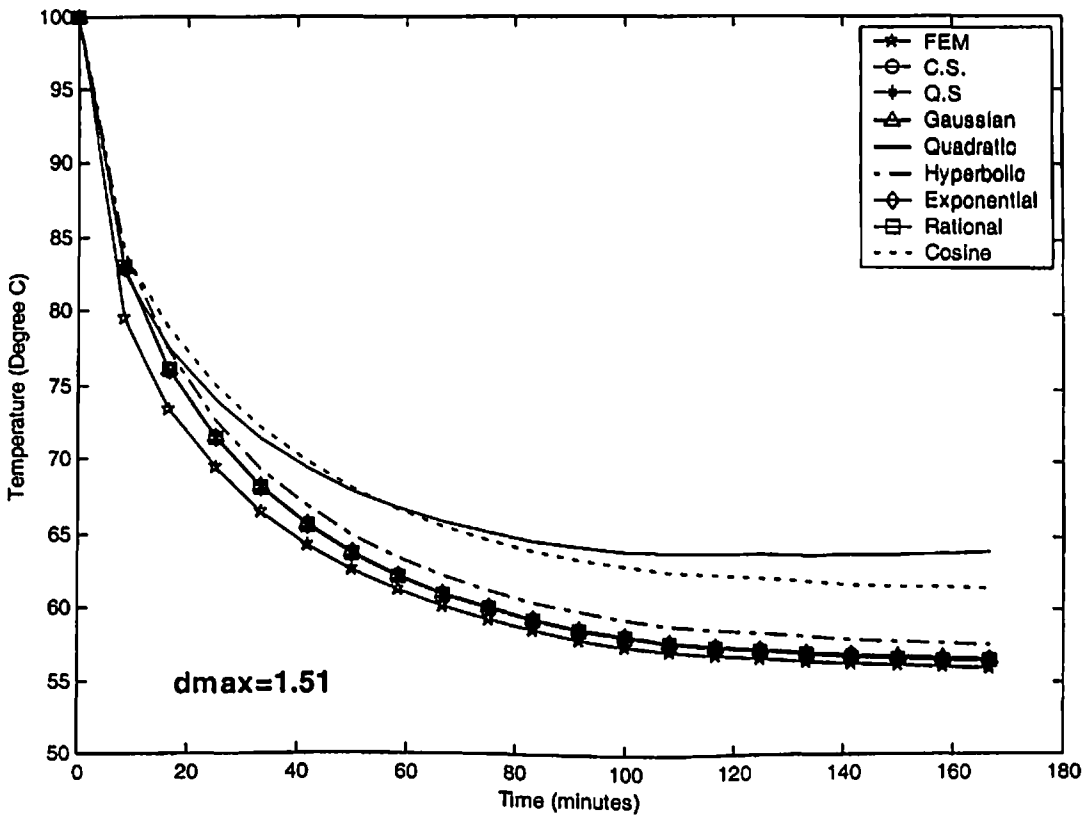
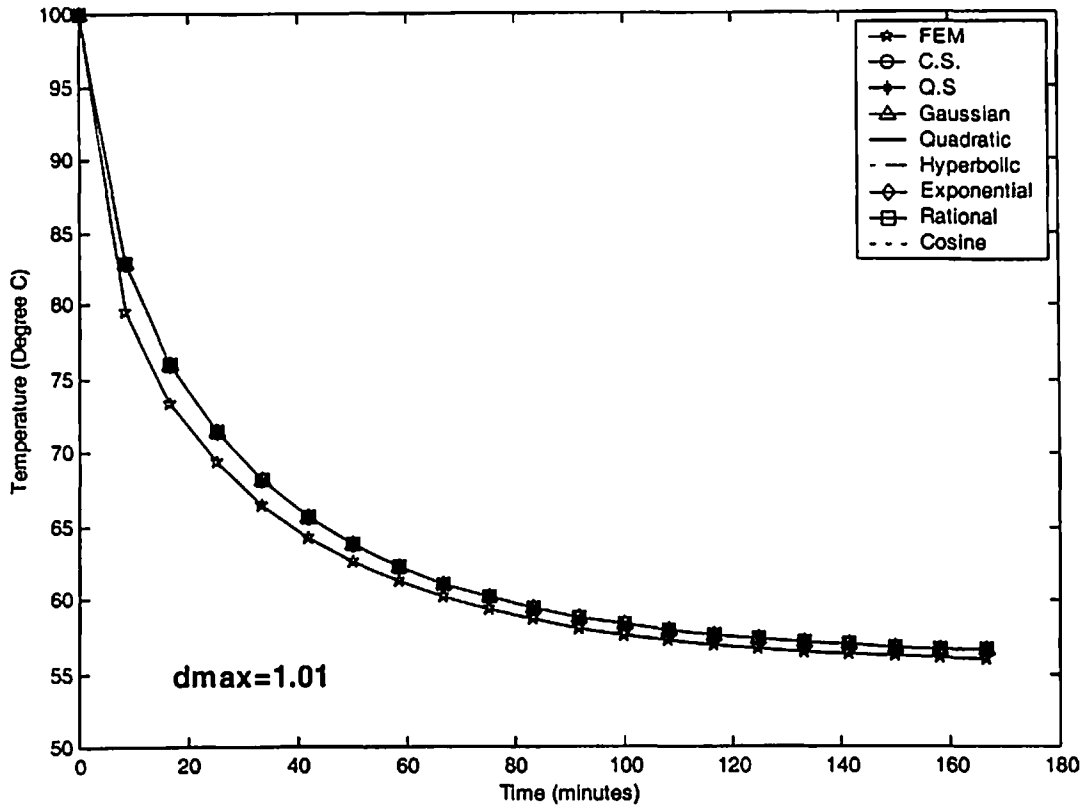


Fig. 4.14 Comparison of EFG results obtained using 11 nodes with FEM at the location ($x = 1\text{ m}$) of the 1-D model shown in Fig. 4.9

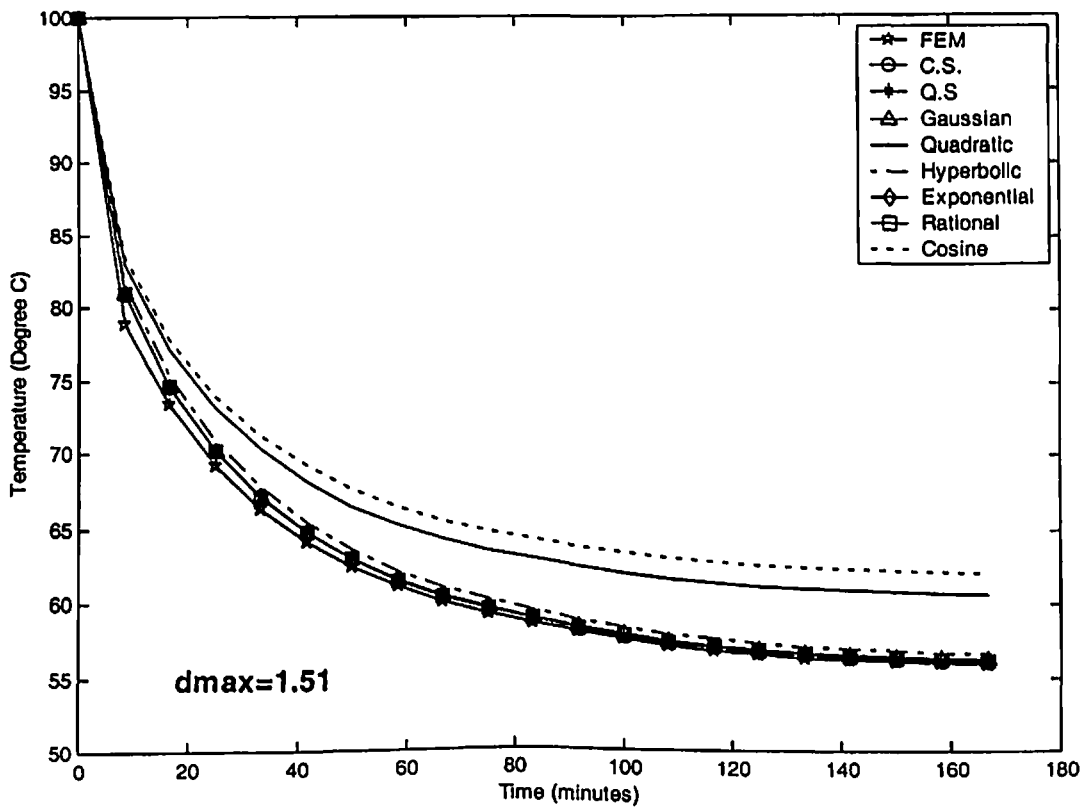
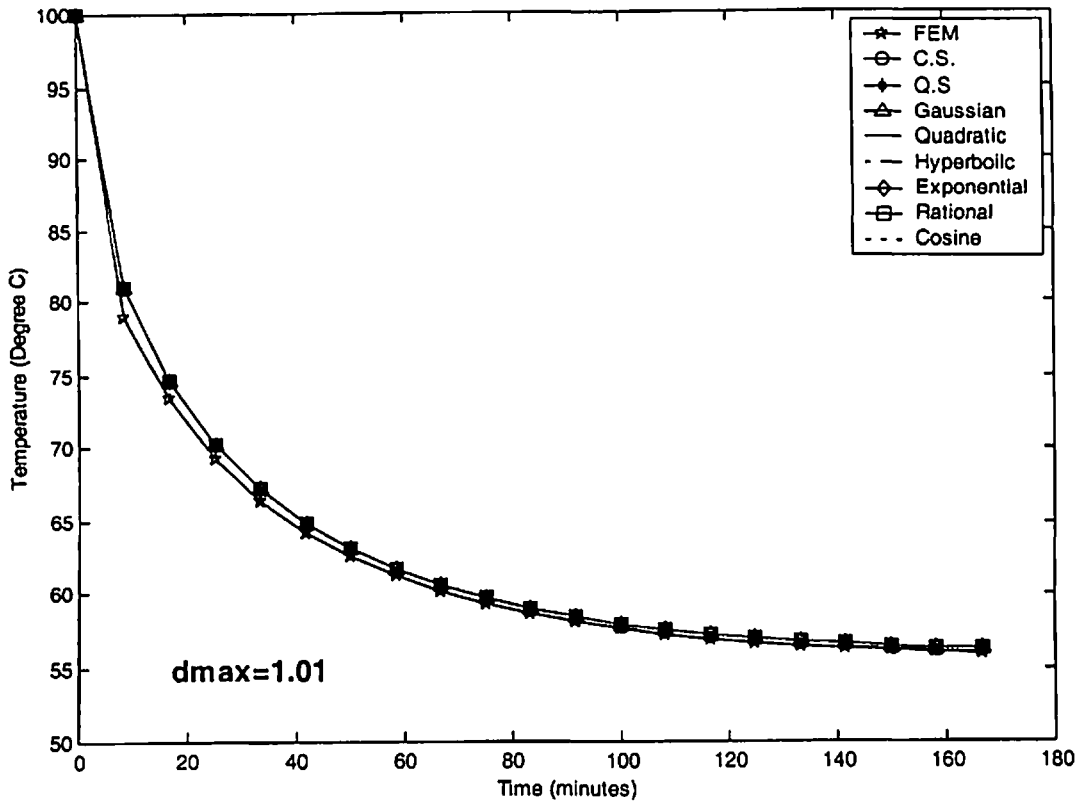


Fig. 4.15 Comparison of EFG results obtained using 21 nodes with FEM at the location ($x = 1$ m) of the 1-D model shown in Fig. 4.9

➤ CASE-III

4.6 DISCRETIZATION OF THE GOVERNING EQUATION

The general form of energy equation for one-dimensional heat transfer in thin fins with thermal properties independent of temperature is given as:

$$k \frac{\partial^2 T}{\partial x^2} - h \left(\frac{P_r}{A_c} \right) (T - T_\infty) + \dot{Q} = \rho c \left(\frac{\partial T}{\partial t} \right) \quad (4.21a)$$

The boundary conditions are

$$\text{at the base of the fin, } x = 0, T = T_l \quad (4.21b)$$

$$\text{at the tip of the fin, } x = L, \frac{dT}{dx} = 0 \quad (4.21c)$$

The weighted integral form of Eq. (4.21a) is given as:

$$\int_0^L w \left\{ k \frac{\partial^2 T}{\partial x^2} - h \left(\frac{P_r}{A_c} \right) T + M + \dot{Q} - \rho c \frac{\partial T}{\partial t} \right\} dx = 0 \quad (4.22)$$

The weak form of Eq. (4.22) will be

$$\int_0^L \left[-k \frac{\partial w}{\partial x} \frac{\partial T}{\partial x} - h \left(\frac{P_r}{A_c} \right) T w \right] dx - \int_0^L \rho c w \dot{T} dx + \int_0^L M w dx + \int_0^L \dot{Q} w dx + \left[w k \frac{\partial T}{\partial x} \right]_0^L = 0 \quad (4.23)$$

The functional $I(T)$ is obtained as:

$$I(T) = \frac{1}{2} \int_0^L \left[k \left(\frac{\partial T}{\partial x} \right)^2 + h \left(\frac{P_r}{A_c} \right) T^2 \right] dx + \int_0^L \rho c \dot{T} T dx - \int_0^L M T dx - \int_0^L \dot{Q} T dx \quad (4.24)$$

Using Lagrange multiplier technique to enforce essential boundary conditions, the functional

$I^*(T)$ is obtained as:

$$I^*(T) = \frac{1}{2} \int_0^L \left[k \left(\frac{\partial T}{\partial x} \right)^2 + h \left(\frac{P_r}{A_c} \right) T^2 \right] dx + \int_0^L \rho c \dot{T} T dx - \int_0^L M T dx - \int_0^L \dot{Q} T dx + \lambda (T - T_l) \quad (4.25)$$

Using Variational method, Eq. (4.25) changes to

$$\delta I^*(T) = \int_0^L \left[k \frac{\partial T}{\partial x} \delta \frac{\partial T}{\partial x} + h \left(\frac{P_r}{A_c} \right) T \delta T \right] dx + \int_0^L \rho c \dot{T} \delta T dx - \int_0^L M \delta T dx - \int_0^L \dot{Q} \delta T dx + \lambda \delta T + \delta \lambda (T - T_L) \quad (4.26)$$

Since δT and $\delta \lambda$ are arbitrary in preceding equation, the following relations are obtained by using Eq. (3.25) and Eq. (4.26)

$$[\mathbf{K}]\{\mathbf{T}\} + [\mathbf{C}]\{\dot{\mathbf{T}}\} + [\mathbf{G}]\{\lambda\} = \{\mathbf{f}\} \quad (4.27a)$$

$$[\mathbf{G}^T]\{\mathbf{T}\} = \{T_L\} \quad (4.27b)$$

where

$$K_{IJ} = \int_0^L \left[k \Phi_{I,x}^T \Phi_{J,x} + h \left(\frac{P_r}{A_c} \right) \Phi_I^T \Phi_J \right] dx \quad (4.28a)$$

$$C_{IJ} = \int_0^L \rho c \Phi_I^T \Phi_J dx \quad (4.28b)$$

$$f_I = \int_0^L \dot{Q} \Phi_I dx + \int_0^L M \Phi_I dx \quad (4.28c)$$

$$G_{IK} = \Phi_K|_{\Gamma_r} \quad (4.28d)$$

Using Crank-Nicolson technique for time approximation, the Eq. (4.27) can be written as:

$$\begin{bmatrix} \mathbf{K}^* + \mathbf{C} & \mathbf{G} \\ \mathbf{G}^T & 0 \end{bmatrix} \begin{bmatrix} \mathbf{T}_N \\ \lambda \end{bmatrix} = \begin{bmatrix} \mathbf{R}_N \\ T_L \end{bmatrix} \quad (4.29)$$

where

$$\mathbf{R}_N = ([\mathbf{C}] - (1 - \alpha)\Delta t [\mathbf{K}]) \{\mathbf{T}\}_{N-1} + \alpha \Delta t \{\mathbf{f}\}_N + (1 - \alpha)\Delta t \{\mathbf{f}\}_{N-1} \quad (4.30a)$$

$$\mathbf{K}^* = \alpha \Delta t [\mathbf{K}] \quad (4.30b)$$

4.7 NUMERICAL RESULTS AND DISCUSSION

The different parameters used for steady-state and transient analysis of one-dimensional model shown in Fig. 4.16 are tabulated in Table 4.44. The EFG results are obtained using different weight functions for two sets of nodes and the FEM results are obtained using linear bar element for same sets of nodes. A comparative analysis is carried out to evaluate the performance of different weight functions.

4.7.1 Steady-state analysis

The results presented in Table 4.45 are obtained using different EFG weight functions for two values of scaling parameter (i.e. $d_{\max} = 1.01$ & $d_{\max} = 1.51$) and it shows a comparison of temperature values obtained using 11 nodes with those obtained by FEM at the location ($x = 0.02$ m). Table 4.46 shows a comparison of temperature values obtained by EFG method using different weight functions for two values of scaling parameter with those obtained by FEM at the same location i.e. ($x = 0.02$ m) for 21 nodes. A comparison of temperature values obtained using different EFG weight functions with FEM for 11 and 21 nodes, is presented in Table 4.47 and Table 4.48 respectively at the location ($x = 0.04$ m). Similar type of comparisons of temperature values are shown in Table 4.49 for 11 nodes at the location ($x = 0.06$ m), in Table 4.50 for 21 nodes at the location ($x = 0.06$ m), in Table 4.51 for 11 nodes at the location ($x = 0.08$ m) and in Table 4.52 for 21 nodes at the location ($x = 0.08$ m). From the results presented in Table 4.45 to Table 4.52, it is observed that EFG results obtained using different weight functions are similar for $d_{\max} = 1.01$. However for $d_{\max} = 1.51$, only cubicspline, quarticspline, Gaussian, exponential and rational weight functions give acceptable results. It is also observed that EFG results obtained using different weight functions are in good agreement with those obtained by finite element method. Moreover with increase in number of nodes EFG results starts converging.

The effect of scaling parameter (d_{\max}) on EFG results obtained using different weight functions is presented in Table 4.53 for 11 nodes and Table 4.54 for 21 nodes respectively at the location ($x = 0.02\text{ m}$). Similar effect of scaling parameter on EFG results is shown in Table 4.55 for 11 nodes and Table 4.56 for 21 nodes at the location ($x = 0.06\text{ m}$). Fig. 4.17 shows the effect of scaling parameter on EFG results obtained using 11 and 21 nodes at the location ($x = 0.04\text{ m}$). Similar effect of scaling parameter on EFG results is observed in Fig. 4.18 at the location ($x = 0.08\text{ m}$). From tables and figures, it is clear that only cubicspline, quarticspline, Gaussian, exponential and rational weight functions give acceptable results in the range $1.0 < d_{\max} < 2.2$ whereas the results obtained using quadratic, hyperbolic and cosine weight functions are varying in abrupt manner with scaling parameter. Therefore EFG results obtained using quadratic, hyperbolic and cosine weight functions are not acceptable in the range $1.0 < d_{\max} < 2.2$. It is also observed that there is minimum variation in EFG results with scaling parameter for exponential weight function.

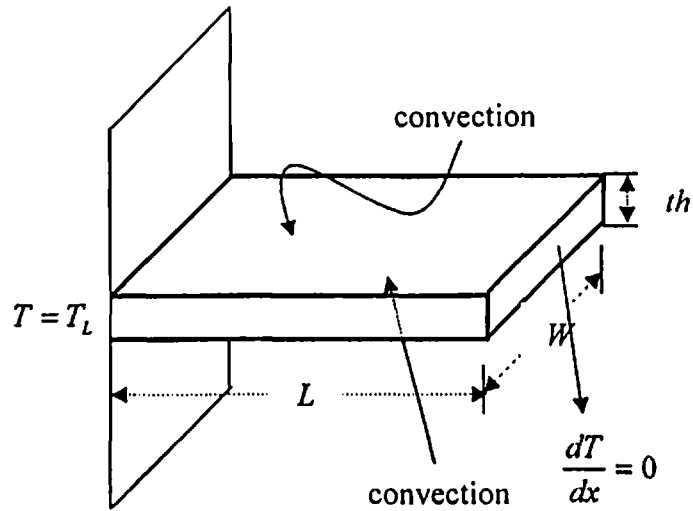


Fig. 4.16 One-dimensional model

Table 4.44 Data for the 1-D model shown in Fig.4.16

Parameters	Value of the parameter
Length (L)	0.10 m
Width (W)	1 m
Thickness (th)	0.001 m
Thermal conductivity (k)	400 W/m-K
Heat transfer coefficient (h)	10000 kg/m ³
Density of the material (ρ)	200 W/m ² -K
Specific heat (c)	400 kJ/kg-K
Rate of internal heat generation (\dot{Q})	0 W/m ³
Surrounding fluid temperature (T_∞)	20 °C
Initial temperature (T_{int})	100 °C
Time step size (Δt)	0.5 sec
Temperature at end, $x = 0$	100 °C

Table 4.45 Comparison of EFG results obtained using 11 nodes with FEM results at the location ($x = 0.02$ m) of the 1-D model shown in Fig.4.16

Weight function	EFG				FEM
	$d_{\max} = 1.01$		$d_{\max} = 1.51$		
	T (°C)	% diff with FEM	T (°C)	% diff with FEM	T (°C)
C. S.	62.4468	-0.2109	62.4459	-0.2124	62.5788
Q. S.	62.4468	-0.2109	62.4451	-0.2137	
Gaussian	62.4468	-0.2109	62.3813	-0.3156	
Quadratic	62.4468	-0.2109	45.9778	-26.528	
Hyperbolic	62.4468	-0.2109	92.7463	48.2072	
Exponential	62.4468	-0.2109	62.5231	-0.0890	
Rational	62.4468	-0.2109	62.3545	-0.3584	
Cosine	62.4468	-0.2109	53.0298	-15.259	

Table 4.46 Comparison of EFG results obtained using 21 nodes with FEM results at the location ($x = 0.02$ m) of the 1-D model shown in Fig.4.16

Weight function	EFG				FEM
	$d_{\max} = 1.01$		$d_{\max} = 1.51$		
	T (°C)	% diff with FEM	T (°C)	% diff with FEM	T (°C)
C. S.	62.6239	-0.0688	62.6237	-0.0691	62.6670
Q. S.	62.6239	-0.0688	62.6235	-0.0694	
Gaussian	62.6239	-0.0688	62.6078	-0.0945	
Quadratic	62.6239	-0.0688	69.6172	11.0907	
Hyperbolic	62.6239	-0.0688	72.6870	15.9893	
Exponential	62.6239	-0.0688	62.6428	-0.0386	
Rational	62.6239	-0.0688	62.6043	-0.1001	
Cosine	62.6239	-0.0688	66.8994	6.7538	

Table 4.47 Comparison of EFG results obtained using 11 nodes with FEM results at the location ($x = 0.04$ m) of the 1-D model shown in Fig.4.16

Weight function	EFG				FEM
	$d_{max} = 1.01$				
	T (°C)	T (°C)	T (°C)	% diff with FEM	T (°C)
C. S.	42.7730	-0.3383	42.7730	-0.3383	42.9182
Q. S.	42.7730	-0.3383	42.7726	-0.3393	
Gaussian	42.7730	-0.3383	42.7505	-0.3907	
Quadratic	42.7730	-0.3383	55.0129	28.1808	
Hyperbolic	42.7730	-0.3383	64.0888	49.3278	
Exponential	42.7730	-0.3383	42.7459	-0.4015	
Rational	42.7730	-0.3383	42.5774	-0.7941	
Cosine	42.7730	-0.3383	47.7639	11.2905	

Table 4.48 Comparison of EFG results obtained using 21 nodes with FEM results at the location ($x = 0.04$ m) of the 1-D model shown in Fig.4.16

Weight function	EFG				FEM
	$d_{max} = 1.01$		$d_{max} = 1.51$		
	T (°C)	% diff with FEM	T (°C)	% diff with FEM	T (°C)
C. S.	42.9679	-0.1107	42.9678	-0.1109	43.0155
Q. S.	42.9679	-0.1107	42.9678	-0.1109	
Gaussian	42.9679	-0.1107	42.9624	-0.1234	
Quadratic	42.9679	-0.1107	47.0072	9.2797	
Hyperbolic	42.9679	-0.1107	44.6084	3.7031	
Exponential	42.9679	-0.1107	42.9614	-0.1258	
Rational	42.9679	-0.1107	42.9181	-0.2264	
Cosine	42.9679	-0.1107	48.4573	12.6508	

Table 4.49 Comparison of EFG results obtained using 11 nodes with FEM results at the location ($x = 0.06$ m) of the 1-D model shown in Fig.4.16

Weight function	EFG				FEM
	$d_{\max} = 1.01$		$d_{\max} = 1.51$		
	T (°C)	% diff with FEM	T (°C)	% diff with FEM	T (°C)
C. S.	32.6916	-0.3830	32.6916	-0.3830	32.8173
Q. S.	32.6916	-0.3830	32.6916	-0.3830	
Gaussian	32.6916	-0.3830	32.6865	-0.3986	
Quadratic	32.6916	-0.3830	22.6100	-31.1030	
Hyperbolic	32.6916	-0.3830	43.7839	33.4171	
Exponential	32.6916	-0.3830	32.6374	-0.5482	
Rational	32.6916	-0.3830	32.4923	-0.9903	
Cosine	32.6916	-0.3830	29.4027	-10.4050	

Table 4.50 Comparison of EFG results obtained using 21 nodes with FEM results at the location ($x = 0.06$ m) of the 1-D model shown in Fig.4.16

Weight function	EFG				FEM
	$d_{\max} = 1.01$		$d_{\max} = 1.51$		
	T (°C)	% diff with FEM	T (°C)	% diff with FEM	T (°C)
C. S.	32.8604	-0.1258	32.8604	-0.1258	32.9018
Q. S.	32.8604	-0.1258	32.8604	-0.1258	
Gaussian	32.8604	-0.1258	32.8591	-0.1298	
Quadratic	32.8604	-0.1258	31.7899	-3.3795	
Hyperbolic	32.8604	-0.1258	32.5448	-1.0850	
Exponential	32.8604	-0.1258	32.8469	-0.1669	
Rational	32.8604	-0.1258	32.8095	-0.2805	
Cosine	32.8604	-0.1258	37.6652	14.4776	

Table 4.51 Comparison of EFG results obtained using 11 nodes with FEM results at the location ($x = 0.08$ m) of the 1-D model shown in Fig.4.16

Weight function	EFG				FEM
	$d_{max} = 1.01$		$d_{max} = 1.51$		
	T (°C)	% diff with FEM	T (°C)	% diff with FEM	T (°C)
C. S.	27.9562	-0.3799	27.9563	-0.3795	28.0628
Q. S.	27.9562	-0.3799	27.9564	-0.3791	
Gaussian	27.9562	-0.3799	27.9571	-0.3767	
Quadratic	27.9562	-0.3799	32.2615	14.9618	
Hyperbolic	27.9562	-0.3799	32.6084	16.198	
Exponential	27.9562	-0.3799	27.9011	-0.5762	
Rational	27.9562	-0.3799	27.7888	-0.9764	
Cosine	27.9562	-0.3799	30.1475	7.4287	

Table 4.52 Comparison of EFG results obtained using 21 nodes with FEM results at the location ($x = 0.08$ m) of the 1-D model shown in Fig.4.16

Weight function	EFG				FEM
	$d_{max} = 1.01$		$d_{max} = 1.51$		
	T (°C)	% diff with FEM	T (°C)	% diff with FEM	T (°C)
C. S.	28.0994	-0.1248	28.0994	-0.1248	28.1345
Q. S.	28.0994	-0.1248	28.0994	-0.1248	
Gaussian	28.0994	-0.1248	28.0997	-0.1237	
Quadratic	28.0994	-0.1248	25.7999	-8.2980	
Hyperbolic	28.0994	-0.1248	27.6251	-1.8106	
Exponential	28.0994	-0.1248	28.0852	-0.1752	
Rational	28.0994	-0.1248	28.0542	-0.2854	
Cosine	28.0994	-0.1248	31.1058	10.5611	

Table 4.53 Effect of scaling parameter on EFG results obtained using 11 nodes at the location ($x = 0.02$ m) of the 1-D model shown in Fig.4.16

Scaling Parameter	Temperature ($^{\circ}$ C)							
	C. S.	Q. S	Gaussian	Quadratic	Hyperbolic	Exponential	Rational	Cosine
1.01	62.4468	62.4468	62.4468	62.4468	62.4468	62.4468	62.4468	62.4468
1.21	62.4468	62.4468	62.4468	62.4468	62.4468	62.4468	62.4468	62.4468
1.41	62.4468	62.4468	62.4468	62.4468	62.4468	62.4468	62.4468	62.4468
1.61	62.3634	62.2966	62.3252	76.0607	106.5288	62.4871	62.2976	79.1641
1.81	62.0709	61.9341	62.1672	229.5207	158.8094	62.4003	62.2492	202.9387
2.01	61.9553	62.3073	62.0587	190.5733	300.6412	62.2911	61.7262	162.9482
2.21	62.3501	64.0679	62.2664	199.5825	208.9537	62.1840	61.5746	154.4928
2.41	63.5514	67.5659	63.1878	181.2273	154.3923	62.0833	61.4734	146.9679
2.61	66.2181	74.8053	65.0693	190.2807	-89.1303	61.8962	57.6535	371.8370
2.81	72.9349	90.0113	69.2839	78.8844	-113.6444	61.6539	56.1378	398.8294
3.01	94.1240	108.2795	77.1075	-544.6138	-120.0956	61.6770	57.9088	-863.5372

Table 4.54 Effect of scaling parameter on EFG results obtained using 21 nodes at the location ($x = 0.02$ m) of the 1-D model shown in Fig.4.16

Scaling Parameter	Temperature ($^{\circ}$ C)							
	C. S.	Q. S	Gaussian	Quadratic	Hyperbolic	Exponential	Rational	Cosine
1.01	62.6239	62.6239	62.6239	62.6239	62.6239	62.6239	62.6239	62.6239
1.21	62.6239	62.6239	62.6239	62.6239	62.6239	62.6239	62.6239	62.6239
1.41	62.6239	62.6239	62.6239	62.6239	62.6239	62.6239	62.6239	62.6239
1.61	62.6036	62.5871	62.5937	43.1539	81.4353	62.6349	62.5858	42.0317
1.81	62.5262	62.4715	62.5486	-143.1593	142.9661	62.6161	62.5493	8.9734
2.01	62.4566	62.4298	62.4889	-0.9526	213.6291	62.5972	62.5111	-17.7296
2.21	62.4358	62.6541	62.4301	15.0019	185.8573	62.5770	62.4766	-58.1347
2.41	62.5734	63.5899	62.4297	23.8681	255.7827	62.5577	62.4414	-18.7726
2.61	63.2137	66.6345	62.4759	234.9098	-8.1729	62.5060	62.1188	152.5833
2.81	65.7805	74.7102	63.0407	39.5104	-68.8118	62.4718	61.8579	-5.2968
3.01	77.4440	83.7523	64.6806	-111.2427	-147.3396	62.2769	60.9765	-169.9595

Table 4.55 Effect of scaling parameter on EFG results obtained using 11 nodes at the location ($x = 0.06$ m) of the 1-D model shown in Fig.4.16

Scaling Parameter	Temperature ($^{\circ}$ C)							
	C. S.	Q. S	Gaussian	Quadratic	Hyperbolic	Exponential	Rational	Cosine
1.01	32.6916	32.6916	32.6916	32.6916	32.6916	32.6916	32.6916	32.6916
1.21	32.6916	32.6916	32.6916	32.6916	32.6916	32.6916	32.6916	32.6916
1.41	32.6916	32.6916	32.6916	32.6916	32.6916	32.6916	32.6916	32.6916
1.61	32.6908	32.6903	32.6815	58.1935	55.6790	32.6267	32.4823	55.7358
1.81	32.6764	32.6676	32.6628	-101.5781	125.5363	32.6040	32.4600	-69.9154
2.01	32.6429	32.6293	32.6291	-85.3389	343.0238	32.5822	32.4468	-42.2040
2.21	32.6060	32.7490	32.5756	-75.6861	180.5734	32.5591	32.4284	-29.3156
2.41	32.6697	33.7501	32.5183	-61.5876	41.0374	32.5367	32.4093	-26.6992
2.61	33.3101	38.2186	32.4528	-45.9238	198.2060	32.4426	32.1598	-187.1563
2.81	36.6129	49.7100	32.6944	-165.9354	269.2409	32.4024	32.2080	-200.0585
3.01	54.0988	58.9406	33.8400	153.9308	453.4171	32.4238	32.5442	304.2495

Table 4.56 Effect of scaling parameter on EFG results obtained using 21 nodes at the location ($x = 0.06$ m) of the 1-D model shown in Fig.4.16

Scaling Parameter	Temperature ($^{\circ}$ C)							
	C. S.	Q. S	Gaussian	Quadratic	Hyperbolic	Exponential	Rational	Cosine
1.01	32.8604	32.8604	32.8604	32.8604	32.8604	32.8604	32.8604	32.8604
1.21	32.8604	32.8604	32.8604	32.8604	32.8604	32.8604	32.8604	32.8604
1.41	32.8604	32.8604	32.8604	32.8604	32.8604	32.8604	32.8604	32.8604
1.61	32.8603	32.8602	32.8579	36.1517	33.7548	32.8442	32.8069	41.6087
1.81	32.8566	32.8540	32.8529	-212.4349	70.7868	32.8385	32.8006	-15.5542
2.01	32.8472	32.8380	32.8433	2.7308	86.2782	32.8330	32.7966	36.3691
2.21	32.8320	32.8118	32.8252	26.1821	-27.8857	32.8270	32.7921	54.8628
2.41	32.8134	32.8005	32.7931	27.7184	-98.4388	32.8211	32.7877	47.7743
2.61	32.8003	33.0449	32.7182	235.1845	131.0141	32.7960	32.6768	261.6194
2.81	32.8967	34.0711	32.6016	218.5305	352.1210	32.7850	32.6496	464.6846
3.01	34.7756	33.7925	32.4315	413.1034	653.8587	32.7252	32.4105	90.1513

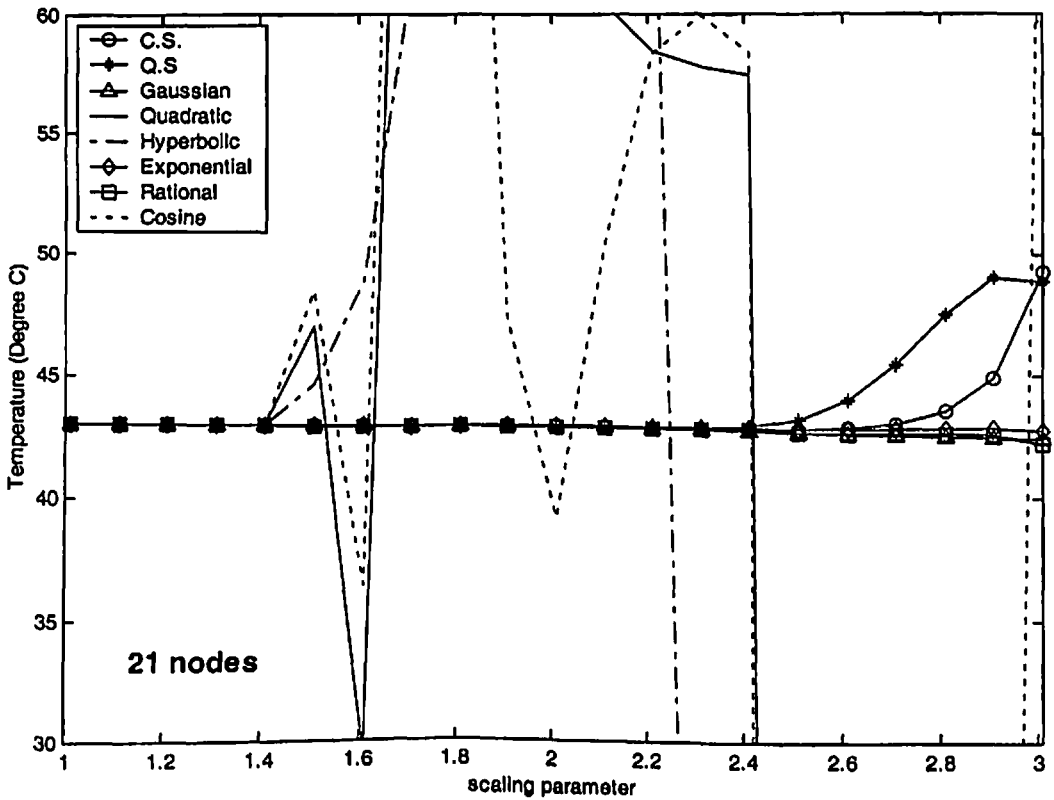
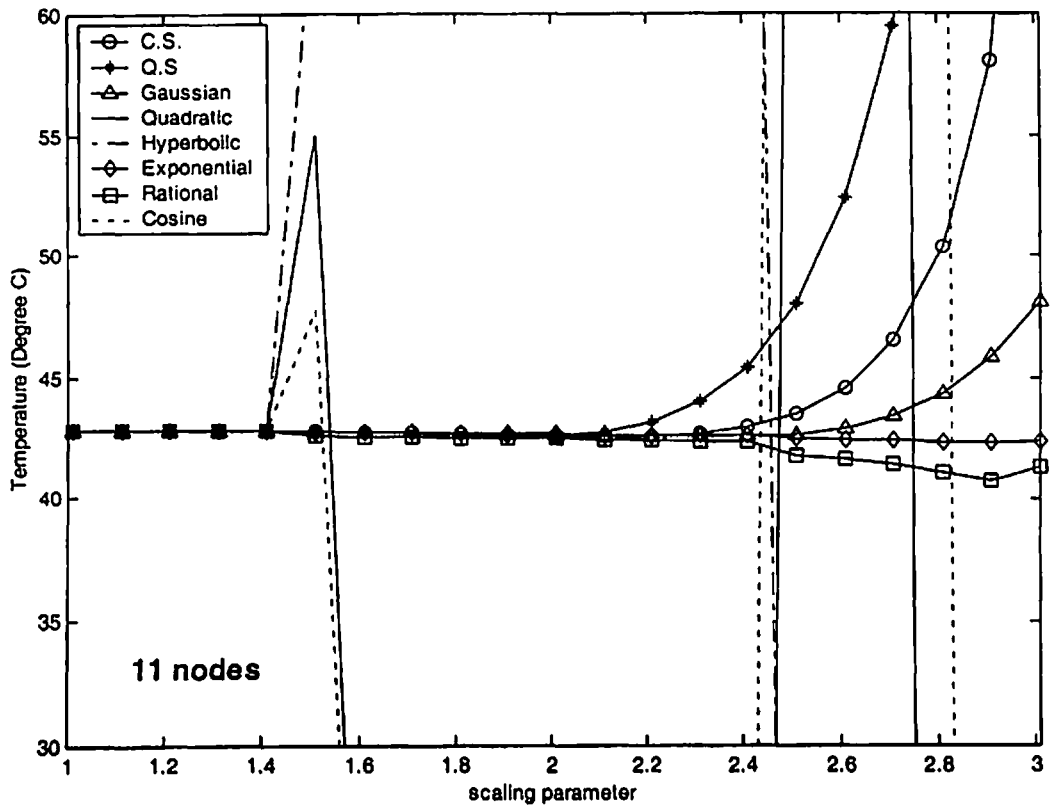


Fig. 4.17 Effect of scaling parameter on EFG results at the location ($x = 0.04$ m) of the 1-D model shown in Fig.4.16

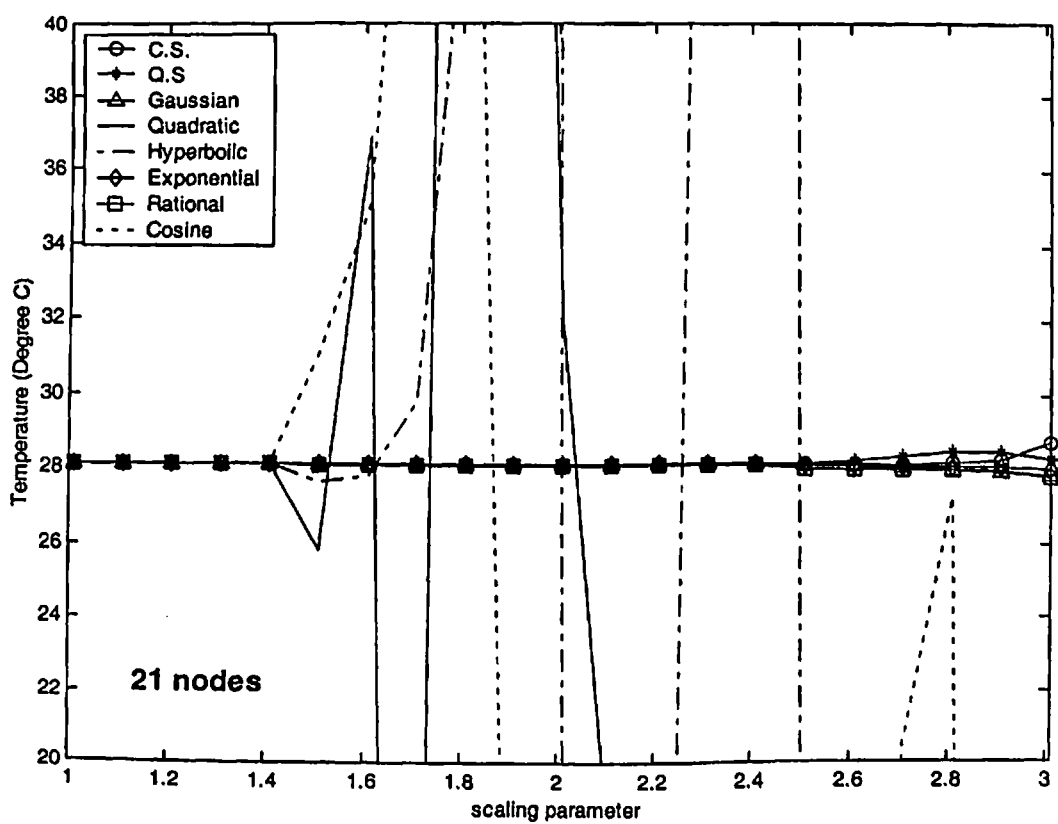
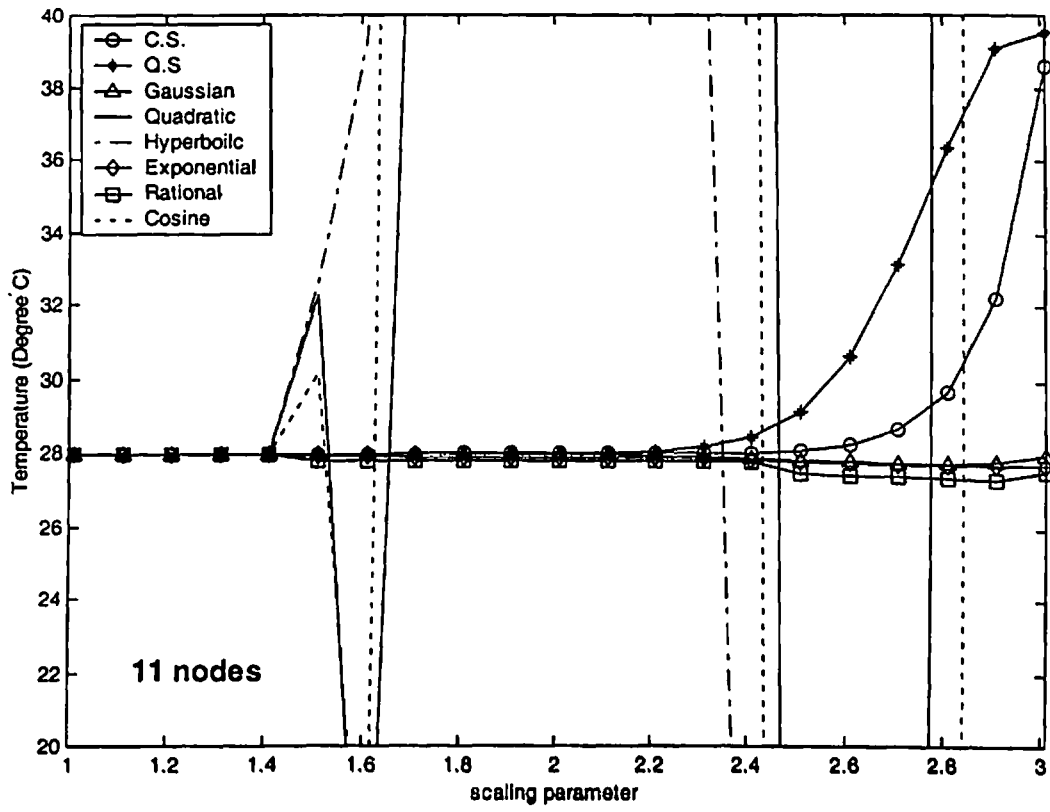


Fig. 4.18 Effect of scaling parameter on EFG results at the location ($x = 0.08\text{m}$) of the 1-D model shown in Fig.4.16

4.7.2 Transient analysis

The transient analysis of 1-D model of thin fins is carried out using different EFG weight functions. Table 4.57 and Table 4.58 show the comparison of temperature values obtained using 11 nodes with FEM results at the location ($x = 0.02$ m) for $d_{\max} = 1.01$ and $d_{\max} = 1.51$ respectively. Similar comparison of temperature values obtained using 21 nodes with FEM results is presented in Table 4.59 and Table 4.60 for $d_{\max} = 1.01$ and $d_{\max} = 1.51$ respectively at the same location i.e. ($x = 0.02$ m). For this case (i.e. CASE-III) of 1-D transient analysis, time step of 0.5 sec has been taken which is less than 1.5% of the total time required to achieve steady state condition. Table 4.61 and Table 4.62 shows the comparison of temperature values obtained using 11 nodes with FEM results at the different location ($x = 0.06$ m) for $d_{\max} = 1.01$ and $d_{\max} = 1.51$ respectively. Similar comparison of temperature values obtained using 21 nodes with FEM results is also presented in Table 4.63 and Table 4.64 for $d_{\max} = 1.01$ and $d_{\max} = 1.51$ respectively at the location i.e. ($x = 0.06$ m). Fig 4.19 shows the comparison of temperature values obtained using 11 nodes with FEM for $d_{\max} = 1.01$ and $d_{\max} = 1.51$ at the location ($x = 0.04$ m). Similar comparison of temperature values obtained using 21 nodes with FEM is shown in Fig. 4.20 at the same location i.e. ($x = 0.04$ m). Fig 4.21 shows the comparison of temperature values obtained using 11 nodes with FEM for $d_{\max} = 1.01$ and $d_{\max} = 1.51$ at the location ($x = 0.10$ m). Similar comparison of temperature values obtained using 21 nodes with FEM is shown in Fig. 4.22 at the same location i.e. ($x = 0.10$ m). From the results presented in tables and figures, it is clear that the EFG results obtained using different weight functions are similar for $d_{\max} = 1.01$ but for $d_{\max} = 1.51$ only cubicspline (C.S.), quarticspline (Q.S), Gaussian, exponential and rational weight functions give acceptable results. It has also been observed that the EFG results are in good agreement with those obtained by FEM.

Table 4.57 Comparison of EFG results obtained using 11 nodes with FEM at the location ($x = 0.02$ m) of the 1-D model shown in Fig.4.16 for $d_{max} = 1.01$

Time (sec)	Temperature ($^{\circ}$ C)								
	$d_{max} = 1.01$								FEM
	C. S.	Q. S	Gaussian	Quadratic	Hyperbolic	Exponential	Rational	Cosine	
0	100.000	100.000	100.000	100.000	100.000	100.000	100.000	100.000	100.000
3	83.2885	83.2885	83.2885	83.2885	83.2885	83.2885	83.2885	83.2885	83.4765
6	75.6102	75.6102	75.6102	75.6102	75.6102	75.6102	75.6102	75.6102	75.7587
9	71.1084	71.1084	71.1084	71.1084	71.1084	71.1084	71.1084	71.1084	71.2416
12	68.2613	68.2613	68.2613	68.2613	68.2613	68.2613	68.2613	68.2613	68.3875
15	66.3922	66.3922	66.3922	66.3922	66.3922	66.3922	66.3922	66.3922	66.5151
18	65.1395	65.1395	65.1395	65.1395	65.1395	65.1395	65.1395	65.1395	65.2610
21	64.2903	64.2903	64.2903	64.2903	64.2903	64.2903	64.2903	64.2903	64.4111
24	63.7109	63.7109	63.7109	63.7109	63.7109	63.7109	63.7109	63.7109	63.8315
27	63.3142	63.3142	63.3142	63.3142	63.3142	63.3142	63.3142	63.3142	63.4347
30	63.0422	63.0422	63.0422	63.0422	63.0422	63.0422	63.0422	63.0422	63.1625
33	62.8554	62.8554	62.8554	62.8554	62.8554	62.8554	62.8554	62.8554	62.9756
36	62.7272	62.7272	62.7272	62.7272	62.7272	62.7272	62.7272	62.7272	62.8472
39	62.6390	62.6390	62.6390	62.6390	62.6390	62.6390	62.6390	62.6390	62.7589
42	62.5785	62.5785	62.5785	62.5785	62.5785	62.5785	62.5785	62.5785	62.6983
45	62.5369	62.5369	62.5369	62.5369	62.5369	62.5369	62.5369	62.5369	62.6566

Table 4.58 Comparison of EFG results obtained using 11 nodes with FEM at the location ($x = 0.02$ m) of the 1-D model shown in Fig.4.16 for $d_{max} = 1.51$

Time (sec)	Temperature ($^{\circ}$ C)								
	$d_{max} = 1.51$								FEM
	C. S.	Q. S	Gaussian	Quadratic	Hyperbolic	Exponential	Rational	Cosine	
0	100.000	100.000	100.000	100.000	100.000	100.000	100.000	100.000	100.000
3	83.2881	83.2877	83.2538	77.9154	100.1056	83.2681	83.0725	79.4123	83.4765
6	75.6095	75.6089	75.5587	65.7425	97.7377	75.6409	75.4617	68.7066	75.7587
9	71.1076	71.1068	71.0500	58.6440	96.1294	71.1611	70.9893	62.8050	71.2416
12	68.2604	68.2597	68.1997	54.2780	95.0564	68.3248	68.1562	59.3198	68.3875
15	66.3913	66.3905	66.3289	51.4908	94.3320	66.4612	66.2934	57.1608	66.5151
18	65.1386	65.1378	65.0754	49.6683	93.8381	65.2114	65.0435	55.7798	65.2610
21	64.2894	64.2886	64.2256	48.4589	93.4993	64.3637	64.1954	54.8775	64.4111
24	63.7100	63.7092	63.6459	47.6494	93.2659	63.7852	63.6166	54.2793	63.8315
27	63.3133	63.3125	63.2491	47.1049	93.1050	63.3891	63.2203	53.8787	63.4347
30	63.0413	63.0405	62.9769	46.7377	92.9938	63.1174	62.9485	53.6083	63.1625
33	62.8545	62.8537	62.7901	46.4898	92.9170	62.9309	62.7620	53.4249	62.9756
36	62.7262	62.7254	62.6618	46.3224	92.8639	62.8028	62.6339	53.3001	62.8472
39	62.6381	62.6373	62.5736	46.2094	92.8271	62.7148	62.5460	53.2148	62.7589
42	62.5776	62.5768	62.5131	46.1331	92.8018	62.6543	62.4856	53.1564	62.6983
45	62.5360	62.5352	62.4715	46.0817	92.7842	62.6128	62.4441	53.1164	62.6566

Table 4.59 Comparison of EFG results obtained using 21 nodes with FEM at the location ($x = 0.02$ m) of the 1-D model shown in Fig.4.16 for $d_{max} = 1.01$

Time (sec)	Temperature (° C)								
	$d_{max} = 1.01$								FEM
	C. S.	Q. S	Gaussian	Quadratic	Hyperbolic	Exponential	Rational	Cosine	
0	100.000	100.000	100.000	100.000	100.000	100.000	100.000	100.000	100.000
3	83.5559	83.5559	83.5559	83.5559	83.5559	83.5559	83.5559	83.5559	83.5903
6	75.8189	75.8189	75.8189	75.8189	75.8189	75.8189	75.8189	75.8189	75.8569
9	71.2957	71.2957	71.2957	71.2957	71.2957	71.2957	71.2957	71.2957	71.3340
12	68.4398	68.4398	68.4398	68.4398	68.4398	68.4398	68.4398	68.4398	68.4771
15	66.5673	66.5673	66.5673	66.5673	66.5673	66.5673	66.5673	66.5673	66.6035
18	65.3136	65.3136	65.3136	65.3136	65.3136	65.3136	65.3136	65.3136	65.3491
21	64.4645	64.4645	64.4645	64.4645	64.4645	64.4645	64.4645	64.4645	64.4992
24	63.8855	63.8855	63.8855	63.8855	63.8855	63.8855	63.8855	63.8855	63.9196
27	63.4892	63.4892	63.4892	63.4892	63.4892	63.4892	63.4892	63.4892	63.5229
30	63.2175	63.2175	63.2175	63.2175	63.2175	63.2175	63.2175	63.2175	63.2508
33	63.0310	63.0310	63.0310	63.0310	63.0310	63.0310	63.0310	63.0310	63.0639
36	62.9030	62.9030	62.9030	62.9030	62.9030	62.9030	62.9030	62.9030	62.9355
39	62.8150	62.8150	62.8150	62.8150	62.8150	62.8150	62.8150	62.8150	62.8473
42	62.7546	62.7546	62.7546	62.7546	62.7546	62.7546	62.7546	62.7546	62.7866
45	62.7131	62.7131	62.7131	62.7131	62.7131	62.7131	62.7131	62.7131	62.7449

Table 4.60 Comparison of EFG results obtained using 21 nodes with FEM at the location ($x = 0.02$ m) of the 1-D model shown in Fig.4.16 for $d_{max} = 1.51$

Time (sec)	Temperature (° C)								
	$d_{max} = 1.51$								FEM
	C. S.	Q. S	Gaussian	Quadratic	Hyperbolic	Exponential	Rational	Cosine	
0	100.0000	100.0000	100.0000	100.0000	100.0000	100.0000	100.0000	100.0000	100.000
3	83.5558	83.5557	83.5472	86.9377	89.7740	83.5555	83.5149	85.6187	83.5903
6	75.8187	75.8185	75.8055	80.7365	83.5849	75.8307	75.7948	78.6057	75.8569
9	71.2955	71.2953	71.2808	77.0839	79.8905	71.3113	71.2754	74.5211	71.3340
12	68.4396	68.4394	68.4243	74.7464	77.5385	68.4569	68.4204	71.9653	68.4771
15	66.5670	66.5668	66.5515	73.1840	75.9892	66.5850	66.5477	70.3059	66.6035
18	65.3134	65.3132	65.2977	72.1129	74.9483	65.3316	65.2936	69.2055	65.3491
21	64.4642	64.4641	64.4485	71.3682	74.2410	64.4825	64.4440	68.4668	64.4992
24	63.8852	63.8850	63.8694	70.8466	73.7573	63.9036	63.8646	67.9671	63.9196
27	63.4890	63.4888	63.4732	70.4799	73.4252	63.5074	63.4681	67.6276	63.5229
30	63.2173	63.2171	63.2015	70.2220	73.1967	63.2357	63.1962	67.3964	63.2508
33	63.0308	63.0306	63.0150	70.0405	73.0393	63.0492	63.0096	67.2385	63.0639
36	62.9027	62.9025	62.8869	69.9129	72.9308	62.9212	62.8815	67.1307	62.9355
39	62.8148	62.8146	62.7989	69.8234	72.8560	62.8333	62.7935	67.0570	62.8473
42	62.7543	62.7541	62.7385	69.7606	72.8044	62.7729	62.7331	67.0066	62.7866
45	62.7128	62.7126	62.6970	69.7166	72.7687	62.7314	62.6916	66.9722	62.7449

Table 4.61 Comparison of EFG results obtained using 11 nodes with FEM at the location ($x = 0.06$ m) of the 1-D model shown in Fig.4.16 for $d_{max} = 1.01$

Time (sec)	Temperature ($^{\circ}$ C)								
	$d_{max} = 1.01$								FEM
	C. S.	Q. S	Gaussian	Quadratic	Hyperbolic	Exponential	Rational	Cosine	
0	100.000	100.000	100.000	100.000	100.000	100.000	100.000	100.000	100.000
3	79.2402	79.2402	79.2402	79.2402	79.2402	79.2402	79.2402	79.2402	79.2725
6	64.4525	64.4525	64.4525	64.4525	64.4525	64.4525	64.4525	64.4525	64.5393
9	54.3944	54.3944	54.3944	54.3944	54.3944	54.3944	54.3944	54.3944	54.4977
12	47.5575	47.5575	47.5575	47.5575	47.5575	47.5575	47.5575	47.5575	47.6677
15	42.8897	42.8897	42.8897	42.8897	42.8897	42.8897	42.8897	42.8897	43.0037
18	39.6932	39.6932	39.6932	39.6932	39.6932	39.6932	39.6932	39.6932	39.8094
21	37.5003	37.5003	37.5003	37.5003	37.5003	37.5003	37.5003	37.5003	37.6178
24	35.9946	35.9946	35.9946	35.9946	35.9946	35.9946	35.9946	35.9946	36.1127
27	34.9602	34.9602	34.9602	34.9602	34.9602	34.9602	34.9602	34.9602	35.0785
30	34.2495	34.2495	34.2495	34.2495	34.2495	34.2495	34.2495	34.2495	34.3677
33	33.7611	33.7611	33.7611	33.7611	33.7611	33.7611	33.7611	33.7611	33.8790
36	33.4255	33.4255	33.4255	33.4255	33.4255	33.4255	33.4255	33.4255	33.5431
39	33.1948	33.1948	33.1948	33.1948	33.1948	33.1948	33.1948	33.1948	33.3121
42	33.0364	33.0364	33.0364	33.0364	33.0364	33.0364	33.0364	33.0364	33.1533
45	32.9276	32.9276	32.9276	32.9276	32.9276	32.9276	32.9276	32.9276	33.0442

Table 4.62 Comparison of EFG results obtained using 11 nodes with FEM at the location ($x = 0.06$ m) of the 1-D model shown in Fig.4.16 for $d_{max} = 1.51$

Time (sec)	Temperature ($^{\circ}$ C)								
	$d_{max} = 1.51$								FEM
	C. S.	Q. S	Gaussian	Quadratic	Hyperbolic	Exponential	Rational	Cosine	
0	100.000	100.000	100.000	100.000	100.000	100.000	100.000	100.000	100.000
3	79.2403	79.2403	79.2425	77.5948	85.6412	79.2197	79.1935	78.4597	79.2725
6	64.4527	64.4528	64.4568	60.7689	73.0725	64.3971	64.3056	62.6030	64.5393
9	54.3945	54.3945	54.3964	48.8494	64.0859	54.3328	54.2145	51.7919	54.4977
12	47.5576	47.5577	47.5574	40.5646	57.8346	47.4962	47.3655	44.5208	47.6677
15	42.8898	42.8898	42.8881	34.8619	53.5050	42.8296	42.6923	39.6405	43.0037
18	39.6932	39.6932	39.6904	30.9569	50.5089	39.6341	39.4931	36.3574	39.8094
21	37.5003	37.5004	37.4968	28.2904	48.4360	37.4421	37.2991	34.1406	37.6178
24	35.9946	35.9946	35.9906	26.4724	47.0020	35.9371	35.7930	32.6380	36.1127
27	34.9603	34.9603	34.9559	25.2343	46.0100	34.9033	34.7585	31.6160	35.0785
30	34.2495	34.2495	34.2449	24.3916	45.3238	34.1930	34.0479	30.9189	34.3677
33	33.7611	33.7611	33.7563	23.8185	44.8491	33.7050	33.5597	30.4423	33.8790
36	33.4255	33.4255	33.4206	23.4288	44.5208	33.3696	33.2243	30.1158	33.5431
39	33.1949	33.1949	33.1899	23.1641	44.2937	33.1392	32.9938	29.8919	33.3121
42	33.0364	33.0364	33.0314	22.9843	44.1366	32.9809	32.8354	29.7381	33.1533
45	32.9276	32.9276	32.9225	22.8624	44.0280	32.8721	32.7267	29.6324	33.0442

Table 4.63 Comparison of EFG results obtained using 21 nodes with FEM at the location ($x = 0.06$ m) of the 1-D model shown in Fig.4.16 for $d_{max} = 1.01$

Time (sec)	Temperature ($^{\circ}$ C)								
	$d_{max} = 1.01$								FEM
	C. S.	Q. S	Gaussian	Quadratic	Hyperbolic	Exponential	Rational	Cosine	
0	100.000	100.000	100.000	100.000	100.000	100.000	100.000	100.000	100.000
3	79.2862	79.2862	79.2862	79.2862	79.2862	79.2862	79.2862	79.2862	79.2924
6	64.5764	64.5764	64.5764	64.5764	64.5764	64.5764	64.5764	64.5764	64.5944
9	54.5438	54.5438	54.5438	54.5438	54.5438	54.5438	54.5438	54.5438	54.5665
12	47.7179	47.7179	47.7179	47.7179	47.7179	47.7179	47.7179	47.7179	47.7427
15	43.0564	43.0564	43.0564	43.0564	43.0564	43.0564	43.0564	43.0564	43.0825
18	39.8636	39.8636	39.8636	39.8636	39.8636	39.8636	39.8636	39.8636	39.8905
21	37.6730	37.6730	37.6730	37.6730	37.6730	37.6730	37.6730	37.6730	37.7004
24	36.1685	36.1685	36.1685	36.1685	36.1685	36.1685	36.1685	36.1685	36.1962
27	35.1347	35.1347	35.1347	35.1347	35.1347	35.1347	35.1347	35.1347	35.1626
30	34.4240	34.4240	34.4240	34.4240	34.4240	34.4240	34.4240	34.4240	34.4520
33	33.9354	33.9354	33.9354	33.9354	33.9354	33.9354	33.9354	33.9354	33.9636
36	33.5994	33.5994	33.5994	33.5994	33.5994	33.5994	33.5994	33.5994	33.6277
39	33.3684	33.3684	33.3684	33.3684	33.3684	33.3684	33.3684	33.3684	33.3967
42	33.2096	33.2096	33.2096	33.2096	33.2096	33.2096	33.2096	33.2096	33.2379
45	33.1003	33.1003	33.1003	33.1003	33.1003	33.1003	33.1003	33.1003	33.1287

Table 4.64 Comparison of EFG results obtained using 21 nodes with FEM at the location ($x = 0.06$ m) of the 1-D model shown in Fig.4.16 for $d_{max} = 1.51$

Time (sec)	Temperature ($^{\circ}$ C)								
	$d_{max} = 1.51$								FEM
	C. S.	Q. S	Gaussian	Quadratic	Hyperbolic	Exponential	Rational	Cosine	
0	100.000	100.000	100.000	100.000	100.000	100.000	100.000	100.000	100.000
3	79.2862	79.2862	79.2870	79.3878	79.5945	79.2804	79.2716	80.1587	79.2924
6	64.5764	64.5764	64.5776	64.4145	64.8656	64.5627	64.5379	66.6307	64.5944
9	54.5438	54.5439	54.5444	54.0493	54.7317	54.5288	54.4978	57.4180	54.5665
12	47.7180	47.7180	47.7180	46.9671	47.8000	47.7030	47.6694	51.1579	47.7427
15	43.0564	43.0564	43.0561	42.1418	43.0469	43.0417	43.0066	46.8948	43.0825
18	39.8637	39.8637	39.8631	38.8548	39.7800	39.8491	39.8131	43.9850	39.8905
21	37.6730	37.6731	37.6723	36.6145	37.5312	37.6587	37.6221	41.9956	37.7004
24	36.1685	36.1685	36.1676	35.0866	35.9819	36.1544	36.1173	40.6339	36.1962
27	35.1347	35.1347	35.1336	34.0437	34.9140	35.1208	35.0834	39.7011	35.1626
30	34.4240	34.4240	34.4229	33.3315	34.1777	34.4102	34.3728	39.0618	34.4520
33	33.9354	33.9354	33.9342	32.8448	33.6700	33.9218	33.8843	38.6235	33.9636
36	33.5994	33.5994	33.5982	32.5120	33.3199	33.5860	33.5485	38.3229	33.6277
39	33.3684	33.3684	33.3671	32.2844	33.0785	33.3550	33.3176	38.1166	33.3967
42	33.2096	33.2096	33.2083	32.1287	32.9120	33.1962	33.1588	37.9751	33.2379
45	33.1003	33.1003	33.0990	32.0221	32.7972	33.0871	33.0497	37.8780	33.1287

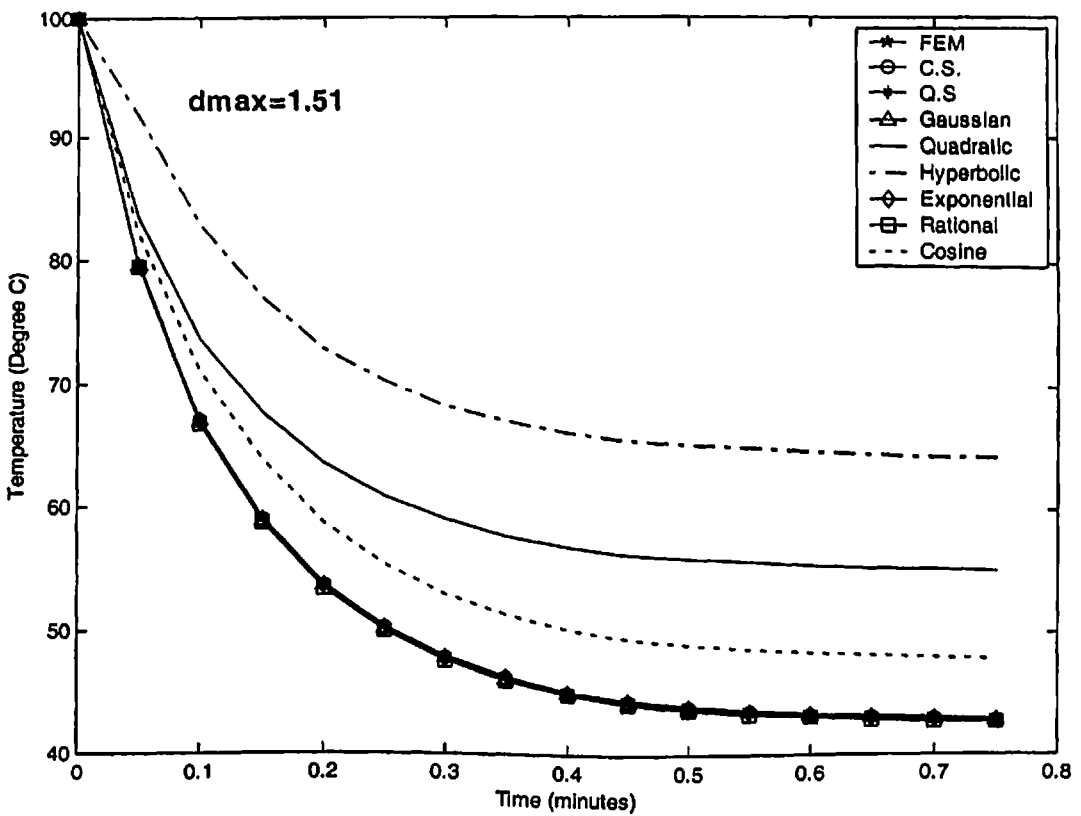
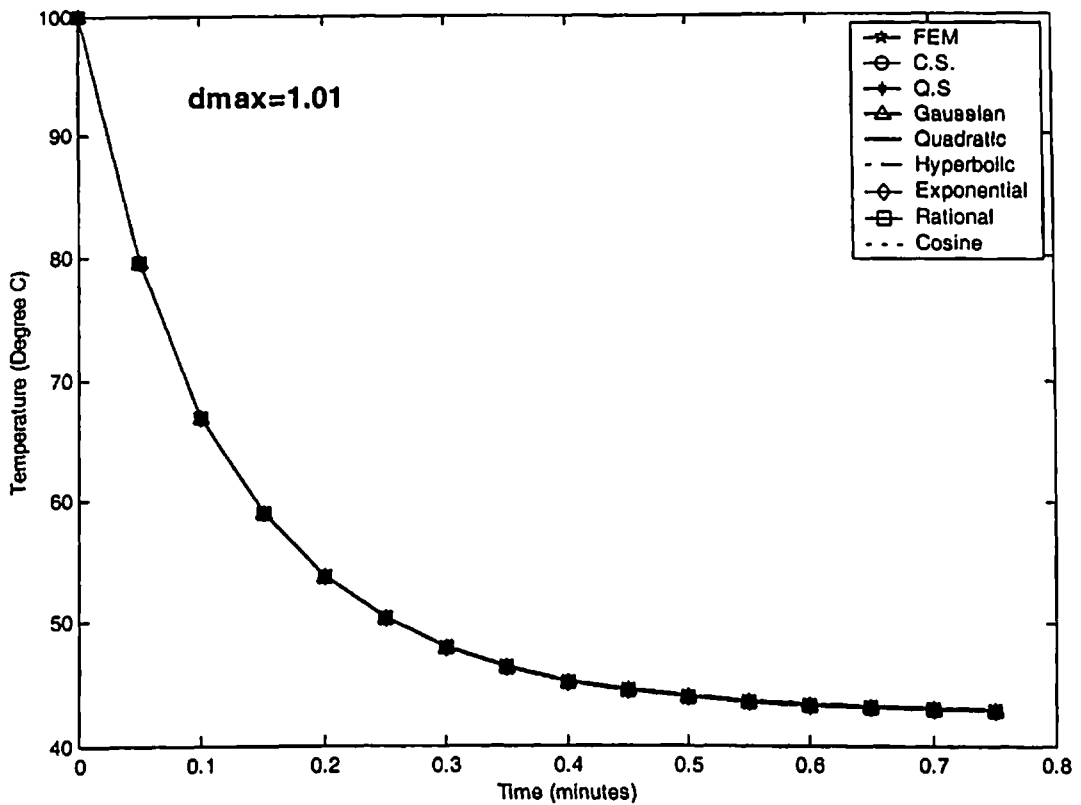


Fig. 4.19 Comparison of EFG results obtained using 11 nodes with FEM at the location ($x = 0.04$ m) of the 1-D model shown in Fig.4.16

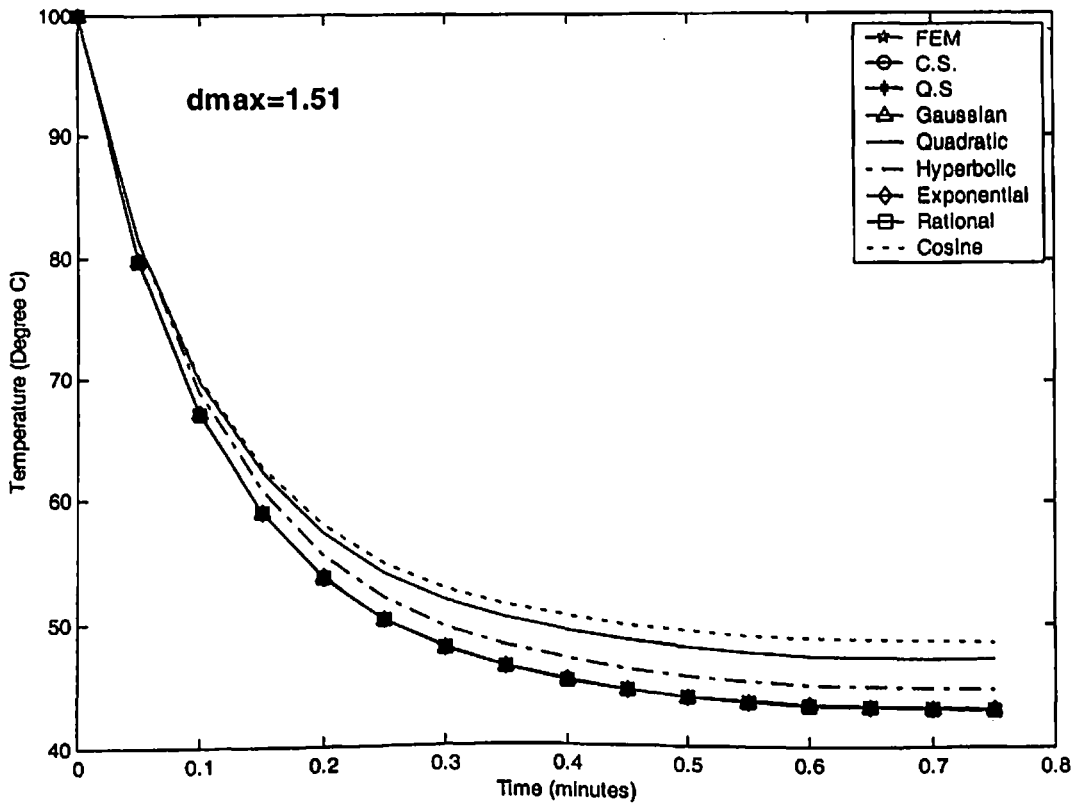
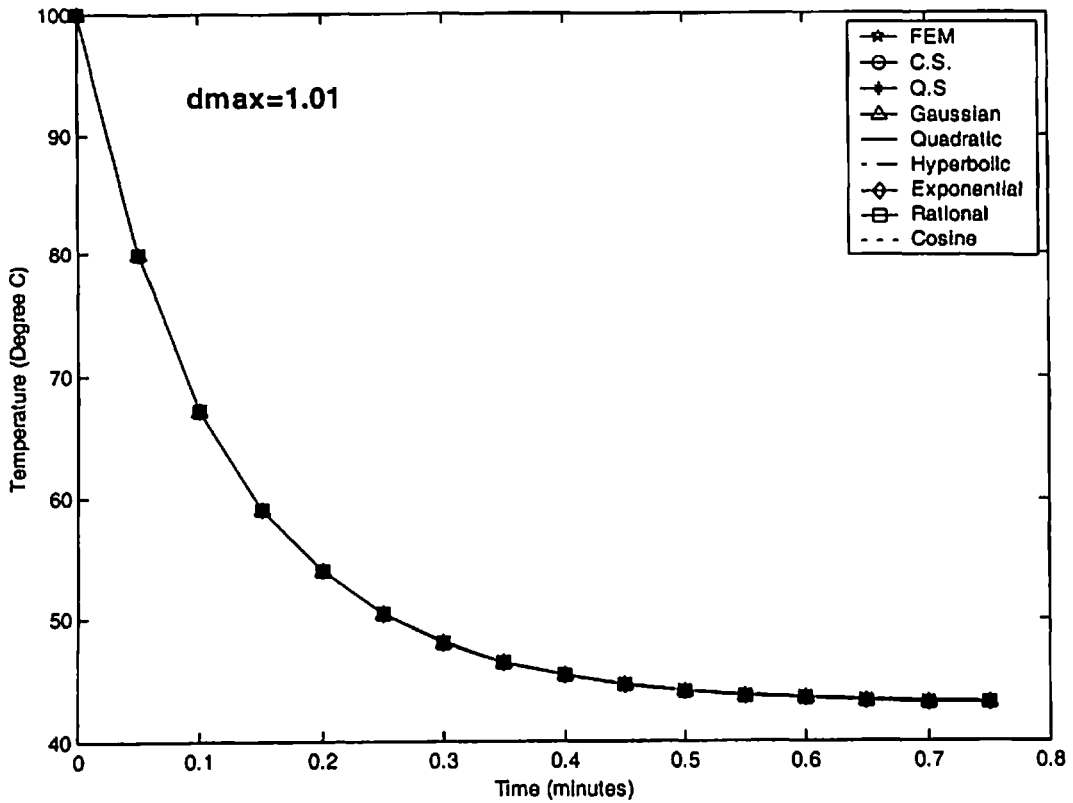


Fig. 4.20 Comparison of EFG results obtained using 21 nodes with FEM at the location ($x = 0.04$ m) of the 1-D model shown in Fig.4.16

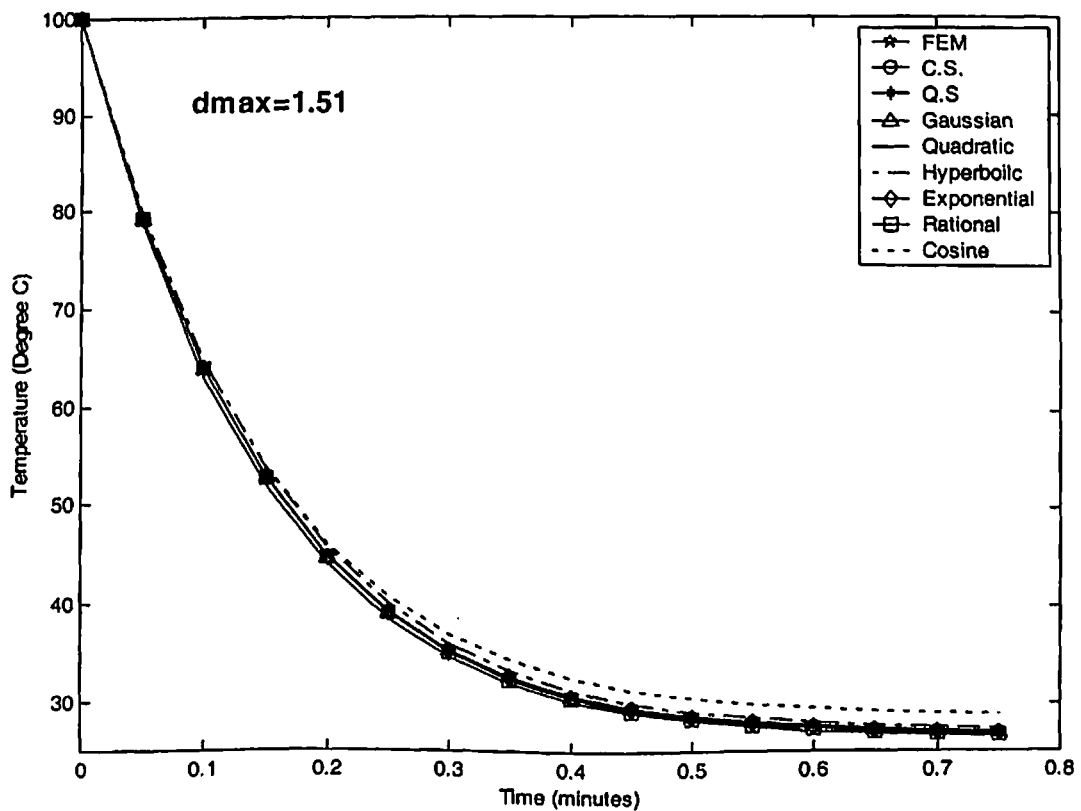
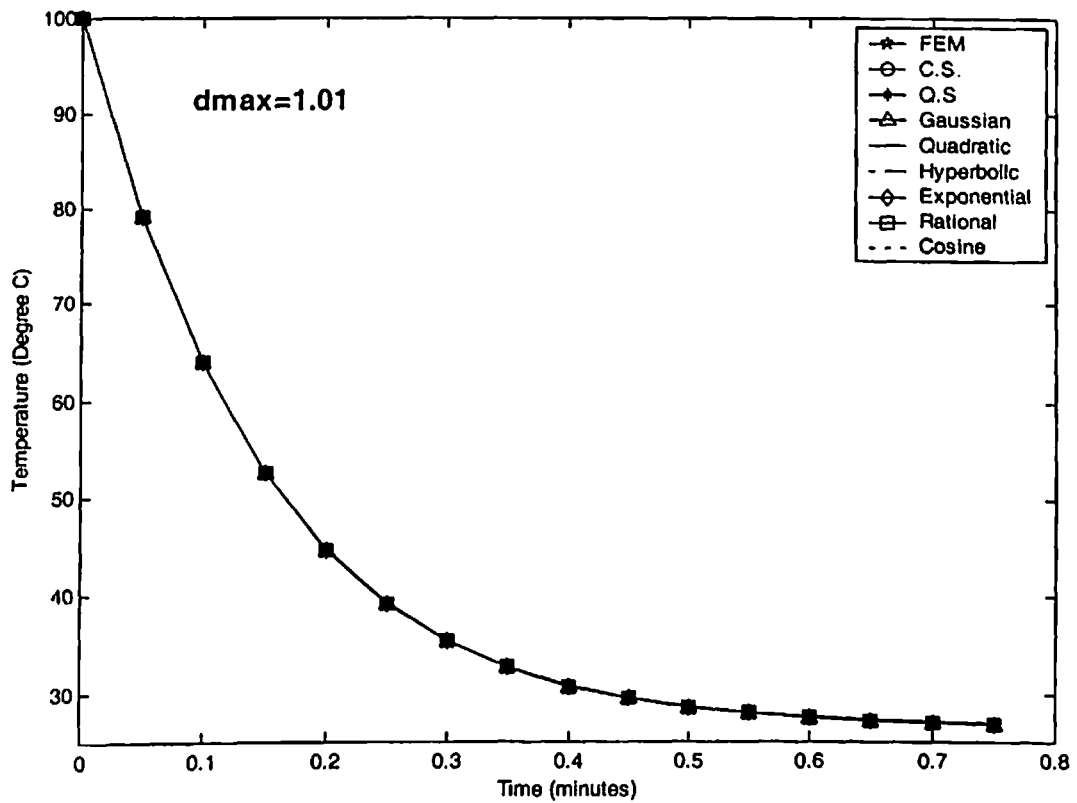


Fig. 4.21 Comparison of EFG results obtained using 11 nodes with FEM at the location ($x = 0.10$ m) of the 1-D model shown in Fig.4.16

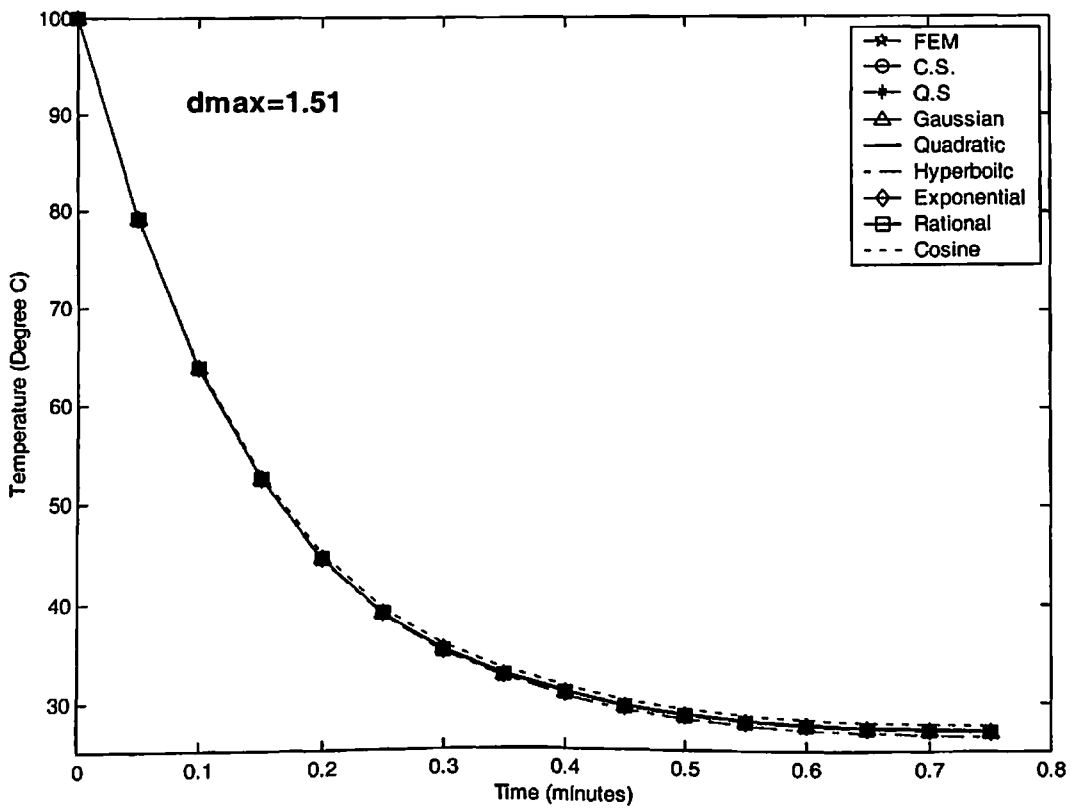
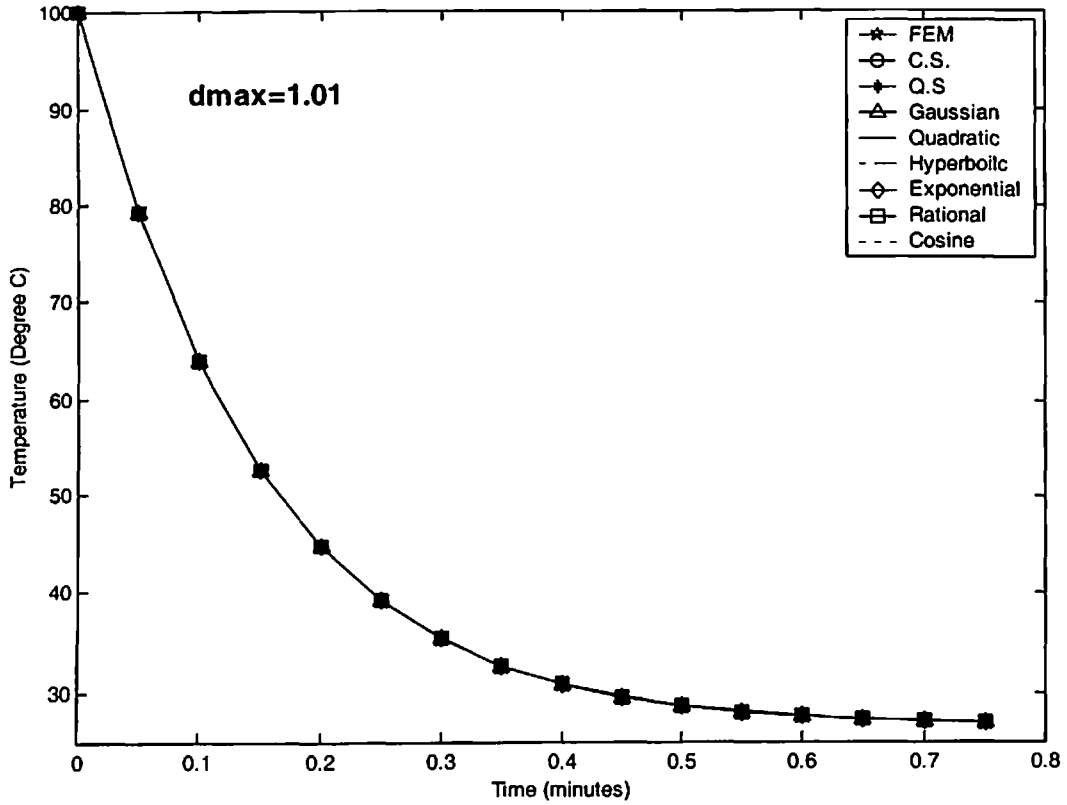


Fig. 4.22 Comparison of EFG results obtained using 21 nodes with FEM at the location ($x = 0.10$ m) of the 1-D model shown in Fig.4.16

➤ **CASE-IV**

4.8 DISCRETIZATION OF THE GOVERNING EQUATION

A general form of energy equation for one-dimensional heat transfer in the cylindrical coordinate system with thermal properties independent of temperature is given as:

$$k_r \frac{\partial^2 T}{\partial r^2} + \frac{k_r}{r} \frac{\partial T}{\partial r} + \dot{Q} = \rho c \frac{\partial T}{\partial t} \quad (4.31)$$

The above equation can be written as:

$$\frac{1}{r} \frac{\partial}{\partial r} \left(k_r r \frac{\partial T}{\partial r} \right) + \dot{Q} = \rho c \frac{\partial T}{\partial t} \quad (4.32a)$$

The initial conditions are:

$$\text{at the time } t = 0 \quad T = T_{ini} \quad (4.32b)$$

The boundary conditions are:

$$\text{at the radius } r = 0 \quad \left(2\pi k_r r \frac{\partial T}{\partial r} \right) \Big|_{r=0} = 0 \quad (4.32c)$$

$$\text{at the outer radius } r = r_o \quad T(r_o) = T_o \quad (4.32d)$$

The weighted integral form of Eq. (4.32a) is given as:

$$\int_0^1 \int_0^{2\pi} \int_0^{r_o} w \left[\frac{1}{r} \frac{\partial}{\partial r} \left(k_r r \frac{\partial T}{\partial r} \right) + \dot{Q} - \rho c \frac{\partial T}{\partial t} \right] r dr d\theta dz = 0 \quad (4.33)$$

The weak form of Eq. (4.33) will be

$$2\pi \int_0^{r_o} \left[\left(k_r \frac{\partial w}{\partial r} \frac{\partial T}{\partial r} \right) - \dot{Q} w + \rho c w \frac{\partial T}{\partial t} \right] r dr - \left[w 2\pi k_r r \frac{\partial T}{\partial r} \right]_0^{r_o} = 0 \quad (4.34)$$

Introducing boundary conditions in Eq. (4.34), the weak form becomes

$$2\pi \int_0^{r_o} \left[\left(k_r \frac{\partial w}{\partial r} \frac{\partial T}{\partial r} \right) - \dot{Q} w + \rho c w \frac{\partial T}{\partial t} \right] r dr - w 2\pi k_r r \frac{\partial T}{\partial r} \Big|_{r_o} = 0 \quad (4.35)$$

The function $I(T)$ can be written as:

$$I(T) = \int_0^{r_0} \frac{2\pi}{2} \left[k_r \left(\frac{\partial T}{\partial r} \right)^2 \right] r dr + 2\pi \int_0^{r_0} \rho c \dot{T} T r dr - 2\pi \int_0^{r_0} \dot{Q} T r dr - Q' T \Big|_{r=r_0} \quad (4.36)$$

where $Q' = 2\pi k_r r \frac{\partial T}{\partial r} \Big|_{r_0}$

Enforcing essential boundary conditions using Lagrange multiplier method, the functional

$I^*(T)$ is obtained as:

$$I^*(T) = \int_0^{r_0} \frac{2\pi}{2} \left[k_r \left(\frac{\partial T}{\partial r} \right)^2 \right] r dr + 2\pi \int_0^{r_0} \rho c \dot{T} T r dr - 2\pi \int_0^{r_0} \dot{Q} T r dr - Q' T \Big|_{r=r_0} + \lambda(T - T_0) \Big|_{r=r_0} \quad (4.37)$$

Using variational principle to obtain the discrete equations:

$$\delta I^*(T) = \int_0^{r_0} 2\pi \left[k_r \left(\frac{\partial T}{\partial r} \right) \delta \left(\frac{\partial T}{\partial r} \right) \right] r dr + 2\pi \int_0^{r_0} \rho c \dot{T} \delta T r dr - 2\pi \int_0^{r_0} \dot{Q} \delta T r dr - Q' \delta T \Big|_{r=r_0} + \lambda \delta T \Big|_{r=r_0} + \delta \lambda (T - T_0) \Big|_{r=r_0} \quad (4.38)$$

since δT and $\delta \lambda$ are arbitrary in the preceding equation, the following set of equations is obtained using Eq. (3.25) and Eq. (4.38)

$$[\mathbf{K}]\{\mathbf{T}\} + [\mathbf{C}]\{\dot{\mathbf{T}}\} + [\mathbf{G}]\{\lambda\} = \{\mathbf{f}\} \quad (4.39a)$$

$$[\mathbf{G}^T]\{\mathbf{T}\} = \{\mathbf{T}_0\} \quad (4.39b)$$

where

$$K_{i,j} = \int_0^{r_0} 2\pi k_r r \Phi_{i,r} \Phi_{j,r} dr \quad (4.40a)$$

$$C_{i,j} = \int_0^{r_0} 2\pi \rho c r \Phi_i^T \Phi_j dr \quad (4.40b)$$

$$f_i = \int_0^{r_0} 2\pi \dot{Q} \Phi_i r dr + Q' \Phi_i \Big|_{r=r_0} \quad (4.40c)$$

$$G_{i,k} = \Phi_k \Big|_{r=r_0} \quad (4.40d)$$

Using Crank-Nicolson technique for time approximation, the Eq. (4.39) can be written as:

$$\begin{bmatrix} \mathbf{K}^* + \mathbf{C} & \mathbf{G} \\ \mathbf{G}^T & 0 \end{bmatrix} \begin{bmatrix} \mathbf{T}_N \\ \lambda \end{bmatrix} = \begin{bmatrix} \mathbf{R}_N \\ T_o \end{bmatrix} \quad (4.41)$$

where

$$\mathbf{R}_N = ([\mathbf{C}] - (1 - \alpha)\Delta t [\mathbf{K}])\{\mathbf{T}\}_{N-1} + \alpha \Delta t \{\mathbf{f}\}_N + (1 - \alpha)\Delta t \{\mathbf{f}\}_{N-1} \quad (4.42a)$$

$$\mathbf{K}^* = \alpha \Delta t [\mathbf{K}] \quad (4.42b)$$

4.9 NUMERICAL RESULTS AND DISCUSSION

The different parameters used for steady-state and transient analysis of one-dimensional model shown in Fig. 4.23 are tabulated in Table 4.65. The EFG results are obtained using different weight functions for two sets of nodes and the FEM results are obtained using linear bar element for same sets of nodes. A comparative analysis is carried out to evaluate the performance of different weight functions.

4.9.1 Steady-state analysis

The results presented in Table 4.66 are obtained using different EFG weight functions for two values of scaling parameter (i.e. $d_{\max} = 1.01$ & $d_{\max} = 1.51$) and it shows a comparison of temperature values obtained using 11 nodes with those obtained by FEM at the location ($r = 0.0\text{m}$). Table 4.67 shows a comparison of temperature values obtained by EFG method using different weight functions for two values of scaling parameter with those obtained by FEM at the same location i.e. ($r = 0.0\text{m}$) for 21 nodes. A comparison of temperature values obtained using different EFG weight functions with FEM for 11 and 21 nodes, is presented in Table 4.68 and Table 4.69 respectively at the location ($r = 0.2\text{m}$). Similar type of comparisons of EFG results are shown in Table 4.70 for 11 nodes at the location ($r = 0.4\text{m}$), in Table 4.71 for 21 nodes at the location ($r = 0.0\text{m}$), in Table 4.72 for 11 nodes at the location ($r = 0.6\text{m}$) and in Table 4.73 for 21 nodes at the location ($r = 0.6\text{m}$). From the results presented in Table 4.66 to Table 4.73, it is observed that EFG results obtained using

different weight functions are similar for $d_{\max} = 1.01$ but for $d_{\max} = 1.51$, only cubicspline, quarticspline, Gaussian, exponential and rational weight functions give acceptable results. It is also observed that EFG results obtained using different weight functions are in good agreement with those obtained by finite element method. Moreover with increase in number of nodes EFG results starts converging.

The effect of scaling parameter (d_{\max}) on EFG results obtained using different weight functions is presented in Table 4.74 for 11 nodes and Table 4.75 for 21 nodes respectively at the location ($r = 0.2$ m). Similar effect of scaling parameter on EFG results is shown in Table 4.76 for 11 nodes and Table 4.77 for 21 nodes at the location ($r = 0.6$ m). Fig. 4.24 shows the effect of scaling parameter on EFG results obtained using 11 and 21 nodes at the location ($r = 0.0$ m). Similar effect of scaling parameter on EFG results is observed in Fig. 4.25 at the location ($r = 0.4$ m). From tables and figures, it is clear that only cubicspline, quarticspline, Gaussian, exponential and rational weight functions give acceptable results in the range $1.0 < d_{\max} < 2.2$ whereas the results obtained using quadratic, hyperbolic and cosine weight functions are varying in abrupt manner with scaling parameter. Therefore EFG results obtained using quadratic, hyperbolic and cosine weight functions are not acceptable in the range $1.0 < d_{\max} < 2.2$. It is also observed that there is minimum variation in EFG results with scaling parameter for exponential weight function.

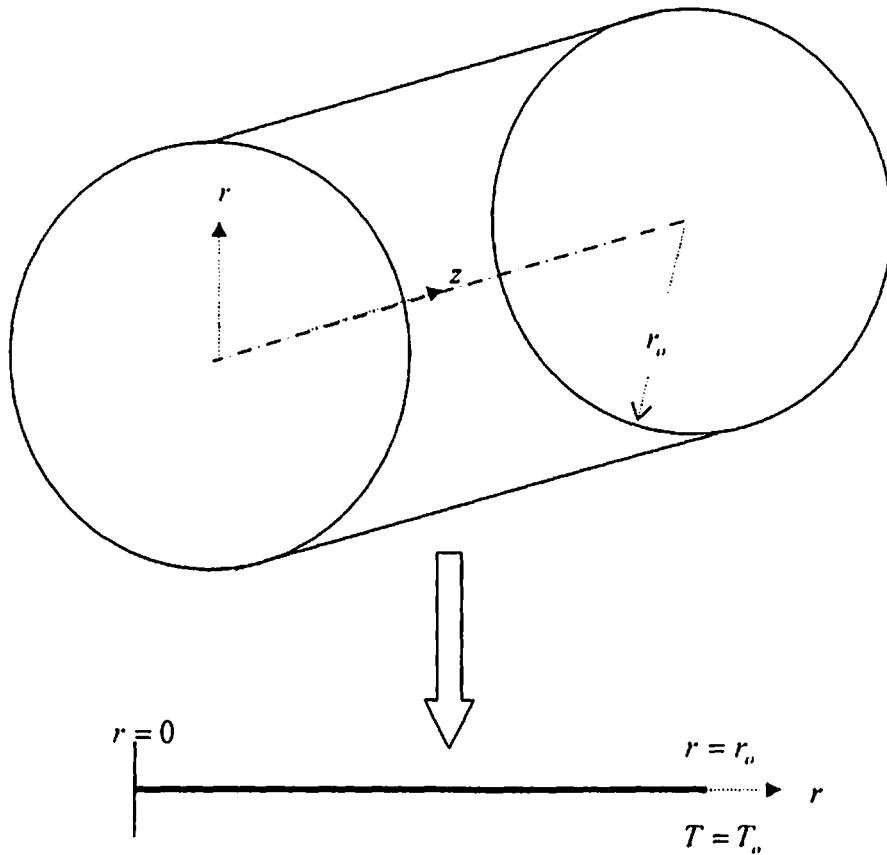


Fig. 4.23 One-dimensional model

Table 4.65 Data for the 1-D model shown in Fig. 4.23

Parameters	Value of the parameter
Radius (r_o)	1 m
Thermal conductivity (k)	400 W/m-K
Specific heat of the material (c)	400 kJ/kg-K
Density of the material (ρ)	10000 kg/m ³
Rate of internal heat generation (\dot{Q})	100000 W/m ³
Heat transfer coefficient (h)	200 W/m ² -K
Initial temperature (T_{ini})	0 °C
Time step size (Δt)	100 sec
Temperature T_o at radius r_o	100 °C

Table 4.66 Comparison of EFG results obtained using 11 nodes with FEM results at the location ($r = 0$) of the 1-D model shown in Fig. 4.23

Weight function	EFG				FEM
	$d_{\max} = 1.01$		$d_{\max} = 1.51$		
	T (°C)	% diff with FEM	T (°C)	% diff with FEM	T (°C)
C. S.	163.8333	0.5455	163.8320	0.5447	162.9444
Q. S.	163.8333	0.5455	163.8310	0.5441	
Gaussian	163.8333	0.5455	163.7698	0.5065	
Quadratic	163.8333	0.5455	199.1402	22.2136	
Hyperbolic	163.8333	0.5455	168.6575	3.5062	
Exponential	163.8333	0.5455	164.1684	0.7512	
Rational	163.8333	0.5455	164.5708	0.9981	
Cosine	163.8333	0.5455	179.7497	10.3135	

Table 4.67 Comparison of EFG results obtained using 21 nodes with FEM results at the location ($r = 0$) of the 1-D model shown in Fig. 4.23

Weight function	EFG				FEM
	$d_{\max} = 1.01$		$d_{\max} = 1.51$		
	T (°C)	% diff with FEM	T (°C)	% diff with FEM	T (°C)
C. S.	162.8874	0.1588	162.8871	0.1586	162.6291
Q. S.	162.8874	0.1588	162.8867	0.1584	
Gaussian	162.8874	0.1588	162.8680	0.1469	
Quadratic	162.8874	0.1588	173.2440	6.5271	
Hyperbolic	162.8874	0.1588	166.0883	2.1270	
Exponential	162.8874	0.1588	162.9907	0.2223	
Rational	162.8874	0.1588	163.1194	0.3015	
Cosine	162.8874	0.1588	151.6105	-6.7753	

Table 4.68 Comparison of EFG results obtained using 11 nodes with FEM results at the location ($r = 0.2$ m) of the 1-D model shown in Fig. 4.23

Weight function	EFG				FEM
	$d_{\max} = 1.01$		$d_{\max} = 1.51$		
	T (°C)	% diff with FEM	T (°C)	% diff with FEM	T (°C)
C. S.	160.5000	0.2081	160.4999	0.2080	160.1667
Q. S.	160.5000	0.2081	160.4999	0.2080	
Gaussian	160.5000	0.2081	160.5032	0.2101	
Quadratic	160.5000	0.2081	8.7300	-94.5494	
Hyperbolic	160.5000	0.2081	158.9631	-0.7515	
Exponential	160.5000	0.2081	160.5645	0.2484	
Rational	160.5000	0.2081	160.7044	0.3357	
Cosine	160.5000	0.2081	128.6542	-19.6748	

Table 4.69 Comparison of EFG results obtained using 21 nodes with FEM results at the location ($r = 0.2$ m) of the 1-D model shown in Fig. 4.23

Weight function	EFG				FEM
	$d_{\max} = 1.01$		$d_{\max} = 1.51$		
	T (°C)	% diff with FEM	T (°C)	% diff with FEM	T (°C)
C. S.	160.1255	0.0523	160.1255	0.0523	160.0418
Q. S.	160.1255	0.0523	160.1255	0.0523	
Gaussian	160.1255	0.0523	160.1264	0.0529	
Quadratic	160.1255	0.0523	189.8748	18.6408	
Hyperbolic	160.1255	0.0523	163.0978	1.9095	
Exponential	160.1255	0.0523	160.1431	0.0633	
Rational	160.1255	0.0523	160.1841	0.0889	
Cosine	160.1255	0.0523	128.9945	-19.3995	

Table 4.70 Comparison of EFG results obtained using 11 nodes with FEM results at the location ($r = 0.4$ m) of the 1-D model shown in Fig. 4.23

Weight function	EFG				FEM
	$d_{\max} = 1.01$		$d_{\max} = 1.51$		
	T (°C)	% diff with FEM	T (°C)	% diff with FEM	T (°C)
C. S.	152.7857	0.1248	152.7859	0.1250	152.5952
Q. S.	152.7857	0.1248	152.7861	0.1251	
Gaussian	152.7857	0.1248	152.8032	0.1363	
Quadratic	152.7857	0.1248	350.8918	129.9490	
Hyperbolic	152.7857	0.1248	145.6080	-4.5789	
Exponential	152.7857	0.1248	152.7780	0.1198	
Rational	152.7857	0.1248	152.8293	0.1534	
Cosine	152.7857	0.1248	184.4544	20.8782	

Table 4.71 Comparison of EFG results obtained using 21 nodes with FEM results at the location ($r = 0.4$ m) of the 1-D model shown in Fig. 4.23

Weight function	EFG				FEM
	$d_{\max} = 1.01$		$d_{\max} = 1.51$		
	T (°C)	% diff with FEM	T (°C)	% diff with FEM	T (°C)
C. S.	152.5715	0.0313	152.5716	0.0313	152.5238
Q. S.	152.5715	0.0313	152.5717	0.0314	
Gaussian	152.5715	0.0313	152.5758	0.0341	
Quadratic	152.5715	0.0313	155.3930	1.8811	
Hyperbolic	152.5715	0.0313	155.1000	1.6890	
Exponential	152.5715	0.0313	152.5709	0.0309	
Rational	152.5715	0.0313	152.5873	0.0416	
Cosine	152.5715	0.0313	117.8554	-22.7298	

Table 4.72 Comparison of EFG results obtained using 11 nodes with FEM results at the location ($r = 0.6$ m) of the 1-D model shown in Fig. 4.23

Weight function	EFG				FEM
	$d_{\max} = 1.01$		$d_{\max} = 1.51$		
	T (°C)	% diff with FEM	T (°C)	% diff with FEM	T (°C)
C. S.	140.1594	0.0759	140.1598	0.0762	140.0531
Q. S.	140.1594	0.0759	140.1602	0.0765	
Gaussian	140.1594	0.0759	140.1850	0.0942	
Quadratic	140.1594	0.0759	-37.7341	-126.9430	
Hyperbolic	140.1594	0.0759	125.5967	-10.3221	
Exponential	140.1594	0.0759	140.1090	0.0399	
Rational	140.1594	0.0759	140.1037	0.0361	
Cosine	140.1594	0.0759	117.3296	-16.2249	

Table 4.73 Comparison of EFG results obtained using 21 nodes with FEM results at the location ($r = 0.6$ m) of the 1-D model shown in Fig. 4.23

Weight function	EFG				FEM
	$d_{\max} = 1.01$		$d_{\max} = 1.51$		
	T (°C)	% diff with FEM	T (°C)	% diff with FEM	T (°C)
C. S.	140.0399	0.0190	140.0400	0.0191	140.0133
Q. S.	140.0399	0.0190	140.0401	0.0191	
Gaussian	140.0399	0.0190	140.0462	0.0235	
Quadratic	140.0399	0.0190	108.6036	-22.4334	
Hyperbolic	140.0399	0.0190	140.6870	0.4812	
Exponential	140.0399	0.0190	140.0285	0.0109	
Rational	140.0399	0.0190	140.0305	0.0123	
Cosine	140.0399	0.0190	110.8593	-20.8223	

Table 4.74 Effect of scaling parameter on EFG results obtained using 11 nodes at the location ($r = 0.2$ m) of the 1-D model shown in Fig. 4.23

Scaling Parameter	Temperature (° C)							
	C. S.	Q. S	Gaussian	Quadratic	Hyperbolic	Exponential	Rational	Cosine
1.01	160.5000	160.5000	160.5000	160.5000	160.5000	160.5000	160.5000	160.5000
1.21	160.5000	160.5000	160.5000	160.5000	160.5000	160.5000	160.5000	160.5000
1.41	160.5000	160.5000	160.5000	160.5000	160.5000	160.5000	160.5000	160.5000
1.61	160.4987	160.4977	160.5065	352.8279	151.2192	160.5754	160.7041	336.0699
1.81	160.5075	160.5127	160.5198	-3252.400	56.7672	160.5969	160.7085	-640.8388
2.01	160.5343	160.5478	160.5512	-442.7000	-2947.000	160.6168	160.7246	184.9188
2.21	160.5754	160.5942	160.6367	-635.0000	-134.0000	160.6346	160.7612	284.8694
2.41	160.6469	160.3278	160.8773	-100.000	1269.400	160.6505	160.8320	284.000
2.61	160.5868	156.4562	161.6613	3000.00	233.600	160.7667	161.5721	43847.0
2.81	158.3879	142.3742	163.3204	5406800	394.800	160.8079	161.9589	81581.0
3.01	133.7563	136.0585	166.4946	121400.0	1339.30	160.8563	162.4865	80113.0

Table 4.75 Effect of scaling parameter on EFG results obtained using 21 nodes at the location ($r = 0.2$ m) of the 1-D model shown in Fig. 4.23

Scaling Parameter	Temperature (° C)							
	C. S.	Q. S	Gaussian	Quadratic	Hyperbolic	Exponential	Rational	Cosine
1.01	160.1255	160.1255	160.1255	160.1255	160.1255	160.1255	160.1255	160.1255
1.21	160.1255	160.1255	160.1255	160.1255	160.1255	160.1255	160.1255	160.1255
1.41	160.1255	160.1255	160.1255	160.1255	160.1255	160.1255	160.1255	160.1255
1.61	160.1251	160.1248	160.1272	99.8940	164.4519	160.1463	160.1836	118.3164
1.81	160.1269	160.1283	160.1306	-140730	144.6884	160.1525	160.1850	-1.9631
2.01	160.1346	160.1432	160.1404	90.0000	100.0000	160.1582	160.1920	2372.000
2.21	160.1519	160.1914	160.1743	410.0000	190.0000	160.1631	160.2094	20128.00
2.41	160.2039	160.3757	160.2830	530.0000	-18146.00	160.1676	160.2441	4921.00
2.61	160.3876	160.9840	160.6435	80720.00	435.000	160.1940	160.4763	7443.00
2.81	161.0939	162.9138	161.4950	8690.000	3223.00	160.2040	160.6441	19591.00
3.01	162.7838	169.5597	163.4248	11171.00	18188.00	160.2169	160.8873	4485.00

Table 4.76 Effect of scaling parameter on EFG results obtained using 11 nodes at the location ($r = 0.6$ m) of the 1-D model shown in Fig. 4.23

Scaling Parameter	Temperature ($^{\circ}$ C)							
	C. S.	Q. S	Gaussian	Quadratic	Hyperbolic	Exponential	Rational	Cosine
1.01	140.1594	140.1594	140.1594	140.1594	140.1594	140.1594	140.1594	140.1594
1.21	140.1594	140.1594	140.1594	140.1594	140.1594	140.1594	140.1594	140.1594
1.41	140.1594	140.1594	140.1594	140.1594	140.1594	140.1594	140.1594	140.1594
1.61	140.1949	140.2239	140.2069	375.2426	110.7276	140.1189	140.1233	555.1746
1.81	140.3237	140.4139	140.2730	4642.200	-16.5432	140.1417	140.1607	1131.000
2.01	140.4246	140.4602	140.3557	1814.000	-4087.000	140.1644	140.1963	491.3000
2.21	140.4351	140.0590	140.4438	1727.100	-1938.000	140.1845	140.2269	664.5000
2.41	140.1276	137.8341	140.4986	2480.000	-635.3000	140.2011	140.2398	1004.70
2.61	138.3431	127.3199	140.6516	3480.000	912.9000	140.2424	141.1326	-2175.50
2.81	129.0979	92.0817	140.1152	-66036.00	2135.700	140.2760	141.9245	-4056.20
3.01	74.2878	36.7714	137.2586	14010.00	7456.900	140.3159	143.1784	2083.10

Table 4.77 Effect of scaling parameter on EFG results obtained using 21 nodes at the location ($r = 0.6$ m) of the 1-D model shown in Fig. 4.23

Scaling Parameter	Temperature ($^{\circ}$ C)							
	C. S.	Q. S	Gaussian	Quadratic	Hyperbolic	Exponential	Rational	Cosine
1.01	140.0399	140.0399	140.0399	140.0399	140.0399	140.0399	140.0399	140.0399
1.21	140.0399	140.0399	140.0399	140.0399	140.0399	140.0399	140.0399	140.0399
1.41	140.0399	140.0399	140.0399	140.0399	140.0399	140.0399	140.0399	140.0399
1.61	140.0486	140.0557	140.0516	215.6581	138.6077	140.0312	140.0345	170.8622
1.81	140.0803	140.1030	140.0681	-228660	81.4392	140.0373	140.0435	-14.1092
2.01	140.1068	140.1297	140.0914	50.0000	-1800.000	140.0432	140.0565	1117.100
2.21	140.1279	140.1591	140.1335	20.0000	480.0000	140.0482	140.0782	9649.000
2.41	140.1676	140.1645	140.2420	260.000	36513.00	140.0522	140.1155	2316.000
2.61	140.2318	139.1689	140.6036	56860.00	137.000	140.0641	140.2967	14006.00
2.81	139.7963	134.4519	141.3918	20840.00	-1750.00	140.0728	140.4620	51770.00
3.01	130.3065	134.3763	143.0060	288640.0	7934.00	140.0836	140.6934	8216.000

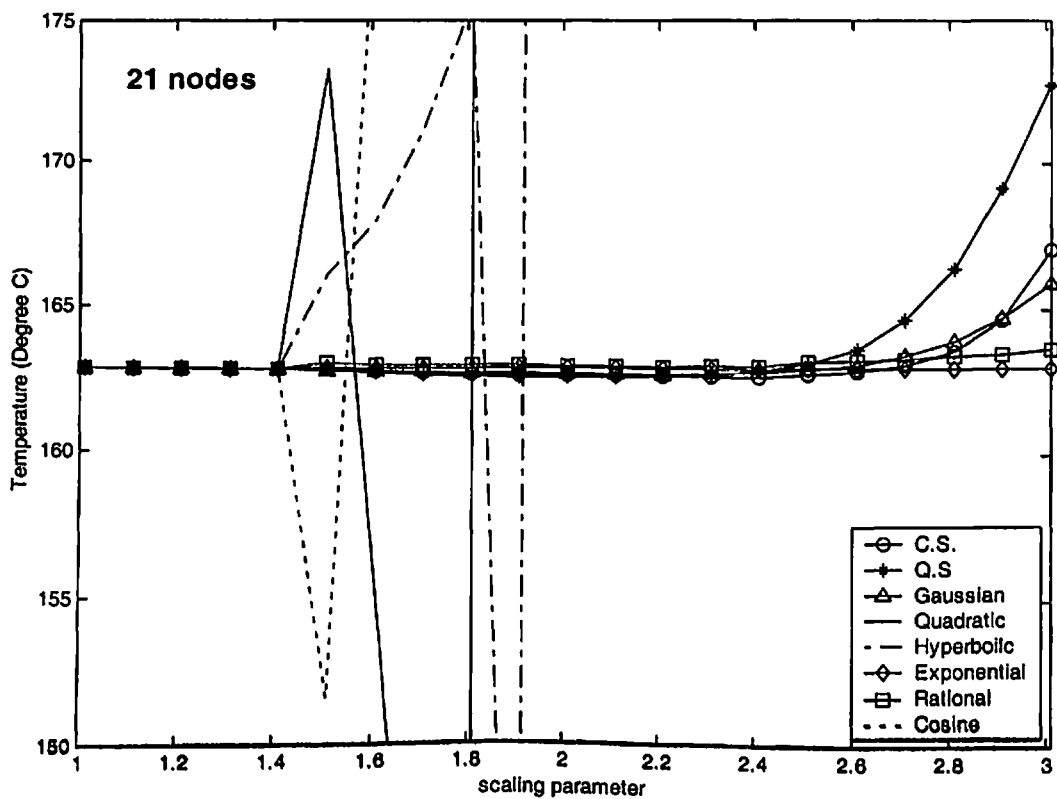
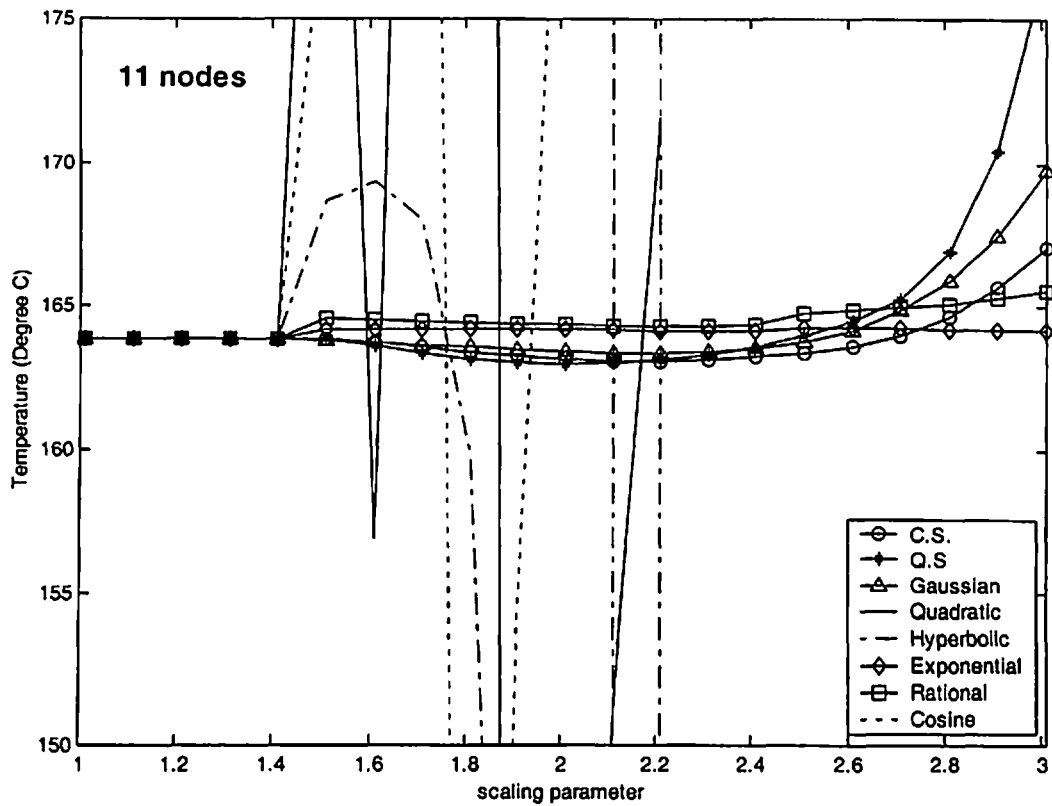


Fig. 4.24 Effect of scaling parameter on EFG results at the location ($r = 0$) of the 1-D model shown in Fig. 4.23

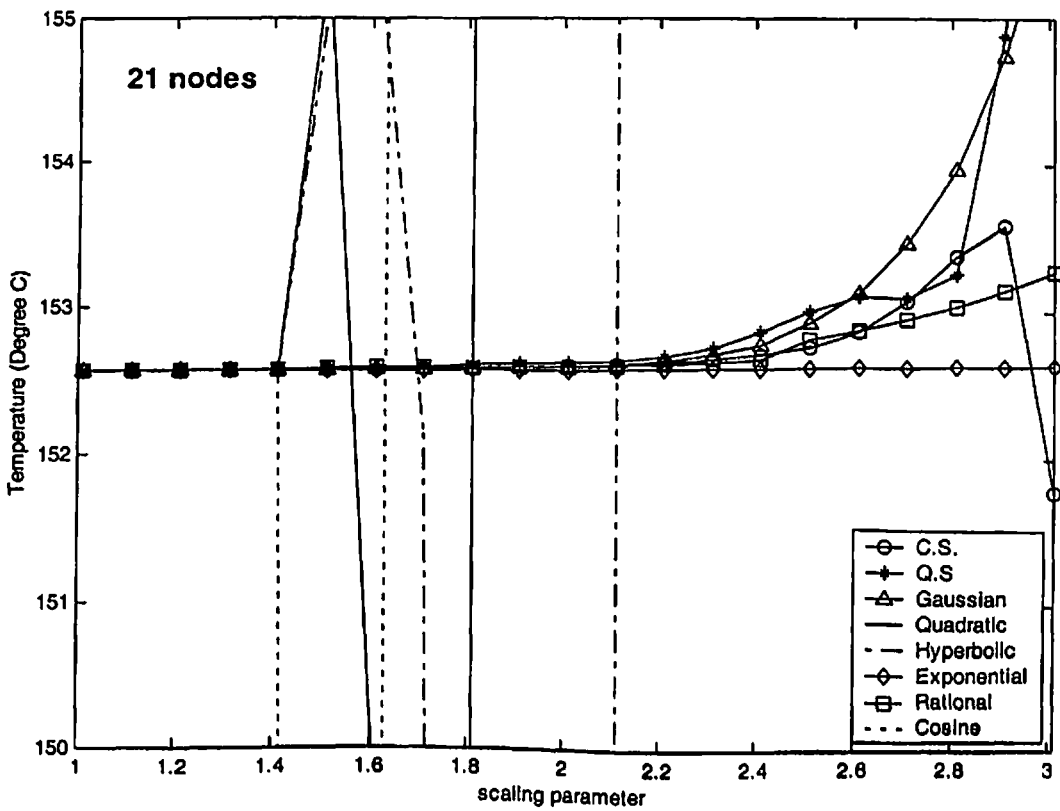
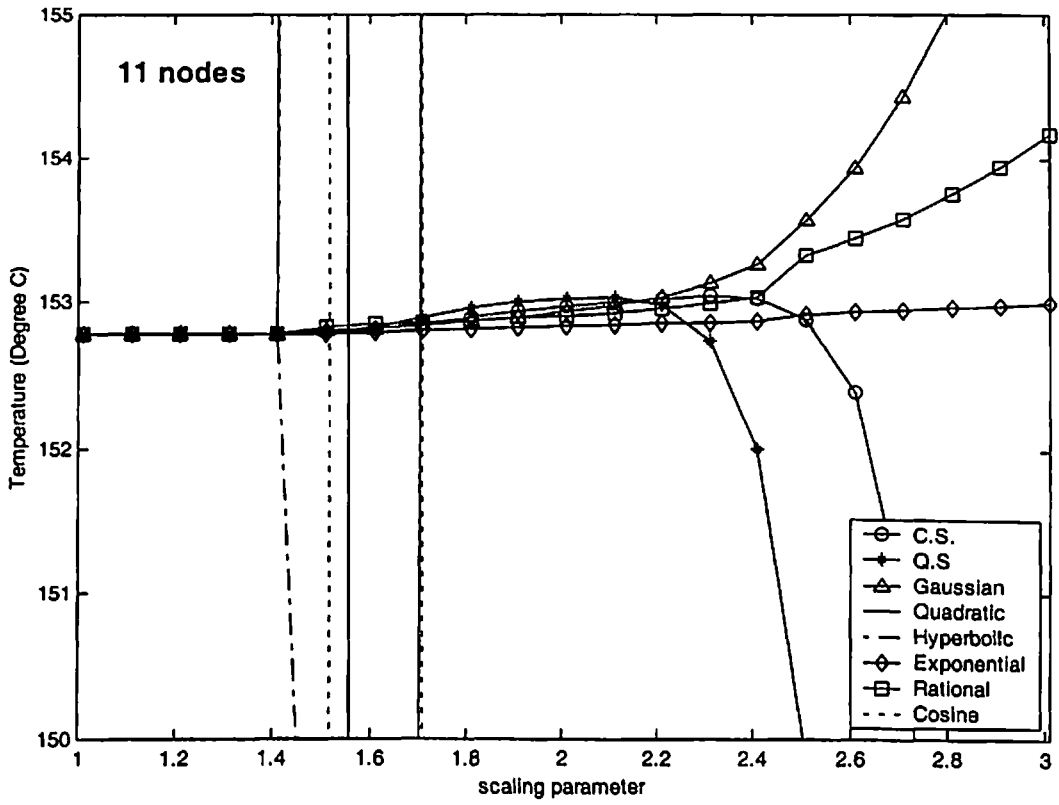


Fig. 4.25 Effect of scaling parameter on EFG results at the location ($r = 0.4$ m) of the 1-D model shown in Fig. 4.23

4.9.2 Transient analysis

The transient analysis of 1-D model as shown in Fig. 4.23 is carried out using different EFG weight functions. Table 4.78 and Table 4.79 show the comparison of temperature values obtained using 11 nodes with FEM results at the location ($r = 0.2\text{m}$) for $d_{\max} = 1.01$ and $d_{\max} = 1.51$ respectively. Similar comparison of temperature values obtained using 21 nodes with FEM results is presented in Table 4.80 and Table 4.81 for $d_{\max} = 1.01$ and $d_{\max} = 1.51$ respectively at the same location i.e. ($r = 0.2\text{m}$). For this case (i.e. CASE-IV) of 1-D transient analysis, time step of 100 sec has been taken which is nearly 1% of the total time required to achieve steady state condition. Table 4.82 and Table 4.83 shows the comparison of temperature values obtained using 11 nodes with FEM results at the different location ($r = 0.6\text{m}$) for $d_{\max} = 1.01$ and $d_{\max} = 1.51$ respectively. Similar comparison of temperature values obtained using 21 nodes with FEM results is also presented in Table 4.84 and Table 4.85 for $d_{\max} = 1.01$ and $d_{\max} = 1.51$ respectively at the same location i.e. ($r = 0.6\text{m}$). Fig. 4.26 shows the comparison of temperature values obtained using 11 nodes with FEM for $d_{\max} = 1.01$ and $d_{\max} = 1.51$ at the location ($r = 0.0$). Similar comparison of temperature values obtained using 21 nodes with FEM is shown in Fig. 4.27 at the same location i.e. ($r = 0.0$). Fig. 4.28 shows the comparison of temperature values obtained using 11 nodes with FEM for $d_{\max} = 1.01$ and $d_{\max} = 1.51$ at the location ($r = 0.4$). Similar comparison of temperature values obtained using 21 nodes with FEM is shown in Fig. 4.29 at the same location i.e. ($r = 0.4$). From the results presented in tables and figures, it is clear that the EFG results obtained using different weight functions are similar for $d_{\max} = 1.01$. However for $d_{\max} = 1.51$ only cubicspline (C.S.), quarticspline (Q.S), Gaussian, exponential and rational weight functions give acceptable results. It has also been observed that the EFG results are in good agreement with those obtained by FEM.

Table 4.78 Comparison of EFG results obtained using 11 nodes with FEM at the location ($r = 0.2$ m) of the 1-D model shown in Fig. 4.23 for $d_{max} = 1.01$

Time (sec) $\times 10^2$	Temperature ($^{\circ}$ C)								
	$d_{max} = 1.01$								FEM
	C. S.	Q. S	Gaussian	Quadratic	Hyperbolic	Exponential	Rational	Cosine	
0	100.0000	100.0000	100.0000	100.0000	100.0000	100.0000	100.0000	100.0000	100.0000
10	123.8373	123.8373	123.8373	123.8373	123.8373	123.8373	123.8373	123.8373	123.5747
20	139.7990	139.7990	139.7990	139.7990	139.7990	139.7990	139.7990	139.7990	139.4319
30	148.8850	148.8850	148.8850	148.8850	148.8850	148.8850	148.8850	148.8850	148.4956
40	153.9870	153.9870	153.9870	153.9870	153.9870	153.9870	153.9870	153.9870	153.6009
50	156.8488	156.8488	156.8488	156.8488	156.8488	156.8488	156.8488	156.8488	156.4732
60	158.4538	158.4538	158.4538	158.4538	158.4538	158.4538	158.4538	158.4538	158.0889
70	159.3539	159.3539	159.3539	159.3539	159.3539	159.3539	159.3539	159.3539	158.9979
80	159.8586	159.8586	159.8586	159.8586	159.8586	159.8586	159.8586	159.8586	159.5092
90	160.1415	160.1415	160.1415	160.1415	160.1415	160.1415	160.1415	160.1415	159.7968
100	160.3000	160.3000	160.3000	160.3000	160.3000	160.3000	160.3000	160.3000	159.9586

Table 4.79 Comparison of EFG results obtained using 11 nodes with FEM at the location ($r = 0.2$ m) of the 1-D model shown in Fig. 4.23 for $d_{max} = 1.51$

Time (sec) $\times 10^2$	Temperature ($^{\circ}$ C)								
	$d_{max} = 1.51$								FEM
	C. S.	Q. S	Gaussian	Quadratic	Hyperbolic	Exponential	Rational	Cosine	
0	100.0000	100.0000	100.0000	100.0000	100.0000	100.0000	100.0000	100.0000	100.0000
10	123.8371	123.8369	123.8283	117.8209	119.6616	123.9030	124.0052	119.9538	123.5747
20	139.7988	139.7986	139.7908	126.5869	135.3410	139.8857	140.0329	131.4836	139.4319
30	148.8848	148.8846	148.8800	129.0806	144.9057	148.9701	149.1231	137.1097	148.4956
40	153.9869	153.9867	153.9847	127.9222	150.6064	154.0676	154.2188	139.2998	153.6009
50	156.8487	156.8486	156.8484	124.7810	153.9961	156.9251	157.0730	139.6644	156.4732
60	158.4538	158.4537	158.4547	120.6267	156.0110	158.5267	158.6717	139.1215	158.0889
70	159.3539	159.3538	159.3556	116.0099	157.2087	159.4243	159.5671	138.1759	158.9979
80	159.8585	159.8585	159.8609	111.2395	157.9205	159.9273	160.0688	137.0976	159.5092
90	160.1414	160.1414	160.1441	106.4864	158.3436	160.2090	160.3498	136.0257	159.7968
100	160.3000	160.2999	160.3028	101.8431	158.5951	160.3668	160.5072	135.0269	159.9586

Table 4.80 Comparison of EFG results obtained using 21 nodes with FEM at the location ($r = 0.2$ m) of the 1-D model shown in Fig. 4.23 for $d_{max} = 1.01$

Time (sec) $\times 10^2$	Temperature ($^{\circ}$ C)								
	$d_{max} = 1.01$								FEM
	C. S.	Q. S	Gaussian	Quadratic	Hyperbolic	Exponential	Rational	Cosine	
0	100.0000	100.0000	100.0000	100.0000	100.0000	100.0000	100.0000	100.0000	100.0000
10	123.7129	123.7129	123.7129	123.7129	123.7129	123.7129	123.7129	123.7129	123.6459
20	139.5594	139.5594	139.5594	139.5594	139.5594	139.5594	139.5594	139.5594	139.4676
30	148.5855	148.5855	148.5855	148.5855	148.5855	148.5855	148.5855	148.5855	148.4890
40	153.6537	153.6537	153.6537	153.6537	153.6537	153.6537	153.6537	153.6537	153.5582
50	156.4961	156.4961	156.4961	156.4961	156.4961	156.4961	156.4961	156.4961	156.4033
60	158.0902	158.0902	158.0902	158.0902	158.0902	158.0902	158.0902	158.0902	158.0000
70	158.9841	158.9841	158.9841	158.9841	158.9841	158.9841	158.9841	158.9841	158.8960
80	159.4854	159.4854	159.4854	159.4854	159.4854	159.4854	159.4854	159.4854	159.3988
90	159.7666	159.7666	159.7666	159.7666	159.7666	159.7666	159.7666	159.7666	159.6810
100	159.9242	159.9242	159.9242	159.9242	159.9242	159.9242	159.9242	159.9242	159.8393

Table 4.81 Comparison of EFG results obtained using 21 nodes with FEM at the location ($r = 0.2$ m) of the 1-D model shown in Fig. 4.23 for $d_{max} = 1.51$

Time (sec) $\times 10^2$	Temperature ($^{\circ}$ C)								
	$d_{max} = 1.51$								FEM
	C. S.	Q. S	Gaussian	Quadratic	Hyperbolic	Exponential	Rational	Cosine	
0	100.0000	100.0000	100.0000	100.0000	100.0000	100.0000	100.0000	100.0000	100.0000
10	123.7129	123.7128	123.7107	126.2568	123.8557	123.7291	123.7546	120.5509	123.6459
20	139.5593	139.5593	139.5571	145.6142	140.3308	139.5825	139.6234	132.7120	139.4676
30	148.5855	148.5854	148.5840	157.7728	149.9843	148.6086	148.6530	138.5975	148.4890
40	153.6536	153.6536	153.6529	165.5620	155.5493	153.6756	153.7202	140.9409	153.5582
50	156.4961	156.4961	156.4959	170.7595	158.7526	156.5169	156.5609	141.4095	156.4033
60	158.0902	158.0902	158.0903	174.3916	160.5963	158.1099	158.1531	140.9332	158.0000
70	158.9841	158.9841	158.9845	177.0505	161.6574	159.0031	159.0457	140.0214	158.8960
80	159.4854	159.4854	159.4860	179.0816	162.2680	159.5040	159.5460	138.9483	159.3988
90	159.7666	159.7666	159.7672	180.6898	162.6194	159.7848	159.8264	137.8571	159.6810
100	159.9242	159.9242	159.9250	181.9995	162.8216	159.9422	159.9836	136.8192	159.8393

Table 4.82 Comparison of EFG results obtained using 11 nodes with FEM at the location ($r = 0.6$ m) of the 1-D model shown in Fig. 4.23 for $d_{max} = 1.01$

Time (sec) $\times 10^2$	Temperature ($^{\circ}$ C)								
	$d_{max} = 1.01$								FEM
	C. S.	Q. S	Gaussian	Quadratic	Hyperbolic	Exponential	Rational	Cosine	
0	100.0000	100.0000	100.0000	100.0000	100.0000	100.0000	100.0000	100.0000	100.0000
10	118.9037	118.9037	118.9037	118.9037	118.9037	118.9037	118.9037	118.9037	118.7962
20	128.3069	128.3069	128.3069	128.3069	128.3069	128.3069	128.3069	128.3069	128.1709
30	133.5148	133.5148	133.5148	133.5148	133.5148	133.5148	133.5148	133.5148	133.3724
40	136.4334	136.4334	136.4334	136.4334	136.4334	136.4334	136.4334	136.4334	136.2952
50	138.0705	138.0705	138.0705	138.0705	138.0705	138.0705	138.0705	138.0705	137.9391
60	138.9887	138.9887	138.9887	138.9887	138.9887	138.9887	138.9887	138.9887	138.8639
70	139.5036	139.5036	139.5036	139.5036	139.5036	139.5036	139.5036	139.5036	139.3842
80	139.7924	139.7924	139.7924	139.7924	139.7924	139.7924	139.7924	139.7924	139.6768
90	139.9543	139.9543	139.9543	139.9543	139.9543	139.9543	139.9543	139.9543	139.8414
100	140.0450	140.0450	140.0450	140.0450	140.0450	140.0450	140.0450	140.0450	139.9340

Table 4.83 Comparison of EFG results obtained using 11 nodes with FEM at the location ($r = 0.6$ m) of the 1-D model shown in Fig. 4.23 for $d_{max} = 1.51$

Time (sec) $\times 10^2$	Temperature ($^{\circ}$ C)								
	$d_{max} = 1.51$								FEM
	C. S.	Q. S	Gaussian	Quadratic	Hyperbolic	Exponential	Rational	Cosine	
0	100.0000	100.0000	100.0000	100.0000	100.0000	100.0000	100.0000	100.0000	100.0000
10	118.9038	118.9039	118.9122	111.2679	108.6144	118.9159	118.9728	115.1485	118.7962
20	128.3071	128.3072	128.3216	112.7249	115.5040	128.2987	128.3405	121.8409	128.1709
30	133.5151	133.5153	133.5332	110.1808	119.6001	133.4933	133.5223	124.7282	133.3724
40	136.4337	136.4340	136.4543	105.6587	122.0336	136.4023	136.4209	125.6360	136.2952
50	138.0708	138.0711	138.0931	100.1748	123.4794	138.0327	138.0436	125.5317	137.9391
60	138.9890	138.9894	139.0124	94.2868	124.3386	138.9465	138.9520	124.9457	138.8639
70	139.5040	139.5043	139.5281	88.3039	124.8492	139.4586	139.4604	124.1655	139.3842
80	139.7928	139.7931	139.8172	82.3960	125.1526	139.7455	139.7450	123.3424	139.6768
90	139.9547	139.9550	139.9794	76.6536	125.3330	139.9062	139.9042	122.5524	139.8414
100	140.0454	140.0457	140.0703	71.1221	125.4401	139.9963	139.9932	121.8300	139.9340

Table 4.84 Comparison of EFG results obtained using 21 nodes with FEM at the location ($r = 0.6$ m) of the 1-D model shown in Fig. 4.23 for $d_{max} = 1.01$

Time (sec) $\times 10^2$	Temperature ($^{\circ}$ C)								
	$d_{max} = 1.01$								FEM
	C. S.	Q. S	Gaussian	Quadratic	Hyperbolic	Exponential	Rational	Cosine	
0	100.0000	100.0000	100.0000	100.0000	100.0000	100.0000	100.0000	100.0000	100.0000
10	118.7895	118.7895	118.7895	118.7895	118.7895	118.7895	118.7895	118.7895	118.7655
20	128.1943	128.1943	128.1943	128.1943	128.1943	128.1943	128.1943	128.1943	128.1624
30	133.4002	133.4002	133.4002	133.4002	133.4002	133.4002	133.4002	133.4002	133.3661
40	136.3165	136.3165	136.3165	136.3165	136.3165	136.3165	136.3165	136.3165	136.2832
50	137.9519	137.9519	137.9519	137.9519	137.9519	137.9519	137.9519	137.9519	137.9200
60	138.8691	138.8691	138.8691	138.8691	138.8691	138.8691	138.8691	138.8691	138.8386
70	139.3835	139.3835	139.3835	139.3835	139.3835	139.3835	139.3835	139.3835	139.3541
80	139.6720	139.6720	139.6720	139.6720	139.6720	139.6720	139.6720	139.6720	139.6433
90	139.8339	139.8339	139.8339	139.8339	139.8339	139.8339	139.8339	139.8339	139.8057
100	139.9247	139.9247	139.9247	139.9247	139.9247	139.9247	139.9247	139.9247	139.8968

Table 4.85 Comparison of EFG results obtained using 21 nodes with FEM at the location ($r = 0.6$ m) of the 1-D model shown in Fig. 4.23 for $d_{max} = 1.51$

Time (sec) $\times 10^2$	Temperature ($^{\circ}$ C)								
	$d_{max} = 1.51$								FEM
	C. S.	Q. S	Gaussian	Quadratic	Hyperbolic	Exponential	Rational	Cosine	
0	100.0000	100.0000	100.0000	100.0000	100.0000	100.0000	100.0000	100.0000	100.0000
10	118.7895	118.7895	118.7912	115.1042	118.0609	118.7936	118.8110	115.4067	118.7655
20	128.1944	128.1944	128.1978	120.9178	127.7391	128.1929	128.2057	121.5751	128.1624
30	133.4002	133.4003	133.4046	122.9883	133.2395	133.3957	133.4057	123.9158	133.3661
40	136.3166	136.3166	136.3216	123.1811	136.4018	136.3096	136.3174	124.3159	136.2832
50	137.9520	137.9520	137.9575	122.4471	138.2216	137.9433	137.9491	123.7468	137.9200
60	138.8692	138.8693	138.8750	121.3009	139.2690	138.8593	138.8637	122.7357	138.8386
70	139.3836	139.3837	139.3896	120.0180	139.8717	139.3730	139.3763	121.5656	139.3541
80	139.6721	139.6722	139.6782	118.7410	140.2185	139.6611	139.6636	120.3843	139.6433
90	139.8340	139.8341	139.8401	117.5395	140.4180	139.8226	139.8247	119.2646	139.8057
100	139.9248	139.9248	139.9310	116.4432	140.5328	139.9132	139.9150	118.2387	139.8968

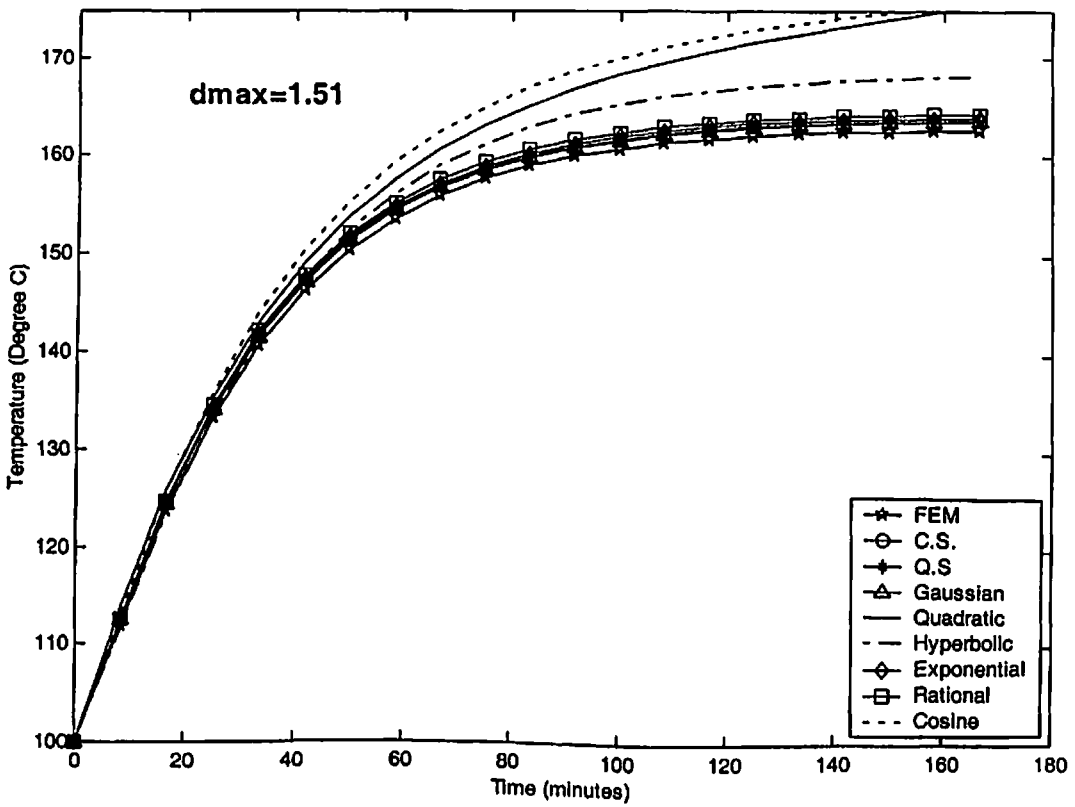
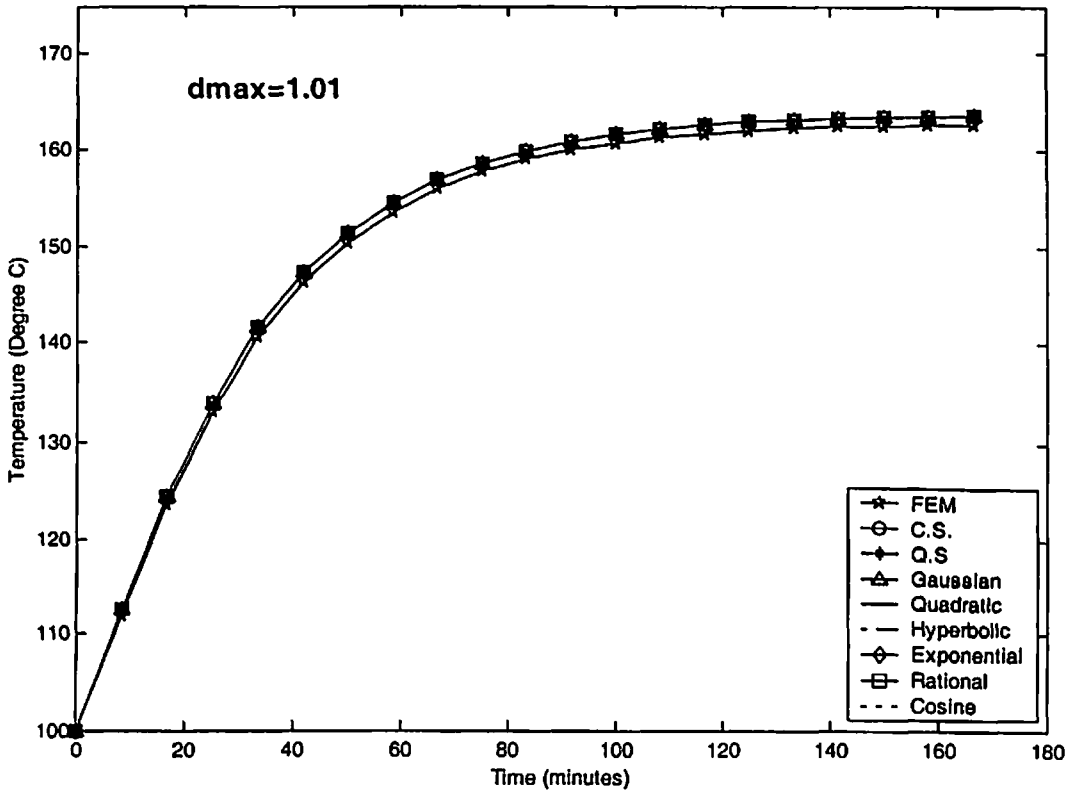


Fig. 4.26 Comparison of EFG results obtained using 11 nodes with FEM at the location ($r = 0$) of the 1-D model shown in Fig. 4.23

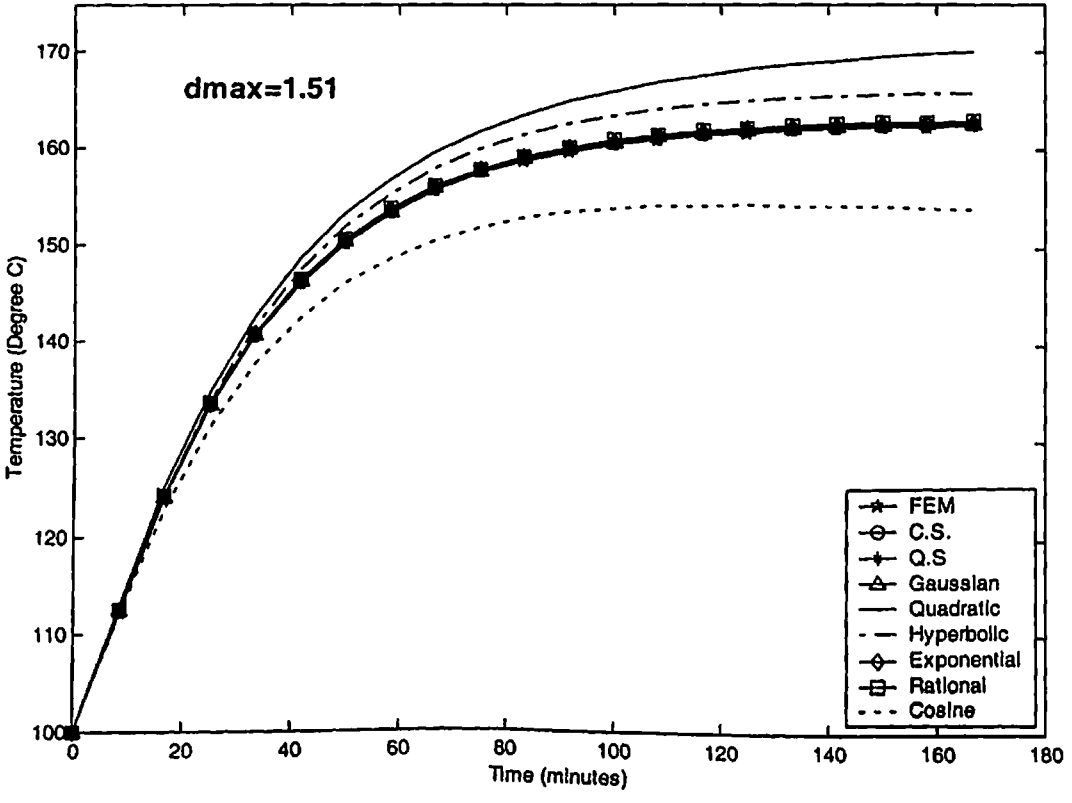
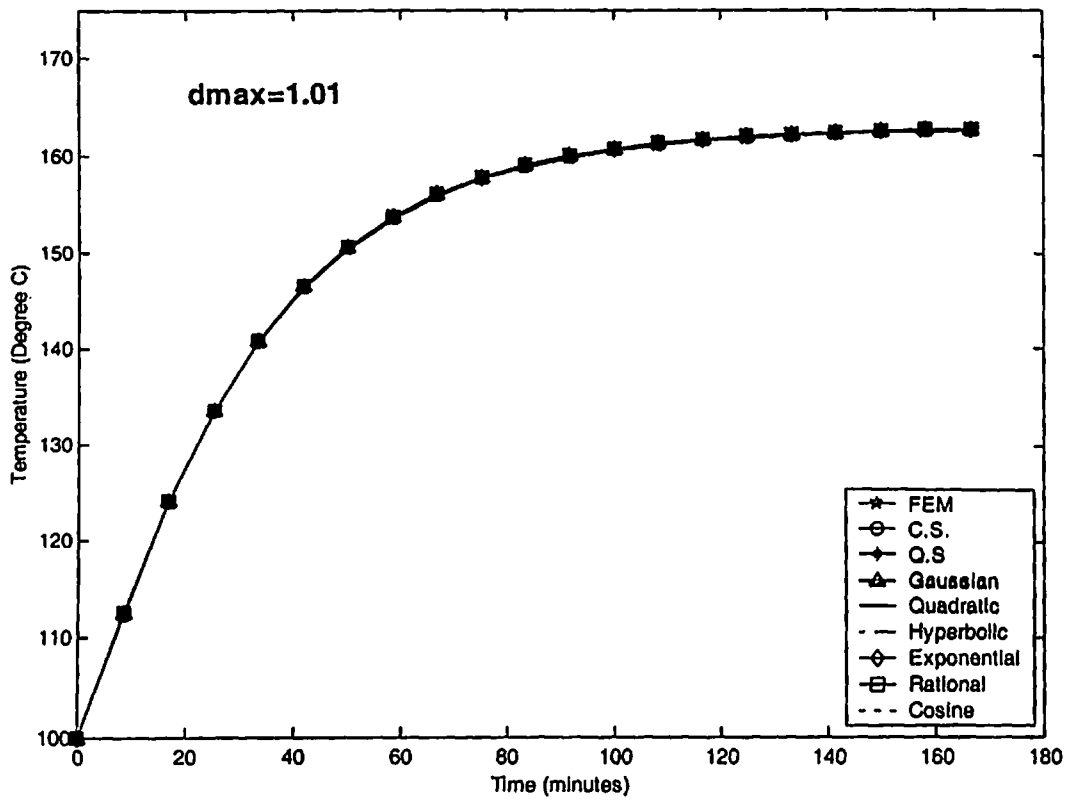


Fig. 4.27 Comparison of EFG results obtained using 21 nodes with FEM at the location ($r = 0$) of the 1-D model shown in Fig. 4.23

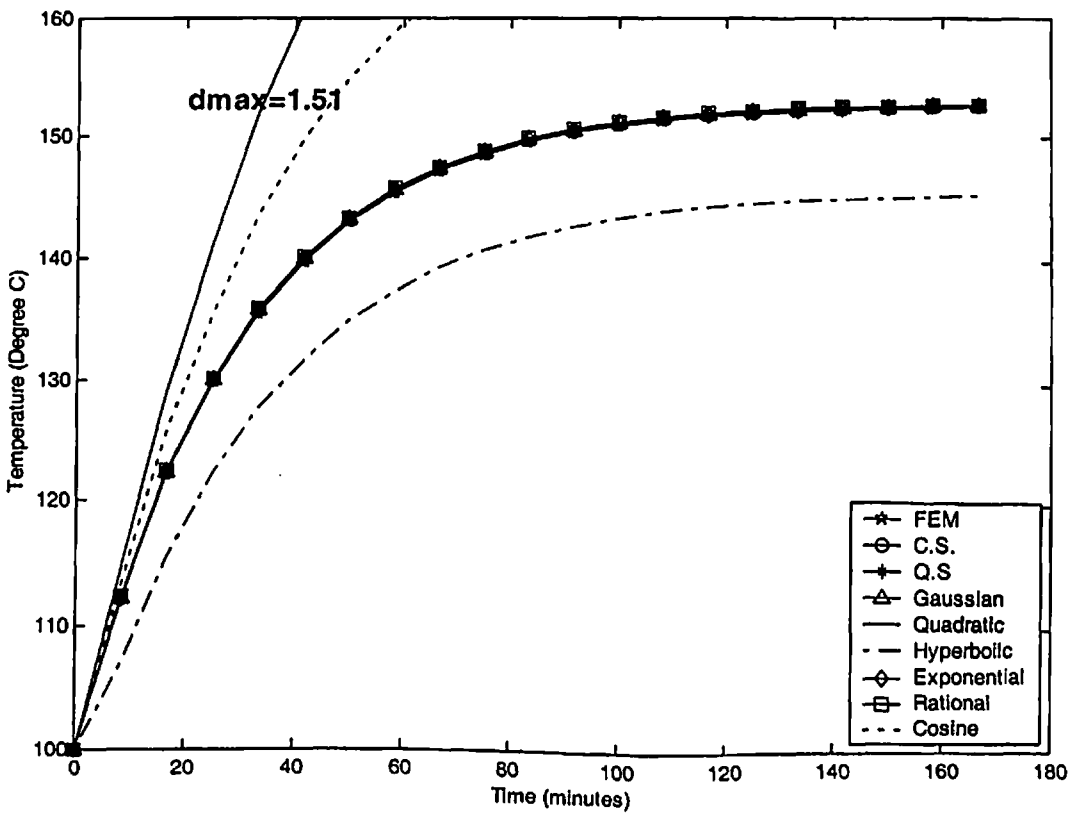
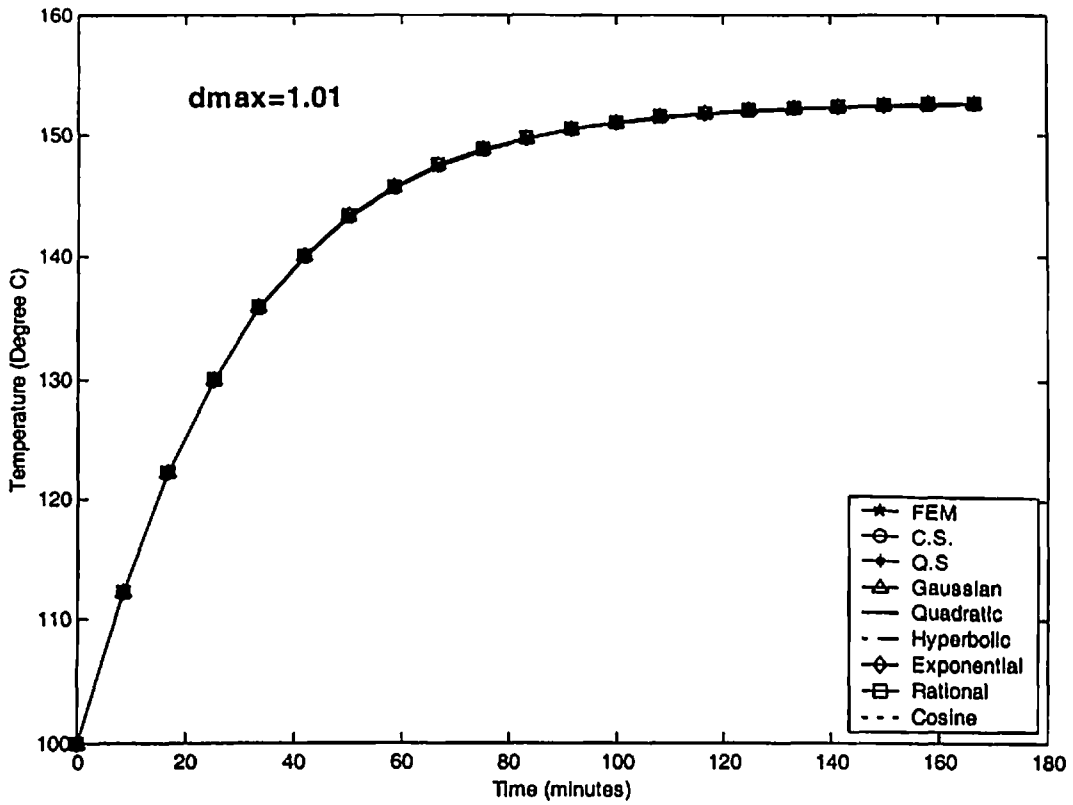


Fig. 4.28 Comparison of EFG results obtained using 11 nodes with FEM at the location ($r = 0.4$ m) of the 1-D model shown in Fig. 4.23

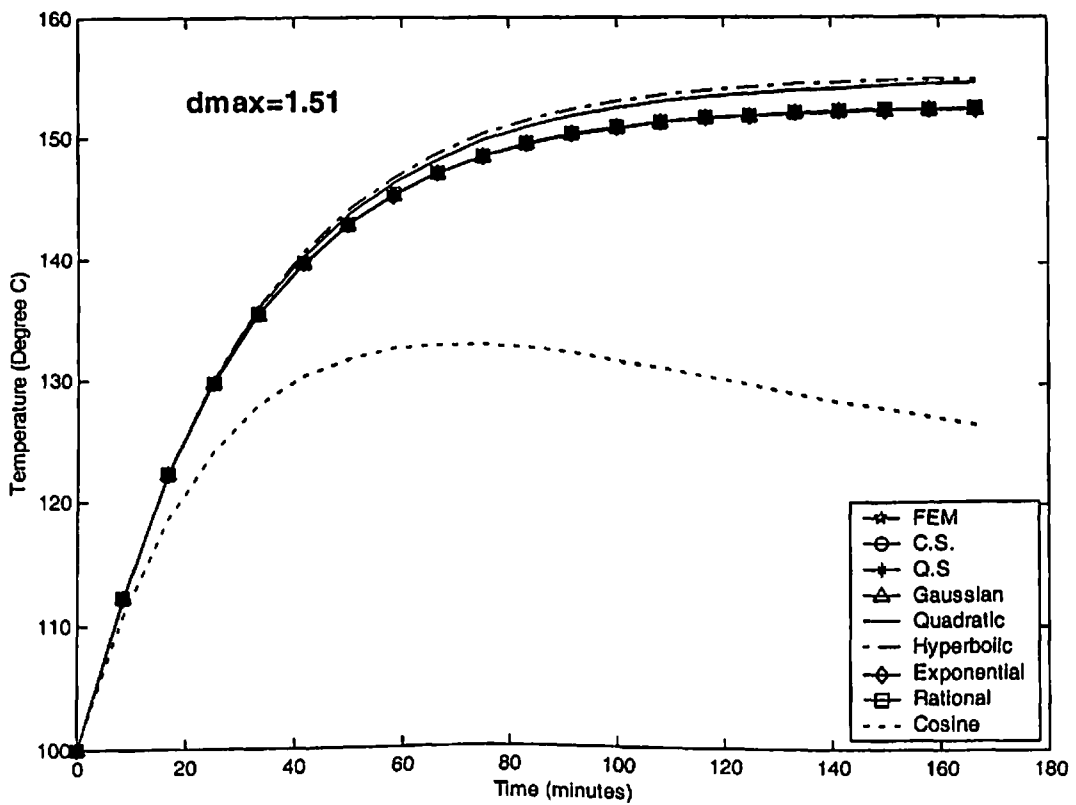
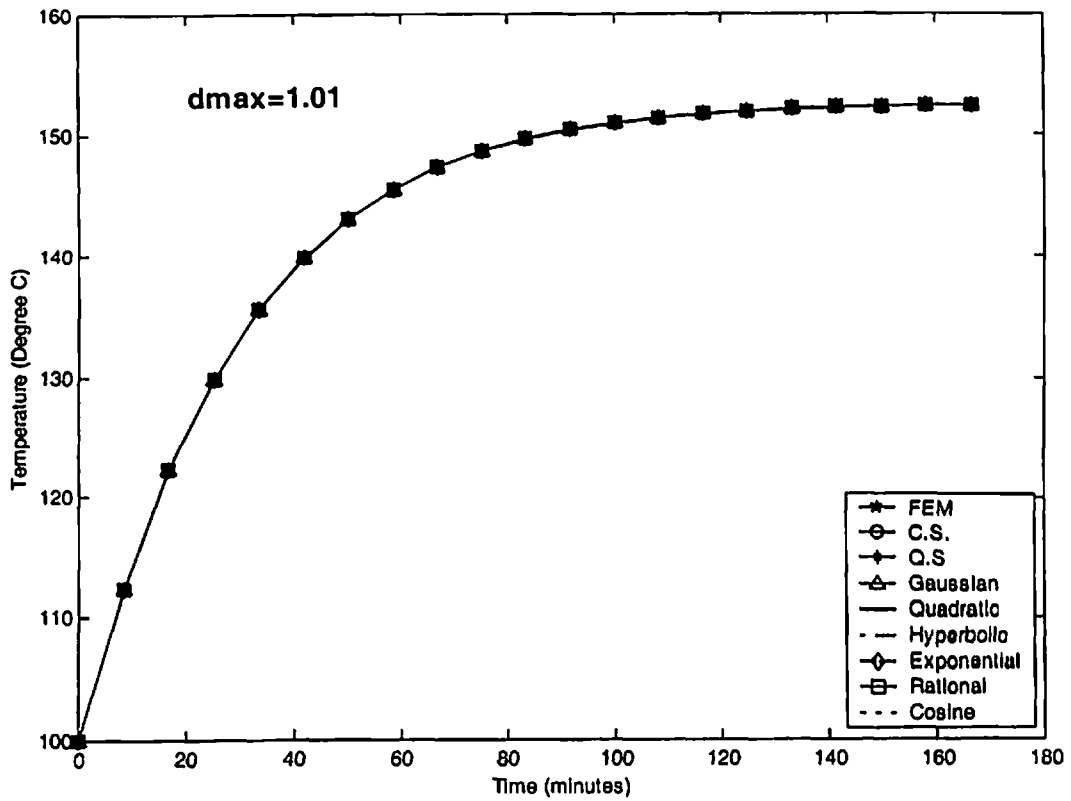


Fig. 4.29 Comparison of EFG results obtained using 21 nodes with FEM at the location ($r = 0.4$ m) of the 1-D model shown in Fig. 4.23

4.10 CONCLUSION

The MATLAB codes have been developed to obtain the numerical solution for the different cases presented in this chapter using different EFG weight functions. The results obtained by EFG method are compared with those obtained by FEM (in Case-I analytical method also) at few typical locations. From the numerical analysis carried out in this chapter, it is clear that the EFG method can be successfully used to obtain the numerical solution of 1-D heat transfer problems. A comparative numerical analysis has been carried out to evaluate the performance of different weight functions. It is found that the EFG results obtained using cubicspline, quarticspline, Gaussian, exponential and rational weight functions are in good agreement with those obtained by FEM. From the analysis carried out in this chapter, it is also observed that only cubicspline, quarticspline, Gaussian, exponential and rational weight functions give acceptable results in the range $1.0 < d_{\max} < 2.0$. Out of all weight functions used, the results obtained using exponential weight function are most reliable as compared to other weight functions used because only exponential weight function has minimum variation in the results with the increase in the value of scaling parameter.

CHAPTER 5

2-D HEAT TRANSFER ANALYSIS

5.1 INTRODUCTION

This chapter describes the application of EFG method in two-dimensional (2-D) heat transfer problems. Four different cases have been chosen to check the applicability of this method in 2-D heat transfer problems. The steady-state and transient analysis of different model problems have been carried out. The effect of scaling parameter on EFG results has also been discussed in detail.

➤ CASE-I

5.2 DISCRETIZATION OF THE GOVERNING EQUATION

The general form of energy equation for two-dimensional heat transfer in isotropic materials with thermal properties independent of temperature is given as:

$$k \left(\frac{\partial^2 T}{\partial x^2} + \frac{\partial^2 T}{\partial y^2} \right) + \dot{Q} - \rho c \frac{\partial T}{\partial t} = 0 \quad (5.1a)$$

The initial conditions are

$$\text{at } t = 0, \quad T = T_{\text{ini}} \quad \text{in } \Omega \quad (5.1b)$$

The boundary conditions are

$$\text{at edge } \Gamma_1, \quad T = T_c \quad (5.1c)$$

$$\text{at edge } \Gamma_2, \quad k \frac{\partial T}{\partial y} = 0 \quad (5.1d)$$

$$\text{at edge } \Gamma_3, \quad -k \frac{\partial T}{\partial x} = h(T - T_\infty) \quad (5.1e)$$

$$\text{at edge } \Gamma_4, \quad -k \frac{\partial T}{\partial y} = h(T - T_\infty) \quad (5.1f)$$

The weighted integral form of Eq. (5.1a) is given as:

$$\int_{\Omega} w \left\{ k \frac{\partial^2 T}{\partial x^2} + k \frac{\partial^2 T}{\partial y^2} + \dot{Q} - \rho c \frac{\partial T}{\partial t} \right\} d\Omega = 0 \quad (5.2)$$

The weak form of Eq. (5.2) is obtained as:

$$\begin{aligned} & \int_{\Omega} \left[-\frac{\partial w}{\partial x} k \frac{\partial T}{\partial x} - \frac{\partial w}{\partial y} k \frac{\partial T}{\partial y} \right] d\Omega - \int_{\Omega} \rho c w \dot{T} d\Omega + \int_{\Omega} \dot{Q} w d\Omega + \\ & \int_{\Gamma} \left[w k \frac{\partial T}{\partial x} \cos(\bar{n}, x) + w k \frac{\partial T}{\partial y} \cos(\bar{n}, y) \right] d\Gamma = 0 \end{aligned} \quad (5.3)$$

Using natural boundary conditions, the functional $I(T)$ is obtained as:

$$\begin{aligned} I(T) = & \frac{1}{2} \int_{\Omega} \left[k \left(\frac{\partial T}{\partial x} \right)^2 + k \left(\frac{\partial T}{\partial y} \right)^2 \right] d\Omega + \int_{\Omega} \rho c \dot{T} T d\Omega - \int_{\Omega} \dot{Q} T d\Omega + \\ & \int_{\Gamma_1} \frac{h}{2} T^2 d\Gamma + \int_{\Gamma_4} \frac{h}{2} T^2 d\Gamma - \int_{\Gamma_1} h T_{\infty} T d\Gamma - \int_{\Gamma_4} h T_{\infty} T d\Gamma \end{aligned} \quad (5.4)$$

Using Lagrange multiplier technique to enforce essential boundary conditions, the functional

$I^*(T)$ is obtained as:

$$\begin{aligned} I^*(T) = & \frac{1}{2} \int_{\Omega} \left[k \left(\frac{\partial T}{\partial x} \right)^2 + k \left(\frac{\partial T}{\partial y} \right)^2 \right] d\Omega + \int_{\Omega} \rho c \dot{T} T d\Omega - \int_{\Omega} \dot{Q} T d\Omega + \\ & \int_{\Gamma_1} \frac{h}{2} T^2 d\Gamma + \int_{\Gamma_4} \frac{h}{2} T^2 d\Gamma - \int_{\Gamma_1} h T_{\infty} T d\Gamma - \int_{\Gamma_4} h T_{\infty} T d\Gamma + \int_{\Gamma_1} \lambda (T - T_e) d\Gamma \end{aligned} \quad (5.5)$$

Using Variational method, Eq. (5.5) reduces to

$$\begin{aligned} \delta I^*(T) = & \int_{\Omega} \left[\left(\frac{\partial T}{\partial x} \right)^T k \delta \left(\frac{\partial T}{\partial x} \right) + \left(\frac{\partial T}{\partial y} \right)^T k \delta \left(\frac{\partial T}{\partial y} \right) \right] d\Omega + \int_{\Omega} \rho c \dot{T} \delta T d\Omega - \int_{\Omega} \dot{Q} \delta T d\Omega + \\ & \int_{\Gamma_1} h T^T \delta T d\Gamma + \int_{\Gamma_4} h T^T \delta T d\Gamma - \int_{\Gamma_1} h T_{\infty} \delta T d\Gamma - \int_{\Gamma_4} h T_{\infty} \delta T d\Gamma + \\ & \int_{\Gamma_1} [\delta \lambda (T - T_e) + \lambda \delta T] d\Gamma \end{aligned} \quad (5.6)$$

Since δT and $\delta \lambda$ are arbitrary in preceding equation, the following relations are obtained

using Eq. (3.25) and Eq. (5.7)

$$[\mathbf{K}]\{\mathbf{T}\} + [\mathbf{C}]\{\dot{\mathbf{T}}\} + [\mathbf{G}]\{\lambda\} = \{\mathbf{f}\} \quad (5.7a)$$

$$[\mathbf{G}^T] \{\mathbf{T}\} = \{\mathbf{q}\} \quad (5.7b)$$

where

$$K_{I,J} = \int_{\Omega} \begin{bmatrix} \Phi_{I,x} \\ \Phi_{I,y} \end{bmatrix}^T \begin{bmatrix} k & 0 \\ 0 & k \end{bmatrix} \begin{bmatrix} \Phi_{J,x} \\ \Phi_{J,y} \end{bmatrix} d\Omega + \int_{\Gamma_1} h \Phi_I^T \Phi_J d\Gamma + \int_{\Gamma_2} h \Phi_I^T \Phi_J d\Gamma \quad (5.8a)$$

$$C_{I,J} = \int_{\Omega} \rho c \Phi_I^T \Phi_J d\Omega \quad (5.8b)$$

$$f_I = \int_{\Omega} \dot{Q} \Phi_I d\Omega + \int_{\Gamma_1} h T_{\infty} \Phi_I d\Gamma + \int_{\Gamma_2} h T_{\infty} \Phi_I d\Gamma \quad (5.8c)$$

$$G_{IK} = \int_{\Gamma_1} \Phi_I N_K d\Gamma \quad (5.8d)$$

$$q_K = \int_{\Gamma_1} T_{\infty} N_K d\Gamma \quad (5.8e)$$

Using Crank-Nicolson technique for time approximation, the Eq. (5.7) can be written as:

$$\begin{bmatrix} \mathbf{K}^* + \mathbf{C} & \mathbf{G} \\ \mathbf{G}^T & 0 \end{bmatrix} \begin{bmatrix} \mathbf{T}_N \\ \lambda \end{bmatrix} = \begin{bmatrix} \mathbf{R}_N \\ \mathbf{q} \end{bmatrix} \quad (5.9)$$

where

$$\mathbf{R}_N = ([\mathbf{C}] - (1 - \alpha) \Delta t [\mathbf{K}]) \{\mathbf{T}\}_{N-1} + \alpha \Delta t \{\mathbf{f}\}_N + (1 - \alpha) \Delta t \{\mathbf{f}\}_{N-1} \quad (5.10a)$$

$$\mathbf{K}^* = \alpha \Delta t [\mathbf{K}] \quad (5.10b)$$

5.3 NUMERICAL RESULTS AND DISCUSSION

The different parameters used for steady-state and transient analysis of two-dimensional model shown in Fig. 5.1 are tabulated in Table 5.1. The EFG results are obtained using different weight functions for two sets of nodes and the FEM results are obtained using 4 node quadrilateral elements (PLANE 55, ANSYS 6.0) for same sets of nodes. Analytical results have also been obtained using an infinite series (Carslaw and Jaeger, 1959). A comparative study is carried out to evaluate the performance of different EFG weight functions.

5.3.1 Steady-state analysis

The EFG results (i.e. temperature values) presented in Table 5.2 are obtained using different weight functions for two values of scaling parameter (i.e. $d_{\max} = 1.01$ & $d_{\max} = 1.51$) at the location $(x = 0.5\text{m}, y = 1\text{m})$ and it shows a comparison of temperature values with those obtained by FEM and analytical methods for 25 nodes. Table 5.3 shows a comparison of temperature values obtained by EFG method using different weight functions for two values of scaling parameter with those obtained by FEM and analytical methods at the same location i.e. $(x = 0.5\text{m}, y = 1\text{m})$ for 81 nodes. A comparison of temperature values obtained using different EFG weight functions with FEM and analytical methods for 25 and 81 nodes, is shown in Table 5.4 and Table 5.5 respectively at the location $(x = 0.5\text{m}, y = 0.5\text{m})$. Similar type of comparisons of temperature values are shown in Table 5.6 for 25 nodes at the location $(x = 1\text{m}, y = 1\text{m})$, in Table 5.7 for 81 nodes at the location $(x = 1\text{m}, y = 1\text{m})$, in Table 5.8 for 25 nodes at the location $(x = 1\text{m}, y = 0.5\text{m})$ and in Table 5.9 for 81 nodes at the location $(x = 1\text{m}, y = 0.5\text{m})$. From the results presented in Table 5.2 to Table 5.9, it is observed that EFG results obtained using different weight functions are almost similar for $d_{\max} = 1.01$. However for $d_{\max} = 1.51$, only cubicspline, quarticspline, Gaussian, exponential and rational weight functions give acceptable results. It is also observed that EFG results obtained using different weight functions are in good agreement with those obtained by FEM and analytical methods. Moreover with the increase in number of nodes EFG results starts converging.

The effect of scaling parameter (d_{\max}) on EFG results obtained using different weight functions is presented in Table 5.10 for 25 nodes and Table 5.11 for 81 nodes respectively at the location $(x = 0.5\text{m}, y = 0.5\text{m})$. Similar effect of scaling parameter on EFG results is shown in Table 5.12 for 25 nodes and Table 5.13 for 81 nodes at the location

$(x = 1\text{ m}, y = 0.5\text{ m})$. Fig. 5.2 shows the effect of scaling parameter on EFG results obtained using 25 and 81 nodes at the location $(x = 0.5\text{ m}, y = 1\text{ m})$. Similar effect of scaling parameter on EFG results is observed in Fig. 5.3 at the location $(x = 1\text{ m}, y = 1\text{ m})$. From tables and figures, it is clear that only cubicspline, quarticspline, Gaussian, exponential and rational weight functions give acceptable results in the range $1.0 < d_{\max} < 2.0$ whereas the results obtained using quadratic, hyperbolic and cosine weight functions are varying in abrupt manner with scaling parameter. Therefore EFG results obtained using quadratic, hyperbolic and cosine weight functions are not acceptable in the range $1.0 < d_{\max} < 2.0$. It is also observed that there is minimum variation in EFG results with scaling parameter for exponential weight function.

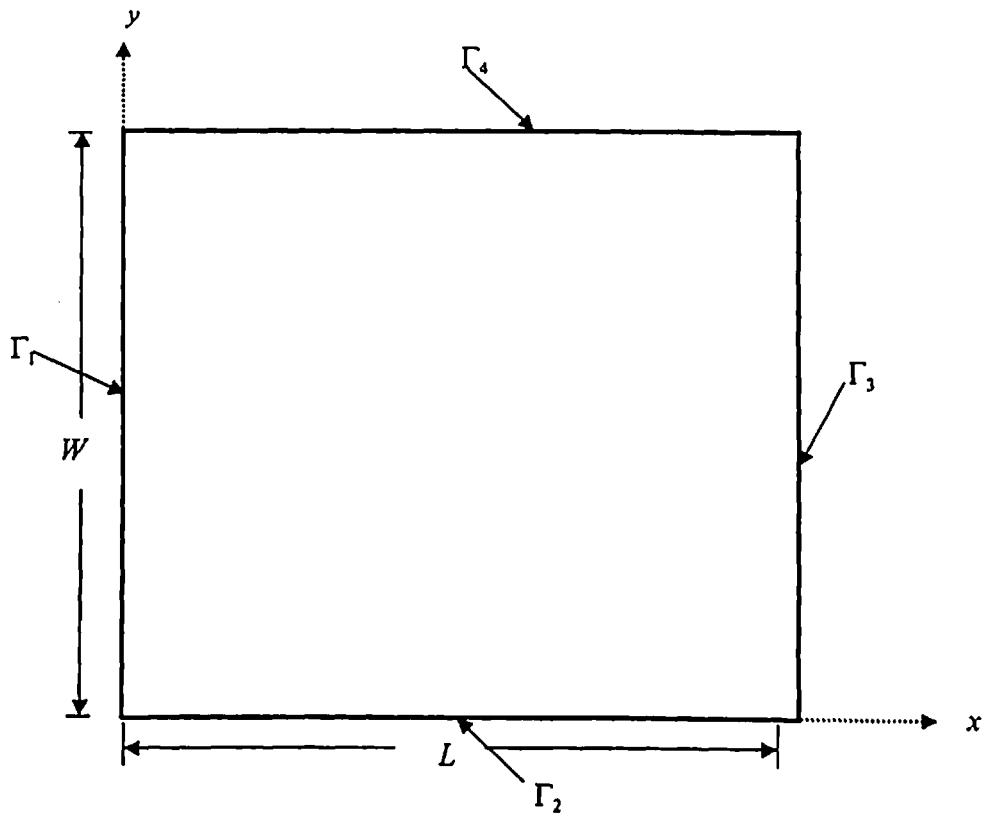


Fig. 5.1 Two-dimensional model

Table 5.1 Data for the 2-D model shown in Fig. 5.1

Parameters	Value of the parameter
Length (L)	1 m
Width (W)	1 m
Thermal conductivity (k)	400 W/m-K
Density of the material (ρ)	10000 kg/m ³
Specific heat (c)	400 kJ/kg-K
Rate of internal heat generation (\dot{Q})	0 W/m ³
Heat transfer coefficient (h)	200 W/m ² -K
Surrounding fluid temperature (T_{∞})	20 °C
Initial temperature (T_{in})	50 °C
Time step size (Δt)	100 sec
Temperature at surface, $x = 0$ or Γ_1	100 °C

Table 5.2 Comparison of EFG results obtained using 25 nodes with FEM and analytical results at the location ($x = 0.5$ m, $y = 1$ m) of the 2-D model shown in Fig. 5.1

Weight function	EFG				FEM		Analytical
	$d_{\max} = 1.01$		$d_{\max} = 1.51$		T (°C)	% error	
	T (°C)	% error	T (°C)	% error			
C. S.	72.0643	-0.0007	71.9548	-0.1526	72.1942	0.1796	72.0648
Q. S.	72.0528	-0.0166	71.9897	-0.1042			
Gaussian	72.1758	0.1540	71.9215	-0.1988			
Quadratic	72.0433	-0.0298	74.7610	3.7413			
Hyperbolic	72.0543	-0.0146	70.0848	-2.7475			
Exponential	72.0508	-0.0194	72.0255	-0.0545			
Rational	72.0444	-0.0283	72.0151	-0.0690			
Cosine	72.0435	-0.0296	75.0249	4.1075			

Table 5.3 Comparison of EFG results obtained using 81 nodes with FEM and analytical results at the location ($x = 0.5$ m, $y = 1$ m) of the 2-D model shown in Fig. 5.1

Weight function	EFG				FEM		Analytical
	$d_{\max} = 1.01$		$d_{\max} = 1.51$		T (°C)	% error	
	T (°C)	% error	T (°C)	% error			
C. S.	72.0659	0.0015	72.0116	-0.0738	72.0970	0.0447	72.0648
Q. S.	72.0623	-0.0035	72.0028	-0.0860			
Gaussian	72.0900	0.0350	72.0079	-0.0790			
Quadratic	72.0583	-0.0090	72.9914	1.2858			
Hyperbolic	72.0472	-0.0244	71.6825	-0.5305			
Exponential	72.0616	-0.0044	72.0510	-0.0192			
Rational	72.0588	-0.0083	72.0249	-0.0554			
Cosine	72.0584	-0.0089	73.6979	2.2662			

Table 5.6 Comparison of EFG results obtained using 25 nodes with FEM and analytical results at the location ($x = 1\text{ m}$, $y = 1\text{ m}$) of the 2-D model shown in Fig. 5.1

Weight function	EFG				FEM		Analytical
	$d_{\max} = 1.01$		$d_{\max} = 1.51$		T (°C)	% error	
	T (°C)	% error	T (°C)	% error			
C. S.	59.1080	-0.0458	59.1362	0.0019	59.5131	0.6392	59.1351
Q. S.	59.1192	-0.0269	59.1447	0.0162			
Gaussian	59.0510	-0.1422	59.0558	-0.1341			
Quadratic	59.1325	-0.0044	60.2170	1.8295			
Hyperbolic	59.1752	0.0678	58.2413	-1.5114			
Exponential	59.1218	-0.0225	59.1304	-0.0080			
Rational	59.1310	-0.0069	59.0988	-0.0614			
Cosine	59.1323	-0.0047	60.3617	2.0742			

Table 5.7 Comparison of EFG results obtained using 81 nodes with FEM and analytical results at the location ($x = 1\text{ m}$, $y = 1\text{ m}$) of the 2-D model shown in Fig. 5.1

Weight function	EFG				FEM		Analytical
	$d_{\max} = 1.01$		$d_{\max} = 1.51$		T (°C)	% error	
	T (°C)	% error	T (°C)	% error			
C. S.	59.1259	-0.0156	59.1346	-0.0008	59.2525	0.1985	59.1351
Q. S.	59.1300	-0.0086	59.1350	-0.0002			
Gaussian	59.1028	-0.0546	59.0959	-0.0663			
Quadratic	59.1348	-0.0005	59.3683	0.3943			
Hyperbolic	59.1484	0.0225	59.1356	0.0008			
Exponential	59.1310	-0.0069	59.1334	-0.0029			
Rational	59.1342	-0.0015	59.1098	-0.0428			
Cosine	59.1347	-0.0007	59.6103	0.8036			

Table 5.10 Effect of scaling parameter on EFG results obtained using 25 nodes at the location ($x = 0.5\text{ m}$, $y = 0.5\text{ m}$) of the 2-D model shown in Fig. 5.1

Scaling Parameter	Temperature ($^{\circ}\text{C}$)							
	C. S.	Q. S	Gaussian	Quadratic	Hyperbolic	Exponential	Rational	Cosine
1.01	80.5157	80.5263	80.4587	80.5392	80.5883	80.5288	80.5376	80.5390
1.21	80.5367	80.5139	80.4075	80.6987	80.7751	80.4639	80.5164	80.6416
1.41	80.4636	80.4543	80.4112	82.0047	79.9297	80.5454	80.6303	81.4301
1.61	80.4292	80.4145	80.4192	77.0261	77.9906	80.5576	80.6504	80.4439
1.81	80.4315	80.4705	80.3954	78.4479	72.3297	80.5697	80.5919	76.1947
2.01	80.4873	80.6341	80.3292	80.1034	86.4314	80.5537	80.6221	79.5585
2.21	80.6666	81.0481	80.1655	77.0585	63.0170	80.5528	80.6507	75.0947
2.41	81.0782	81.9046	79.7934	77.7466	46.2038	80.5795	80.6793	84.6521
2.61	81.9293	83.5618	79.0712	46.1396	49.1487	80.5909	80.7082	43.0280
2.81	83.6319	86.5485	77.7109	83.3270	-9.8936	80.5885	80.8484	76.6830
3.01	86.8907	91.3258	75.3694	-80.9019	78.8697	80.6303	81.1256	58.4485

Table 5.11 Effect of scaling parameter on EFG results obtained using 81 nodes at the location ($x = 0.5\text{ m}$, $y = 0.5\text{ m}$) of the 2-D model shown in Fig. 5.1

Scaling Parameter	Temperature ($^{\circ}\text{C}$)							
	C. S.	Q. S	Gaussian	Quadratic	Hyperbolic	Exponential	Rational	Cosine
1.01	80.4165	80.4185	80.4041	80.4207	80.4271	80.4189	80.4204	80.4206
1.21	80.4209	80.4137	80.3888	80.4370	80.4537	80.4000	80.4103	80.4287
1.41	80.3995	80.3967	80.3887	80.8832	80.4114	80.4214	80.4334	80.6725
1.61	80.3905	80.3866	80.3897	80.2008	80.4477	80.4233	80.4334	80.1874
1.81	80.3884	80.3901	80.3854	80.8653	80.0677	80.4289	80.4394	80.3360
2.01	80.3897	80.4036	80.3751	83.8084	112.9042	80.4240	80.4420	82.2226
2.21	80.4055	80.4783	80.3485	77.1066	80.9886	80.4196	80.4492	80.4467
2.41	80.4756	80.7445	80.2748	81.7076	74.4751	80.4294	80.4524	81.2068
2.61	80.7221	81.5416	80.1044	76.4458	75.8857	80.4320	80.4505	72.4678
2.81	81.5339	83.3744	79.6983	80.3373	113.0560	80.4301	80.4684	79.9340
3.01	83.9883	84.9101	78.8260	73.3900	95.5460	80.4347	80.3339	74.2754

Table 5.12 Effect of scaling parameter on EFG results obtained using 25 nodes at the location ($x = 1\text{ m}$, $y = 0.5\text{ m}$) of the 2-D model shown in Fig. 5.1

Scaling Parameter	Temperature ($^{\circ}\text{C}$)							
	C. S.	Q. S	Gaussian	Quadratic	Hyperbolic	Exponential	Rational	Cosine
1.01	66.2404	66.2395	66.2429	66.2383	66.2358	66.2394	66.2386	66.2384
1.21	66.2359	66.2498	66.2689	66.3360	66.3823	66.2689	66.2904	66.3165
1.41	66.2783	66.2892	66.2869	67.2049	66.0613	66.2518	66.3187	66.9079
1.61	66.3064	66.3159	66.3005	64.9684	65.7874	66.2649	66.3439	66.1503
1.81	66.3262	66.3404	66.2655	65.8258	65.5136	66.3048	66.3906	65.5898
2.01	66.3523	66.4021	66.0972	66.1206	55.5320	66.3442	66.4613	66.3873
2.21	66.4290	66.5789	65.6793	64.9235	37.0261	66.4013	66.5526	63.7341
2.41	66.6037	66.9223	64.8466	69.2933	9.5380	66.4325	66.6811	75.6949
2.61	66.9574	67.5326	63.3189	18.9042	-5.7137	66.4696	66.6326	26.0591
2.81	67.6014	68.4733	60.7350	66.8601	-48.8286	66.5614	66.6309	61.2361
3.01	68.7675	69.7453	56.4658	84.1884	102.3911	66.6787	67.6563	75.5777

Table 5.13 Effect of scaling parameter on EFG results obtained using 81 nodes at the location ($x = 1\text{ m}$, $y = 0.5\text{ m}$) of the 2-D model shown in Fig. 5.1

Scaling Parameter	Temperature ($^{\circ}\text{C}$)							
	C. S.	Q. S	Gaussian	Quadratic	Hyperbolic	Exponential	Rational	Cosine
1.01	66.1846	66.1845	66.1850	66.1844	66.1834	66.1845	66.1844	66.1844
1.21	66.1838	66.1866	66.1904	66.1999	66.2120	66.1904	66.1961	66.1986
1.41	66.1928	66.1955	66.1951	66.3820	66.3134	66.1878	66.2044	66.3146
1.61	66.2007	66.2052	66.2022	66.2624	66.2643	66.1911	66.2103	66.3155
1.81	66.2085	66.2127	66.2096	66.0790	65.7203	66.2022	66.2281	66.3015
2.01	66.2159	66.2199	66.2006	63.9896	66.3409	66.2128	66.2551	65.8594
2.21	66.2247	66.2381	66.1379	68.2255	68.0830	66.2239	66.2827	66.4784
2.41	66.2434	66.2898	65.9426	66.4435	58.0575	66.2332	66.3083	69.4903
2.61	66.2946	66.4209	65.4744	73.2930	56.4908	66.2422	66.3150	78.1173
2.81	66.4334	66.6279	64.4853	65.6535	66.2402	66.2555	66.3094	66.6333
3.01	66.8270	66.5873	62.5656	50.8536	28.3875	66.2828	66.5715	58.5267

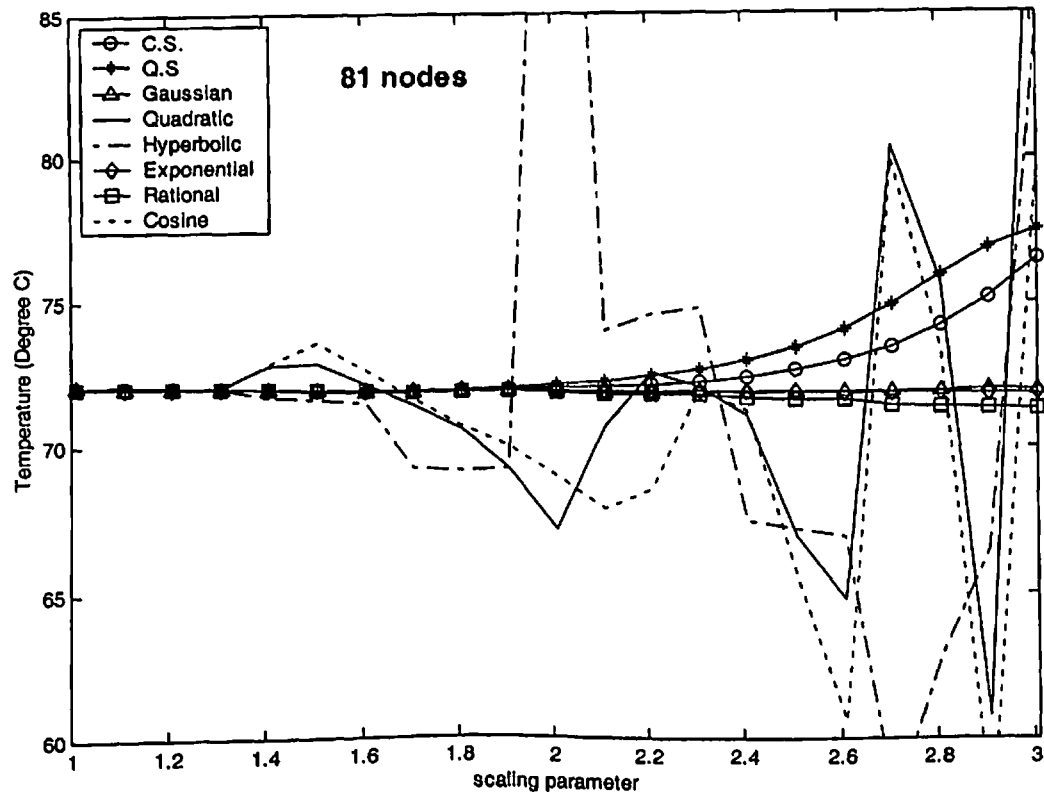
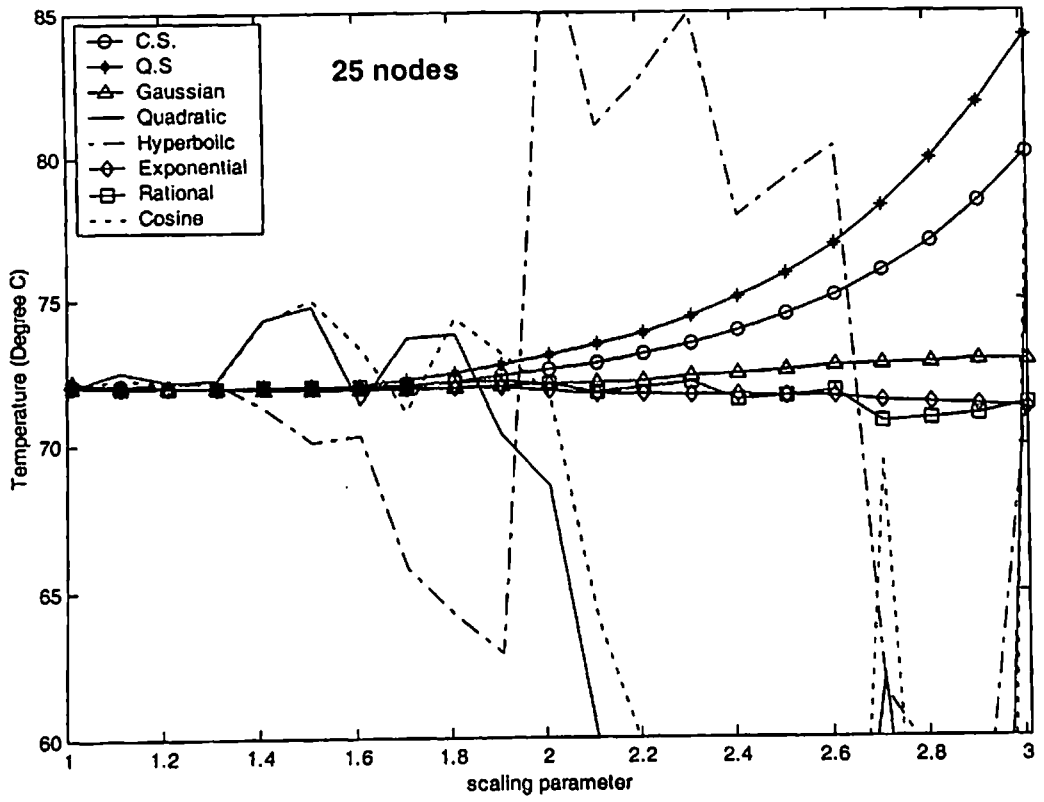


Fig. 5.2 Effect of scaling parameter on EFG results at the location ($x = 0.5\text{ m}$, $y = 1\text{ m}$) of the 2-D model shown in Fig. 5.1

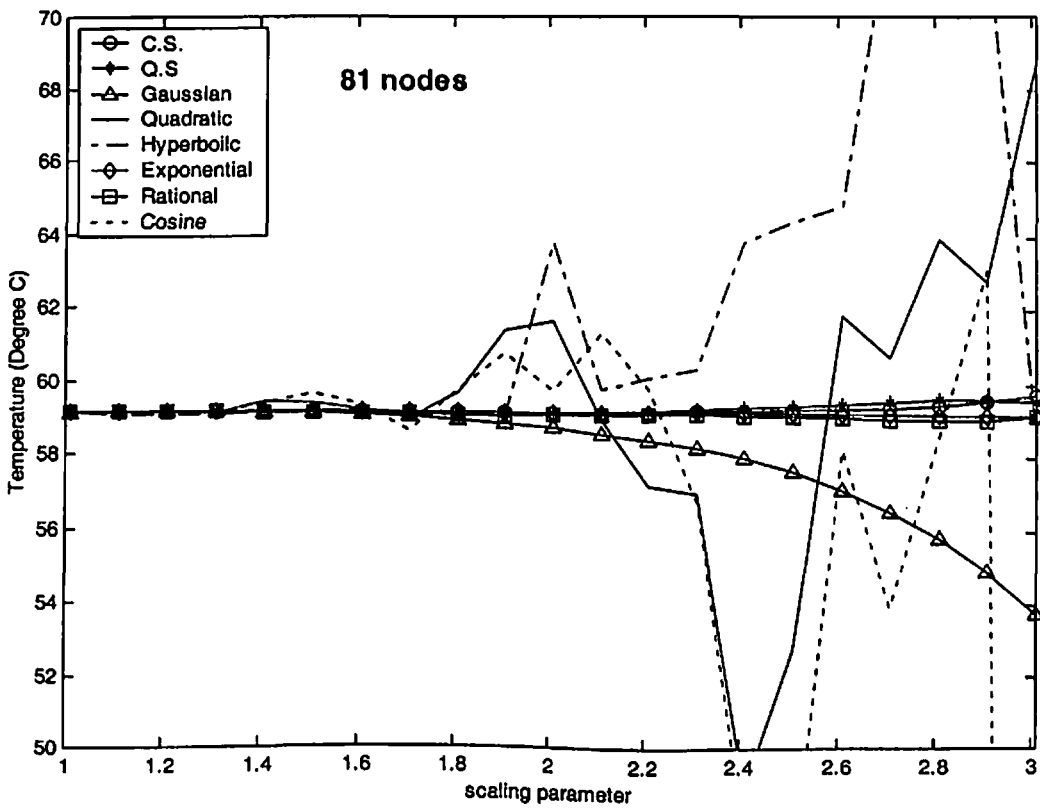
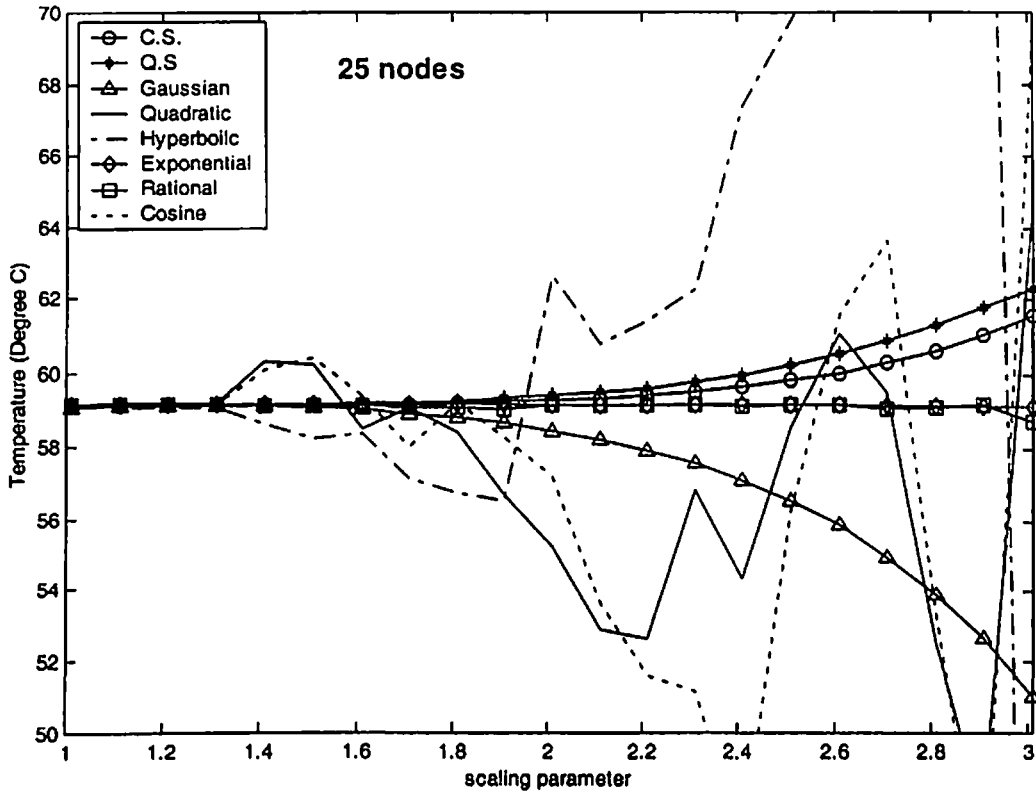


Fig. 5.3 Effect of scaling parameter on EFG results at the location $(x = 1 \text{ m}, y = 1 \text{ m})$ of the 2-D model shown in Fig. 5.1

5.3.2 Transient analysis

The transient analysis of 2-D model is carried out using different EFG weight functions. Table 5.14 and Fig. 5.4 show the convergence study using different time steps at two different locations. The solution with 1000 sec time step continues to oscillate with decreasing amplitude until it converges at 20000 sec. This time step (1000 sec) is nearly 10% of the total time required to achieve steady state condition in first two time steps (i.e. 100 sec and 500 sec). For time steps up to 500 sec, the EFG results are well converged and this time step is nearly 5% of the total time required to achieve steady state. For this (i.e. CASE-I) of 2-D transient analysis, time step of 100 sec has been taken which is nearly 1% of the total time required to achieve steady state condition.

Table 5.15 and Table 5.16 show the comparison of EFG results (i.e. temperature values) obtained using 25 nodes with FEM results at the location $(x = 0.5\text{ m}, y = 0.5\text{ m})$ for $d_{\max} = 1.01$ and $d_{\max} = 1.51$ respectively. Similar comparison of temperature values obtained using 81 nodes is presented in Table 5.17 and Table 5.18 for $d_{\max} = 1.01$ and $d_{\max} = 1.51$ respectively at the same location i.e. $(x = 0.5\text{ m}, y = 0.5\text{ m})$. Table 5.19 and Table 5.20 show the comparison of EFG results (i.e. temperature values) obtained using 25 nodes with FEM results at the location $(x = 1\text{ m}, y = 0.5\text{ m})$ for $d_{\max} = 1.01$ and $d_{\max} = 1.51$ respectively. Similar comparison of temperature values obtained using 81 nodes is also presented in Table 5.21 and Table 5.22 for $d_{\max} = 1.01$ and $d_{\max} = 1.51$ respectively at the same location i.e. $(x = 1\text{ m}, y = 0.5\text{ m})$. Fig 5.5 shows the comparison of EFG results (i.e. temperature values) obtained using 25 nodes with FEM results for $d_{\max} = 1.01$ and $d_{\max} = 1.51$ at the location $(x = 0.5\text{ m}, y = 1\text{ m})$. Similar comparison of temperature values obtained using 81 nodes is shown in Fig. 5.6 at the same location i.e. $(x = 0.5\text{ m}, y = 1\text{ m})$. Fig 5.7 shows the comparison of EFG results (i.e. temperature values) obtained using 25 nodes with FEM results for $d_{\max} = 1.01$ and $d_{\max} = 1.51$ at the location $(x = 1\text{ m}, y = 1\text{ m})$. Similar comparison of temperature values obtained using 81 nodes is shown in Fig. 5.8 at the same location i.e. $(x = 1\text{ m}, y = 1\text{ m})$. From the results presented in tables and figures, it is clear that the EFG

results obtained using different weight functions are almost similar for $d_{\max} = 1.01$ but for $d_{\max} = 1.51$ only cubicspline, quarticspline, Gaussian, exponential and rational weight functions give acceptable results. It has also been observed that the EFG results are in good agreement with those obtained by finite element method.

Table 5.14 Convergence analysis of EFG results obtained using different time step at the location ($x = 1\text{ m}$, $y = 1\text{ m}$) of the 2-D model shown in Fig. 5.1

Time (sec) $\times 10^2$	Time Step Size		
	100 sec	500 sec	1000 sec
0	50.0000	50.0000	50.0000
10	42.9842	43.3114	39.6466
20	46.8562	46.0226	44.9475
30	50.6176	50.0909	46.6710
40	53.2997	52.9778	53.0454
50	55.1450	54.9470	53.1493
60	56.4072	56.2880	56.5524
70	57.2695	57.2014	56.1211
80	57.8583	57.8231	58.1794
90	58.2604	58.2457	57.5057
100	58.5349	58.5325	58.9080

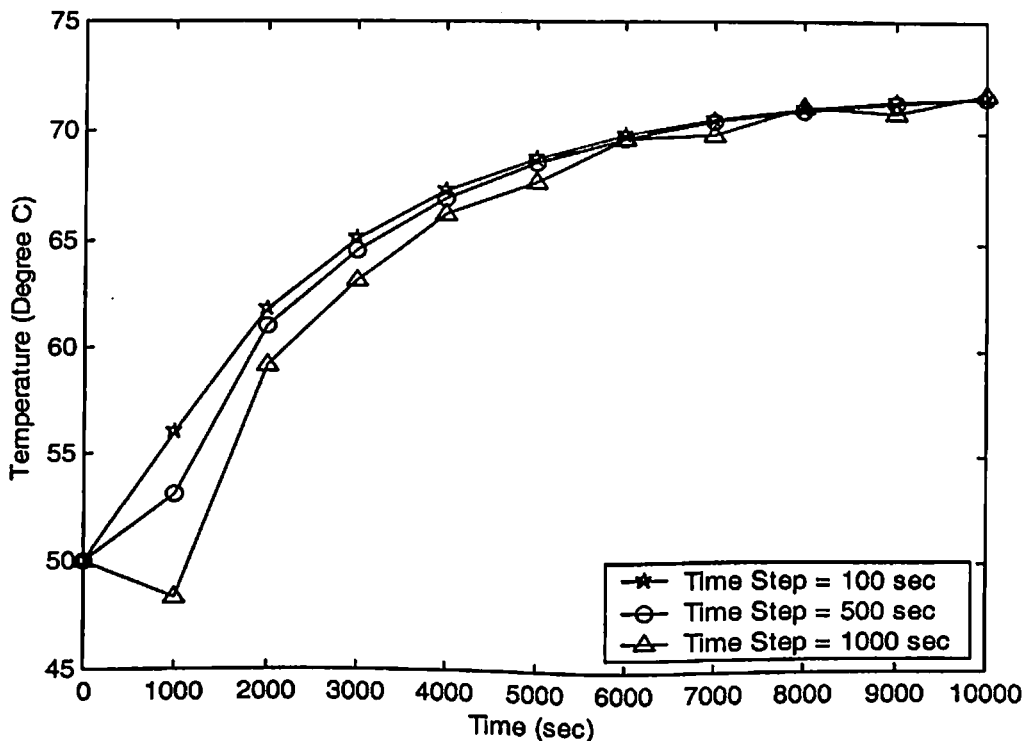


Fig. 5.4 Convergence analysis of EFG results obtained using different time step at the location ($x = 0.5\text{ m}$, $y = 1\text{ m}$) of the 2-D model shown in Fig. 5.1

Table 5.15 Comparison of EFG results obtained using 25 nodes with FEM at the location ($x = 0.5$ m, $y = 0.5$ m) of the 2-D model shown in Fig. 5.1 for $d_{max} = 1.01$

Time (sec) $\times 10^2$	Temperature ($^{\circ}$ C)								
	$d_{max} = 1.01$								FEM
	C. S.	Q. S	Gaussian	Quadratic	Hyperbolic	Exponential	Rational	Cosine	
0	50.0000	50.0000	50.0000	50.0000	50.0000	50.0000	50.0000	50.0000	50.000055
5	53.8028	53.8061	53.7895	53.8104	53.8381	53.8068	53.8096	53.8102	.8689
10	61.0458	61.0520	61.0151	61.0599	61.0968	61.0535	61.0588	61.0597	61.5713
15	65.1682	65.1755	65.1313	65.1847	65.2251	65.1773	65.1835	65.1846	65.5277
20	68.0464	68.0543	68.0062	68.0641	68.1061	68.0561	68.0629	68.0639	68.3777
25	70.2832	70.2915	70.2406	70.3018	70.3449	70.2935	70.3005	70.3016	70.5609
30	72.0920	72.1006	72.0475	72.1113	72.1552	72.1026	72.1099	72.1111	72.3024
35	73.5741	73.5830	73.5278	73.5939	73.6386	73.5851	73.5926	73.5937	73.7219
40	74.7937	74.8028	74.7459	74.8140	74.8592	74.8049	74.8126	74.8138	74.8910
45	75.7985	75.8078	75.7495	75.8193	75.8651	75.8100	75.8179	75.8191	75.8588
50	76.6268	76.6363	76.5766	76.6480	76.6942	76.6385	76.6465	76.6478	76.6616

Table 5.16 Comparison of EFG results obtained using 25 nodes with FEM at the location ($x = 0.5$ m, $y = 0.5$ m) of the 2-D model shown in Fig. 5.1 for $d_{max} = 1.51$

Time (sec) $\times 10^2$	Temperature ($^{\circ}$ C)								
	$d_{max} = 1.51$								FEM
	C. S.	Q. S	Gaussian	Quadratic	Hyperbolic	Exponential	Rational	Cosine	
0	50.0000	50.0000	50.0000	50.0000	50.0000	50.0000	50.0000	50.0000	50.0000
5	53.2594	53.0879	53.2634	55.1730	46.8329	53.6314	53.0611	54.0173	55.8689
10	60.5244	60.3788	60.4855	60.8192	56.4818	60.9974	60.8535	61.9973	61.5713
15	64.8063	64.7144	64.7724	66.0241	61.1947	65.1468	65.0816	66.6373	65.5277
20	67.7607	67.6929	67.7302	69.0355	64.3318	68.0372	68.0064	69.6744	68.3777
25	70.0326	69.9754	70.0029	71.4152	66.7314	70.2830	70.2777	71.9873	70.5609
30	71.8612	71.8096	71.8312	73.3157	68.6668	72.0990	72.1146	73.8435	72.3024
35	73.3581	73.3104	73.3278	74.8720	70.2491	73.5870	73.6195	75.3608	73.7219
40	74.5910	74.5464	74.5603	76.1509	71.5481	74.8113	74.8572	76.6082	74.8910
45	75.6085	75.5667	75.5776	77.2037	72.6157	75.8200	75.8763	77.6356	75.8588
50	76.4489	76.4097	76.4179	78.0707	73.4932	76.6513	76.7157	78.4823	76.6616

Table 5.17 Comparison of EFG results obtained using 81 nodes with FEM at the location ($x = 0.5$ m, $y = 0.5$ m) of the 2-D model shown in Fig. 5.1 for $d_{max} = 1.01$

Time (sec) $\times 10^2$	Temperature ($^{\circ}$ C)								
	$d_{max} = 1.01$								FEM
	C. S.	Q. S	Gaussian	Quadratic	Hyperbolic	Exponential	Rational	Cosine	
0	50.0000	50.0000	50.0000	50.0000	50.0000	50.0000	50.0000	50.0000	50.0000
5	54.1991	54.1994	54.1972	54.1998	54.2012	54.1995	54.1997	54.1997	55.2724
10	61.0047	61.0056	60.9992	61.0066	61.0097	61.0058	61.0065	61.0066	61.2584
15	65.1343	65.1355	65.1270	65.1368	65.1409	65.1357	65.1366	65.1367	65.2887
20	68.0111	68.0124	68.0029	68.0138	68.0184	68.0126	68.0136	68.0138	68.1486
25	70.2305	70.2319	70.2218	70.2335	70.2383	70.2322	70.2333	70.2335	70.3379
30	72.0184	72.0199	72.0091	72.0215	72.0266	72.0202	72.0213	72.0215	72.0890
35	73.4824	73.4839	73.4727	73.4856	73.4909	73.4842	73.4854	73.4856	73.5193
40	74.6882	74.6898	74.6781	74.6916	74.6970	74.6901	74.6914	74.6916	74.6985
45	75.6835	75.6851	75.6731	75.6870	75.6925	75.6855	75.6868	75.6870	75.6745
50	76.5056	76.5073	76.4950	76.5092	76.5149	76.5077	76.5090	76.5092	76.4839

Table 5.18 Comparison of EFG results obtained using 81 nodes with FEM at the location ($x = 0.5$ m, $y = 0.5$ m) of the 2-D model shown in Fig. 5.1 for $d_{max} = 1.51$

Time (sec) $\times 10^2$	Temperature ($^{\circ}$ C)								
	$d_{max} = 1.51$								FEM
	C. S.	Q. S	Gaussian	Quadratic	Hyperbolic	Exponential	Rational	Cosine	
0	50.0000	50.0000	50.0000	50.0000	50.0000	50.0000	50.0000	50.0000	50.0000
5	54.1001	54.0722	54.0928	55.4786	53.9481	54.1778	54.2382	57.2905	55.2724
10	60.8719	60.8370	60.8648	59.7098	60.7064	60.9843	60.8730	60.8839	61.2584
15	65.0377	65.0136	65.0313	64.9799	64.9868	65.1251	65.1111	66.5022	65.2887
20	67.9359	67.9175	67.9304	67.3847	67.9121	68.0051	67.9836	68.7340	68.1486
25	70.1651	70.1495	70.1598	69.8879	70.1404	70.2270	70.2150	71.3641	70.3379
30	71.9580	71.9440	71.9526	71.5524	71.9607	72.0168	72.0098	72.9540	72.0890
35	73.4253	73.4125	73.4198	73.0995	73.4360	73.4823	73.4793	74.5544	73.5193
40	74.6341	74.6222	74.6285	74.2761	74.6596	74.6893	74.6900	75.7012	74.6985
45	75.6322	75.6211	75.6265	75.2982	75.6638	75.6856	75.6888	76.7451	75.6745
50	76.4571	76.4467	76.4514	76.1152	76.4958	76.5086	76.5139	77.5517	76.4839

Table 5.19 Comparison of EFG results obtained using 25 nodes with FEM at the location ($x = 1$ m, $y = 0.5$ m) of the 2-D model shown in Fig. 5.1 for $d_{max} = 1.01$

Time (sec) $\times 10^2$	Temperature ($^{\circ}$ C)								
	$d_{max} = 1.01$								FEM
	C. S.	Q. S	Gaussian	Quadratic	Hyperbolic	Exponential	Rational	Cosine	
0	50.0000	50.0000	50.0000	50.0000	50.0000	50.0000	50.0000	50.0000	50.0000
5	46.2661	46.2654	46.2711	46.2647	46.2676	46.2652	46.2648	46.2647	47.4387
10	46.0098	46.0073	46.0244	46.0045	46.0000	46.0068	46.0049	46.0045	48.0320
15	48.5008	48.4977	48.5180	48.4942	48.4872	48.4971	48.4947	48.4942	49.9815
20	51.3334	51.3303	51.3502	51.3268	51.3194	51.3297	51.3273	51.3269	52.2732
25	53.8757	53.8728	53.8912	53.8694	53.8623	53.8722	53.8699	53.8695	54.4579
30	56.0265	56.0238	56.0406	56.0207	56.0140	56.0233	56.0211	56.0208	56.3855
35	57.8144	57.8119	57.8271	57.8090	57.8028	57.8114	57.8094	57.8091	58.0313
40	59.2923	59.2900	59.3037	59.2873	59.2816	59.2896	59.2878	59.2874	59.4164
45	60.5118	60.5097	60.5220	60.5072	60.5019	60.5093	60.5076	60.5073	60.5743
50	61.5175	61.5156	61.5267	61.5133	61.5083	61.5152	61.5137	61.5133	61.5392

Table 5.20 Comparison of EFG results obtained using 25 nodes with FEM at the location ($x = 1$ m, $y = 0.5$ m) of the 2-D model shown in Fig. 5.1 for $d_{max} = 1.51$

Time (sec) $\times 10^2$	Temperature ($^{\circ}$ C)								
	$d_{max} = 1.51$								FEM
	C. S.	Q. S	Gaussian	Quadratic	Hyperbolic	Exponential	Rational	Cosine	
0	50.0000	50.0000	50.0000	50.0000	50.0000	50.0000	50.0000	50.0000	50.0000
5	46.5673	46.6026	46.5646	48.4141	44.2703	46.2835	46.2985	47.5584	47.4387
10	46.4899	46.5854	46.5347	46.0007	44.3846	45.9791	45.8755	46.8778	48.0320
15	48.8006	48.8646	48.8348	48.9793	47.2067	48.4841	48.4466	49.4477	49.9815
20	51.5090	51.5484	51.5317	51.8682	50.2567	51.3287	51.3380	52.3104	52.2732
25	53.9817	54.0068	53.9970	54.4966	52.9154	53.8784	53.9145	54.8770	54.4579
30	56.0931	56.1101	56.1037	56.7027	55.1383	56.0339	56.0861	57.0465	56.3855
35	57.8575	57.8697	57.8651	58.5341	56.9741	57.8250	57.8874	58.8491	58.0313
40	59.3212	59.3305	59.3267	60.0456	58.4854	59.3052	59.3745	60.3388	59.4164
45	60.5322	60.5398	60.5362	61.2916	59.7283	60.5263	60.6004	61.5678	60.5743
50	61.5333	61.5399	61.5363	62.3181	60.7502	61.5333	61.6104	62.5811	61.5392

Table 5.21 Comparison of EFG results obtained using 81 nodes with FEM at the location ($x = 1$ m, $y = 0.5$ m) of the 2-D model shown in Fig. 5.1 for $d_{max} = 1.01$

Time (sec) $\times 10^2$	Temperature ($^{\circ}$ C)								
	$d_{max} = 1.01$								FEM
	C. S.	Q. S	Gaussian	Quadratic	Hyperbolic	Exponential	Rational	Cosine	
0	50.0000	50.0000	50.0000	50.0000	50.0000	50.0000	50.0000	50.0000	50.0000
5	46.4328	46.4326	46.4340	46.4324	46.4318	46.4326	46.4325	46.4324	46.9714
10	46.4842	46.4837	46.4872	46.4831	46.4813	46.4836	46.4832	46.4831	47.4712
15	48.7729	48.7723	48.7768	48.7716	48.7693	48.7722	48.7717	48.7716	49.4933
20	51.4576	51.4569	51.4614	51.4562	51.4538	51.4568	51.4563	51.4562	51.8949
25	53.9144	53.9138	53.9180	53.9132	53.9108	53.9137	53.9133	53.9132	54.1658
30	56.0154	56.0149	56.0187	56.0142	56.0120	56.0148	56.0143	56.0143	56.1523
35	57.7725	57.7721	57.7755	57.7715	57.7694	57.7720	57.7716	57.7715	57.8378
40	59.2308	59.2304	59.2334	59.2298	59.2279	59.2303	59.2299	59.2299	59.2502
45	60.4377	60.4373	60.4401	60.4368	60.4350	60.4372	60.4369	60.4368	60.4276
50	61.4355	61.4352	61.4377	61.4348	61.4330	61.4351	61.4348	61.4348	61.4067

Table 5.22 Comparison of EFG results obtained using 81 nodes with FEM at the location ($x = 1$ m, $y = 0.5$ m) of the 2-D model shown in Fig. 5.1 for $d_{max} = 1.51$

Time (sec) $\times 10^2$	Temperature ($^{\circ}$ C)								
	$d_{max} = 1.51$								FEM
	C. S.	Q. S	Gaussian	Quadratic	Hyperbolic	Exponential	Rational	Cosine	
0	50.0000	50.0000	50.0000	50.0000	50.0000	50.0000	50.0000	50.0000	50.0000
5	46.4677	46.4733	46.4718	47.1788	46.3958	46.4314	46.4157	48.0032	46.9714
10	46.6115	46.6344	46.6236	46.1453	46.4853	46.4773	46.4494	46.2151	47.4712
15	48.8603	48.8771	48.8699	48.9207	48.7067	48.7688	48.7588	49.4651	49.4933
20	51.5095	51.5202	51.5161	51.3874	51.5001	51.4564	51.4541	51.6696	51.8949
25	53.9452	53.9522	53.9499	53.9902	53.9620	53.9152	53.9226	54.4049	54.1658
30	56.0339	56.0390	56.0375	56.0321	56.0985	56.0175	56.0291	56.3630	56.1523
35	57.7838	57.7876	57.7866	57.8363	57.8601	57.7755	57.7903	58.2096	57.8378
40	59.2377	59.2408	59.2400	59.2794	59.3328	59.2343	59.2512	59.6240	59.2502
45	60.4419	60.4446	60.4439	60.5026	60.5429	60.4417	60.4598	60.8611	60.4276
50	61.4383	61.4407	61.4400	61.4975	61.5470	61.4398	61.4589	61.8460	61.4067

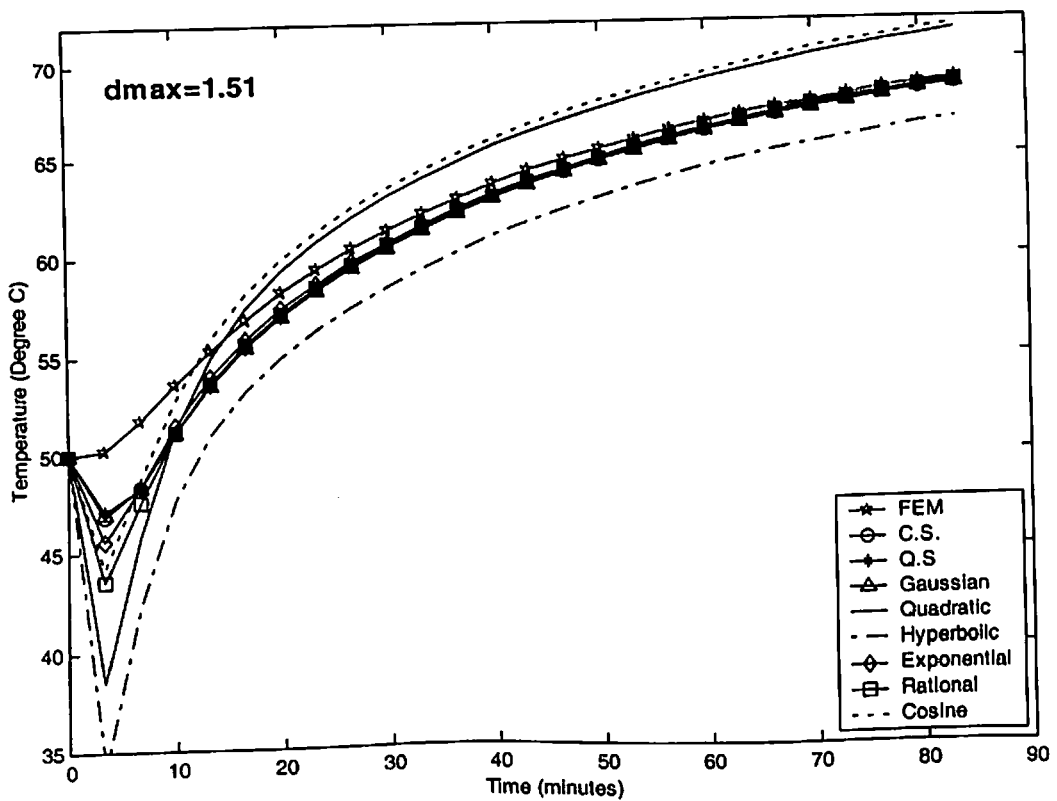
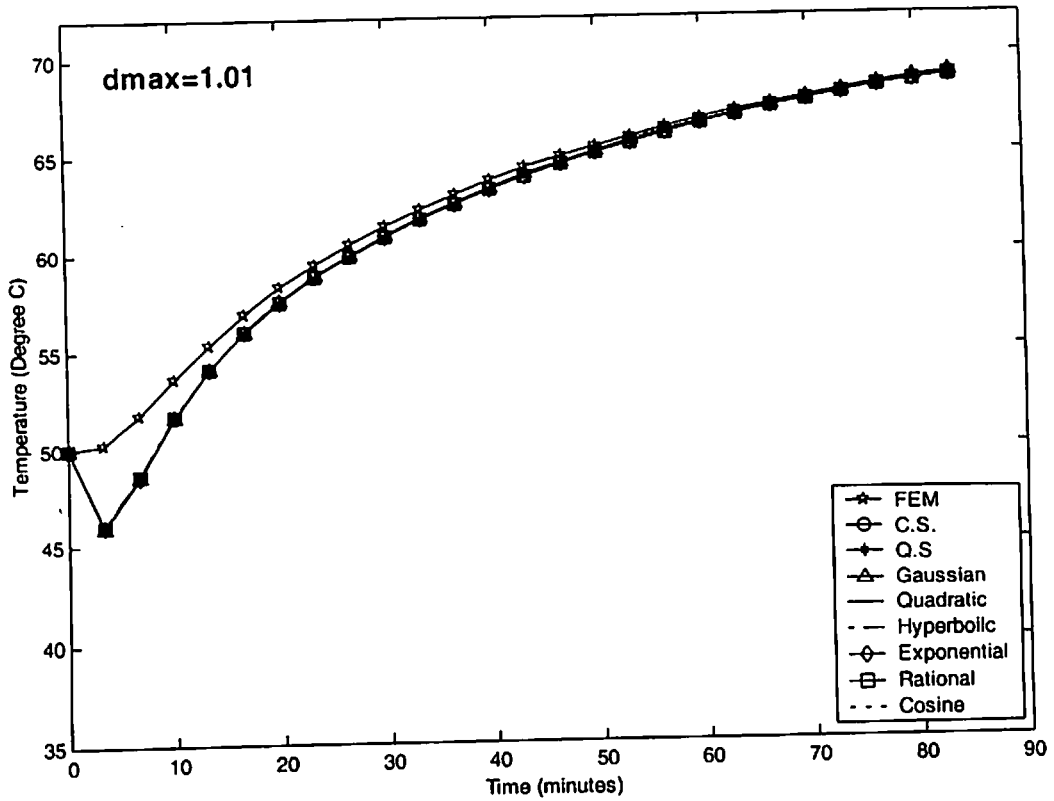


Fig. 5.5 Comparison of EFG results obtained using 25 nodes with FEM at the location ($x = 0.5\text{ m}$, $y = 1\text{ m}$) of the 2-D model shown in Fig. 5.1

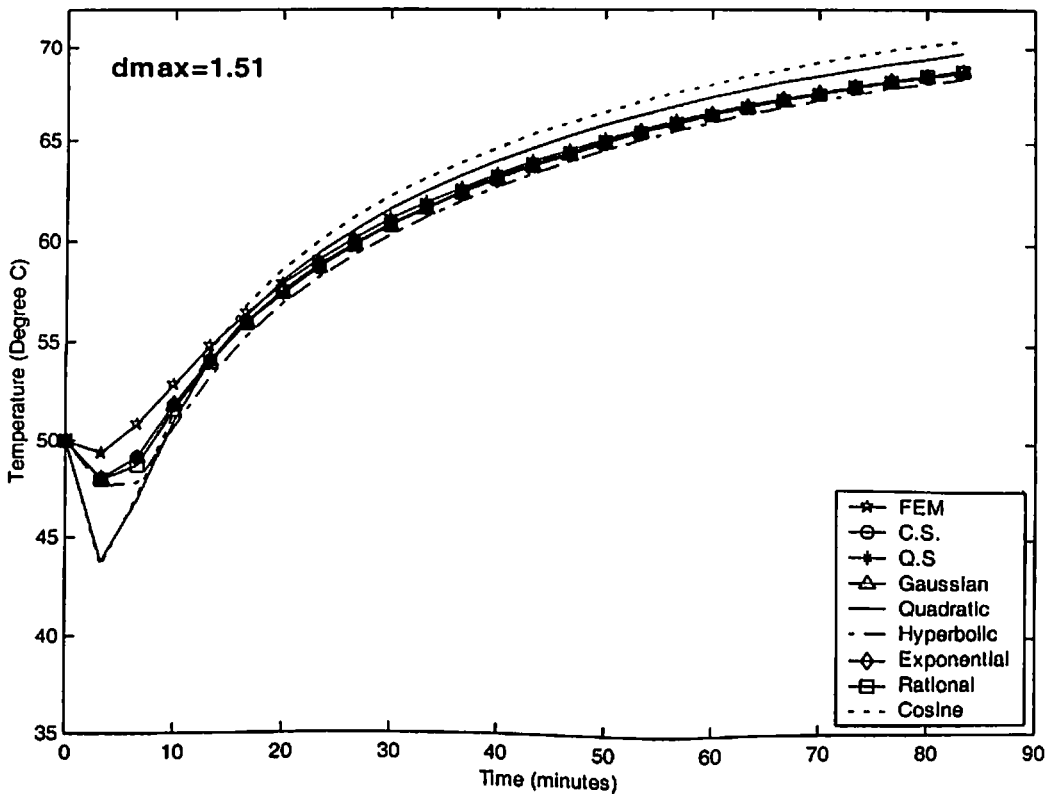
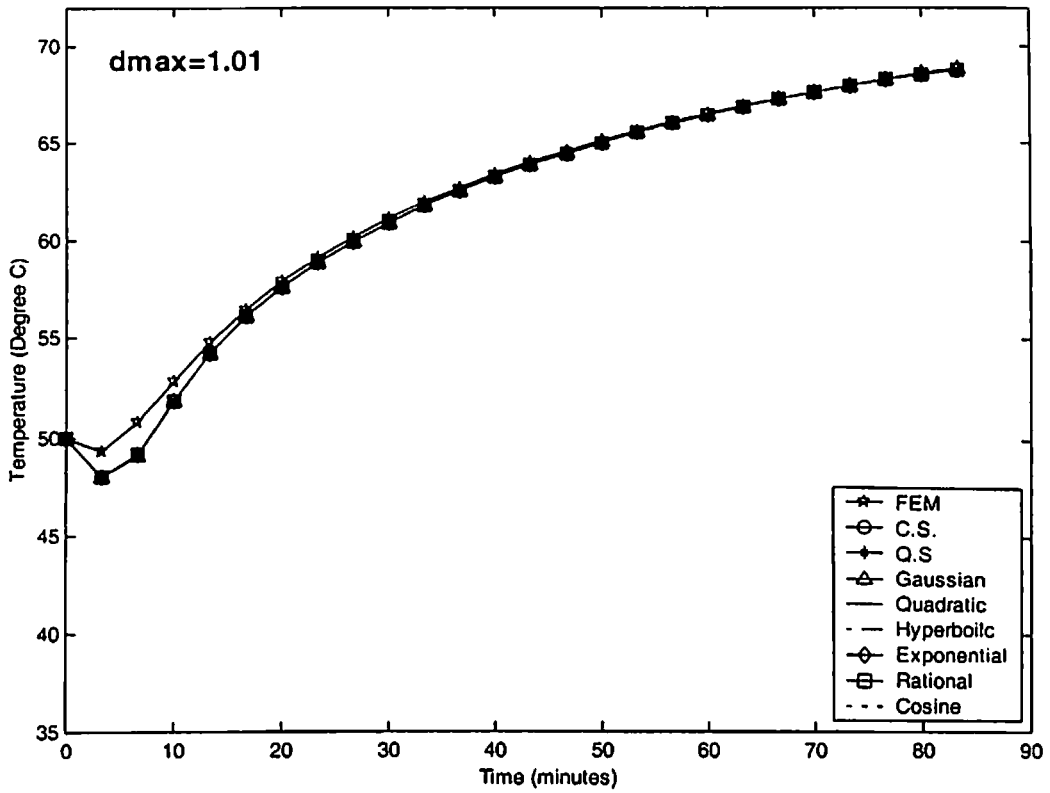


Fig. 5.6 Comparison of EFG results obtained using 81 nodes with FEM at the location ($x = 0.5$ m, $y = 1$ m) of the 2-D model shown in Fig. 5.1

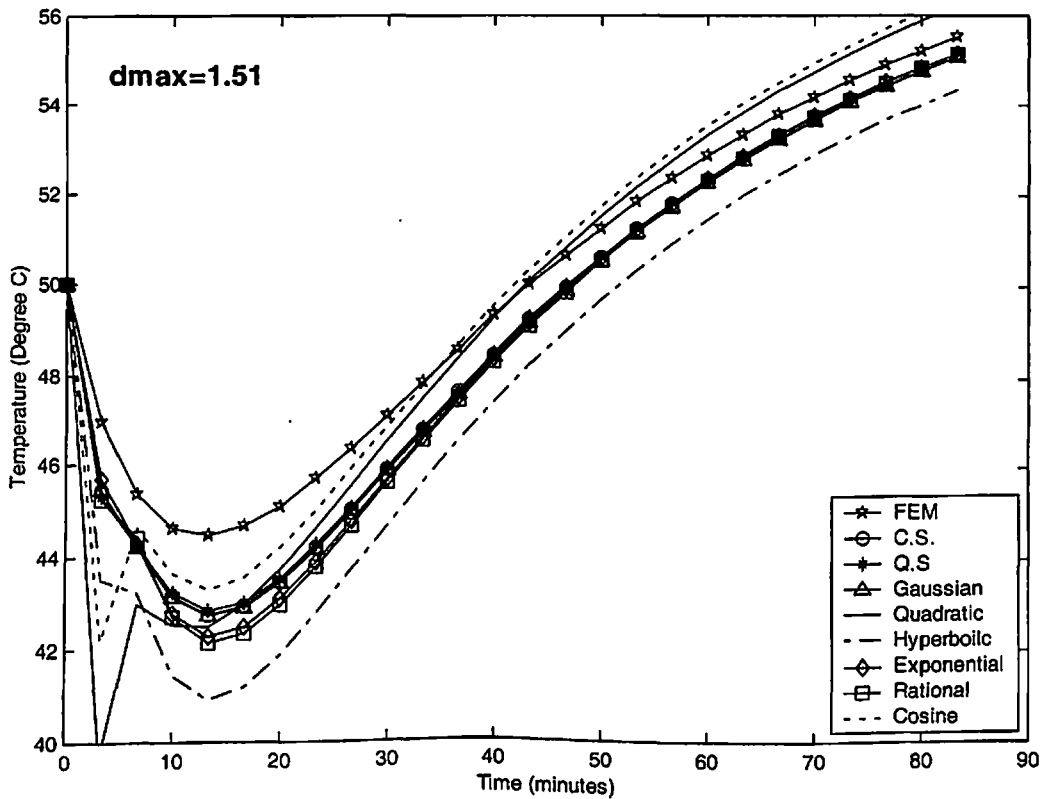
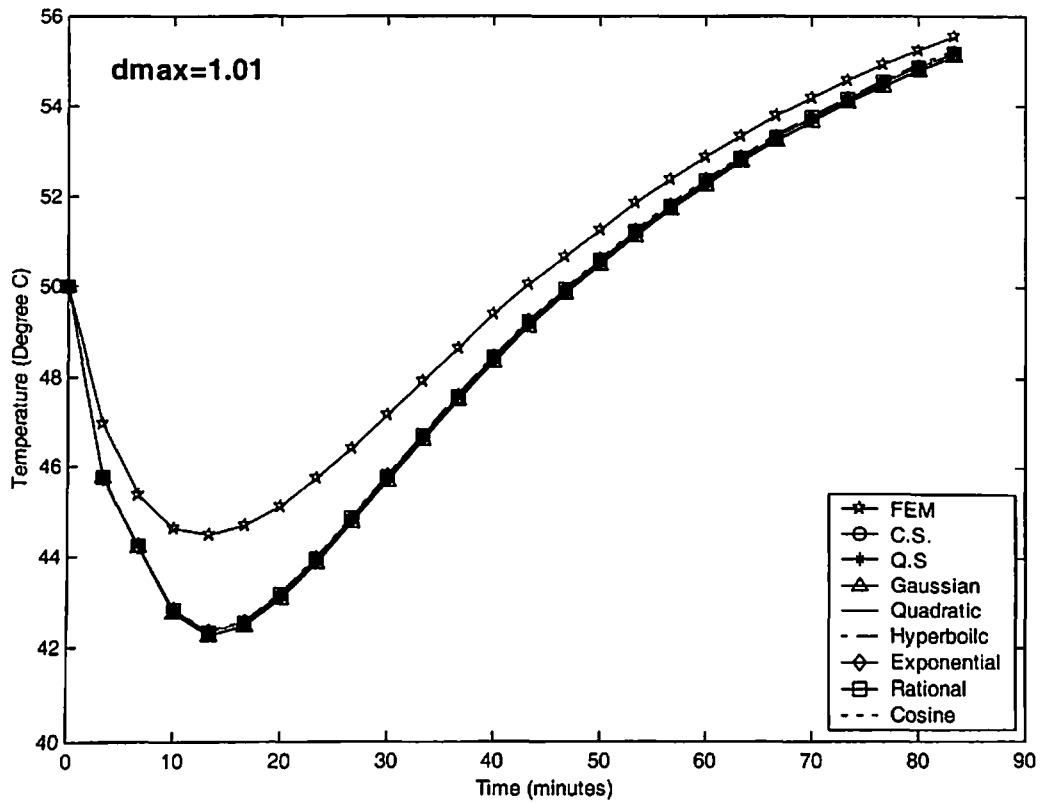


Fig. 5.7 Comparison of EFG results obtained using 25 nodes with FEM at the location $(x = 1\text{ m}, y = 1\text{ m})$ of the 2-D model shown in Fig. 5.1

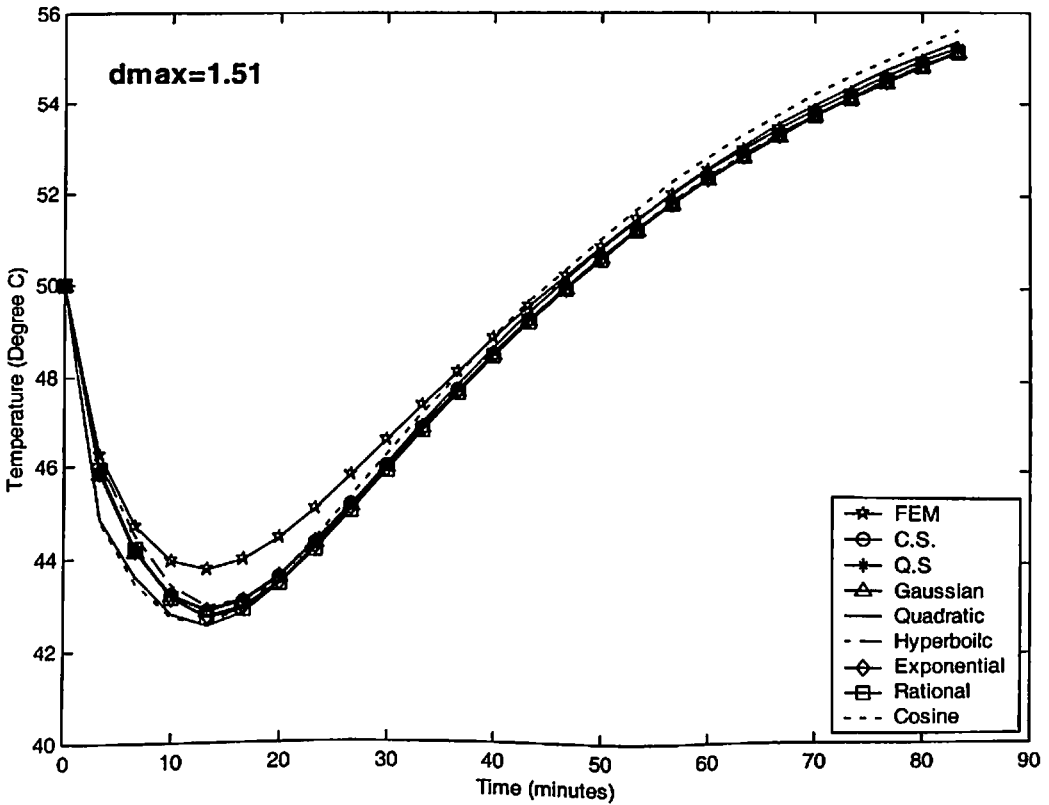
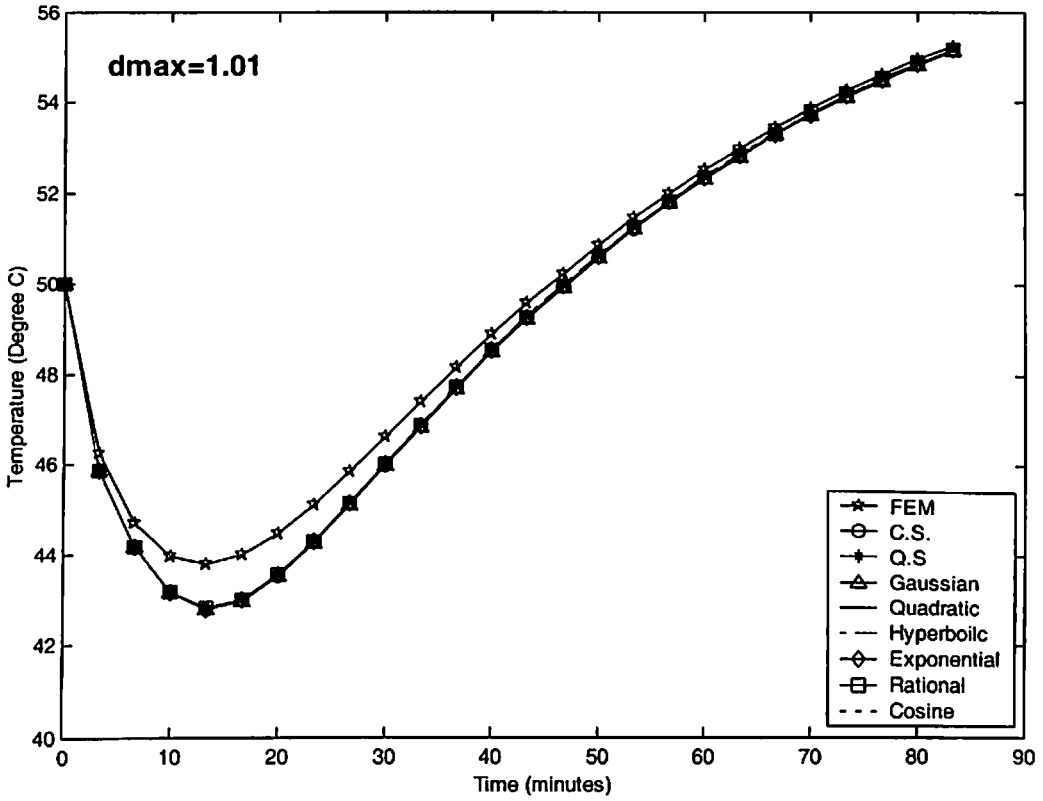


Fig. 5.8 Comparison of EFG results obtained using 81 nodes with FEM at the location $(x = 1\text{ m}, y = 1\text{ m})$ of the 2-D model shown in Fig. 5.1

➤ *CASE-II*

5.4 DISCRETIZATION OF THE GOVERNING EQUATION

The general form of energy equation for two-dimensional heat transfer in thin fins with thermal properties independent of temperature is given as:

$$k \left(\frac{\partial^2 T}{\partial x^2} + \frac{\partial^2 T}{\partial y^2} \right) - h \left(\frac{P_r}{A_c} \right) (T - T_\infty) + \dot{Q} - \rho c \frac{\partial T}{\partial t} = 0 \quad (5.11a)$$

The Initial conditions are

$$\text{at } t = 0, \quad T = T_{\text{ini}} \quad \text{in } \Omega \quad (5.11b)$$

The boundary conditions are

$$\text{at edge } \Gamma_1, \quad T = T_c \quad (5.11c)$$

$$\text{at edge } \Gamma_2, \quad k \frac{\partial T}{\partial y} = h(T - T_\infty) \quad (5.11d)$$

$$\text{at edge } \Gamma_3, \quad -k \frac{\partial T}{\partial x} = h(T - T_\infty) \quad (5.11e)$$

$$\text{at edge } \Gamma_4, \quad -k \frac{\partial T}{\partial y} = h(T - T_\infty) \quad (5.11f)$$

The weighted integral form of Eq. (5.11a) is given as:

$$\int_{\Omega} w \left\{ k \frac{\partial^2 T}{\partial x^2} + k \frac{\partial^2 T}{\partial y^2} - h \left(\frac{P_r}{A_c} \right) T + M + \dot{Q} - \rho c \frac{\partial T}{\partial t} \right\} d\Omega = 0 \quad (5.12)$$

The weak form of Eq. (5.12) will be obtained as:

$$\int_{\Omega} \left[-\frac{\partial w}{\partial x} k \frac{\partial T}{\partial x} - \frac{\partial w}{\partial y} k \frac{\partial T}{\partial y} - h \left(\frac{P_r}{A_c} \right) T w \right] d\Omega - \int_{\Omega} \rho c w \dot{T} d\Omega + \int_{\Omega} (M + \dot{Q}) w d\Omega + \int_{\Gamma} \left[w k \frac{\partial T}{\partial x} \cos(\bar{n}, x) + w k \frac{\partial T}{\partial y} \cos(\bar{n}, y) \right] d\Gamma = 0 \quad (5.13)$$

Using natural boundary conditions, the functional $I(T)$ is obtained as:

$$I(T) = \frac{1}{2} \int_{\Omega} \left[k \left(\frac{\partial T}{\partial x} \right)^2 + k \left(\frac{\partial T}{\partial y} \right)^2 \right] d\Omega + \int_{\Omega} \frac{h}{2} \left(\frac{P_r}{A_c} \right) T^2 + \int_{\Omega} \rho c \dot{T} T d\Omega - \int_{\Omega} (M + \dot{Q}) T d\Omega + \int_{\Gamma_2} \frac{h}{2} T^2 d\Gamma + \int_{\Gamma_1} \frac{h}{2} T^2 d\Gamma + \int_{\Gamma_4} \frac{h}{2} T^2 d\Gamma - \int_{\Gamma_1} h T_{\infty} T d\Gamma - \int_{\Gamma_1} h T_{\infty} T d\Gamma - \int_{\Gamma_4} h T_{\infty} T d\Gamma \quad (5.14)$$

Using Lagrange multiplier technique to enforce essential boundary conditions, the functional $I^*(T)$ is obtained as:

$$I^*(T) = \frac{1}{2} \int_{\Omega} \left[k \left(\frac{\partial T}{\partial x} \right)^2 + k \left(\frac{\partial T}{\partial y} \right)^2 \right] d\Omega + \int_{\Omega} \frac{h}{2} \left(\frac{P_r}{A_c} \right) T^2 + \int_{\Omega} \rho c \dot{T} T d\Omega - \int_{\Omega} (M + \dot{Q}) T d\Omega + \int_{\Gamma_2} \frac{h}{2} T^2 d\Gamma + \int_{\Gamma_1} \frac{h}{2} T^2 d\Gamma + \int_{\Gamma_4} \frac{h}{2} T^2 d\Gamma - \int_{\Gamma_2} h T_{\infty} T d\Gamma - \int_{\Gamma_1} h T_{\infty} T d\Gamma - \int_{\Gamma_4} h T_{\infty} T d\Gamma + \int_{\Gamma_1} \lambda (T - T_c) d\Gamma \quad (5.15)$$

Using Variational method, Eq. (5.15) can be written as:

$$\delta I^*(T) = \int_{\Omega} \left[\left(\frac{\partial T}{\partial x} \right)^T k \delta \left(\frac{\partial T}{\partial x} \right) + \left(\frac{\partial T}{\partial y} \right)^T k \delta \left(\frac{\partial T}{\partial y} \right) \right] d\Omega + \int_{\Omega} h \left(\frac{P_r}{A_c} \right) T^T \delta T d\Omega + \int_{\Omega} \rho c \dot{T} \delta T d\Omega - \int_{\Omega} (M + \dot{Q}) \delta T d\Omega + \int_{\Gamma_2} h T^T \delta T d\Gamma + \int_{\Gamma_1} h T^T \delta T d\Gamma + \int_{\Gamma_4} h T^T \delta T d\Gamma - \int_{\Gamma_2} h T_{\infty} \delta T d\Gamma - \int_{\Gamma_1} h T_{\infty} \delta T d\Gamma - \int_{\Gamma_4} h T_{\infty} \delta T d\Gamma + \int_{\Gamma_1} h T_{\infty} \delta T d\Gamma - \int_{\Gamma_1} h T_{\infty} \delta T d\Gamma + \int_{\Gamma_1} [\delta \lambda (T - T_c) + \lambda \delta T] d\Gamma \quad (5.16)$$

Since δT and $\delta \lambda$ are arbitrary in preceding equation, the following relations are obtained using Eq. (3.25) and Eq. (5.16)

$$[\mathbf{K}]\{\mathbf{T}\} + [\mathbf{C}]\{\dot{\mathbf{T}}\} + [\mathbf{G}]\{\lambda\} = \{\mathbf{f}\} \quad (5.17a)$$

$$[\mathbf{G}^T]\{\mathbf{T}\} = \{\mathbf{q}\} \quad (5.17b)$$

where

$$K_{i,j} = \int_{\Omega} \begin{bmatrix} \Phi_{i,x} \\ \Phi_{j,y} \end{bmatrix}^T \begin{bmatrix} k & 0 \\ 0 & k \end{bmatrix} \begin{bmatrix} \Phi_{i,x} \\ \Phi_{j,y} \end{bmatrix} d\Omega + \int_{\Omega} h \left(\frac{P_r}{A_c} \right) \Phi_i^T \Phi_j d\Omega + \int_{\Gamma_2} h \Phi_i^T \Phi_j d\Gamma + \int_{\Gamma_1} h \Phi_i^T \Phi_j d\Gamma + \int_{\Gamma_4} h \Phi_i^T \Phi_j d\Gamma \quad (5.18a)$$

$$C_{IJ} = \int_{\Omega} \rho c \Phi_I^T \Phi_J d\Omega \quad (5.18b)$$

$$f_I = \int_{\Omega} (M + \dot{Q}) \Phi_I d\Omega + \int_{\Gamma_1} h T_{\infty} \Phi_I d\Gamma + \int_{\Gamma_2} h T_{\infty} \Phi_I d\Gamma + \int_{\Gamma_3} h T_{\infty} \Phi_I d\Gamma \quad (5.18c)$$

$$G_{IK} = \int_{\Gamma_1} \Phi_I N_K d\Gamma \quad (5.18d)$$

$$q_K = \int_{\Gamma_1} T_c N_K d\Gamma \quad (5.18e)$$

Using Crank-Nicolson technique for time approximation, the Eq. (5.17) can be written as:

$$\begin{bmatrix} \mathbf{K}^* + \mathbf{C} & \mathbf{G} \\ \mathbf{G}^T & 0 \end{bmatrix} \begin{bmatrix} \mathbf{T}_N \\ \lambda \end{bmatrix} = \begin{bmatrix} \mathbf{R}_N \\ \mathbf{q} \end{bmatrix} \quad (5.19)$$

where

$$\mathbf{R}_N = ((\mathbf{C}) - (1 - \alpha) \Delta t [\mathbf{K}]) \{\mathbf{T}\}_{N-1} + \alpha \Delta t \{\mathbf{f}\}_N + (1 - \alpha) \Delta t \{\mathbf{f}\}_{N-1} \quad (5.20a)$$

$$\mathbf{K}^* = \alpha \Delta t [\mathbf{K}] \quad (5.20b)$$

5.5 NUMERICAL RESULTS AND DISCUSSION

The different parameters used for steady-state and transient analysis of two-dimensional fin model shown in Fig. 5.9 are tabulated in Table 5.23. The EFG results are obtained using different weight functions for two sets of nodes and the FEM results are obtained using 4 node quadrilateral elements (PLANE 55, ANSYS 6.0) for same sets of nodes. A comparative study is carried out to evaluate the performance of different EFG weight functions.

5.5.1 Steady-state analysis

The results (i.e. temperature values) presented in Table 5.24 are obtained using different EFG weight functions for two values of scaling parameter (i.e. $d_{\max} = 1.01$ & $d_{\max} = 1.51$) at the location ($x = 0.025$ m, $y = 0$ m) and it shows a comparison of temperature values obtained by EFG method using different weight functions with FEM for 25 nodes. Table 5.25 shows a

comparison of temperature values obtained by EFG method using different functions for two values of scaling parameter with FEM at the same location i.e. ($x = 0.025$ m, $y = 0$ m) for 81 nodes. A comparison of temperature values obtained using different EFG weight functions with FEM for 25 and 81 nodes, is shown in Table 5.26 and Table 5.27 respectively at the location ($x = 0.05$ m, $y = 0$ m). Similar type of comparisons of temperature values are shown in Table 5.28 for 25 nodes at the location ($x = 0.075$ m, $y = 0$ m), in Table 5.29 for 81 nodes at the location ($x = 0.075$ m, $y = 0$ m), in Table 5.30 for 25 nodes at the location ($x = 0.1$ m, $y = 0$ m) and in Table 5.31 for 81 nodes at the location ($x = 0.1$ m, $y = 0$ m). From the results presented in Table 5.24 to Table 5.31, it is observed that EFG results obtained using different weight functions are almost similar for $d_{\max} = 1.01$. However for $d_{\max} = 1.51$, only cubicspline, quarticspline, Gaussian, exponential and rational weight functions give acceptable results. It is also observed that EFG results obtained using different weight functions are in good agreement with those obtained by FEM. Moreover with the increase in number of nodes EFG results starts converging.

The effect of scaling parameter (d_{\max}) on EFG results obtained using different weight functions is presented in Table 5.32 for 25 nodes and Table 5.33 for 81 nodes respectively at the location ($x = 0.025$ m, $y = 0$ m). The similar effect of scaling parameter on EFG results is shown in Table 5.34 for 25 nodes and Table 5.35 for 81 nodes at the location ($x = 0.075$ m, $y = 0.0$ m). Fig. 5.10 shows the effect of scaling parameter on EFG results obtained using 25 and 81 nodes at the location ($x = 0.05$ m, $y = 0$ m). The similar effect of scaling parameter on EFG results is observed in Fig. 5.11 at the location ($x = 0.1$ m, $y = 0$ m). From tables and figures, it is clear that only cubicspline, quarticspline, Gaussian, exponential and rational weight functions give acceptable results in the range $1.0 < d_{\max} < 2.2$ whereas the results obtained using quadratic, hyperbolic and cosine weight functions are varying in abrupt

manner with scaling parameter. Therefore EFG results obtained using quadratic, hyperbolic and cosine weight functions are not acceptable in the range $1.0 < d_{\text{max}} < 2.2$. It is also observed that there is minimum variation in EFG results with scaling parameter for exponential weight function.

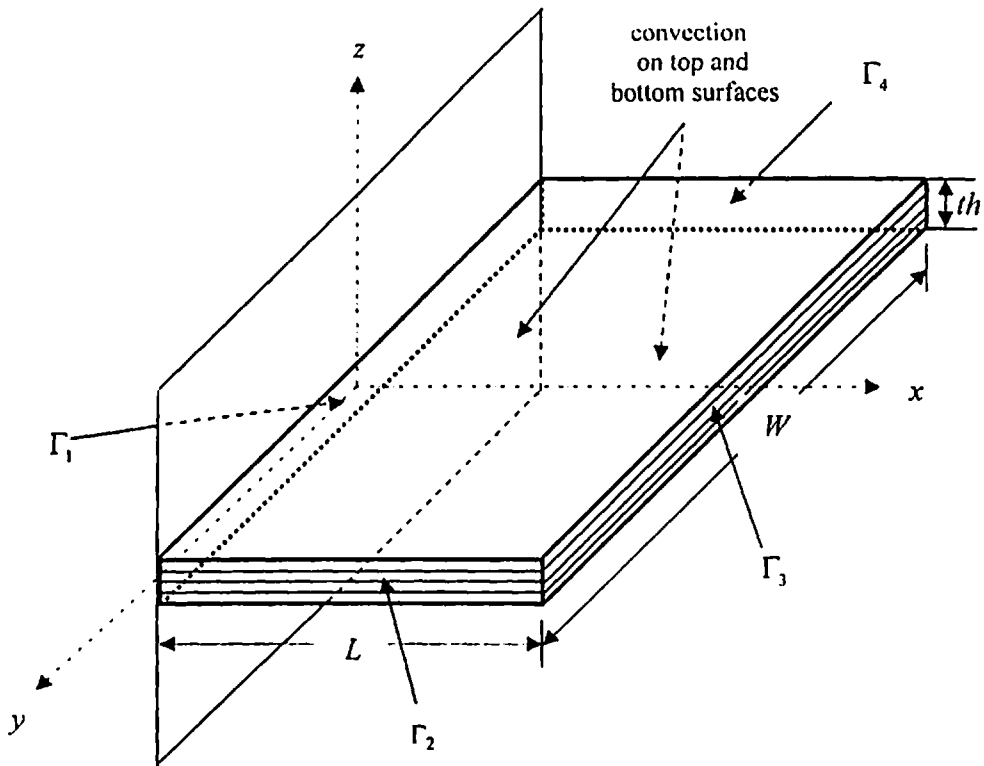


Fig. 5.9 Two-dimensional fin model

Table 5.23 Data for the 2-D model shown in Fig. 5.9

Parameters	Value of the parameter
Length (L)	0.1 m
Width (W)	0.5 m
Thickness (th)	0.005 m
Thermal conductivity (k)	400 W/m-K
Density of the material (ρ)	10000 kg/m ³
Specific heat (c)	400 kJ/kg-K
Rate of internal heat generation (\dot{Q})	0 W/m ³
Heat transfer coefficient (h)	200 W/m ² -K
Surrounding fluid temperature (T_{∞})	20 °C
Initial temperature (T_{in})	100 °C
Time step size (Δt)	1 sec
Temperature at surface, $x = 0$ or Γ_1	100 °C

Table 5.24 Comparison of EFG results obtained using 25 nodes with FEM results at the location ($x = 0.025$ m, $y = 0$ m) of the 2-D model shown in Fig. 5.9

Weight function	EFG				FEM
	$d_{\max} = 1.01$		$d_{\max} = 1.51$		
	T (°C)	% diff with FEM	T (°C)	% diff with FEM	T (°C)
C. S.	78.9253	-0.0100	78.2290	-0.8922	78.9332
Q. S.	78.9219	-0.0143	77.9781	-1.2100	
Gaussian	78.9339	0.0009	78.1674	-0.9702	
Quadratic	78.9173	-0.0201	78.6725	-0.3303	
Hyperbolic	78.9033	-0.0379	80.6879	2.22302	
Exponential	78.9208	-0.0157	78.8023	-0.1658	
Rational	78.9176	-0.0198	78.5387	-0.4998	
Cosine	78.9173	-0.0201	76.8266	-2.6688	

Table 5.25 Comparison of EFG results obtained using 81 nodes with FEM results at the location ($x = 0.025$ m, $y = 0$ m) of the 2-D model shown in Fig. 5.9

Weight function	EFG				FEM
	$d_{\max} = 1.01$		$d_{\max} = 1.51$		
	T (°C)	% diff with FEM	T (°C)	% diff with FEM	T (°C)
C. S.	79.0316	0.0020	78.9000	-0.1645	79.0300
Q. S.	79.0317	0.0022	78.8690	-0.2037	
Gaussian	79.0310	0.0013	78.8944	-0.1716	
Quadratic	79.0317	0.0022	77.7539	-1.6147	
Hyperbolic	79.0311	0.0014	77.3418	-2.1362	
Exponential	79.0317	0.0022	79.0067	-0.0295	
Rational	79.0317	0.0022	78.9291	-0.1277	
Cosine	79.0317	0.0022	78.2422	-0.9968	

Table 5.26 Comparison of EFG results obtained using 25 nodes with FEM results at the location ($x = 0.05$ m, $y = 0$ m) of the 2-D model shown in Fig. 5.9

Weight function	EFG				FEM
	$d_{\max} = 1.01$		$d_{\max} = 1.51$		
	T (°C)	% diff with FEM	T (°C)	% diff with FEM	T (°C)
C. S.	65.4678	0.0003	65.1003	-0.5610	65.4676
Q. S.	65.4665	-0.0017	65.0158	-0.6901	
Gaussian	65.4704	0.0043	65.0533	-0.6328	
Quadratic	65.4646	-0.0046	62.6604	-4.2879	
Hyperbolic	65.4539	-0.0209	51.0138	-22.0778	
Exponential	65.4661	-0.0023	65.3739	-0.1431	
Rational	65.4648	-0.0043	64.9276	-0.8248	
Cosine	65.4646	-0.0046	64.4427	-1.5655	

Table 5.27 Comparison of EFG results obtained using 81 nodes with FEM results at the location ($x = 0.05$ m, $y = 0$ m) of the 2-D model shown in Fig. 5.9

Weight function	EFG				FEM
	$d_{\max} = 1.01$		$d_{\max} = 1.51$		
	T (°C)	% diff with FEM	T (°C)	% diff with FEM	T (°C)
C. S.	65.6157	0.0040	65.5305	-0.1259	65.6131
Q. S.	65.6159	0.0043	65.5061	-0.1631	
Gaussian	65.6146	0.0023	65.5273	-0.1308	
Quadratic	65.6161	0.0046	64.7220	-1.3581	
Hyperbolic	65.6171	0.0061	64.7906	-1.2536	
Exponential	65.6160	0.0044	65.5957	-0.0265	
Rational	65.6161	0.0046	65.5360	-0.1175	
Cosine	65.6161	0.0046	65.1452	-0.7131	

Table 5.28 Comparison of EFG results obtained using 25 nodes with FEM results at the location ($x = 0.075$ m, $y = 0$ m) of the 2-D model shown in Fig. 5.9

Weight function	EFG				FEM
	$d_{\max} = 1.01$		$d_{\max} = 1.51$		
	T (°C)	% diff with FEM	T (°C)	% diff with FEM	T (°C)
C. S.	57.8746	0.0147	57.5384	-0.5663	57.8661
Q. S.	57.8752	0.0157	57.3988	-0.8075	
Gaussian	57.8712	0.0088	57.4837	-0.6608	
Quadratic	57.8760	0.0171	56.4201	-2.4989	
Hyperbolic	57.8796	0.0233	53.0406	-8.3391	
Exponential	57.8753	0.0159	57.7956	-0.1218	
Rational	57.8759	0.0169	57.3988	-0.8075	
Cosine	57.8760	0.0171	55.5802	-3.9503	

Table 5.29 Comparison of EFG results obtained using 81 nodes with FEM results at the location ($x = 0.075$ m, $y = 0$ m) of the 2-D model shown in Fig. 5.9

Weight function	EFG				FEM
	$d_{\max} = 1.01$		$d_{\max} = 1.51$		
	T (°C)	% diff with FEM	T (°C)	% diff with FEM	T (°C)
C. S.	58.0365	0.0057	57.9781	-0.0949	58.0332
Q. S.	58.0367	0.0060	57.9624	-0.1220	
Gaussian	58.0351	0.0033	57.9770	-0.0968	
Quadratic	58.0370	0.0065	57.4874	-0.9405	
Hyperbolic	58.0376	0.0076	57.5142	-0.8943	
Exponential	58.0368	0.0062	58.0192	-0.0241	
Rational	58.0369	0.0064	57.9694	-0.1099	
Cosine	58.0370	0.0065	57.7993	-0.4031	

Table 5.30 Comparison of EFG results obtained using 25 nodes with FEM results at the location ($x = 0.1$ m, $y = 0$ m) of the 2-D model shown in Fig. 5.9

Weight function	EFG				FEM
	$d_{\max} = 1.01$		$d_{\max} = 1.51$		
	T (°C)	% diff with FEM	T (°C)	% diff with FEM	T (°C)
C. S.	55.1611	0.0218	55.2817	0.2404	55.1491
Q. S.	55.1624	0.0241	55.2864	0.2490	
Gaussian	55.1556	0.0118	55.2547	0.1915	
Quadratic	55.1643	0.0276	53.7781	-2.4860	
Hyperbolic	55.1735	0.0442	50.7471	-7.9820	
Exponential	55.1627	0.0247	55.1501	0.0018	
Rational	55.1640	0.0270	54.9228	-0.4103	
Cosine	55.1642	0.0274	54.6856	-0.8404	

Table 5.31 Comparison of EFG results obtained using 81 nodes with FEM results at the location ($x = 0.1$ m, $y = 0$ m) of the 2-D model shown in Fig. 5.9

Weight function	EFG				FEM
	$d_{\max} = 1.01$		$d_{\max} = 1.51$		
	T (°C)	% diff with FEM	T (°C)	% diff with FEM	T (°C)
C. S.	55.3251	0.0063	55.3679	0.0837	55.3216
Q. S.	55.3253	0.0067	55.3751	0.0967	
Gaussian	55.3236	0.0036	55.3720	0.0911	
Quadratic	55.3255	0.0071	54.9866	-0.6055	
Hyperbolic	55.3260	0.0079	54.9078	-0.7480	
Exponential	55.3253	0.0067	55.3227	0.0020	
Rational	55.3255	0.0071	55.3112	-0.0188	
Cosine	55.3255	0.0071	55.1836	-0.2494	

Table 5.32 Effect of scaling parameter on EFG results obtained using 25 nodes at the location ($x = 0.025$ m, $y = 0$ m) of the 2-D model shown in Fig. 5.9

Scaling Parameter	Temperature (° C)							
	C. S.	Q. S	Gaussian	Quadratic	Hyperbolic	Exponential	Rational	Cosine
1.01	78.9253	78.9219	78.9339	78.9173	78.9033	78.9208	78.9176	78.9173
1.21	78.9458	78.7933	78.5050	78.6012	79.2879	78.5410	78.4830	78.5456
1.41	78.4441	78.3065	78.3016	74.3942	89.8743	78.8364	78.5891	74.6343
1.61	77.9953	77.6535	77.9865	77.4406	73.2692	78.7639	78.5147	82.4519
1.81	77.4911	77.0788	77.1818	71.0002	65.4923	78.6177	77.3549	71.9522
2.01	76.8503	76.2601	75.7782	73.6565	-97.0165	78.1779	76.5716	73.9996
2.21	76.1158	75.3736	73.7862	54.6754	61.0360	77.9004	75.9728	62.1502
2.41	75.2633	74.2509	71.4025	81.5800	103.2780	77.7040	74.8151	52.8964
2.61	74.1258	72.7110	69.5912	11.3831	70.7815	77.4478	74.0315	-59.8030
2.81	72.5850	70.7921	69.4777	72.3416	14.4284	76.9627	71.6726	58.7438
3.01	70.8114	68.7511	74.1502	118.2802	74.0396	76.9264	73.4991	-57.5047

Table 5.33 Effect of scaling parameter on EFG results obtained using 81 nodes at the location ($x = 0.025$ m, $y = 0$ m) of the 2-D model shown in Fig. 5.9

Scaling Parameter	Temperature (° C)							
	C. S.	Q. S	Gaussian	Quadratic	Hyperbolic	Exponential	Rational	Cosine
1.01	79.0316	79.0317	79.0310	79.0317	79.0311	79.0317	79.0317	79.0317
1.21	79.0378	79.0033	78.9385	78.9707	78.8983	78.9508	78.9427	78.9628
1.41	78.9341	78.9120	78.9083	80.2224	76.8851	79.0139	78.9484	79.7083
1.61	78.8711	78.8431	78.8795	76.7918	77.9148	78.9986	78.9089	75.6180
1.81	78.8294	78.8079	78.8328	80.9034	110.7047	78.9471	79.0005	79.4189
2.01	78.7901	78.7537	78.7850	78.1114	121.8266	78.8941	78.8991	77.9872
2.21	78.7299	78.6476	78.6811	75.5662	125.5869	78.7876	78.5628	74.3729
2.41	78.6422	78.5493	78.3339	75.1932	341.3382	78.7636	78.2353	107.0409
2.61	78.5178	78.4129	77.2444	189.6853	396.7575	78.7117	78.1005	99.0273
2.81	78.5161	78.5490	73.8098	75.5172	53.0444	78.5863	78.2738	71.3211
3.01	78.5948	78.6267	64.4641	74.9076	148.0824	78.5494	78.6318	78.3582

Table 5.34 Effect of scaling parameter on EFG results obtained using 25 nodes at the location ($x = 0.075$ m, $y = 0.0$ m) of the 2-D model shown in Fig. 5.9

Scaling Parameter	Temperature ($^{\circ}$ C)							
	C. S.	Q. S	Gaussian	Quadratic	Hyperbolic	Exponential	Rational	Cosine
1.01	57.8746	57.8752	57.8712	57.8760	57.8796	57.8753	57.8759	57.8760
1.21	57.8889	57.8185	57.6887	57.6012	57.2401	57.7056	57.6119	57.6058
1.41	57.6493	57.5742	57.5781	56.4102	54.6994	57.8225	57.4733	56.2455
1.61	57.4062	57.2068	57.3359	53.4502	52.0929	57.7691	57.2295	57.0393
1.81	57.0901	56.8010	56.6598	58.9142	59.0655	57.5950	56.9348	57.6480
2.01	56.6639	56.2500	55.3539	57.3769	181.0480	57.4303	56.8183	58.5884
2.21	56.1767	55.6995	53.1823	62.6744	368.5014	57.3079	57.0419	58.0965
2.41	55.5990	54.9900	50.1893	-54.4344	420.9001	57.1865	57.9848	-84.8511
2.61	54.9406	54.2434	46.7893	334.4398	464.7938	57.0977	58.5314	380.4588
2.81	54.0734	53.3547	44.4117	77.6047	291.1382	57.0111	60.3150	61.4879
3.01	53.2122	52.8916	46.2044	133.9311	112.5215	56.7765	56.2352	-24.0250

Table 5.35 Effect of scaling parameter on EFG results obtained using 81 nodes at the location ($x = 0.075$ m, $y = 0.0$ m) of the 2-D model shown in Fig. 5.9

Scaling Parameter	Temperature ($^{\circ}$ C)							
	C. S.	Q. S	Gaussian	Quadratic	Hyperbolic	Exponential	Rational	Cosine
1.01	58.0365	58.0367	58.0351	58.0370	58.0376	58.0368	58.0369	58.0370
1.21	58.0398	58.0252	57.9987	57.9927	57.9982	58.0041	57.9910	57.9908
1.41	57.9948	57.9834	57.9845	58.4387	57.6270	58.0245	57.9779	58.4096
1.61	57.9628	57.9474	57.9685	56.8013	57.3960	58.0134	57.9619	56.5798
1.81	57.9374	57.9240	57.9342	57.7705	64.8813	57.9851	57.9181	57.6485
2.01	57.9101	57.8881	57.8577	57.5227	121.4559	57.9439	57.9120	57.9942
2.21	57.8746	57.8369	57.6812	59.6280	86.6050	57.9046	57.8965	60.4621
2.41	57.8277	57.7833	57.3167	52.1799	-7.6435	57.8817	57.6801	69.7560
2.61	57.7717	57.7114	56.6642	149.8567	7.9674	57.8580	57.6700	101.5847
2.81	57.7532	57.6707	55.4230	52.5576	79.3609	57.7824	57.1237	52.9092
3.01	57.7581	57.4344	52.7549	56.9843	-436.7320	57.7212	56.5333	55.9333

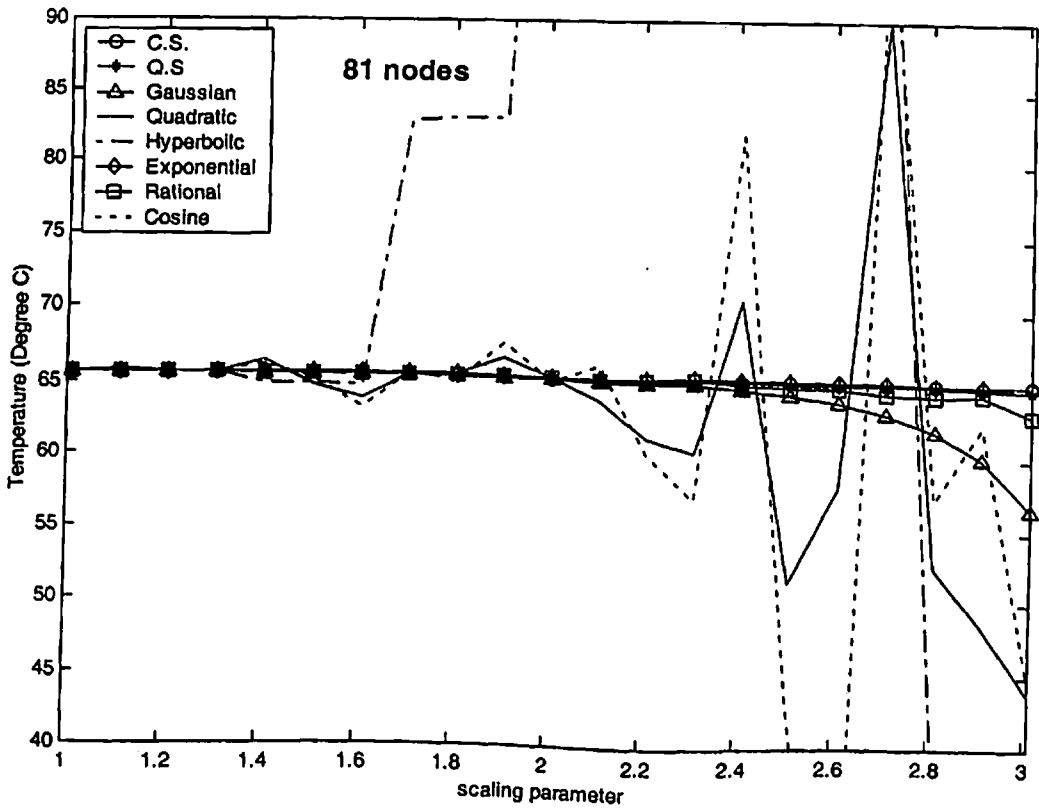
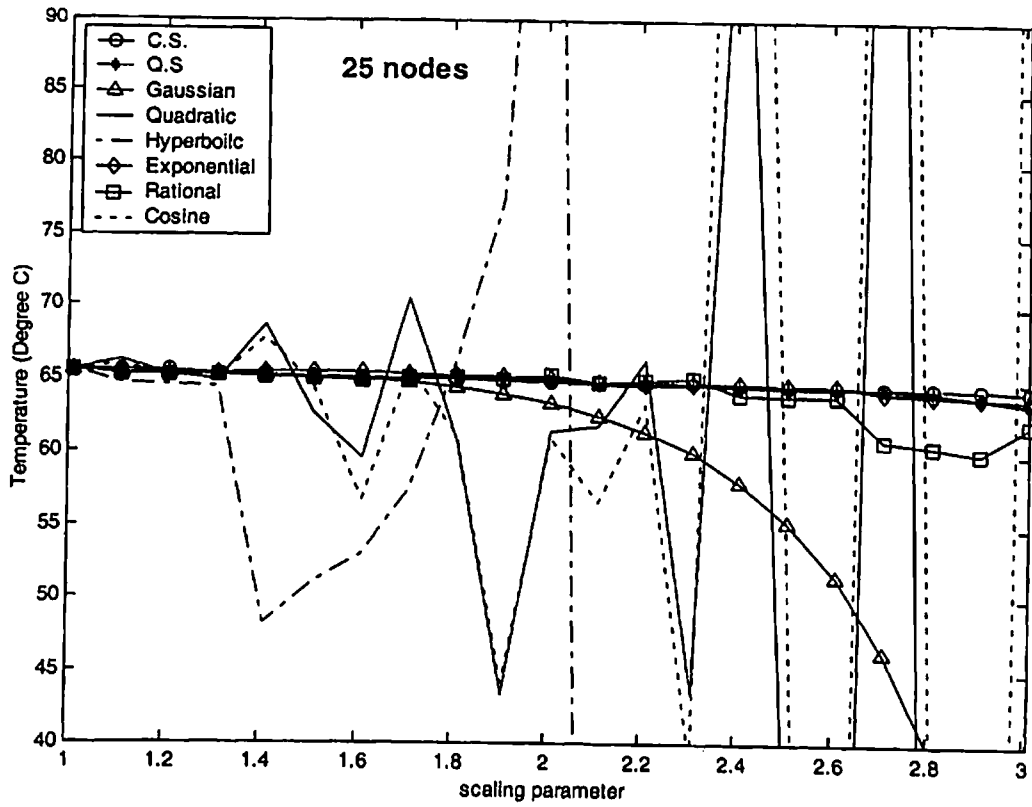


Fig. 5.10 Effect of scaling parameter on EFG results at the location ($x = 0.05$ m, $y = 0$ m) of the 2-D model shown in Fig. 5.9

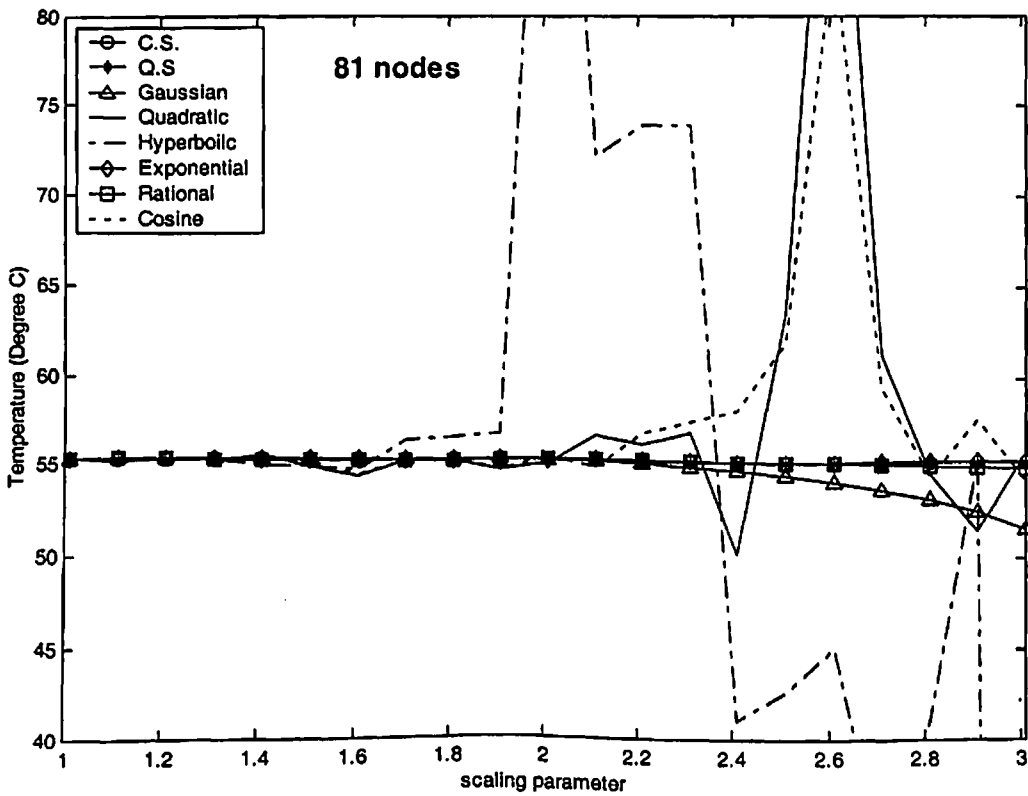
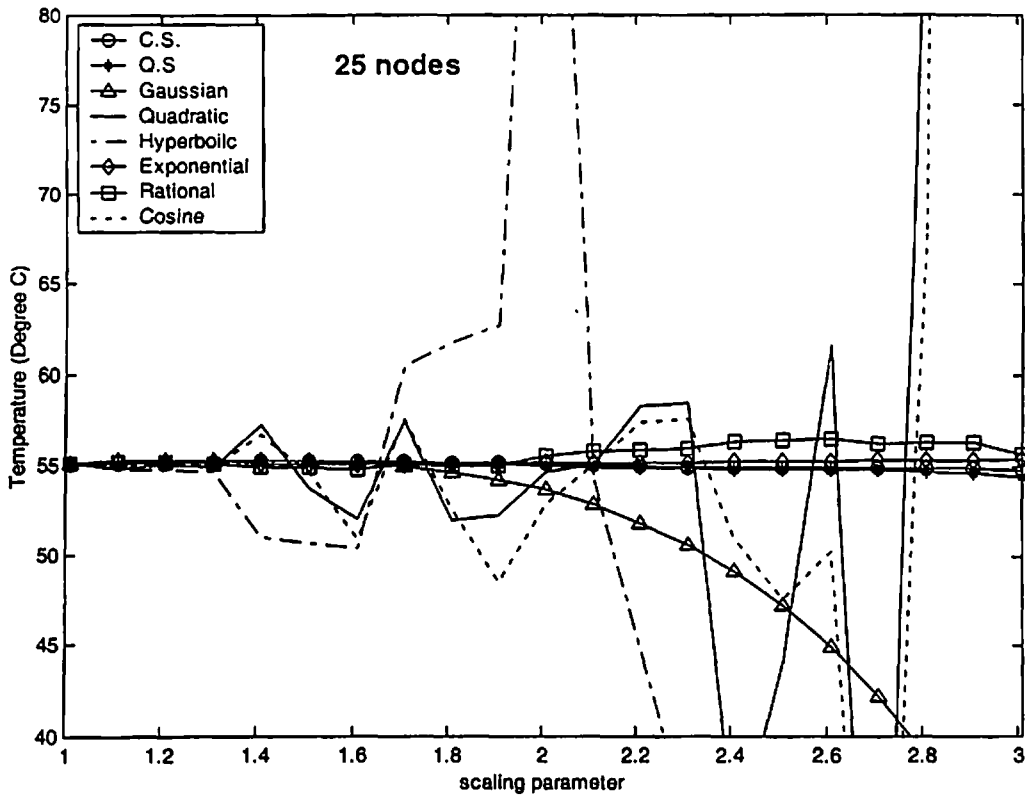


Fig. 5.11 Effect of scaling parameter on EFG results at the location ($x = 0.1 \text{ m}$, $y = 0 \text{ m}$) of the 2-D model shown in Fig. 5.9

5.5.2 Transient analysis

The transient analysis of 2-D model, shown in Fig. 5.9, is carried out using different EFG weight functions. Table 5.36 and Table 5.37 show the comparison of EFG results (i.e. temperature values) obtained using 25 nodes with FEM results at the location ($x = 0.025$ m, $y = 0$ m) for $d_{\max} = 1.01$ and $d_{\max} = 1.51$ respectively. Similar comparison of temperature values obtained using 81 nodes is presented in Table 5.38 and Table 5.39 for $d_{\max} = 1.01$ and $d_{\max} = 1.51$ respectively at the same location i.e. ($x = 0.025$ m, $y = 0$ m). For this case (i.e. CASE-II) of 2-D transient analysis, time step of 1 sec has been taken which is nearly 1% of the total time required to achieve steady state condition. Table 5.40 and Table 5.41 show the comparison of EFG results (i.e. temperature values) obtained using 25 nodes with FEM results at the location ($x = 0.075$ m, $y = 0$ m) for $d_{\max} = 1.01$ and $d_{\max} = 1.51$ respectively. Similar comparison of temperature values obtained using 81 nodes is also presented in Table 5.42 and Table 5.43 for $d_{\max} = 1.01$ and $d_{\max} = 1.51$ respectively at the same location i.e. ($x = 0.075$ m, $y = 0$ m). Fig 5.12 shows the comparison of EFG results (i.e. temperature values) obtained using 25 nodes with FEM results for $d_{\max} = 1.01$ and $d_{\max} = 1.51$ at the location ($x = 0.05$ m, $y = 0$ m). Similar comparison of temperature values obtained using 81 nodes is shown in Fig. 5.13 at the same location i.e. ($x = 0.05$ m, $y = 0$ m). Fig 5.14 shows the comparison of EFG results (i.e. temperature values) obtained using 25 nodes with FEM results for $d_{\max} = 1.01$ and $d_{\max} = 1.51$ at the location ($x = 0.1$ m, $y = 0$ m). Similar comparison of temperature values obtained using 81 nodes is shown in Fig. 5.15 at the same location i.e. ($x = 0.1$ m, $y = 0$ m). From the results presented in tables and figures, it is clear that the EFG results obtained using different weight functions are almost similar for $d_{\max} = 1.01$ but for $d_{\max} = 1.51$ only cubicspline, quarticspline, Gaussian, exponential and rational weight functions give acceptable results. It is also observed that the EFG results are in good agreement with those obtained by FEM.

Table 5.36 Comparison of EFG results obtained using 25 nodes with FEM at the location ($x = 0.025$ m, $y = 0$ m) of the 2-D model shown in Fig. 5.9 for $d_{max} = 1.01$

Time (sec)	Temperature ($^{\circ}$ C)								
	$d_{max} = 1.01$								FEM
	C. S.	Q. S	Gaussian	Quadratic	Hyperbolic	Exponential	Rational	Cosine	
0	100.0000	100.0000	100.0000	100.0000	100.0000	100.0000	100.0000	100.0000	100.0000
10	90.4700	90.4658	90.4858	90.4606	90.4481	90.4645	90.4609	90.4606	90.4927
20	86.1218	86.1172	86.1381	86.1112	86.0969	86.1157	86.1116	86.1112	86.1427
30	83.4600	83.4557	83.4738	83.4500	83.4353	83.4543	83.4503	83.4500	83.4758
40	81.7853	81.7814	81.7965	81.7762	81.7616	81.7801	81.7765	81.7761	81.7969
50	80.7285	80.7249	80.7380	80.7200	80.7057	80.7238	80.7203	80.7200	80.7376
60	80.0617	80.0583	80.0703	80.0536	80.0395	80.0572	80.0539	80.0536	80.0696
70	79.6412	79.6378	79.6494	79.6332	79.6193	79.6367	79.6335	79.6332	79.6487
80	79.3761	79.3728	79.3842	79.3682	79.3543	79.3717	79.3685	79.3682	79.3837
90	79.2091	79.2058	79.2172	79.2012	79.1873	79.2047	79.2015	79.2012	79.2168
100	79.1039	79.1006	79.1121	79.0960	79.0821	79.0995	79.0963	79.0960	79.1118

Table 5.37 Comparison of EFG results obtained using 25 nodes with FEM at the location ($x = 0.025$ m, $y = 0$ m) of the 2-D model shown in Fig. 5.9 for $d_{max} = 1.51$

Time (sec)	Temperature ($^{\circ}$ C)								
	$d_{max} = 1.51$								FEM
	C. S.	Q. S	Gaussian	Quadratic	Hyperbolic	Exponential	Rational	Cosine	
0	100.0000	100.0000	100.0000	100.0000	100.0000	100.0000	100.0000	100.0000	100.0000
10	89.9657	89.7626	89.9320	89.5162	90.3862	90.3597	89.9835	88.0928	90.4927
20	85.5286	85.3005	85.4812	85.4522	86.5907	86.0046	85.6638	83.8406	86.1427
30	82.8340	82.5981	82.7798	82.9580	84.3403	83.3406	83.0265	81.2605	83.4758
40	81.1396	80.8994	81.0816	81.3808	82.9539	81.6648	81.3674	79.6310	81.7969
50	80.0687	79.8256	80.0088	80.3823	82.0963	80.6073	80.3208	78.5987	80.7376
60	79.3915	79.1462	79.3306	79.7510	81.5647	79.9399	79.6609	77.9454	80.0696
70	78.9633	78.7164	78.9020	79.3522	81.2345	79.5190	79.2450	77.5324	79.6487
80	78.6927	78.4446	78.6312	79.1006	81.0291	79.2536	78.9831	77.2716	79.3837
90	78.5217	78.2727	78.4601	78.9420	80.9011	79.0864	78.8182	77.1070	79.2168
100	78.4137	78.1642	78.3521	78.8421	80.8212	78.9811	78.7144	77.0032	79.1118

Table 5.38 Comparison of EFG results obtained using 81 nodes with FEM at the location ($x = 0.025$ m, $y = 0$ m) of the 2-D model shown in Fig. 5.9 for $d_{max} = 1.01$

Time (sec)	Temperature ($^{\circ}$ C)								
	$d_{max} = 1.01$								FEM
	C. S.	Q. S	Gaussian	Quadratic	Hyperbolic	Exponential	Rational	Cosine	
0	100.0000	100.0000	100.0000	100.0000	100.0000	100.0000	100.0000	100.0000	100.000
10	90.6136	90.6136	90.6133	90.6136	90.6126	90.6136	90.6136	90.6136	90.6130
20	86.2451	86.2451	86.2453	86.2450	86.2440	86.2450	86.2450	86.2450	86.2452
30	83.5811	83.5810	83.5813	83.5809	83.5799	83.5810	83.5809	83.5809	83.5810
40	81.9057	81.9057	81.9057	81.9057	81.9047	81.9057	81.9057	81.9057	81.9051
50	80.8474	80.8475	80.8471	80.8475	80.8467	80.8475	80.8475	80.8475	80.8462
60	80.1786	80.1786	80.1781	80.1787	80.1779	80.1786	80.1787	80.1787	80.1769
70	79.7559	79.7559	79.7553	79.7560	79.7553	79.7560	79.7560	79.7560	79.7540
80	79.4888	79.4889	79.4882	79.4890	79.4883	79.4889	79.4890	79.4890	79.4869
90	79.3202	79.3203	79.3196	79.3203	79.3197	79.3203	79.3203	79.3203	79.3183
100	79.2137	79.2138	79.2131	79.2139	79.2132	79.2138	79.2139	79.2139	79.2118

Table 5.39 Comparison of EFG results obtained using 81 nodes with FEM at the location ($x = 0.025$ m, $y = 0$ m) of the 2-D model shown in Fig. 5.9 for $d_{max} = 1.51$

Time (sec)	Temperature ($^{\circ}$ C)								
	$d_{max} = 1.51$								FEM
	C. S.	Q. S	Gaussian	Quadratic	Hyperbolic	Exponential	Rational	Cosine	
0	100.0000	100.0000	100.0000	100.0000	100.0000	100.0000	100.0000	100.0000	100.000
10	90.5333	90.5141	90.5303	89.7130	89.5714	90.5946	90.5364	90.1219	90.6130
20	86.1433	86.1193	86.1391	85.1994	84.9452	86.2229	86.1538	85.6527	86.2452
30	83.4693	83.4429	83.4647	82.4491	82.1316	83.5575	83.4842	82.9184	83.5810
40	81.7879	81.7600	81.7830	80.7198	80.3646	81.8816	81.8062	81.1973	81.9051
50	80.7255	80.6966	80.7203	79.6275	79.2496	80.8230	80.7465	80.1096	80.8462
60	80.0538	80.0242	80.0485	78.9372	78.5458	80.1539	80.0768	79.4219	80.1769
70	79.6290	79.5990	79.6236	78.5010	78.1014	79.7311	79.6537	78.9872	79.7540
80	79.3605	79.3302	79.3551	78.2254	77.8210	79.4640	79.3864	78.7126	79.4869
90	79.1909	79.1603	79.1854	78.0515	77.6441	79.2953	79.2177	78.5391	79.3183
100	79.0837	79.0530	79.0782	77.9416	77.5324	79.1888	79.1112	78.4295	79.2118

Table 5.40 Comparison of EFG results obtained using 25 nodes with FEM at the location ($x = 0.075$ m, $y = 0$ m) of the 2-D model shown in Fig. 5.9 for $d_{max} = 1.01$

Time (sec)	Temperature ($^{\circ}$ C)									
	$d_{max} = 1.01$								FEM	
	C. S.	Q. S	Gaussian	Quadratic	Hyperbolic	Exponential	Rational	Cosine		
0	100.0000	100.0000	100.0000	100.0000	100.0000	100.0000	100.0000	100.0000	100.0000	100.000
10	85.0782	85.0768	85.0891	85.0756	85.0733	85.0765	85.0758	85.0756	85.0756	85.1042
20	75.0613	75.0589	75.0761	75.0564	75.0503	75.0584	75.0567	75.0564	75.0564	75.0837
30	68.7198	68.7181	68.7289	68.7162	68.7114	68.7177	68.7164	68.7162	68.7162	68.7290
40	64.7157	64.7150	64.7185	64.7142	64.7122	64.7147	64.7142	64.7142	64.7142	64.7141
50	62.1880	62.1880	62.1867	62.1881	62.1887	62.1880	62.1880	62.1880	62.1880	62.1805
60	60.5930	60.5934	60.5895	60.5940	60.5962	60.5935	60.5939	60.5940	60.5940	60.5829
70	59.5870	59.5877	59.5827	59.5885	59.5917	59.5878	59.5884	59.5885	59.5885	59.5764
80	58.9529	58.9537	58.9485	58.9546	58.9582	58.9538	58.9545	58.9546	58.9546	58.9425
90	58.5535	58.5542	58.5491	58.5552	58.5589	58.5543	58.5550	58.5551	58.5551	58.5434
100	58.3019	58.3026	58.2977	58.3035	58.3073	58.3027	58.3034	58.3035	58.3035	58.2923

Table 5.41 Comparison of EFG results obtained using 81 nodes with FEM at the location ($x = 0.075$ m, $y = 0$ m) of the 2-D model shown in Fig. 5.9 for $d_{max} = 1.51$

Time (sec)	Temperature ($^{\circ}$ C)									
	$d_{max} = 1.51$								FEM	
	C. S.	Q. S	Gaussian	Quadratic	Hyperbolic	Exponential	Rational	Cosine		
0	100.0000	100.0000	100.0000	100.0000	100.0000	100.0000	100.0000	100.0000	100.0000	100.000
10	85.0798	85.0466	85.0857	83.5122	85.4979	85.0400	84.8231	83.0880	83.0880	85.1042
20	74.9739	74.9075	74.9607	73.5710	73.4823	75.0028	74.6890	72.9758	72.9758	75.0837
30	68.5613	68.4728	68.5311	67.2702	65.8008	68.6540	68.2874	66.5916	66.5916	68.7290
40	64.5066	64.4033	64.4657	63.2755	61.0051	64.6461	64.2474	62.5443	62.5443	64.7141
50	61.9423	61.8287	61.8955	60.7469	58.0161	62.1161	61.6985	59.9801	59.9801	62.1805
60	60.3205	60.1996	60.2707	59.1486	56.1516	60.5194	60.0913	58.3576	58.3576	60.5829
70	59.2951	59.1690	59.2437	58.1395	54.9872	59.5123	59.0786	57.3321	57.3321	59.5764
80	58.6469	58.5172	58.5948	57.5030	54.2595	58.8775	58.4408	56.6846	56.6846	58.9425
90	58.2374	58.1052	58.1850	57.1018	53.8042	58.4774	58.0393	56.2761	56.2761	58.5434
100	57.9788	57.8449	57.9262	56.8490	53.5192	58.2255	57.7867	56.0185	56.0185	58.2923

Table 5.42 Comparison of EFG results obtained using 81 nodes with FEM at the location ($x = 0.075$ m, $y = 0$ m) of the 2-D model shown in Fig. 5.9 for $d_{max} = 1.01$

Time (sec)	Temperature ($^{\circ}$ C)								
	$d_{max} = 1.01$								FEM
	C. S.	Q. S	Gaussian	Quadratic	Hyperbolic	Exponential	Rational	Cosine	
0	100.0000	100.0000	100.0000	100.0000	100.0000	100.0000	100.0000	100.0000	100.000
10	85.2227	85.2228	85.2224	85.2229	85.2231	85.2228	85.2228	85.2229	85.2220
20	75.2492	75.2491	75.2495	75.2491	75.2490	75.2491	75.2491	75.2491	75.2499
30	68.9153	68.9152	68.9158	68.9151	68.9148	68.9152	68.9151	68.9151	68.9160
40	64.9111	64.9111	64.9109	64.9111	64.9110	64.9111	64.9111	64.9111	64.9102
50	62.3799	62.3800	62.3791	62.3801	62.3804	62.3800	62.3801	62.3801	62.3777
60	60.7800	60.7802	60.7787	60.7804	60.7809	60.7802	60.7803	60.7804	60.7768
70	59.7689	59.7692	59.7675	59.7694	59.7701	59.7692	59.7694	59.7694	59.7653
80	59.1302	59.1304	59.1286	59.1307	59.1314	59.1305	59.1307	59.1307	59.1264
90	58.7268	58.7270	58.7252	58.7273	58.7280	58.7271	58.7273	58.7273	58.7230
100	58.4721	58.4724	58.4705	58.4726	58.4733	58.4724	58.4726	58.4726	58.4684

Table 5.43 Comparison of EFG results obtained using 81 nodes with FEM at the location ($x = 0.075$ m, $y = 0$ m) of the 2-D model shown in Fig. 5.9 for $d_{max} = 1.51$

Time (sec)	Temperature ($^{\circ}$ C)								
	$d_{max} = 1.51$								FEM
	C. S.	Q. S	Gaussian	Quadratic	Hyperbolic	Exponential	Rational	Cosine	
0	100.0000	100.0000	100.0000	100.0000	100.0000	100.0000	100.0000	100.0000	100.000
10	85.2384	85.2389	85.2393	84.9086	85.1217	85.2201	85.2152	85.0579	85.2220
20	75.2540	75.2523	75.2555	74.8719	74.9598	75.2386	75.2058	75.1003	75.2499
30	68.9024	68.8966	68.9034	68.4789	68.5279	68.9014	68.8592	68.7417	68.9160
40	64.8847	64.8758	64.8850	64.4345	64.4675	64.8957	64.8495	64.7169	64.9102
50	62.3442	62.3332	62.3439	61.8770	61.9036	62.3638	62.3155	62.1712	62.3777
60	60.7377	60.7252	60.7370	60.2601	60.2845	60.7634	60.7141	60.5615	60.7768
70	59.7219	59.7084	59.7210	59.2382	59.2622	59.7521	59.7022	59.5438	59.7653
80	59.0797	59.0655	59.0787	58.5925	58.6170	59.1131	59.0631	58.9008	59.1264
90	58.6739	58.6592	58.6728	58.1848	58.2098	58.7096	58.6596	58.4946	58.7230
100	58.4175	58.4025	58.4164	57.9274	57.9529	58.4549	58.4048	58.2381	58.4684

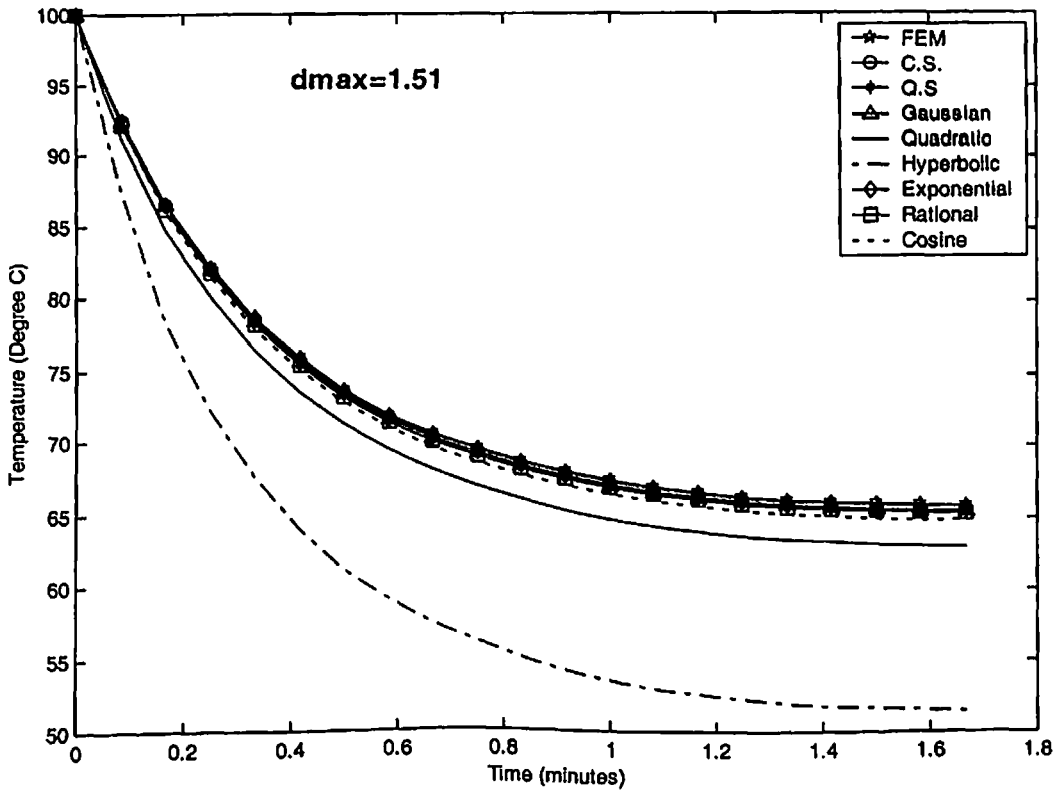
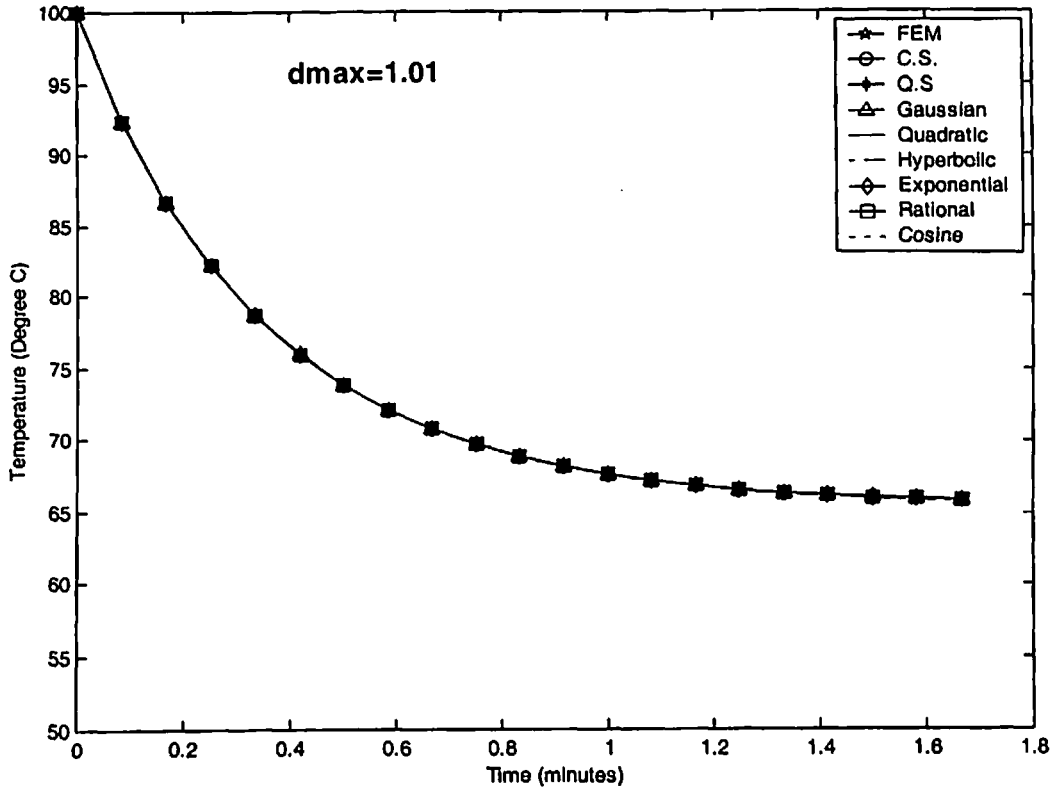


Fig. 5.12 Comparison of EFG results obtained using 25 nodes with FEM at the location ($x = 0.05$ m, $y = 0$ m) of the 2-D model shown in Fig. 5.9

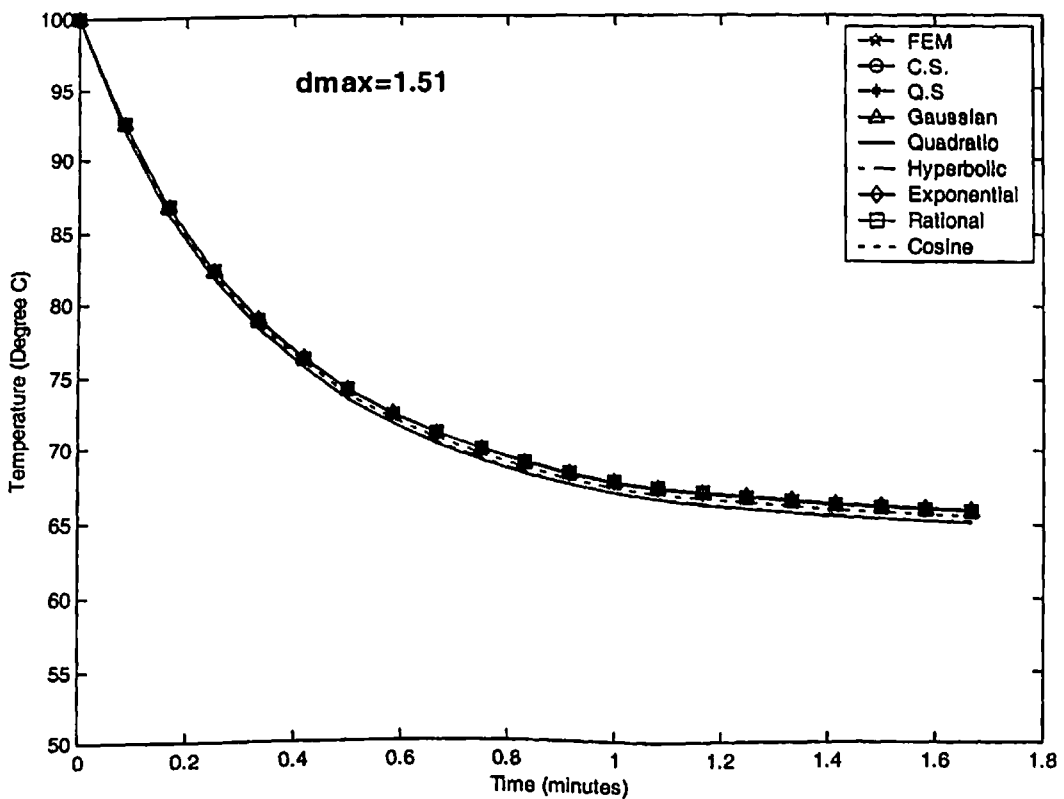
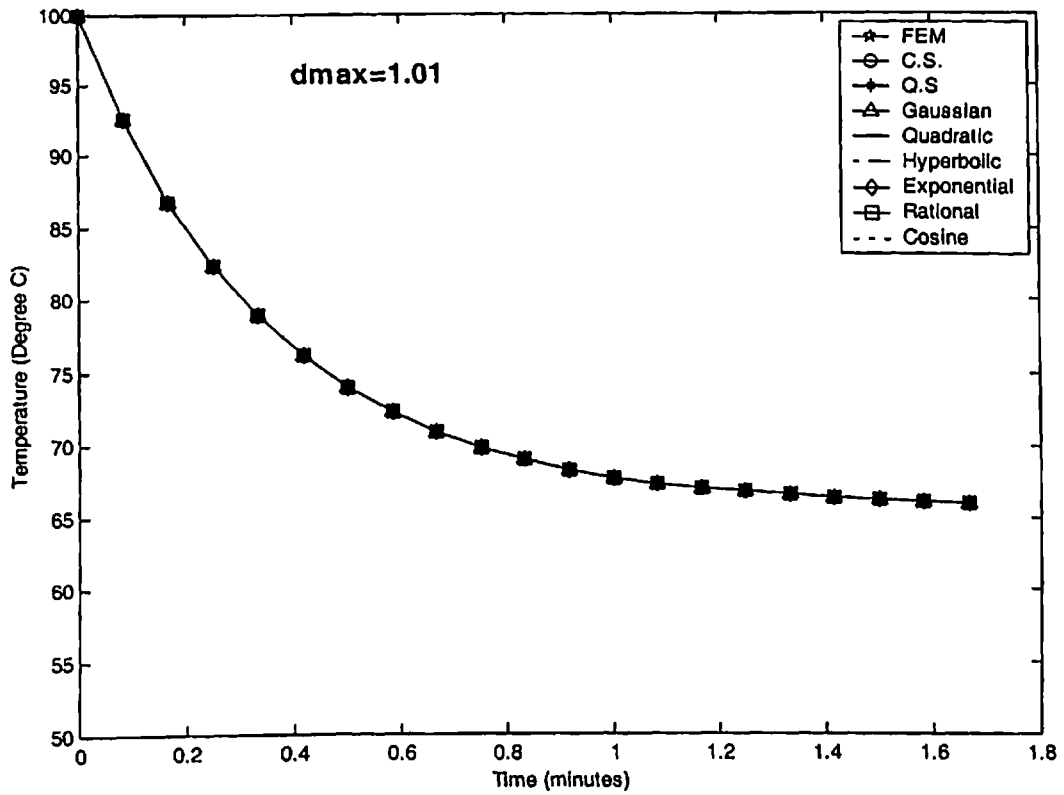


Fig. 5.13 Comparison of EFG results obtained using 81 nodes with FEM at the location ($x = 0.05$ m, $y = 0$ m) of the 2-D model shown in Fig. 5.9

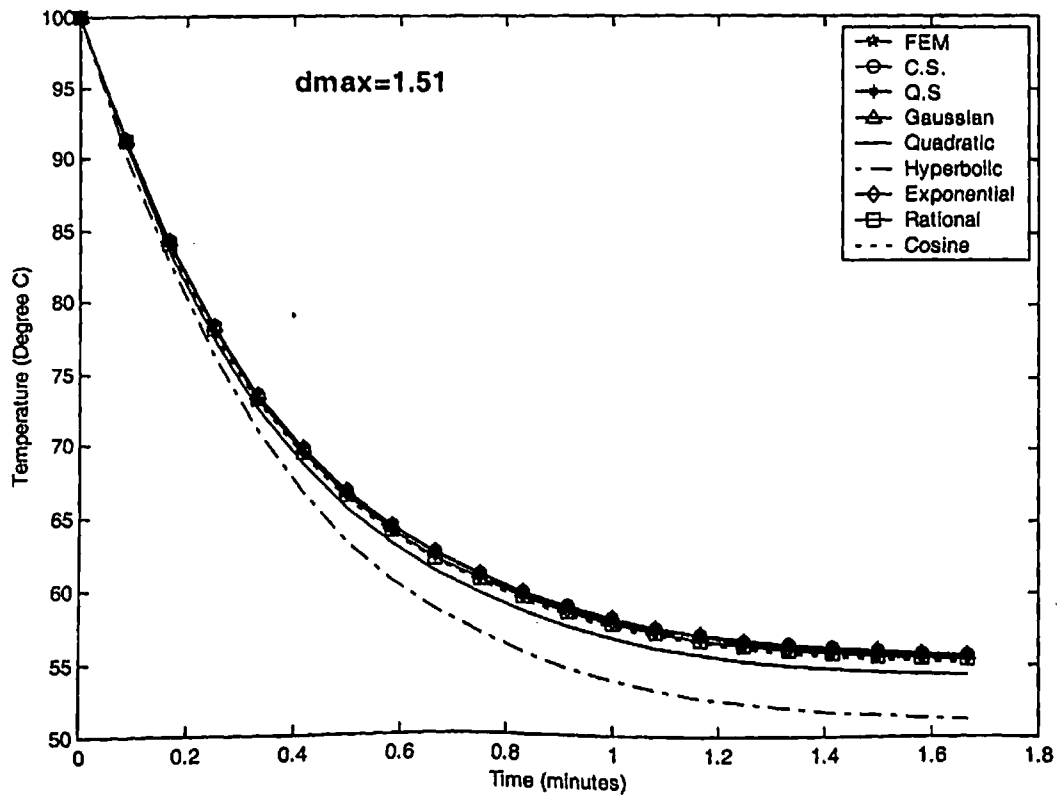
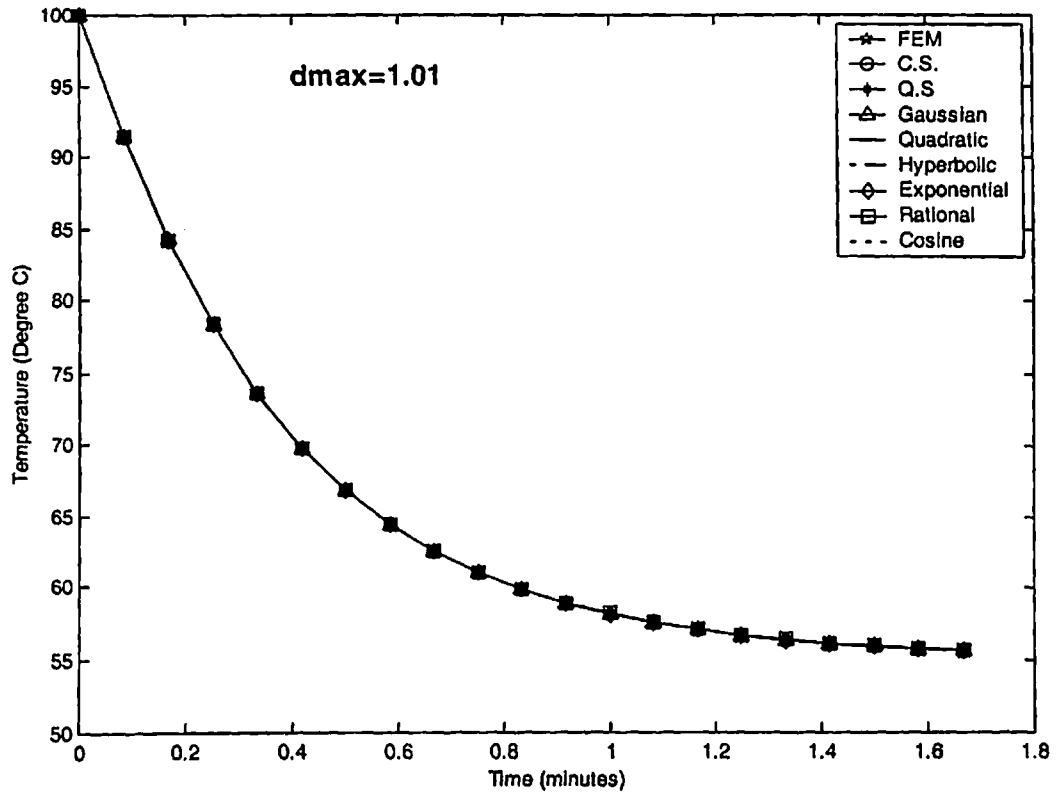


Fig. 5.14 Comparison of EFG results obtained using 25 nodes with FEM at the location $(x = 0.1 \text{ m}, y = 0 \text{ m})$ of the 2-D model shown in Fig. 5.9

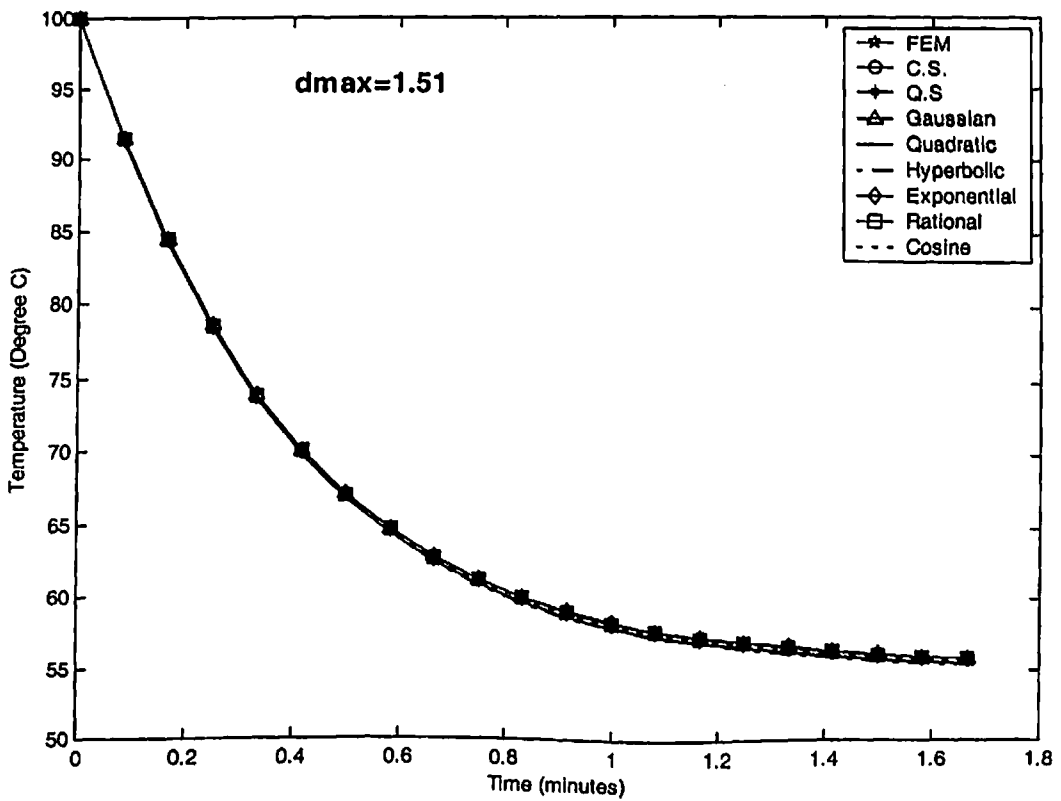
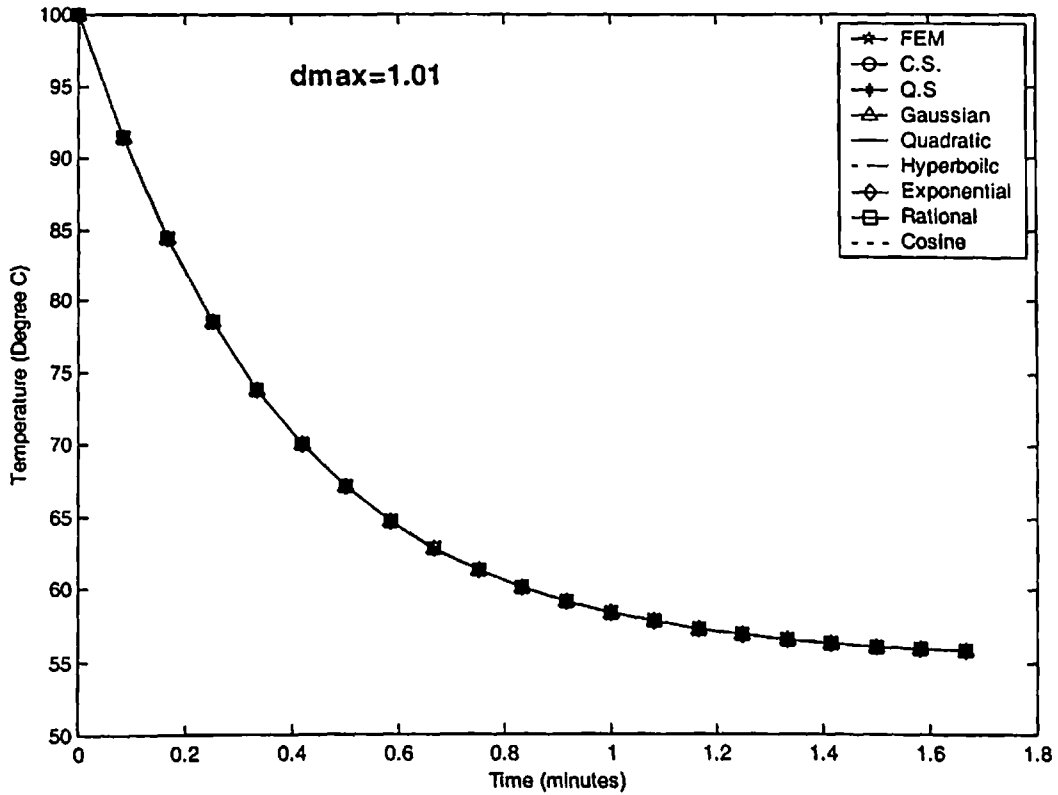


Fig. 5.15 Comparison of EFG results obtained using 81 nodes with FEM at the location ($x = 0.1\text{ m}$, $y = 0\text{ m}$) of the 2-D model shown in Fig. 5.9

➤ **CASE-III**

5.6 DISCRETIZATION OF THE GOVERNING EQUATION

A general form of energy equation for two-dimensional heat transfer in composite slabs with thermal properties independent of temperature is given as:

$$k \left(\frac{\partial^2 T}{\partial x^2} + \frac{\partial^2 T}{\partial y^2} \right) + \dot{Q} = \rho c \dot{T} \quad (5.21a)$$

with boundary and initial conditions:

$$\text{at } t = 0 \quad T = T_{ini} \quad \text{on } \Omega \quad (5.21b)$$

$$\text{at the edge of slab 1 } x = 0 \text{ or } \Gamma_1 \quad T = T_{e1} \quad (5.21c)$$

$$\text{at the edge of slab 1 } y = W_2 - W_1 \text{ or } \Gamma_2 \quad k \frac{\partial T}{\partial y} = h(T - T_{\infty}) \quad (5.21d)$$

$$\text{at the edge of slab 2 } x = L_1 \text{ or } \Gamma_3 \quad k \frac{\partial T}{\partial x} = h(T - T_{\infty}) \quad (5.21e)$$

$$\text{at the edge of slab 2 } y = 0 \text{ or } \Gamma_4 \quad k \frac{\partial T}{\partial y} = h(T - T_{\infty}) \quad (5.21f)$$

$$\text{at the edge of slab 2 } x = L_1 + L_2 \text{ or } \Gamma_5 \quad -k \frac{\partial T}{\partial x} = h(T - T_{\infty}) \quad (5.21g)$$

$$\text{at the edge of slab 2 } y = W_2 \text{ or } \Gamma_6 \quad -k \frac{\partial T}{\partial y} = h(T - T_{\infty}) \quad (5.21h)$$

$$\text{at the edge of slab 1 } y = W_2 \text{ or } \Gamma_7 \quad -k \frac{\partial T}{\partial y} = h(T - T_{\infty}) \quad (5.21i)$$

Compatibility requirement at the interface of two slabs is given as:

$$-k \left(\frac{\partial T}{\partial x} \right)_{x=L_1} \Big|_{\text{slab 1}} = -k \left(\frac{\partial T}{\partial x} \right)_{x=L_1} \Big|_{\text{slab 2}} \quad (5.21j)$$

The weighted integral form of Eq. (5.21a) is

$$\int_{\Omega} w \left[k \left(\frac{\partial^2 T}{\partial x^2} + \frac{\partial^2 T}{\partial y^2} \right) + \dot{Q} - \rho c \dot{T} \right] d\Omega = 0 \quad (5.22)$$

The weak of the Eq. (5.22) with natural boundary conditions is obtained as:

$$\begin{aligned} & \int_{\Omega} [k(w_{,x}T_{,x} + w_{,y}T_{,y})] d\Omega - \int_{\Omega} w \dot{Q} d\Omega + \int_{\Omega} w \rho c \dot{T} d\Omega + \int_{\Gamma_2} w h(T - T_{\infty}) d\Gamma + \int_{\Gamma_3} w h(T - T_{\infty}) d\Gamma + \\ & \int_{\Gamma_4} w h(T - T_{\infty}) d\Gamma + \int_{\Gamma_5} w h(T - T_{\infty}) d\Gamma + \int_{\Gamma_6} w h(T - T_{\infty}) d\Gamma + \int_{\Gamma_7} w h(T - T_{\infty}) d\Gamma = 0 \end{aligned} \quad (5.23)$$

The functional $I(T)$ can be written as:

$$\begin{aligned}
I(T) = & \int_{\Omega} \frac{k}{2} [T_{,x}^2 + T_{,y}^2] d\Omega - \int_{\Omega} T \dot{Q} d\Omega + \int_{\Omega} \rho c \dot{T} T d\Omega + \int_{\Gamma_2} \frac{hT^2}{2} d\Gamma + \int_{\Gamma_1} \frac{hT^2}{2} d\Gamma + \\
& \int_{\Gamma_4} \frac{hT^2}{2} d\Gamma + \int_{\Gamma_5} \frac{hT^2}{2} d\Gamma + \int_{\Gamma_6} \frac{hT^2}{2} d\Gamma + \int_{\Gamma_7} \frac{hT^2}{2} d\Gamma + \int_{\Gamma_2} hT_{\infty} T d\Gamma + \int_{\Gamma_1} hT_{\infty} T d\Gamma + \\
& \int_{\Gamma_4} hT_{\infty} T d\Gamma + \int_{\Gamma_5} hT_{\infty} T d\Gamma + \int_{\Gamma_6} hT_{\infty} T d\Gamma + \int_{\Gamma_7} hT_{\infty} T d\Gamma
\end{aligned} \tag{5.24}$$

Enforcing essential boundary conditions using Lagrange multiplier the functional $I^*(T)$ is obtained as:

$$\begin{aligned}
I^*(T) = & \int_{\Omega} \frac{k}{2} [T_{,x}^2 + T_{,y}^2] d\Omega - \int_{\Omega} T \dot{Q} d\Omega + \int_{\Omega} \rho c \dot{T} T d\Omega + \int_{\Gamma_2} \frac{hT^2}{2} d\Gamma + \int_{\Gamma_1} \frac{hT^2}{2} d\Gamma + \\
& \int_{\Gamma_4} \frac{hT^2}{2} d\Gamma + \int_{\Gamma_5} \frac{hT^2}{2} d\Gamma + \int_{\Gamma_6} \frac{hT^2}{2} d\Gamma + \int_{\Gamma_7} \frac{hT^2}{2} d\Gamma + \int_{\Gamma_2} hT_{\infty} T d\Gamma + \int_{\Gamma_1} hT_{\infty} T d\Gamma + \\
& \int_{\Gamma_4} hT_{\infty} T d\Gamma + \int_{\Gamma_5} hT_{\infty} T d\Gamma + \int_{\Gamma_6} hT_{\infty} T d\Gamma + \int_{\Gamma_7} hT_{\infty} T d\Gamma + \int_{\Gamma_1} \lambda (T - T_{e_1}) d\Gamma
\end{aligned} \tag{5.25}$$

Using variational principle to obtain the discrete equations:

$$\begin{aligned}
\delta I^*(T) = & \int_{\Omega} k [T_{,x} \delta T_{,x} + T_{,y} \delta T_{,y}] d\Omega - \int_{\Omega} \dot{Q} \delta T d\Omega + \int_{\Omega} \rho c \dot{T} \delta T d\Omega + \int_{\Gamma_2} hT \delta T d\Gamma + \\
& \int_{\Gamma_4} hT \delta T d\Gamma + \int_{\Gamma_5} hT \delta T d\Gamma + \int_{\Gamma_6} hT \delta T d\Gamma + \int_{\Gamma_7} hT \delta T d\Gamma + \int_{\Gamma_1} hT_{\infty} \delta T d\Gamma + \\
& \int_{\Gamma_2} hT_{\infty} \delta T d\Gamma + \int_{\Gamma_4} hT_{\infty} \delta T d\Gamma + \int_{\Gamma_5} hT_{\infty} \delta T d\Gamma + \int_{\Gamma_6} hT_{\infty} \delta T d\Gamma + \int_{\Gamma_7} hT_{\infty} \delta T d\Gamma + \\
& \int_{\Gamma_1} hT_{\infty} \delta T d\Gamma + \int_{\Gamma_1} (T - T_{e_1}) \delta \lambda d\Gamma + \int_{\Gamma_1} \lambda \delta T d\Gamma
\end{aligned} \tag{5.26}$$

Since δT and $\delta \lambda$ are arbitrary in preceding equation, the following relations are obtained by using Eq. (3.25) and Eq. (5.26)

$$[\mathbf{K}]\{\mathbf{T}\} + [\mathbf{C}]\{\dot{\mathbf{T}}\} + [\mathbf{G}]\{\lambda\} = \{\mathbf{f}\} \tag{5.27a}$$

$$[\mathbf{G}^T]\{\mathbf{T}\} = \{\mathbf{q}\} \tag{5.27b}$$

where

$$\begin{aligned}
K_{i,j} = & \int_{\Omega} \begin{bmatrix} \Phi_{i,x} \\ \Phi_{i,y} \end{bmatrix}^T \begin{bmatrix} k & 0 \\ 0 & k \end{bmatrix} \begin{bmatrix} \Phi_{j,x} \\ \Phi_{j,y} \end{bmatrix} dV + \int_{\Gamma_2} h\Phi_i^T \Phi_j d\Gamma + \int_{\Gamma_1} h\Phi_i^T \Phi_j d\Gamma + \\
& \int_{\Gamma_4} h\Phi_i^T \Phi_j d\Gamma + \int_{\Gamma_5} h\Phi_i^T \Phi_j d\Gamma + \int_{\Gamma_6} h\Phi_i^T \Phi_j d\Gamma + \int_{\Gamma_7} h\Phi_i^T \Phi_j d\Gamma
\end{aligned} \tag{5.28a}$$

$$C_{IJ} = \int_{\Omega} \rho c \Phi_I^T \Phi_J d\Omega \quad (5.28b)$$

$$f_I = \int_{\Omega} \dot{Q} \Phi_I d\Omega + \int_{\Gamma_1} h T_{\infty} \Phi_I d\Gamma + \int_{\Gamma_2} h T_{\infty} \Phi_I d\Gamma + \int_{\Gamma_3} h T_{\infty} \Phi_I d\Gamma + \int_{\Gamma_4} h T_{\infty} \Phi_I d\Gamma + \int_{\Gamma_5} h T_{\infty} \Phi_I d\Gamma + \int_{\Gamma_6} h T_{\infty} \Phi_I d\Gamma \quad (5.28c)$$

$$G_{IK} = \int_{\Gamma_1} \Phi_I N_K d\Gamma \quad (5.28d)$$

$$q_K = \int_{\Gamma_1} T_{e1} N_K d\Gamma \quad (5.28e)$$

Using backward difference method for time approximation, the Eq. (5.27) can be written as:

$$\begin{bmatrix} \mathbf{K}^* + \mathbf{C} & \mathbf{G} \\ \mathbf{G}^T & 0 \end{bmatrix} \begin{Bmatrix} \mathbf{T}_N \\ \lambda \end{Bmatrix} = \begin{Bmatrix} \mathbf{R}_N \\ \mathbf{q} \end{Bmatrix} \quad (5.29)$$

where

$$\mathbf{R}_N = ([\mathbf{C}] - (1 - \alpha) \Delta t [\mathbf{K}]) \{\mathbf{T}\}_{N-1} + \alpha \Delta t \{\mathbf{f}\}_N + (1 - \alpha) \Delta t \{\mathbf{f}\}_{N-1} \quad (5.30a)$$

$$\mathbf{K}^* = \alpha \Delta t [\mathbf{K}] \quad (5.30b)$$

5.7 NUMERICAL RESULTS AND DISCUSSION

The different parameters used for steady-state and transient analysis of two-dimensional composite slab model shown in Fig. 5.16 are tabulated in Table 5.44. The EFG results (temperature values) are obtained using different weight functions for two sets of nodes and FEM results are obtained using 4 node quadrilateral elements (PLANE 55, ANSYS 6.0) for same sets of nodes. A comparative study is carried out to evaluate the performance of different EFG weight functions.

5.7.1 Steady-state analysis

The results (i.e. temperature values) presented in Table 5.45 are obtained using different EFG weight functions for two values of scaling parameter (i.e. $d_{\max} = 1.01$ & $d_{\max} = 1.51$) at the location ($x = 0.2$ m, $y = 0.4$ m) and it shows a comparison of temperature values obtained by EFG method using different weight functions with FEM for 65 nodes. Table 5.46 shows a

comparison of temperature values obtained by EFG method using different functions for two values of scaling parameter with FEM at the same location i.e. ($x = 0.2 \text{ m}$, $y = 0.4 \text{ m}$) for 225 nodes. A comparison of temperature values obtained using different EFG weight functions with FEM for 65 and 81 nodes, is shown in Table 5.47 and Table 5.48 respectively at the location ($x = 0.2 \text{ m}$, $y = 0 \text{ m}$). Similar type of comparisons of temperature values are shown in Table 5.49 for 65 nodes at the location ($x = 0.4 \text{ m}$, $y = 0.4 \text{ m}$), in Table 5.50 for 225 nodes at the location ($x = 0.4 \text{ m}$, $y = 0.4 \text{ m}$), in Table 5.51 for 65 nodes at the location ($x = 0.4 \text{ m}$, $y = 0 \text{ m}$) and in Table 5.52 for 225 nodes at the location ($x = 0.4 \text{ m}$, $y = 0 \text{ m}$). From the results presented in Table 5.45 to Table 5.52, it is observed that EFG results obtained using cubicspline, quarticspline, Gaussian, exponential and rational weight functions are acceptable for $d_{\max} = 1.01$. However for $d_{\max} = 1.51$, only exponential and rational weight functions give acceptable results. It is also observed that the EFG results obtained using different weight functions are in good agreement with those obtained by FEM. Moreover with the increase in number of nodes EFG results starts converging.

The effect of scaling parameter (d_{\max}) on EFG results obtained using different weight functions is presented in Table 5.53 for 65 nodes and Table 5.54 for 225 nodes respectively at the location ($x = 0.4 \text{ m}$, $y = 0 \text{ m}$). Similar effect of scaling parameter on EFG results is shown in Table 5.55 for 25 nodes and Table 5.56 for 225 nodes at the location ($x = 0.2 \text{ m}$, $y = 0 \text{ m}$). Fig. 5.17 shows the effect of scaling parameter on EFG results obtained using 65 and 225 nodes at the location ($x = 0.2 \text{ m}$, $y = 0.4 \text{ m}$). Similar effect of scaling parameter on EFG results is observed in Fig. 5.18 at the location ($x = 0.4 \text{ m}$, $y = 0.4 \text{ m}$). From tables and figures, it is clear that only cubicspline, exponential and rational weight functions give acceptable results in the range $1.0 < d_{\max} < 1.5$ whereas the results obtained

using quarticspline, Gaussian, quadratic, hyperbolic and cosine weight functions acceptable in the range $1.0 < d_{\max} < 1.5$. It is also observed that there is minimum variation in EFG results with scaling parameter for exponential weight function. Therefore exponential weight function gives most reliable results for this case.

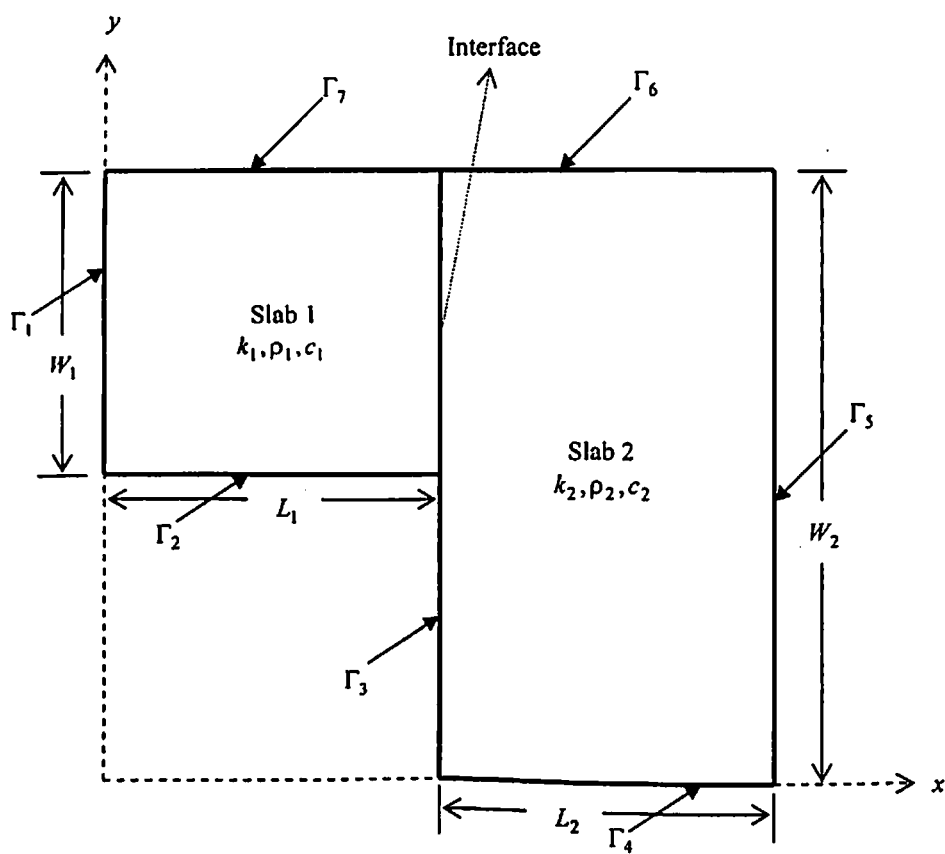


Fig. 5.16 Two-dimensional model of composite slabs

Table 5.44 Data for the 2-D model shown in Fig. 5.16

Parameters	Value of the parameter
Length (L_1)	0.2 m
Width (W_1)	0.2 m
Length (L_2)	0.2 m
Width (W_2)	0.4 m
Thermal conductivity of slab 1 (k_1)	400 W/m-K
Thermal conductivity of slab 2 (k_2)	100 W/m-K
Specific heat of slab 1 (c_1)	400 kJ/kg-K
Specific heat of slab 2 (c_2)	300 kJ/kg-K
Density of slab 1 (ρ_1)	10000 kg/m ³
Density of slab 2 (ρ_2)	8000 kg/m ³
Rate of internal heat generation (\dot{Q})	0 W/m ³
Heat transfer coefficient (h)	200 W/m ² -K
Initial temperature (T_{ini})	0 °C
Surrounding fluid temperature (T_∞)	20 °C
Time step size (Δt)	100 sec
Temperature (T_L) at surface, $x = 0$ or Γ_1	100 °C
Convection at all other edges	$-k \frac{\partial T}{\partial n'} = h(T - T_\infty)$ on Γ_i , where $n' = x, y$ and $i = 2, 3 \dots 7$

Table 5.45 Comparison of EFG results obtained using 65 nodes with FEM results at the location ($x = 0.2$ m, $y = 0.4$ m) of the 2-D model shown in Fig. 5.16

Weight function	EFG				FEM
	$d_{\max} = 1.01$		$d_{\max} = 1.51$		
	T (°C)	% diff with FEM	T (°C)	% diff with FEM	T (°C)
C. S.	79.9504	1.77102	89.7237	14.2117	78.5591
Q. S.	80.6513	2.6632	95.1367	21.1021	
Gaussian	79.6047	1.3310	86.7078	10.3727	
Quadratic	79.7142	1.4704	76.4645	-2.6663	
Hyperbolic	95.7775	21.9178	113.0261	43.8740	
Exponential	79.3664	1.0276	81.1409	3.2864	
Rational	80.7683	2.8121	85.1812	8.4295	
Cosine	79.0537	0.6296	92.1504	17.3007	

Table 5.46 Comparison of EFG results obtained using 225 nodes with FEM results at the location ($x = 0.2$ m, $y = 0.4$ m) of the 2-D model shown in Fig. 5.16

Weight function	EFG				FEM
	$d_{\max} = 1.01$		$d_{\max} = 1.51$		
	T (°C)	% diff with FEM	T (°C)	% diff with FEM	T (°C)
C. S.	79.4096	1.0569	86.8840	10.5688	78.5791
Q. S.	79.7782	1.5260	91.0416	15.8598	
Gaussian	79.2562	0.8617	83.5254	6.2947	
Quadratic	80.4302	2.3557	79.2643	0.8720	
Hyperbolic	88.8976	13.1313	-40.3535	-151.3540	
Exponential	79.0656	0.6191	80.1558	2.0065	
Rational	79.8701	1.6429	82.8744	5.4662	
Cosine	79.7061	1.4342	266.1567	238.7118	

Table 5.47 Comparison of EFG results obtained using 65 nodes with FEM results at the location ($x = 0.2$ m, $y = 0$ m) of the 2-D model shown in Fig. 5.16

Weight function	EFG				FEM
	$d_{\max} = 1.01$		$d_{\max} = 1.51$		T (°C)
	T (°C)	% diff with FEM	T (°C)	% diff with FEM	
C. S.	40.6239	0.9159	36.5568	-9.1874	40.2552
Q. S.	40.7086	1.1263	38.6135	-4.0782	
Gaussian	39.9705	-0.7072	36.3247	-9.7640	
Quadratic	29.7008	-26.2187	96.0034	138.4870	
Hyperbolic	14.3799	-64.2782	190.8448	374.0873	
Exponential	40.1289	-0.3137	40.1184	-0.3398	
Rational	40.0453	-0.5214	41.7291	3.6614	
Cosine	27.7201	-31.1391	85.8364	113.2306	

Table 5.48 Comparison of EFG results obtained using 225 nodes with FEM results at the location ($x = 0.2$ m, $y = 0$ m) of the 2-D model shown in Fig. 5.16

Weight function	EFG				FEM
	$d_{\max} = 1.01$		$d_{\max} = 1.51$		T (°C)
	T (°C)	% diff with FEM	T (°C)	% diff with FEM	
C. S.	40.0219	0.5010	38.0388	-4.4789	39.8224
Q. S.	40.0614	0.6002	40.3879	1.4201	
Gaussian	39.7039	-0.2976	37.4706	-5.9057	
Quadratic	43.3486	8.8548	31.3763	-21.2094	
Hyperbolic	29.6207	-25.6180	53.5133	34.3799	
Exponential	39.8103	-0.0304	39.8200	-0.0060	
Rational	39.8681	0.1148	39.9443	0.3061	
Cosine	48.8383	22.6403	52.1856	31.0458	

Table 5.49 Comparison of EFG results obtained using 65 nodes with FEM results at the location ($x = 0.4$ m, $y = 0.4$ m) of the 2-D model shown in Fig. 5.16

Weight function	EFG				FEM
	$d_{\max} = 1.01$		$d_{\max} = 1.51$		
	T (°C)	% diff with FEM	T (°C)	% diff with FEM	T (°C)
C. S.	50.1622	0.6394	50.7805	1.8799	49.8435
Q. S.	50.2721	0.8599	50.5418	1.4010	
Gaussian	49.5347	-0.6195	45.0758	-9.5653	
Quadratic	47.8174	-4.0649	42.1558	-15.4237	
Hyperbolic	47.0348	-5.6350	46.1453	-7.4196	
Exponential	49.6950	-0.2979	49.6804	-0.3272	
Rational	49.7987	-0.0899	50.0376	0.3894	
Cosine	45.7981	-8.1162	22.0185	-55.8247	

Table 5.50 Comparison of EFG results obtained using 225 nodes with FEM results at the location ($x = 0.4$ m, $y = 0.4$ m) of the 2-D model shown in Fig. 5.16

	EFG				FEM
	$d_{\max} = 1.01$		$d_{\max} = 1.51$		
	T (°C)	% diff with FEM	T (°C)	% diff with FEM	
C. S.	49.8180	0.3881	49.9874	0.7295	49.6254
Q. S.	49.8477	0.4480	49.7870	0.3256	
Gaussian	49.4995	-0.2537	46.4959	-6.3063	
Quadratic	51.9808	4.7464	46.1086	-7.0867	
Hyperbolic	46.7986	-5.6963	59.4386	19.7745	
Exponential	49.5934	-0.0645	49.5837	-0.0840	
Rational	49.6582	0.0660	49.7144	0.1793	
Cosine	52.0317	4.8489	-54.0874	-208.9910	

Table 5.51 Comparison of EFG results obtained using 65 nodes with FEM results at the location ($x = 0.4 \text{ m}$, $y = 0 \text{ m}$) of the 2-D model shown in Fig. 5.16

Weight function	EFG				FEM
	$d_{\max} = 1.01$		$d_{\max} = 1.51$		
	T (°C)	% diff with FEM	T (°C)	% diff with FEM	T (°C)
C. S.	39.4342	0.2830	37.9358	-3.5275	39.3229
Q. S.	39.5041	0.4608	38.1421	-3.0028	
Gaussian	38.8999	-1.0757	34.5210	-12.2115	
Quadratic	46.6551	18.6461	170.0518	332.4498	
Hyperbolic	26.2517	-33.2407	-1.0483	-102.6660	
Exponential	39.2293	-0.2380	39.2552	-0.1722	
Rational	39.4090	0.21896	39.8008	1.2153	
Cosine	47.2096	20.0562	59.0975	50.2877	

Table 5.52 Comparison of EFG results obtained using 225 nodes with FEM results at the location ($x = 0.4 \text{ m}$, $y = 0 \text{ m}$) of the 2-D model shown in Fig. 5.16

Weight function	EFG				FEM
	$d_{\max} = 1.01$		$d_{\max} = 1.51$		
	T (°C)	% diff with FEM	T (°C)	% diff with FEM	T (°C)
C. S.	38.9808	0.3584	38.7545	-0.2242	38.8416
Q. S.	39.0137	0.4431	39.1299	0.7422	
Gaussian	38.7094	-0.3404	36.6317	-5.6895	
Quadratic	40.9643	5.4650	49.7855	28.1757	
Hyperbolic	37.7532	-2.8021	56.3286	45.0213	
Exponential	38.8337	-0.0203	38.8528	0.0288	
Rational	38.9199	0.2016	39.0392	0.5087	
Cosine	43.8072	12.7842	49.1057	26.4255	

Table 5.53 Effect of scaling parameter on EFG results obtained using 65 nodes at the location ($x = 0.2$ m, $y = 0$ m) of the 2-D model shown in Fig. 5.16

Scaling Parameter	Temperature ($^{\circ}$ C)							
	C. S.	Q. S	Gaussian	Quadratic	Hyperbolic	Exponential	Rational	Cosine
1.01	40.6239	40.7086	39.9705	29.7008	14.3799	40.1289	40.0453	27.7201
1.11	40.6847	40.5745	39.8064	59.6787	33.2217	40.1262	40.1277	55.2568
1.21	40.5760	40.2024	39.4956	83.7116	41.4072	40.1309	40.0482	83.4669
1.31	40.1318	39.5110	38.9326	87.9533	44.0757	40.1149	39.9541	86.4258
1.41	38.9748	38.6236	37.8917	96.2095	40.1618	40.1260	40.1158	100.3115
1.51	36.5568	38.6135	36.3247	96.0034	190.8448	40.1184	41.7291	85.8364
1.61	31.7109	41.2929	33.2342	32.4889	150.6641	40.1113	41.1733	15.9954
1.71	21.1038	42.8771	27.4618	-49.8207	100.7315	40.0923	40.5871	-82.4493
1.81	-1.9012	35.8486	18.0151	-39.9418	100.3692	40.0634	40.8275	-79.5731

Table 5.54 Effect of scaling parameter on EFG results obtained using 225 nodes at the location ($x = 0.2$ m, $y = 0$ m) of the 2-D model shown in Fig. 5.16

Scaling Parameter	Temperature ($^{\circ}$ C)							
	C. S.	Q. S	Gaussian	Quadratic	Hyperbolic	Exponential	Rational	Cosine
1.01	40.0219	40.0614	39.7039	43.3486	29.6207	39.8103	39.8681	48.8383
1.11	40.0624	40.0409	39.5802	37.9975	38.6908	39.8108	39.9116	33.2767
1.21	40.0608	39.9187	39.3703	61.1176	41.9356	39.8158	39.9193	57.8945
1.31	39.9337	39.5754	39.0290	61.2245	42.7508	39.8129	39.9292	55.1249
1.41	39.4281	39.2296	38.4311	52.6959	42.3442	39.8228	39.9241	61.0530
1.51	38.0388	40.3879	37.4706	31.3763	53.5133	39.8200	39.9443	52.1856
1.61	34.6491	43.2466	35.7257	24.1185	57.0369	39.8153	39.9946	44.9348
1.71	25.5969	45.5680	32.4140	-20.4640	41.8201	39.8150	39.9318	51.9478
1.81	0.5785	46.3589	26.4984	-31.3753	38.6162	39.8096	39.9116	0.2937

Table 5.55 Effect of scaling parameter on EFG results obtained using 65 nodes at the location ($x = 0.4 \text{ m}$, $y = 0 \text{ m}$) of the 2-D model shown in Fig. 5.16

Scaling Parameter	Temperature ($^{\circ} \text{C}$)							
	C. S.	Q. S	Gaussian	Quadratic	Hyperbolic	Exponential	Rational	Cosine
1.01	39.4342	39.5041	38.8999	46.6551	26.2517	39.2293	39.4090	47.2096
1.11	39.5068	39.5020	38.6616	31.6056	37.2412	39.2191	39.4925	36.6919
1.21	39.5313	39.4237	38.2463	11.3560	42.0765	39.2467	39.5395	0.7732
1.31	39.4386	39.1662	37.5605	2.0021	42.5737	39.2516	39.5747	-6.5217
1.41	39.0337	38.6437	36.3833	20.2117	45.7407	39.2597	39.6419	-13.1051
1.51	37.9358	38.1421	34.5210	170.0518	-1.0483	39.2552	39.8008	59.0975
1.61	35.2978	38.3516	31.4316	137.9602	17.9737	39.2412	39.9918	174.0952
1.71	28.8263	38.7454	26.1492	36.7537	28.6484	39.2271	40.1090	275.6187
1.81	13.5925	36.8590	17.5839	-56.3368	25.4852	39.2271	40.4127	151.4979

Table 5.56 Effect of scaling parameter on EFG results obtained using 225 nodes at the location ($x = 0.4 \text{ m}$, $y = 0 \text{ m}$) of the 2-D model shown in Fig. 5.16

Scaling Parameter	Temperature ($^{\circ} \text{C}$)							
	C. S.	Q. S	Gaussian	Quadratic	Hyperbolic	Exponential	Rational	Cosine
1.01	38.9808	39.0137	38.7094	40.9643	37.7532	38.8337	38.9199	43.8072
1.11	39.0163	39.0194	38.5927	40.1892	39.6008	38.8319	38.9644	37.0622
1.21	39.0431	39.0235	38.3905	26.8943	40.4982	38.8434	38.9862	48.1982
1.31	39.0546	39.0017	38.0669	24.7255	41.2575	38.8448	39.0009	30.6172
1.41	39.0040	38.9681	37.5143	37.5437	41.9914	38.8535	39.0211	26.1682
1.51	38.7545	39.1299	36.6317	49.7855	56.3286	38.8528	39.0392	49.1057
1.61	37.8951	39.4956	35.2326	23.9546	51.2763	38.8505	39.0845	38.9393
1.71	34.9781	40.0229	32.8875	-28.7164	40.5204	38.8543	39.1492	-16.8248
1.81	25.3948	39.9934	28.9751	6.5386	41.9597	38.8565	39.2070	-15.5878

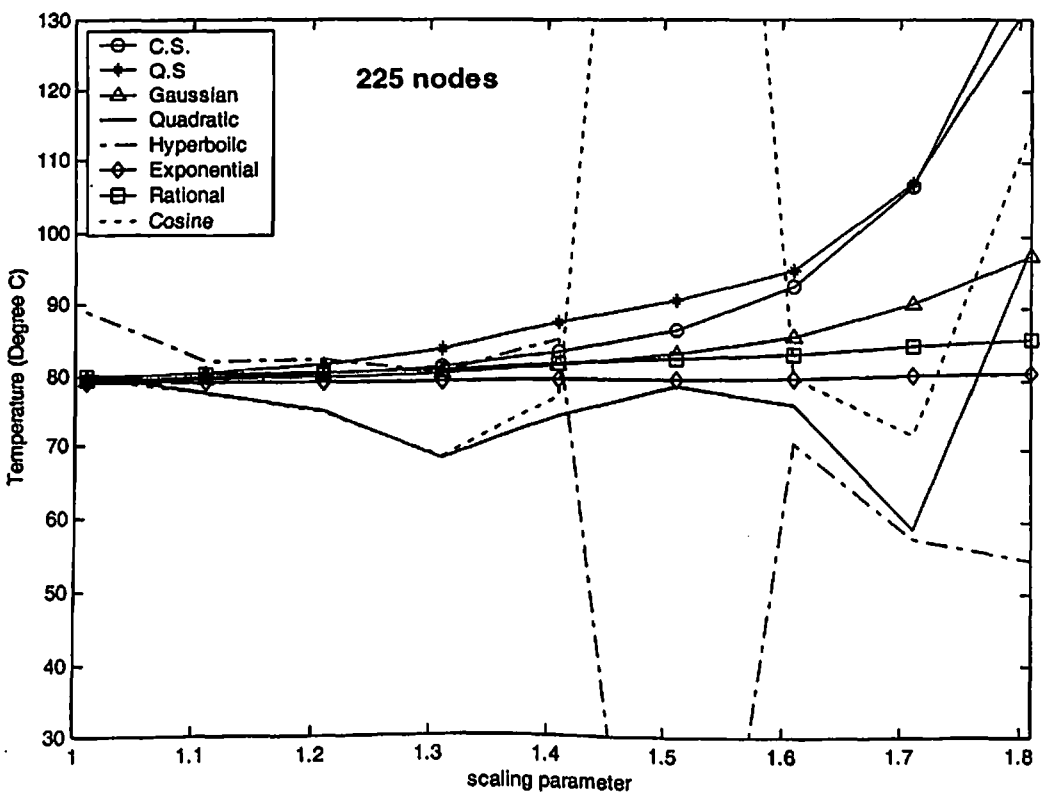
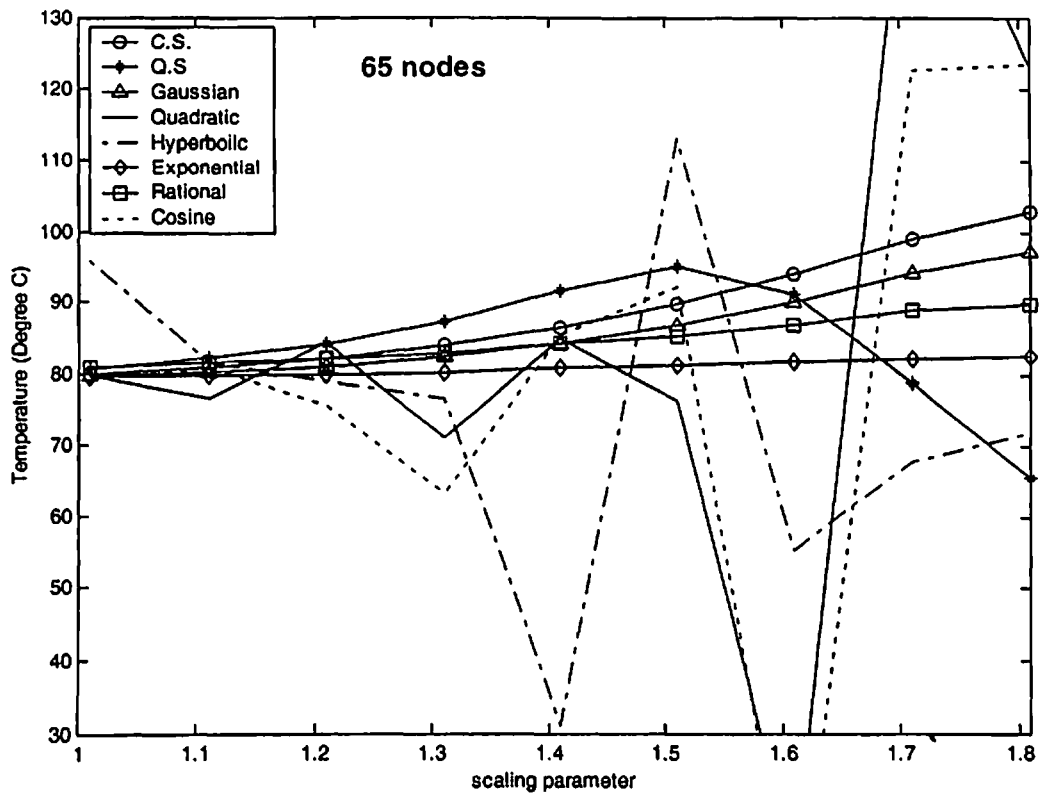


Fig. 5.17 Effect of scaling parameter on EFG results at the location ($x = 0.2$ m, $y = 0.4$ m) of the 2-D model shown in Fig. 5.16

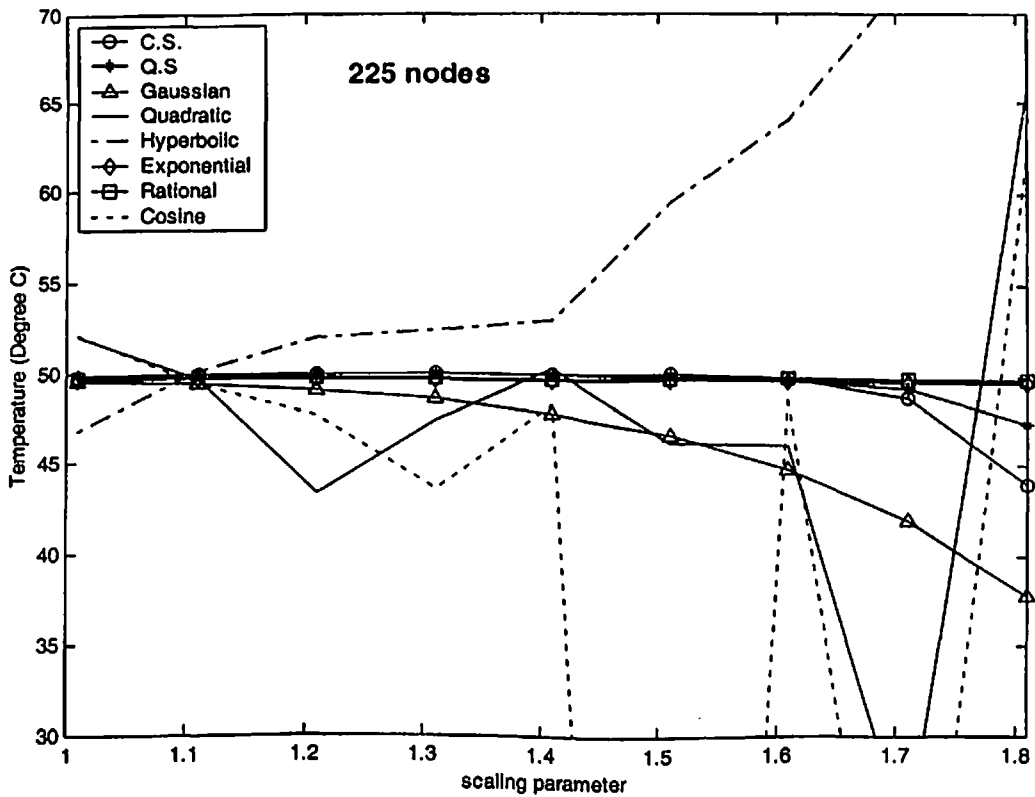
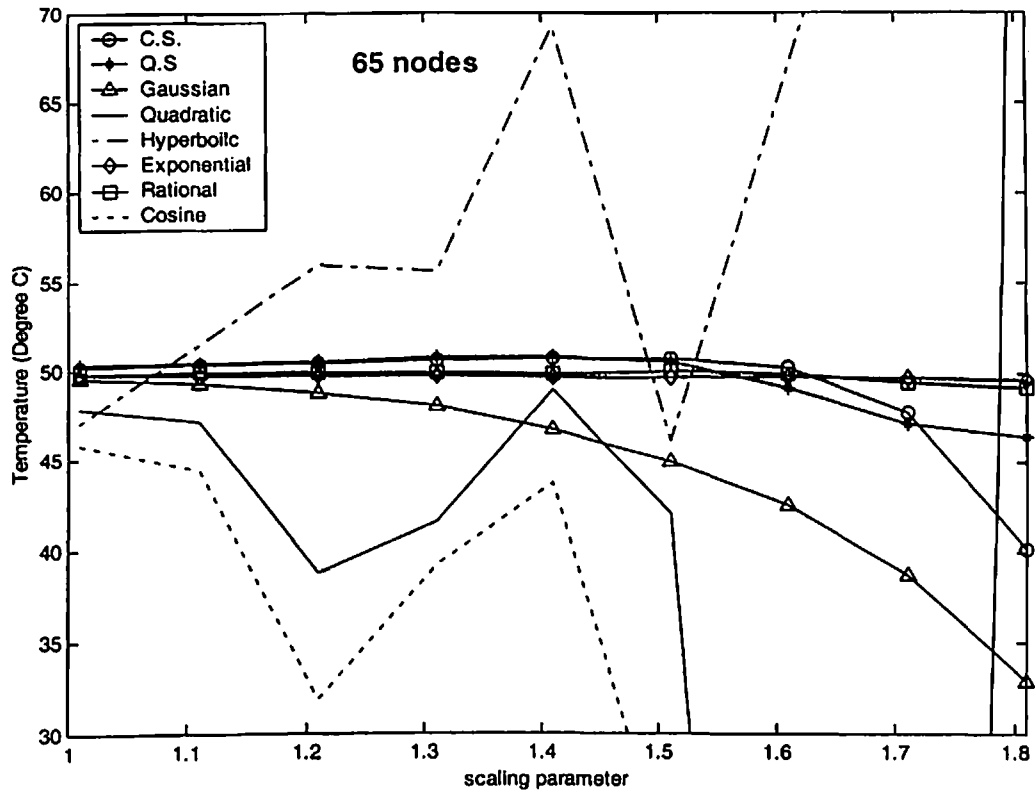


Fig. 5.18 Effect of scaling parameter on EFG results at the location ($x = 0.4$ m, $y = 0.4$ m) of the 2-D model shown in Fig. 5.16

5.7.2 Transient analysis

The transient analysis of 2-D model, shown in Fig. 5.16, is carried out using different EFG weight functions. Table 5.57 and Table 5.58 show the comparison of EFG results (i.e. temperature values) obtained using 65 nodes with FEM results at the location $(x = 0.2 \text{ m}, y = 0 \text{ m})$ for $d_{\max} = 1.01$ and $d_{\max} = 1.51$ respectively. Similar comparison of temperature values obtained using 225 nodes is presented in Table 5.59 and Table 5.60 for $d_{\max} = 1.01$ and $d_{\max} = 1.51$ respectively at the same location i.e. $(x = 0.2 \text{ m}, y = 0 \text{ m})$. For this case (i.e. CASE-III) of 2-D transient analysis, time step of 100 sec has been taken which is nearly 3% of the total time required to achieve steady state condition. Table 5.61 and Table 5.62 show the comparison of EFG results (i.e. temperature values) obtained using 65 nodes with FEM results at the location $(x = 0.4 \text{ m}, y = 0.4 \text{ m})$ for $d_{\max} = 1.01$ and $d_{\max} = 1.51$ respectively. Similar comparison of temperature values obtained using 225 nodes is also presented in Table 5.63 and Table 5.64 for $d_{\max} = 1.01$ and $d_{\max} = 1.51$ respectively at the same location i.e. $(x = 0.4 \text{ m}, y = 0.4 \text{ m})$. Fig 5.19 shows the comparison of EFG results (i.e. temperature values) obtained using 65 nodes with FEM results for $d_{\max} = 1.01$ and $d_{\max} = 1.51$ at the location $(x = 0.4 \text{ m}, y = 0.2 \text{ m})$. Similar comparison of temperature values obtained using 225 nodes is shown in Fig. 5.20 at the same location i.e. $(x = 0.4 \text{ m}, y = 0.2 \text{ m})$. Fig 5.21 shows the comparison of EFG results (i.e. temperature values) obtained using 65 nodes with FEM results for $d_{\max} = 1.01$ and $d_{\max} = 1.51$ at the location $(x = 0.4 \text{ m}, y = 0 \text{ m})$. Similar comparison of temperature values obtained using 225 nodes is shown in Fig. 5.22 at the same location i.e. $(x = 0.4 \text{ m}, y = 0 \text{ m})$. From the results presented in tables and figures, it is clear that EFG results obtained using cubicspline, quarticspline, Gaussian, exponential and rational weight functions are acceptable for $d_{\max} = 1.01$. However for $d_{\max} = 1.51$ only exponential and rational weight functions give acceptable results. It has also been observed that the EFG results are in good agreement with those obtained by FEM.

Table 5.57 Comparison of EFG results obtained using 65 nodes with FEM at the location ($x = 0.2$ m, $y = 0$ m) of the 2-D model shown in Fig. 5.16 for $d_{\max} = 1.01$

Time (sec) $\times 10^2$	Temperature ($^{\circ}$ C)								
	$d_{\max} = 1.01$								FEM
	C. S.	Q. S	Gaussian	Quadratic	Hyperbolic	Exponential	Rational	Cosine	
0	0.0000	0.0000	0.0000	0.0000	0.0000	0.0000	0.0000	0.0000	0.0000
3	10.7865	10.8215	10.7815	-2.4247	1.0716	10.3237	10.1798	-5.4426	10.5622
6	19.6682	19.7224	19.3703	5.2386	0.3408	19.0806	18.9732	2.2806	19.3525
9	26.9194	26.9937	26.4495	13.5292	4.1779	26.3260	26.2842	10.8794	26.5179
12	31.9899	32.0749	31.4281	19.5230	7.6220	31.4163	31.3994	17.1124	31.5519
15	35.2890	35.3783	34.6793	23.4341	10.0605	34.7361	34.7183	21.1833	34.8467
18	37.3605	37.4507	36.7265	25.8829	11.6630	36.8243	36.7955	23.7343	36.9281
21	38.6380	38.7277	37.9921	27.3870	12.6841	38.1143	38.0726	25.3025	38.2194
24	39.4187	39.5074	38.7672	28.3023	13.3254	38.9039	38.8509	26.2576	39.0130
27	39.8935	39.9812	39.2397	28.8566	13.7255	39.3850	39.3231	26.8366	39.4983
30	40.1815	40.2684	39.5270	29.1916	13.9742	39.6775	39.6088	27.1867	39.7944

Table 5.58 Comparison of EFG results obtained using 65 nodes with FEM at the location ($x = 0.2$ m, $y = 0$ m) of the 2-D model shown in Fig. 5.16 for $d_{\max} = 1.51$

Time (sec) $\times 10^2$	Temperature ($^{\circ}$ C)								
	$d_{\max} = 1.51$								FEM
	C. S.	Q. S	Gaussian	Quadratic	Hyperbolic	Exponential	Rational	Cosine	
0	0.0000	0.0000	0.0000	0.0000	0.0000	0.0000	0.0000	0.0000	0.0000
3	5.3130	8.4701	13.6071	71.0879	149.7724	10.3344	11.2739	59.8015	10.5622
6	13.6293	16.5048	19.7625	91.0725	172.3374	19.1143	20.5884	76.9729	19.3525
9	21.4546	24.0143	25.2543	94.7349	179.3384	26.3626	28.0550	81.6653	26.5179
12	27.0443	29.4013	29.2413	95.6118	183.6405	31.4429	33.1886	83.5676	31.5519
15	30.6922	32.9267	31.8910	95.8618	186.3603	34.7514	36.4878	84.5281	34.8467
18	32.9798	35.1415	33.5805	95.9443	188.0630	36.8308	38.5408	85.0637	36.9281
21	34.3870	36.5056	34.6360	95.9755	189.1224	38.1147	39.7983	85.3752	38.2194
24	35.2443	37.3374	35.2886	95.9889	189.7792	38.9003	40.5624	85.5597	39.0130
27	35.7640	37.8421	35.6900	95.9954	190.1859	39.3789	41.0249	85.6701	39.4983
30	36.0783	38.1476	35.9362	95.9988	190.4375	39.6697	41.3043	85.7363	39.7944

Table 5.59 Comparison of EFG results obtained using 225 nodes with FEM at the location ($x = 0.2$ m, $y = 0$ m) of the 2-D model shown in Fig. 5.16 for $d_{max} = 1.01$

Time (sec) $\times 10^2$	Temperature ($^{\circ}$ C)								
	$d_{max} = 1.01$								FEM
	C. S.	Q. S	Gaussian	Quadratic	Hyperbolic	Exponential	Rational	Cosine	
0	0.0000	0.0000	0.0000	0.0000	0.0000	0.0000	0.0000	0.0000	0.0000
3	10.4866	10.5007	10.4995	14.4063	4.9593	10.3662	10.3783	21.4032	10.4110
6	19.1443	19.1753	19.0175	23.1739	10.7083	18.9376	18.9881	30.6208	18.9830
9	26.2790	26.3193	26.0638	30.0818	16.9042	26.0394	26.1194	36.9760	26.0618
12	31.3104	31.3542	31.0454	34.9362	21.4793	31.0636	31.1537	41.3331	31.0713
15	34.6075	34.6520	34.3157	38.1184	24.5244	34.3636	34.4528	44.1739	34.3658
18	36.6911	36.7351	36.3853	40.1303	26.4657	36.4532	36.5372	45.9678	36.4549
21	37.9837	38.0268	37.6708	41.3789	27.6784	37.7521	37.8301	47.0809	37.7552
24	38.7781	38.8204	38.4618	42.1465	28.4284	38.5519	38.6245	47.7653	38.5570
27	39.2640	39.3055	38.9462	42.6160	28.8898	39.0420	39.1103	48.1841	39.0489
30	39.5604	39.6013	39.2420	42.9024	29.1730	39.3415	39.4066	48.4397	39.3499

Table 5.60 Comparison of EFG results obtained using 225 nodes with FEM at the location ($x = 0.2$ m, $y = 0$ m) of the 2-D model shown in Fig. 5.16 for $d_{max} = 1.51$

Time (sec) $\times 10^2$	Temperature ($^{\circ}$ C)								
	$d_{max} = 1.51$								FEM
	C. S.	Q. S	Gaussian	Quadratic	Hyperbolic	Exponential	Rational	Cosine	
0	0.0000	0.0000	0.0000	0.0000	0.0000	0.0000	0.0000	0.0000	0.0000
3	7.7462	10.9097	11.3543	-3.4747	15.3900	10.3717	10.4438	21.6234	10.4110
6	16.2828	19.6196	18.8448	4.0845	27.4878	18.9519	19.0903	30.4622	18.9830
9	23.6898	26.7418	25.1319	12.9155	36.2533	26.0591	26.2493	37.6483	26.0618
12	28.9474	31.7489	29.6078	19.5808	42.4027	31.0834	31.2866	42.8919	31.0713
15	32.3941	35.0243	32.5604	24.0340	46.4831	34.3816	34.5771	46.3899	34.3658
18	34.5703	37.0915	34.4363	26.8641	49.1060	36.4691	36.6503	48.6180	36.4549
21	35.9189	38.3726	35.6057	28.6211	50.7641	37.7662	37.9331	50.0042	37.7552
24	36.7467	39.1592	36.3277	29.6995	51.8031	38.5646	38.7196	50.8564	38.5570
27	37.2524	39.6398	36.7712	30.3575	52.4510	39.0537	39.1995	51.3772	39.0489
30	37.5605	39.9328	37.0429	30.7579	52.8540	39.3526	39.4917	51.6943	39.3499

Table 5.61 Comparison of EFG results obtained using 65 nodes with FEM at the location ($x = 0.4$ m, $y = 0.4$ m) of the 2-D model shown in Fig. 5.16 for $d_{max} = 1.01$

Time (sec) $\times 10^2$	Temperature ($^{\circ}$ C)								
	$d_{max} = 1.01$								FEM
	C. S.	Q. S	Gaussian	Quadratic	Hyperbolic	Exponential	Rational	Cosine	
0	0.0000	0.0000	0.0000	0.0000	0.0000	0.0000	0.0000	0.0000	0.0000
3	15.1465	15.2048	15.1089	11.6186	37.9456	14.5669	14.5890	9.7432	15.0467
6	29.2601	29.3556	28.9595	26.3080	38.2419	28.6309	28.7937	23.9586	28.8943
9	38.2332	38.3425	37.7857	35.6443	41.5936	37.6545	37.8508	33.3323	37.7862
12	43.2704	43.3845	42.7407	40.8297	43.8156	42.7252	42.9096	38.6089	42.8359
15	46.1087	46.2239	45.5332	43.7280	45.1099	45.5863	45.7524	41.5793	45.7019
18	47.7479	47.8628	47.1473	45.3923	45.8674	47.2422	47.3920	43.2918	47.3654
21	48.7135	48.8276	48.0995	46.3682	46.3200	48.2199	48.3569	44.2984	48.3496
24	49.2895	49.4025	48.6683	46.9478	46.5947	48.8044	48.9317	44.8972	48.9391
27	49.6353	49.7475	49.0105	47.2945	46.7631	49.1561	49.2762	45.2558	49.2948
30	49.8437	49.9553	49.2172	47.5026	46.8668	49.3686	49.4836	45.4713	49.5101

Table 5.62 Comparison of EFG results obtained using 65 nodes with FEM at the location ($x = 0.4$ m, $y = 0.4$ m) of the 2-D model shown in Fig. 5.16 for $d_{max} = 1.51$

Time (sec) $\times 10^2$	Temperature ($^{\circ}$ C)								
	$d_{max} = 1.51$								FEM
	C. S.	Q. S	Gaussian	Quadratic	Hyperbolic	Exponential	Rational	Cosine	
0	0.0000	0.0000	0.0000	0.0000	0.0000	0.0000	0.0000	0.0000	0.0000
3	15.2078	15.1137	16.6223	-7.9844	-30.5130	14.6404	15.0084	25.9592	15.0467
6	29.4554	29.0364	28.0261	11.0799	9.0351	28.6991	29.4016	16.7255	28.8943
9	38.5784	38.1309	35.2540	22.5828	26.3658	37.6880	38.3322	4.6559	37.7862
12	43.7257	43.3244	39.3451	29.9876	34.6620	42.7359	43.2871	4.8838	42.8359
15	46.6361	46.2848	41.6712	34.6935	39.2264	45.5854	46.0718	11.3579	45.7019
18	48.3190	48.0053	43.0272	37.6183	41.9144	47.2354	47.6797	15.4889	47.3654
21	49.3096	49.0214	43.8338	39.4097	43.5425	48.2100	48.6262	18.0503	48.3496
24	49.8992	49.6275	44.3197	40.4980	44.5400	48.7926	49.1898	19.6165	48.9391
27	50.2523	49.9910	44.6145	41.1562	45.1541	49.1433	49.5274	20.5675	49.2948
30	50.4645	50.2097	44.7940	41.5535	45.5330	49.3551	49.7303	21.1428	49.5101

Table 5.63 Comparison of EFG results obtained using 225 nodes with FEM at the location ($x = 0.4$ m, $y = 0.4$ m) of the 2-D model shown in Fig. 5.16 for $d_{max} = 1.01$

Time (sec) $\times 10^2$	Temperature ($^{\circ}$ C)								
	$d_{max} = 1.01$								FEM
	C. S.	Q. S	Gaussian	Quadratic	Hyperbolic	Exponential	Rational	Cosine	
0	0.0000	0.0000	0.0000	0.0000	0.0000	0.0000	0.0000	0.0000	0.0000
3	14.9896	15.0035	14.9912	17.3642	13.2268	14.7772	14.8064	17.1327	14.8907
6	28.9491	28.9756	28.8120	31.2783	26.8085	28.6698	28.7594	31.2681	28.7244
9	37.8634	37.8948	37.6439	40.1217	35.2792	37.5830	37.6889	40.1438	37.6040
12	42.8837	42.9166	42.6185	45.0995	40.0650	42.6125	42.7146	45.1321	42.6292
15	45.7214	45.7544	45.4311	47.9138	42.7912	45.4606	45.5550	47.9523	45.4797
18	47.3663	47.3988	47.0623	49.5459	44.3839	47.1149	47.2020	49.5884	47.1370
21	48.3395	48.3714	48.0282	50.5119	45.3330	48.0956	48.1767	50.5572	48.1203
24	48.9226	48.9540	48.6075	51.0910	45.9055	48.6845	48.7609	51.1381	48.7112
27	49.2745	49.3055	48.9575	51.4406	46.2532	49.0406	49.1135	51.4890	49.0688
30	49.4878	49.5183	49.1698	51.6525	46.4652	49.2568	49.3272	51.7017	49.2862

Table 5.64 Comparison of EFG results obtained using 225 nodes with FEM at the location ($x = 0.4$ m, $y = 0.4$ m) of the 2-D model shown in Fig. 5.16 for $d_{max} = 1.51$

Time (sec) $\times 10^2$	Temperature ($^{\circ}$ C)								
	$d_{max} = 1.51$								FEM
	C. S.	Q. S	Gaussian	Quadratic	Hyperbolic	Exponential	Rational	Cosine	
0	0.0000	0.0000	0.0000	0.0000	0.0000	0.0000	0.0000	0.0000	0.0000
3	15.0045	14.9585	15.5115	11.5018	6.9750	14.7738	14.8902	120.642	14.8907
6	29.0358	28.8984	27.8449	24.8043	27.5273	28.6702	28.9079	115.222	28.7244
9	37.9879	37.8103	35.7667	33.8025	40.8259	37.5812	37.8268	-95.479	37.6040
12	43.0296	42.8367	40.2481	38.9443	48.3559	42.6078	42.8290	-80.318	42.6292
15	45.8797	45.6810	42.7905	41.8724	52.7249	45.4542	45.6514	-70.328	45.4797
18	47.5312	47.3306	44.2695	43.5756	55.3288	47.1075	47.2859	-64.041	47.1370
21	48.5077	48.3065	45.1478	44.5840	56.9078	48.0876	48.2520	-60.159	48.1203
24	49.0923	48.8910	45.6761	45.1876	57.8748	48.6760	48.8302	-57.783	48.7112
27	49.4447	49.2436	45.9962	45.5512	58.4704	49.0318	49.1787	-56.333	49.0688
30	49.6580	49.4571	46.1910	45.7709	58.8383	49.2477	49.3895	-55.452	49.2862

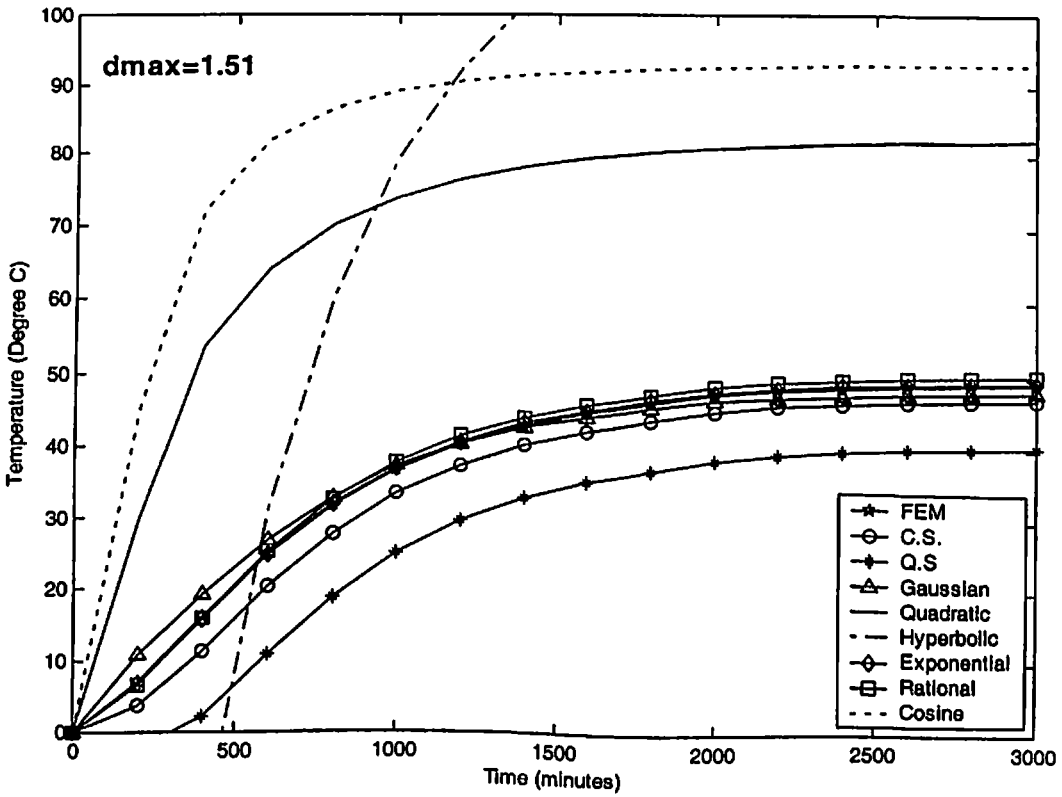
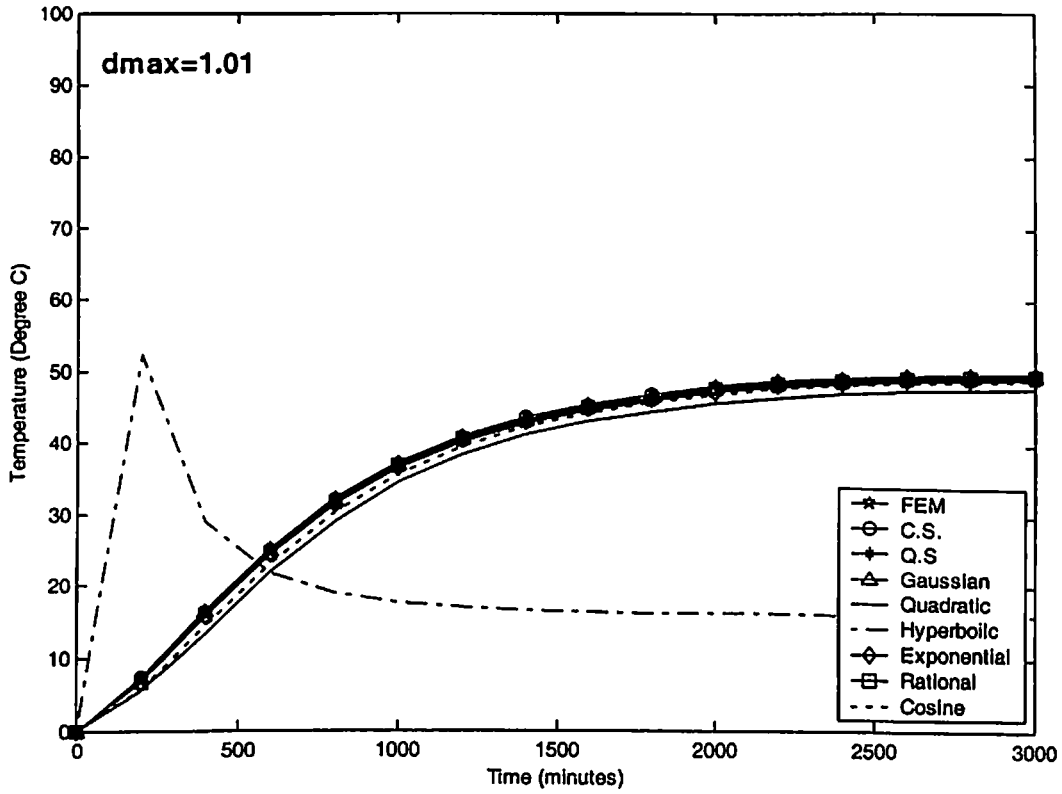


Fig. 5.19 Comparison of EFG results obtained using 65 nodes with FEM at the location ($x = 0.4$ m, $y = 0.2$ m) of the 2-D model shown in Fig. 5.16

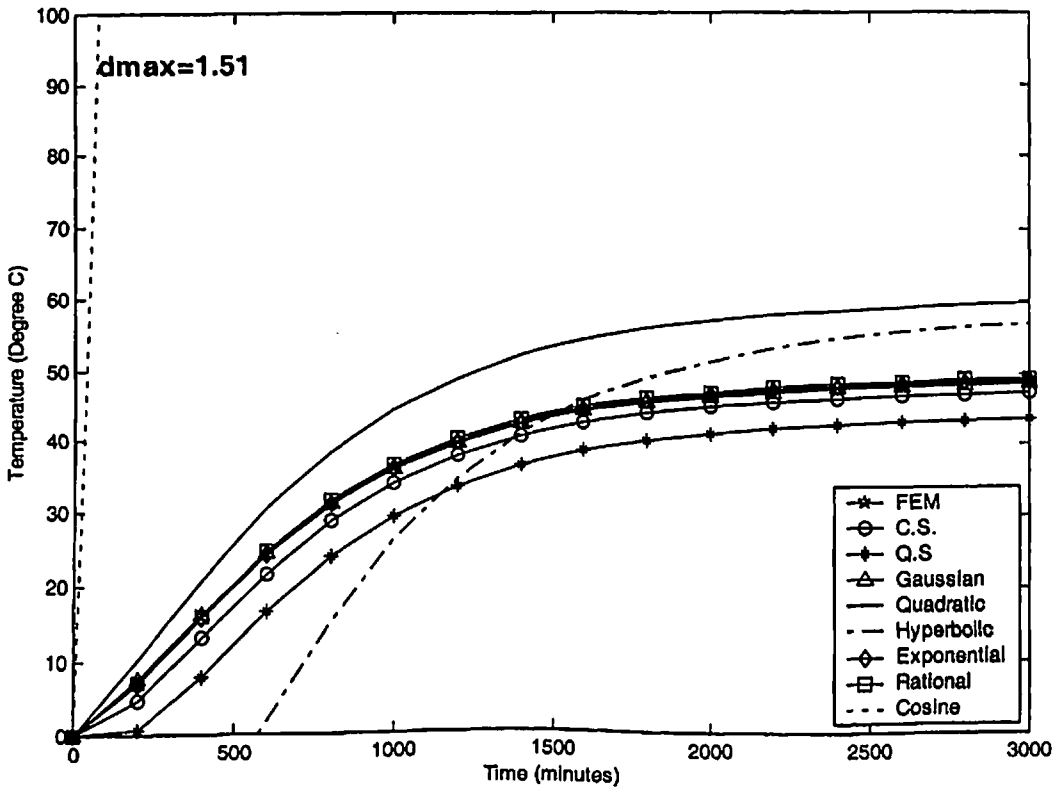
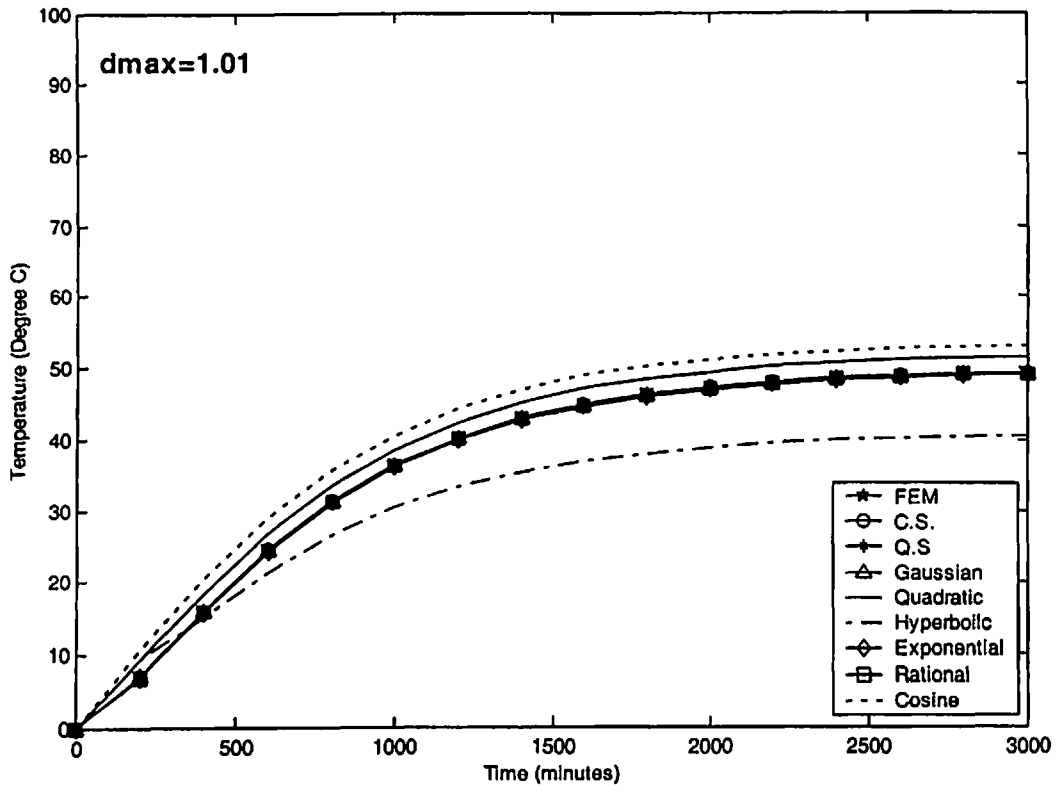


Fig. 5.20 Comparison of EFG results obtained using 225 nodes with FEM at the location ($x = 0.4$ m, $y = 0.2$ m) of the 2-D model shown in Fig. 5.16

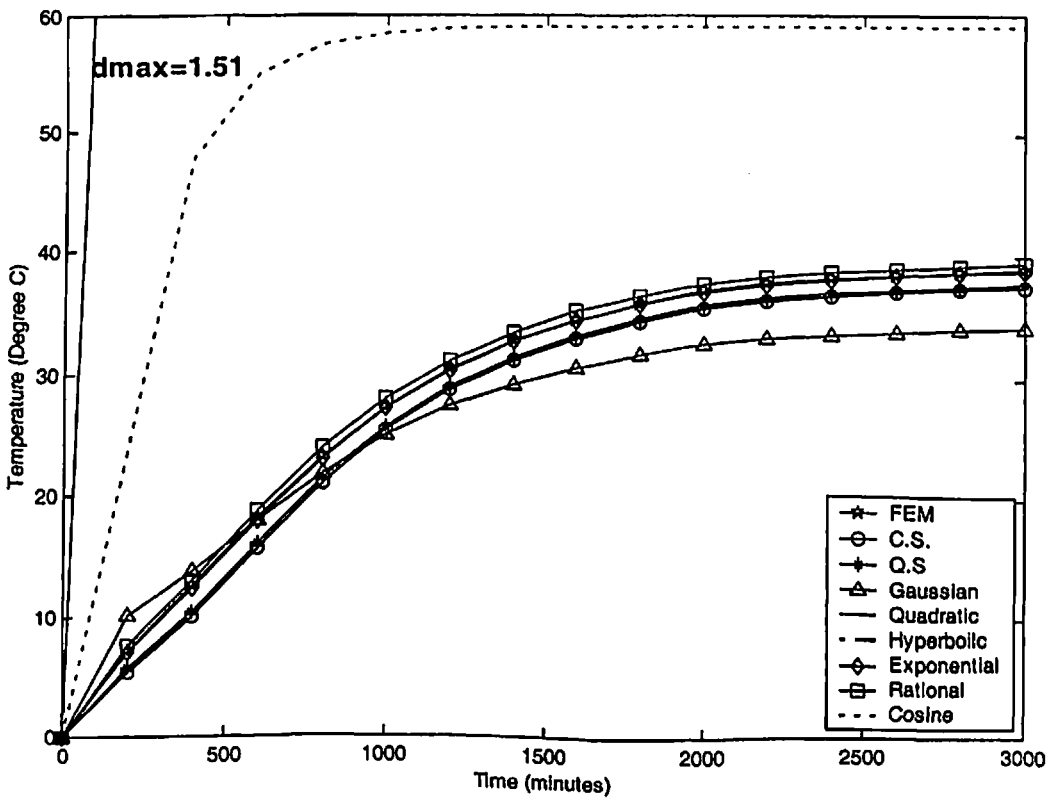
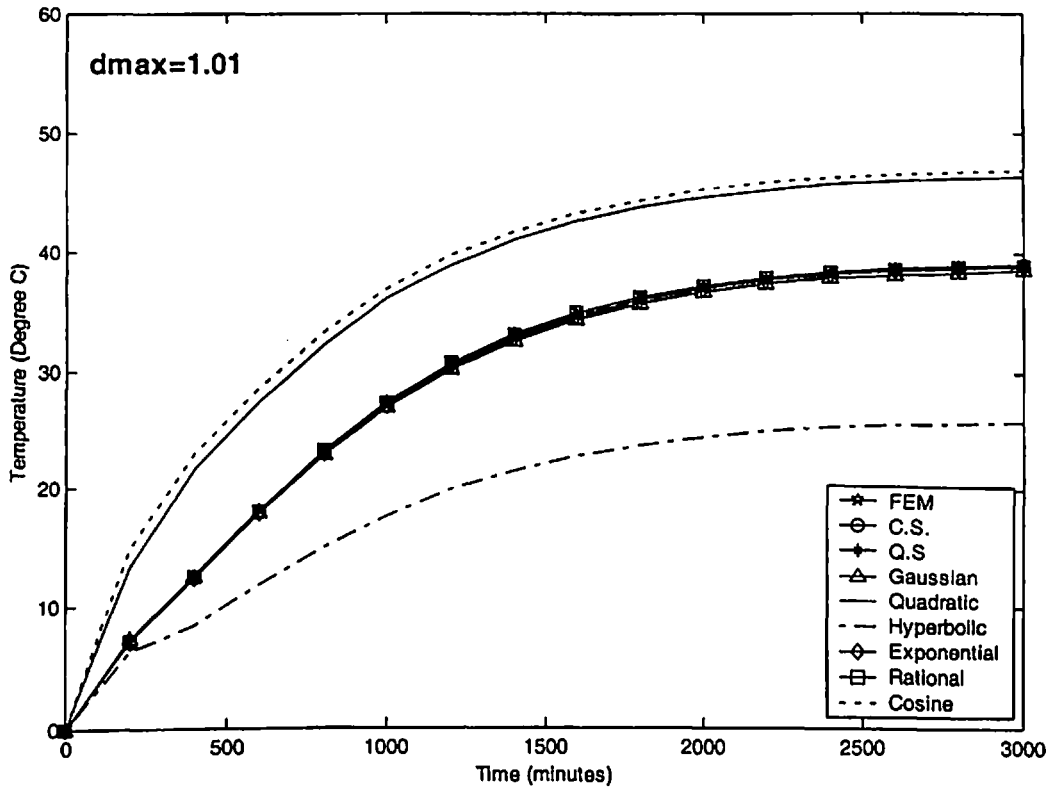


Fig. 5.21 Comparison of EFG results obtained using 65 nodes with FEM at the location ($x = 0.4$ m, $y = 0$ m) of the 2-D model shown in Fig. 5.16

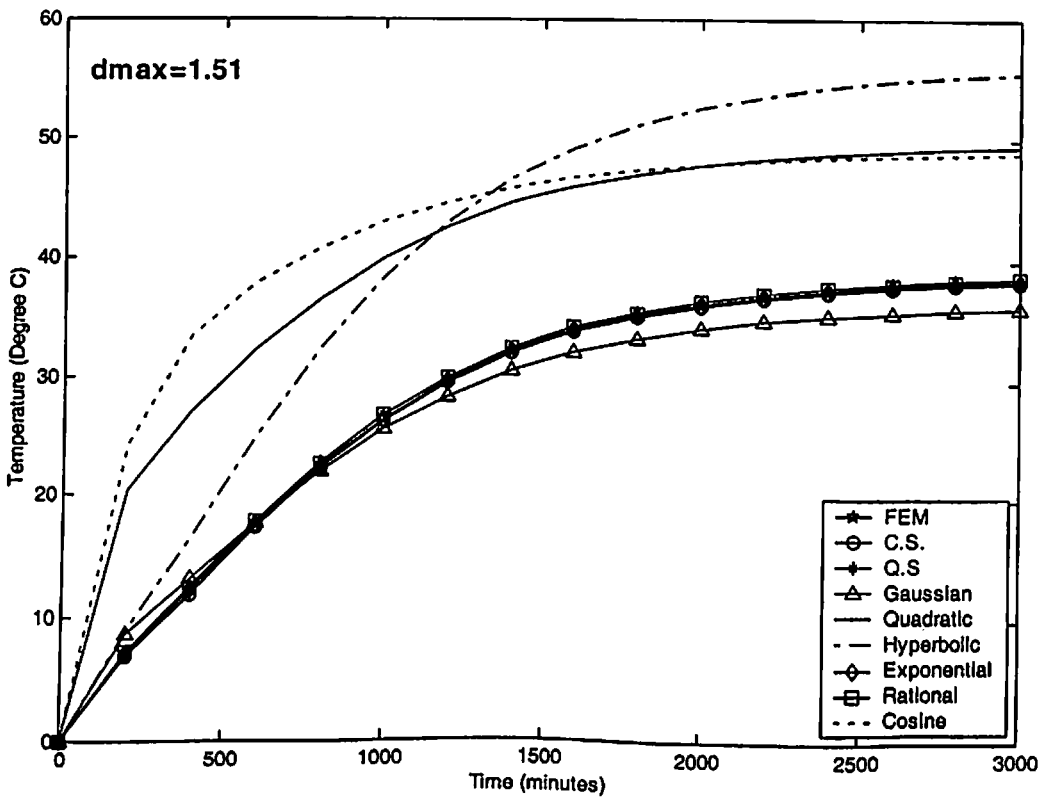
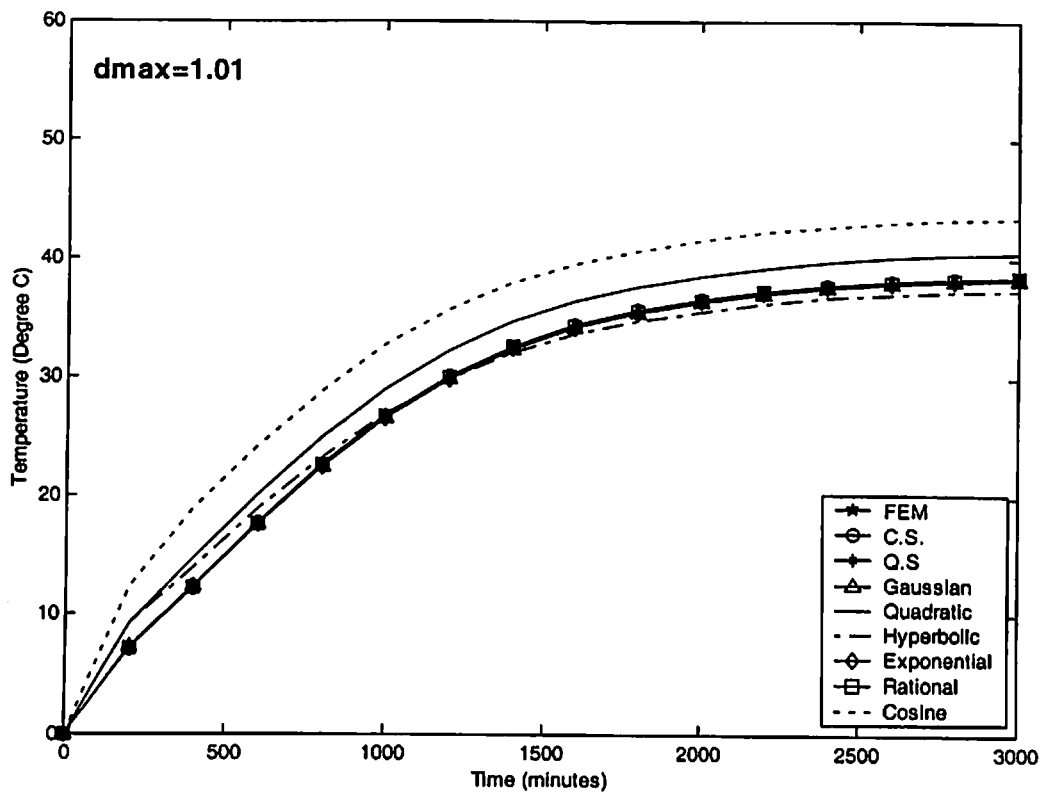


Fig. 5.22 Comparison of EFG results obtained using 225 nodes with FEM at the location ($x = 0.4$ m, $y = 0$ m) of the 2-D model shown in Fig. 5.16

➤ *CASE-IV*

5.8 DISCRETIZATION OF THE GOVERNING EQUATION

A general form of energy equation for two-dimensional heat transfer in the cylindrical coordinate system with thermal properties independent of temperature is given as:

$$k_r \frac{\partial^2 T}{\partial r^2} + \frac{k_r}{r} \frac{\partial T}{\partial r} + k_z \frac{\partial^2 T}{\partial z^2} + \dot{Q} = \rho c \frac{\partial T}{\partial t} \quad (5.31)$$

The above equation can be written as:

$$\frac{1}{r} \frac{\partial}{\partial r} \left(k_r r \frac{\partial T}{\partial r} \right) + \frac{\partial}{\partial z} \left(k_z \frac{\partial T}{\partial z} \right) + \dot{Q} = \rho c \frac{\partial T}{\partial t} \quad (5.32a)$$

The initial conditions are:

$$\text{at the time } t = 0 \quad T = T_{in} \quad \text{on} \quad \Omega \quad (5.32b)$$

The essential boundary conditions are:

$$\text{at } z = 0 \quad T = T_b \quad (5.32c)$$

The natural boundary conditions are:

$$\text{at } r = r_o \quad q_n = -hr(T - T_\infty) \quad (5.32d)$$

$$\text{at } r = 0 \quad q_n = 0 \quad (5.32e)$$

$$\text{at } z = L \quad q_n = -hr(T - T_\infty) \quad (5.32f)$$

The weighted integral form of Eq. (5.32a) is given as:

$$\int_0^L \int_0^{2\pi} \int_0^{r_o} w \left[\frac{1}{r} \frac{\partial}{\partial r} \left(k_r r \frac{\partial T}{\partial r} \right) + \frac{\partial}{\partial z} \left(k_z \frac{\partial T}{\partial z} \right) + \dot{Q} - \rho c \frac{\partial T}{\partial t} \right] r dr d\theta dz = 0 \quad (5.33)$$

Using divergence theorem to obtain the weak form of Eq. (5.33)

$$2\pi \iint_{\Omega} \left[\left(k_r \frac{\partial w}{\partial r} \frac{\partial T}{\partial r} + k_z \frac{\partial w}{\partial z} \frac{\partial T}{\partial z} \right) - \dot{Q} w + \rho c w \frac{\partial T}{\partial t} \right] r dr dz - 2\pi \int_{\Gamma} w q_n d\Gamma = 0 \quad (5.34)$$

where $q_n = r \left[k_r \frac{\partial T}{\partial r} n_r + k_z \frac{\partial T}{\partial z} n_z \right]$

Introducing natural boundary conditions in Eq. (5.34), the weak form becomes

$$\int_{\Omega} \left[\left(k_r \frac{\partial w}{\partial r} \frac{\partial T}{\partial r} + k_z \frac{\partial w}{\partial z} \frac{\partial T}{\partial z} \right) - \dot{Q} w + \rho c w \frac{\partial T}{\partial t} \right] r dr dz + \int_{\Gamma_1} w h r (T - T_{\infty}) d\Gamma + \int_{\Gamma_2} w h r (T - T_{\infty}) d\Gamma = 0 \quad (5.35)$$

The functional $I(T)$ can be written as:

$$I(T) = 2\pi \int_{\Omega} \frac{1}{2} \left[k_r \left(\frac{\partial T}{\partial r} \right)^2 + k_z \left(\frac{\partial T}{\partial z} \right)^2 \right] r dr dz + 2\pi \int_{\Omega} \rho c \dot{T} T r dr dz - 2\pi \int_{\Omega} \dot{Q} T r dr dz + 2\pi \int_{\Gamma_1} \frac{h r T^2}{2} d\Gamma + 2\pi \int_{\Gamma_2} \frac{h r T^2}{2} d\Gamma - 2\pi \int_{\Gamma_1} h r T T_{\infty} d\Gamma - 2\pi \int_{\Gamma_2} h r T T_{\infty} d\Gamma \quad (5.36)$$

Enforcing essential boundary conditions using Lagrange multiplier method, the functional

$I^*(T)$ is obtained as:

$$I^*(T) = 2\pi \int_{\Omega} \frac{1}{2} \left[k_r \left(\frac{\partial T}{\partial r} \right)^2 + k_z \left(\frac{\partial T}{\partial z} \right)^2 \right] r dr dz + 2\pi \int_{\Omega} \rho c \dot{T} T r dr dz - 2\pi \int_{\Omega} \dot{Q} T r dr dz + 2\pi \int_{\Gamma_1} \frac{h r T^2}{2} d\Gamma + 2\pi \int_{\Gamma_2} \frac{h r T^2}{2} d\Gamma - 2\pi \int_{\Gamma_1} h r T T_{\infty} d\Gamma - 2\pi \int_{\Gamma_2} h r T T_{\infty} d\Gamma + \int_{\Gamma_2} \lambda (T - T_b) d\Gamma \quad (5.37)$$

Using variational principle to obtain the discrete equations:

$$\delta I^*(T) = 2\pi \int_{\Omega} \left[k_r \left(\frac{\partial T}{\partial r} \right)^T \delta \left(\frac{\partial T}{\partial r} \right) + k_z \left(\frac{\partial T}{\partial z} \right)^T \delta \left(\frac{\partial T}{\partial z} \right) \right] r dr dz + \int_{\Omega} \rho c \dot{T} \delta T r dr dz - 2\pi \int_{\Omega} \dot{Q} \delta T r dr dz + 2\pi \int_{\Gamma_1} h r T^T \delta T d\Gamma + 2\pi \int_{\Gamma_2} h r T^T \delta T d\Gamma - 2\pi \int_{\Gamma_1} h r T_{\infty} \delta T d\Gamma - 2\pi \int_{\Gamma_2} h r T_{\infty} \delta T d\Gamma + \int_{\Gamma_2} \lambda \delta T d\Gamma + \int_{\Gamma_2} \delta \lambda (T - T_b) d\Gamma \quad (5.38)$$

since δT and $\delta \lambda$ are arbitrary in the preceding equation, the following set of equations is

obtained using Eq. (3.25) and Eq. (5.38)

$$[\mathbf{K}]\{\mathbf{T}\} + [\mathbf{C}]\{\dot{\mathbf{T}}\} + [\mathbf{G}]\{\lambda\} = \{\mathbf{f}\} \quad (5.39a)$$

$$[\mathbf{G}^T]\{\mathbf{T}\} = \{\mathbf{q}\} \quad (5.39b)$$

where

$$K_{IJ} = 2\pi \int_{\Omega} \begin{bmatrix} \Phi_{I,r} \\ \Phi_{I,z} \end{bmatrix}^T \begin{bmatrix} k_r & 0 \\ 0 & k_z \end{bmatrix} \begin{bmatrix} \Phi_{I,r} \\ \Phi_{I,z} \end{bmatrix} r \, dr dz + 2\pi \int_{\Gamma_3} h r \Phi_i^T \Phi_j \, d\Gamma + 2\pi \int_{\Gamma_4} h r \Phi_i^T \Phi_j \, d\Gamma \quad (5.40a)$$

$$C_{IJ} = 2\pi \int_{\Omega} \rho c \Phi_i^T \Phi_j \, r \, dr dz \quad (5.40b)$$

$$f_i = 2\pi \int_{\Omega} \dot{Q} \Phi_i \, r \, dr dz + 2\pi \int_{\Gamma_3} h r T_{\infty} \Phi_i \, d\Gamma + 2\pi \int_{\Gamma_4} h r T_{\infty} \Phi_i \, d\Gamma \quad (5.40c)$$

$$G_{IK} = \int_{\Gamma_3} \Phi_i N_K \, d\Gamma \quad (5.40d)$$

$$q_K = \int_{\Gamma_3} T_b N_K \, d\Gamma \quad (5.40e)$$

Using backward difference technique for time approximation, the Eq. (5.39) can be written

as:

$$\begin{bmatrix} \mathbf{K}^* + \mathbf{C} & \mathbf{G} \\ \mathbf{G}^T & 0 \end{bmatrix} \begin{Bmatrix} \mathbf{T}_N \\ \boldsymbol{\lambda} \end{Bmatrix} = \begin{Bmatrix} \mathbf{R}_N \\ \mathbf{q} \end{Bmatrix} \quad (5.41)$$

where

$$\mathbf{R}_N = ([\mathbf{C}] - (1 - \alpha) \Delta t [\mathbf{K}]) \{\mathbf{T}\}_{N-1} + \alpha \Delta t \{\mathbf{f}\}_N + (1 - \alpha) \Delta t \{\mathbf{f}\}_{N-1} \quad (5.42a)$$

$$\mathbf{K}^* = \alpha \Delta t [\mathbf{K}] \quad (5.42b)$$

5.9 NUMERICAL RESULTS AND DISCUSSION

The different parameters used for steady-state and transient analysis of two-dimensional model shown in Fig. 5.23 are tabulated in Table 5.65. The EFG results are obtained using different weight functions for two sets of nodes and the FEM results are obtained using ANSYS 6.0 for same sets of nodes. A comparative analysis is carried out to evaluate the performance of different EFG weight functions.

5.9.1 Steady-state analysis

The results (i.e. temperature values) presented in Table 5.66 are obtained using different EFG weight functions for two values of scaling parameter (i.e. $d_{\max} = 1.01$ & $d_{\max} = 1.51$) at the location ($r = 0.5\text{ m}$ & $z = 1\text{ m}$) and it shows a comparison of temperature values obtained by EFG method using different weight functions with FEM for 25 nodes. Table 5.67 shows a comparison of temperature values obtained by EFG method using different functions for two values of scaling parameter with FEM at the same location i.e. ($r = 0.5\text{ m}$ & $z = 1\text{ m}$) for 81 nodes. A comparison of temperature values obtained using different EFG weight functions with FEM for 25 and 81 nodes, is shown in Table 5.68 and Table 5.69 respectively at the location ($r = 0.5\text{ m}$ & $z = 0.75\text{ m}$). Similar type of comparisons of temperature values are shown in Table 5.70 for 25 nodes at the location ($r = 0.5\text{ m}$ & $z = 0.5\text{ m}$), in Table 5.71 for 81 nodes at the location ($r = 0.5\text{ m}$ & $z = 0.5\text{ m}$), in Table 5.72 for 25 nodes at the location ($r = 0.5\text{ m}$ & $z = 0.25\text{ m}$) and in Table 5.73 for 81 nodes at the location ($r = 0.5\text{ m}$ & $z = 0.25\text{ m}$). From the results presented in Table 5.66 to Table 5.73, it is observed that EFG results obtained using different weight functions are almost similar for $d_{\max} = 1.01$. However for $d_{\max} = 1.51$, only cubicspline, quarticspline, Gaussian, exponential and rational weight functions give acceptable results. It is also observed that EFG results obtained using different weight functions are in good agreement with those obtained by FEM. Moreover with the increase in number of nodes EFG results starts converging.

The effect of scaling parameter (d_{\max}) on EFG results obtained using different weight functions is presented in Table 5.74 for 25 nodes and Table 5.75 for 81 nodes respectively at the location ($r = 0.5\text{ m}$ & $z = 1\text{ m}$). Similar effect of scaling parameter on EFG results is shown in Table 5.76 for 25 nodes and Table 5.77 for 81 nodes at the location ($r = 0.5\text{ m}$ & $z = 0.5\text{ m}$). Fig. 5.24 shows the effect of scaling parameter on EFG results

obtained using 25 and 81 nodes at the location ($r = 0.5 \text{ m}$ & $z = 0.75 \text{ m}$). Similar effect of scaling parameter on EFG results is observed in Fig. 5.25 at the location ($r = 0.5 \text{ m}$ & $z = 0.25 \text{ m}$). From tables and figures, it is clear that only cubicspline, quarticspline, Gaussian, exponential and rational weight functions give acceptable results in the range $1.0 < d_{\max} < 1.8$ whereas the results obtained using quadratic, hyperbolic and cosine weight functions are varying in abrupt manner with scaling parameter. Therefore EFG results obtained using quadratic, hyperbolic and cosine weight functions are not acceptable in the range $1.0 < d_{\max} < 1.8$. It is also observed that there is minimum variation in EFG results with scaling parameter for exponential weight function.

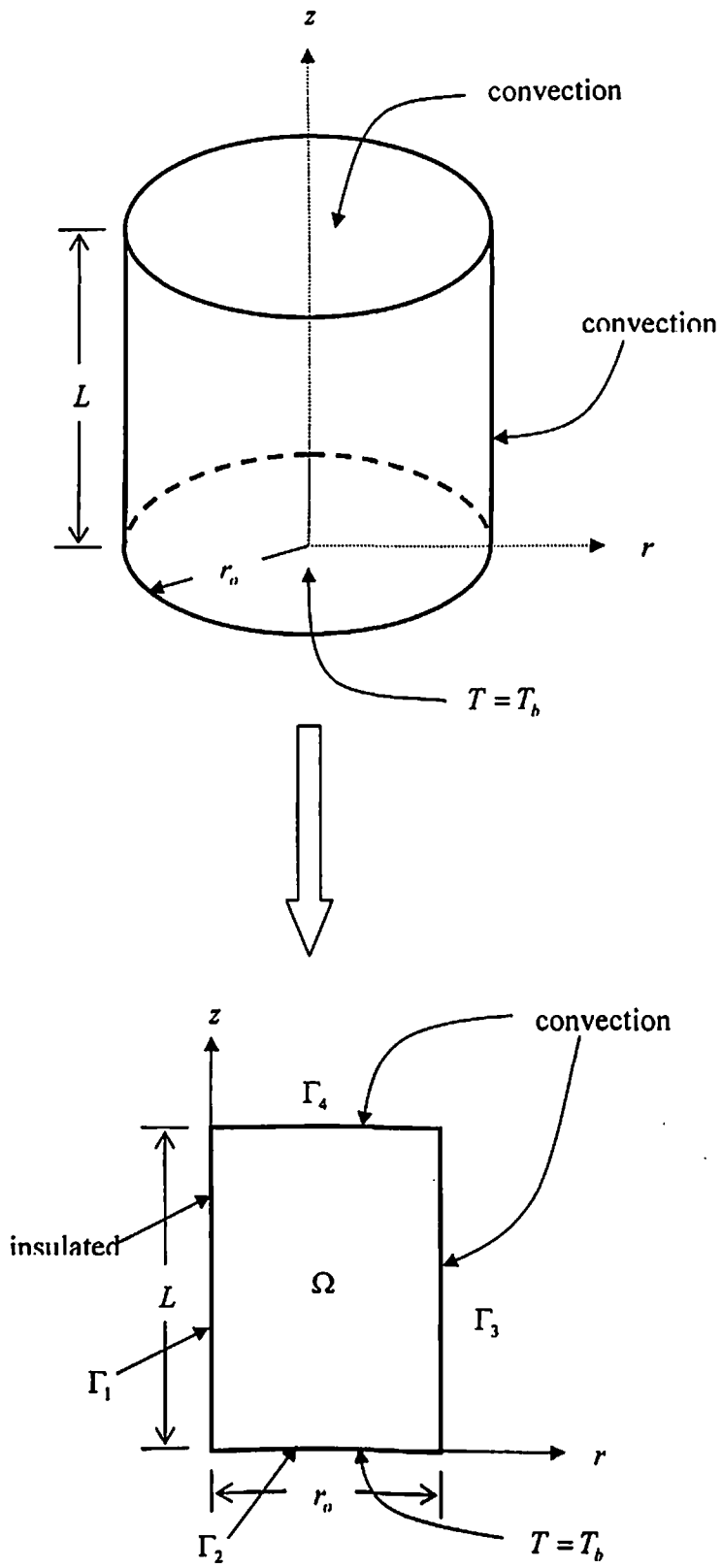


Fig. 5.23 Two-dimensional model

Table 5.65 Data for 2-D model shown in Fig 5.23

Parameters	Value of the parameter
Radius (r)	0.5 m
Length (L)	1 m
Thermal conductivity (k)	400 W/m-K
Specific heat (c)	400 kJ/kg-K
Density of material (ρ)	10000 kg/m ³
Rate of internal heat generation (\dot{Q})	10000 W/m ³
Heat transfer coefficient (h)	200 W/m ² -K
Initial temperature (T_{mi})	100 °C
Time step size (Δt)	100 sec
Surrounding fluid temperature (T_{∞})	20 °C
Temperature T_b at $z = 0$	100 °C

Table 5.66 Comparison of EFG results obtained using 25 nodes with FEM results at the location ($r = 0.5 \text{ m}$ & $z = 1 \text{ m}$) of 2-D model shown in Fig 5.23

Weight function	EFG				FEM
	$d_{\max} = 1.01$		$d_{\max} = 1.51$		
	T (°C)	% diff with FEM	T (°C)	% diff with FEM	T (°C)
C. S.	51.9724	-0.5861	52.0755	-0.3889	52.2788
Q. S.	51.9781	-0.5752	52.1028	-0.3367	
Gaussian	51.9458	-0.6370	52.0378	-0.4610	
Quadratic	51.9886	-0.5551	52.9217	1.2297	
Hyperbolic	52.0311	-0.4738	51.4061	-1.6693	
Exponential	51.9810	-0.5696	51.9876	-0.5570	
Rational	51.9875	-0.5572	51.9734	-0.5842	
Cosine	51.9885	-0.5553	53.1896	1.7422	

Table 5.67 Comparison of EFG results obtained using 81 nodes with FEM results at the location ($r = 0.5 \text{ m}$ & $z = 1 \text{ m}$) of 2-D model shown in Fig 5.23

Weight function	EFG				FEM
	$d_{\max} = 1.01$		$d_{\max} = 1.51$		
	T (°C)	% diff with FEM	T (°C)	% diff with FEM	T (°C)
C. S.	52.0586	-0.1481	52.0833	-0.1007	52.1358
Q. S.	52.0602	-0.1450	52.0869	-0.0938	
Gaussian	52.0497	-0.1651	52.0641	-0.1375	
Quadratic	52.0630	-0.1396	52.2684	0.2543	
Hyperbolic	52.0683	-0.1295	51.9931	-0.2737	
Exponential	52.0610	-0.1435	52.0618	-0.1419	
Rational	52.0627	-0.1402	52.0416	-0.1807	
Cosine	52.0630	-0.1396	52.4961	0.6912	

Table 5.68 Comparison of EFG results obtained using 25 nodes with FEM results at the location ($r = 0.5$ m & $z = 0.75$ m) of 2-D model shown in Fig 5.23

Weight function	EFG				FEM
	$d_{\max} = 1.01$		$d_{\max} = 1.51$		
	T (°C)	% diff with FEM	T (°C)	% diff with FEM	T (°C)
C. S.	57.2216	-0.2616	56.9963	-0.6543	57.3717
Q. S.	57.2206	-0.2634	56.8957	-0.8297	
Gaussian	57.2159	-0.2716	57.0134	-0.6245	
Quadratic	57.2187	-0.2667	54.7609	-4.5507	
Hyperbolic	57.1697	-0.3521	57.4664	0.1651	
Exponential	57.2210	-0.2627	57.1739	-0.3448	
Rational	57.2195	-0.2653	56.9861	-0.6721	
Cosine	57.2190	-0.2662	54.4003	-5.1792	

Table 5.69 Comparison of EFG results obtained using 81 nodes with FEM results at the location ($r = 0.5$ m & $z = 0.75$ m) of 2-D model shown in Fig 5.23

Weight function	EFG				FEM
	$d_{\max} = 1.01$		$d_{\max} = 1.51$		
	T (°C)	% diff with FEM	T (°C)	% diff with FEM	T (°C)
C. S.	57.3156	-0.0457	57.2779	-0.1114	57.3418
Q. S.	57.3160	-0.0450	57.2681	-0.1285	
Gaussian	57.3134	-0.0495	57.2739	-0.1184	
Quadratic	57.3168	-0.0436	57.9015	0.9761	
Hyperbolic	57.3181	-0.0413	57.2833	-0.1020	
Exponential	51.3163	-10.508	57.3074	-0.0600	
Rational	57.3168	-0.0436	57.2796	-0.1085	
Cosine	57.3168	-0.0436	58.3452	1.7499	

Table 5.70 Comparison of EFG results obtained using 25 nodes with FEM results at the location ($r = 0.5 \text{ m}$ & $z = 0.5 \text{ m}$) of 2-D model shown in Fig 5.23

Weight function	EFG				FEM
	$d_{\max} = 1.01$		$d_{\max} = 1.51$		
	T (°C)	% diff with FEM	T (°C)	% diff with FEM	T (°C)
C. S.	65.4849	-0.2349	65.3907	-0.3784	65.6391
Q. S.	65.4953	-0.2191	65.4240	-0.3277	
Gaussian	65.4684	-0.2601	65.3341	-0.4647	
Quadratic	65.5127	-0.1926	68.0051	3.6046	
Hyperbolic	65.6079	-0.0475	64.7891	-1.2950	
Exponential	65.4990	-0.2134	65.4852	-0.2345	
Rational	65.5106	-0.1958	65.5052	-0.2040	
Cosine	65.5125	-0.1929	68.3967	4.2011	

Table 5.71 Comparison of EFG results obtained using 81 nodes with FEM results at the location ($r = 0.5 \text{ m}$ & $z = 0.5 \text{ m}$) of 2-D model shown in Fig 5.23

Weight function	EFG				FEM
	$d_{\max} = 1.01$		$d_{\max} = 1.51$		
	T (°C)	% diff with FEM	T (°C)	% diff with FEM	T (°C)
C. S.	65.5568	-0.0392	65.5011	-0.1241	65.5825
Q. S.	65.5565	-0.0396	65.4899	-0.1412	
Gaussian	65.5601	-0.0342	65.4950	-0.1334	
Quadratic	65.5569	-0.0390	66.5047	1.4062	
Hyperbolic	65.5608	-0.0331	65.2554	-0.4988	
Exponential	65.5568	-0.0392	65.5452	-0.0569	
Rational	65.5569	-0.0390	65.5156	-0.1020	
Cosine	65.5570	-0.0389	67.0829	2.2878	

Table 5.72 Comparison of EFG results obtained using 25 nodes with FEM results at the location ($r = 0.5 \text{ m}$ & $z = 0.25 \text{ m}$) of 2-D model shown in Fig 5.23

Weight function	EFG				FEM
	$d_{\max} = 1.01$		$d_{\max} = 1.51$		
	T (°C)	% diff with FEM	T (°C)	% diff with FEM	T (°C)
C. S.	77.6008	-0.4289	76.6960	-1.5899	77.9351
Q. S.	77.5378	-0.5098	76.3730	-2.0044	
Gaussian	77.9315	-0.0046	76.7610	-1.5065	
Quadratic	77.4662	-0.6017	73.2077	-6.0658	
Hyperbolic	77.1910	-0.9548	76.1959	-2.2316	
Exponential	77.5254	-0.5257	77.3028	-0.8113	
Rational	77.4757	-0.5895	76.6005	-1.7125	
Cosine	77.4677	-0.5997	72.8537	-6.5200	

Table 5.73 Comparison of EFG results obtained using 81 nodes with FEM results at the location ($r = 0.5 \text{ m}$ & $z = 0.25 \text{ m}$) of 2-D model shown in Fig 5.23

Weight function	EFG				FEM
	$d_{\max} = 1.01$		$d_{\max} = 1.51$		
	T (°C)	% diff with FEM	T (°C)	% diff with FEM	T (°C)
C. S.	78.0171	-0.0404	77.9763	-0.0926	78.0486
Q. S.	78.0175	-0.0398	77.9951	-0.0685	
Gaussian	78.0388	-0.0126	77.9542	-0.1210	
Quadratic	78.0207	-0.0357	79.3513	1.6691	
Hyperbolic	78.0535	0.0063	77.7723	-0.3540	
Exponential	78.0182	-0.0390	78.0108	-0.0484	
Rational	78.0203	-0.0363	78.0236	-0.0320	
Cosine	78.0207	-0.0357	79.9654	2.4559	

Table 5.74 Effect of scaling parameter on EFG results obtained using 25 nodes at the location ($r = 0.5 \text{ m}$ & $z = 1 \text{ m}$) of 2-D model shown in Fig 5.23

Scaling Parameter	Temperature ($^{\circ} \text{C}$)							
	C. S.	Q. S	Gaussian	Quadratic	Hyperbolic	Exponential	Rational	Cosine
1.01	51.9724	51.9781	51.9458	51.9886	52.0311	51.9810	51.9875	51.9885
1.21	51.9813	52.0062	52.0439	52.0568	51.9870	52.0433	52.0295	52.0461
1.41	52.0525	52.0666	52.0513	53.0275	51.6315	51.9886	51.9682	52.8641
1.61	52.0985	52.1388	52.0143	51.8687	51.3681	51.9868	51.9786	52.3269
1.81	52.1542	52.2264	51.9293	51.3742	47.9994	51.9778	51.8954	52.4155
2.01	52.2478	52.3760	51.7990	49.5650	58.6151	52.0019	52.0840	51.0818
2.21	52.3937	52.5915	51.6035	48.1764	54.9746	52.0192	52.0796	46.7262
2.41	52.6361	52.9602	51.3104	47.8151	53.8061	52.0190	52.0592	44.5070
2.61	53.0334	53.5400	50.9136	41.5072	58.9456	52.0251	52.0901	45.1478
2.81	53.6470	54.3384	50.3435	44.0963	30.6739	52.0530	52.0271	40.9436
3.01	54.5642	55.2914	49.6702	56.6924	66.8051	52.1450	52.5032	58.1813

Table 5.75 Effect of scaling parameter on EFG results obtained using 81 nodes at the location ($r = 0.5 \text{ m}$ & $z = 1 \text{ m}$) of 2-D model shown in Fig 5.23

Scaling Parameter	Temperature ($^{\circ} \text{C}$)							
	C. S.	Q. S	Gaussian	Quadratic	Hyperbolic	Exponential	Rational	Cosine
1.01	52.0586	52.0602	52.0497	52.0630	52.0683	52.0610	52.0627	52.0630
1.21	52.0614	52.0678	52.0821	52.0531	52.0018	52.0775	52.0675	52.0580
1.41	52.0789	52.0811	52.0769	52.3297	51.9761	52.0626	52.0439	52.2604
1.61	52.0862	52.0898	52.0443	52.0735	52.0255	52.0608	52.0389	52.1799
1.81	52.0891	52.0933	51.9723	52.3024	51.7262	52.0580	52.0012	52.1115
2.01	52.0953	52.1095	51.8563	53.0548	57.2243	52.0637	52.0455	51.9960
2.21	52.1116	52.1458	51.6750	50.9800	52.9895	52.0668	52.0435	52.5714
2.41	52.1498	52.2214	51.3827	43.9217	57.9337	52.0624	52.0268	45.5785
2.61	52.2320	52.3583	50.9327	53.3454	58.8348	52.0606	52.0198	50.4178
2.81	52.3896	52.5306	50.2148	55.0448	67.5001	52.0630	51.9848	51.8628
3.01	52.6858	52.5274	49.1693	49.5605	37.0879	52.0869	52.1632	-17.9625

Table 5.76 Effect of scaling parameter on EFG results obtained using 25 nodes at the location ($r = 0.5 \text{ m}$ & $z = 0.5 \text{ m}$) of 2-D model shown in Fig 5.23

Scaling Parameter	Temperature ($^{\circ} \text{C}$)							
	C. S.	Q. S	Gaussian	Quadratic	Hyperbolic	Exponential	Rational	Cosine
1.01	65.4849	65.4953	65.4684	65.5127	65.6079	65.4990	65.5106	65.5125
1.21	65.5112	65.4694	65.3351	65.6983	65.7218	65.4011	65.4549	65.6328
1.41	65.3991	65.3986	65.3250	67.5991	65.3914	65.4917	65.4899	67.5109
1.61	65.4195	65.5345	65.3539	66.0335	64.7328	65.4789	65.5305	66.9814
1.81	65.6173	65.9214	65.4258	67.9842	56.6171	65.3823	65.6971	68.9462
2.01	66.0056	66.5172	65.6147	62.8794	90.5172	65.2628	65.6508	65.5032
2.21	66.5389	67.2197	65.9749	53.7560	79.6929	65.0879	65.4661	56.4788
2.41	67.2740	68.2528	66.5815	33.3267	58.0434	65.0494	64.8532	26.6914
2.61	68.3200	69.8062	67.6762	28.0725	58.0623	64.9913	65.1100	28.5397
2.81	69.9463	72.2070	69.2782	30.1317	-9.8611	64.6808	63.4438	29.5945
3.01	72.4066	75.4949	71.9136	46.4411	94.6125	64.5374	64.8542	56.2453

Table 5.77 Effect of scaling parameter on EFG results obtained using 81 nodes at the location ($r = 0.5 \text{ m}$ & $z = 0.5 \text{ m}$) of 2-D model shown in Fig 5.23

Scaling Parameter	Temperature ($^{\circ} \text{C}$)							
	C. S.	Q. S	Gaussian	Quadratic	Hyperbolic	Exponential	Rational	Cosine
1.01	65.5568	65.5565	65.5601	65.5569	65.5608	65.5568	65.5569	65.5570
1.21	65.5594	65.5449	65.5191	65.5595	65.5681	65.5229	65.5203	65.5456
1.41	65.5156	65.5065	65.5027	66.2806	65.3240	65.5490	65.5202	66.2391
1.61	65.4902	65.4872	65.4877	65.8175	65.1989	65.5411	65.5131	66.2070
1.81	65.4915	65.5366	65.4673	64.5122	64.1298	65.5143	65.4635	65.0520
2.01	65.5459	65.6907	65.4580	62.6984	104.2801	65.4744	65.4009	63.5118
2.21	65.6872	65.9803	65.4794	64.7419	66.7819	65.4347	65.2973	63.0350
2.41	65.9687	66.4999	65.5671	65.1123	54.0624	65.4173	65.0859	66.5635
2.61	66.4928	67.4201	65.8533	48.0361	52.1084	65.3919	64.9714	49.2464
2.81	67.4874	68.9329	66.3941	64.9417	33.2469	65.3397	64.5082	65.1021
3.01	69.3397	70.2641	67.5454	82.9377	114.9206	65.3083	65.0588	71.7502

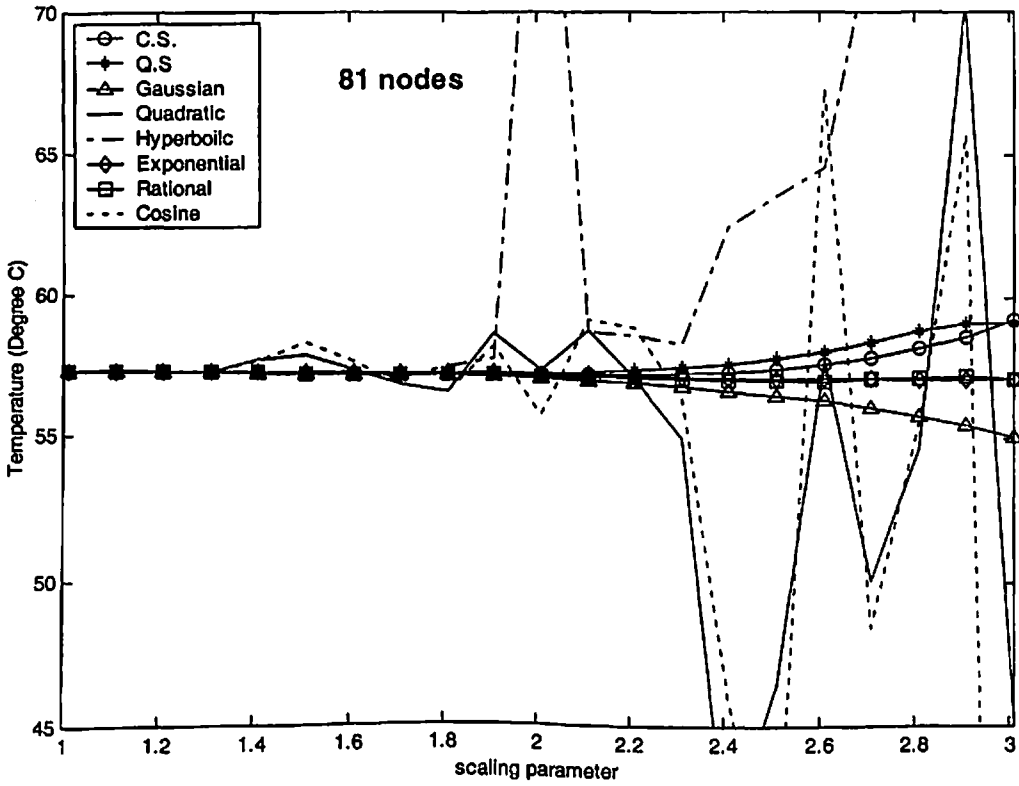
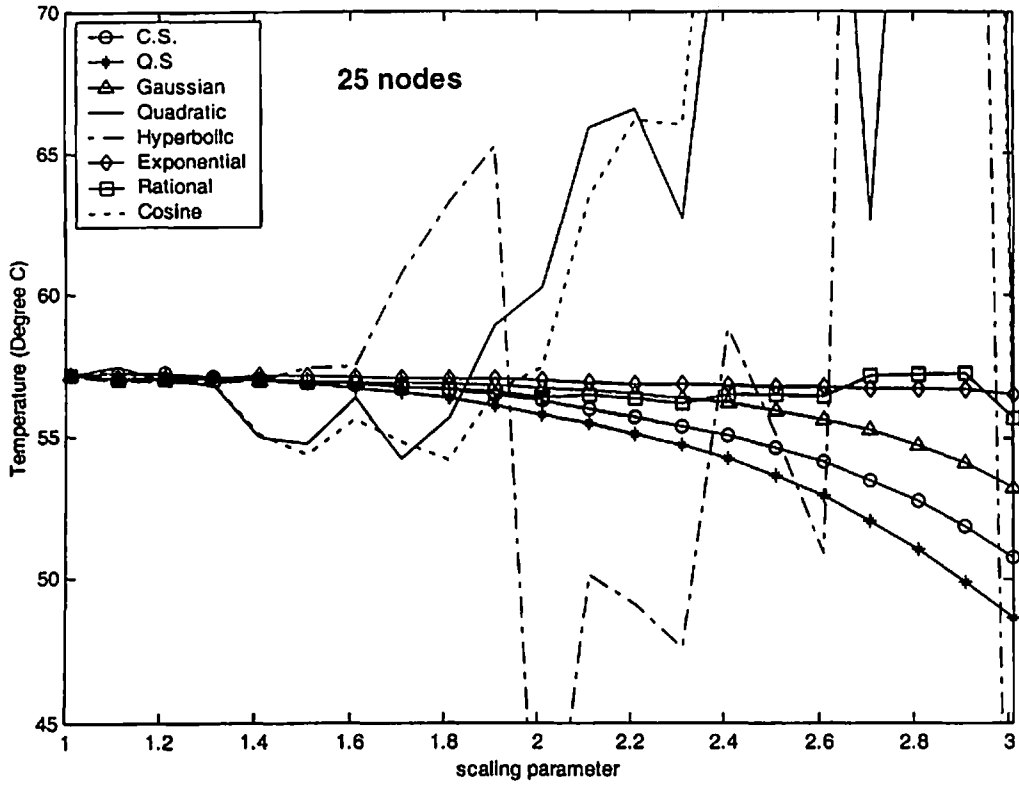


Fig. 5.24 Effect of scaling parameter on EFG results at the location ($r = 0.5$ m & $z = 0.75$ m) of 2-D model shown in Fig 5.23

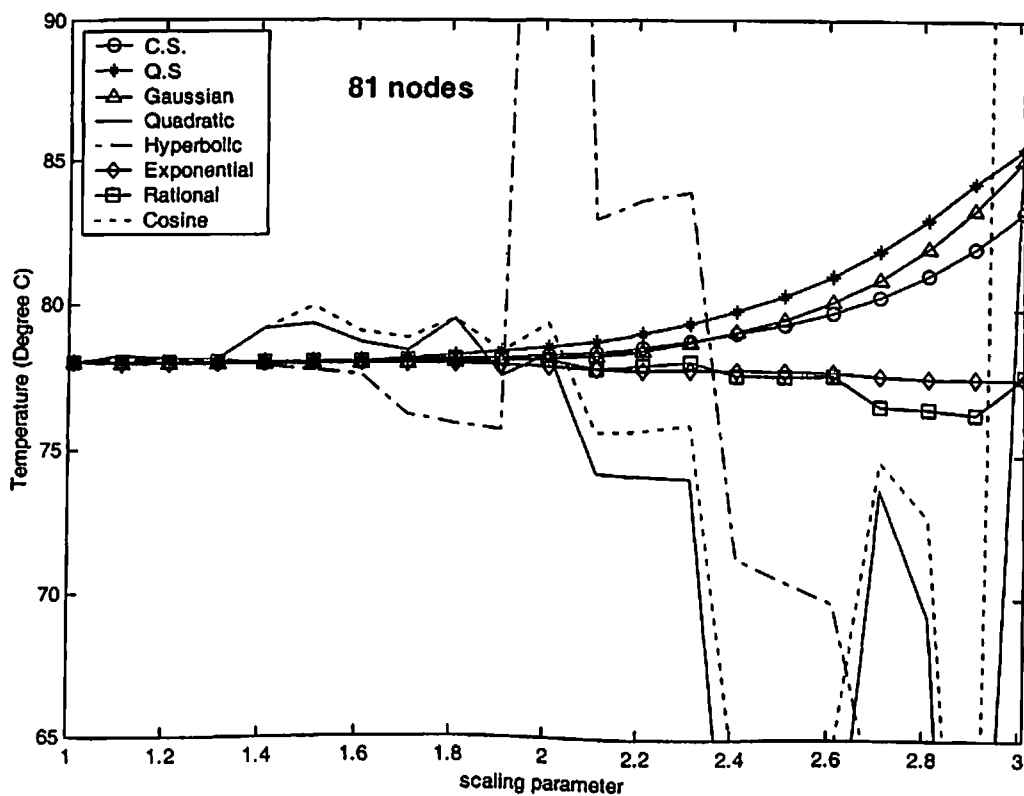
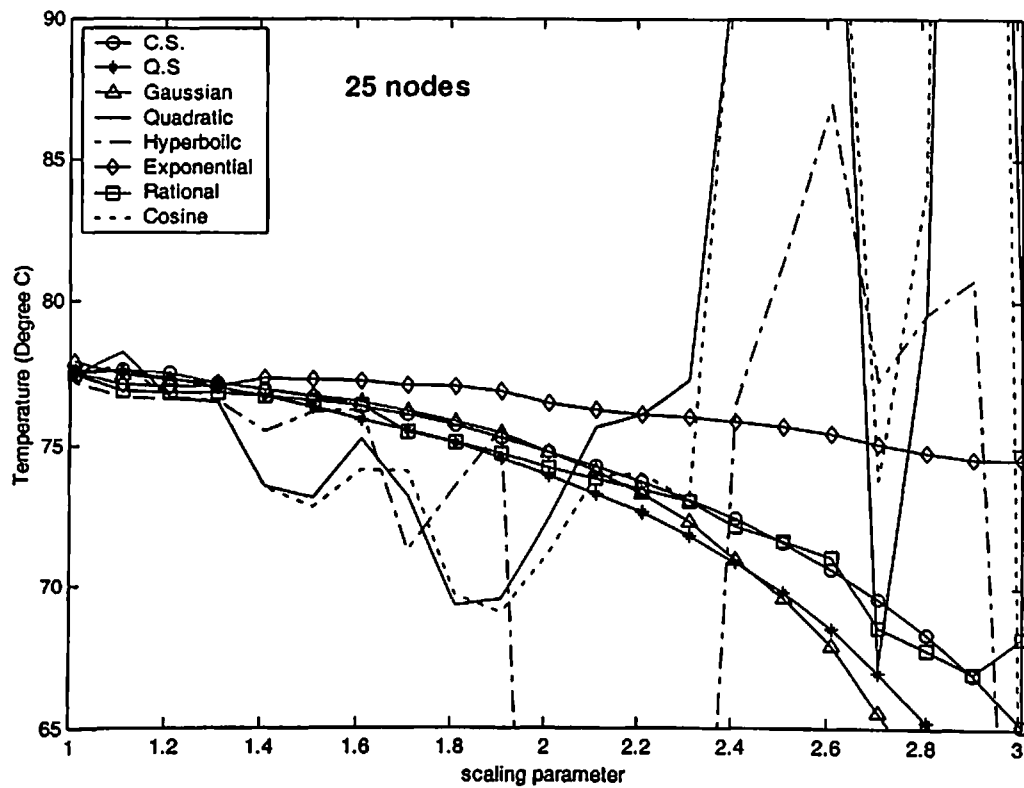


Fig. 5.25 Effect of scaling parameter on EFG results at the location ($r = 0.5 \text{ m}$ & $z = 0.25 \text{ m}$) of 2-D model shown in Fig 5.23

5.9.2 Transient analysis

The transient analysis of 2-D model, shown in Fig. 5.23, is carried out using different EFG weight functions. Table 5.78 and Table 5.79 show the comparison of EFG results (i.e. temperature values) obtained using 25 nodes with FEM results at the location ($r = 0.5 \text{ m}$ & $z = 1 \text{ m}$) for $d_{\max} = 1.01$ and $d_{\max} = 1.51$ respectively. Similar comparison of temperature values obtained using 81 nodes is presented in Table 5.80 and Table 5.81 for $d_{\max} = 1.01$ and $d_{\max} = 1.51$ respectively at the same location i.e. ($r = 0.5 \text{ m}$ & $z = 1 \text{ m}$). For this case (i.e. CASE-IV) of 2-D transient analysis, time step of 100 sec has been taken which is nearly 1.5% of the total time required to achieve steady state condition. Table 5.82 and Table 5.83 show the comparison of EFG results (i.e. temperature values) obtained using 25 nodes with FEM results at the location ($r = 0.5 \text{ m}$ & $z = 0.5 \text{ m}$) for $d_{\max} = 1.01$ and $d_{\max} = 1.51$ respectively. Similar comparison of temperature values obtained using 81 nodes is also presented in Table 5.84 and Table 5.85 for $d_{\max} = 1.01$ and $d_{\max} = 1.51$ respectively at the same location i.e. ($r = 0.5 \text{ m}$ & $z = 0.5 \text{ m}$). Fig 5.26 shows the comparison of EFG results (i.e. temperature values) obtained using 25 nodes with FEM results for $d_{\max} = 1.01$ and $d_{\max} = 1.51$ at the location ($r = 0.5 \text{ m}$ & $z = 0.75 \text{ m}$). Similar comparison of temperature values obtained using 81 nodes is shown in Fig. 5.27 at the same location i.e. ($r = 0.5 \text{ m}$ & $z = 0.75 \text{ m}$). Fig 5.28 shows the comparison of EFG results (i.e. temperature values) obtained using 25 nodes with FEM results for $d_{\max} = 1.01$ and $d_{\max} = 1.51$ at the location ($r = 0.5 \text{ m}$ & $z = 0.25 \text{ m}$). Similar comparison of temperature values obtained using 81 nodes is shown in Fig. 5.29 at the same location i.e. ($r = 0.5 \text{ m}$ & $z = 0.25 \text{ m}$). From the results presented in tables and figures, it is clear that EFG results obtained using different weight functions are almost similar for $d_{\max} = 1.01$ but for $d_{\max} = 1.51$ only cubicspline (C.S.), quarticspline (Q.S), Gaussian, exponential and rational weight functions give acceptable results. It has also been observed that the EFG results are in good agreement with those obtained by finite element method.

Table 5.78 Comparison of EFG results obtained using 25 nodes with FEM at the location ($r = 0.5$ m & $z = 1$ m) of 2-D model shown in Fig 5.23 for $d_{\max} = 1.01$

Time (sec) $\times 10^2$	Temperature ($^{\circ}$ C)								
	$d_{\max} = 1.01$								FEM
	C. S.	Q. S	Gaussian	Quadratic	Hyperbolic	Exponential	Rational	Cosine	
0	100.0000	100.0000	100.0000	100.0000	100.0000	100.0000	100.0000	100.0000	100.000
6	80.1885	80.1939	80.1689	80.2053	80.2546	80.1969	80.2043	80.2053	81.4703
12	72.2689	72.2742	72.2479	72.2849	72.3321	72.2771	72.2838	72.2849	73.1683
18	66.6961	66.7013	66.6742	66.7119	66.7571	66.7043	66.7108	66.7118	67.5336
24	62.6700	62.6753	62.6474	62.6859	62.7299	62.6783	62.6848	62.6858	63.4646
30	59.7478	59.7532	59.7245	59.7638	59.8070	59.7562	59.7627	59.7637	60.4925
36	57.6244	57.6298	57.6004	57.6404	57.6832	57.6328	57.6394	57.6404	58.3137
42	56.0810	56.0864	56.0564	56.0970	56.1396	56.0894	56.0960	56.0970	56.7141
48	54.9590	54.9645	54.9340	54.9751	55.0175	54.9675	54.9741	54.9751	55.5389
54	54.1434	54.1490	54.1181	54.1596	54.2019	54.1520	54.1585	54.1596	54.6752
60	53.5506	53.5562	53.5250	53.5667	53.6091	53.5591	53.5657	53.5667	54.0404

Table 5.79 Comparison of EFG results obtained using 25 nodes with FEM at the location ($r = 0.5$ m & $z = 1$ m) of 2-D model shown in Fig 5.23 for $d_{\max} = 1.51$

Time (sec) $\times 10^2$	Temperature ($^{\circ}$ C)								
	$d_{\max} = 1.51$								FEM
	C. S.	Q. S	Gaussian	Quadratic	Hyperbolic	Exponential	Rational	Cosine	
0	100.0000	100.0000	100.0000	100.0000	100.0000	100.0000	100.0000	100.0000	100.000
6	80.1004	80.0932	80.0151	81.4098	80.2943	80.2345	80.3062	81.3583	81.4703
12	72.2913	72.3045	72.2267	73.4457	72.1270	72.2977	72.3149	73.5103	73.1683
18	66.7773	66.8016	66.7233	67.7968	66.3606	66.7174	66.7109	67.9452	67.5336
24	62.7839	62.8140	62.7364	63.7137	62.2131	62.6874	62.6692	63.9147	63.4646
30	59.8785	59.9116	59.8352	60.7539	59.2215	59.7629	59.7390	60.9858	60.4925
36	57.7620	57.7963	57.7214	58.6067	57.0609	57.6383	57.6121	58.8563	58.3137
42	56.2198	56.2542	56.1808	57.0486	55.4991	56.0943	56.0679	57.3081	56.7141
48	55.0959	55.1298	55.0578	55.9177	54.3694	54.9723	54.9465	56.1828	55.5389
54	54.2767	54.3099	54.2392	55.0969	53.5519	54.1568	54.1323	55.3649	54.6752
60	53.6798	53.7121	53.6425	54.5010	52.9601	53.5641	53.5410	54.7704	54.0404

Table 5.80 Comparison of EFG results obtained using 81 nodes with FEM at the location ($r = 0.5$ m & $z = 1$ m) of 2-D model shown in Fig 5.23 for $d_{max} = 1.01$

Time (sec) $\times 10^2$	Temperature ($^{\circ}$ C)								
	$d_{max} = 1.01$								FEM
	C. S.	Q. S	Gaussian	Quadratic	Hyperbolic	Exponential	Rational	Cosine	
0	100.0000	100.0000	100.0000	100.0000	100.0000	100.0000	100.0000	100.0000	100.000
6	80.3046	80.3063	80.2948	80.3094	80.3168	80.3072	80.3090	80.3094	80.6358
12	72.3546	72.3563	72.3455	72.3593	72.3658	72.3571	72.3589	72.3592	72.7572
18	66.7964	66.7980	66.7876	66.8010	66.8070	66.7989	66.8007	66.8010	67.2486
24	62.7860	62.7876	62.7773	62.7906	62.7963	62.7885	62.7903	62.7906	63.2383
30	59.8733	59.8749	59.8646	59.8778	59.8833	59.8758	59.8776	59.8778	60.2980
36	57.7533	57.7549	57.7445	57.7578	57.7632	57.7558	57.7575	57.7578	58.1379
42	56.2090	56.2106	56.2002	56.2134	56.2188	56.2114	56.2132	56.2134	56.5498
48	55.0837	55.0853	55.0749	55.0881	55.0934	55.0861	55.0879	55.0881	55.3821
54	54.2636	54.2652	54.2548	54.2680	54.2733	54.2660	54.2677	54.2680	54.5233
60	53.6658	53.6674	53.6570	53.6702	53.6755	53.6683	53.6700	53.6702	53.8917

Table 5.81 Comparison of EFG results obtained using 81 nodes with FEM at the location ($r = 0.5$ m & $z = 1$ m) of 2-D model shown in Fig 5.23 for $d_{max} = 1.51$

Time (sec) $\times 10^2$	Temperature ($^{\circ}$ C)								
	$d_{max} = 1.51$								FEM
	C. S.	Q. S	Gaussian	Quadratic	Hyperbolic	Exponential	Rational	Cosine	
0	100.0000	100.0000	100.0000	100.0000	100.0000	100.0000	100.0000	100.0000	100.000
6	80.2914	80.2971	80.2467	80.6297	80.3205	80.3248	80.3537	80.7626	80.6358
12	72.3588	72.3631	72.3213	72.6163	72.3328	72.3677	72.3724	72.7802	72.7572
18	66.8141	66.8188	66.7827	67.0361	66.7584	66.8055	66.7995	67.2202	67.2486
24	62.8127	62.8177	62.7856	63.0150	62.7399	62.7924	62.7798	63.2118	63.2383
30	59.9050	59.9104	59.8809	60.0950	59.8223	59.8780	59.8609	60.3002	60.2980
36	57.7872	57.7927	57.7650	57.9699	57.6992	57.7569	57.7371	58.1808	58.1379
42	56.2435	56.2489	56.2224	56.4222	56.1529	56.2121	56.1907	56.6371	56.5498
48	55.1177	55.1230	55.0974	55.2948	55.0263	55.0866	55.0644	55.5125	55.3821
54	54.2967	54.3018	54.2768	54.4734	54.2053	54.2664	54.2440	54.6932	54.5233
60	53.6978	53.7027	53.6782	53.8750	53.6069	53.6686	53.6463	54.0964	53.8917

Table 5.82 Comparison of EFG results obtained using 25 nodes with FEM at the location ($r = 0.5 \text{ m}$ & $z = 0.5 \text{ m}$) of 2-D model shown in Fig 5.23 for $d_{\max} = 1.01$

Time (sec) $\times 10^2$	Temperature ($^{\circ} \text{C}$)								
	$d_{\max} = 1.01$								FEM
	C. S.	Q. S	Gaussian	Quadratic	Hyperbolic	Exponential	Rational	Cosine	
0	100.0000	100.0000	100.0000	100.0000	100.0000	100.0000	100.0000	100.0000	100.000
6	88.2679	88.2779	88.2594	88.2954	88.3924	88.2814	88.2941	88.2956	88.8114
12	82.1211	82.1300	82.1146	82.1451	82.2403	82.1329	82.1432	82.1449	82.6370
18	77.5981	77.6071	77.5904	77.6225	77.7172	77.6102	77.6205	77.6223	78.1497
24	74.2941	74.3034	74.2847	74.3194	74.4138	74.3067	74.3173	74.3191	74.8391
30	71.8893	71.8988	71.8783	71.9152	72.0096	71.9022	71.9131	71.9150	72.4022
36	70.1406	70.1503	70.1283	70.1670	70.2614	70.1538	70.1649	70.1668	70.6104
42	68.8693	68.8792	68.8559	68.8961	68.9905	68.8827	68.8940	68.8959	69.2933
48	67.9451	67.9551	67.9310	67.9722	68.0667	67.9587	67.9701	67.9720	68.3252
54	67.2733	67.2834	67.2586	67.3006	67.3952	67.2871	67.2985	67.3004	67.6136
60	66.7849	66.7951	66.7698	66.8124	66.9071	66.7988	66.8102	66.8122	67.0906

Table 5.83 Comparison of EFG results obtained using 25 nodes with FEM at the location ($r = 0.5 \text{ m}$ & $z = 0.5 \text{ m}$) of 2-D model shown in Fig 5.23 for $d_{\max} = 1.51$

Time (sec) $\times 10^2$	Temperature ($^{\circ} \text{C}$)								
	$d_{\max} = 1.51$								FEM
	C. S.	Q. S	Gaussian	Quadratic	Hyperbolic	Exponential	Rational	Cosine	
0	100.0000	100.0000	100.0000	100.0000	100.0000	100.0000	100.0000	100.0000	100.000
6	88.4304	88.5239	88.3803	91.0585	89.0811	88.3446	88.5807	91.0770	88.8114
12	82.2608	82.3486	82.2165	84.9811	82.5313	82.1691	82.3330	85.1361	82.6370
18	77.7074	77.7870	77.6625	80.3811	77.6152	77.6298	77.7425	80.6325	78.1497
24	74.3717	74.4433	74.3255	76.9994	74.0464	74.3152	74.3944	77.3098	74.8391
30	71.9370	72.0015	71.8893	74.5361	71.4749	71.9033	71.9606	74.8809	72.4022
36	70.1619	70.2202	70.1127	72.7464	69.6220	70.1498	70.1928	73.1113	70.6104
42	68.8680	68.9212	68.8174	71.4471	68.2850	68.8753	68.9091	71.8238	69.2933
48	67.9250	67.9740	67.8733	70.5039	67.3192	67.9490	67.9769	70.8875	68.3252
54	67.2377	67.2834	67.1850	69.8193	66.6208	67.2759	67.3000	70.2069	67.6136
60	66.7368	66.7798	66.6833	69.3223	66.1154	66.7866	66.8084	69.7123	67.0906

Table 5.84 Comparison of EFG results obtained using 81 nodes with FEM at the location ($r = 0.5$ m & $z = 0.5$ m) of 2-D model shown in Fig 5.23 for $d_{max} = 1.01$

Time (sec) $\times 10^2$	Temperature ($^{\circ}$ C)								
	$d_{max} = 1.01$								FEM
	C. S.	Q. S	Gaussian	Quadratic	Hyperbolic	Exponential	Rational	Cosine	
0	100.0000	100.0000	100.0000	100.0000	100.0000	100.0000	100.0000	100.0000	100.000
6	88.4023	88.4013	88.4100	88.4007	88.4009	88.4012	88.4009	88.4008	88.3986
12	82.1955	82.1947	82.2026	82.1946	82.1963	82.1948	82.1949	82.1947	82.4152
18	77.6796	77.6790	77.6856	77.6792	77.6816	77.6792	77.6794	77.6793	77.9892
24	74.3887	74.3883	74.3939	74.3886	74.3914	74.3885	74.3887	74.3886	74.7149
30	71.9921	71.9917	71.9967	71.9921	71.9952	71.9920	71.9922	71.9921	72.3011
36	70.2465	70.2461	70.2506	70.2465	70.2498	70.2464	70.2466	70.2466	70.5243
42	68.9747	68.9744	68.9786	68.9748	68.9782	68.9747	68.9749	68.9749	69.2171
48	68.0480	68.0477	68.0517	68.0481	68.0516	68.0480	68.0482	68.0481	68.2557
54	67.3726	67.3723	67.3761	67.3727	67.3763	67.3726	67.3728	67.3728	67.5485
60	66.8803	66.8801	66.8838	66.8805	66.8841	66.8803	66.8805	66.8805	67.0284

Table 5.85 Comparison of EFG results obtained using 81 nodes with FEM at the location ($r = 0.5$ m & $z = 0.5$ m) of 2-D model shown in Fig 5.23 for $d_{max} = 1.51$

Time (sec) $\times 10^2$	Temperature ($^{\circ}$ C)								
	$d_{max} = 1.51$								FEM
	C. S.	Q. S	Gaussian	Quadratic	Hyperbolic	Exponential	Rational	Cosine	
0	100.0000	100.0000	100.0000	100.0000	100.0000	100.0000	100.0000	100.0000	100.000
6	88.4201	88.4352	88.4155	89.3608	88.3866	88.4144	88.4610	89.7030	88.3986
12	82.1974	82.2055	82.1920	83.1347	82.1214	82.2023	82.2326	83.5312	82.4152
18	77.6726	77.6759	77.6677	78.6098	77.5433	77.6807	77.6927	79.0541	77.9892
24	74.3748	74.3747	74.3703	75.3178	74.2051	74.3855	74.3839	75.7981	74.7149
30	71.9716	71.9692	71.9673	72.9218	71.7740	71.9858	71.9746	73.4277	72.3011
36	70.2200	70.2157	70.2156	71.1775	70.0037	70.2383	70.2204	71.7017	70.5243
42	68.9429	68.9371	68.9383	69.9074	68.7144	68.9653	68.9429	70.4448	69.2171
48	68.0115	68.0046	68.0067	68.9826	67.7753	68.0377	68.0125	69.5297	68.2557
54	67.3323	67.3244	67.3272	68.3092	67.0913	67.3618	67.3347	68.8635	67.5485
60	66.8368	66.8282	66.8315	67.8188	66.5930	66.8693	66.8410	68.3785	67.0284

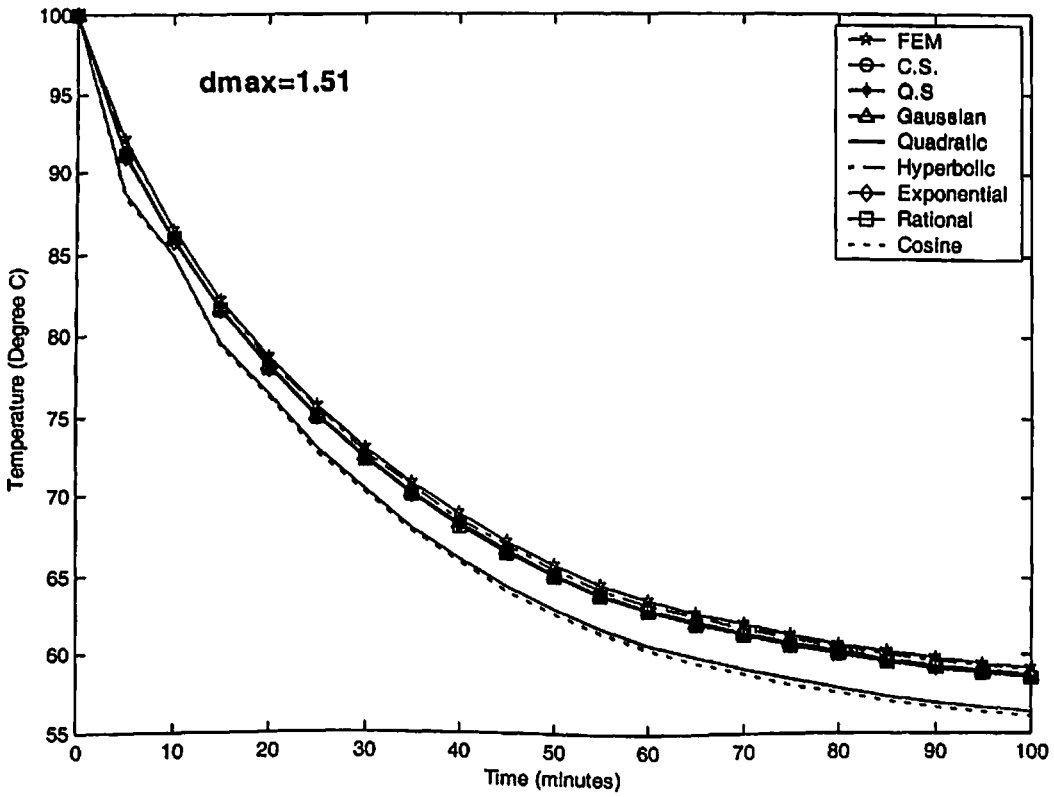
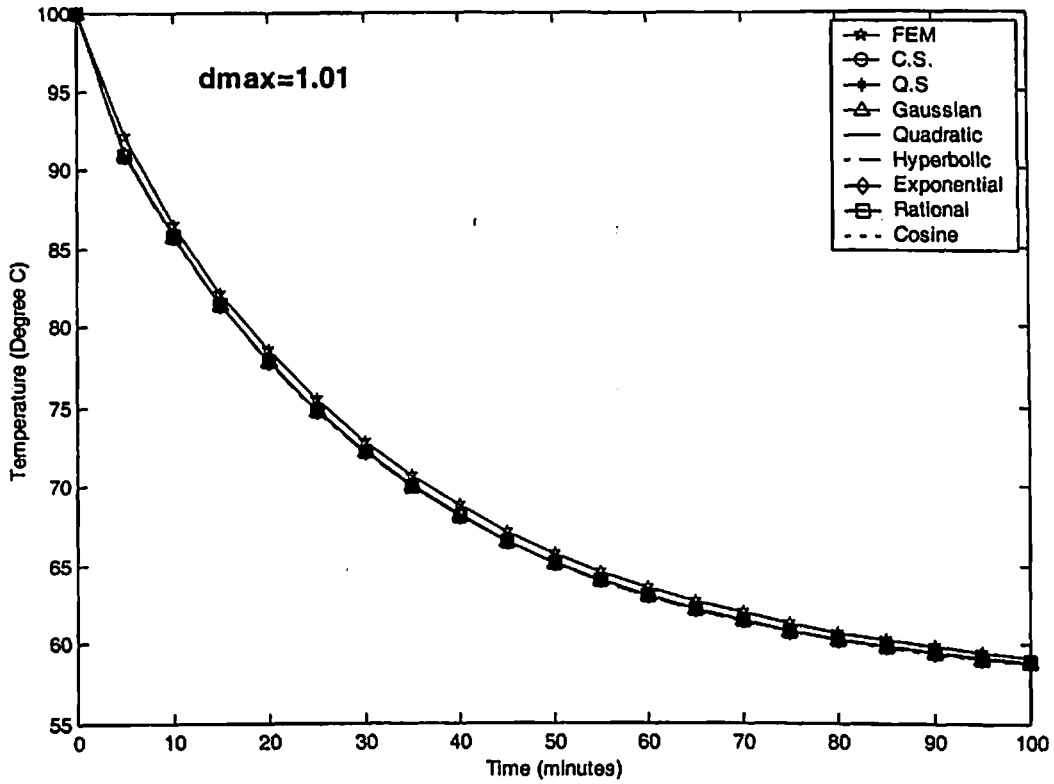


Fig. 5.26 Comparison of EFG results obtained using 25 nodes with FEM at the location ($r = 0.5$ m & $z = 0.75$ m) of 2-D model shown in Fig 5.23

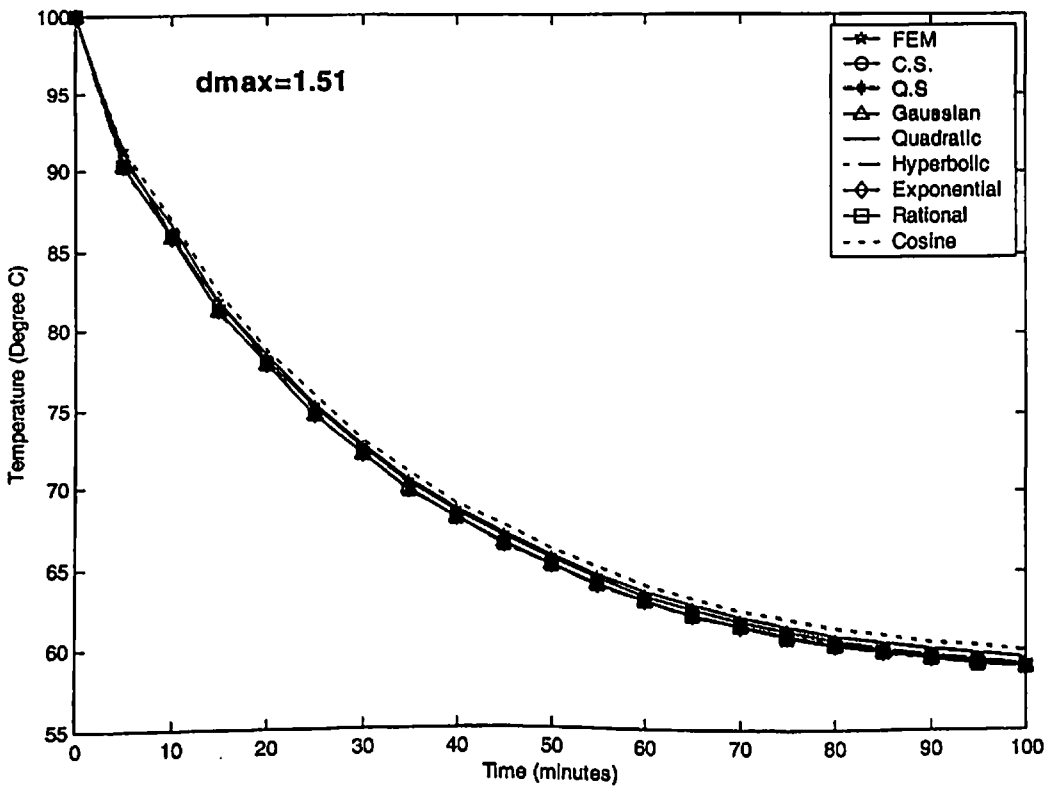
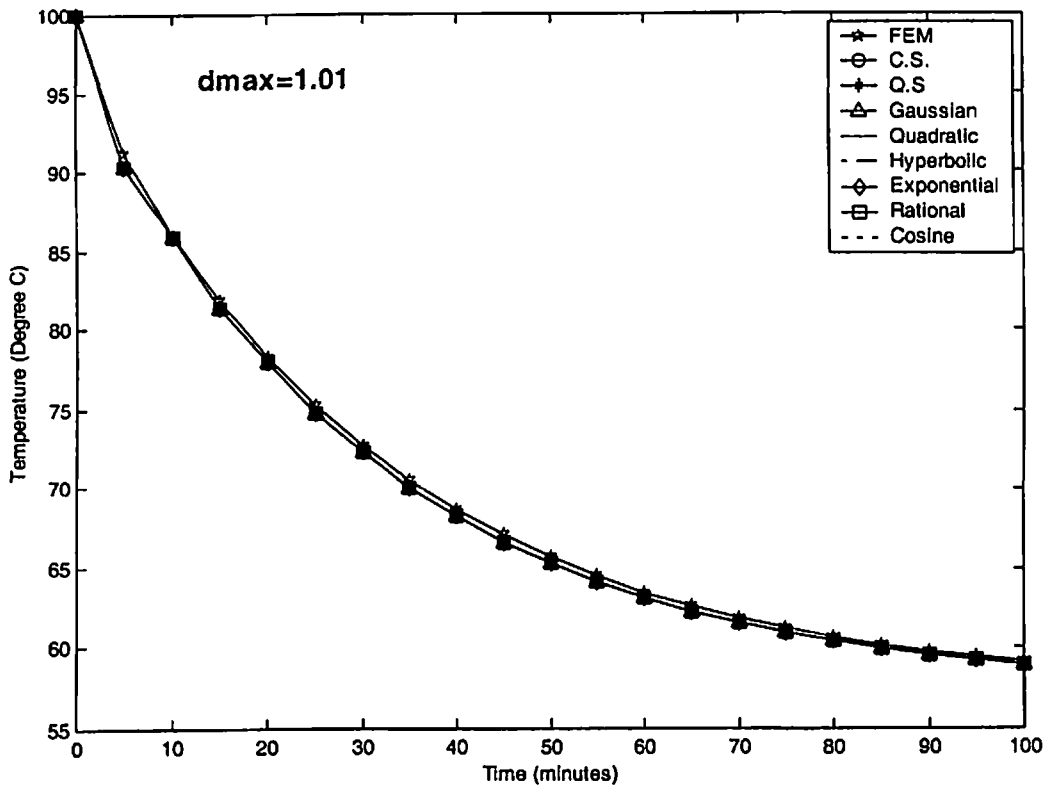


Fig. 5.27 Comparison of EFG results obtained using 81 nodes with FEM at the location ($r = 0.5\text{ m}$ & $z = 0.75\text{ m}$) of 2-D model shown in Fig 5.23

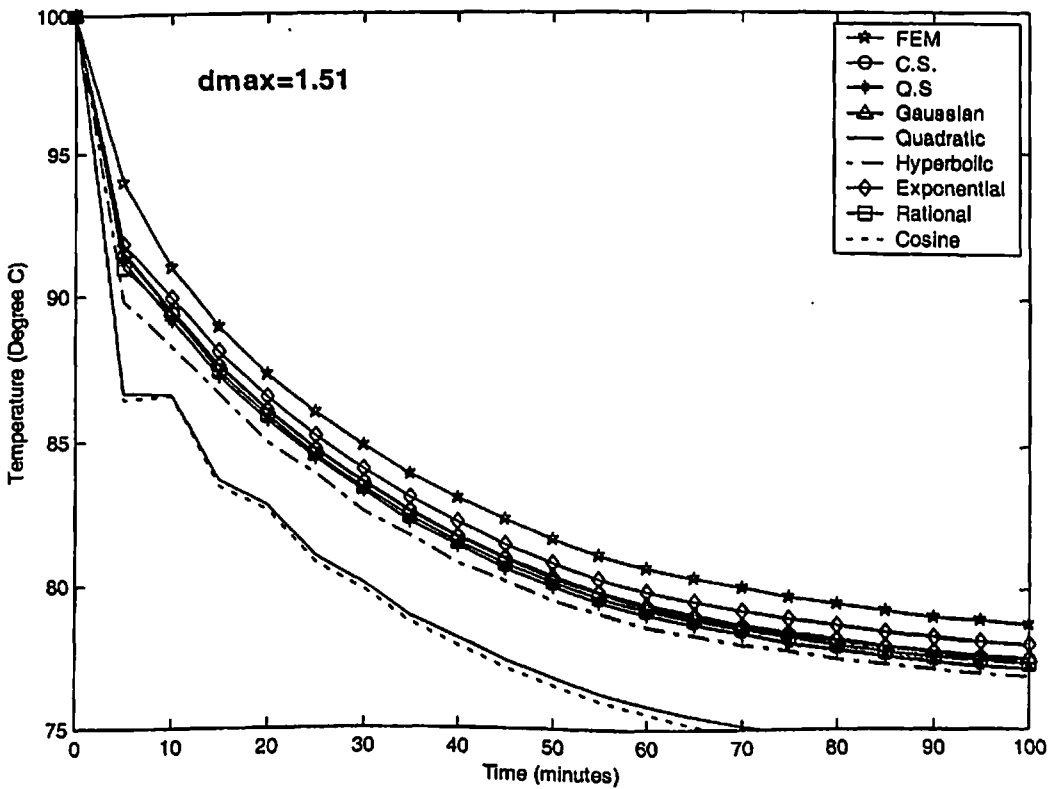
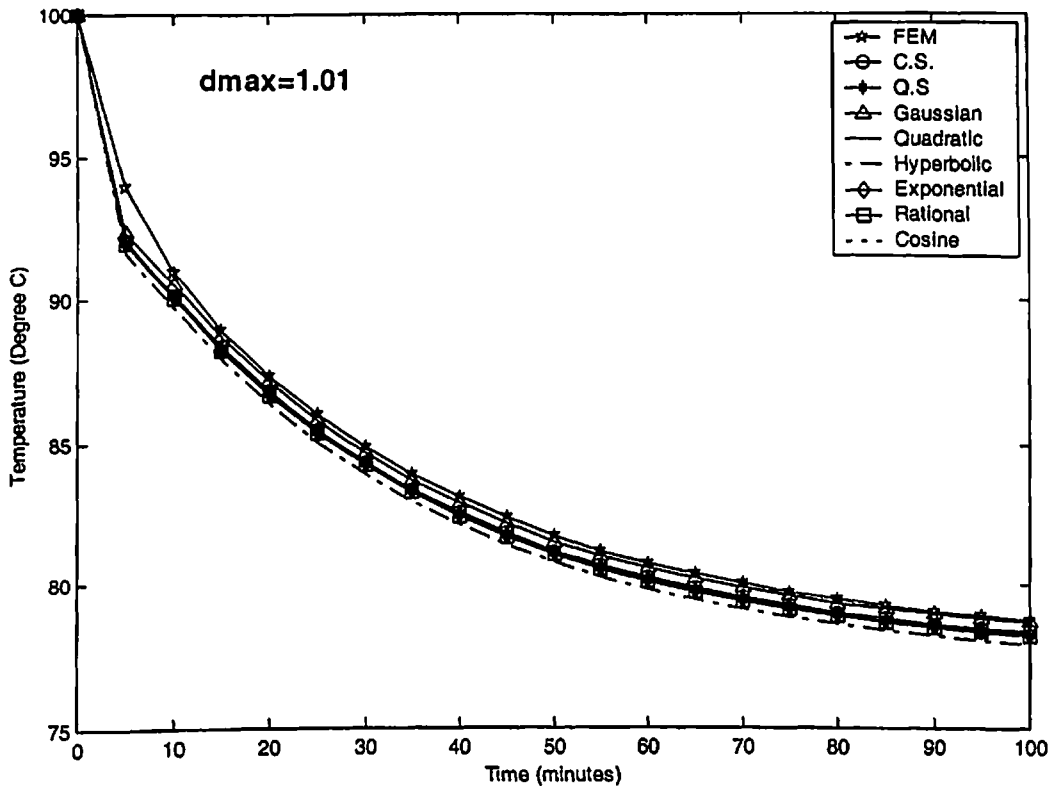


Fig. 5.28 Comparison of EFG results obtained using 25 nodes with FEM at the location ($r = 0.5$ m & $z = 0.25$ m) of 2-D model shown in Fig 5.23

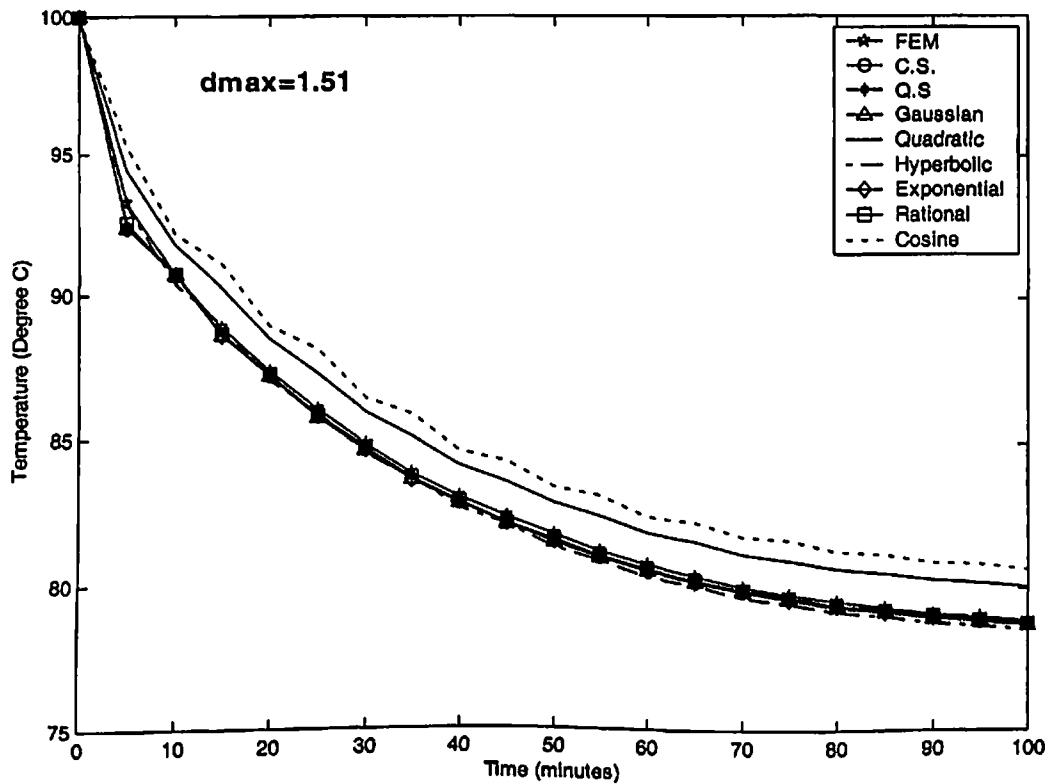
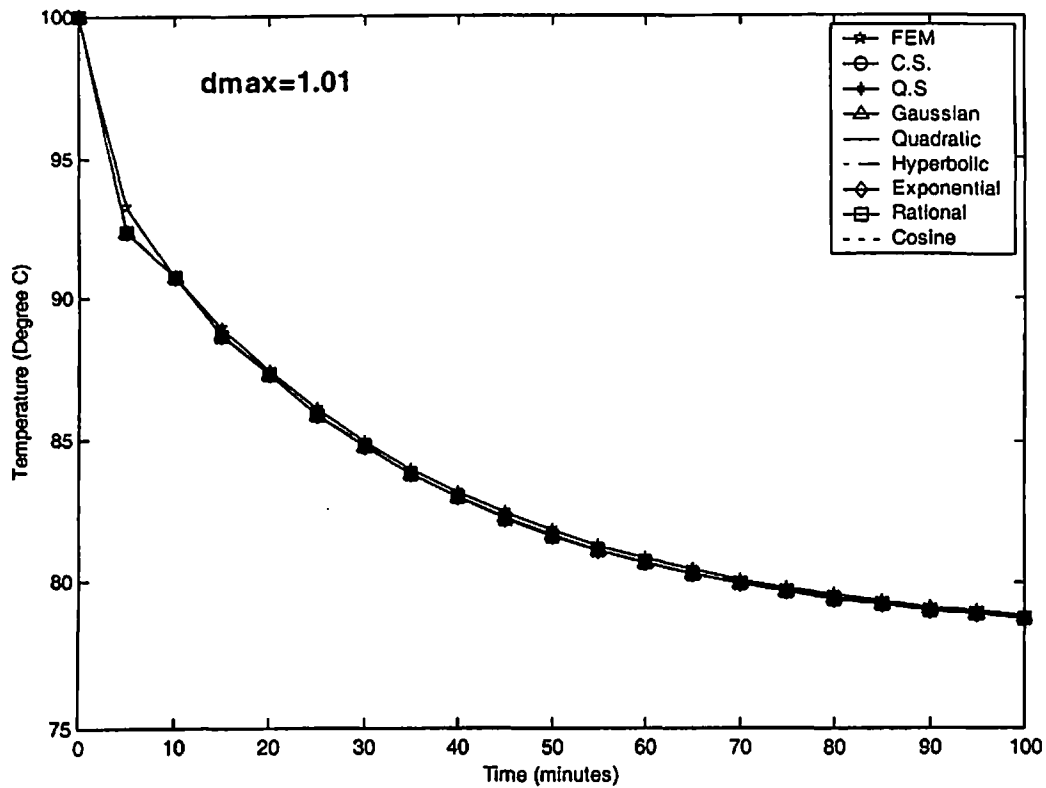


Fig. 5.29 Comparison of EFG results obtained using 81 nodes with FEM at the location ($r = 0.5$ m & $z = 0.25$ m) of 2-D model shown in Fig 5.23

5.10 CONCLUSION

2-D MATLAB codes have been developed to obtain the numerical solution for the different cases presented in this chapter using different EFG weight functions. The results obtained by EFG method have been compared with those obtained by FEM (in Case-I, analytical method also) at few typical locations. From the numerical analysis carried out in this chapter, it is clear that the EFG method can be successfully used to obtain the numerical solution of 2-D heat transfer problems. A comparative numerical analysis has been carried out to evaluate the performance of different weight functions. It is found that the EFG results obtained using cubicspline, quarticspline, Gaussian, exponential and rational weight functions are in good agreement with those obtained by FEM. From the analysis carried out in this chapter, it is also observed that only cubicspline, quarticspline, Gaussian, exponential and rational weight functions give acceptable results in the range $1.0 < d_{\max} < 1.5$. Out of all the weight functions used, the results obtained using exponential weight function are most reliable as compared to other weight functions used because only exponential weight function has minimum variation in the results (temperature values) with the change in the value of scaling parameter.

CHAPTER 6

3-D HEAT TRANSFER ANALYSIS

6.1 INTRODUCTION

This chapter describes the application of EFG method in three-dimensional (3-D) heat transfer problems. Four different cases have been chosen to check the applicability of this method in 3-D heat transfer problems. The steady-state and transient analysis of different model problems have been carried out. The effect of scaling parameter on EFG results has also been discussed in detail.

➤ CASE-I

6.2 DISCRETIZATION OF THE GOVERNING EQUATION

A general form of energy equation for three-dimensional heat transfer in isotropic materials with thermal properties independent of temperature is given as:

$$k_x \frac{\partial^2 T}{\partial x^2} + k_y \frac{\partial^2 T}{\partial y^2} + k_z \frac{\partial^2 T}{\partial z^2} + \dot{Q} = \rho c \dot{T} \quad (6.1a)$$

With initial and boundary conditions are:

$$\text{at the time } t = 0 \quad T = T_{ini} \quad \text{on} \quad V \quad (6.1b)$$

$$\text{at surface } x = 0 \ (S_1), \quad T = T_{s_1} \quad (6.1c)$$

$$\text{at surface } x = L \ (S_2), \quad k_x \frac{\partial T}{\partial x} = -h(T - T_\infty) \quad (6.1d)$$

$$\text{at surface } y = 0 \ (S_3), \quad k_y \frac{\partial T}{\partial y} = h(T - T_\infty) \quad (6.1e)$$

$$\text{at surface } y = W \ (S_4), \quad k_y \frac{\partial T}{\partial y} = -h(T - T_\infty) \quad (6.1f)$$

$$\text{at surface } z = 0 \ (S_5), \quad k_z \frac{\partial T}{\partial z} = h(T - T_\infty) \quad (6.1g)$$

$$\text{at surface } z = H \ (S_6), \quad k_z \frac{\partial T}{\partial z} = -h(T - T_\infty) \quad (6.1h)$$

The weighted integral form of Eq. (6.1a) is obtained as:

$$\int_V w \left[\left(k_x \frac{\partial^2 T}{\partial x^2} + k_y \frac{\partial^2 T}{\partial y^2} + k_z \frac{\partial^2 T}{\partial z^2} \right) + \dot{Q} - \rho c \dot{T} \right] dV = 0 \quad (6.2)$$

The weak form of the Eq. (6.2) will be

$$\begin{aligned} & \int_V \left[\left\{ k_x \frac{\partial w}{\partial x} \frac{\partial T}{\partial x} + k_y \frac{\partial w}{\partial y} \frac{\partial T}{\partial y} + k_z \frac{\partial w}{\partial z} \frac{\partial T}{\partial z} \right\} \right] dV - \int_V w \dot{Q} dV + \int_V w \rho c \dot{T} dV - \\ & \int_S \left[w k \frac{\partial T}{\partial x} \cos(\bar{n}, x) + w k \frac{\partial T}{\partial y} \cos(\bar{n}, y) + w k \frac{\partial T}{\partial z} \cos(\bar{n}, z) \right] dS = 0 \end{aligned} \quad (6.3)$$

Introducing natural boundary conditions in weak form, the Eq. (6.3) changes to

$$\begin{aligned} & \int_V \left[\left(k_x \frac{\partial w}{\partial x} \frac{\partial T}{\partial x} + k_y \frac{\partial w}{\partial y} \frac{\partial T}{\partial y} + k_z \frac{\partial w}{\partial z} \frac{\partial T}{\partial z} \right) \right] dV - \int_V w \dot{Q} dV + \int_V w \rho c \dot{T} dV + \int_{s_2} w h (T - T_\infty) dS + \\ & \int_{s_3} w h (T - T_\infty) dS + \int_{s_4} w h (T - T_\infty) dS + \int_{s_5} w h (T - T_\infty) dS + \int_{s_6} w h (T - T_\infty) dS = 0 \end{aligned} \quad (6.4)$$

The functional $I(T)$ can be written as:

$$\begin{aligned} I(T) = & \int_V \frac{1}{2} \left[k_x \left(\frac{\partial T}{\partial x} \right)^2 + k_y \left(\frac{\partial T}{\partial y} \right)^2 + k_z \left(\frac{\partial T}{\partial z} \right)^2 \right] + \int_V \rho c T \dot{T} dV - \int_V \dot{Q} dV + \\ & \int_{s_2} \frac{h T^2}{2} dS + \int_{s_3} \frac{h T^2}{2} dS + \int_{s_4} \frac{h T^2}{2} dS + \int_{s_5} \frac{h T^2}{2} dS + \int_{s_6} \frac{h T^2}{2} dS - \\ & \int_{s_2} h T T_\infty dS - \int_{s_3} h T T_\infty dS - \int_{s_4} h T T_\infty dS - \int_{s_5} h T T_\infty dS - \int_{s_6} h T T_\infty dS \end{aligned} \quad (6.5)$$

Enforcing essential boundary conditions, the functional $I^*(T)$ is obtained as:

$$\begin{aligned} I^*(T) = & \int_V \frac{1}{2} \left[k_x \left(\frac{\partial T}{\partial x} \right)^2 + k_y \left(\frac{\partial T}{\partial y} \right)^2 + k_z \left(\frac{\partial T}{\partial z} \right)^2 \right] + \int_V \rho c T \dot{T} dV - \int_V \dot{Q} dV + \\ & \int_{s_2} \frac{h T^2}{2} dS + \int_{s_3} \frac{h T^2}{2} dS + \int_{s_4} \frac{h T^2}{2} dS + \int_{s_5} \frac{h T^2}{2} dS + \int_{s_6} \frac{h T^2}{2} dS - \int_{s_2} h T T_\infty dS - \\ & \int_{s_3} h T T_\infty dS - \int_{s_4} h T T_\infty dS - \int_{s_5} h T T_\infty dS + \int_{s_1} \lambda (T - T_{s_1}) dS \end{aligned} \quad (6.6)$$

Using Variational method, Eq. (6.6) changes to

$$\begin{aligned}
\delta I^*(T) = & \int_V \left[k_x \frac{\partial T}{\partial x} \delta \frac{\partial T}{\partial x} + k_y \frac{\partial T}{\partial y} \delta \frac{\partial T}{\partial y} + k_z \frac{\partial T}{\partial z} \delta \frac{\partial T}{\partial z} \right] dV + \int_V \rho c \dot{T} \delta T dV - \int_V \dot{Q} \delta T dV + \\
& \int_{s_2} h T \delta T dS + \int_{s_3} h T \delta T dS + \int_{s_4} h T \delta T dS + \int_{s_5} h T \delta T dS + \int_{s_6} h T \delta T dS - \int_{s_2} h T_\infty \delta T dS - \quad (6.7) \\
& \int_{s_3} h T_\infty \delta T dS - \int_{s_4} h T_\infty \delta T dS - \int_{s_5} h T_\infty \delta T dS - \int_{s_6} h T_\infty \delta T dS + \int_{s_1} \lambda \delta T dS + \int_{s_1} \delta \lambda (T - T_{s_1}) dS
\end{aligned}$$

Since δT and $\delta \lambda$ are arbitrary in preceding equation, the following relations are obtained using Eqs. (3.25) and (6.7)

$$[\mathbf{K}]\{\mathbf{T}\} + [\mathbf{C}]\{\dot{\mathbf{T}}\} + [\mathbf{G}]\{\lambda\} = \{\mathbf{f}\} \quad (6.8a)$$

$$[\mathbf{G}^T]\{\mathbf{T}\} = \{\mathbf{q}\} \quad (6.8b)$$

where

$$\begin{aligned}
K_{IJ} = & \int_V \begin{bmatrix} \Phi_{I,x} \\ \Phi_{I,y} \\ \Phi_{I,z} \end{bmatrix}^T \begin{bmatrix} k_x & 0 & 0 \\ 0 & k_y & 0 \\ 0 & 0 & k_z \end{bmatrix} \begin{bmatrix} \Phi_{I,x} \\ \Phi_{I,y} \\ \Phi_{I,z} \end{bmatrix} dV + \int_{s_2} h \Phi_I^T \Phi_J dS + \\
& \int_{s_3} h \Phi_I^T \Phi_J dS + \int_{s_4} h \Phi_I^T \Phi_J dS + \int_{s_5} h \Phi_I^T \Phi_J dS + \int_{s_6} h \Phi_I^T \Phi_J dS \quad (6.9a)
\end{aligned}$$

$$C_{IJ} = \int_V \rho c \Phi_I^T \Phi_J dV \quad (6.9b)$$

$$f_I = \int_V \dot{Q} \Phi_I dV + \int_{s_2} h T_\infty \Phi_I dS + \int_{s_3} h T_\infty \Phi_I dS + \int_{s_4} h T_\infty \Phi_I dS + \int_{s_5} h T_\infty \Phi_I dS + \int_{s_6} h T_\infty \Phi_I dS \quad (6.9c)$$

$$G_{IK} = \int_{s_1} \Phi_I N_K dS \quad (6.9d)$$

$$q_K = \int_{s_1} T_{s_1} N_K dS \quad (6.9e)$$

Using Crank-Nicolson technique for time approximation, the Eq. (6.8) can be written as:

$$\left[\begin{array}{c|c} \mathbf{K}' + \mathbf{C} & \mathbf{G} \\ \hline \mathbf{G}^T & 0 \end{array} \right] \begin{Bmatrix} \mathbf{T}_N \\ \lambda \end{Bmatrix} = \begin{Bmatrix} \mathbf{R}_N \\ \mathbf{q} \end{Bmatrix} \quad (6.10)$$

where

$$\mathbf{R}_N = ([\mathbf{C}] - (1 - \alpha) \Delta t [\mathbf{K}]) \{\mathbf{T}\}_{N-1} + \alpha \Delta t \{\mathbf{f}\}_N + (1 - \alpha) \Delta t \{\mathbf{f}\}_{N-1} \quad (6.11a)$$

$$\mathbf{K}' = \alpha \Delta t [\mathbf{K}] \quad (6.11b)$$

6.3 NUMERICAL RESULTS AND DISCUSSION

The different parameters used for steady-state and transient analysis of three-dimensional model shown in Fig. 6.1 are tabulated in Table 6.1. The EFG results are obtained using different weight functions for two sets of nodes and the FEM results are obtained using 8 node brick element (SOLID 70, ANSYS 6.0) for same sets of nodes. Analytical solution has also obtained using an infinite series (Carslaw and Jaeger, 1959). A comparative study is carried out to evaluate the performance of different EFG weight functions.

6.3.1 Steady-state analysis

The results (i.e. temperature values) presented in Table 6.2 are obtained using different EFG weight functions for two values of scaling parameter (i.e. $d_{\max} = 1.01$ & $d_{\max} = 1.51$) at the location ($x = 0.5$ m, $y = 1$ m & $z = 1$ m) and it shows a comparison of temperature values obtained by EFG method using different weight functions with FEM and analytical methods for 27 nodes. Table 6.3 shows a comparison of temperature values obtained by EFG method using different functions for two values of scaling parameter with FEM and analytical methods at the same location i.e. ($x = 0.5$ m, $y = 1$ m & $z = 1$ m) for 125 nodes. A comparison of temperature values obtained using different EFG weight functions with FEM and analytical methods for 27 and 125 nodes, is shown in Table 6.4 and Table 6.5 respectively at the location ($x = 0.5$ m, $y = 1$ m & $z = 0.5$ m). Similar type of comparisons of temperature values are shown in Table 6.6 for 27 nodes at the location ($x = 1$ m, $y = 1$ m & $z = 1$ m), in Table 6.7 for 125 nodes at the location ($x = 1$ m, $y = 1$ m & $z = 1$ m), in Table 6.8 for 27 nodes at the location ($x = 1$ m, $y = 1$ m & $z = 0.5$ m) and in Table 6.9 for 125 nodes at the location ($x = 1$ m, $y = 1$ m & $z = 0.5$ m). From the results presented in Table 6.2 to Table 6.9,

it is observed that EFG results obtained using different weight functions are almost similar for $d_{\max} = 1.01$. However for $d_{\max} = 1.51$, only cubicspline, quarticspline, Gaussian, exponential and rational weight functions give acceptable results. It is also observed that EFG results obtained using different weight functions are in good agreement with those obtained by FEM and analytical methods. Moreover with the increase in number of nodes EFG results starts converging.

The effect of scaling parameter (d_{\max}) on EFG results obtained using different weight functions is presented in Table 6.10 for 27 nodes and in Table 6.11 for 125 nodes respectively at the location ($x = 0.5 \text{ m}$, $y = 1 \text{ m}$ & $z = 0.5 \text{ m}$). Similar effect of scaling parameter on EFG results is shown in Table 6.12 for 27 nodes and in Table 6.13 for 125 nodes at the location ($x = 1 \text{ m}$, $y = 1 \text{ m}$ & $z = 0.5 \text{ m}$). Fig. 6.2 shows the effect of scaling parameter on EFG results obtained using 27 and 125 nodes at the location ($x = 0.5 \text{ m}$, $y = 1 \text{ m}$ & $z = 1 \text{ m}$). Similar effect of scaling parameter on EFG results is observed in Fig. 6.3 at the location ($x = 1 \text{ m}$, $y = 1 \text{ m}$ & $z = 1 \text{ m}$). From tables and figures, it is clear that only cubicspline, quarticspline, Gaussian, exponential and rational weight functions give acceptable results in the range $1.0 < d_{\max} < 1.6$ whereas the results obtained using quadratic, hyperbolic and cosine weight functions are varying in abrupt manner with scaling parameter. Therefore EFG results obtained using quadratic, hyperbolic and cosine weight functions are not acceptable in the range $1.0 < d_{\max} < 1.6$. It is also observed that there is minimum variation in EFG results with scaling parameter for exponential weight function.

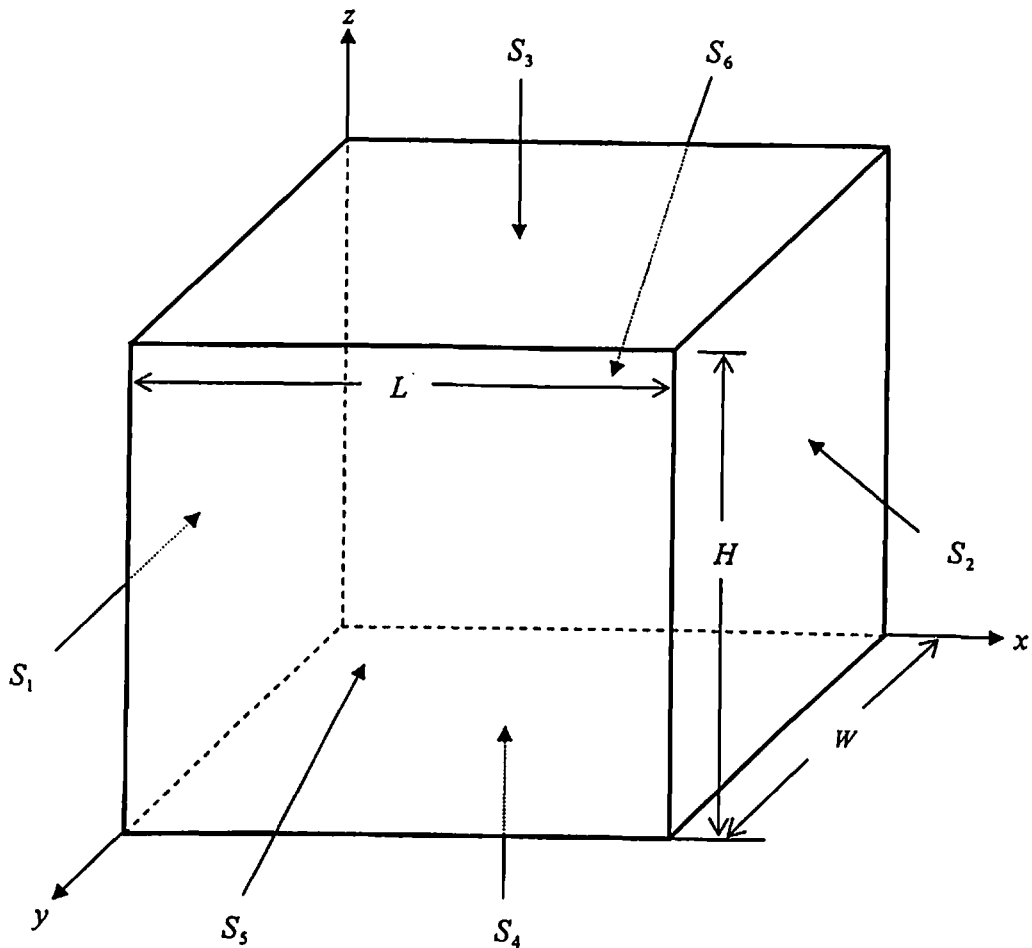


Fig. 6.1 Three-dimensional model

Table 6.1 Data for the 3-D model shown in Fig. 6.1

Parameters	Value of the parameter
Length (L)	1 m
Width (W)	1 m
Height (H)	1 m
Thermal conductivity (k)	400 W/m-K
Density of the material (ρ)	10000 kg/m ³
Specific heat (c)	400 kJ/kg-K
Rate of internal heat generation (\dot{Q})	0 W/m ³
Heat transfer coefficient (h)	200 W/m ² -K
Surrounding fluid temperature (T_∞)	20 °C
Initial temperature (T_{ini})	100 °C
Time step size (Δt)	100 sec
Temperature at surface, $x = 0$ or S_1	100 °C
Convection at all other surfaces	$-k \frac{\partial T}{\partial n'} = h(T - T_\infty)$ where $n' = x, y, z$ & $i = 2, 3, 4, 5, 6$

Table 6.2 Comparison of EFG results obtained using 27 nodes with FEM and analytical results at the location ($x = 0.5\text{ m}$, $y = 1\text{ m}$ & $z = 1\text{ m}$) of the 3-D model shown in Fig. 6.1

Weight function	EFG				FEM		Analytical
	$d_{\max} = 1.01$		$d_{\max} = 1.51$		T (°C)	% error	
	T (°C)	% error	T (°C)	% error			
C. S.	57.4355	0.3230	54.4565	5.4929	59.4238	-3.1276	57.6216
Q. S.	57.3447	0.4805	53.3230	7.4600			
Gaussian	57.9915	-0.6419	54.2764	5.8086			
Quadratic	57.3395	0.4896	36.0593	37.4205			
Hyperbolic	57.0785	0.9425	54.4567	5.4926			
Exponential	57.3646	0.4460	56.8520	1.3356			
Rational	57.3310	0.5043	55.0520	4.4594			
Cosine	57.3299	0.5062	41.9399	27.2150			

Table 6.3 Comparison of EFG results obtained using 125 nodes with FEM and analytical results at the location ($x = 0.5\text{ m}$, $y = 1\text{ m}$ & $z = 1\text{ m}$) of the 3-D model shown in Fig. 6.1

Weight function	EFG				FEM		Analytical
	$d_{\max} = 1.01$		$d_{\max} = 1.51$		T (°C)	% error	
	T (°C)	% error	T (°C)	% error			
C. S.	57.6348	-0.0229	57.4094	0.3683	58.2697	-1.1248	57.6216
Q. S.	57.6424	-0.0361	57.4484	0.3006			
Gaussian	57.6647	-0.0748	57.2657	0.6177			
Quadratic	57.6562	-0.0600	62.0657	-7.7126			
Hyperbolic	57.7670	-0.2523	57.0288	1.0288			
Exponential	57.6450	-0.0406	57.6103	0.0196			
Rational	57.6541	-0.0564	57.4712	0.2610			
Cosine	57.6559	-0.0595	59.9490	-4.0391			

Table 6.4 Comparison of EFG results obtained using 27 nodes with FEM and analytical results at the location ($x = 0.5$ m, $y = 1$ m & $z = 0.5$ m) of the 3-D model shown in Fig. 6.1

Weight function	EFG				FEM		Analytical
	$d_{\max} = 1.01$		$d_{\max} = 1.51$		T (°C)	% error	
	T (°C)	% error	T (°C)	% error			
C. S.	62.8557	-1.1711	60.9171	1.9492	63.9721	-2.9681	62.1281
Q. S.	62.8172	-1.1092	60.3020	2.9392			
Gaussian	62.8790	-1.2086	61.0070	1.8045			
Quadratic	62.6622	-0.8597	66.1792	-6.5206			
Hyperbolic	62.3820	-0.4087	57.1049	8.0852			
Exponential	62.7668	-1.0280	62.4927	-0.5869			
Rational	62.6854	-0.8970	61.7196	0.6575			
Cosine	62.6715	-0.8746	60.7759	2.1765			

Table 6.5 Comparison of EFG results obtained using 125 nodes with FEM and analytical results at the location ($x = 0.5$ m, $y = 1$ m & $z = 0.5$ m) of the 3-D model shown in Fig. 6.1

Weight function	EFG				FEM		Analytical
	$d_{\max} = 1.01$		$d_{\max} = 1.51$		T (°C)	% error	
	T (°C)	% error	T (°C)	% error			
C. S.	62.3105	-0.2936	62.0145	-0.1828	62.6783	-0.8856	62.1281
Q. S.	62.3178	-0.3053	61.9700	0.2545			
Gaussian	62.2895	-0.2598	61.9605	0.2698			
Quadratic	62.3225	-0.3129	67.0820	-7.9737			
Hyperbolic	62.3559	-0.3667	64.1584	-3.2679			
Exponential	62.3180	-0.3057	62.3056	-0.2857			
Rational	62.3228	-0.3134	62.2613	-0.2144			
Cosine	62.3231	-0.3139	62.8464	-1.1562			

Table 6.6 Comparison of EFG results obtained using 27 nodes with FEM and analytical results at the location ($x = 1\text{ m}$, $y = 1\text{ m}$ & $z = 1\text{ m}$) of the 3-D model shown in Fig. 6.1

Weight function	EFG				FEM		Analytical
	$d_{\max} = 1.01$		$d_{\max} = 1.51$		T (°C)	% error	
	T (°C)	% error	T (°C)	% error			
C. S.	44.8227	-0.1267	45.2945	-1.1806	47.4016	-5.8875	44.7660
Q. S.	44.9460	-0.4021	45.4757	-1.5854			
Gaussian	44.3704	0.8837	44.8850	0.2658			
Quadratic	45.0544	-0.6442	58.9115	-31.5988			
Hyperbolic	45.6527	-1.9807	50.1505	-12.0281			
Exponential	44.9587	0.4305	45.1037	-0.7544			
Rational	45.0454	-0.6241	45.2674	-1.1200			
Cosine	45.0577	-0.6516	53.0279	18.4557			

Table 6.7 Comparison of EFG results obtained using 125 nodes with FEM and analytical results at the location ($x = 1\text{ m}$, $y = 1\text{ m}$ & $z = 1\text{ m}$) of the 3-D model shown in Fig. 6.1

Weight function	EFG				FEM		Analytical
	$d_{\max} = 1.01$		$d_{\max} = 1.51$		T (°C)	% error	
	T (°C)	% error	T (°C)	% error			
C. S.	44.7419	0.0538	44.7855	-0.0436	45.5761	-1.8096	44.7660
Q. S.	44.7709	-0.0109	44.7962	-0.0675			
Gaussian	44.5800	0.4155	44.6303	0.3031			
Quadratic	44.8039	-0.0847	46.5444	-3.9727			
Hyperbolic	44.9115	-0.3250	44.6675	0.2200			
Exponential	44.7771	-0.0248	44.7996	-0.0751			
Rational	44.7999	-0.0757	44.7569	0.0203			
Cosine	44.8004	-0.0768	45.5955	-1.8530			

Table 6.8 Comparison of EFG results obtained using 27 nodes with FEM and analytical results at the location ($x = 1\text{ m}$, $y = 1\text{ m}$ & $z = 0.5\text{ m}$) of the 3-D model shown in Fig. 6.1

Weight function	EFG				FEM		Analytical
	$d_{\max} = 1.01$		$d_{\max} = 1.51$		$T (^{\circ}\text{C})$	% error	
	$T (^{\circ}\text{C})$	% error	$T (^{\circ}\text{C})$	% error			$T (^{\circ}\text{C})$
C. S.	48.1029	-0.4188	48.8215	-1.9189	49.8064	-3.9750	47.9023
Q. S.	48.1092	-0.4319	49.0645	-2.4262			
Gaussian	48.0950	-0.4023	48.8792	-2.0394			
Quadratic	48.1754	-0.5701	43.7350	8.6996			
Hyperbolic	48.3454	-0.9250	40.7083	15.0181			
Exponential	48.1288	-0.4728	48.2751	-0.7783			
Rational	48.1617	-0.5415	48.7267	-1.7210			
Cosine	48.1690	-0.5568	48.8323	-1.9415			

Table 6.9 Comparison of EFG results obtained using 125 nodes with FEM and analytical results at the location ($x = 1\text{ m}$, $y = 1\text{ m}$ & $z = 0.5\text{ m}$) of the 3-D model shown in Fig. 6.1

Weight function	EFG				FEM		Analytical
	$d_{\max} = 1.01$		$d_{\max} = 1.51$		$T (^{\circ}\text{C})$	% error	
	$T (^{\circ}\text{C})$	% error	$T (^{\circ}\text{C})$	% error			$T (^{\circ}\text{C})$
C. S.	47.9464	-0.0921	48.0561	-0.3211	48.4485	-1.1402	47.9023
Q. S.	47.9529	-0.1056	48.0805	-0.3720			
Gaussian	47.9108	-0.0177	48.0116	-0.2282			
Quadratic	47.9604	-0.1213	50.0474	-4.4781			
Hyperbolic	47.9756	-0.1530	48.7558	-1.7818			
Exponential	47.9547	-0.1094	47.9824	-0.1672			
Rational	47.9599	-0.1202	48.0487	-0.3056			
Cosine	47.9604	-0.1213	48.1845	-0.5891			

Table 6.10 Effect of scaling parameter on EFG results obtained using 27 nodes at the location ($x = 0.5 \text{ m}$, $y = 1 \text{ m}$ & $z = 0.5 \text{ m}$) of the 3-D model shown in Fig. 6.1

Scaling Parameter	Temperature ($^{\circ} \text{C}$)							
	C. S.	Q. S	Gaussian	Quadratic	Hyperbolic	Exponential	Rational	Cosine
1.01	62.8557	62.8172	62.8790	62.7000	62.3821	62.7668	62.6854	62.7000
1.11	63.0606	62.9534	61.8703	65.1000	62.8174	61.7233	61.5964	64.0000
1.21	62.7877	62.3632	61.6882	62.3000	62.9734	61.7040	61.6468	62.0000
1.31	61.9817	61.6103	61.5661	62.7000	63.1503	61.7096	61.7003	62.3000
1.41	61.4567	61.1222	61.2106	61.5000	57.5485	62.5506	61.9595	59.5000
1.51	60.9171	60.3020	61.0070	66.2000	57.1049	62.4927	61.7196	60.8000
1.61	60.3491	59.5550	60.8280	86.5000	56.9386	62.4248	61.4870	65.2000
1.71	59.8345	59.0872	60.4927	259.9000	24.8117	62.1475	59.6866	111.900
1.81	59.2545	58.5105	60.3060	148.3000	21.1614	61.9992	59.0567	249.000
1.91	58.6573	57.8220	60.1925	-371.500	17.8449	61.8341	58.3806	3048.80
2.01	58.0736	57.1112	59.9617	-847.000	3.6402	61.1738	57.1889	62.800
2.11	57.4804	56.3738	59.9551	-381.600	-5.1947	60.9569	56.4539	190.000
2.21	56.8166	55.4546	60.0659	-947.200	-14.9839	60.7303	55.6674	-142.000
2.31	56.0262	54.2199	60.3212	-1942.900	-25.7859	60.4946	54.8227	-283.200
2.41	55.0484	52.5535	60.7534	-3616.000	-37.6593	60.2503	53.9119	-291.600

Table 6.11 Effect of scaling parameter on EFG results obtained using 125 nodes at the location ($x = 0.5 \text{ m}$, $y = 1 \text{ m}$ & $z = 0.5 \text{ m}$) of the 3-D model shown in Fig. 6.1

Scaling Parameter	Temperature ($^{\circ} \text{C}$)							
	C. S.	Q. S	Gaussian	Quadratic	Hyperbolic	Exponential	Rational	Cosine
1.01	62.3105	62.3178	62.2895	62.3225	62.3559	62.3180	62.3228	62.3231
1.11	62.3833	62.3761	62.0582	63.1507	62.3448	62.0971	62.1426	62.7725
1.21	62.3324	62.2454	62.0325	62.3219	62.3741	62.1036	62.1605	62.2961
1.31	62.1650	62.1032	62.0246	62.3209	62.4128	62.1140	62.1779	62.2954
1.41	62.0793	62.0433	61.9776	62.3803	64.6399	62.3085	62.2885	62.0935
1.51	62.0145	61.9700	61.9605	67.0820	64.1584	62.3056	62.2613	62.8464
1.61	61.9768	61.9614	61.9437	63.7777	63.7709	62.3015	62.2359	69.8380
1.71	61.9758	62.0079	61.8845	61.7092	63.5426	62.2775	62.3487	62.3757
1.81	61.9822	62.0207	61.8335	56.1193	68.6358	62.2713	62.3414	55.4572
1.91	61.9955	61.9974	61.7638	51.5102	66.1741	62.2659	62.3351	49.9689
2.01	62.0003	61.9157	61.6415	60.2051	75.8115	62.1271	62.1973	56.3566
2.11	61.9661	61.7127	61.4835	69.6853	21.6286	61.9796	61.9310	53.8888
2.21	61.8508	61.2924	61.3140	94.7015	31.4805	61.9685	61.9762	81.6243
2.31	61.6177	60.5465	61.1143	104.5584	39.3649	61.9603	62.0243	135.4578
2.41	61.1817	59.2303	60.8049	95.5498	113.5150	61.9601	61.4197	240.0242

Table 6.12 Effect of scaling parameter on EFG results obtained using 27 nodes at the location ($x = 1\text{ m}$, $y = 1\text{ m}$ & $z = 0.5\text{ m}$) of the 3-D model shown in Fig. 6.1

Scaling Parameter	Temperature ($^{\circ}\text{C}$)							
	C. S.	Q. S	Gaussian	Quadratic	Hyperbolic	Exponential	Rational	Cosine
1.01	48.1029	48.1092	48.0950	48.2000	48.3454	48.1288	48.1617	48.2000
1.11	48.0223	48.0624	48.4135	47.5000	48.0458	48.5022	48.6005	47.8000
1.21	48.1188	48.2777	48.4833	48.5000	47.8824	48.5165	48.5912	48.6000
1.31	48.4170	48.5567	48.5469	48.2000	47.6862	48.5210	48.5810	48.4000
1.41	48.6146	48.7476	48.7199	49.6000	43.4566	48.2407	48.6161	50.3000
1.51	48.8215	49.0645	48.8792	43.7000	40.7083	48.2751	48.7267	48.8000
1.61	49.0485	49.3719	49.0785	18.7000	37.0448	48.3147	48.8325	42.0000
1.71	49.2706	49.6061	49.4206	-64.3000	32.6357	48.4511	49.5856	29.9000
1.81	49.5298	49.9002	49.7667	-65.3000	25.4716	48.5291	49.8086	-105.800
1.91	49.8109	50.2562	50.1590	159.000	17.1063	48.6145	50.0301	-2279.60
2.01	50.1081	50.6484	50.6992	137.100	72.5605	48.9585	51.2120	100.000
2.11	50.4383	51.1055	51.2008	348.600	75.8769	49.0841	51.5758	444.100
2.21	50.8390	51.7109	51.6965	746.500	79.5545	49.2157	51.9612	-112.000
2.31	51.3389	52.5252	52.1357	1425.50	83.6198	49.3528	52.3708	-473.000
2.41	51.9654	53.5927	52.4469	2532.20	88.0998	49.4950	52.8073	-423.000

Table 6.13 Effect of scaling parameter on EFG results obtained using 125 nodes at the location ($x = 1\text{ m}$, $y = 1\text{ m}$ & $z = 0.5\text{ m}$) of the 3-D model shown in Fig. 6.1

Scaling Parameter	Temperature ($^{\circ}\text{C}$)							
	C. S.	Q. S	Gaussian	Quadratic	Hyperbolic	Exponential	Rational	Cosine
1.01	47.9464	47.9529	47.9108	47.9604	47.9756	47.9547	47.9599	47.9604
1.11	47.9354	47.9427	47.9877	47.7856	48.0272	48.0134	48.0299	47.8843
1.21	47.9532	47.9798	48.0046	48.0374	48.0376	48.0150	48.0300	48.0432
1.31	48.0016	48.0225	48.0133	48.0370	48.0528	48.0157	48.0300	48.0368
1.41	48.0301	48.0479	48.0228	48.2573	49.0190	47.9755	48.0355	48.1706
1.51	48.0561	48.0805	48.0116	50.0474	48.7558	47.9824	48.0487	48.1845
1.61	48.0791	48.1021	47.9811	47.7298	48.6028	47.9900	48.0600	51.3305
1.71	48.0967	48.1149	47.9100	47.4786	49.6180	48.0337	48.1061	46.7611
1.81	48.1161	48.1364	47.7983	45.2386	49.6661	48.0439	48.1071	45.2096
1.91	48.1345	48.1505	47.6253	44.5143	48.9379	48.0534	48.1044	42.9541
2.01	48.1496	48.1465	47.3764	47.7315	30.2545	48.0965	48.2493	41.5753
2.11	48.1625	48.1212	47.0470	52.2472	36.5362	48.1550	48.3807	49.9608
2.21	48.1692	48.0538	46.5996	41.8277	51.1653	48.1714	48.3932	46.7199
2.31	48.1480	47.8827	46.0340	45.3600	67.2515	48.1873	48.4050	30.9884
2.41	48.0720	47.5306	45.3821	24.2564	171.5653	48.2119	48.6796	36.1823

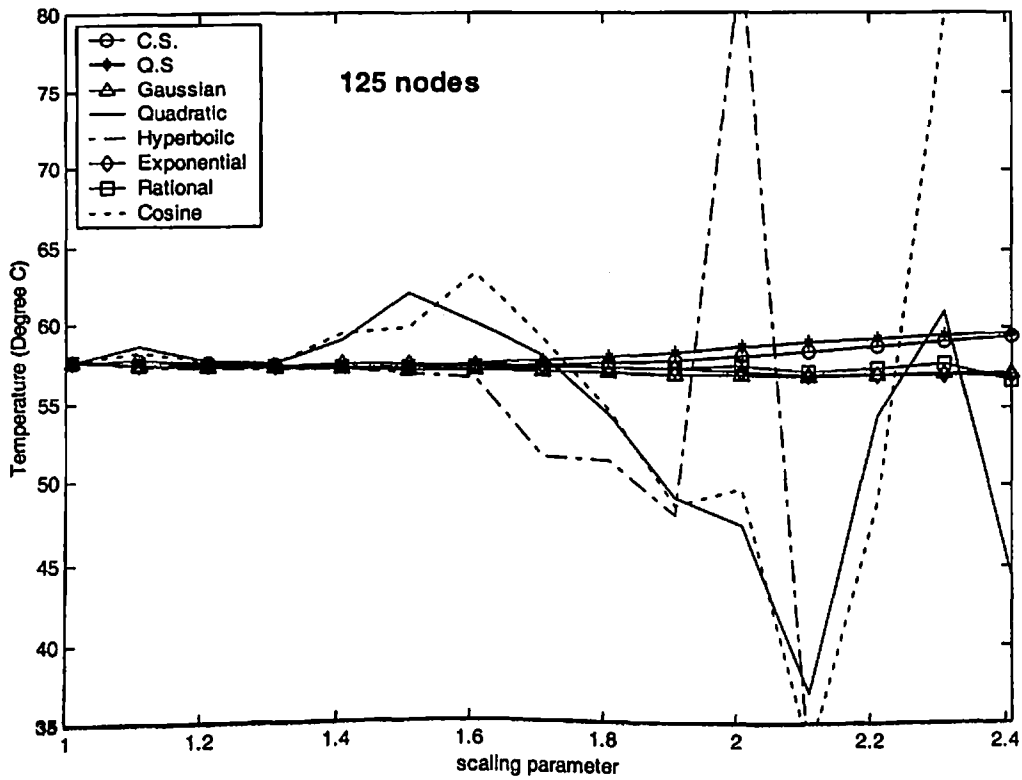
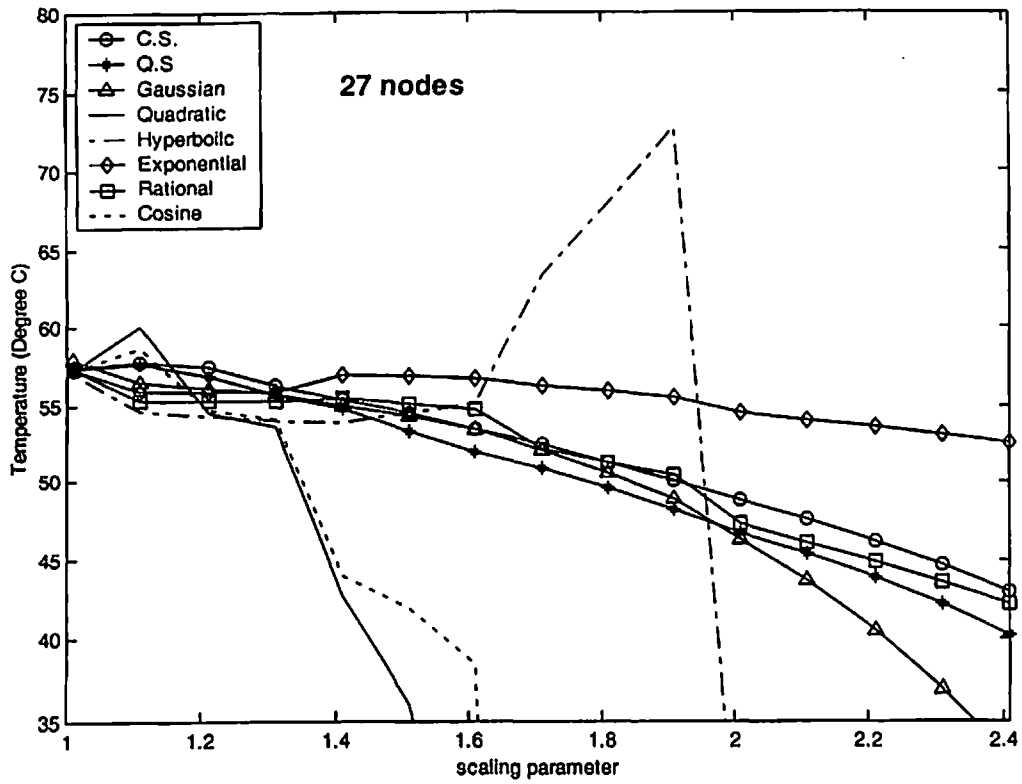


Fig. 6.2 Effect of scaling parameter on EFG results at the location ($x = 0.5\text{ m}$, $y = 1\text{ m}$ & $z = 1\text{ m}$) of the 3-D model shown in Fig. 6.1

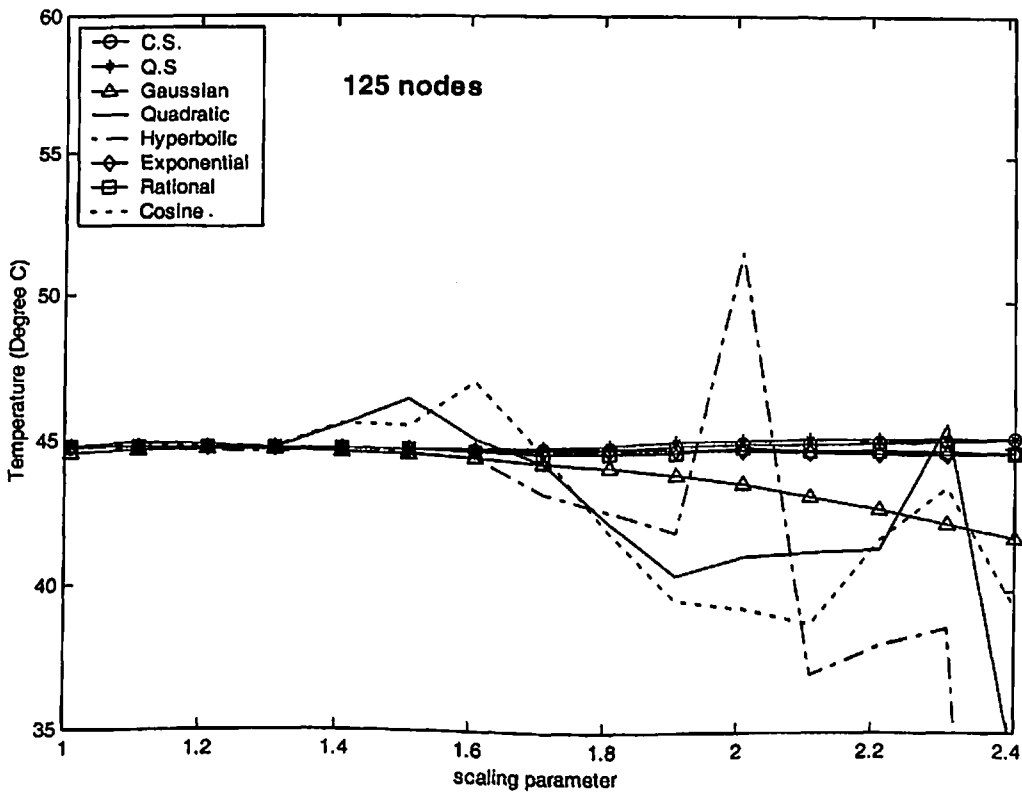
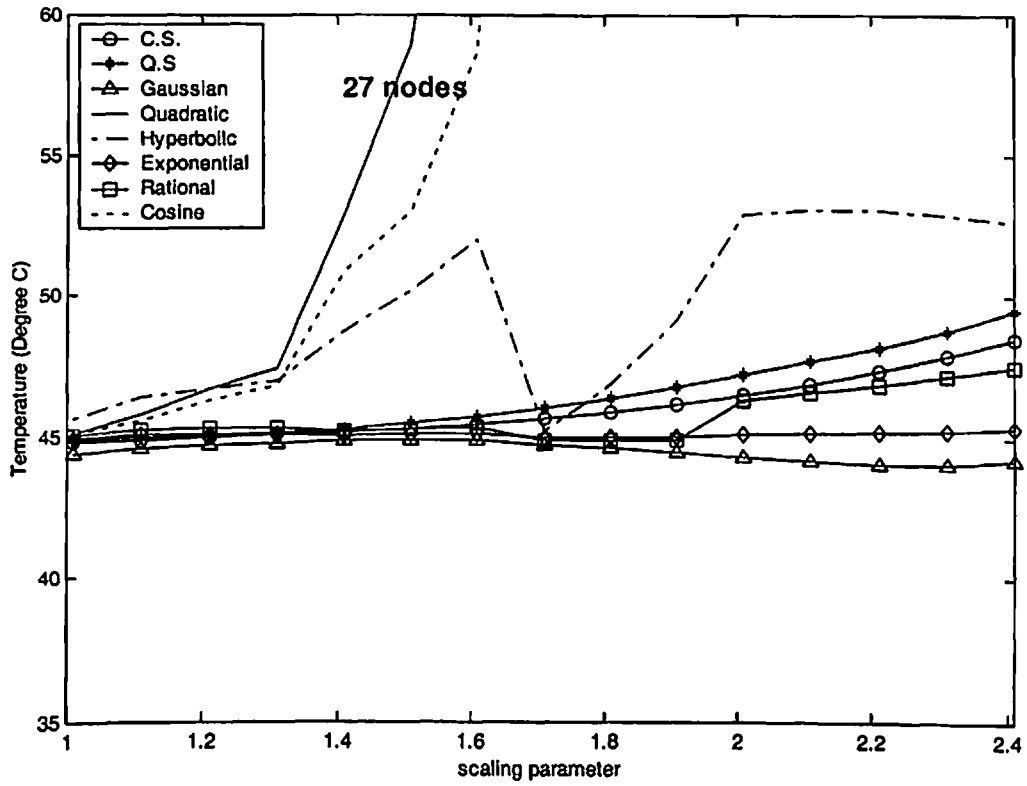


Fig. 6.3 Effect of scaling parameter on EFG results at the location ($x = 1\text{ m}$, $y = 1\text{ m}$ & $z = 1\text{ m}$) of the 3-D model shown in Fig. 6.1

6.3.2 Transient analysis

The transient analysis of 3-D model is carried out using different EFG weight functions. Table 6.14 and Fig. 6.4 show the convergence study using different time steps at two different locations. The solution with 1000 sec time step continues to oscillate with decreasing amplitude until it converges at 20000 sec. This time step (1000 sec) is nearly 10% of the total time required to achieve steady state condition in first two time steps (i.e. 100 sec and 500 sec). For time steps up to 500 sec, the EFG results are well converged and this time step is nearly 5% of the total time required for achieving steady state. For this case (i.e. CASE-I) of 3-D transient analysis, the time step of 100 sec has been taken which is nearly 1% of the total time required to achieve steady state condition.

Table 6.15 and Table 6.16 show the comparison of EFG results (i.e. temperature values) obtained using 27 nodes with FEM results at the location ($x = 0.5\text{ m}$, $y = 1\text{ m}$ & $z = 0.5\text{ m}$) for $d_{\max} = 1.01$ and $d_{\max} = 1.51$ respectively. Similar comparison of temperature values obtained using 125 nodes is presented in Table 6.17 and Table 6.18 for $d_{\max} = 1.01$ and $d_{\max} = 1.51$ respectively at the same location i.e. ($x = 0.5\text{ m}$, $y = 1\text{ m}$ & $z = 0.5\text{ m}$). Table 6.19 and Table 6.20 show the comparison of EFG results (i.e. temperature values) obtained using 27 nodes with FEM results at the location ($x = 1\text{ m}$, $y = 1\text{ m}$ & $z = 0.5\text{ m}$) for $d_{\max} = 1.01$ and $d_{\max} = 1.51$ respectively. Similar comparison of temperature values obtained using 125 nodes is also presented in Table 6.21 and Table 6.22 for $d_{\max} = 1.01$ and $d_{\max} = 1.51$ respectively at the same location i.e. ($x = 1\text{ m}$, $y = 1\text{ m}$ & $z = 0.5\text{ m}$). Fig 6.5 shows the comparison of EFG results (i.e. temperature values) obtained using 27 nodes with FEM results for $d_{\max} = 1.01$ and $d_{\max} = 1.51$ at the location ($x = 0.5\text{ m}$, $y = 0.5\text{ m}$ & $z = 1\text{ m}$). Similar comparison of temperature values obtained using 125 nodes is shown in Fig. 6.6 at the same location i.e. ($x = 0.5\text{ m}$, $y = 0.5\text{ m}$ & $z = 1\text{ m}$). Fig 6.7 shows the comparison of EFG results (i.e. temperature values) obtained using 27 nodes with FEM results for $d_{\max} = 1.01$ and $d_{\max} = 1.51$ at the location ($x = 1\text{ m}$, $y = 1\text{ m}$ & $z = 1\text{ m}$). Similar comparison of temperature values obtained using 125 nodes is shown in Fig. 6.8 at the same location i.e.

($x = 1\text{ m}$, $y = 1\text{ m}$ & $z = 1\text{ m}$). From the results presented in tables and figures, it is clear that EFG results obtained using different weight functions are almost similar for $d_{\max} = 1.01$. However for $d_{\max} = 1.51$ only cubicspline, quarticspline, Gaussian, exponential and rational weight functions give acceptable results. It has also been observed that the EFG results are in good agreement with those obtained by FEM.

Table 6.14 Convergence study of EFG results obtained using different time step at the location ($x = 1\text{ m}$, $y = 1\text{ m}$ & $z = 1\text{ m}$) of the 3-D model shown in Fig. 6.1

Time (sec) $\times 10^2$	Time Step Size		
	100 sec	500 sec	1000 sec
0	100.0000	100.0000	100.0000
10	68.0961	70.1553	58.4668
20	58.4484	59.1564	63.6492
30	52.8170	53.0930	48.8266
40	49.5006	49.6273	51.9693
50	47.5462	47.6207	45.5044
60	46.3945	46.4505	47.8038
70	45.7158	45.7651	44.5739
80	45.3159	45.3625	46.1859
90	45.0802	45.1256	44.4201
100	44.9412	44.9861	45.4973

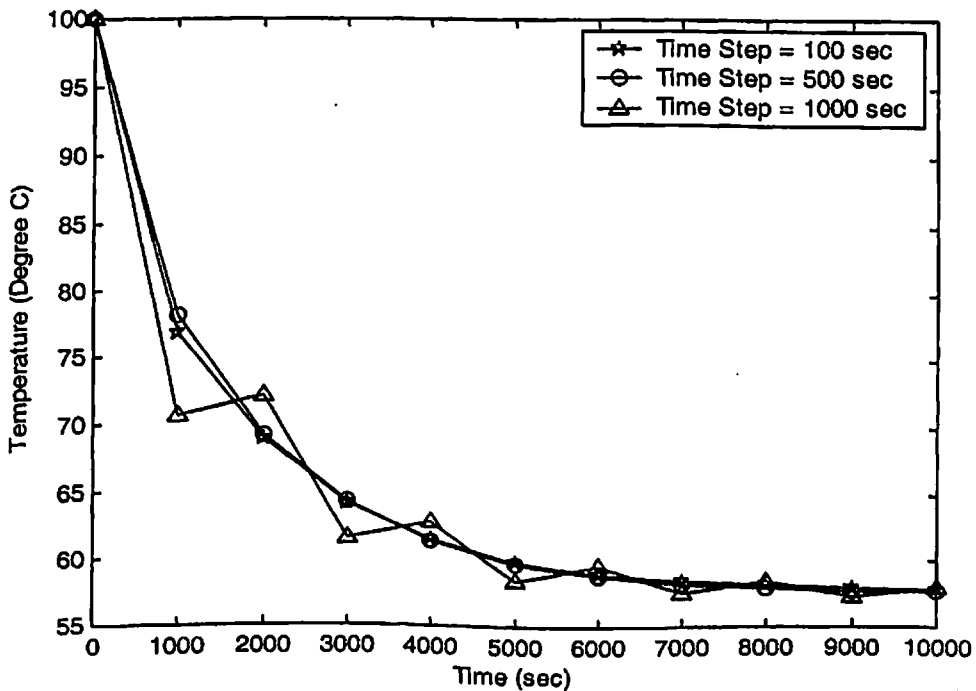


Fig. 6.4 Convergence analysis of EFG results obtained using different time step at the location ($x = 0.5\text{ m}$, $y = 1\text{ m}$ & $z = 1\text{ m}$) of the 3-D model shown in Fig. 6.1

Table 6.15 Comparison of EFG results obtained using 27 nodes with FEM at the location ($x = 0.5$ m, $y = 1$ m & $z = 0.5$ m) of the 3-D model shown in Fig. 6.1 for $d_{max} = 1.01$

Time (sec) $\times 10^2$	Temperature ($^{\circ}$ C)								
	$d_{max} = 1.01$								FEM
	C. S.	Q. S	Gaussian	Quadratic	Hyperbolic	Exponential	Rational	Cosine	
0	100.000	100.000	100.000	100.000	100.000	100.000	100.000	100.000	100.000
10	85.4179	85.3653	85.4936	85.1820	84.8450	85.3062	85.2076	85.1918	86.5292
20	75.9030	75.8582	75.9457	75.6887	75.3782	75.8033	75.7132	75.6984	77.7232
30	70.3809	70.3398	70.4091	70.1777	69.8812	70.2872	70.2016	70.1872	72.3004
40	67.1954	67.1560	67.2180	66.9977	66.7087	67.1045	67.0212	67.0071	69.0124
50	65.3584	65.3197	65.3792	65.1632	64.8784	65.2688	65.1865	65.1726	67.0249
60	64.2990	64.2606	64.3196	64.1050	63.8223	64.2099	64.1282	64.1143	65.8230
70	63.6880	63.6497	63.7091	63.4945	63.2130	63.5992	63.5177	63.5038	65.0953
80	63.3357	63.2974	63.3573	63.1423	62.8615	63.2469	63.1655	63.1516	64.6542
90	63.1325	63.0941	63.1546	62.9392	62.6587	63.0437	62.9623	62.9485	64.3865
100	63.0153	62.9769	63.0378	62.8220	62.5417	62.9265	62.8451	62.8313	64.2240

Table 6.16 Comparison of EFG results obtained using 27 nodes with FEM at the location ($x = 0.5$ m, $y = 1$ m & $z = 0.5$ m) of the 3-D model shown in Fig. 6.1 for $d_{max} = 1.51$

Time (sec) $\times 10^2$	Temperature ($^{\circ}$ C)								
	$d_{max} = 1.51$								FEM
	C. S.	Q. S	Gaussian	Quadratic	Hyperbolic	Exponential	Rational	Cosine	
0	100.000	100.000	100.000	100.000	100.000	100.000	100.000	100.000	100.000
10	85.1576	85.2016	85.3984	90.1614	69.8081	85.3415	85.6758	88.6472	86.5292
20	75.1726	75.0024	75.3640	79.9706	64.3097	75.6905	75.4778	76.9069	77.7232
30	69.2684	68.9455	69.4231	74.1088	61.1920	70.0974	69.6084	70.0999	72.3004
40	65.8084	65.3829	65.9393	70.7386	59.4235	66.8741	66.2428	66.1654	69.0124
50	63.7818	63.2887	63.8975	68.8008	58.4202	65.0170	64.3131	63.8911	67.0249
60	62.5949	62.0577	62.7010	67.6866	57.8511	63.9471	63.2066	62.5765	65.8230
70	61.8998	61.3340	61.9997	67.0459	57.5282	63.3306	62.5722	61.8167	65.0953
80	61.4926	60.9087	61.5888	66.6775	57.3451	62.9754	62.2085	61.3775	64.6542
90	61.2542	60.6586	61.3479	66.4657	57.2411	62.7708	61.9999	61.1236	64.3865
100	61.1145	60.5117	61.2068	66.3439	57.1822	62.6529	61.8803	60.9769	64.2240

Table 6.17 Comparison of EFG results obtained using 125 nodes with FEM at the location ($x = 0.5$ m, $y = 1$ m & $z = 0.5$ m) of the 3-D model shown in Fig. 6.1 for $d_{max} = 1.01$

Time (sec) $\times 10^2$	Temperature ($^{\circ}$ C)								
	$d_{max} = 1.01$								FEM
	C. S.	Q. S	Gaussian	Quadratic	Hyperbolic	Exponential	Rational	Cosine	
0	100.000	100.000	100.000	100.0000	100.0000	100.0000	100.0000	100.0000	100.000
10	83.8643	83.8655	83.8802	83.8625	83.8826	83.8640	83.8634	83.8631	84.3225
20	75.0401	75.0443	75.0371	75.0452	75.0717	75.0437	75.0458	75.0459	75.7728
30	69.8139	69.8198	69.8013	69.8226	69.8526	69.8195	69.8230	69.8233	70.5826
40	66.7325	66.7391	66.7151	66.7430	66.7748	66.7391	66.7433	66.7436	67.4466
50	64.9164	64.9235	64.8968	64.9278	64.9605	64.9236	64.9281	64.9284	65.5544
60	63.8462	63.8534	63.8256	63.8580	63.8911	63.8536	63.8583	63.8586	64.4130
70	63.2155	63.2228	63.1945	63.2275	63.2608	63.2230	63.2277	63.2281	63.7246
80	62.8438	62.8512	62.8227	62.8559	62.8893	62.8514	62.8561	62.8565	63.3094
90	62.6248	62.6322	62.6036	62.6369	62.6703	62.6324	62.6371	62.6375	63.0589
100	62.4957	62.5031	62.4746	62.5078	62.5412	62.5033	62.5080	62.5084	62.9079

Table 6.18 Comparison of EFG results obtained using 125 nodes with FEM at the location ($x = 0.5$ m, $y = 1$ m & $z = 0.5$ m) of the 3-D model shown in Fig. 6.1 for $d_{max} = 1.51$

Time (sec) $\times 10^2$	Temperature ($^{\circ}$ C)								
	$d_{max} = 1.51$								FEM
	C. S.	Q. S	Gaussian	Quadratic	Hyperbolic	Exponential	Rational	Cosine	
0	100.0000	100.0000	100.0000	100.0000	100.0000	100.0000	100.0000	100.0000	100.000
10	83.8049	83.8200	83.7721	85.7313	83.0276	83.9316	84.1813	84.3545	84.3225
20	74.9508	74.9551	74.9113	78.8453	75.2960	75.0750	75.1832	75.6344	75.7728
30	69.6779	69.6694	69.6335	74.0971	70.6888	69.8304	69.8627	70.3870	70.5826
40	66.5532	66.5341	66.5055	71.2199	67.9847	66.7390	66.7320	67.2887	67.4466
50	64.7024	64.6755	64.6525	69.5171	66.4000	64.9176	64.8907	65.4631	65.5544
60	63.6064	63.5737	63.5550	68.5143	65.4716	63.8445	63.8077	64.3878	64.4130
70	62.9573	62.9206	62.9049	67.9243	64.9277	63.2122	63.1708	63.7543	63.7246
80	62.5729	62.5335	62.5199	67.5774	64.6091	62.8398	62.7962	63.3812	63.3094
90	62.3452	62.3041	62.2918	67.3733	64.4224	62.6203	62.5759	63.1614	63.0589
100	62.2104	62.1680	62.1568	67.2533	64.3131	62.4910	62.4463	63.0320	62.9079

Table 6.19 Comparison of EFG results obtained using 27 nodes with FEM at the location ($x = 1\text{ m}$, $y = 1\text{ m}$ & $z = 0.5\text{ m}$) of the 3-D model shown in Fig. 6.1 for $d_{\max} = 1.01$

Time (sec) $\times 10^2$	Temperature ($^{\circ}\text{C}$)								
	$d_{\max} = 1.01$								FEM
	C. S.	Q. S	Gaussian	Quadratic	Hyperbolic	Exponential	Rational	Cosine	
0	100.000	100.000	100.000	100.000	100.0000	100.0000	100.0000	100.0000	100.000
10	75.6655	75.6579	75.7181	75.7085	75.8553	75.6733	75.6950	75.7016	77.9517
20	63.9410	63.9411	63.9563	64.0000	64.1571	63.9587	63.9863	63.9933	66.3217
30	57.2350	57.2391	57.2330	57.3026	57.4663	57.2579	57.2888	57.2960	59.7070
40	53.3692	53.3750	53.3604	53.4405	53.6076	53.3943	53.4267	53.4340	55.7982
50	51.1399	51.1463	51.1290	51.2126	51.3814	51.1659	51.1989	51.2062	53.4471
60	49.8543	49.8609	49.8432	49.9275	50.0970	49.8806	49.9137	49.9211	52.0219
70	49.1129	49.1195	49.1023	49.1861	49.3560	49.1392	49.1724	49.1797	51.1553
80	48.6853	48.6919	48.6754	48.7584	48.9284	48.7116	48.7447	48.7521	50.6277
90	48.4388	48.4453	48.4294	48.5117	48.6818	48.4649	48.4980	48.5054	50.3064
100	48.2966	48.3030	48.2877	48.3694	48.5395	48.3227	48.3557	48.3630	50.1108

Table 6.20 Comparison of EFG results obtained using 27 nodes with FEM at the location ($x = 1\text{ m}$, $y = 1\text{ m}$ & $z = 0.5\text{ m}$) of the 3-D model shown in Fig. 6.1 for $d_{\max} = 1.51$

Time (sec) $\times 10^2$	Temperature ($^{\circ}\text{C}$)								
	$d_{\max} = 1.51$								FEM
	C. S.	Q. S	Gaussian	Quadratic	Hyperbolic	Exponential	Rational	Cosine	
0	100.000	100.000	100.000	100.000	100.000	100.000	100.000	100.000	100.000
10	76.1152	76.3647	76.1892	75.3856	81.8405	75.9648	76.9659	77.6551	77.9517
20	64.7156	65.0177	64.7887	61.9266	64.0419	64.1796	64.8939	65.4704	66.3217
30	58.1273	58.4389	58.1994	54.1952	53.9455	57.4373	57.9961	58.4494	59.7070
40	54.2717	54.5749	54.3411	49.7496	48.2177	53.5538	54.0415	54.3912	55.7982
50	52.0136	52.3036	52.0801	47.1933	44.9683	51.3164	51.7740	52.0455	53.4471
60	50.6911	50.9685	50.7551	45.7235	43.1250	50.0273	50.4739	50.6896	52.0219
70	49.9165	50.1837	49.9785	44.8784	42.0793	49.2846	49.7285	49.9058	51.1553
80	49.4628	49.7224	49.5234	44.3924	41.4860	48.8567	49.3011	49.4528	50.6277
90	49.1971	49.4512	49.2567	44.1130	41.1495	48.6102	49.0560	49.1909	50.3064
100	49.0415	49.2918	49.1004	43.9524	40.9586	48.4682	48.9155	49.0396	50.1108

Table 6.21 Comparison of EFG results obtained using 125 nodes with FEM at the location ($x = 1\text{ m}$, $y = 1\text{ m}$ & $z = 0.5\text{ m}$) of the 3-D model shown in Fig. 6.1 for $d_{\max} = 1.01$

Time (sec) $\times 10^2$	Temperature ($^{\circ}\text{C}$)								
	$d_{\max} = 1.01$								FEM
	C. S.	Q. S.	Gaussian	Quadratic	Hyperbolic	Exponential	Rational	Cosine	
0	100.000	100.000	100.000	100.000	100.000	100.000	100.000	100.000	100.000
10	74.2550	74.2587	74.2429	74.2634	74.2768	74.2599	74.2632	74.2635	75.0824
20	63.4071	63.4124	63.3822	63.4188	63.4338	63.4139	63.4184	63.4189	64.3651
30	57.0551	57.0613	57.0232	57.0686	57.0845	57.0630	57.0681	57.0686	58.0344
40	53.3141	53.3207	53.2791	53.3283	53.3445	53.3225	53.3278	53.3284	54.2284
50	51.1096	51.1164	51.0735	51.1241	51.1401	51.1182	51.1235	51.1242	51.9343
60	49.8105	49.8173	49.7741	49.8250	49.8409	49.8191	49.8244	49.8250	50.5509
70	49.0450	49.0516	49.0085	49.0593	49.0750	49.0534	49.0588	49.0594	49.7165
80	48.5938	48.6004	48.5575	48.6081	48.6237	48.6022	48.6075	48.6081	49.2133
90	48.3279	48.3345	48.2918	48.3421	48.3576	48.3363	48.3416	48.3422	48.9098
100	48.1712	48.1778	48.1352	48.1854	48.2008	48.1796	48.1848	48.1854	48.7267

Table 6.22 Comparison of EFG results obtained using 125 nodes with FEM at the location ($x = 1\text{ m}$, $y = 1\text{ m}$ & $z = 0.5\text{ m}$) of the 3-D model shown in Fig. 6.1 for $d_{\max} = 1.51$

Time (sec) $\times 10^2$	Temperature ($^{\circ}\text{C}$)								
	$d_{\max} = 1.51$								FEM
	C. S.	Q. S.	Gaussian	Quadratic	Hyperbolic	Exponential	Rational	Cosine	
0	100.000	100.000	100.000	100.000	100.000	100.000	100.000	100.000	100.000
10	74.1818	74.1759	74.0934	74.3691	73.8844	74.3282	74.5527	74.4305	75.0824
20	63.4874	63.5101	63.4207	64.7533	63.4631	63.4605	63.5939	63.6377	64.3651
30	57.1920	57.2236	57.1355	58.7554	57.3728	57.0988	57.1891	57.2880	58.0344
40	53.4664	53.5000	53.4155	55.1768	53.8041	53.3532	53.4243	53.5470	54.2284
50	51.2602	51.2930	51.2124	53.0651	51.7132	51.1466	51.2103	51.3432	51.9343
60	49.9537	49.9847	49.9074	51.8222	50.4883	49.8466	49.9082	50.0451	50.5509
70	49.1799	49.2093	49.1345	51.0912	49.7708	49.0807	49.1423	49.2805	49.7165
80	48.7217	48.7496	48.6767	50.6613	49.3504	48.6294	48.6919	48.8301	49.2133
90	48.4503	48.4771	48.4055	50.4084	49.1041	48.3636	48.4270	48.5648	48.9098
100	48.2896	48.3156	48.2449	50.2597	48.9599	48.2070	48.2712	48.4085	48.7267

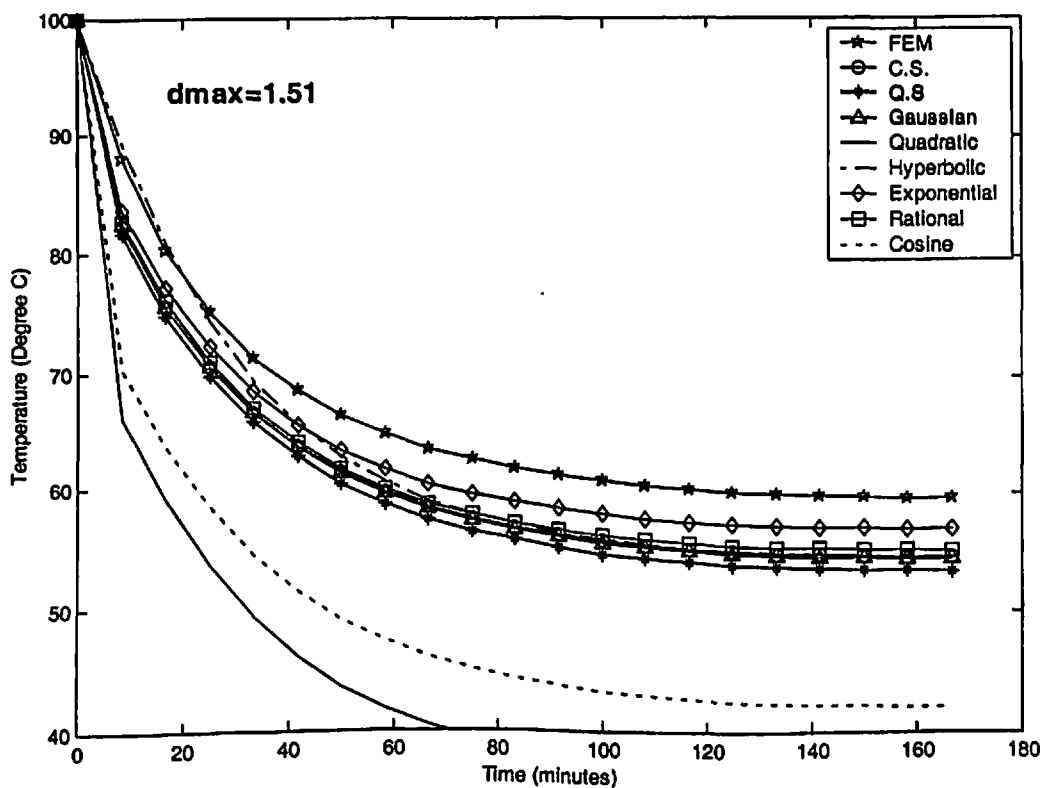
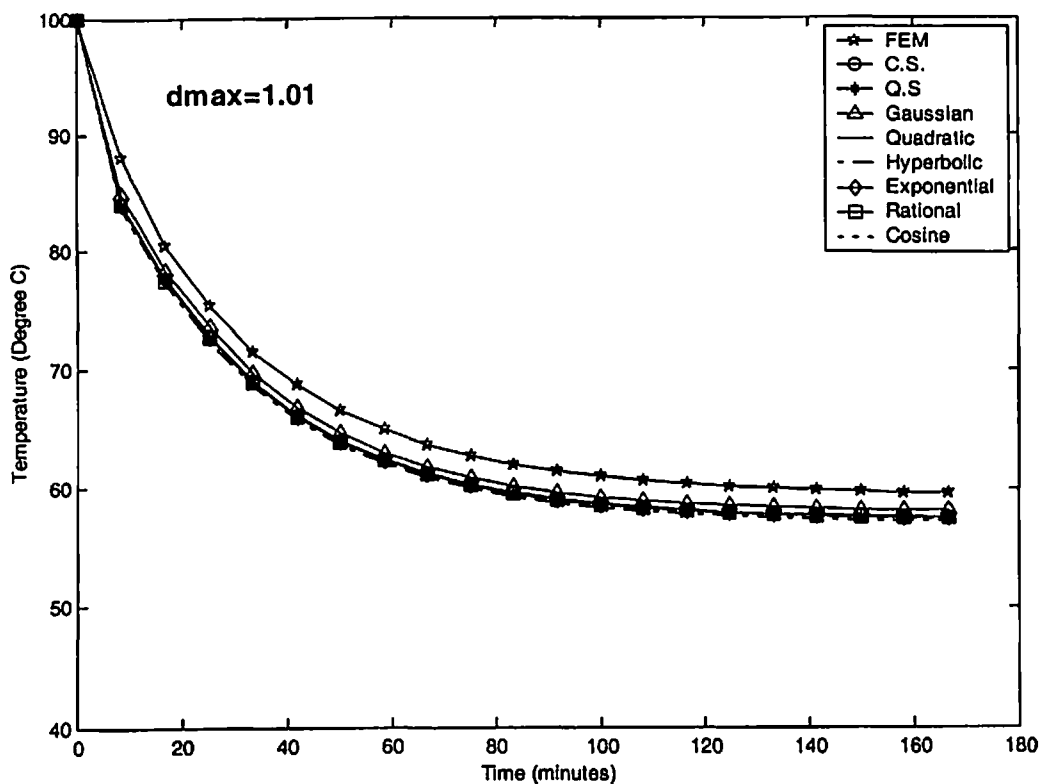


Fig. 6.5 Comparison of EFG results obtained using 27 nodes with FEM at the location ($x = 0.5$ m, $y = 0.5$ m & $z = 1$ m) of the 3-D model shown in Fig. 6.1

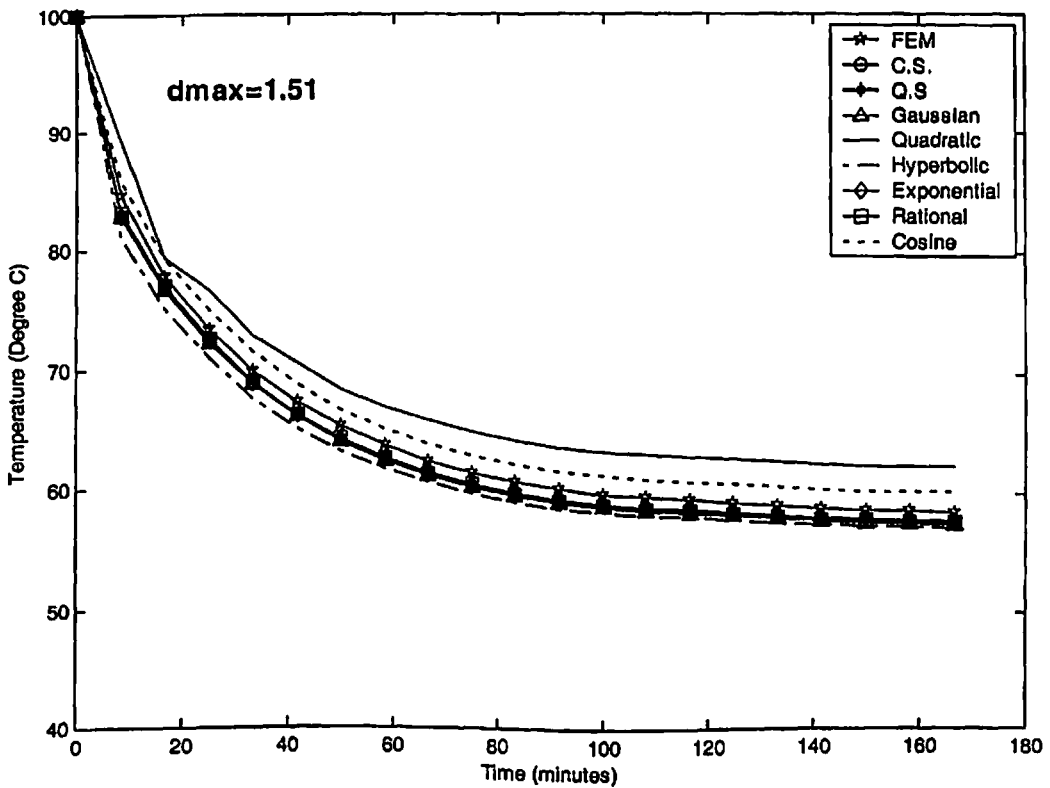
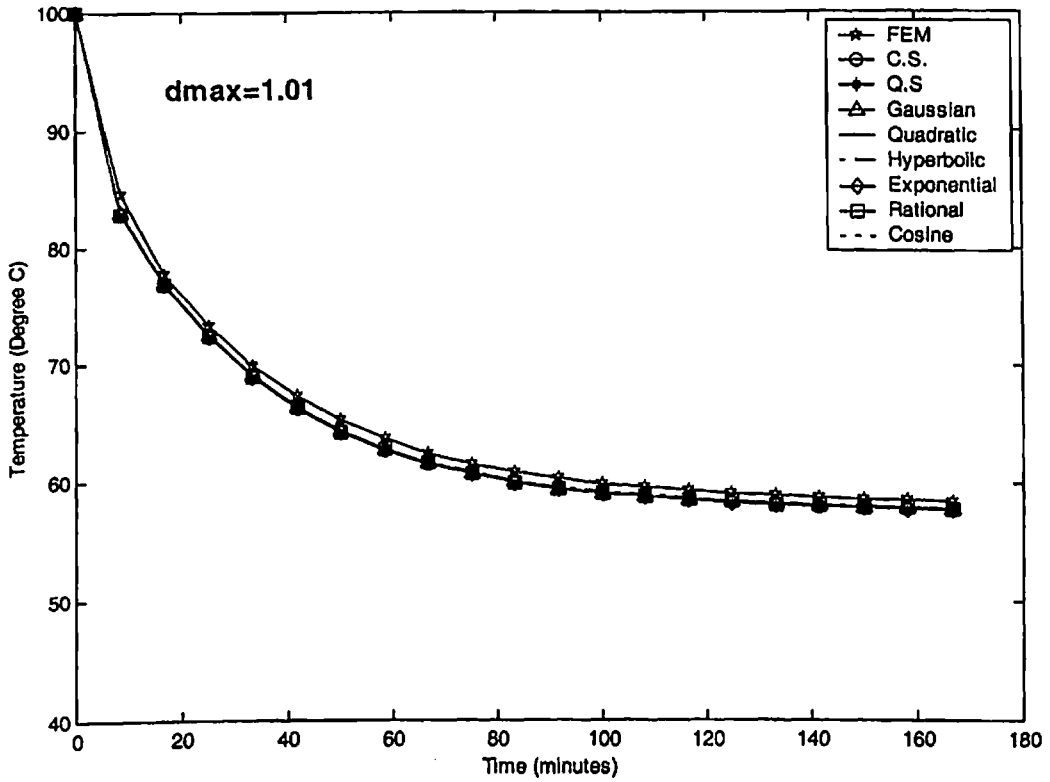


Fig. 6.6 Comparison of EFG results obtained using 125 nodes with FEM at the location ($x = 0.5$ m, $y = 0.5$ m & $z = 1$ m) of the 3-D model shown in Fig. 6.1

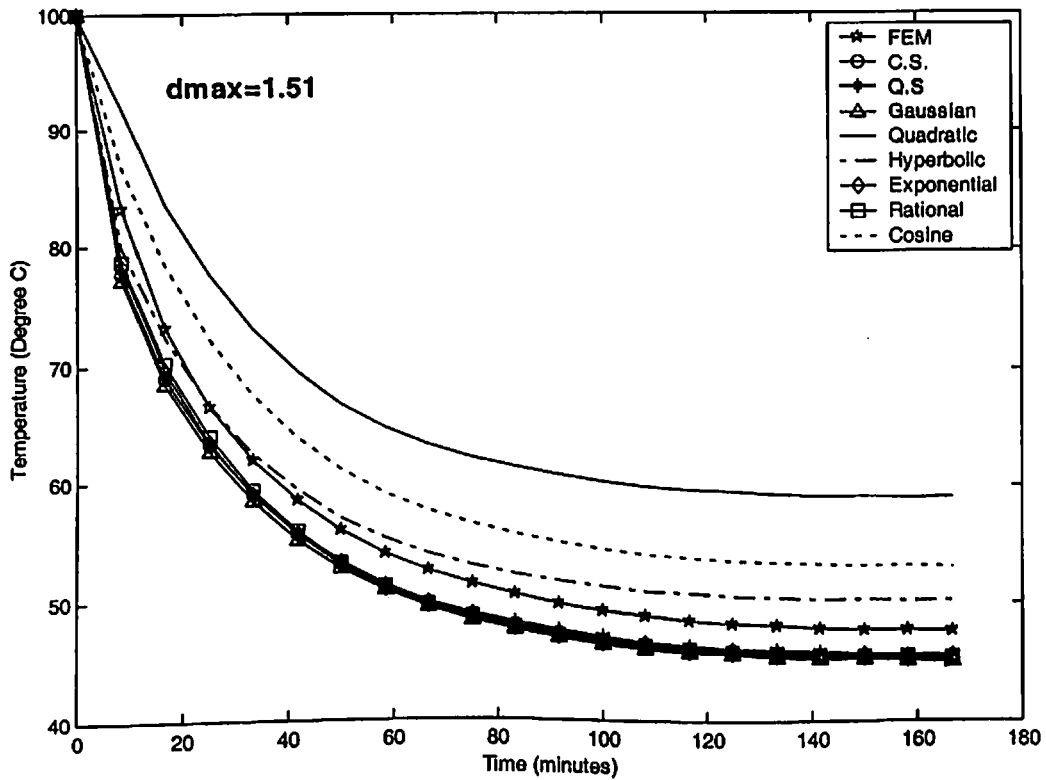
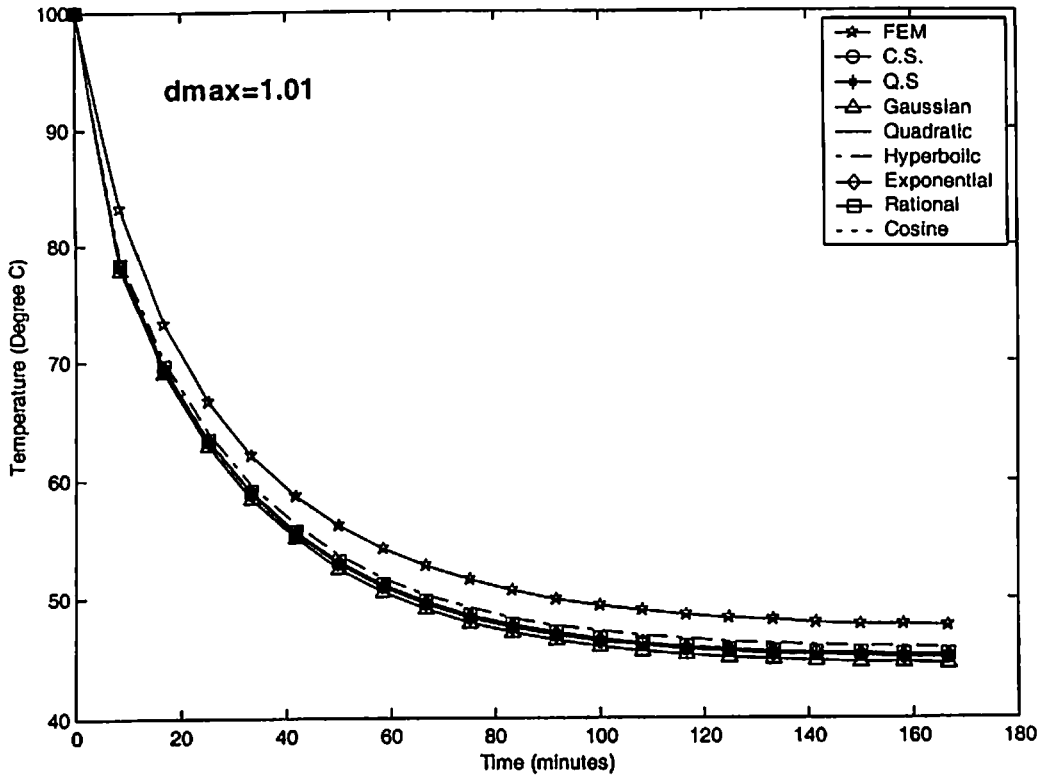


Fig. 6.7 Comparison of EFG results obtained using 27 nodes with FEM at the location ($x = 1\text{ m}$, $y = 1\text{ m}$ & $z = 1\text{ m}$) of the 3-D model shown in Fig. 6.1

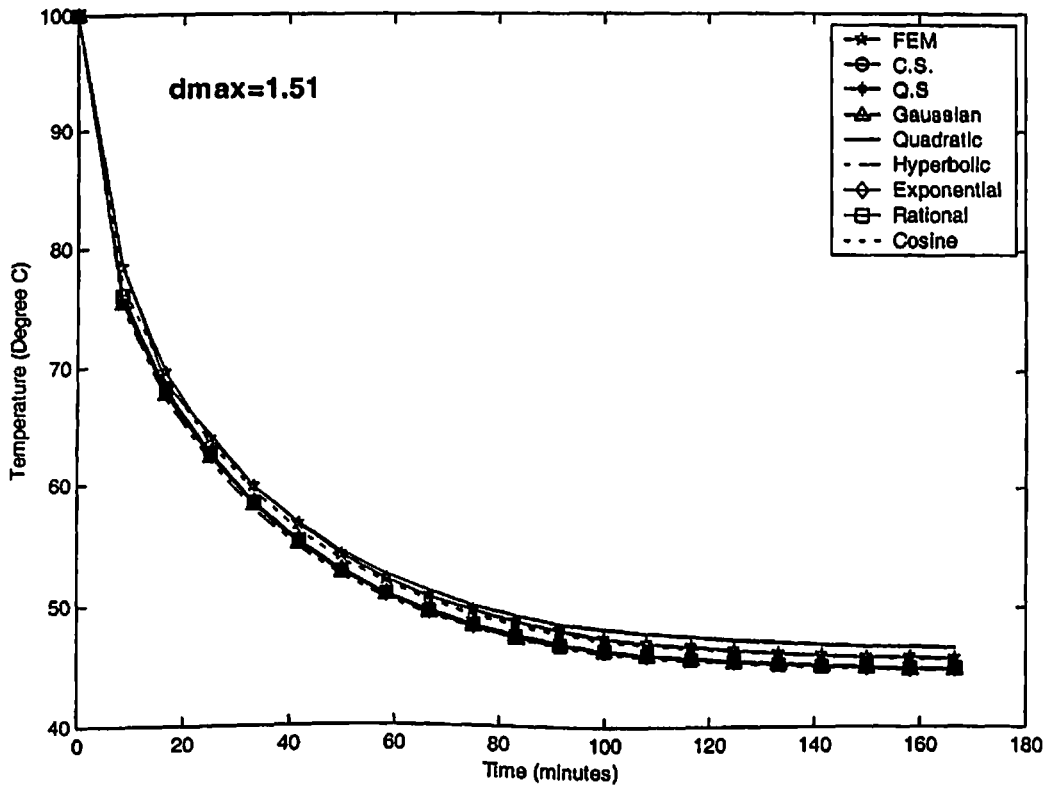
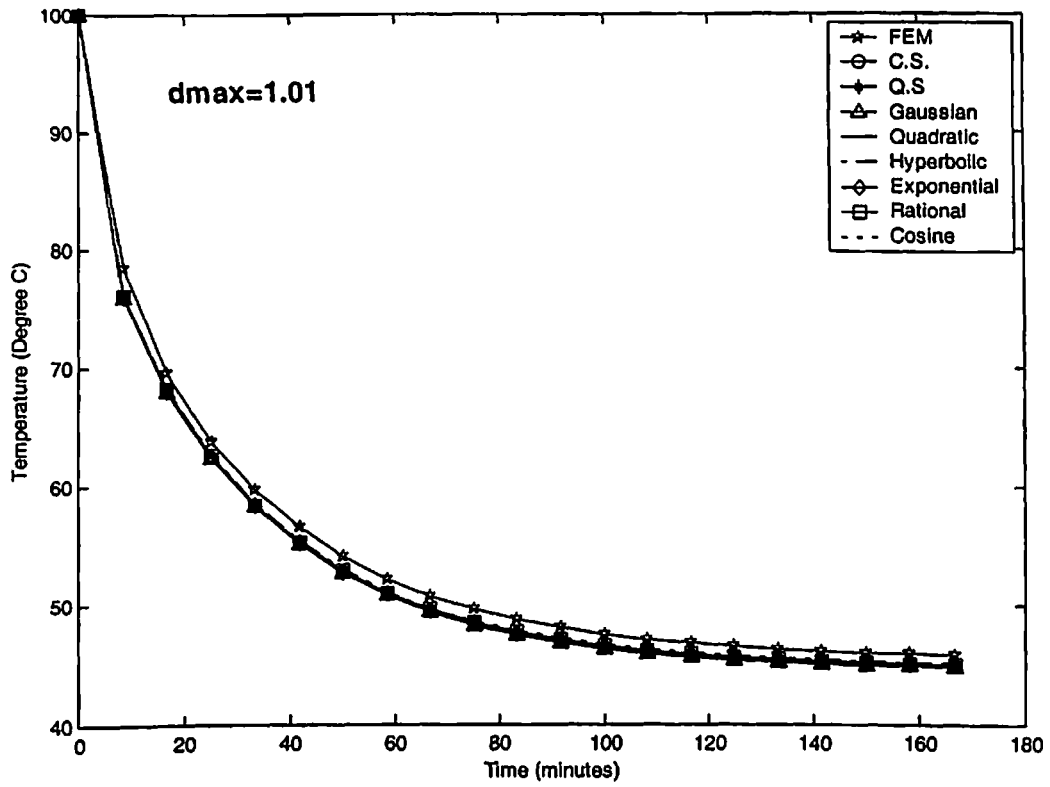


Fig. 6.8 Comparison of EFG results obtained using 125 nodes with FEM at the location ($x = 1\text{ m}$, $y = 1\text{ m}$ & $z = 1\text{ m}$) of the 3-D model shown in Fig. 6.1

➤ **CASE-II**

6.4 DISCRETIZATION OF THE GOVERNING EQUATION

The general form of energy equation for three-dimensional heat transfer in composite model with thermal properties independent of temperature is given as:

$$k \left(\frac{\partial^2 T}{\partial x^2} + \frac{\partial^2 T}{\partial y^2} + \frac{\partial^2 T}{\partial z^2} \right) + \dot{Q} = \rho c \dot{T} \quad (6.12a)$$

The initial conditions are:

$$\text{at the time } t = 0 \quad T = T_{in} \quad \text{on } V \quad (6.12b)$$

The essential boundary conditions are:

$$\text{at the surface of material 1 } y = W \text{ or } S_{1F} \quad T = T_{1F} \quad (6.12c)$$

$$\text{at the surface of material 2 } y = W \text{ or } S_{2F} \quad T = T_{2F} \quad (6.12d)$$

The natural boundary conditions are:

$$\text{at the surface of material 2, } x = 0 \text{ or } S_{2L} \quad k \frac{\partial T}{\partial x} = h(T - T_\infty) \quad (6.12e)$$

$$\text{at the surface of material 1, } x = \frac{(L_3 - L_1)}{2} \text{ or } S_{1L} \quad -k \frac{\partial T}{\partial x} = h(T - T_\infty) \quad (6.12f)$$

$$\text{at the surface of material 1, } x = \left(\frac{(L_3 - L_1)}{2} + L_1 \right) \text{ or } S_{1R} \quad k \frac{\partial T}{\partial x} = h(T - T_\infty) \quad (6.12g)$$

$$\text{at the surface of material 2 } x = L_3 \text{ or } S_{2R} \quad -k \frac{\partial T}{\partial x} = h(T - T_\infty) \quad (6.12h)$$

$$\text{at the surface of material 2, } z = 0 \text{ or } S_{2B} \quad k \frac{\partial T}{\partial z} = h(T - T_\infty) \quad (6.12i)$$

$$\text{at the surface of material 1, } z = \frac{(H_3 - H_1)}{2} \text{ or } S_{1B} \quad -k \frac{\partial T}{\partial z} = h(T - T_\infty) \quad (6.12j)$$

$$\text{at the surface of material 1, } z = \left(\frac{(H_3 - H_1)}{2} + H_1 \right) \text{ or } S_{1T} \quad k \frac{\partial T}{\partial z} = h(T - T_\infty) \quad (6.12k)$$

$$\text{at the surface of material 2 } z = H_3 \text{ or } S_{2T} \quad -k \frac{\partial T}{\partial z} = h(T - T_\infty) \quad (6.12l)$$

$$\text{at the surface of material 1 } y = 0 \text{ or } S_{1BS} \quad k \frac{\partial T}{\partial y} = h(T - T_\infty) \quad (6.12m)$$

$$\text{at the surface of material 2 } y = 0 \text{ or } S_{2BS} \quad k \frac{\partial T}{\partial y} = h(T - T_\infty) \quad (6.12n)$$

Compatibility requirements at the interface of two materials are given as:

$$-k \left(\frac{\partial T}{\partial x} \right)_{x=\left(\frac{L_1-L_2}{2}\right)} \Big|_{\text{mat 2}} = -k \left(\frac{\partial T}{\partial x} \right)_{x=\left(\frac{L_2-L_1}{2}\right)} \Big|_{\text{mat 1}} \quad (6.12p)$$

$$-k \left(\frac{\partial T}{\partial x} \right)_{x=\left(\frac{L_2-L_1+L_1}{2}\right)} \Big|_{\text{mat 2}} = -k \left(\frac{\partial T}{\partial x} \right)_{x=\left(\frac{L_2-L_2+L_2}{2}\right)} \Big|_{\text{mat 1}} \quad (6.12q)$$

$$-k \left(\frac{\partial T}{\partial z} \right)_{x=\left(\frac{H_1-H_2}{2}\right)} \Big|_{\text{mat 2}} = -k \left(\frac{\partial T}{\partial z} \right)_{x=\left(\frac{H_2-H_1}{2}\right)} \Big|_{\text{mat 1}} \quad (6.12r)$$

$$-k \left(\frac{\partial T}{\partial z} \right)_{x=\left(\frac{H_2-H_1+L_1}{2}\right)} \Big|_{\text{mat 2}} = -k \left(\frac{\partial T}{\partial z} \right)_{x=\left(\frac{H_2-H_2+L_2}{2}\right)} \Big|_{\text{mat 1}} \quad (6.12s)$$

The weighted integral form of Eq. (6.12a) is obtained as:

$$\int_V w \left[k \left(\frac{\partial^2 T}{\partial x^2} + \frac{\partial^2 T}{\partial y^2} + \frac{\partial^2 T}{\partial z^2} \right) + \dot{Q} - \rho c \dot{T} \right] dV = 0 \quad (6.13)$$

The weak form of the Eq. (6.13) will be

$$\begin{aligned} & \int_V w \left\{ k \left[\frac{\partial w}{\partial x} \frac{\partial T}{\partial x} + \frac{\partial w}{\partial y} \frac{\partial T}{\partial y} + \frac{\partial w}{\partial z} \frac{\partial T}{\partial z} \right] \right\} dV - \int_V w \dot{Q} dV + \int_V w \rho c \dot{T} dV - \\ & \int_S \left[w k \frac{\partial T}{\partial x} \cos(\bar{n}, x) + w k \frac{\partial T}{\partial y} \cos(\bar{n}, y) + w k \frac{\partial T}{\partial z} \cos(\bar{n}, z) \right] dS = 0 \end{aligned} \quad (6.14)$$

Introducing natural boundary conditions in weak form, the Eq. (6.14) changes to

$$\begin{aligned}
& \int_{V_1} \left[k_1 \left(\frac{\partial w}{\partial x} \frac{\partial T}{\partial x} + \frac{\partial w}{\partial y} \frac{\partial T}{\partial y} + \frac{\partial w}{\partial z} \frac{\partial T}{\partial z} \right) \right] dV + \int_{V_2} \left[k_2 \left(\frac{\partial w}{\partial x} \frac{\partial T}{\partial x} + \frac{\partial w}{\partial y} \frac{\partial T}{\partial y} + \frac{\partial w}{\partial z} \frac{\partial T}{\partial z} \right) \right] dV - \\
& \int_{V_1} w \dot{Q}_1 dV - \int_{V_2} w \dot{Q}_2 dV + \int_{V_1} w \rho_1 c_1 \dot{T} dV + \int_{V_2} w \rho_2 c_2 \dot{T} dV + \int_{S_{2L}} w h (T - T_\infty) dS + \\
& \int_{S_{1L}} w h (T - T_\infty) dS + \int_{S_{1R}} w h (T - T_\infty) dS + \int_{S_{2R}} w h (T - T_\infty) dS + \int_{S_{2B}} w h (T - T_\infty) dS + \\
& \int_{S_{1B}} w h (T - T_\infty) dS + \int_{S_{1T}} w h (T - T_\infty) dS + \int_{S_{2T}} w h (T - T_\infty) dS + \int_{S_{1BS}} w h (T - T_\infty) dS + \\
& \int_{S_{2BS}} w h (T - T_\infty) dS = 0
\end{aligned} \tag{6.15}$$

The functional $I(T)$ can be written as:

$$\begin{aligned}
I(T) = & \int_{V_1} \frac{1}{2} k_1 \left[\left(\frac{\partial T}{\partial x} \right)^2 + \left(\frac{\partial T}{\partial y} \right)^2 + \left(\frac{\partial T}{\partial z} \right)^2 \right] dV + \int_{V_2} \frac{1}{2} k_2 \left[\left(\frac{\partial T}{\partial x} \right)^2 + \left(\frac{\partial T}{\partial y} \right)^2 + \left(\frac{\partial T}{\partial z} \right)^2 \right] dV + \\
& \int_{V_1} \rho_1 c_1 T \dot{T} dV + \int_{V_2} \rho_2 c_2 T \dot{T} dV - \int_{V_1} T \dot{Q}_1 dV - \int_{V_2} T \dot{Q}_2 dV + \int_{S_{2L}} \frac{hT^2}{2} dS + \int_{S_{1L}} \frac{hT^2}{2} dS + \\
& \int_{S_{1R}} \frac{hT^2}{2} dS + \int_{S_{2R}} \frac{hT^2}{2} dS + \int_{S_{2B}} \frac{hT^2}{2} dS + \int_{S_{1B}} \frac{hT^2}{2} dS + \int_{S_{1T}} \frac{hT^2}{2} dS + \int_{S_{2T}} \frac{hT^2}{2} dS + \\
& \int_{S_{1BS}} \frac{hT^2}{2} dS + \int_{S_{2BS}} \frac{hT^2}{2} dS - \int_{S_{2L}} hTT_\infty dS - \int_{S_{1L}} hTT_\infty dS - \int_{S_{1R}} hTT_\infty dS - \int_{S_{2R}} hTT_\infty dS - \\
& \int_{S_{2B}} hTT_\infty dS - \int_{S_{1B}} hTT_\infty dS - \int_{S_{1T}} hTT_\infty dS - \int_{S_{2T}} hTT_\infty dS - \int_{S_{1BS}} hTT_\infty dS - \int_{S_{2BS}} hTT_\infty dS
\end{aligned} \tag{6.16}$$

Enforce essential boundary conditions, the functional $I^*(T)$ is obtained as:

$$\begin{aligned}
I^*(T) = & \int_{V_1} \frac{1}{2} k_1 \left[\left(\frac{\partial T}{\partial x} \right)^2 + \left(\frac{\partial T}{\partial y} \right)^2 + \left(\frac{\partial T}{\partial z} \right)^2 \right] dV + \int_{V_1} \frac{1}{2} k_2 \left[\left(\frac{\partial T}{\partial x} \right)^2 + \left(\frac{\partial T}{\partial y} \right)^2 + \left(\frac{\partial T}{\partial z} \right)^2 \right] dV + \\
& \int_{V_1} \rho_1 c_1 T \dot{T} dV + \int_{V_1} \rho_2 c_2 T \dot{T} dV - \int_{V_1} T \dot{Q}_1 dV - \int_{V_1} T \dot{Q}_2 dV + \int_{S_{2L}} \frac{hT^2}{2} dS + \int_{S_{1L}} \frac{hT^2}{2} dS + \\
& \int_{S_{1R}} \frac{hT^2}{2} dS + \int_{S_{2R}} \frac{hT^2}{2} dS + \int_{S_{2B}} \frac{hT^2}{2} dS + \int_{S_{1B}} \frac{hT^2}{2} dS + \int_{S_{1T}} \frac{hT^2}{2} dS + \int_{S_{2T}} \frac{hT^2}{2} dS + \\
& \int_{S_{1BS}} \frac{hT^2}{2} dS + \int_{S_{2BS}} \frac{hT^2}{2} dS - \int_{S_{2L}} hT T_\infty dS - \int_{S_{1L}} hT T_\infty dS - \int_{S_{1R}} hT T_\infty dS - \int_{S_{2R}} hT T_\infty dS - \\
& \int_{S_{2B}} hT T_\infty dS - \int_{S_{1B}} hT T_\infty dS - \int_{S_{1T}} hT T_\infty dS - \int_{S_{2T}} hT T_\infty dS - \int_{S_{1BS}} hT T_\infty dS - \int_{S_{2BS}} hT T_\infty dS + \\
& \int_{S_{1F}} \lambda (T - T_{S_{1F}}) dS + \int_{S_{2F}} \lambda' (T - T_{S_{2F}}) dS
\end{aligned} \tag{6.17}$$

Using variational method, Eq. (6.17) can be written as:

$$\begin{aligned}
\delta I^*(T) = & \int_{V_1} k_1 \left[\frac{\partial T}{\partial x} \delta \frac{\partial T}{\partial x} + \frac{\partial T}{\partial y} \delta \frac{\partial T}{\partial y} + \frac{\partial T}{\partial z} \delta \frac{\partial T}{\partial z} \right] dV + \int_{V_1} \rho_1 c_1 \dot{T} \delta T dV + \\
& \int_{V_1} k_2 \left[\frac{\partial T}{\partial x} \delta \frac{\partial T}{\partial x} + \frac{\partial T}{\partial y} \delta \frac{\partial T}{\partial y} + \frac{\partial T}{\partial z} \delta \frac{\partial T}{\partial z} \right] dV + \int_{V_1} \rho_2 c_2 \dot{T} \delta T dV - \int_{V_1} \dot{Q}_1 \delta T dV - \\
& \int_{V_1} \dot{Q}_2 \delta T dV + \int_{S_{2L}} hT \delta T dS + \int_{S_{1L}} hT \delta T dS + \int_{S_{1R}} hT \delta T dS + \int_{S_{2R}} hT \delta T dS + \\
& \int_{S_{2B}} hT \delta T dS + \int_{S_{1B}} hT \delta T dS + \int_{S_{1T}} hT \delta T dS + \int_{S_{2T}} hT \delta T dS + \int_{S_{1BS}} hT \delta T dS + \\
& \int_{S_{2BS}} hT \delta T dS - \int_{S_{2L}} hT_\infty \delta T dS - \int_{S_{1L}} hT_\infty \delta T dS - \int_{S_{1R}} hT_\infty \delta T dS - \int_{S_{2R}} hT_\infty \delta T dS - \\
& \int_{S_{2B}} hT_\infty \delta T dS - \int_{S_{1B}} hT_\infty \delta T dS - \int_{S_{1T}} hT_\infty \delta T dS - \int_{S_{2T}} hT_\infty \delta T dS - \int_{S_{1BS}} hT_\infty \delta T dS - \\
& \int_{S_{2BS}} hT_\infty \delta T dS + \int_{S_{1F}} \lambda \delta T dS + \int_{S_{1F}} \delta \lambda (T - T_{S_{1F}}) dS + \int_{S_{2F}} \lambda' \delta T dS + \int_{S_{2F}} \delta \lambda' (T - T_{S_{2F}}) dS
\end{aligned} \tag{6.18}$$

Since δT , $\delta \lambda$ and $\delta \lambda'$ are arbitrary in preceding equation, the following relations are obtained

using Eqs. (3.25) and (6.18)

$$[\mathbf{K}]\{\mathbf{T}\} + [\mathbf{C}]\{\dot{\mathbf{T}}\} + [\mathbf{G}]\{\lambda\} + [\mathbf{G}']\{\lambda'\} = \{\mathbf{f}\} \tag{6.19a}$$

$$[\mathbf{G}^T]\{\mathbf{T}\} = \{\mathbf{q}\} \tag{6.19b}$$

$$[\mathbf{G}'^T]\{\mathbf{T}\} = \{\mathbf{q}'\} \tag{6.19c}$$

where

$$\begin{aligned}
 K_{IJ} = & \int_{V_1} \begin{bmatrix} \Phi_{I,x} \\ \Phi_{I,y} \\ \Phi_{I,z} \end{bmatrix}^T \begin{bmatrix} k_1 & 0 & 0 \\ 0 & k_1 & 0 \\ 0 & 0 & k_1 \end{bmatrix} \begin{bmatrix} \Phi_{I,x} \\ \Phi_{I,y} \\ \Phi_{I,z} \end{bmatrix} dV + \int_{S_{2L}} h \Phi_I^T \Phi_J dS + \\
 & \int_{V_2} \begin{bmatrix} \Phi_{I,x} \\ \Phi_{I,y} \\ \Phi_{I,z} \end{bmatrix}^T \begin{bmatrix} k_2 & 0 & 0 \\ 0 & k_2 & 0 \\ 0 & 0 & k_2 \end{bmatrix} \begin{bmatrix} \Phi_{I,x} \\ \Phi_{I,y} \\ \Phi_{I,z} \end{bmatrix} dV + \int_{S_{1L}} h \Phi_I^T \Phi_J dS + \\
 & \int_{S_{1R}} h \Phi_I^T \Phi_J dS + \int_{S_{2R}} h \Phi_I^T \Phi_J dS + \int_{S_{2B}} h \Phi_I^T \Phi_J dS + \int_{S_{1B}} h \Phi_I^T \Phi_J dS + \\
 & \int_{S_{1T}} h \Phi_I^T \Phi_J dS + \int_{S_{2T}} h \Phi_I^T \Phi_J dS + \int_{S_{1BS}} h \Phi_I^T \Phi_J dS + \int_{S_{2BS}} h \Phi_I^T \Phi_J dS
 \end{aligned} \tag{6.20a}$$

$$C_{IJ} = \int_{V_1} \rho_1 c_1 \Phi_I^T \Phi_J dV + \int_{V_2} \rho_2 c_2 \Phi_I^T \Phi_J dV \tag{6.20b}$$

$$\begin{aligned}
 f_I = & \int_{V_1} \dot{Q}_1 \Phi_I dV + \int_{V_2} \dot{Q}_2 \Phi_I dV + \int_{S_{2L}} h T_\infty \Phi_I dS + \int_{S_{1L}} h T_\infty \Phi_I dS + \\
 & \int_{S_{1R}} h T_\infty \Phi_I dS + \int_{S_{2R}} h T_\infty \Phi_I dS + \int_{S_{2B}} h T_\infty \Phi_I dS + \int_{S_{1B}} h T_\infty \Phi_I dS + \\
 & \int_{S_{1T}} h T_\infty \Phi_I dS + \int_{S_{2T}} h T_\infty \Phi_I dS + \int_{S_{1BS}} h T_\infty \Phi_I dS + \int_{S_{2BS}} h T_\infty \Phi_I dS
 \end{aligned} \tag{6.20c}$$

$$G_{IK} = \int_{S_{1F}} \Phi_I N_K dS \tag{6.20d}$$

$$G'_{IK} = \int_{S_{2F}} \Phi_I N_K dS \tag{6.20e}$$

$$q_K = \int_{S_{1F}} T_{S_{1F}} N_K dS \tag{6.20f}$$

$$q'_K = \int_{S_{2F}} T_{S_{2F}} N_K dS \tag{6.20g}$$

Using Crank-Nicolson technique for time approximation, the Eq. (6.19) can be written as:

$$\begin{bmatrix} \mathbf{K}' + \mathbf{C} & \mathbf{G} & \mathbf{G}' \\ \mathbf{G}^T & 0 & 0 \\ \mathbf{G}'^T & 0 & 0 \end{bmatrix} \begin{bmatrix} \mathbf{T}_N \\ \lambda \\ \lambda' \end{bmatrix} = \begin{bmatrix} \mathbf{R}_N \\ \mathbf{q} \\ \mathbf{q}' \end{bmatrix} \quad (6.21)$$

where

$$\mathbf{R}_N = ([\mathbf{C}] - (1 - \alpha) \Delta t [\mathbf{K}]) \{\mathbf{T}\}_{N-1} + \alpha \Delta t \{\mathbf{f}\}_N + (1 - \alpha) \Delta t \{\mathbf{f}\}_{N-1} \quad (6.22a)$$

$$\mathbf{K}' = \alpha \Delta t [\mathbf{K}] \quad (6.22b)$$

6.5 NUMERICAL RESULTS AND DISCUSSION

The different parameters used for steady-state and transient analysis of three-dimensional composite model shown in Fig. 6.9 are tabulated in Table 6.23. The EFG results are obtained using different weight functions for two sets of nodes and the FEM results are obtained using 8 node brick element (SOLID 70, ANSYS 6.0) for same sets of nodes. A comparative study is carried out to evaluate the performance of different EFG weight functions.

6.5.1 Steady-state analysis

The results (i.e. temperature values) presented in Table 6.24 are obtained using different EFG weight functions for two values of scaling parameter (i.e. $d_{\max} = 1.01$ & $d_{\max} = 1.51$) at the location ($x = 0.2\text{ m}$, $y = 0\text{ m}$ & $z = 0.2\text{ m}$) and it shows a comparison of temperature values obtained by EFG method using different weight functions with FEM for 96 nodes. Table 6.25 shows a comparison of temperature values obtained by EFG method using different functions for two values of scaling parameter with FEM at the same location i.e. ($x = 0.2\text{ m}$, $y = 0\text{ m}$ & $z = 0.2\text{ m}$) for 144 nodes. A comparison of temperature values obtained using different EFG weight functions with FEM for 96 and 144 nodes, is shown in Table 6.26 and Table 6.27 respectively at the location ($x = 0.4\text{ m}$, $y = 0\text{ m}$ & $z = 0.3\text{ m}$). Similar type of comparisons of temperature values are shown in Table 6.28 for 96 nodes at the location ($x = 0.5\text{ m}$, $y = 0\text{ m}$ & $z = 0.1\text{ m}$), in Table 6.29 for 144 nodes at the location

($x = 0.5\text{ m}$, $y = 0\text{ m}$ & $z = 0.1\text{ m}$), in Table 6.30 for 96 nodes at the location ($x = 0.6\text{ m}$, $y = 0\text{ m}$ & $z = 0.3\text{ m}$) and in Table 6.31 for 144 nodes at the location ($x = 0.6\text{ m}$, $y = 0\text{ m}$ & $z = 0.3\text{ m}$). From the results presented in Table 6.24 to Table 6.31, it is observed that EFG results obtained using different weight functions are almost similar for $d_{\max} = 1.01$. However for $d_{\max} = 1.51$, only cubicspline, quarticspline, Gaussian, exponential and rational weight functions give acceptable results. It is also observed that EFG results obtained using different weight functions are in good agreement with those obtained by FEM. Moreover with the increase in number of nodes EFG results starts converging.

The effect of scaling parameter (d_{\max}) on EFG results obtained using different weight functions is presented in Table 6.32 for 96 nodes and Table 6.33 for 144 nodes respectively at the location ($x = 0.2\text{ m}$, $y = 0\text{ m}$ & $z = 0.2\text{ m}$). Similar effect of scaling parameter on EFG results is shown in Table 6.34 for 96 nodes and Table 6.35 for 144 nodes at the location ($x = 0.5\text{ m}$, $y = 0\text{ m}$ & $z = 0.1\text{ m}$). Fig. 6.10 shows the effect of scaling parameter on EFG results obtained using 96 and 144 nodes at the location ($x = 0.4\text{ m}$, $y = 0\text{ m}$ & $z = 0.3\text{ m}$). Similar effect of scaling parameter on EFG results is observed in Fig. 6.11 at the location ($x = 0.6\text{ m}$, $y = 0\text{ m}$ & $z = 0.3\text{ m}$). From tables and figures, it is clear that only cubicspline, quarticspline, Gaussian, exponential and rational weight functions give acceptable results in the range $1.0 < d_{\max} < 1.6$ whereas the results obtained using quadratic, hyperbolic and cosine weight functions are varying in abrupt manner with scaling parameter. Therefore EFG results obtained using quadratic, hyperbolic and cosine weight functions are not acceptable in the range $1.0 < d_{\max} < 1.6$. It is also observed that there is minimum variation in EFG results with scaling parameter for exponential weight function.

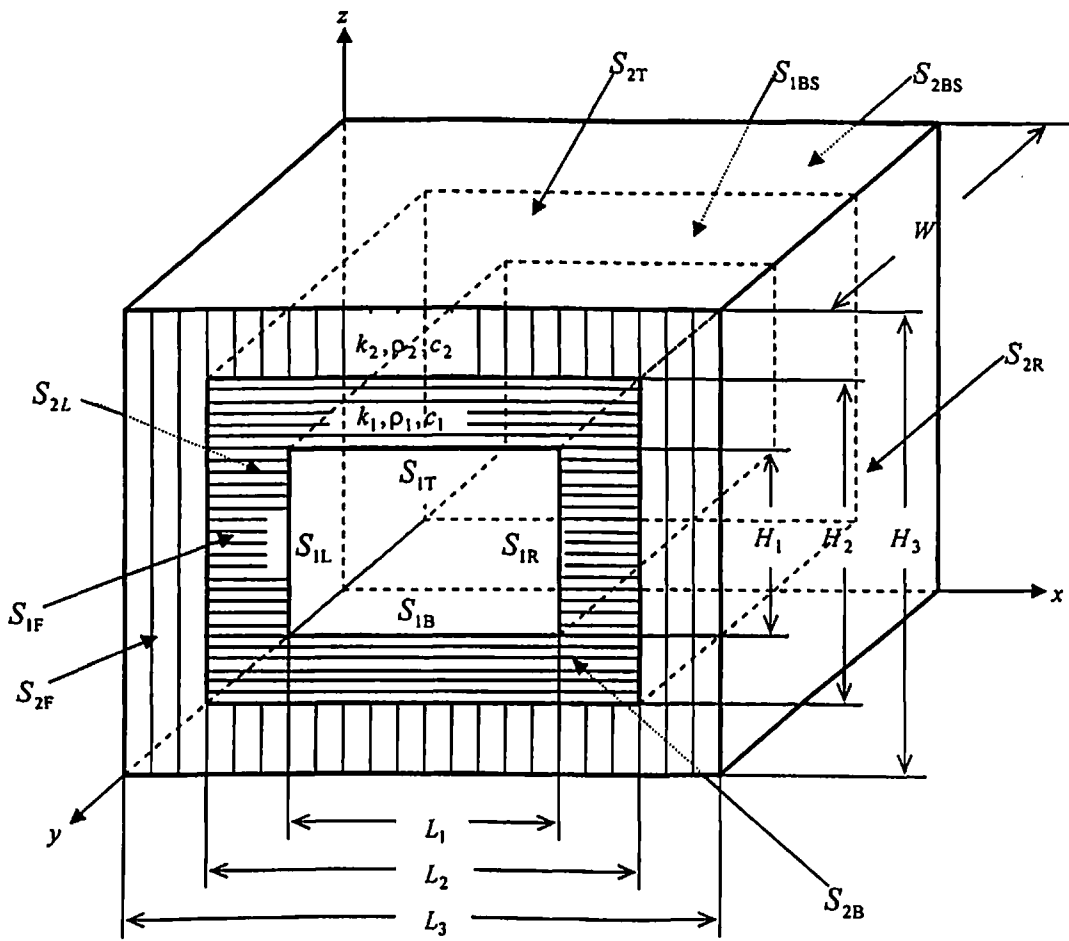


Fig. 6.9 Three-dimensional model of composites

Table 6.23 Data for the 3-D model shown in Fig 6.9

Parameters	Value of the parameter
Length (L_1)	0.2 m
Length (L_2)	0.4 m
Length (L_3)	0.6 m
Depth (W)	0.3 m
Height (H_1)	0.2 m
Height (H_2)	0.4 m
Height (H_3)	0.6 m
Thermal conductivity of material 1 (k_1)	400 W/m-K
Thermal conductivity of material 1 (k_2)	100 W/m-K
Specific heat of material 1 (c_1)	400 kJ/kg-K
Specific heat of material 2 (c_2)	300 kJ/kg-K
Density of material 1 (ρ_1)	10000 kg/m ³
Density of material 2 (ρ_2)	8000 kg/m ³
Rate of internal heat generation (\dot{Q})	0 W/m ³
Heat transfer coefficient (h)	200 W/m ² -K
Initial temperature (T_{in})	0°C
Time step size (Δt)	100 sec
Surrounding fluid temperature (T_∞)	20 °C
Temperature ($T_{S_{1F}}$ & $T_{S_{2F}}$) at surfaces S_{1F} & S_{2F}	100 °C
Convection at all other surfaces	$-k \frac{\partial T}{\partial n'} = h(T - T_\infty)$ where $n' = x, y, z$

Table 6.24 Comparison of EFG results obtained using 96 nodes with FEM results at the location ($x = 0.2$ m, $y = 0$ m & $z = 0.2$ m) of the 3-D model shown in Fig 6.9

Weight function	EFG				FEM
	$d_{\max} = 1.01$		$d_{\max} = 1.51$		
	T (°C)	% diff with FEM	T (°C)	% diff with FEM	T (°C)
C. S.	69.6814	3.0306	70.0358	2.5375	71.8592
Q. S.	69.8559	2.7878	70.0201	2.5593	
Gaussian	68.7470	4.3310	69.8325	2.8204	
Quadratic	70.0992	2.4492	66.2145	7.8552	
Hyperbolic	71.2336	0.8706	69.5592	3.2007	
Exponential	69.9146	2.7061	70.1085	2.4363	
Rational	70.2198	2.2814	70.3975	2.0341	
Cosine	70.0872	2.4659	68.8278	4.2185	

Table 6.25 Comparison of EFG results obtained using 144 nodes with FEM results at the location ($x = 0.2$ m, $y = 0$ m & $z = 0.2$ m) of the 3-D model shown in Fig 6.9

Weight function	EFG				FEM
	$d_{\max} = 1.01$		$d_{\max} = 1.51$		
	T (°C)	% diff with FEM	T (°C)	% diff with FEM	T (°C)
C. S.	69.7622	1.0388	69.8073	0.9748	70.4945
Q. S.	69.8002	0.9849	69.7664	1.0328	
Gaussian	69.5263	1.3734	69.7414	1.0683	
Quadratic	69.8810	0.8703	77.2801	-9.6257	
Hyperbolic	70.4315	0.0894	68.3606	3.0270	
Exponential	69.8285	0.9448	69.8714	0.8839	
Rational	69.9945	0.7093	69.8784	0.8740	
Cosine	69.8725	0.8823	69.2338	1.7884	

Table 6.26 Comparison of EFG results obtained using 96 nodes with FEM results at the location ($x = 0.4$ m, $y = 0$ m & $z = 0.3$ m) of the 3-D model shown in Fig 6.9

Weight function	EFG				FEM
	$d_{\max} = 1.01$		$d_{\max} = 1.51$		
	T (°C)	% diff with FEM	T (°C)	% diff with FEM	T (°C)
C. S.	69.1685	3.2171	68.9394	3.5377	71.4677
Q. S.	69.3115	3.0170	68.7693	3.7757	
Gaussian	68.4647	4.2019	68.7963	3.7379	
Quadratic	69.4831	2.7769	69.3593	2.9501	
Hyperbolic	69.6856	2.4936	69.1617	3.2266	
Exponential	69.3381	2.9798	69.3720	2.9324	
Rational	69.3554	2.9556	69.3068	3.0236	
Cosine	69.4818	2.7787	68.4756	4.1866	

Table 6.27 Comparison of EFG results obtained using 144 nodes with FEM results at the location ($x = 0.4$ m, $y = 0$ m & $z = 0.3$ m) of the 3-D model shown in Fig 6.9

Weight function	EFG				FEM
	$d_{\max} = 1.01$		$d_{\max} = 1.51$		
	T (°C)	% diff with FEM	T (°C)	% diff with FEM	T (°C)
C. S.	69.6657	1.0893	69.3667	1.5138	70.4329
Q. S.	69.7128	1.0224	69.2297	1.7083	
Gaussian	69.4172	1.4421	69.2996	1.6090	
Quadratic	69.7429	0.9797	65.8763	6.4694	
Hyperbolic	69.6529	1.1074	70.8645	-0.6128	
Exponential	69.7091	1.0276	69.6925	1.0512	
Rational	69.6673	1.0870	69.6533	1.1069	
Cosine	69.7468	0.9741	69.0582	1.9518	

Table 6.28 Comparison of EFG results obtained using 96 nodes with FEM results at the location ($x = 0.5$ m, $y = 0$ m & $z = 0.1$ m) of the 3-D model shown in Fig 6.9

Weight function	EFG				FEM
	$d_{\max} = 1.01$		$d_{\max} = 1.51$		
	T (°C)	% diff with FEM	T (°C)	% diff with FEM	T (°C)
C. S.	65.2701	4.7558	66.0662	3.5941	68.5292
Q. S.	65.2947	4.7199	66.4053	3.0993	
Gaussian	65.2220	4.8260	66.0943	3.5531	
Quadratic	65.3966	4.5712	69.4435	-1.3342	
Hyperbolic	66.6384	2.7591	71.5153	-4.3574	
Exponential	65.3127	4.6936	65.5851	4.2961	
Rational	65.3881	4.5836	66.6257	2.7776	
Cosine	65.3797	4.5959	69.3822	-1.2447	

Table 6.29 Comparison of EFG results obtained using 144 nodes with FEM results at the location ($x = 0.5$ m, $y = 0$ m & $z = 0.1$ m) of the 3-D model shown in Fig 6.9

Weight function	EFG				FEM
	$d_{\max} = 1.01$		$d_{\max} = 1.51$		
	T (°C)	% diff with FEM	T (°C)	% diff with FEM	T (°C)
C. S.	65.4975	0.7185	65.8320	0.2115	65.9715
Q. S.	65.4281	0.8237	65.9509	0.0312	
Gaussian	65.7886	0.2772	66.0163	-0.0679	
Quadratic	65.3323	0.9689	63.0606	4.4124	
Hyperbolic	64.9817	1.5003	68.0141	-3.0962	
Exponential	65.4118	0.8484	65.4694	0.7611	
Rational	65.3726	0.9078	65.9133	0.0882	
Cosine	65.3352	0.9645	61.6468	6.5554	

Table 6.30 Comparison of EFG results obtained using 96 nodes with FEM results at the location ($x = 0.6$ m, $y = 0$ m & $z = 0.3$ m) of the 3-D model shown in Fig 6.9

Weight function	EFG				FEM
	$d_{max} = 1.01$		$d_{max} = 1.51$		
	T (°C)	% diff with FEM	T (°C)	% diff with FEM	T (°C)
C. S.	57.2931	6.1191	56.8968	6.7684	61.0274
Q. S.	57.1835	6.2986	56.9359	6.7044	
Gaussian	58.0514	4.8765	56.9463	6.6873	
Quadratic	57.0867	6.4573	54.1032	11.3461	
Hyperbolic	56.8980	6.7665	56.7676	6.9801	
Exponential	57.1761	6.3108	57.3276	6.0625	
Rational	57.0582	6.5040	57.5125	5.7595	
Cosine	57.0825	6.4641	53.5871	12.1917	

Table 6.31 Comparison of EFG results obtained using 144 nodes with FEM results at the location ($x = 0.6$ m, $y = 0$ m & $z = 0.3$ m) of the 3-D model shown in Fig 6.9

Weight function	EFG				FEM
	$d_{max} = 1.01$		$d_{max} = 1.51$		
	T (°C)	% diff with FEM	T (°C)	% diff with FEM	T (°C)
C. S.	59.3372	2.1921	59.4493	2.0073	60.6671
Q. S.	59.3395	2.1883	59.5585	1.8273	
Gaussian	59.3744	2.1308	59.3493	2.1722	
Quadratic	59.3283	2.2068	60.5436	0.2036	
Hyperbolic	58.9241	2.8731	59.4515	2.0037	
Exponential	59.3352	2.1954	59.5671	1.8132	
Rational	59.3106	2.2360	60.1109	0.9168	
Cosine	59.3328	2.1994	60.5700	0.1601	

Table 6.32 Effect of scaling parameter on EFG results obtained using 96 nodes at the location ($x = 0.2 \text{ m}$, $y = 0 \text{ m}$ & $z = 0.2 \text{ m}$) of the 3-D model shown in Fig 6.9

Scaling Parameter	Temperature ($^{\circ} \text{C}$)							
	C. S.	Q. S	Gaussian	Quadratic	Hyperbolic	Exponential	Rational	Cosine
1.01	69.6814	69.8559	68.7470	70.0992	71.2336	69.9146	70.2198	70.0872
1.11	69.8749	69.9921	68.8647	69.7757	71.4085	69.8989	70.2053	69.7568
1.21	69.9938	70.0532	69.0979	71.2776	71.4398	69.9467	70.2717	70.8908
1.31	70.0390	70.0454	69.3489	72.0136	71.4634	69.9885	70.3435	71.5779
1.41	70.0448	70.0531	69.5790	75.1559	68.8323	70.0702	70.3739	73.6472
1.51	70.0358	70.0201	69.8325	66.2145	69.5592	70.1085	70.3975	68.8278
1.61	70.0101	69.9105	70.0832	64.8373	70.3148	70.1450	70.4106	64.3830
1.71	69.9574	69.7506	70.3014	84.8320	51.9305	70.1061	69.6094	84.8667
1.81	69.8489	69.5147	70.5115	90.4010	49.7907	70.1183	69.3933	88.7365
1.91	69.6746	69.2008	70.6956	85.8398	47.0927	70.1250	69.1041	85.9372
2.01	69.4572	68.9415	70.9348	200.0383	-251.0259	70.2386	69.2368	179.9973
2.11	69.2840	69.1168	71.1634	54.9363	-46.0624	70.3317	69.5501	68.3182
2.21	69.2761	70.1341	71.3831	45.7752	-49.8714	70.3384	69.0438	49.4954
2.31	69.5819	72.2938	71.6377	27.6879	-52.0982	70.3370	68.3591	23.7556
2.41	70.4023	75.8669	72.2316	90.3990	60.2864	70.3883	71.1334	65.7887

Table 6.33 Effect of scaling parameter on EFG results obtained using 144 nodes at the location ($x = 0.2 \text{ m}$, $y = 0 \text{ m}$ & $z = 0.2 \text{ m}$) of the 3-D model shown in Fig 6.9

Scaling Parameter	Temperature ($^{\circ} \text{C}$)							
	C. S.	Q. S	Gaussian	Quadratic	Hyperbolic	Exponential	Rational	Cosine
1.01	69.7622	69.8002	69.5263	69.8810	70.4315	69.8285	69.9945	69.8725
1.11	69.8133	69.8402	69.5272	69.2691	71.1781	69.7805	69.9000	69.4062
1.21	69.8488	69.8601	69.5828	70.0406	71.5128	69.7957	69.9321	69.9690
1.31	69.8477	69.8373	69.6441	70.7989	71.8830	69.8116	69.9670	70.4416
1.41	69.8315	69.8210	69.6889	72.6063	68.1916	69.8558	69.9003	69.1976
1.51	69.8073	69.7664	69.7414	77.2801	68.3606	69.8714	69.8784	69.2338
1.61	69.7617	69.6445	69.7833	79.6075	68.6813	69.8846	69.8470	74.8385
1.71	69.6827	69.4703	69.7977	89.9595	98.6489	69.8745	69.4805	93.9422
1.81	69.5572	69.2433	69.7760	95.1976	104.0035	69.8739	69.3316	96.4449
1.91	69.3805	68.9537	69.6921	109.7309	108.5163	69.8681	69.1498	116.5362
2.01	69.1639	68.6529	69.6113	115.7373	-263.4159	70.0389	69.6027	-9.9285
2.11	68.9530	68.5170	69.4219	26.8723	-85.4597	70.1149	69.8908	5.0000
2.21	68.7924	68.6821	69.0756	-36.1904	-102.3341	70.1253	69.5818	-31.000
2.31	68.7127	69.1719	68.5567	-95.9047	-116.5132	70.1299	69.1700	-89.000
2.41	68.7614	70.0248	68.0867	-181.4461	-12.8605	70.1654	70.5231	-25.000

Table 6.34 Effect of scaling parameter on EFG results obtained using 96 nodes at the location ($x = 0.5 \text{ m}$, $y = 0 \text{ m}$ & $z = 0.1 \text{ m}$) of the 3-D model shown in Fig 6.9

Scaling Parameter	Temperature ($^{\circ} \text{C}$)							
	C. S.	Q. S	Gaussian	Quadratic	Hyperbolic	Exponential	Rational	Cosine
1.01	65.2701	65.2947	65.2220	65.3966	66.6384	65.3127	65.3881	65.3797
1.11	65.1918	65.2405	65.5338	63.7792	67.1631	65.6373	65.8368	64.0212
1.21	65.2858	65.4674	65.6081	66.3749	67.3492	65.6630	65.8743	66.1522
1.31	65.6026	65.7462	65.6758	67.2630	67.5354	65.6843	65.9174	66.8925
1.41	65.8024	65.9591	65.8897	66.7333	71.2317	65.4776	66.4089	65.3792
1.51	66.0662	66.4053	66.0943	69.4435	71.5153	65.5851	66.6257	69.3822
1.61	66.4183	66.9129	66.3601	69.4305	71.6664	65.7031	66.8425	69.6526
1.71	66.8159	67.3803	66.8256	71.4900	130.7711	66.2410	68.8733	66.7970
1.81	67.3083	67.9771	67.3176	90.6450	139.1832	66.4477	69.3915	80.6481
1.91	67.8812	68.7169	67.9129	106.4591	145.6547	66.6645	69.9561	97.3552
2.01	68.5268	69.5909	68.7957	309.6332	200.9514	67.2940	71.9022	199.4708
2.11	69.2744	70.6811	69.7938	97.6029	127.2347	67.6313	72.5475	99.1303
2.21	70.1919	72.2049	71.0345	115.5707	118.9625	67.9229	73.3246	104.3752
2.31	71.3712	74.4090	72.6151	110.3517	110.2966	68.2219	74.1727	88.2042
2.41	72.9380	77.5522	74.6972	364.0192	97.9427	68.6005	75.1589	301.0513

Table 6.35 Effect of scaling parameter on EFG results obtained using 144 nodes at the location ($x = 0.5 \text{ m}$, $y = 0 \text{ m}$ & $z = 0.1 \text{ m}$) of the 3-D model shown in Fig 6.9

Scaling Parameter	Temperature ($^{\circ} \text{C}$)							
	C. S.	Q. S	Gaussian	Quadratic	Hyperbolic	Exponential	Rational	Cosine
1.01	65.4975	65.4281	65.7886	65.3323	64.9817	65.4118	65.3726	65.3352
1.11	65.3358	65.2977	66.0157	63.2457	65.9025	65.6425	65.6599	63.6647
1.21	65.3573	65.4582	65.9827	64.9190	66.0568	65.6372	65.6537	64.9879
1.31	65.5705	65.6501	65.9315	65.4741	66.2459	65.6339	65.6462	65.3163
1.41	65.6928	65.7440	65.9897	64.1941	67.0919	65.4166	65.8207	62.7500
1.51	65.8320	65.9509	66.0163	63.0606	68.0141	65.4694	65.9133	61.6468
1.61	65.9802	66.1070	66.0686	74.7428	68.7068	65.5277	65.9951	67.2945
1.71	66.0950	66.1346	66.2590	75.9779	81.2125	65.9008	67.1506	79.4287
1.81	66.2018	66.1314	66.4340	81.7540	85.7784	66.0172	67.3286	75.7092
1.91	66.2689	66.0590	66.6520	101.9692	90.6335	66.1367	67.4975	99.3016
2.01	66.2588	65.8512	67.0619	103.8000	-17.6972	66.6484	68.5127	-200270
2.11	66.1487	65.4883	67.5020	-196.100	33.8821	66.8697	68.9848	-150.00
2.21	65.9482	65.0684	68.0334	-360.000	39.0119	67.0414	69.1034	-240.00
2.31	65.6617	64.6482	68.7079	-273.900	44.8138	67.2115	69.1808	-340.00
2.41	65.2763	64.2434	69.6594	-2403.80	-11.4020	67.4767	69.8681	-290.00

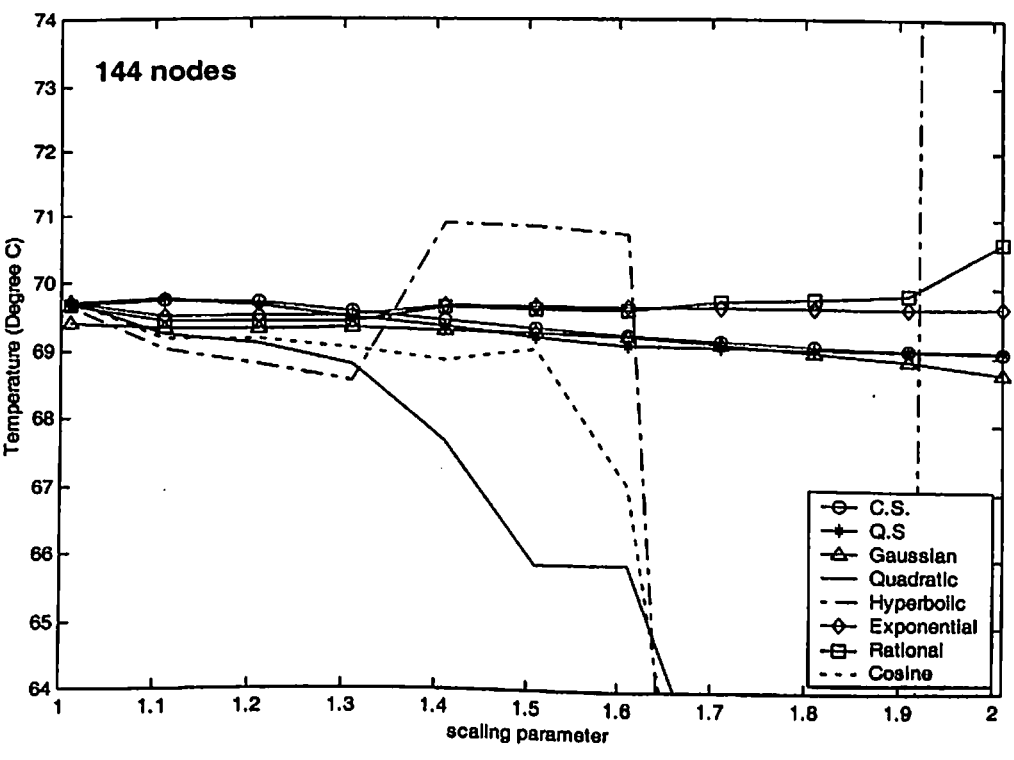
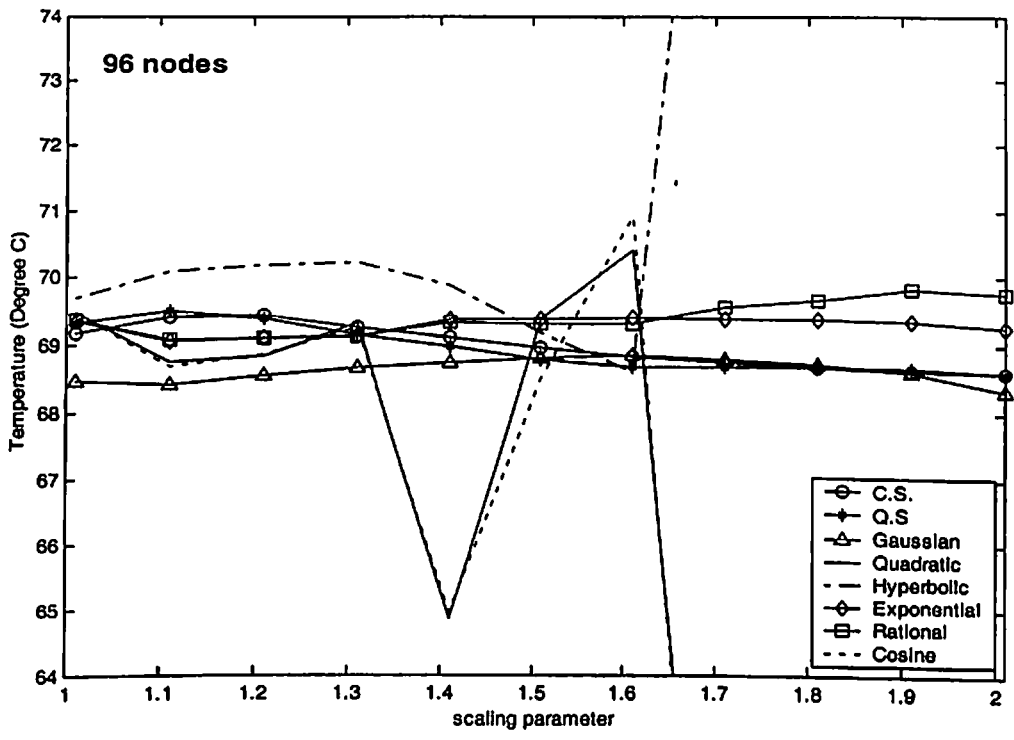


Fig. 6.10 Effect of scaling parameter on EFG results at the location ($x = 0.4 \text{ m}$, $y = 0 \text{ m}$ & $z = 0.3 \text{ m}$) of the 3-D model shown in Fig 6.9

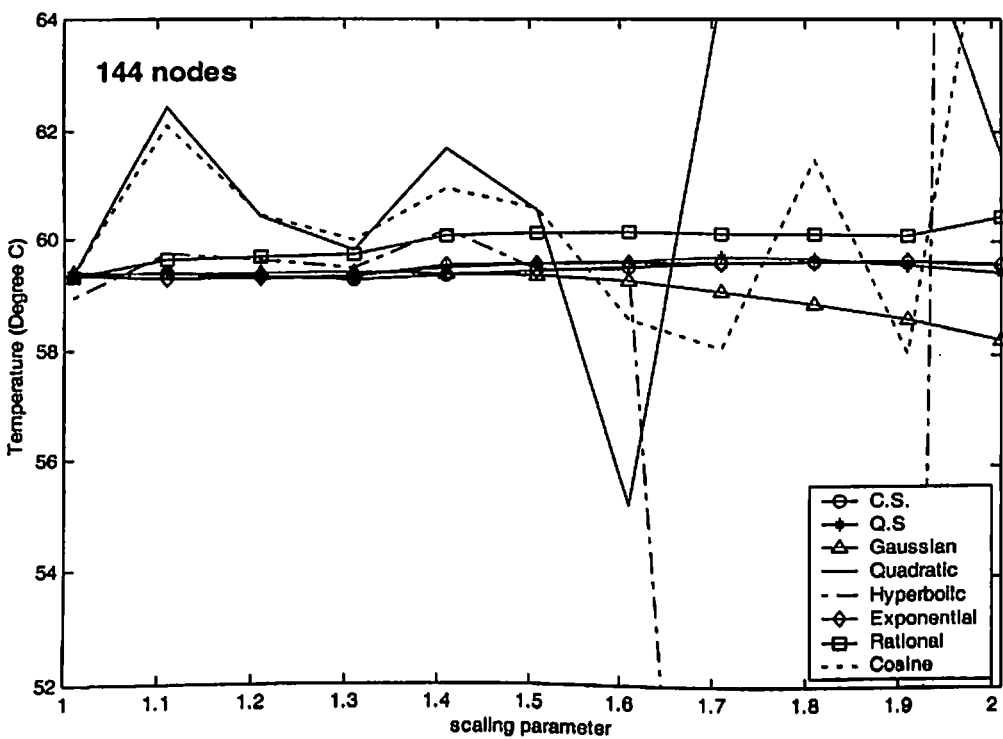
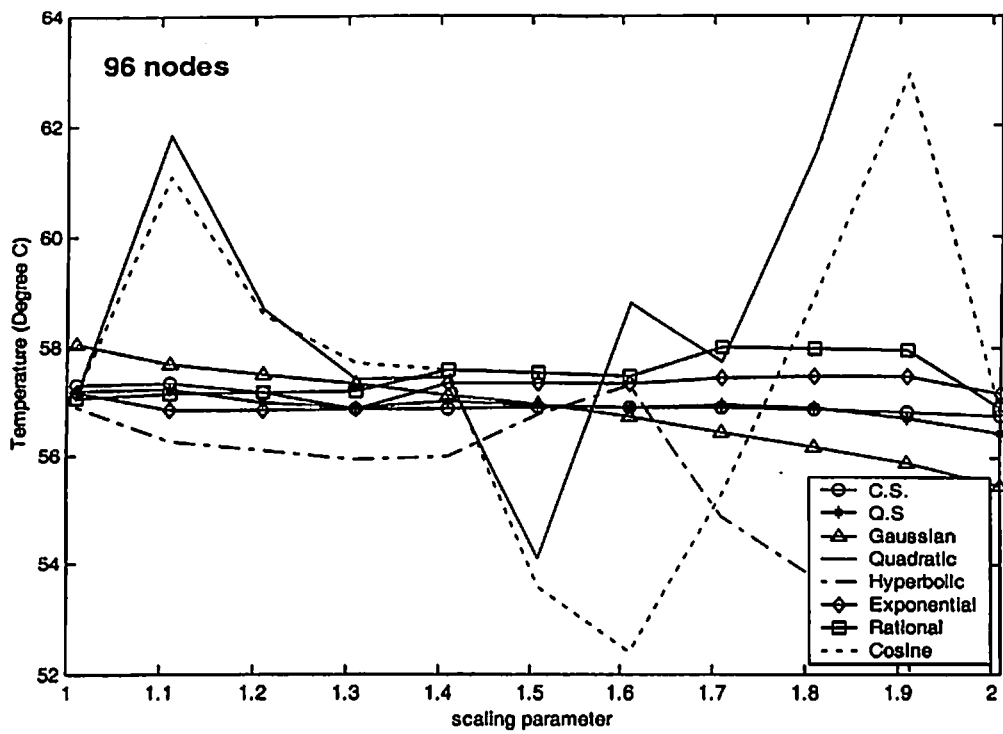


Fig. 6.11 Effect of scaling parameter on EFG results at the location ($x = 0.6$ m, $y = 0$ m & $z = 0.3$ m) of the 3-D model shown in Fig 6.9

6.5.2 Transient analysis

The transient analysis of 3-D model, shown in Fig. 6.9, is carried out using different EFG weight functions. Table 6.36 and Table 6.37 show the comparison of EFG results (i.e. temperature values) obtained using 96 nodes with FEM results at the location ($x = 0.4\text{ m}$, $y = 0\text{ m}$ & $z = 0.2\text{ m}$) for $d_{\max} = 1.01$ and $d_{\max} = 1.51$ respectively. Similar comparison of temperature values obtained using 144 nodes is presented in Table 6.38 and Table 6.39 for $d_{\max} = 1.01$ and $d_{\max} = 1.51$ respectively at the same location i.e. ($x = 0.4\text{ m}$, $y = 0\text{ m}$ & $z = 0.2\text{ m}$). For this case (i.e. CASE-II) of 3-D transient analysis, time step of 100 sec has been taken which is nearly 3% of the total time required to achieve steady state condition. Table 6.40 and Table 6.41 show the comparison of EFG results (i.e. temperature values) obtained using 96 nodes with FEM results at the location ($x = 0.5\text{ m}$, $y = 0\text{ m}$ & $z = 0.1\text{ m}$) for $d_{\max} = 1.01$ and $d_{\max} = 1.51$ respectively. Similar comparison of temperature values obtained using 81 nodes is also presented in Table 6.42 and Table 6.43 for $d_{\max} = 1.01$ and $d_{\max} = 1.51$ respectively at the same location i.e. ($x = 0.5\text{ m}$, $y = 0\text{ m}$ & $z = 0.1\text{ m}$). Fig 6.12 shows the comparison of EFG results (i.e. temperature values) obtained using 96 nodes with FEM results for $d_{\max} = 1.01$ and $d_{\max} = 1.51$ at the location ($x = 0.6\text{ m}$, $y = 0\text{ m}$ & $z = 0.2\text{ m}$). Similar comparison of temperature values obtained using 144 nodes is shown in Fig. 6.13 at the same location i.e. ($x = 0.6\text{ m}$, $y = 0\text{ m}$ & $z = 0.2\text{ m}$). Fig 6.14 shows the comparison of EFG results (i.e. temperature values) obtained using 96 nodes with FEM results for $d_{\max} = 1.01$ and $d_{\max} = 1.51$ at the location ($x = 0.6\text{ m}$, $y = 0\text{ m}$ & $z = 0.3\text{ m}$). Similar comparison of temperature values obtained using 144 nodes is shown in Fig. 6.15 at the same location i.e. ($x = 0.6\text{ m}$, $y = 0\text{ m}$ & $z = 0.3\text{ m}$). From the results presented in tables and figures, it is clear that the EFG results obtained using different weight functions are almost similar for $d_{\max} = 1.01$. However for $d_{\max} = 1.51$ only cubicspline, quarticspline, Gaussian, exponential and rational weight functions give acceptable results. It has also been observed that the EFG results are in good agreement with those obtained by FEM.

Table 6.36 Comparison of EFG results obtained using 96 nodes with FEM at the location ($x = 0.4$ m, $y = 0$ m & $z = 0.2$ m) of the 3-D model shown in Fig 6.9 for $d_{max} = 1.01$

Time (sec) $\times 10^2$	Temperature ($^{\circ}$ C)								
	$d_{max} = 1.01$								FEM
	C. S.	Q. S	Gaussian	Quadratic	Hyperbolic	Exponential	Rational	Cosine	
0	0.0000	0.0000	0.0000	0.0000	0.0000	0.0000	0.0000	0.0000	0.0000
3	25.3345	25.5048	24.4405	25.7137	26.5095	25.5403	25.7261	25.7058	37.9128
6	52.4294	52.6056	51.4934	52.8404	53.8647	52.6560	52.9196	52.8300	55.2100
9	62.9407	63.1156	62.0072	63.3553	64.4474	63.1709	63.4602	63.3439	63.6469
12	67.0460	67.2204	66.1132	67.4620	68.5795	67.2777	67.5766	67.4502	67.8024
15	68.6509	68.8253	67.7177	69.0677	70.1954	68.8834	69.1861	69.0559	69.8543
18	69.2785	69.4529	68.3448	69.6958	70.8274	69.5113	69.8155	69.6838	70.8682
21	69.5239	69.6983	68.5898	69.9414	71.0747	69.7569	70.0617	69.9295	71.3693
24	69.6198	69.7943	68.6856	70.0375	71.1714	69.8530	70.1580	70.0255	71.6170
27	69.6573	69.8318	68.7230	70.0751	71.2093	69.8905	70.1956	70.0631	71.7395
30	69.6720	69.8465	68.7376	70.0898	71.2241	69.9052	70.2103	70.0778	71.8000

Table 6.37 Comparison of EFG results obtained using 96 nodes with FEM at the location ($x = 0.4$ m, $y = 0$ m & $z = 0.2$ m) of the 3-D model shown in Fig 6.9 for $d_{max} = 1.51$

Time (sec) $\times 10^2$	Temperature ($^{\circ}$ C)								
	$d_{max} = 1.51$								FEM
	C. S.	Q. S	Gaussian	Quadratic	Hyperbolic	Exponential	Rational	Cosine	
0	0.0000	0.0000	0.0000	0.0000	0.0000	0.0000	0.0000	0.0000	0.0000
3	25.8472	25.9543	25.6531	34.2501	23.5621	25.7571	26.0760	36.2574	37.9128
6	52.8428	52.8721	52.6407	53.7453	51.5526	52.8619	53.1690	56.1387	55.2100
9	63.3134	63.3141	63.1110	61.3292	62.5171	63.3696	63.6672	63.8565	63.6469
12	67.4053	67.3956	67.2026	64.3003	66.8053	67.4734	67.7663	66.8793	67.8024
15	69.0063	68.9928	68.8034	65.4645	68.4823	69.0779	69.3687	68.0641	69.8543
18	69.6329	69.6180	69.4298	65.9206	69.1381	69.7054	69.9952	68.5284	70.8682
21	69.8781	69.8627	69.6749	66.0993	69.3946	69.9508	70.2402	68.7105	71.3693
24	69.9741	69.9585	69.7708	66.1694	69.4948	70.0468	70.3360	68.7818	71.6170
27	70.0116	69.9960	69.8084	66.1968	69.5340	70.0844	70.3734	68.8098	71.7395
30	70.0263	70.0107	69.8231	66.2075	69.5494	70.0990	70.3881	68.8208	71.8000

Table 6.38 Comparison of EFG results obtained using 144 nodes with FEM at the location ($x = 0.4$ m, $y = 0$ m & $z = 0.2$ m) of the 3-D model shown in Fig 6.9 for $d_{\max} = 1.01$

Time (sec) $\times 10^2$	Temperature ($^{\circ}$ C)								
	$d_{\max} = 1.01$								FEM
	C. S.	Q. S	Gaussian	Quadratic	Hyperbolic	Exponential	Rational	Cosine	
0	0.0000	0.0000	0.0000	0.0000	0.0000	0.0000	0.0000	0.0000	0.0000
3	27.7777	27.7756	27.7462	27.7800	27.7289	27.7804	27.7987	27.7775	31.0311
6	51.1260	51.1522	50.9515	51.2070	51.5229	51.1714	51.2790	51.2011	52.1403
9	61.5773	61.6096	61.3708	61.6785	62.1247	61.6339	61.7744	61.6712	61.9275
12	66.1682	66.2034	65.9469	66.2786	66.7820	66.2298	66.3846	66.2705	66.5053
15	68.1840	68.2206	67.9553	68.2988	68.8280	68.2481	68.4091	68.2905	68.6377
18	69.0692	69.1065	68.8368	69.1861	69.7269	69.1344	69.2982	69.1777	69.6303
21	69.4579	69.4956	69.2237	69.5758	70.1219	69.5237	69.6887	69.5673	70.0923
24	69.6286	69.6664	69.3935	69.7470	70.2954	69.6947	69.8602	69.7385	70.3073
27	69.7035	69.7415	69.4680	69.8222	70.3717	69.7697	69.9355	69.8136	70.4074
30	69.7365	69.7744	69.5008	69.8552	70.4052	69.8027	69.9686	69.8467	70.4539

Table 6.39 Comparison of EFG results obtained using 144 nodes with FEM at the location ($x = 0.4$ m, $y = 0$ m & $z = 0.2$ m) of the 3-D model shown in Fig 6.9 for $d_{\max} = 1.51$

Time (sec) $\times 10^2$	Temperature ($^{\circ}$ C)								
	$d_{\max} = 1.51$								FEM
	C. S.	Q. S	Gaussian	Quadratic	Hyperbolic	Exponential	Rational	Cosine	
0	0.0000	0.0000	0.0000	0.0000	0.0000	0.0000	0.0000	0.0000	0.0000
3	28.5827	28.7961	28.6839	36.4238	8.6876	27.6985	27.2910	34.0727	31.0311
6	51.1169	51.0966	51.0776	59.7803	42.9939	51.2045	51.1816	53.7799	52.1403
9	61.4391	61.3686	61.3700	69.6179	57.4475	61.6850	61.7254	62.4151	61.9275
12	66.0621	65.9906	65.9884	73.9208	63.6642	66.2814	66.3225	66.2236	66.5053
15	68.1311	68.0687	68.0588	75.8071	66.3394	68.2970	68.3274	67.9048	68.6377
18	69.0571	69.0030	68.9871	76.6342	67.4907	69.1809	69.2019	68.6470	69.6303
21	69.4715	69.4231	69.4032	76.9969	67.9862	69.5686	69.5833	68.9747	70.0923
24	69.6570	69.6120	69.5898	77.1559	68.1995	69.7386	69.7497	69.1194	70.3073
27	69.7400	69.6970	69.6734	77.2257	68.2912	69.8131	69.8223	69.1833	70.4074
30	69.7772	69.7352	69.7109	77.2563	68.3307	69.8458	69.8540	69.2115	70.4539

Table 6.40 Comparison of EFG results obtained using 96 nodes with FEM at the location ($x = 0.5$ m, $y = 0$ m & $z = 0.1$ m) of the 3-D model shown in Fig 6.9 for $d_{max} = 1.01$

Time (sec) $\times 10^2$	Temperature ($^{\circ}$ C)								
	$d_{max} = 1.01$								FEM
	C. S.	Q. S	Gaussian	Quadratic	Hyperbolic	Exponential	Rational	Cosine	
0	0.0000	0.0000	0.0000	0.0000	0.0000	0.0000	0.0000	0.0000	0.0000
3	19.0642	19.0501	19.2231	19.0987	19.9184	19.0591	19.0796	19.0836	33.4291
6	47.1405	47.1436	47.2035	47.2172	48.2906	47.1563	47.2060	47.2009	51.0674
9	58.1759	58.1907	58.1778	58.2797	59.4532	58.2062	58.2707	58.2631	59.8836
12	62.4957	62.5161	62.4690	62.6124	63.8268	62.5330	62.6039	62.5956	64.2533
15	64.1852	64.2080	64.1461	64.3076	65.5384	64.2256	64.2991	64.2907	66.4151
18	64.8459	64.8697	64.8015	64.9706	66.2081	64.8875	64.9622	64.9538	67.4840
21	65.1042	65.1285	65.0577	65.2300	66.4701	65.1464	65.2215	65.2131	68.0125
24	65.2052	65.2297	65.1578	65.3314	66.5726	65.2477	65.3229	65.3146	68.2738
27	65.2447	65.2693	65.1969	65.3711	66.6126	65.2873	65.3626	65.3542	68.4029
30	65.2602	65.2848	65.2122	65.3866	66.6283	65.3028	65.3781	65.3697	68.4668

Table 6.41 Comparison of EFG results obtained using 96 nodes with FEM at the location ($x = 0.5$ m, $y = 0$ m & $z = 0.1$ m) of the 3-D model shown in Fig 6.9 for $d_{max} = 1.51$

Time (sec) $\times 10^2$	Temperature ($^{\circ}$ C)								
	$d_{max} = 1.51$								FEM
	C. S.	Q. S	Gaussian	Quadratic	Hyperbolic	Exponential	Rational	Cosine	
0	0.0000	0.0000	0.0000	0.0000	0.0000	0.0000	0.0000	0.0000	0.0000
3	19.1934	19.2793	19.2665	16.7078	20.8456	19.1936	19.7432	17.5522	33.4291
6	47.6355	47.8670	47.6872	48.5714	51.6277	47.3714	48.2265	48.8968	51.0674
9	58.8450	59.1402	58.8838	61.2475	63.7346	58.4556	59.4254	61.3381	59.8836
12	63.2393	63.5607	63.2720	66.2305	68.4725	62.7962	63.8098	66.2279	64.2533
15	64.9597	65.2917	64.9898	68.1844	70.3255	64.4943	65.5246	68.1457	66.4151
18	65.6331	65.9694	65.6620	68.9501	71.0501	65.1585	66.1951	68.8975	67.4840
21	65.8967	66.2346	65.9251	69.2501	71.3334	65.4183	66.4573	69.1922	68.0125
24	65.9998	66.3385	66.0281	69.3677	71.4442	65.5199	66.5599	69.3078	68.2738
27	66.0402	66.3791	66.0684	69.4138	71.4875	65.5596	66.5999	69.3530	68.4029
30	66.0560	66.3950	66.0841	69.4318	71.5044	65.5751	66.6156	69.3708	68.4668

Table 6.42 Comparison of EFG results obtained using 144 nodes with FEM at the location ($x = 0.5$ m, $y = 0$ m & $z = 0.1$ m) of the 3-D model shown in Fig 6.9 for $d_{max} = 1.01$

Time (sec) $\times 10^2$	Temperature ($^{\circ}$ C)								
	$d_{max} = 1.01$								FEM
	C. S.	Q. S	Gaussian	Quadratic	Hyperbolic	Exponential	Rational	Cosine	
0	0.0000	0.0000	0.0000	0.0000	0.0000	0.0000	0.0000	0.0000	0.0000
3	23.1684	23.1120	23.4060	23.0260	22.5584	23.0971	23.0466	23.0289	27.8851
6	46.3783	46.3083	46.6795	46.2101	45.7917	46.2914	46.2438	46.2132	47.4500
9	57.0841	57.0132	57.3863	56.9147	56.5293	56.9963	56.9528	56.9177	57.2622
12	61.8022	61.7317	62.1001	61.6343	61.2669	61.7151	61.6738	61.6372	61.9078
15	63.8747	63.8047	64.1696	63.7080	63.3494	63.7882	63.7481	63.7109	64.0790
18	64.7849	64.7151	65.0780	64.6189	64.2645	64.6987	64.6591	64.6218	65.0906
21	65.1845	65.1150	65.4767	65.0190	64.6666	65.0986	65.0592	65.0218	65.5615
24	65.3601	65.2906	65.6517	65.1947	64.8433	65.2743	65.2349	65.1976	65.7807
27	65.4371	65.3677	65.7285	65.2719	64.9209	65.3514	65.3121	65.2748	65.8827
30	65.4710	65.4016	65.7622	65.3058	64.9550	65.3853	65.3460	65.3087	65.9302

Table 6.43 Comparison of EFG results obtained using 144 nodes with FEM at the location ($x = 0.5$ m, $y = 0$ m & $z = 0.1$ m) of the 3-D model shown in Fig 6.9 for $d_{max} = 1.51$

Time (sec) $\times 10^2$	Temperature ($^{\circ}$ C)								
	$d_{max} = 1.51$								FEM
	C. S.	Q. S	Gaussian	Quadratic	Hyperbolic	Exponential	Rational	Cosine	
0	0.0000	0.0000	0.0000	0.0000	0.0000	0.0000	0.0000	0.0000	0.0000
3	23.8911	23.9874	24.1099	16.8855	19.3014	22.9096	22.3984	15.0885	27.8851
6	46.4178	46.4121	46.5858	42.2527	46.8328	46.2786	46.4715	40.4511	47.4500
9	57.1181	57.1396	57.2800	53.9115	58.8902	57.0360	57.4204	52.2651	57.2622
12	61.9307	61.9878	62.0983	59.0469	64.0868	61.7701	62.2082	57.5031	61.9078
15	64.0858	64.1689	64.2597	61.3004	66.3239	63.8470	64.2971	59.8171	64.0790
18	65.0505	65.1496	65.2287	62.2887	67.2867	64.7579	65.2083	60.8389	65.0906
21	65.4822	65.5906	65.6632	62.7221	67.7010	65.1574	65.6058	61.2901	65.5615
24	65.6754	65.7889	65.8580	62.9122	67.8794	65.3326	65.7792	61.4893	65.7807
27	65.7619	65.8781	65.9453	62.9955	67.9561	65.4094	65.8548	61.5772	65.8827
30	65.8006	65.9181	65.9845	63.0320	67.9891	65.4431	65.8878	61.6161	65.9302

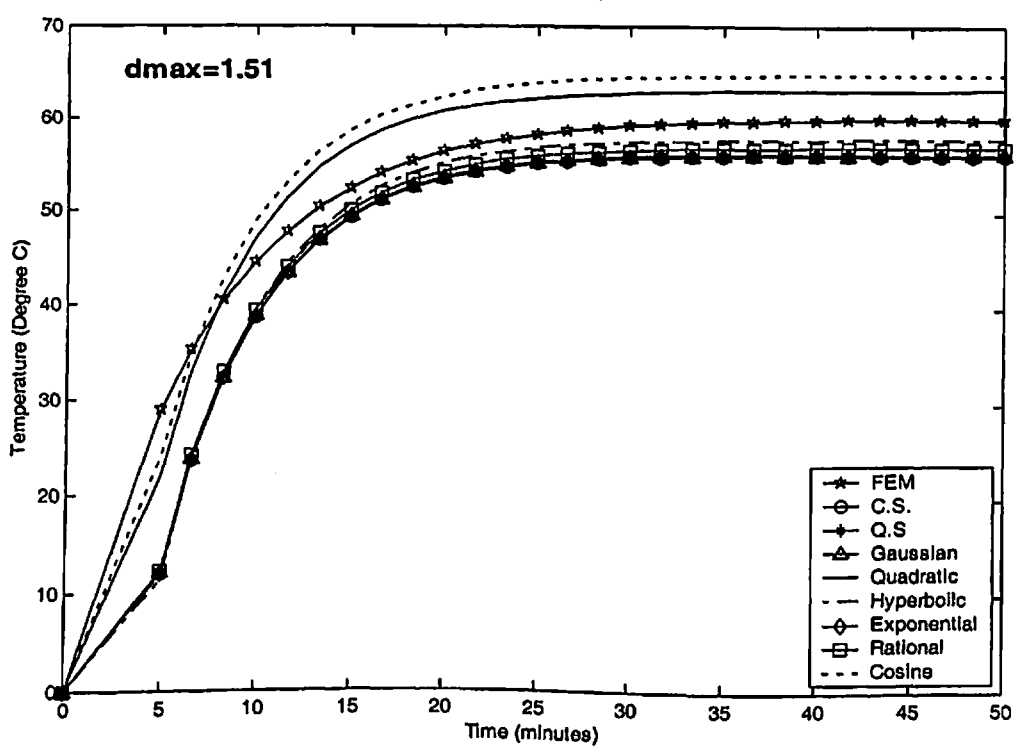
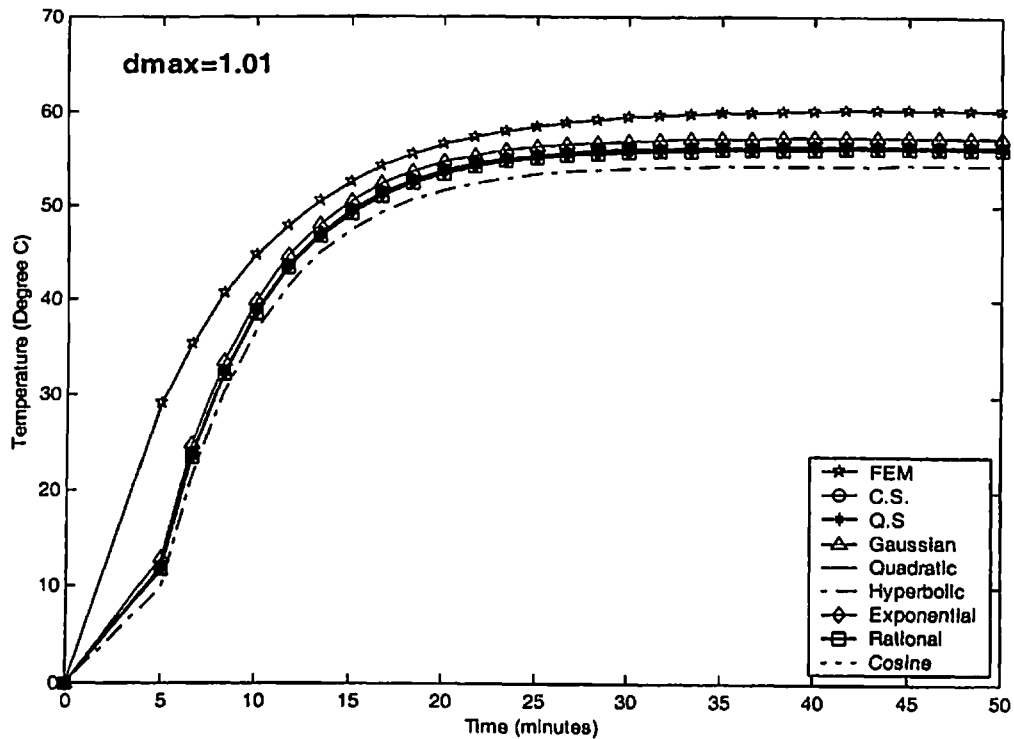


Fig. 6.12 Comparison of EFG results obtained using 96 nodes with FEM at the location ($x = 0.6$ m, $y = 0$ m & $z = 0.2$ m) of the 3-D model shown in Fig 6.9

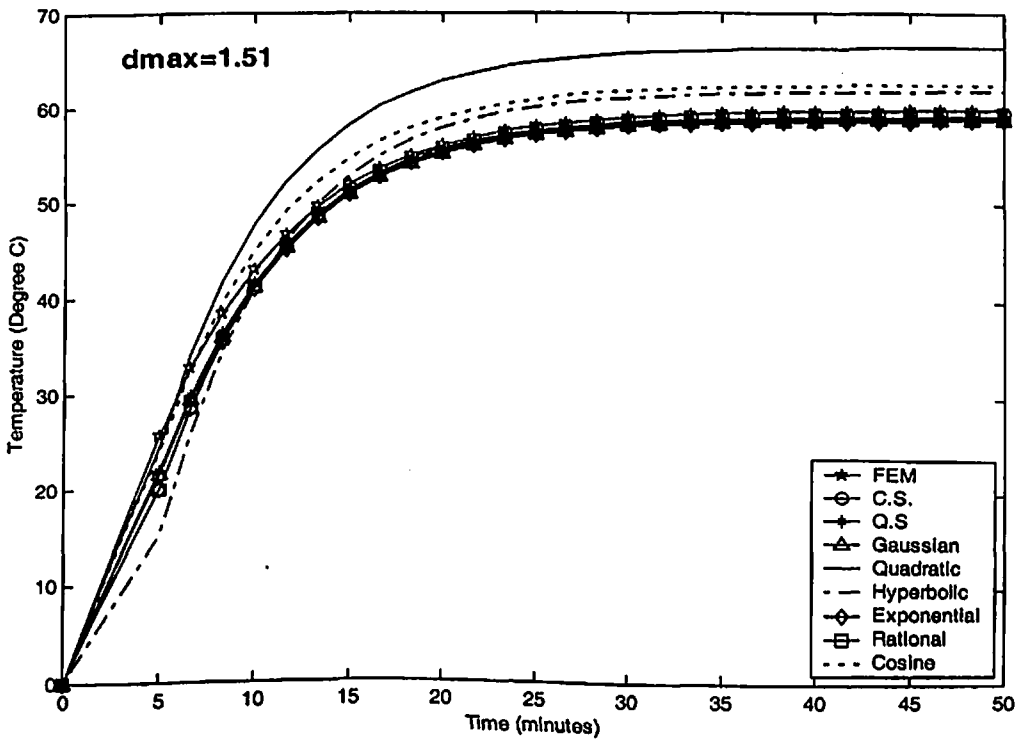
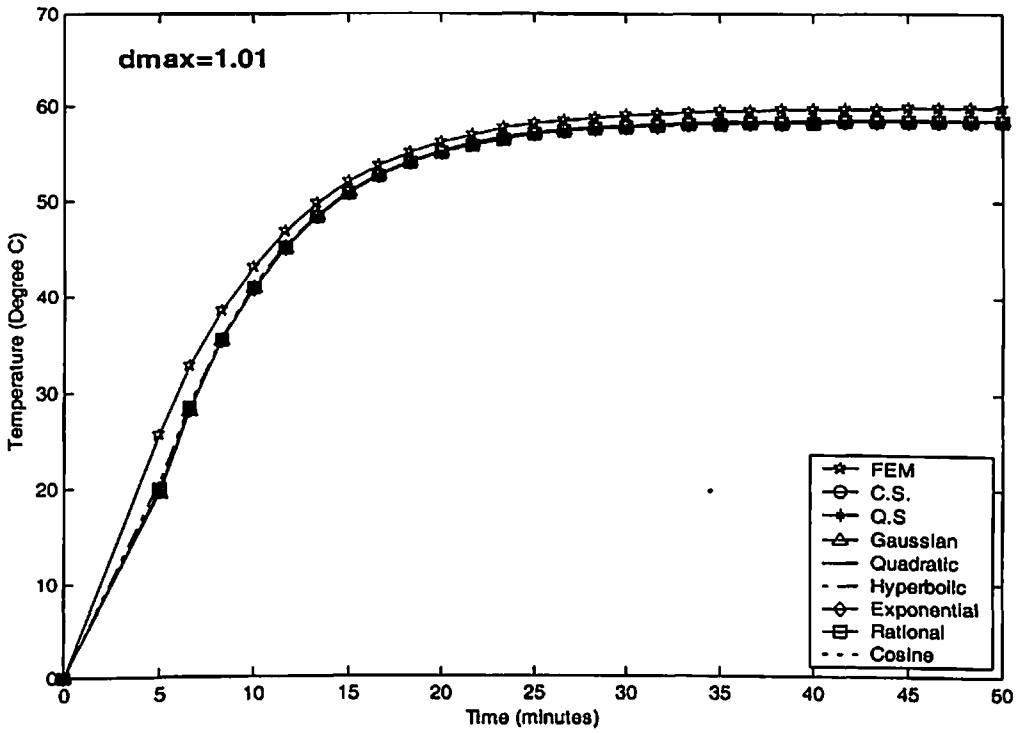


Fig. 6.13 Comparison of EFG results obtained using 144 nodes with FEM at the location ($x = 0.6$ m, $y = 0$ m & $z = 0.2$ m) of the 3-D model shown in Fig 6.9

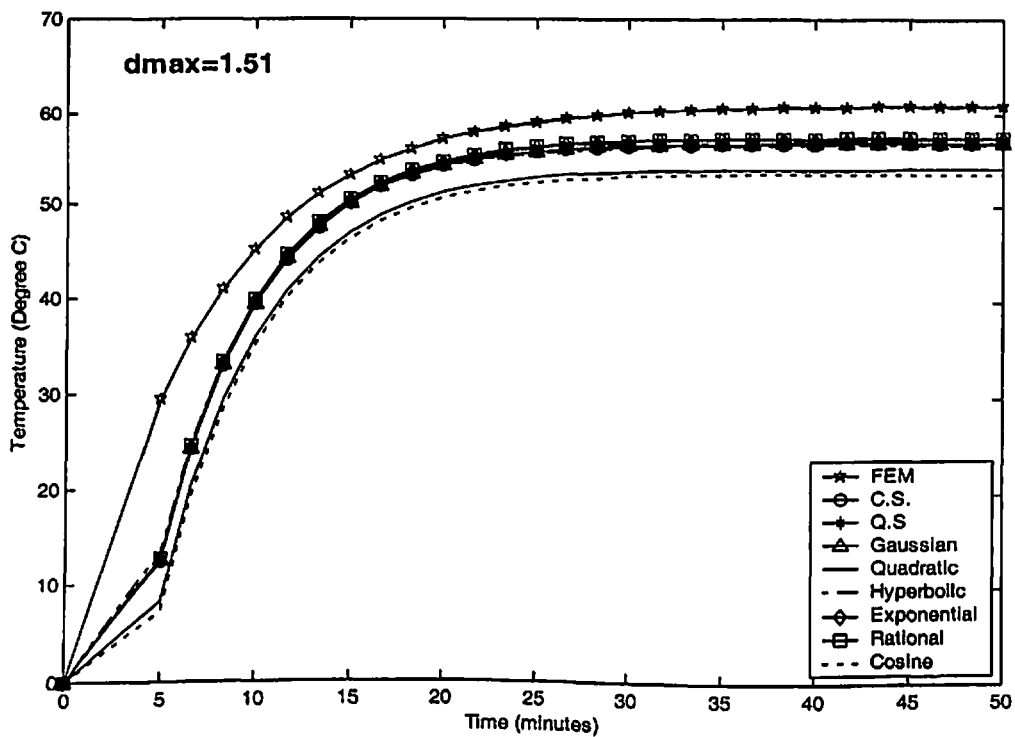
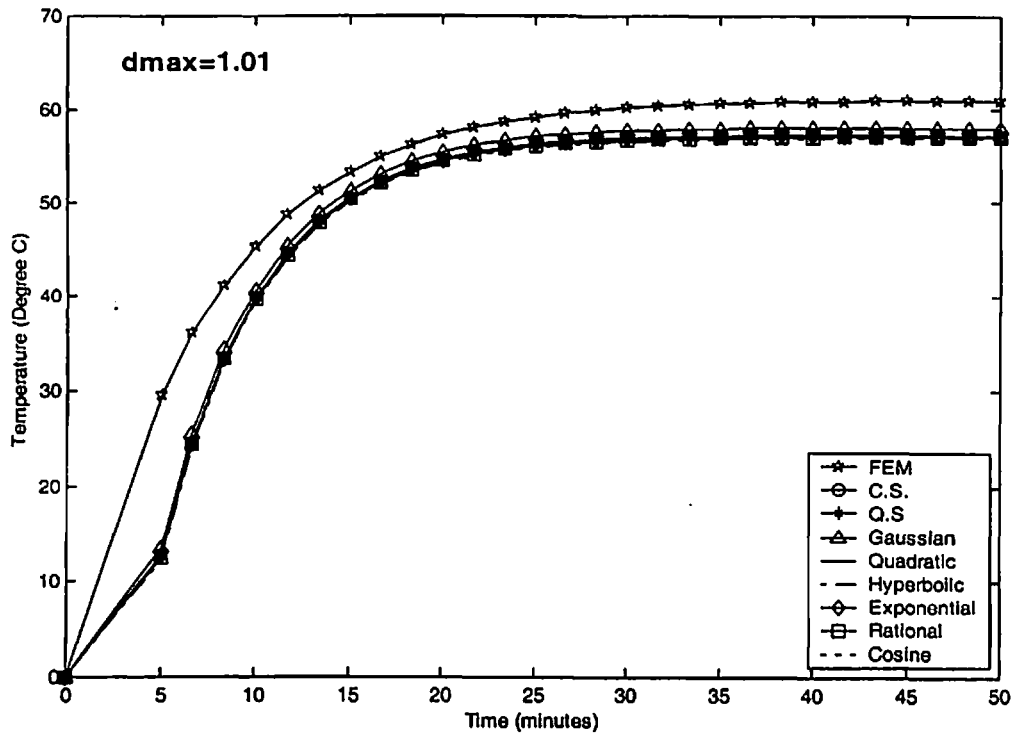


Fig. 6.14 Comparison of EFG results obtained using 96 nodes with FEM at the location ($x = 0.6 \text{ m}$, $y = 0 \text{ m}$ & $z = 0.3 \text{ m}$) of the 3-D model shown in Fig 6.9

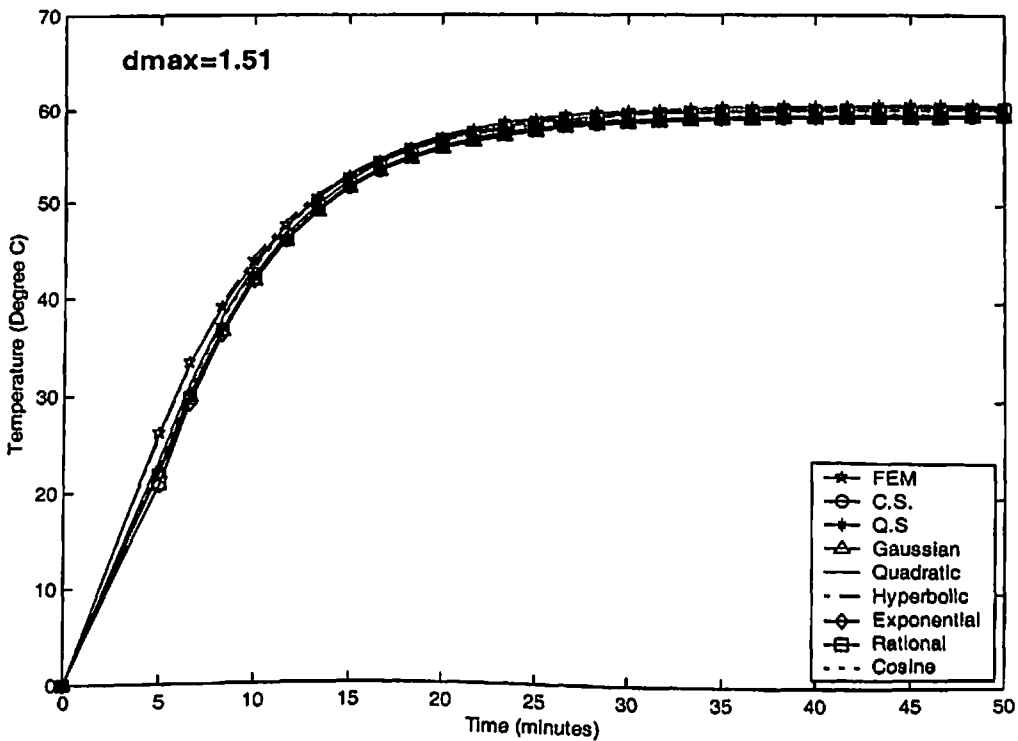
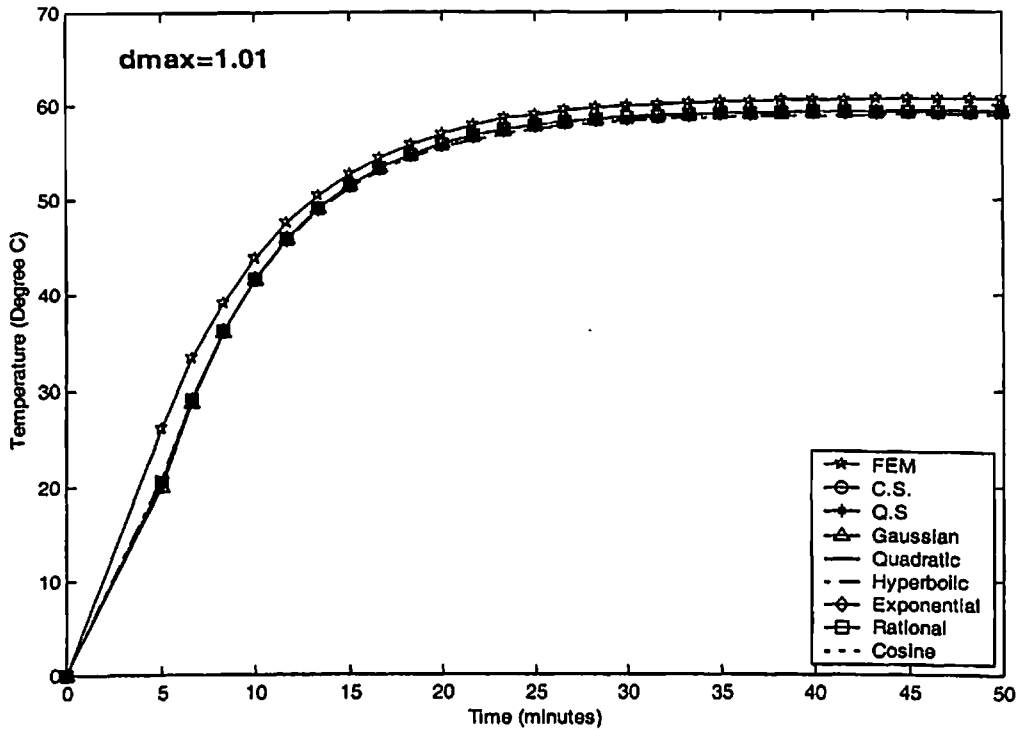


Fig. 6.15 Comparison of EFG results obtained using 144 nodes with FEM at the location ($x = 0.6$ m, $y = 0$ m & $z = 0.3$ m) of the 3-D model shown in Fig 6.9

➤ **CASE-III**

6.6 DISCRETIZATION OF THE GOVERNING EQUATION

A general form of energy equation for three-dimensional steady-state heat transfer in composite slabs with thermal properties independent of temperature is given as:

$$k \left(\frac{\partial^2 T}{\partial x^2} + \frac{\partial^2 T}{\partial y^2} + \frac{\partial^2 T}{\partial z^2} \right) + \dot{Q} = \rho c \dot{T} \quad (6.23a)$$

The initial conditions are:

$$\text{at the time } t = 0 \quad T = T_{in} \quad \text{on } V \quad (6.23b)$$

The essential boundary conditions are:

$$\text{at the surface of slab 1 } x = 0 \text{ or } S_1 \quad T = T_s \quad (6.23c)$$

The natural boundary conditions are:

$$\text{at the surface of slab 1 } z = H/2 \text{ or } S_2 \quad k \frac{\partial T}{\partial z} = h(T - T_\infty) \quad (6.23d)$$

$$\text{at the surface of slab 2 } x = L/2 \text{ or } S_3, \quad k \frac{\partial T}{\partial x} = h(T - T_\infty) \quad (6.23e)$$

$$\text{at the surface of slab 2 } z = 0 \text{ or } S_4 \quad k \frac{\partial T}{\partial z} = h(T - T_\infty) \quad (6.23f)$$

$$\text{at the surface of slab 2 } x = L \text{ or } S_5 \quad -k \frac{\partial T}{\partial x} = h(T - T_\infty) \quad (6.23g)$$

$$\text{at the surface of slab 2 } z = H \text{ or } S_6 \quad -k \frac{\partial T}{\partial z} = h(T - T_\infty) \quad (6.23h)$$

$$\text{at the surface of slab 1 } z = H \text{ or } S_7 \quad -k \frac{\partial T}{\partial z} = h(T - T_\infty) \quad (6.23i)$$

$$\text{at the surface of slab 1 } y = W \text{ or } S_8 \quad -k \frac{\partial T}{\partial y} = h(T - T_\infty) \quad (6.23j)$$

$$\text{at the surface of slab 2 } y = W \text{ or } S_9 \quad -k \frac{\partial T}{\partial y} = h(T - T_\infty) \quad (6.23k)$$

$$\text{at the surface of slab 1 } y = 0 \text{ or } S_{10} \quad k \frac{\partial T}{\partial y} = h(T - T_\infty) \quad (6.23l)$$

$$\text{at the surface of slab 2 } y = 0 \text{ or } S_{11} \quad k \frac{\partial T}{\partial y} = h(T - T_{\infty}) \quad (6.23m)$$

Compatibility requirement at the interface of two slabs is given as:

$$-k \left(\frac{\partial T}{\partial x} \right) \Big|_{x=L/2} \Big|_{\text{slab1}} = -k \left(\frac{\partial T}{\partial x} \right) \Big|_{x=L/2} \Big|_{\text{slab2}} \quad (6.23n)$$

The weak of the Eq. (6.23a) with natural boundary conditions is obtained as:

$$\begin{aligned} & \int_V [k(w_{,x}T_{,x} + w_{,y}T_{,y} + w_{,z}T_{,z})]dV - \int_V w \dot{Q} dV + \int_V w \rho c \dot{T} dV + \int_{S_2} w h(T - T_{\infty})dS + \\ & \int_{S_3} w h(T - T_{\infty})dS + \int_{S_4} w h(T - T_{\infty})dS + \int_{S_5} w h(T - T_{\infty})dS + \\ & \int_{S_6} w h(T - T_{\infty})dS + \int_{S_7} w h(T - T_{\infty})dS + \int_{S_8} w h(T - T_{\infty})dS + \int_{S_9} w h(T - T_{\infty})dS + \\ & \int_{S_{10}} w h(T - T_{\infty})dS + \int_{S_{11}} w h(T - T_{\infty})dS = 0 \end{aligned} \quad (6.24)$$

The functional $I(T)$ can be written as:

$$\begin{aligned} I(T) = & \int_V \frac{k}{2} [T_{,x}^2 + T_{,y}^2 + T_{,z}^2] dV - \int_V T \dot{Q} dV + \int_V \rho c \dot{T} T dV + \int_{S_2} \frac{hT^2}{2} dS + \int_{S_3} \frac{hT^2}{2} dS + \\ & \int_{S_4} \frac{hT^2}{2} dS + \int_{S_5} \frac{hT^2}{2} dS + \int_{S_6} \frac{hT^2}{2} dS + \int_{S_7} \frac{hT^2}{2} dS + \int_{S_8} \frac{hT^2}{2} dS + \\ & \int_{S_9} \frac{hT^2}{2} dS + \int_{S_{10}} \frac{hT^2}{2} dS + \int_{S_{11}} hT_{\infty} T dS + \int_{S_2} hT_{\infty} T dS + \int_{S_3} hT_{\infty} T dS + \int_{S_4} hT_{\infty} T dS + \\ & \int_{S_5} hT_{\infty} T dS + \int_{S_6} hT_{\infty} T dS + \int_{S_7} hT_{\infty} T dS + \int_{S_8} hT_{\infty} T dS + \int_{S_9} hT_{\infty} T dS + \int_{S_{10}} hT_{\infty} T dS + \\ & \int_{S_{11}} hT_{\infty} T dS \end{aligned} \quad (6.25)$$

Enforcing essential boundary conditions using Lagrange multiplier the functional $I'(T)$ is obtained as:

$$\begin{aligned}
I^*(T) = & \int_V \frac{k}{2} [T_{,x}^2 + T_{,y}^2 + T_{,z}^2] dV - \int_V T \dot{Q} dV + \int_{s_1} \frac{hT^2}{2} dS + \int_{s_1} \frac{hT^2}{2} dS + \int_{s_4} \frac{hT^2}{2} dS + \\
& \int_{s_5} \frac{hT^2}{2} dS + \int_{s_6} \frac{hT^2}{2} dS + \int_{s_7} \frac{hT^2}{2} dS + \int_{s_8} \frac{hT^2}{2} dS + \int_{s_9} \frac{hT^2}{2} dS + \int_{s_{10}} \frac{hT^2}{2} dS + \\
& \int_{s_{11}} \frac{hT^2}{2} dS + \int_{s_2} hT_{\infty} T dS + \int_{s_3} hT_{\infty} T dS + \int_{s_4} hT_{\infty} T dS + \int_{s_5} hT_{\infty} T dS + \int_{s_6} hT_{\infty} T dS + \\
& \int_{s_7} hT_{\infty} T dS + \int_{s_8} hT_{\infty} T dS + \int_{s_9} hT_{\infty} T dS + \int_{s_{10}} hT_{\infty} T dS + \int_{s_{11}} hT_{\infty} T dS + \int_{s_1} \lambda (T - T_{s_1}) dS
\end{aligned} \tag{6.26}$$

Using variational principle for obtaining the discrete equations:

$$\begin{aligned}
\delta I^*(T) = & \int_V [T_{,x} \delta T_{,x} + T_{,y} \delta T_{,y} + T_{,z} \delta T_{,z}] dV - \int_V \dot{Q} \delta T dV + \int_V \rho c \dot{T} \delta T dV + \\
& \int_{s_2} hT \delta T dS + \int_{s_3} hT \delta T dS + \int_{s_4} hT \delta T dS + \int_{s_5} hT \delta T dS + \int_{s_6} hT \delta T dS + \\
& \int_{s_7} hT \delta T dS + \int_{s_8} hT \delta T dS + \int_{s_9} hT \delta T dS + \int_{s_{10}} hT \delta T dS + \int_{s_{11}} hT \delta T dS + \\
& \int_{s_2} hT_{\infty} \delta T dS + \int_{s_3} hT_{\infty} \delta T dS + \int_{s_4} hT_{\infty} \delta T dS + \int_{s_5} hT_{\infty} \delta T dS + \int_{s_6} hT_{\infty} \delta T dS + \\
& \int_{s_7} hT_{\infty} \delta T dS + \int_{s_8} hT_{\infty} \delta T dS + \int_{s_9} hT_{\infty} \delta T dS + \int_{s_{10}} hT_{\infty} \delta T dS + \int_{s_{11}} hT_{\infty} \delta T dS + \\
& \int_{s_1} (T - T_{s_1}) \delta \lambda dS + \int_{s_1} \lambda \delta T dS
\end{aligned} \tag{6.27}$$

Since δT and $\delta \lambda$ are arbitrary in preceding equation, the following relations are obtained by using Eq. (3.25) and Eq. (6.27)

$$[\mathbf{K}]\{\mathbf{T}\} + [\mathbf{C}]\{\dot{\mathbf{T}}\} + [\mathbf{G}]\{\lambda\} = \{\mathbf{f}\} \tag{6.28a}$$

$$[\mathbf{G}^T]\{\mathbf{T}\} = \{\mathbf{q}\} \tag{6.28b}$$

where

$$K_{IJ} = \int_{\Omega} \begin{bmatrix} \Phi_{I,x} \\ \Phi_{I,y} \\ \Phi_{I,z} \end{bmatrix}^T \begin{bmatrix} k & 0 & 0 \\ 0 & k & 0 \\ 0 & 0 & k \end{bmatrix} \begin{bmatrix} \Phi_{J,x} \\ \Phi_{J,y} \\ \Phi_{J,z} \end{bmatrix} dV + \int_{S_1} h \Phi_I^T \Phi_J dS + \int_{S_2} h \Phi_I^T \Phi_J dS + \int_{S_3} h \Phi_I^T \Phi_J dS + \int_{S_4} h \Phi_I^T \Phi_J dS + \int_{S_5} h \Phi_I^T \Phi_J dS + \int_{S_6} h \Phi_I^T \Phi_J dS + \int_{S_7} h \Phi_I^T \Phi_J dS + \int_{S_8} h \Phi_I^T \Phi_J dS + \int_{S_9} h \Phi_I^T \Phi_J dS + \int_{S_{10}} h \Phi_I^T \Phi_J dS + \int_{S_{11}} h \Phi_I^T \Phi_J dS \quad (6.29a)$$

$$C_{IJ} = \int_V \rho c \Phi_I^T \Phi_J dV \quad (6.29b)$$

$$f_I = \int_V \dot{Q} \Phi_I dV + \int_{S_2} h T_{\infty} \Phi_I dS + \int_{S_3} h T_{\infty} \Phi_I dS + \int_{S_4} h T_{\infty} \Phi_I dS + \int_{S_5} h T_{\infty} \Phi_I dS + \int_{S_6} h T_{\infty} \Phi_I dS + \int_{S_7} h T_{\infty} \Phi_I dS + \int_{S_8} h T_{\infty} \Phi_I dS + \int_{S_9} h T_{\infty} \Phi_I dS + \int_{S_{10}} h T_{\infty} \Phi_I dS + \int_{S_{11}} h T_{\infty} \Phi_I dS \quad (6.29c)$$

$$G_{IK} = \int_{S_i} \Phi_I N_K dS \quad (6.29d)$$

$$q_K = \int_{S_i} T_{S_i} N_K dS \quad (6.29e)$$

Using backward difference method for time approximation, the Eq. (6.28) can be written as:

$$\left[\begin{array}{c|c} \mathbf{K}^* + \mathbf{C} & \mathbf{G} \\ \hline \mathbf{G}^T & 0 \end{array} \right] \begin{Bmatrix} \mathbf{T}_N \\ \boldsymbol{\lambda} \end{Bmatrix} = \begin{Bmatrix} \mathbf{R}_N \\ \mathbf{q} \end{Bmatrix} \quad (6.30)$$

where

$$\mathbf{R}_N = ([\mathbf{C}] - (1 - \alpha) \Delta t [\mathbf{K}]) \{\mathbf{T}\}_{N-1} + \alpha \Delta t \{\mathbf{f}\}_N + (1 - \alpha) \Delta t \{\mathbf{f}\}_{N-1} \quad (6.31a)$$

$$\mathbf{K}^* = \alpha \Delta t [\mathbf{K}] \quad (6.31b)$$

6.7 NUMERICAL RESULTS AND DISCUSSION

The different parameters used for three-dimensional steady-state and transient analysis of the composite slab model shown in Fig. 6.16 are tabulated in Table 6.44. The EFG results (temperature values) are obtained using different weight functions for two sets of nodes and the FEM results are obtained using 8 node brick elements (SOLID 70, ANSYS 6.0) for same

sets of nodes. A comparative study is carried out to evaluate the performance of different EFG weight functions.

6.7.1 Steady-state analysis

The results (i.e. temperature values) presented in Table 6.45 are obtained using different EFG weight functions for two values of scaling parameter (i.e. $d_{\max} = 1.01$ & $d_{\max} = 1.51$) at the location ($x = 0.2$ m, $y = 0.4$ m & $z = 0.4$ m) and it shows a comparison of temperature values obtained by EFG method using different weight functions with FEM for 63 nodes. Table 6.46 shows a comparison of temperature values obtained by EFG method using different functions for two values of scaling parameter with FEM at the same location i.e. ($x = 0.2$ m, $y = 0.4$ m & $z = 0.4$ m) for 325 nodes. A comparison of temperature values obtained using different EFG weight functions with FEM for 63 and 325 nodes, is shown in Table 6.47 and Table 6.48 respectively at the location ($x = 0.2$ m, $y = 0.4$ m & $z = 0$ m). Similar type of comparisons of temperature values are shown in Table 6.49 for 63 nodes at the location ($x = 0.4$ m, $y = 0.4$ m & $z = 0.4$ m), in Table 6.50 for 325 nodes at the location ($x = 0.4$ m, $y = 0.4$ m & $z = 0.4$ m), in Table 6.51 for 63 nodes at the location ($x = 0.4$ m, $y = 0.2$ m & $z = 0.2$ m) and in Table 6.52 for 325 nodes at the location ($x = 0.4$ m, $y = 0.2$ m & $z = 0.2$ m). From the results presented in Table 6.45 to Table 6.52, it is observed that EFG results obtained using cubicspline, quarticspline, Gaussian, exponential and rational weight functions are acceptable for $d_{\max} = 1.01$. However for $d_{\max} = 1.51$, only exponential and rational weight functions give acceptable results. It is also observed that EFG results obtained using different weight functions are in good agreement with those obtained by FEM. Moreover with the increase in number of nodes EFG results starts converging.

The effect of scaling parameter (d_{\max}) on EFG results obtained using different weight functions is presented in Table 6.53 for 63 nodes and Table 6.54 for 325 nodes respectively at

the location ($x = 0.2 \text{ m}$, $y = 0.4 \text{ m}$ & $z = 0.4 \text{ m}$). Similar effect of scaling parameter on EFG results is shown in Table 6.55 for 63 nodes and Table 6.56 for 325 nodes at the location ($x = 0.4 \text{ m}$, $y = 0.2 \text{ m}$ & $z = 0.2 \text{ m}$). Fig. 6.17 shows the effect of scaling parameter on EFG results obtained using 63 and 325 nodes at the location ($x = 0.2 \text{ m}$, $y = 0.4 \text{ m}$ & $z = 0 \text{ m}$). Similar effect of scaling parameter on EFG results is observed in Fig. 6.18 at the location ($x = 0.4 \text{ m}$, $y = 0.4 \text{ m}$ & $z = 0 \text{ m}$). From tables and figures, it is clear that only cubicspline, exponential and rational weight functions give acceptable results in the range $1.0 < d_{\max} < 1.5$ whereas the results obtained using quarticspline, Gaussian, quadratic, hyperbolic and cosine weight functions acceptable in the range $1.0 < d_{\max} < 1.5$. It is also observed that there is minimum variation in EFG results with scaling parameter for exponential weight function. Therefore exponential weight function gives most reliable results for this case.

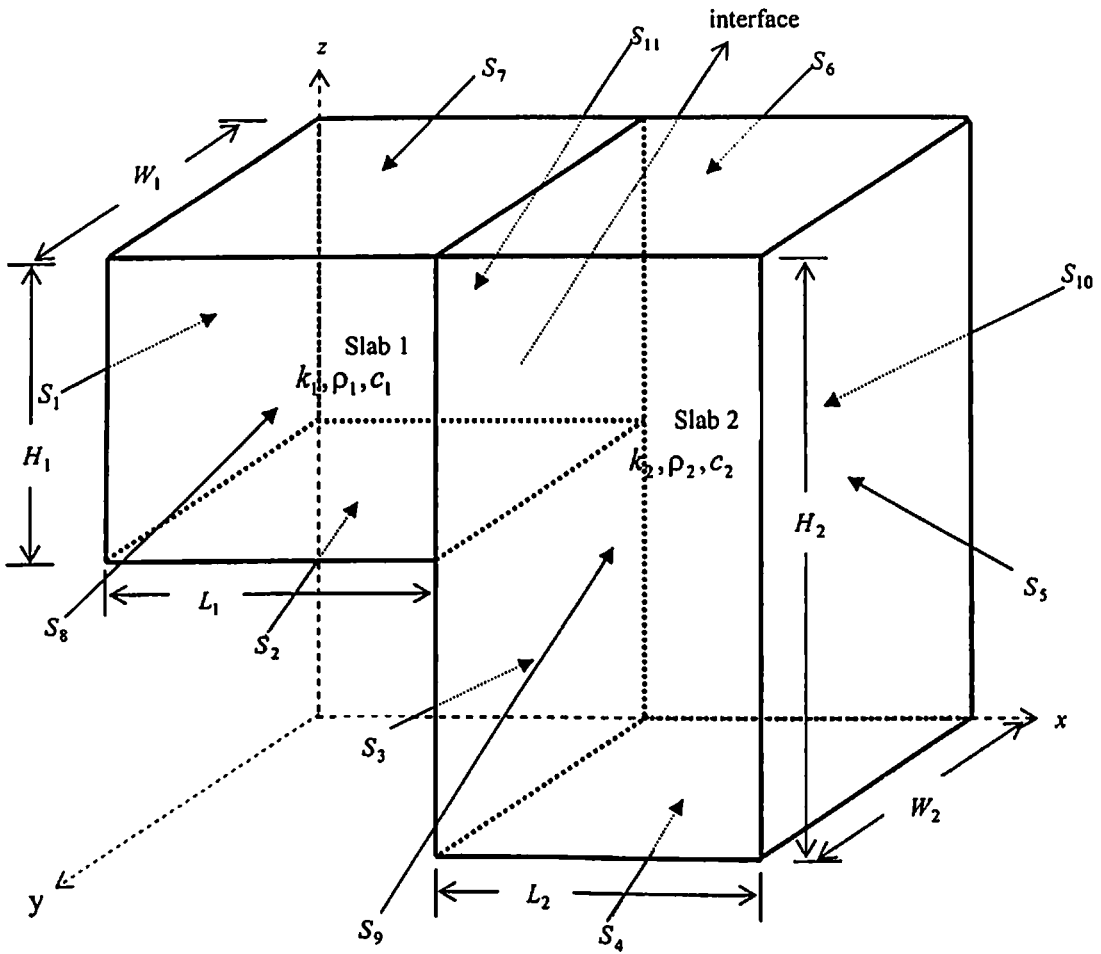


Fig. 6.16 Three-dimensional model of composite slabs

Table 6.44 Data for the 3-D model shown in Fig. 6.16

Parameters	Value of the parameter
Length (L_1)	0.2 m
Width (W_1)	0.2 m
Height (H_1)	0.2 m
Length (L_2)	0.2 m
Width (W_2)	0.2 m
Height (H_2)	0.4 m
Thermal conductivity (k_1)	400 W/m-K
Thermal conductivity (k_2)	100 W/m-K
Specific heat of material 1 (c_1)	400 kJ/kg-K
Specific heat of material 2 (c_2)	300 kJ/kg-K
Density of material 1 (ρ_1)	10000 kg/m ³
Density of material 2 (ρ_2)	8000 kg/m ³
Rate of internal heat generation (\dot{Q})	0 W/m ³
Heat transfer coefficient (h)	200 W/m ² -K
Initial temperature (T_{ini})	0 °C
Time step size (Δt)	100 sec
Surrounding fluid temperature (T_∞)	20 °C
Temperature (T_{S_1}) at surface, $x = 0$ or S_1	100 °C
Convection at all other surfaces	$-k \frac{\partial T}{\partial n^i} = h(T - T_\infty)$ where $n^i = x, y, z$ and $i = 2, 3 \dots 11$

Table 6.45 Comparison of EFG results obtained using 63 nodes with FEM results at the location ($x = 0.2$ m, $y = 0.4$ m & $z = 0.4$ m) of the 3-D model shown in Fig. 6.16

Weight function	EFG				FEM
	$d_{max} = 1.01$		$d_{max} = 1.51$		
	T (°C)	% diff with FEM	T (°C)	% diff with FEM	T (°C)
C. S.	72.0836	0.0333	71.8689	0.3310	72.1076
Q. S.	72.0783	0.0406	71.9337	0.2412	
Gaussian	72.0868	0.0288	71.6962	0.5705	
Quadratic	72.0736	0.0472	72.1119	-0.0059	
Hyperbolic	72.0802	0.0380	85.2667	-18.2493	
Exponential	72.0791	0.0395	72.1576	-0.0693	
Rational	72.0952	0.0172	72.6504	-0.7528	
Cosine	72.0727	0.0484	70.5069	2.2199	

Table 6.46 Comparison of EFG results obtained using 325 nodes with FEM results at the location ($x = 0.2$ m, $y = 0.4$ m & $z = 0.4$ m) of the 3-D model shown in Fig. 6.16

Weight function	EFG				FEM
	$d_{max} = 1.01$		$d_{max} = 1.51$		
	T (°C)	% diff with FEM	T (°C)	% diff with FEM	T (°C)
C. S.	71.7094	-0.0008	71.8714	-0.2268	71.7088
Q. S.	71.7110	-0.0031	71.9562	-0.3450	
Gaussian	71.7049	0.0054	71.8008	-0.1283	
Quadratic	71.7158	-0.0098	72.0733	-0.5083	
Hyperbolic	71.7613	-0.0732	73.5531	-2.5719	
Exponential	71.7126	-0.0053	71.7939	-0.1187	
Rational	71.7240	-0.0212	72.1966	-0.6803	
Cosine	71.7151	-0.0088	70.3502	1.8946	

Table 6.47 Comparison of EFG results obtained using 63 nodes with FEM results at the location ($x = 0.2$ m, $y = 0.4$ m & $z = 0$ m) of the 3-D model shown in Fig. 6.16

Weight function	EFG				FEM
	$d_{\max} = 1.01$		$d_{\max} = 1.51$		
	T (°C)	% diff with FEM	T (°C)	% diff with FEM	T (°C)
C. S.	33.7943	3.2070	34.2717	1.8397	34.9140
Q. S.	33.7837	3.2374	34.5623	1.0073	
Gaussian	34.1829	2.0940	34.0132	2.5801	
Quadratic	33.7828	3.2340	21.9455	37.1441	
Hyperbolic	34.1522	2.1819	45.9308	-31.5541	
Exponential	33.7754	3.2612	33.9742	2.6918	
Rational	33.6915	3.5015	34.2871	1.7956	
Cosine	33.7860	3.2308	28.8124	17.4761	

Table 6.48 Comparison of EFG results obtained using 325 nodes with FEM results at the location ($x = 0.2$ m, $y = 0.4$ m & $z = 0$ m) of the 3-D model shown in Fig. 6.16

Weight function	EFG				FEM
	$d_{\max} = 1.01$		$d_{\max} = 1.51$		
	T (°C)	% diff with FEM	T (°C)	% diff with FEM	T (°C)
C. S.	33.1885	1.0952	33.2631	0.8729	33.5560
Q. S.	33.1725	1.1429	33.3597	0.5850	
Gaussian	33.2907	0.7906	33.1957	1.0737	
Quadratic	33.1463	1.2209	21.5736	35.7087	
Hyperbolic	32.9993	1.6590	31.5330	6.0287	
Exponential	33.1660	1.1622	33.2315	0.9670	
Rational	33.1269	1.2788	33.3182	0.7087	
Cosine	33.1485	1.2144	27.4954	18.0612	

Table 6.49 Comparison of EFG results obtained using 63 nodes with FEM results at the location ($x = 0.4$ m, $y = 0.4$ m & $z = 0.4$ m) of the 3-D model shown in Fig. 6.16

Weight function	EFG				FEM
	$d_{\max} = 1.01$		$d_{\max} = 1.51$		
	T (°C)	% diff with FEM	T (°C)	% diff with FEM	T (°C)
C. S.	41.4907	3.3601	41.9136	2.3751	42.9333
Q. S.	41.5103	3.3144	42.1021	1.9360	
Gaussian	41.5524	3.2164	41.6164	3.0673	
Quadratic	41.5444	3.2350	48.0177	-11.8426	
Hyperbolic	41.9466	2.2982	48.1197	-12.0801	
Exponential	41.5169	3.2991	41.6858	2.9057	
Rational	41.5493	3.2236	41.8300	2.5698	
Cosine	41.5438	3.2364	44.4286	-3.4828	

Table 6.50 Comparison of EFG results obtained using 325 nodes with FEM results at the location ($x = 0.4$ m, $y = 0.4$ m & $z = 0.4$ m) of the 3-D model shown in Fig. 6.16

Weight function	EFG				FEM
	$d_{\max} = 1.01$		$d_{\max} = 1.51$		
	T (°C)	% diff with FEM	T (°C)	% diff with FEM	T (°C)
C. S.	41.1661	1.3241	41.3411	0.9046	41.7185
Q. S.	41.1767	1.2987	41.4295	0.6927	
Gaussian	41.1220	1.4298	41.2157	1.2052	
Quadratic	41.1891	1.2690	44.1812	-5.9031	
Hyperbolic	41.2269	1.1784	40.5565	2.7853	
Exponential	41.1792	1.2927	41.2658	1.0851	
Rational	41.1881	1.2714	41.3239	0.9459	
Cosine	41.1890	1.2692	42.0819	-0.8711	

Table 6.51 Comparison of EFG results obtained using 63 nodes with FEM results at the location ($x = 0.4$ m, $y = 0.2$ m & $z = 0.2$ m) of the 3-D model shown in Fig. 6.16

Weight function	EFG				FEM
	$d_{\max} = 1.01$		$d_{\max} = 1.51$		
	T (°C)	% diff with FEM	T (°C)	% diff with FEM	T (°C)
C. S.	45.6609	-0.5357	46.7496	-2.9328	45.4176
Q. S.	45.5928	-0.3858	47.2577	-4.0515	
Gaussian	46.0974	-1.4968	46.9958	-3.4749	
Quadratic	45.5011	-0.1839	31.5409	30.5536	
Hyperbolic	45.2759	0.3120	35.7449	21.2973	
Exponential	45.5697	-0.3349	45.8703	-0.9968	
Rational	45.4678	-0.1105	47.1471	-3.8080	
Cosine	45.5063	-0.1953	42.8579	5.6359	

Table 6.52 Comparison of EFG results obtained using 325 nodes with FEM results at the location ($x = 0.4$ m, $y = 0.2$ m & $z = 0.2$ m) of the 3-D model shown in Fig. 6.16

Weight function	EFG				FEM
	$d_{\max} = 1.01$		$d_{\max} = 1.51$		
	T (°C)	% diff with FEM	T (°C)	% diff with FEM	T (°C)
C. S.	44.5655	-0.0991	44.8158	-0.6613	44.5214
Q. S.	44.5369	-0.0348	44.9590	-0.9829	
Gaussian	44.7340	-0.4775	44.8587	-0.7576	
Quadratic	44.4988	0.0508	49.3276	-10.7953	
Hyperbolic	44.3328	0.4236	44.5155	0.0133	
Exponential	44.5289	-0.0169	44.6470	-0.2821	
Rational	44.4904	0.0696	44.9660	-0.9986	
Cosine	44.5007	0.0465	45.9950	-3.3099	

Table 6.53 Effect of scaling parameter on EFG results obtained using 63 nodes at the location ($x = 0.2\text{ m}$, $y = 0.4\text{ m}$ & $z = 0.4\text{ m}$) of the 3-D model shown in Fig. 6.16

Scaling Parameter	Temperature ($^{\circ}\text{C}$)							
	C. S.	Q. S	Gaussian	Quadratic	Hyperbolic	Exponential	Rational	Cosine
1.01	72.0836	72.0783	72.0868	72.0736	72.0802	72.0791	72.0952	72.0727
1.11	72.1172	72.1053	71.8990	69.8348	72.0737	71.8370	71.9423	69.8075
1.21	72.0746	72.0223	71.8423	71.3442	71.9874	71.8574	71.9728	71.3676
1.31	71.9558	71.8747	71.7842	71.5786	71.9040	71.8879	71.9992	71.6976
1.41	71.8669	71.8014	71.7364	67.7612	81.7366	72.0845	72.5598	70.7631
1.51	71.8689	71.9337	71.6962	72.1119	85.2667	72.1576	72.6504	70.5069
1.61	72.0143	72.3138	71.6719	96.1384	88.9310	72.2367	72.7447	77.8140
1.71	72.3025	72.8348	71.6522	71.7472	108.4763	72.7322	74.2718	64.1796
1.81	72.7422	73.5082	71.6525	110.9659	113.5461	72.8836	74.4838	126.4728
1.91	73.3229	74.3232	71.6504	123.8523	117.0967	73.0393	74.7075	194.0194
2.01	73.9988	75.2152	71.5923	-5.9122	132.2401	73.1502	76.2352	56788.00

Table 6.54 Effect of scaling parameter on EFG results obtained using 325 nodes at the location ($x = 0.2\text{ m}$, $y = 0.4\text{ m}$ & $z = 0.4\text{ m}$) of the 3-D model shown in Fig. 6.16

Scaling Parameter	Temperature ($^{\circ}\text{C}$)							
	C. S.	Q. S	Gaussian	Quadratic	Hyperbolic	Exponential	Rational	Cosine
1.01	71.7094	71.7110	71.7049	71.7158	71.7613	71.7126	71.7240	71.7151
1.11	71.6776	71.6848	71.7729	69.9773	71.9140	71.7590	71.8103	70.1339
1.21	71.6985	71.7467	71.7669	71.2855	71.8871	71.7698	71.8186	71.3350
1.31	71.7770	71.7867	71.7515	71.5160	71.8585	71.7830	71.8252	71.5720
1.41	71.8050	71.8032	71.7839	68.9346	73.7391	71.7413	72.1088	70.8572
1.51	71.8714	71.9562	71.8008	72.0733	73.5531	71.7939	72.1966	70.3502
1.61	72.0005	72.1948	71.8305	73.3707	73.3255	71.8516	72.2842	74.9196
1.71	72.1792	72.4626	71.9029	71.4584	77.1060	72.1751	73.2005	70.7679
1.81	72.4393	72.8570	71.9804	70.6209	76.6513	72.2808	73.3695	73.2730
1.91	72.7785	73.3832	72.0792	70.5563	76.3056	72.3894	73.5480	69.4792
2.01	73.1900	74.0277	72.2096	67.9141	106.2116	72.5839	74.1613	70.0314

Table 6.55 Effect of scaling parameter on EFG results obtained using 63 nodes at the location ($x = 0.4$ m, $y = 0.2$ m & $z = 0.2$ m) of the 3-D model shown in Fig. 6.16

Scaling	Temperature (° C)							
Parameter	C. S.	Q. S	Gaussian	Quadratic	Hyperbolic	Exponential	Rational	Cosine
1.01	45.6609	45.5928	46.0974	45.5011	45.2759	45.5697	45.4678	45.5063
1.11	45.4525	45.4289	46.4550	47.0927	46.8207	46.1094	46.5552	47.4404
1.21	45.4993	45.6838	46.4841	47.4255	46.8319	46.1230	46.5967	47.4355
1.31	45.9182	46.2166	46.5322	47.2497	46.8153	46.1327	46.6385	47.2421
1.41	46.3220	46.6832	46.7568	47.3492	38.3795	45.8079	46.9037	47.9454
1.51	46.7496	47.2577	46.9958	31.5409	35.7449	45.8703	47.1471	42.8579
1.61	47.1825	47.7817	47.3247	1.2534	34.0330	45.9430	47.3915	28.1100
1.71	47.5881	48.1667	47.8912	-19.9416	23.8942	46.1652	48.0146	1.3652
1.81	48.0052	48.5354	48.5051	-79.5028	23.9432	46.2745	48.3188	-95.6148
1.91	48.3861	48.8230	49.2343	-47.4759	25.3097	46.3918	48.6173	-170.915
2.01	48.6942	48.9424	50.1957	-3.8032	-35.1840	46.7895	50.3369	46.0000

Table 6.56 Effect of scaling parameter on EFG results obtained using 325 nodes at the location ($x = 0.4$ m, $y = 0.2$ m & $z = 0.2$ m) of the 3-D model shown in Fig. 6.16

Scaling	Temperature (° C)							
Parameter	C. S.	Q. S	Gaussian	Quadratic	Hyperbolic	Exponential	Rational	Cosine
1.01	44.5655	44.5369	44.7340	44.4988	44.3328	44.5289	44.4904	44.5007
1.11	44.5216	44.5039	44.7922	46.1682	44.9909	44.6335	44.8169	46.0752
1.21	44.5114	44.5318	44.7932	45.5791	45.0560	44.6389	44.8370	45.5030
1.31	44.5821	44.6742	44.8034	45.4263	45.1218	44.6439	44.8569	45.3566
1.41	44.6987	44.8297	44.8308	45.1070	44.8545	44.6360	44.9268	45.9752
1.51	44.8158	44.9590	44.8587	49.3276	44.5155	44.6470	44.9660	45.9950
1.61	44.9190	45.0667	44.8879	48.9231	44.3904	44.6590	45.0076	49.6449
1.71	45.0111	45.1658	44.9090	43.7173	43.4577	44.7289	45.0892	44.4816
1.81	45.0967	45.2630	44.9116	42.5576	43.5263	44.7475	45.0979	45.0651
1.91	45.1798	45.3652	44.8813	40.3816	43.5696	44.7657	45.1013	43.4233
2.01	45.2713	45.4965	44.7976	34.3778	142.0687	44.7999	45.1803	22.1583

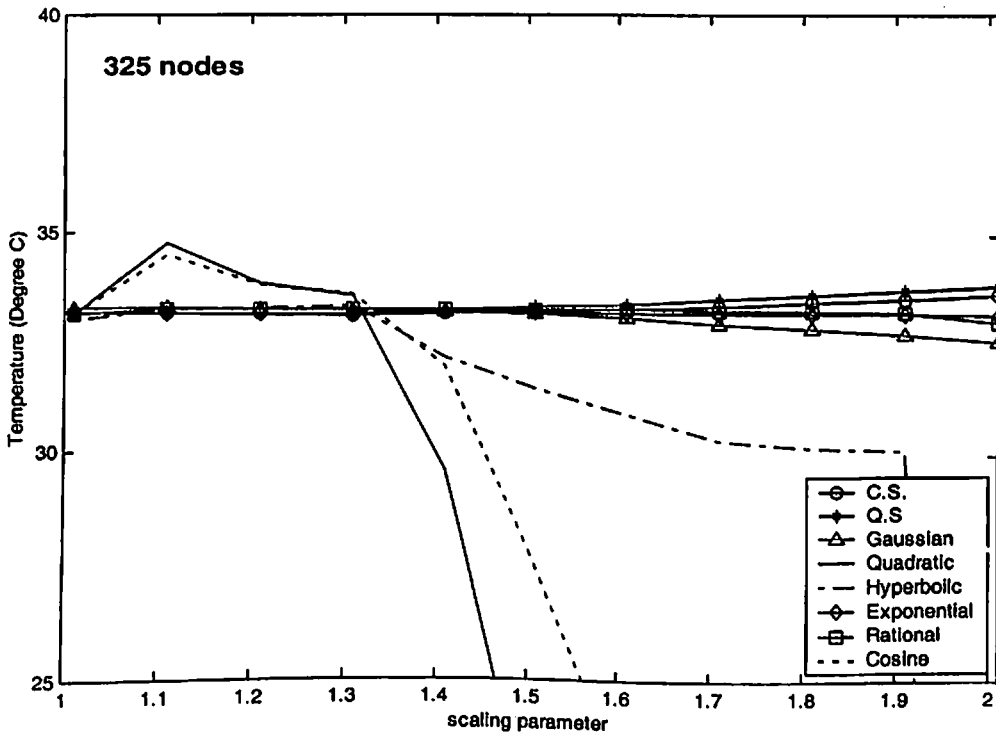
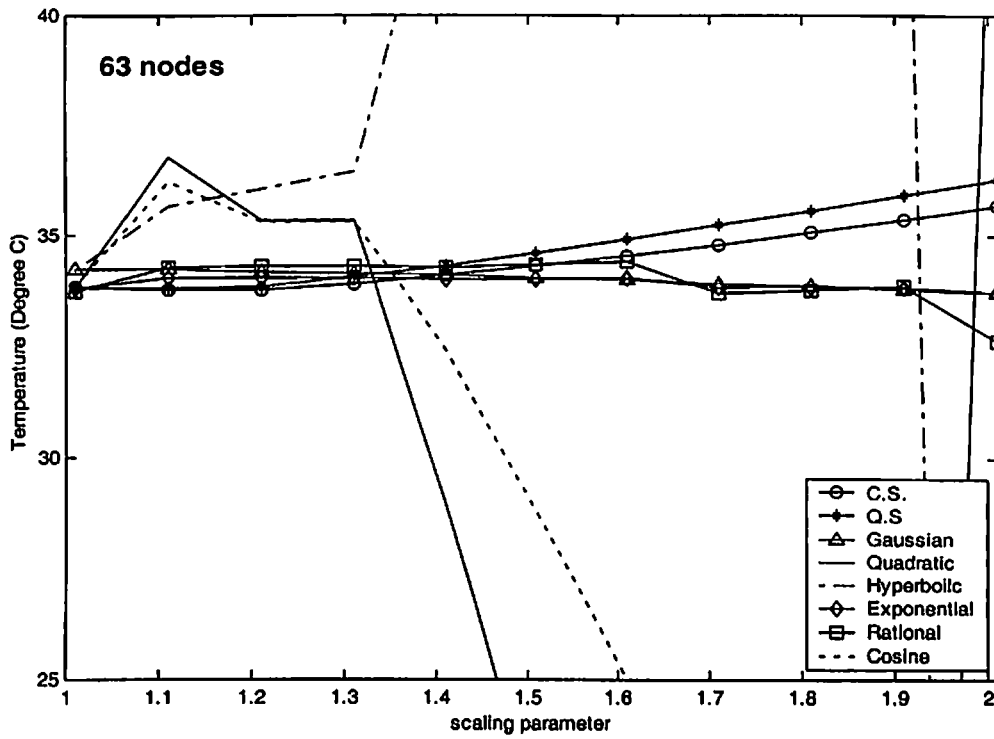


Fig. 6.17 Effect of scaling parameter on EFG results at the location ($x = 0.2$ m, $y = 0.4$ m & $z = 0$ m) of the 3-D model shown in Fig. 6.16

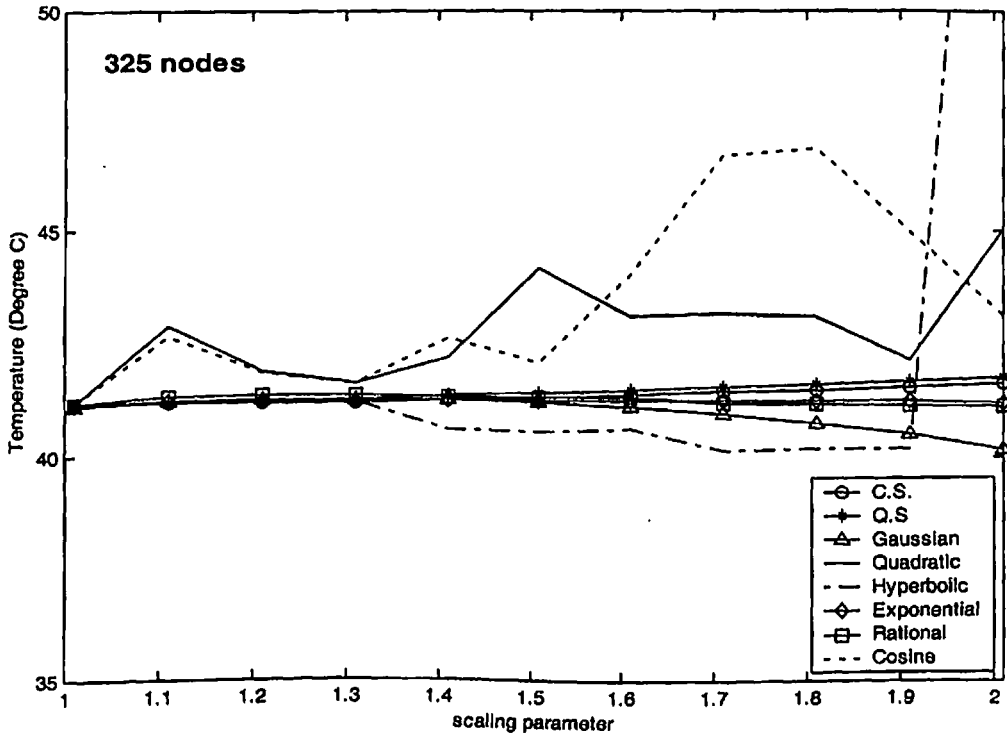
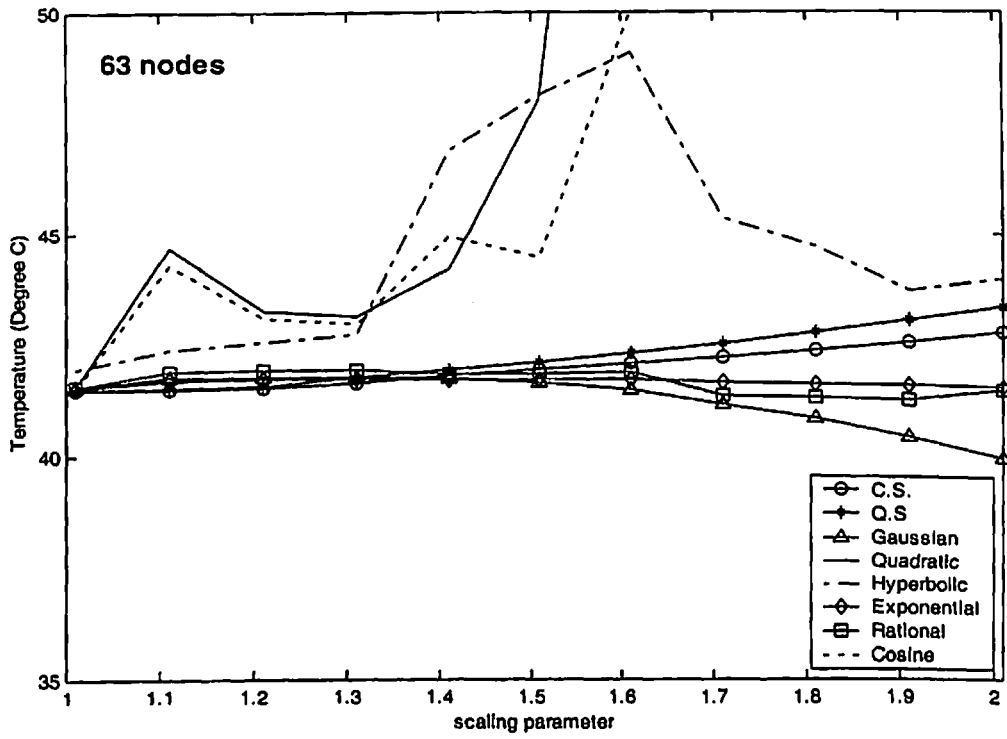


Fig. 6.18 Effect of scaling parameter on EFG results at the location ($x = 0.4\text{m}$, $y = 0.4\text{m}$ & $z = 0\text{m}$) of the 3-D model shown in Fig. 6.16

6.7.2 Transient analysis

The transient analysis of 3-D model, shown in Fig. 6.16, is carried out using different EFG weight functions. Table 6.57 and Table 6.58 show the comparison of EFG results (i.e. temperature values) obtained using 63 nodes with FEM results at the location ($x = 0.4\text{ m}$, $y = 0.4\text{ m}$ & $z = 0\text{ m}$) for $d_{\max} = 1.01$ and $d_{\max} = 1.51$ respectively. Similar comparison of temperature values obtained using 325 nodes is presented in Table 6.59 and Table 6.60 for $d_{\max} = 1.01$ and $d_{\max} = 1.51$ respectively at the same location i.e. ($x = 0.4\text{ m}$, $y = 0.4\text{ m}$ & $z = 0\text{ m}$). For this case (i.e. CASE-III) of 3-D transient analysis, time step of 100 sec has been taken which is nearly 3% of the total time required to achieve steady state condition. Table 6.61 and Table 6.62 show the comparison of EFG results (i.e. temperature values) obtained using 63 nodes with FEM results at the location ($x = 0.4\text{ m}$, $y = 0.2\text{ m}$ & $z = 0.2\text{ m}$) for $d_{\max} = 1.01$ and $d_{\max} = 1.51$ respectively. Similar comparison of temperature values obtained using 325 nodes is also presented in Table 6.63 and Table 6.64 for $d_{\max} = 1.01$ and $d_{\max} = 1.51$ respectively at the same location i.e. ($x = 0.4\text{ m}$, $y = 0.2\text{ m}$ & $z = 0.2\text{ m}$). Fig 6.19 shows the comparison of EFG results (i.e. temperature values) obtained using 63 nodes with FEM results for $d_{\max} = 1.01$ and $d_{\max} = 1.51$ at the location ($x = 0.2\text{ m}$, $y = 0.4\text{ m}$ & $z = 0\text{ m}$). Similar comparison of temperature values obtained using 325 nodes is shown in Fig. 6.20 at the same location i.e. ($x = 0.2\text{ m}$, $y = 0.4\text{ m}$ & $z = 0\text{ m}$). Fig 6.21 shows the comparison of EFG results (i.e. temperature values) obtained using 63 nodes with FEM results for $d_{\max} = 1.01$ and $d_{\max} = 1.51$ at the location ($x = 0.4\text{ m}$, $y = 0.4\text{ m}$ & $z = 0.4\text{ m}$). Similar comparison of temperature values obtained using 325 nodes is shown in Fig. 6.22 at the same location i.e. ($x = 0.4\text{ m}$, $y = 0.4\text{ m}$ & $z = 0.4\text{ m}$). From the results presented in tables and figures, it is clear that the EFG results obtained using different weight functions are almost similar for $d_{\max} = 1.01$. However for $d_{\max} = 1.51$ only cubicspline, quarticspline, Gaussian, exponential and rational weight functions give acceptable results. It has also been observed that the EFG results are in good agreement with those obtained by finite element method.

Table 6.57 Comparison of EFG results obtained using 63 nodes with FEM at the location ($x = 0.4\text{ m}$, $y = 0.4\text{ m}$ & $z = 0\text{ m}$) of the 3-D model shown in Fig. 6.16 for $d_{\max} = 1.01$

Time (sec) $\times 10^2$	Temperature ($^{\circ}\text{C}$)								
	$d_{\max} = 1.01$								FEM
	C. S.	Q. S	Gaussian	Quadratic	Hyperbolic	Exponential	Rational	Cosine	
0	0.0000	0.0000	0.0000	0.0000	0.0000	0.0000	0.0000	0.0000	0.0000
3	11.3581	11.4291	11.0039	11.5158	12.2932	11.4384	11.4940	11.5123	11.9491
6	18.8453	18.9450	18.3384	19.0620	19.8802	18.9584	19.0173	19.0597	20.1656
9	24.6494	24.7432	24.1926	24.8510	25.5574	24.7549	24.7941	24.8499	25.9313
12	28.3681	28.4561	27.9538	28.5557	29.1858	28.4663	28.4916	28.5552	29.5461
15	30.5502	30.6359	30.1542	30.7318	31.3228	30.6453	30.6632	30.7317	31.6764
18	31.7818	31.8671	31.3912	31.9619	32.5343	31.8762	31.8902	31.9619	32.8931
21	32.4645	32.5500	32.0741	32.6447	33.2087	32.5590	32.5711	32.6449	33.5768
24	32.8396	32.9255	32.4478	33.0205	33.5807	32.9345	32.9456	33.0207	33.9578
27	33.0448	33.1311	32.6514	33.2264	33.7850	33.1401	33.1507	33.2266	34.1690
30	33.1568	33.2434	32.7622	33.3389	33.8970	33.2524	33.2627	33.3392	34.2859

Table 6.58 Comparison of EFG results obtained using 63 nodes with FEM at the location ($x = 0.4\text{ m}$, $y = 0.4\text{ m}$ & $z = 0\text{ m}$) of the 3-D model shown in Fig. 6.16 for $d_{\max} = 1.51$

Time (sec) $\times 10^2$	Temperature ($^{\circ}\text{C}$)								
	$d_{\max} = 1.51$								FEM
	C. S.	Q. S	Gaussian	Quadratic	Hyperbolic	Exponential	Rational	Cosine	
0	0.0000	0.0000	0.0000	0.0000	0.0000	0.0000	0.0000	0.0000	0.0000
3	11.7154	11.8140	11.6636	1.9157	21.2359	11.5296	11.7655	6.7880	11.9491
6	19.0624	19.1428	18.8895	8.1756	28.5235	19.1201	19.4588	13.4197	20.1656
9	24.6898	24.7538	24.4590	15.2547	34.0648	24.9527	25.3789	20.0696	25.9313
12	28.3103	28.3636	28.0511	19.9632	37.6034	28.6774	29.1411	24.4354	29.5461
15	30.4499	30.4968	30.1750	22.7063	39.6548	30.8595	31.3312	26.9736	31.6764
18	31.6662	31.7095	31.3822	24.2262	40.7959	32.0898	32.5581	28.3816	32.8931
21	32.3450	32.3862	32.0556	25.0503	41.4191	32.7711	33.2335	29.1468	33.5768
24	32.7204	32.7604	32.4278	25.4927	41.7564	33.1451	33.6021	29.5588	33.9578
27	32.9270	32.9664	32.6325	25.7291	41.9384	33.3495	33.8024	29.7795	34.1690
30	33.0405	33.0795	32.7448	25.8551	42.0363	33.4611	33.9111	29.8976	34.2859

Table 6.59 Comparison of EFG results obtained using 325 nodes with FEM at the location ($x = 0.4\text{ m}$, $y = 0.4\text{ m}$ & $z = 0\text{ m}$) of the 3-D model shown in Fig. 6.16 for $d_{\max} = 1.01$

Time (sec) $\times 10^2$	Temperature ($^{\circ}\text{C}$)								
	$d_{\max} = 1.01$								FEM
	C. S.	Q. S	Gaussian	Quadratic	Hyperbolic	Exponential	Rational	Cosine	
0	0.0000	0.0000	0.0000	0.0000	0.0000	0.0000	0.0000	0.0000	0.0000
3	11.5417	11.5426	11.5220	11.5425	11.5484	11.5422	11.5413	11.5425	11.6110
6	18.4741	18.4794	18.4242	18.4824	18.4776	18.4793	18.4768	18.4826	18.8028
9	23.8821	23.8870	23.8361	23.8881	23.8604	23.8863	23.8792	23.8887	24.2370
12	27.4206	27.4254	27.3772	27.4257	27.3851	27.4244	27.4142	27.4265	27.7708
15	29.5428	29.5482	29.4978	29.5486	29.5029	29.5470	29.5353	29.5495	29.8935
18	30.7656	30.7716	30.7174	30.7725	30.7253	30.7704	30.7580	30.7735	31.1208
21	31.4566	31.4633	31.4055	31.4647	31.4174	31.4621	31.4493	31.4658	31.8170
24	31.8434	31.8506	31.7899	31.8524	31.8055	31.8495	31.8365	31.8535	32.2082
27	32.0589	32.0664	32.0037	32.0686	32.0219	32.0653	32.0522	32.0696	32.4268
30	32.1787	32.1864	32.1223	32.1887	32.1424	32.1853	32.1721	32.1898	32.5487

Table 6.60 Comparison of EFG results obtained using 325 nodes with FEM at the location ($x = 0.4\text{ m}$, $y = 0.4\text{ m}$ & $z = 0\text{ m}$) of the 3-D model shown in Fig. 6.16 for $d_{\max} = 1.51$

Time (sec) $\times 10^2$	Temperature ($^{\circ}\text{C}$)								
	$d_{\max} = 1.51$								FEM
	C. S.	Q. S	Gaussian	Quadratic	Hyperbolic	Exponential	Rational	Cosine	
0	0.0000	0.0000	0.0000	0.0000	0.0000	0.0000	0.0000	0.0000	0.0000
3	11.6378	11.6676	11.6698	2.5513	11.5387	11.5516	11.5720	6.9245	11.6110
6	18.5529	18.6015	18.5410	9.2093	18.4467	18.5226	18.5954	13.7474	18.8028
9	23.9267	23.9845	23.8870	15.4489	23.8842	23.9509	24.0634	19.7101	24.2370
12	27.4434	27.5034	27.3870	19.5794	27.4216	27.4982	27.6267	23.6356	27.7708
15	29.5548	29.6142	29.4884	22.0347	29.5237	29.6236	29.7548	25.9698	29.8935
18	30.7728	30.8307	30.7003	23.4311	30.7228	30.8472	30.9759	27.2989	31.1208
21	31.4619	31.5184	31.3858	24.2093	31.3937	31.5382	31.6632	28.0407	31.8170
24	31.8480	31.9034	31.7697	24.6387	31.7656	31.9247	32.0464	28.4505	32.2082
27	32.0633	32.1179	31.9837	24.8745	31.9706	32.1398	32.2591	28.6759	32.4268
30	32.1830	32.2371	32.1027	25.0036	32.0835	32.2593	32.3768	28.7994	32.5487

Table 6.61 Comparison of EFG results obtained using 63 nodes with FEM at the location ($x = 0.4$ m, $y = 0.2$ m & $z = 0.2$ m) of the 3-D model shown in Fig. 6.16 for $d_{max} = 1.01$

Time (sec) $\times 10^2$	Temperature ($^{\circ}$ C)								
	$d_{max} = 1.01$								FEM
	C. S.	Q. S	Gaussian	Quadratic	Hyperbolic	Exponential	Rational	Cosine	
0	0.0000	0.0000	0.0000	0.0000	0.0000	0.0000	0.0000	0.0000	0.0000
3	10.4371	10.3934	10.8258	10.3612	10.5700	10.3854	10.3632	10.3627	12.1656
6	24.5425	24.4574	25.1347	24.3647	24.3091	24.4365	24.3598	24.3683	25.0233
9	33.9709	33.8824	34.5563	33.7775	33.6119	33.8585	33.7650	33.7819	33.7831
12	39.2877	39.2036	39.8324	39.0996	38.8929	39.1795	39.0808	39.1043	38.9376
15	42.1934	42.1142	42.7023	42.0132	41.7910	42.0903	41.9897	42.0182	41.8353
18	43.7740	43.6986	44.2570	43.6004	43.3730	43.6749	43.5734	43.6055	43.4415
21	44.6337	44.5609	45.0993	44.4650	44.2364	44.5374	44.4357	44.4701	44.3280
24	45.1015	45.0306	45.5560	44.9361	44.7079	45.0072	44.9053	44.9413	44.8169
27	45.3563	45.2864	45.8036	45.1930	44.9655	45.2632	45.1612	45.1982	45.0864
30	45.4950	45.4258	45.9380	45.3330	45.1062	45.4026	45.3006	45.3383	45.2350

Table 6.62 Comparison of EFG results obtained using 63 nodes with FEM at the location ($x = 0.4$ m, $y = 0.2$ m & $z = 0.2$ m) of the 3-D model shown in Fig. 6.16 for $d_{max} = 1.51$

Time (sec) $\times 10^2$	Temperature ($^{\circ}$ C)								
	$d_{max} = 1.51$								FEM
	C. S.	Q. S	Gaussian	Quadratic	Hyperbolic	Exponential	Rational	Cosine	
0	0.0000	0.0000	0.0000	0.0000	0.0000	0.0000	0.0000	0.0000	0.0000
3	11.3799	11.6214	11.5655	-18.8831	-20.7714	10.3686	10.5941	-0.2549	12.1656
6	25.4541	25.8328	25.7475	2.0346	6.0072	24.5633	25.4157	17.4998	25.0233
9	34.8822	35.3225	35.1743	15.7827	20.0189	34.0812	35.2114	29.1943	33.7831
12	40.2415	40.7136	40.5192	23.2089	27.3673	39.4473	40.6821	35.5852	38.9376
15	43.1889	43.6778	43.4552	27.1280	31.2629	42.3782	43.6511	38.9871	41.8353
18	44.8012	45.2990	45.0598	29.1989	33.3418	43.9714	45.2561	40.7954	43.4415
21	45.6829	46.1855	45.9367	30.2965	34.4551	44.8373	46.1239	41.7582	44.3280
24	46.1655	46.6706	46.4163	30.8793	35.0522	45.3082	46.5933	42.2713	44.8169
27	46.4297	46.9362	46.6786	31.1890	35.3728	45.5644	46.8473	42.5449	45.0864
30	46.5744	47.0816	46.8222	31.3537	35.5450	45.7038	46.9848	42.6909	45.2350

Table 6.63 Comparison of EFG results obtained using 325 nodes with FEM at the location ($x = 0.4$ m, $y = 0.2$ m & $z = 0.2$ m) of the 3-D model shown in Fig. 6.16 for $d_{max} = 1.01$

Time (sec) $\times 10^2$	Temperature ($^{\circ}$ C)								
	$d_{max} = 1.01$								FEM
	C. S.	Q. S.	Gaussian	Quadratic	Hyperbolic	Exponential	Rational	Cosine	
0	0.0000	0.0000	0.0000	0.0000	0.0000	0.0000	0.0000	0.0000	0.0000
3	11.2862	11.2709	11.3824	11.2533	11.2007	11.2678	11.2557	11.2538	11.6871
6	24.3485	24.3195	24.5246	24.2848	24.1616	24.3132	24.2869	24.2860	24.4557
9	33.1671	33.1343	33.3628	33.0941	32.9410	33.1269	33.0941	33.0956	33.1296
12	38.2427	38.2099	38.4375	38.1687	38.0047	38.2020	38.1664	38.1703	38.1731
15	41.0669	41.0349	41.2558	40.9941	40.8265	41.0269	40.9900	40.9958	40.9964
18	42.6292	42.5982	42.8123	42.5580	42.3897	42.5901	42.5525	42.5598	42.5644
21	43.4934	43.4631	43.6717	43.4236	43.2554	43.4551	43.4170	43.4254	43.4345
24	43.9716	43.9419	44.1466	43.9029	43.7352	43.9339	43.8957	43.9047	43.9175
27	44.2365	44.2072	44.4091	44.1685	44.0013	44.1992	44.1608	44.1703	44.1858
30	44.3832	44.3541	44.5543	44.3157	44.1489	44.3462	44.3077	44.3175	44.3349

Table 6.64 Comparison of EFG results obtained using 325 nodes with FEM at the location ($x = 0.4$ m, $y = 0.2$ m & $z = 0.2$ m) of the 3-D model shown in Fig. 6.16 for $d_{max} = 1.51$

Time (sec) $\times 10^2$	Temperature ($^{\circ}$ C)								
	$d_{max} = 1.51$								FEM
	C. S.	Q. S.	Gaussian	Quadratic	Hyperbolic	Exponential	Rational	Cosine	
0	0.0000	0.0000	0.0000	0.0000	0.0000	0.0000	0.0000	0.0000	0.0000
3	11.5672	11.6624	11.6176	15.8688	10.1515	11.2722	11.2754	12.1001	11.6871
6	24.6161	24.7477	24.6790	28.9483	23.5893	24.3791	24.5580	25.1141	24.4557
9	33.4162	33.5624	33.4759	37.8892	32.7878	33.2281	33.5056	34.2399	33.1296
12	38.4876	38.6378	38.5424	43.0357	38.0593	38.3175	38.6332	39.5189	38.1731
15	41.3119	41.4620	41.3626	45.8839	40.9728	41.1472	41.4749	42.4459	40.9964
18	42.8753	43.0240	42.9232	47.4453	42.5722	42.7115	43.0411	44.0527	42.5644
21	43.7407	43.8878	43.7867	48.2992	43.4493	43.5761	43.9042	44.9325	43.4345
24	44.2199	44.3657	44.2647	48.7658	43.9304	44.0542	44.3801	45.4138	43.9175
27	44.4855	44.6304	44.5295	49.0207	44.1944	44.3188	44.6426	45.6771	44.1858
30	44.6327	44.7769	44.6762	49.1600	44.3393	44.4653	44.7875	45.8211	44.3349

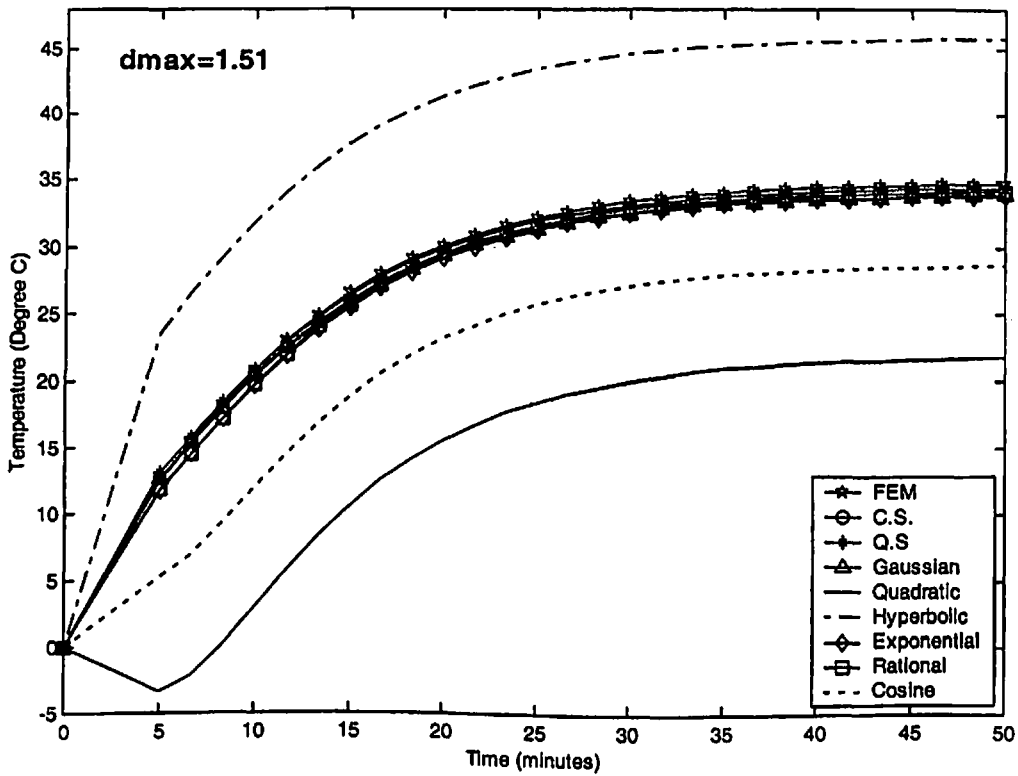
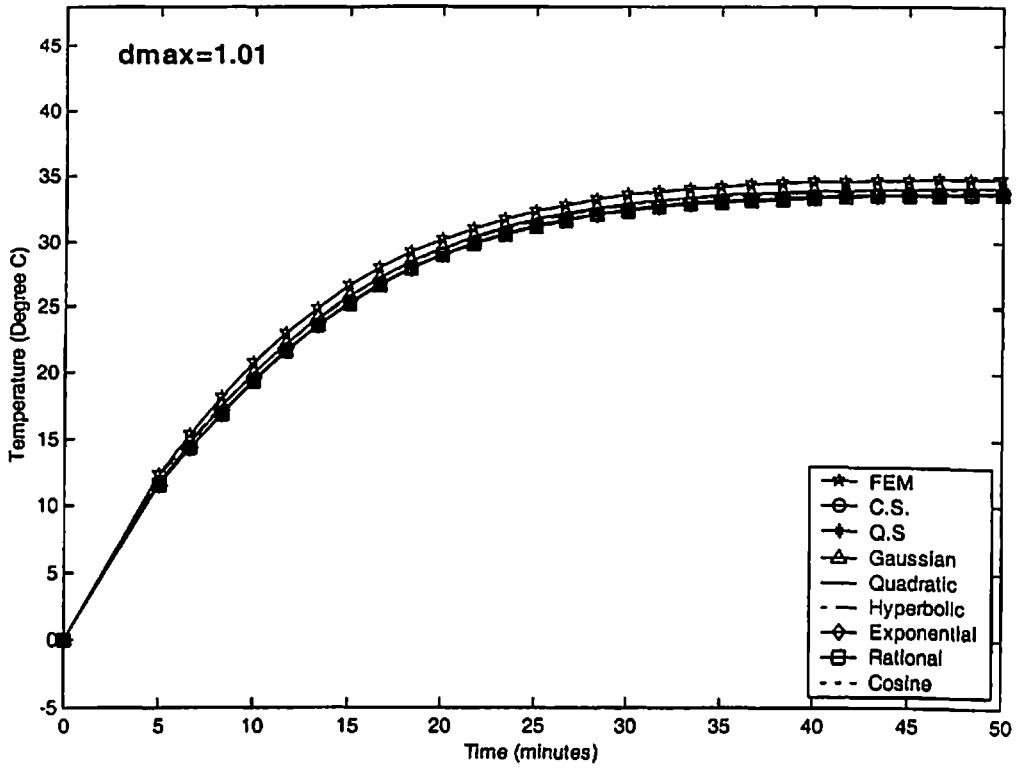


Fig. 6.19 Comparison of EFG results obtained using 63 nodes with FEM at the location ($x = 0.2$ m, $y = 0.4$ m & $z = 0$ m) of the 3-D model shown in Fig. 6.16

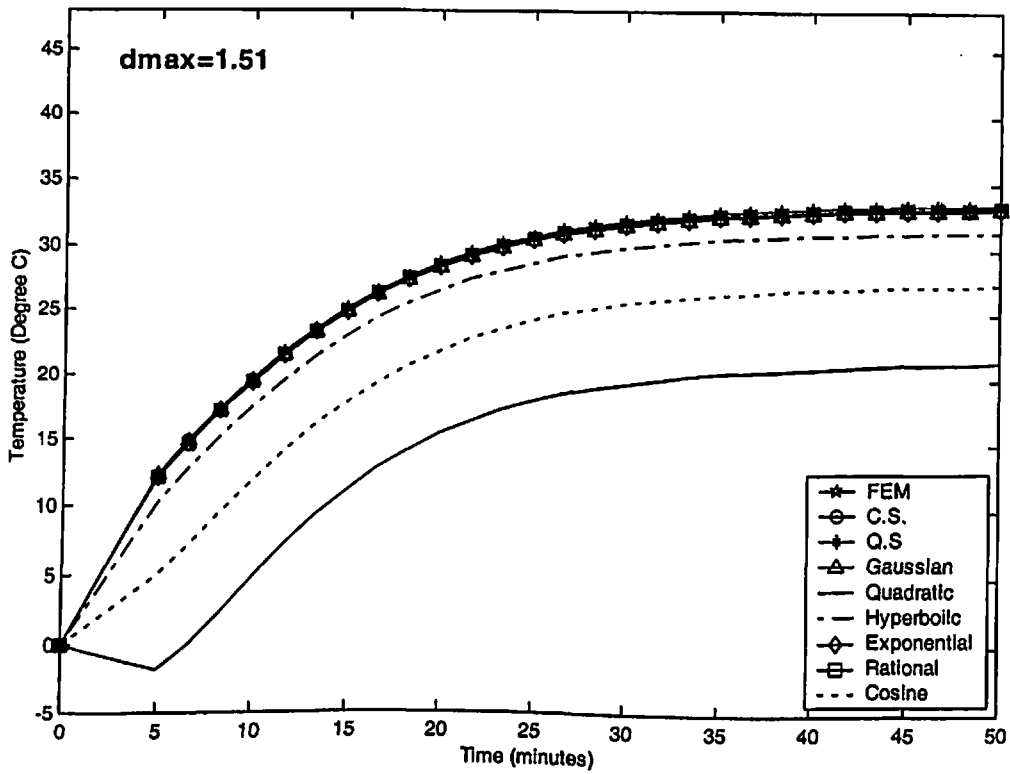
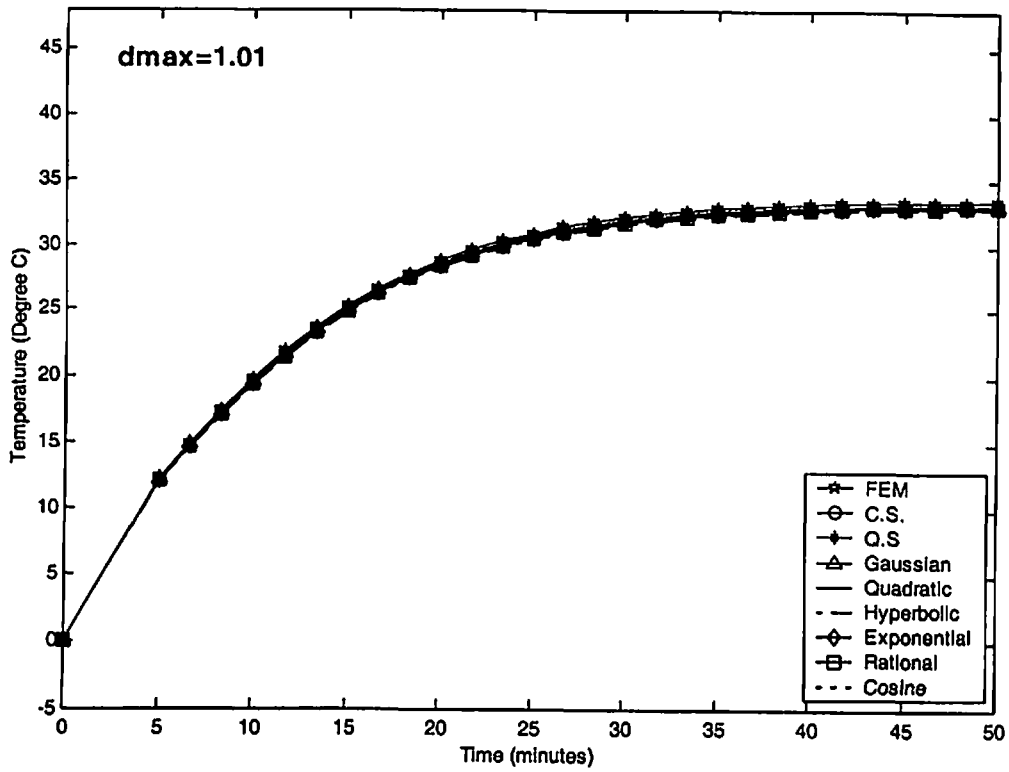


Fig. 6.20 Comparison of EFG results obtained using 325 nodes with FEM at the location ($x = 0.2$ m, $y = 0.4$ m & $z = 0$ m) of the 3-D model shown in Fig. 6.16

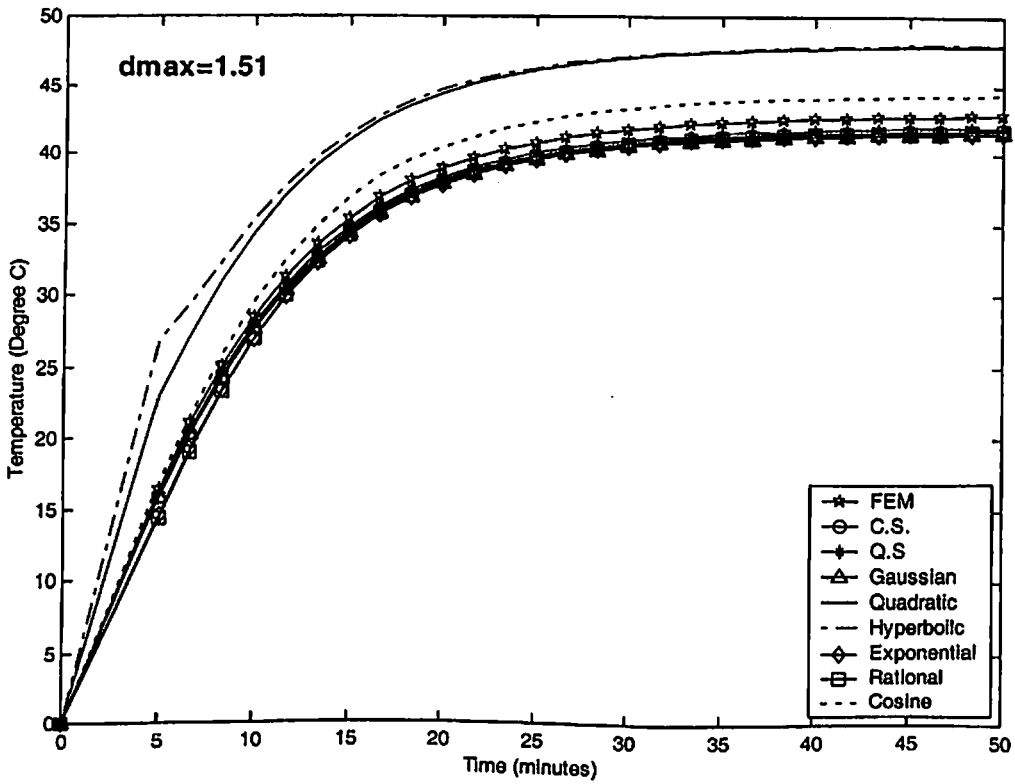
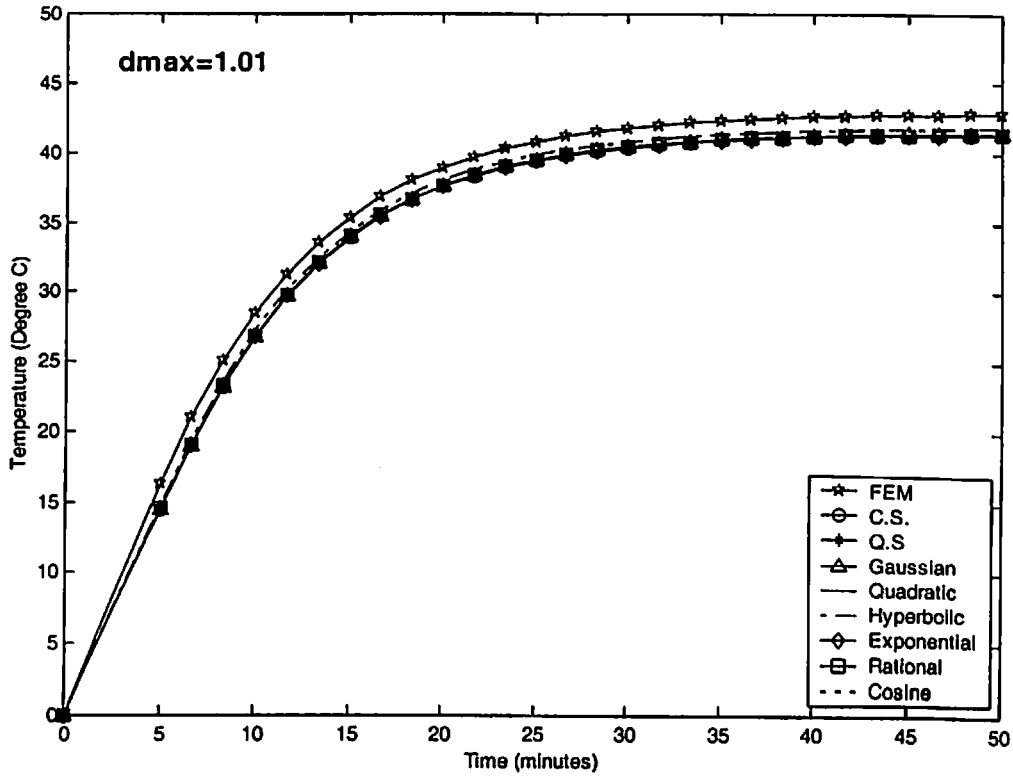


Fig. 6.21 Comparison of EFG results obtained using 63 nodes with FEM at the location ($x = 0.4$ m, $y = 0.4$ m & $z = 0.4$ m) of the 3-D model shown in Fig. 6.16

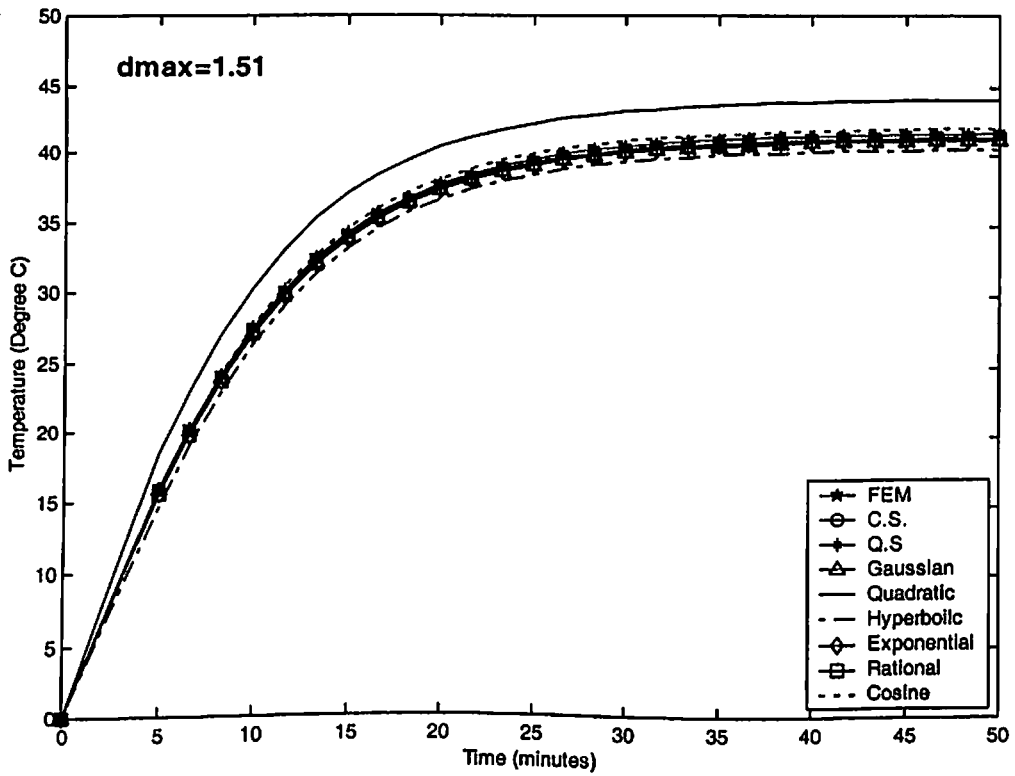
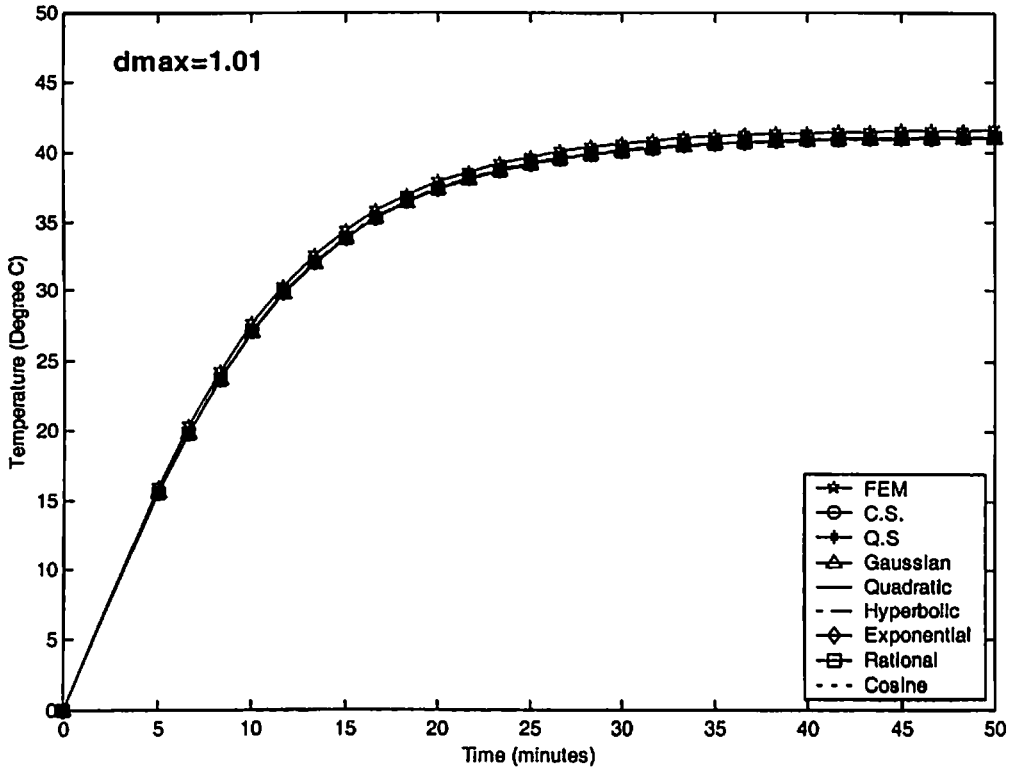


Fig. 6.22 Comparison of EFG results obtained using 325 nodes with FEM at the location ($x = 0.4$ m, $y = 0.4$ m & $z = 0.4$ m) of the 3-D model shown in Fig. 6.16

➤ **CASE-IV**

6.8 DISCRETIZATION OF THE GOVERNING EQUATION

A general form of energy equation for three-dimensional heat transfer in the cylindrical coordinate system with thermal properties independent of temperature is given as:

$$k_r \frac{\partial^2 T}{\partial r^2} + \frac{k_r}{r} \frac{\partial T}{\partial r} + \frac{k_\theta}{r^2} \frac{\partial^2 T}{\partial \theta^2} + k_z \frac{\partial^2 T}{\partial z^2} + \dot{Q} = \rho c \frac{\partial T}{\partial t} \quad (6.32)$$

The above equation can be written as:

$$\frac{1}{r} \frac{\partial}{\partial r} \left(k_r r \frac{\partial T}{\partial r} \right) + \frac{\partial}{\partial \theta} \left(\frac{k_\theta}{r^2} \frac{\partial T}{\partial \theta} \right) + \frac{\partial}{\partial z} \left(k_z \frac{\partial T}{\partial z} \right) + \dot{Q} = \rho c \frac{\partial T}{\partial t} \quad (6.33a)$$

The initial conditions are:

$$\text{at the time } t = 0 \quad T = T_{in} \quad \text{on } V \quad (6.33b)$$

The essential boundary conditions are:

$$\text{at the surface of material 1 } r = r_i \text{ or } S_i \quad T = T_{s_i} \quad (6.33c)$$

The natural boundary conditions are:

$$\text{at the outer surface of material 2, } r = r_o \text{ or } S_o \quad q_n = -hr(T - T_\infty) \quad (6.33d)$$

$$\text{at the left surface of material 1, } z = 0 \text{ or } S_{1L} \quad q_n = hr(T - T_\infty) \quad (6.33e)$$

$$\text{at the left surface of material 2, } z = 0 \text{ or } S_{2L} \quad q_n = hr(T - T_\infty) \quad (6.33f)$$

$$\text{at the right surface of material 1, } z = L \text{ or } S_{1R} \quad q_n = 0 \quad (6.33g)$$

$$\text{at the right surface of material 2, } z = L \text{ or } S_{2R} \quad q_n = 0 \quad (6.33h)$$

The weighted integral form of Eq. (6.33a) is given as:

$$\int_V w \left[\frac{1}{r} \frac{\partial}{\partial r} \left(k_r r \frac{\partial T}{\partial r} \right) + \frac{\partial}{\partial \theta} \left(\frac{k_\theta}{r^2} \frac{\partial T}{\partial \theta} \right) + \frac{\partial}{\partial z} \left(k_z \frac{\partial T}{\partial z} \right) + \dot{Q} - \rho c \frac{\partial T}{\partial t} \right] r dr d\theta dz = 0 \quad (6.34)$$

Using divergence theorem to obtain the weak form of Eq. (6.34)

$$\begin{aligned}
& \int_{V_1} \left[\left(k_{1r} \frac{\partial w}{\partial r} \frac{\partial T}{\partial r} + \frac{k_{1\theta}}{r^2} \frac{\partial w}{\partial \theta} \frac{\partial T}{\partial \theta} + k_{1z} \frac{\partial w}{\partial z} \frac{\partial T}{\partial z} \right) - \dot{Q}_1 w + \rho_1 c_1 w \frac{\partial T}{\partial t} \right] r dr d\theta dz + \\
& \int_{V_2} \left[\left(k_{2r} \frac{\partial w}{\partial r} \frac{\partial T}{\partial r} + \frac{k_{2\theta}}{r^2} \frac{\partial w}{\partial \theta} \frac{\partial T}{\partial \theta} + k_{2z} \frac{\partial w}{\partial z} \frac{\partial T}{\partial z} \right) - \dot{Q}_2 w + \rho_2 c_2 w \frac{\partial T}{\partial t} \right] r dr d\theta dz - \\
& \int_S w q_n dS = 0
\end{aligned} \tag{6.35}$$

$$\text{where } q_n = r \left[k_r \frac{\partial T}{\partial r} n_{r,i} + \frac{k_\theta}{r^2} \frac{\partial T}{\partial \theta} n_{\theta,j} + k_z \frac{\partial T}{\partial z} n_{z,k} \right]$$

Introducing natural boundary conditions in Eq. (6.35), the weak form becomes

$$\begin{aligned}
& \int_{V_1} \left[\left(k_{1r} \frac{\partial w}{\partial r} \frac{\partial T}{\partial r} + \frac{k_{1\theta}}{r^2} \frac{\partial w}{\partial \theta} \frac{\partial T}{\partial \theta} + k_{1z} \frac{\partial w}{\partial z} \frac{\partial T}{\partial z} \right) - \dot{Q}_1 w + \rho_1 c_1 w \frac{\partial T}{\partial t} \right] r dr d\theta dz + \\
& \int_{V_2} \left[\left(k_{2r} \frac{\partial w}{\partial r} \frac{\partial T}{\partial r} + \frac{k_{2\theta}}{r^2} \frac{\partial w}{\partial \theta} \frac{\partial T}{\partial \theta} + k_{2z} \frac{\partial w}{\partial z} \frac{\partial T}{\partial z} \right) - \dot{Q}_2 w + \rho_2 c_2 w \frac{\partial T}{\partial t} \right] r dr d\theta dz + \\
& \int_{S_{1L}} whr(T - T_\infty) dS + \int_{S_{2L}} whr(T - T_\infty) dS + \int_{S_o} whr(T - T_\infty) dS = 0
\end{aligned} \tag{6.36}$$

The functional $I(T)$ can be written as:

$$\begin{aligned}
I(T) = & \int_{V_1} \frac{1}{2} \left[k_{1r} \left(\frac{\partial T}{\partial r} \right)^2 + \frac{k_{1\theta}}{r^2} \left(\frac{\partial T}{\partial \theta} \right)^2 + k_{1z} \left(\frac{\partial T}{\partial z} \right)^2 \right] r dr d\theta dz - \int_{V_1} \dot{Q}_1 T r dr d\theta dz + \\
& \int_{V_2} \frac{1}{2} \left[k_{2r} \left(\frac{\partial T}{\partial r} \right)^2 + \frac{k_{2\theta}}{r^2} \left(\frac{\partial T}{\partial \theta} \right)^2 + k_{2z} \left(\frac{\partial T}{\partial z} \right)^2 \right] r dr d\theta dz - \int_{V_2} \dot{Q}_2 T r dr d\theta dz + \\
& \int_{V_1} \rho_1 c_1 \dot{T} T r dr d\theta dz + \int_{V_2} \rho_2 c_2 \dot{T} T r dr d\theta dz + \int_{S_{1L}} \frac{hr T^2}{2} dS + \int_{S_{2L}} \frac{hr T^2}{2} dS + \\
& \int_{S_o} \frac{hr T^2}{2} dS - \int_{S_{1L}} hr T T_\infty dS - \int_{S_{2L}} hr T T_\infty dS - \int_{S_o} hr T T_\infty dS
\end{aligned} \tag{6.37}$$

Enforcing essential boundary conditions using Lagrange multiplier method, the functional

$I'(T)$ is obtained as:

$$\begin{aligned}
I^*(T) = & \int_{V_1} \frac{1}{2} \left[k_{1r} \left(\frac{\partial T}{\partial r} \right)^2 + \frac{k_{1\theta}}{r^2} \left(\frac{\partial T}{\partial \theta} \right)^2 + k_{1z} \left(\frac{\partial T}{\partial z} \right)^2 \right] r dr d\theta dz - \int_{V_1} \dot{Q}_1 T r dr d\theta dz + \\
& \int_{V_2} \frac{1}{2} \left[k_{2r} \left(\frac{\partial T}{\partial r} \right)^2 + \frac{k_{2\theta}}{r^2} \left(\frac{\partial T}{\partial \theta} \right)^2 + k_{2z} \left(\frac{\partial T}{\partial z} \right)^2 \right] r dr d\theta dz - \int_{V_2} \dot{Q}_2 T r dr d\theta dz + \\
& \int_{V_1} \rho_1 c_1 \dot{T} T r dr d\theta dz + \int_{V_2} \rho_2 c_2 \dot{T} T r dr d\theta dz + \int_{S_{iL}} \frac{hrT^2}{2} dS + \int_{S_{iL}} \frac{hrT^2}{2} dS + \\
& \int_{S_o} \frac{hrT^2}{2} dS - \int_{S_{iL}} hrTT_\infty dS - \int_{S_{iL}} hrTT_\infty dS - \int_{S_o} hrTT_\infty dS + \int_{S_i} \lambda(T - T_{S_i}) dS
\end{aligned} \tag{6.38}$$

Using variational principle to obtain the discrete equations:

$$\begin{aligned}
\delta I^*(T) = & \int_{V_1} \left[k_{1r} \left(\frac{\partial T}{\partial r} \right)^T \delta \left(\frac{\partial T}{\partial r} \right) + \frac{k_{1\theta}}{r^2} \left(\frac{\partial T}{\partial \theta} \right)^T \delta \left(\frac{\partial T}{\partial \theta} \right) + k_{1z} \left(\frac{\partial T}{\partial z} \right)^T \delta \left(\frac{\partial T}{\partial z} \right) \right] r dr d\theta dz + \\
& \int_{V_2} \left[k_{2r} \left(\frac{\partial T}{\partial r} \right)^T \delta \left(\frac{\partial T}{\partial r} \right) + \frac{k_{2\theta}}{r^2} \left(\frac{\partial T}{\partial \theta} \right)^T \delta \left(\frac{\partial T}{\partial \theta} \right) + k_{2z} \left(\frac{\partial T}{\partial z} \right)^T \delta \left(\frac{\partial T}{\partial z} \right) \right] r dr d\theta dz + \\
& \int_{V_1} \rho_1 c_1 \dot{T} \delta T r dr d\theta dz + \int_{V_2} \rho_2 c_2 \dot{T} \delta T r dr d\theta dz - \int_{V_1} \dot{Q}_1 \delta T r dr d\theta dz - \\
& \int_{V_2} \dot{Q}_2 \delta T r dr d\theta dz + \int_{S_{iL}} hrT^T \delta T dS + \int_{S_{iL}} hrT^T \delta T dS + \int_{S_o} hrT^T \delta T dS - \\
& \int_{S_{iL}} hrT_\infty \delta T dS - \int_{S_{iL}} hrT_\infty \delta T dS - \int_{S_o} hrT_\infty \delta T dS + \int_{S_i} \lambda \delta T dS + \int_{S_i} \delta \lambda (T - T_{S_i}) dS
\end{aligned} \tag{6.39}$$

since δT and $\delta \lambda$ are arbitrary in the preceding equation, the following set of equations is obtained using Eq. (3.25) and Eq. (6.39)

$$[\mathbf{K}]\{\mathbf{T}\} + [\mathbf{C}]\{\dot{\mathbf{T}}\} + [\mathbf{G}]\{\lambda\} = \{\mathbf{f}\} \tag{6.40a}$$

$$[\mathbf{G}^T]\{\mathbf{T}\} = \{\mathbf{q}\} \tag{6.40b}$$

where

$$\begin{aligned}
K_{IJ} = & \int_{V_1} \begin{bmatrix} \Phi_{I,r} \\ \Phi_{I,\theta} \\ \Phi_{I,z} \end{bmatrix}^T \begin{bmatrix} k_{1r} & 0 & 0 \\ 0 & \frac{k_{1\theta}}{r^2} & 0 \\ 0 & 0 & k_{1z} \end{bmatrix} \begin{bmatrix} \Phi_{I,r} \\ \Phi_{I,\theta} \\ \Phi_{I,z} \end{bmatrix} r dr d\theta dz + \\
& \int_{V_2} \begin{bmatrix} \Phi_{I,r} \\ \Phi_{I,\theta} \\ \Phi_{I,z} \end{bmatrix}^T \begin{bmatrix} k_{2r} & 0 & 0 \\ 0 & \frac{k_{2\theta}}{r^2} & 0 \\ 0 & 0 & k_{2z} \end{bmatrix} \begin{bmatrix} \Phi_{I,r} \\ \Phi_{I,\theta} \\ \Phi_{I,z} \end{bmatrix} r dr d\theta dz + \\
& \int_{S_{1L}} hr \Phi_I^T \Phi_J dS + \int_{S_{2L}} hr \Phi_I^T \Phi_J dS + \int_{S_o} hr \Phi_I^T \Phi_J dS +
\end{aligned} \tag{6.41a}$$

$$C_{IJ} = \int_{V_1} \rho_1 c_1 \Phi_I^T \Phi_J r dr d\theta dz + \int_{V_2} \rho_2 c_2 \Phi_I^T \Phi_J r dr d\theta dz \tag{6.41b}$$

$$\begin{aligned}
f_I = & \int_{V_1} \dot{Q}_1 \Phi_I r dr d\theta dz + \int_{V_2} \dot{Q}_2 \Phi_I r dr d\theta dz + \int_{S_{1L}} hr T_\infty \Phi_I dS + \\
& \int_{S_{2L}} hr T_\infty \Phi_I dS + \int_{S_o} hr T_\infty \Phi_I dS
\end{aligned} \tag{6.41c}$$

$$G_{IK} = \int_S \Phi_I N_K dS \tag{6.41d}$$

$$q_K = \int_S T_S N_K dS \tag{6.41e}$$

Using backward difference technique for time approximation, the Eq. (6.40) can be written as

$$\left[\begin{array}{c|c} \mathbf{K}^* + \mathbf{C} & \mathbf{G} \\ \hline \mathbf{G}^T & \mathbf{0} \end{array} \right] \begin{Bmatrix} \mathbf{T}_N \\ \boldsymbol{\lambda} \end{Bmatrix} = \begin{Bmatrix} \mathbf{R}_N \\ \mathbf{q} \end{Bmatrix} \tag{6.42}$$

where

$$\mathbf{R}_N = ([\mathbf{C}] - (1 - \alpha) \Delta t [\mathbf{K}]) \{\mathbf{T}\}_{N-1} + \alpha \Delta t \{\mathbf{f}\}_N + (1 - \alpha) \Delta t \{\mathbf{f}\}_{N-1} \tag{6.43a}$$

$$\mathbf{K}^* = \alpha \Delta t [\mathbf{K}] \tag{6.43b}$$

6.9 NUMERICAL RESULTS AND DISCUSSION

The different parameters used for three-dimensional steady-state and transient analysis of the composite cylinder model shown in Fig. 6.23 are tabulated in Table 6.65. The EFG results

(temperature values) are obtained using different weight functions for two sets of nodes and the FEM results are obtained using 8 node brick elements (SOLID 70, ANSYS 6.0) for same sets of nodes. A comparative study is carried out to evaluate the performance of different EFG weight functions.

6.9.1 Steady-state analysis

The results (i.e. temperature values) presented in Table 6.66 are obtained using different EFG weight functions for two values of scaling parameter (i.e. $d_{\max} = 1.01$ & $d_{\max} = 1.51$) at the location ($r = 0.5$ m, $\theta = 0$ m & $z = 0$ m) and it shows a comparison of temperature values obtained by EFG method using different weight functions with FEM for 72 nodes. Table 6.67 shows a comparison of temperature values obtained by EFG method using different functions for two values of scaling parameter with FEM at the same location i.e. ($r = 0.5$ m, $\theta = 0$ m & $z = 0$ m) for 216 nodes. A comparison of temperature values obtained using different EFG weight functions with FEM for 72 and 216 nodes, is shown in Table 6.68 and Table 6.69 respectively at the location ($r = 0.5$ m, $\theta = 0$ m & $z = 0.25$ m). Similar type of comparisons of temperature values are shown in Table 6.70 for 72 nodes at the location ($r = 0.5$ m, $\theta = 0$ m & $z = 0.5$ m) and in Table 6.71 for 216 nodes at the same location i.e. ($r = 0.5$ m, $\theta = 0$ m & $z = 0.5$ m). From the results presented in Table 6.66 to Table 6.71, it is observed that EFG results obtained using cubicspline, quarticspline, Gaussian, exponential and rational weight functions are acceptable for $d_{\max} = 1.01$. However for $d_{\max} = 1.51$, only exponential and rational weight functions give acceptable results. It is also observed that EFG results obtained using different weight functions are in good agreement with those obtained by FEM. Moreover with the increase in number of nodes EFG results starts converging.

The effect of scaling parameter (d_{max}) on EFG results obtained using different weight functions is presented in Table 6.72 for 72 nodes and Table 6.73 for 216 nodes respectively at the location ($r = 0.5\text{ m}$, $\theta = 0\text{ m}$ & $z = 0.25\text{ m}$). Fig. 6.24 shows the effect of scaling parameter on EFG results obtained using 72 and 216 nodes at the location ($r = 0.5\text{ m}$, $\theta = 0\text{ m}$ & $z = 0\text{ m}$). Similar effect of scaling parameter on EFG results is observed in Fig. 6.25 at the location ($r = 0.5\text{ m}$, $\theta = 0\text{ m}$ & $z = 0.5\text{ m}$). From tables and figures, it is clear that only cubicspline, exponential and rational weight functions give acceptable results in the range $1.0 < d_{max} < 1.6$ whereas the results obtained using quarticspline, Gaussian, quadratic, hyperbolic and cosine weight functions acceptable in the range $1.0 < d_{max} < 1.6$. It is also observed that there is minimum variation in EFG results with scaling parameter for exponential weight function. Therefore exponential weight function gives most reliable results for this case.

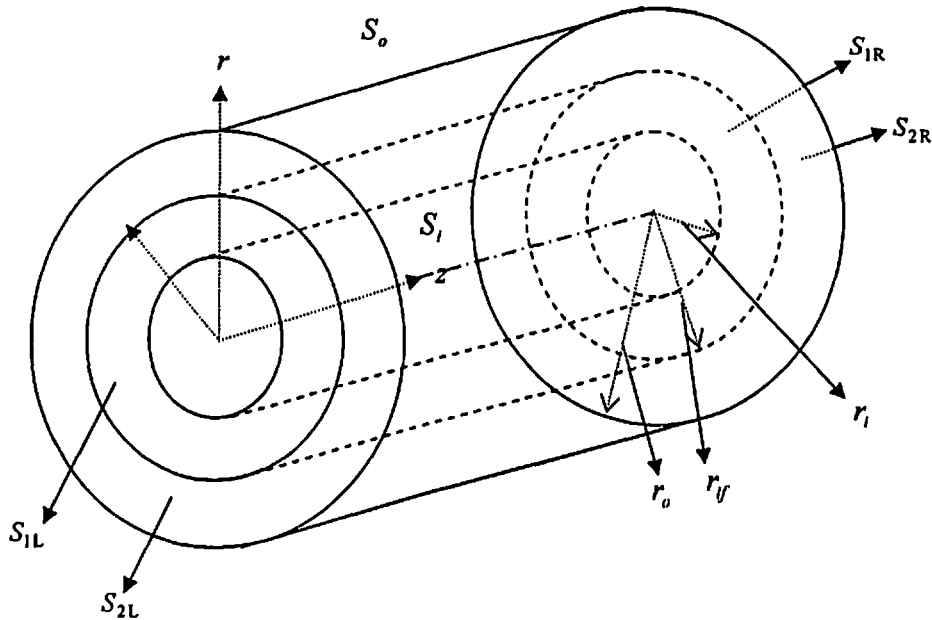


Fig. 6.23 Three-dimensional model of composite cylinder

Table 6.65 Data for the 3-D model shown in Fig. 6.23

Parameters	Value of the parameter
Inner radius (r_i)	0.1 m
Interface radius (r_f)	0.3 m
Outer radius (r_o)	0.5 m
Thermal conductivity of material 1 ($k_{1r} = k_{1\theta}$)	400 W/m-K
Thermal conductivity of material 2 ($k_{2r} = k_{2\theta}$)	100 W/m-K
Specific heat of material 1 (c_1)	400 kJ/kg-K
Specific heat of material 2 (c_2)	300 kJ/kg-K
Density of material 1 (ρ_1)	10000 kg/m ³
Density of material 2 (ρ_2)	8000 kg/m ³
Rate of internal heat generation (\dot{Q})	0 W/m ³
Heat transfer coefficient (h)	200 W/m ² -K
Initial temperature (T_{mi})	0 °C
Time step size (Δt)	100 sec
Surrounding fluid temperature (T_∞)	20 °C
Temperature T_{R1} & T_{R2} at surfaces, $z = 0$	100 °C
Convection at all other surfaces	$-k \frac{\partial T}{\partial n'} = h(T - T_\infty)$, $n' = r, \theta, z$

Table 6.66 Comparison of EFG results obtained using 72 nodes with FEM results at the location ($r = 0.5$ m, $\theta = 0$ m & $z = 0$ m) of the 3-D model shown in Fig. 6.23

Weight function	EFG				FEM
	$d_{\max} = 1.01$		$d_{\max} = 1.51$		
	T (°C)	% diff with FEM	T (°C)	% diff with FEM	T (°C)
C. S.	64.6076	2.6381	64.9271	2.1566	66.3582
Q. S.	64.6482	2.5769	65.0170	2.0212	
Gaussian	64.3586	3.0133	64.7201	2.4686	
Quadratic	64.6898	2.5142	67.9554	-2.4069	
Hyperbolic	64.5920	2.6616	61.1716	7.8161	
Exponential	64.6541	2.5680	64.9847	2.0698	
Rational	64.6840	2.5230	65.2280	1.7032	
Cosine	64.6890	2.5154	66.8392	-0.7249	

Table 6.67 Comparison of EFG results obtained using 216 nodes with FEM results at the location ($r = 0.5$ m, $\theta = 0$ m & $z = 0$ m) of the 3-D model shown in Fig. 6.23

Weight function	EFG				FEM
	$d_{\max} = 1.01$		$d_{\max} = 1.51$		
	T (°C)	% diff with FEM	T (°C)	% diff with FEM	T (°C)
C. S.	64.1964	2.8893	64.8640	1.8794	66.1064
Q. S.	64.2161	2.8595	65.0472	1.6023	
Gaussian	64.0709	3.0792	64.8488	1.9024	
Quadratic	64.2270	2.8430	66.2092	-0.1555	
Hyperbolic	64.4093	2.5672	65.6486	0.6925	
Exponential	64.2216	2.8512	64.5704	2.3235	
Rational	64.2333	2.8335	65.1671	1.4209	
Cosine	64.2296	2.8391	65.9651	0.2137	

Table 6.68 Comparison of EFG results obtained using 72 nodes with FEM results at the location ($r = 0.5$ m, $\theta = 0$ m & $z = 0.25$ m) of the 3-D model shown in Fig. 6.23

Weight function	EFG				FEM
	$d_{\max} = 1.01$		$d_{\max} = 1.51$		
	T (°C)	% diff with FEM	T (°C)	% diff with FEM	T (°C)
C. S.	63.0395	2.5744	64.3467	0.5542	64.7053
Q. S.	63.0817	2.5092	64.8116	-0.1643	
Gaussian	62.7736	2.9854	64.5396	0.2561	
Quadratic	63.1241	2.4437	64.5934	0.1729	
Hyperbolic	63.2552	2.2411	74.7160	-15.4712	
Exponential	63.0856	2.5032	63.6005	1.7074	
Rational	63.1153	2.4573	65.0589	-0.5465	
Cosine	63.1220	2.4469	65.8480	-1.7660	

Table 6.69 Comparison of EFG results obtained using 216 nodes with FEM results at the location ($r = 0.5$ m, $\theta = 0$ m & $z = 0.25$ m) of the 3-D model shown in Fig. 6.23

Weight function	EFG				FEM
	$d_{\max} = 1.01$		$d_{\max} = 1.51$		
	T (°C)	% diff with FEM	T (°C)	% diff with FEM	T (°C)
C. S.	62.3237	3.2793	63.0628	2.1323	64.4368
Q. S.	62.3397	3.2545	63.2790	1.7968	
Gaussian	62.2207	3.4392	63.0915	2.0878	
Quadratic	62.3499	3.2387	64.2886	0.2300	
Hyperbolic	62.4193	3.1310	64.2393	0.3065	
Exponential	62.3432	3.2491	62.6888	2.7127	
Rational	62.3524	3.2348	63.2371	1.8618	
Cosine	62.3510	3.2370	63.9816	0.7064	

Table 6.70 Comparison of EFG results obtained using 72 nodes with FEM results at the location ($r = 0.5$ m, $\theta = 0$ m & $z = 0.5$ m) of the 3-D model shown in Fig. 6.23

Weight function	EFG				FEM
	$d_{\max} = 1.01$		$d_{\max} = 1.51$		
	T (°C)	% diff with FEM	T (°C)	% diff with FEM	T (°C)
C. S.	52.5359	7.0118	53.0791	6.0504	56.4974
Q. S.	52.4523	7.1598	53.2978	5.6633	
Gaussian	53.0747	6.0582	52.9877	6.2121	
Quadratic	52.3677	7.3095	56.5131	-0.0278	
Hyperbolic	52.1090	7.7674	47.8728	15.2655	
Exponential	52.4452	7.1724	52.7506	6.6318	
Rational	52.3858	7.2775	52.9348	6.3058	
Cosine	52.3720	7.3019	55.4725	1.8141	

Table 6.71 Comparison of EFG results obtained using 216 nodes with FEM results at the location ($r = 0.5$ m, $\theta = 0$ m & $z = 0.5$ m) of the 3-D model shown in Fig. 6.23

Weight function	EFG				FEM
	$d_{\max} = 1.01$		$d_{\max} = 1.51$		
	T (°C)	% diff with FEM	T (°C)	% diff with FEM	T (°C)
C. S.	51.5256	6.4788	52.3453	4.9910	55.0951
Q. S.	51.4740	6.5725	52.5348	4.6471	
Gaussian	51.8752	5.8443	52.3484	4.9854	
Quadratic	51.4266	6.6585	54.0628	1.8737	
Hyperbolic	51.1872	7.0930	52.2146	5.2282	
Exponential	51.4762	6.5685	51.8169	5.9501	
Rational	51.4417	6.6311	52.2955	5.0814	
Cosine	51.4306	6.6512	53.8403	2.2775	

Table 6.72 Effect of scaling parameter on EFG results obtained using 72 nodes at the location ($r = 0.5$ m, $\theta = 0$ m & $z = 0.25$ m) of the 3-D model shown in Fig. 6.23

Scaling Parameter	Temperature (° C)							
	C. S.	Q. S	Gaussian	Quadratic	Hyperbolic	Exponential	Rational	Cosine
1.01	63.0395	63.0817	62.7736	63.1241	63.2552	63.0856	63.1153	63.1220
1.11	62.9492	62.9950	63.2817	64.4755	65.3543	63.6366	64.2328	64.7820
1.21	63.0632	63.2896	63.5009	64.9378	65.5297	63.6795	64.3015	64.9672
1.31	63.5276	63.8492	63.7392	65.0198	65.6905	63.7131	64.3720	64.9937
1.41	63.9435	64.2994	64.1175	64.2869	73.4630	63.5223	64.7919	65.5072
1.51	64.3467	64.8116	64.5396	64.5934	74.7160	63.6005	65.0589	65.8480
1.61	64.7505	65.3030	65.0692	65.8863	76.0394	63.6880	65.3379	66.8779
1.71	65.1419	65.7135	65.8541	50.5408	84.4933	63.8841	66.3478	58.1389
1.81	65.5362	66.1057	66.7527	49.0768	85.8860	64.0098	66.7944	58.3424
1.91	65.9193	66.4932	67.8460	57.6565	87.0658	64.1475	67.2722	57.9078
2.01	66.2946	66.8738	69.2016	68.6639	73.8054	64.1133	65.9016	95.5692
2.11	66.6539	67.2435	70.7760	76.7908	74.6475	64.2204	66.1593	75.6630
2.21	66.9958	67.6193	72.6211	87.9532	75.3073	64.3305	66.4199	164.4999
2.31	67.3306	68.0144	74.7670	102.4906	75.9635	64.4431	66.6843	168.8044
2.41	67.6641	68.4358	77.2452	120.7314	76.9972	64.5582	66.9540	132.6184

Table 6.73 Effect of scaling parameter on EFG results obtained using 216 nodes at the location ($r = 0.5$ m, $\theta = 0$ m & $z = 0.25$ m) of the 3-D model shown in Fig. 6.23

Scaling Parameter	Temperature (° C)							
	C. S.	Q. S	Gaussian	Quadratic	Hyperbolic	Exponential	Rational	Cosine
1.01	62.3237	62.3397	62.2207	62.3499	62.4193	62.3432	62.3524	62.3510
1.11	62.2705	62.2909	62.5879	64.2283	63.1636	62.6927	63.0305	64.2209
1.21	62.3303	62.4511	62.7089	63.7723	63.2074	62.7118	63.0580	63.7199
1.31	62.5962	62.8010	62.8244	63.5782	63.2470	62.7251	63.0828	63.5378
1.41	62.8517	63.0668	62.9654	63.8538	64.1517	62.6679	63.1671	63.7723
1.51	63.0628	63.2790	63.0915	64.2886	64.2393	62.6888	63.2371	63.9816
1.61	63.2339	63.4463	63.2184	64.8083	64.3228	62.7116	63.3077	64.4094
1.71	63.3706	63.5682	63.3422	63.8294	64.5150	62.7141	63.3625	63.9417
1.81	63.4752	63.6448	63.4642	64.0705	64.6577	62.7363	63.4320	64.3208
1.91	63.5550	63.6895	63.5811	62.8976	64.8004	62.7608	63.5007	64.6257
2.01	63.6200	63.7155	63.6526	65.2348	56.6898	62.5597	62.6279	64.1800
2.11	63.6671	63.7232	63.7351	65.8732	58.7372	62.5620	62.7108	65.7038
2.21	63.6873	63.6997	63.7891	65.8462	58.0227	62.5576	62.7020	66.4318
2.31	63.6755	63.6351	63.8076	65.3693	57.3013	62.5528	62.6880	66.4340
2.41	63.6319	63.5233	63.8060	64.6086	54.6586	62.5600	62.8313	65.1968

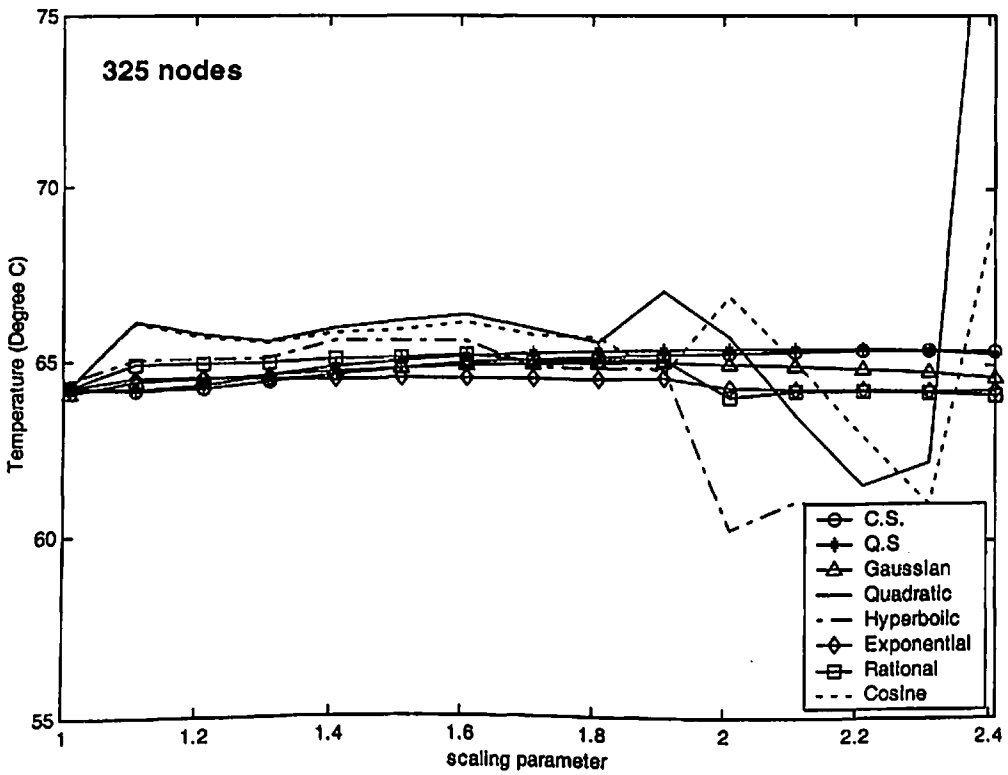
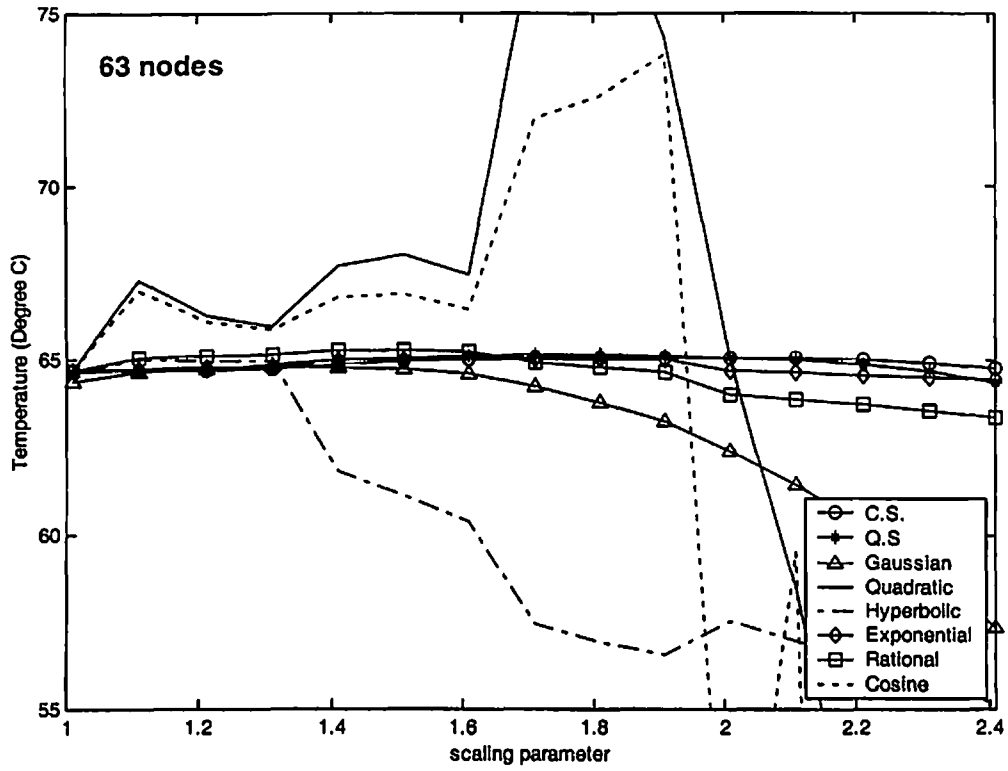


Fig. 6.24 Effect of scaling parameter on EFG results at the location ($r = 0.5 \text{ m}$, $\theta = 0 \text{ m}$ & $z = 0 \text{ m}$) of the 3-D model shown in Fig. 6.23

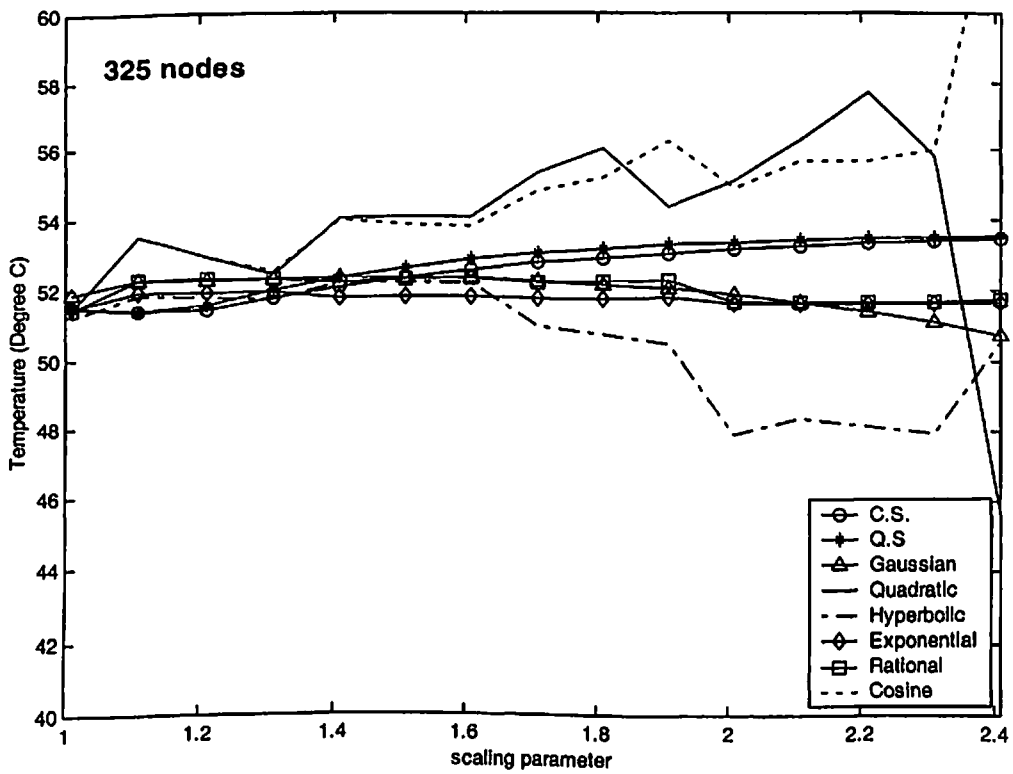
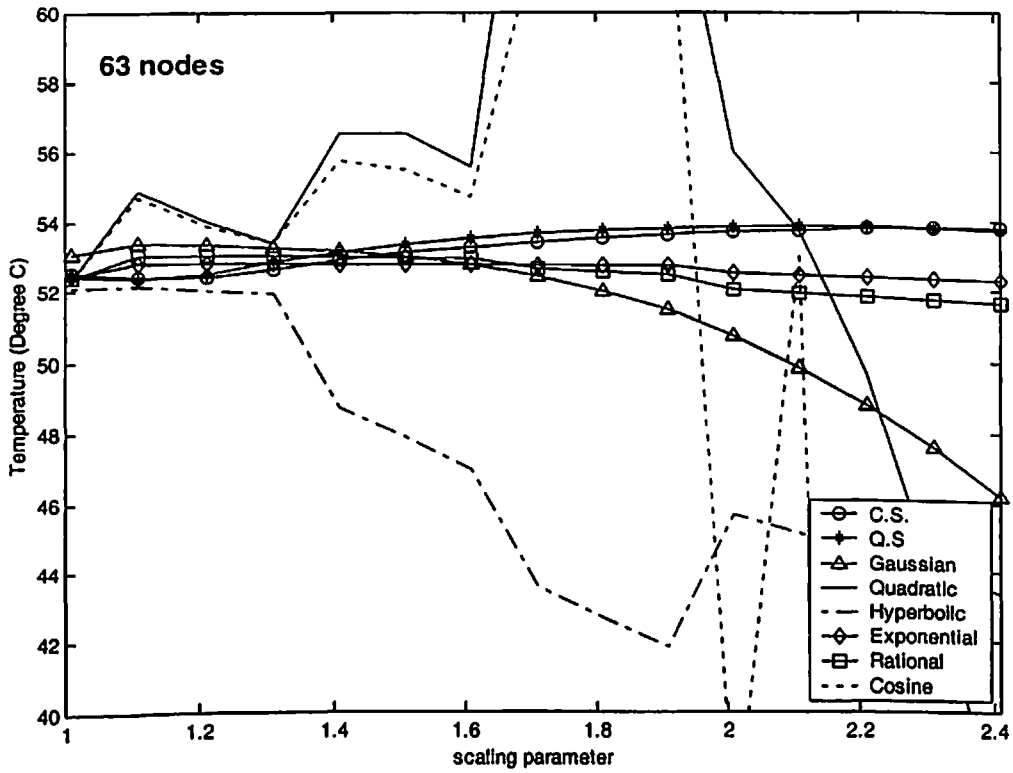


Fig. 6.25 Effect of scaling parameter on EFG results at the location ($r = 0.5 \text{ m}$, $\theta = 0 \text{ m}$ & $z = 0.5 \text{ m}$) of the 3-D model shown in Fig. 6.23

6.9.2 Transient analysis

The transient analysis of 3-D cylindrical composite model, shown in Fig. 6.23, is carried out using different EFG weight functions. Table 6.74 and Table 6.75 show the comparison of EFG results (i.e. temperature values) obtained using 72 nodes with FEM results at the location ($r = 0.5\text{ m}$, $\theta = 0\text{ m}$ & $z = 0.25\text{ m}$) for $d_{\max} = 1.01$ and $d_{\max} = 1.51$ respectively. Similar comparison of temperature values obtained using 216 nodes is presented in Table 6.76 and Table 6.77 for $d_{\max} = 1.01$ and $d_{\max} = 1.51$ respectively at the same location i.e. ($r = 0.5\text{ m}$, $\theta = 0\text{ m}$ & $z = 0.25\text{ m}$). For this case (i.e. CASE-IV) of 3-D transient analysis, time step of 100 sec has also been taken which is nearly 3% of the total time required to achieve steady state condition. Fig 6.26 shows the comparison of EFG results (i.e. temperature values) obtained using 72 nodes with FEM results for $d_{\max} = 1.01$ and $d_{\max} = 1.51$ at the location ($r = 0.2\text{ m}$, $\theta = 0\text{ m}$ & $z = 0.5\text{ m}$). Similar comparison of temperature values obtained using 216 nodes is shown in Fig. 6.27 at the same location i.e. ($r = 0.2\text{ m}$, $\theta = 0\text{ m}$ & $z = 0.5\text{ m}$). Fig 6.28 shows the comparison of EFG results (i.e. temperature values) obtained using 72 nodes with FEM results for $d_{\max} = 1.01$ and $d_{\max} = 1.51$ at the location ($r = 0.2\text{ m}$, $\theta = 0\text{ m}$ & $z = 0\text{ m}$). Similar comparison of temperature values obtained using 216 nodes is shown in Fig. 6.29 at the same location i.e. ($r = 0.2\text{ m}$, $\theta = 0\text{ m}$ & $z = 0\text{ m}$). From the results presented in tables and figures, it is clear that the EFG results obtained using different weight functions are almost similar for $d_{\max} = 1.01$. However for $d_{\max} = 1.51$ only cubicspline, quarticspline, Gaussian, exponential and rational weight functions give acceptable results. It has also been observed that the EFG results are in good agreement with those obtained by FEM.

Table 6.74 Comparison of EFG results obtained using 72 nodes with FEM at the location ($r = 0.5$ m, $\theta = 0$ m & $z = 0.25$ m) of the 3-D model shown in Fig. 6.23 for $d_{max} = 1.01$

Time (sec) $\times 10^2$	Temperature ($^{\circ}$ C)								
	$d_{max} = 1.01$								FEM
	C. S.	Q. S	Gaussian	Quadratic	Hyperbolic	Exponential	Rational	Cosine	
0	100.000	100.000	100.000	100.000	100.000	100.000	100.000	100.000	100.000
3	89.7666	89.8062	89.5282	89.8376	89.9669	89.8083	89.8246	89.8326	84.1228
6	83.1632	83.2209	82.8256	83.2822	83.5216	83.2272	83.2694	83.2791	75.7436
9	78.7431	78.8022	78.3962	78.8667	79.1242	78.8089	78.8545	78.8641	71.0728
12	75.5417	75.5980	75.2081	75.6592	75.9038	75.6044	75.6477	75.6568	68.4012
15	73.0931	73.1464	72.7743	73.2035	73.4293	73.1523	73.1926	73.2011	66.8560
18	71.1632	71.2140	70.8562	71.2678	71.4760	71.2195	71.2573	71.2655	65.9582
21	69.6192	69.6681	69.3207	69.7193	69.9127	69.6732	69.7093	69.7171	65.4356
24	68.3748	68.4224	68.0827	68.4718	68.6530	68.4273	68.4619	68.4695	65.1311
27	67.3685	67.4150	67.0809	67.4630	67.6344	67.4197	67.4534	67.4608	64.9537
30	66.5531	66.5989	66.2692	66.6458	66.8093	66.6034	66.6364	66.6436	64.8502

Table 6.75 Comparison of EFG results obtained using 72 nodes with FEM at the location ($r = 0.5$ m, $\theta = 0$ m & $z = 0.25$ m) of the 3-D model shown in Fig. 6.23 for $d_{max} = 1.51$

Time (sec) $\times 10^2$	Temperature ($^{\circ}$ C)								
	$d_{max} = 1.51$								FEM
	C. S.	Q. S	Gaussian	Quadratic	Hyperbolic	Exponential	Rational	Cosine	
0	100.000	100.000	100.000	100.000	100.000	100.000	100.000	100.000	100.000
3	90.0803	90.2906	90.0997	91.9039	93.8663	90.1077	91.1854	92.7101	84.1228
6	83.6932	84.0080	83.7531	85.9461	89.1092	83.6792	85.1117	87.0145	75.7436
9	79.4900	79.8887	79.5795	81.9755	86.1919	79.3484	80.9543	83.0933	71.0728
12	76.4977	76.9612	76.6119	78.9478	84.0288	76.1900	77.8655	80.1041	68.4012
15	74.2272	74.7372	74.3629	76.5100	82.3148	73.7591	75.4498	77.7017	66.8560
18	72.4356	72.9768	72.5891	74.5101	80.9302	71.8336	73.5153	75.7304	65.9582
21	70.9917	71.5521	71.1592	72.8573	79.8043	70.2872	71.9509	74.0992	65.4356
24	69.8151	70.3860	69.9932	71.4864	78.8858	69.0370	70.6801	72.7439	65.1311
27	68.8511	69.4260	69.0370	70.3467	78.1350	68.0232	69.6458	71.6151	64.9537
30	68.0589	68.6333	68.2504	69.3977	77.5207	67.1996	68.8029	70.6733	64.8502

Table 6.76 Comparison of EFG results obtained using 216 nodes with FEM at the location ($r = 0.5$ m, $\theta = 0$ m & $z = 0.25$ m) of the 3-D model shown in Fig. 6.23 for $d_{max} = 1.01$

Time (sec) $\times 10^2$	Temperature ($^{\circ}$ C)								
	$d_{max} = 1.01$								FEM
	C. S.	Q. S	Gaussian	Quadratic	Hyperbolic	Exponential	Rational	Cosine	
0	100.0000	100.0000	100.0000	100.0000	100.0000	100.0000	100.0000	100.0000	100.0000
3	88.4019	88.4031	88.3880	88.4017	88.3898	88.4042	88.4041	88.4026	84.0903
6	81.9961	82.0086	81.9125	82.0165	82.0651	82.0110	82.0179	82.0172	75.5218
9	77.7179	77.7348	77.6079	77.7468	77.8207	77.7384	77.7486	77.7477	70.7662
12	74.6072	74.6252	74.4915	74.6377	74.7209	74.6291	74.6398	74.6387	68.0825
15	72.2143	72.2323	72.0983	72.2447	72.3308	72.2364	72.2471	72.2458	66.5480
18	70.3218	70.3395	70.2076	70.3516	70.4376	70.3438	70.3542	70.3527	65.6631
21	68.8046	68.8221	68.6923	68.8338	68.9185	68.8263	68.8365	68.8350	65.1503
24	67.5806	67.5978	67.4697	67.6093	67.6922	67.6020	67.6120	67.6104	64.8523
27	66.5900	66.6069	66.4803	66.6183	66.6994	66.6111	66.6210	66.6194	64.6789
30	65.7871	65.8039	65.6784	65.8151	65.8944	65.8081	65.8178	65.8162	64.5779

Table 6.77 Comparison of EFG results obtained using 216 nodes with FEM at the location ($r = 0.5$ m, $\theta = 0$ m & $z = 0.25$ m) of the 3-D model shown in Fig. 6.23 for $d_{max} = 1.51$

Time (sec) $\times 10^2$	Temperature ($^{\circ}$ C)								
	$d_{max} = 1.51$								FEM
	C. S.	Q. S	Gaussian	Quadratic	Hyperbolic	Exponential	Rational	Cosine	
0	100.000	100.000	100.000	100.000	100.000	100.000	100.000	100.000	100.000
3	88.0993	88.0013	88.1114	87.1240	88.7870	88.4079	88.3092	86.4232	84.0903
6	81.7702	81.7511	81.7578	83.8603	84.0251	82.1869	82.6085	83.4127	75.5218
9	77.7099	77.7837	77.6917	79.9156	80.3148	78.0304	78.6589	79.2043	70.7662
12	74.8358	74.9878	74.8233	77.5672	77.4655	74.9895	75.7416	77.0433	68.0825
15	72.6503	72.8598	72.6489	75.2886	75.0597	72.6321	73.4080	74.7434	66.5480
18	70.9204	71.1699	70.9305	73.5189	73.1121	70.7564	71.5314	73.0616	65.6631
21	69.5225	69.7982	69.5425	71.9887	71.5079	69.2457	70.0048	71.5516	65.1503
24	68.3814	68.6733	68.4090	70.7302	70.1973	68.0224	68.7618	70.3345	64.8523
27	67.4453	67.7459	67.4784	69.6712	69.1229	67.0292	67.7482	69.2957	64.6789
30	66.6754	66.9794	66.7122	68.7891	68.2432	66.2219	66.9210	68.4351	64.5779

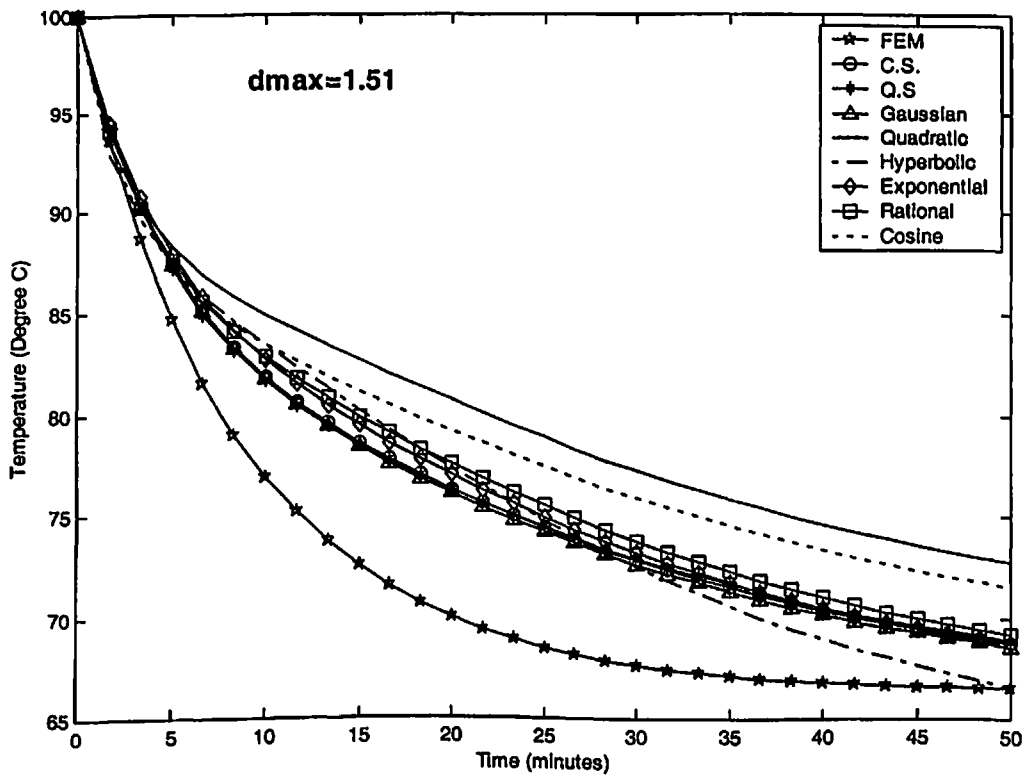
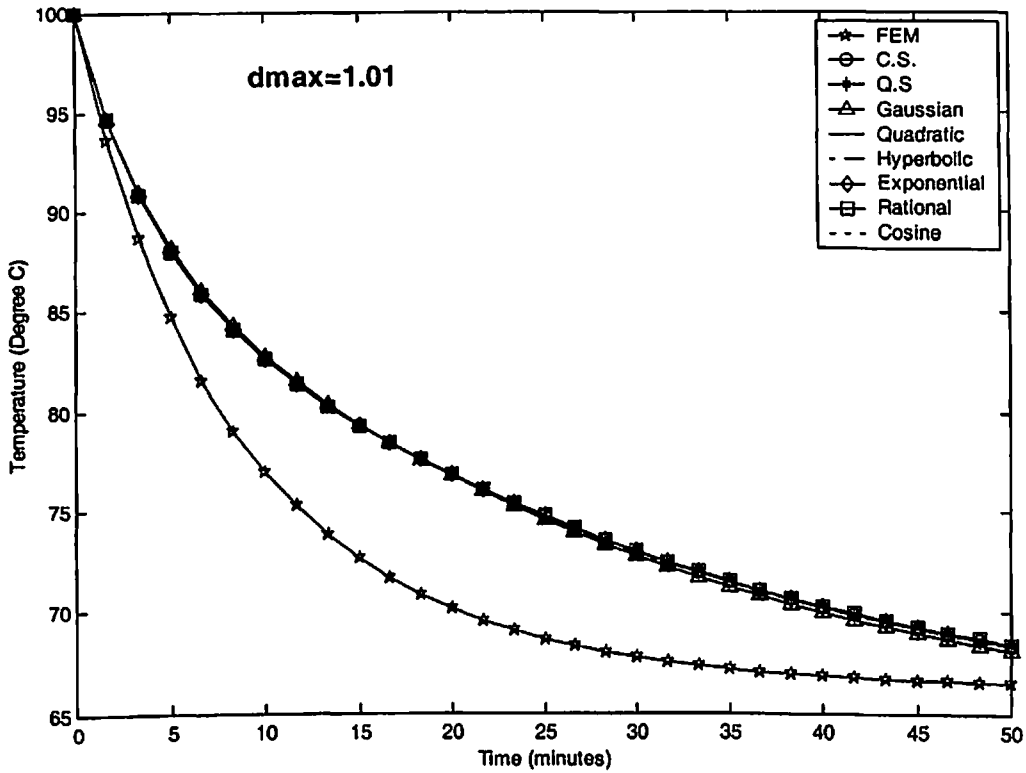


Fig. 6.26 Comparison of EFG results obtained using 72 nodes with FEM at the location ($r = 0.2$ m, $\theta = 0$ m & $z = 0.5$ m) of the 3-D model shown in Fig. 6.23

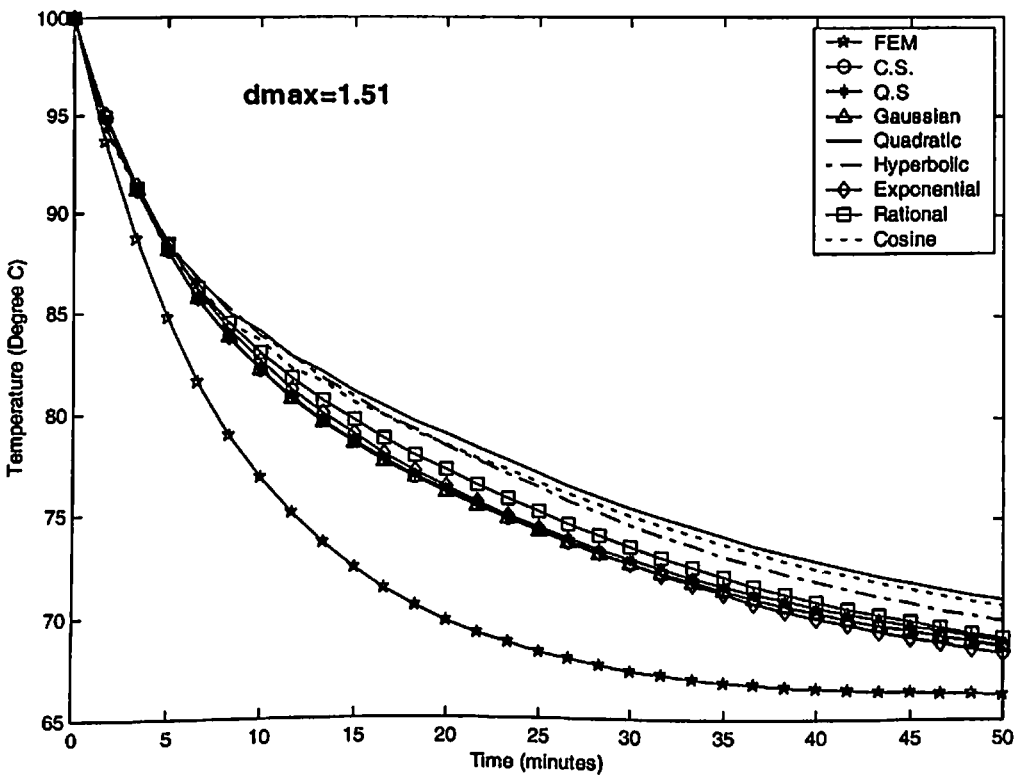
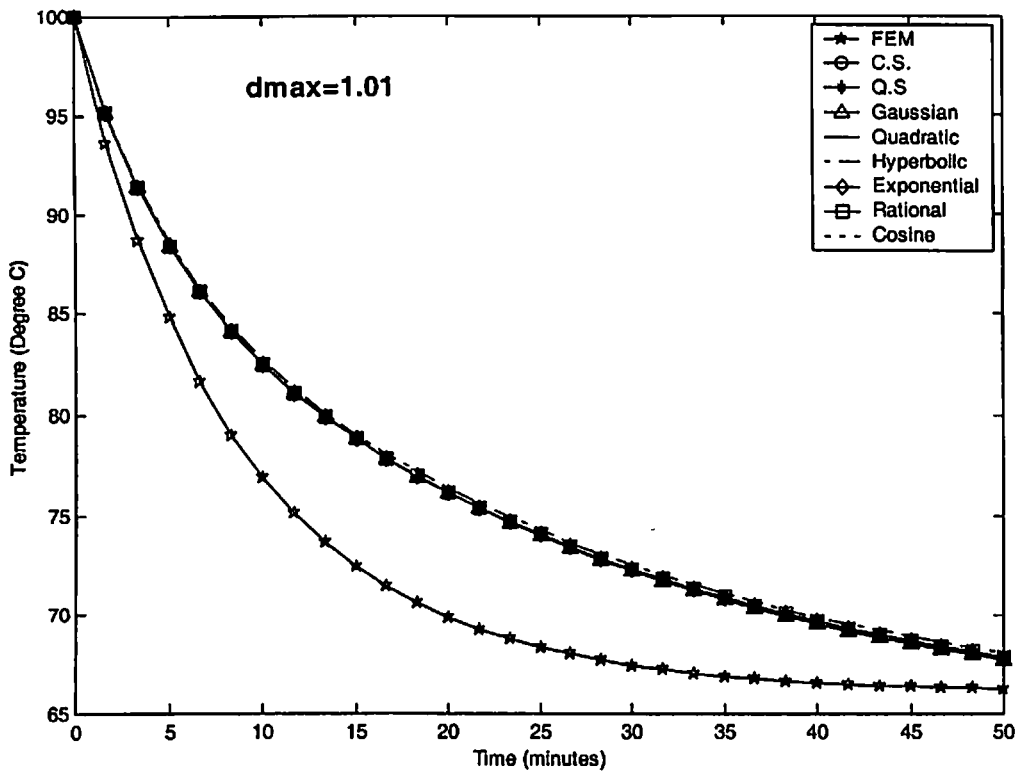


Fig. 6.27 Comparison of EFG results obtained using 216 nodes with FEM at the location ($r = 0.2$ m, $\theta = 0$ m & $z = 0.5$ m) of the 3-D model shown in Fig. 6.23

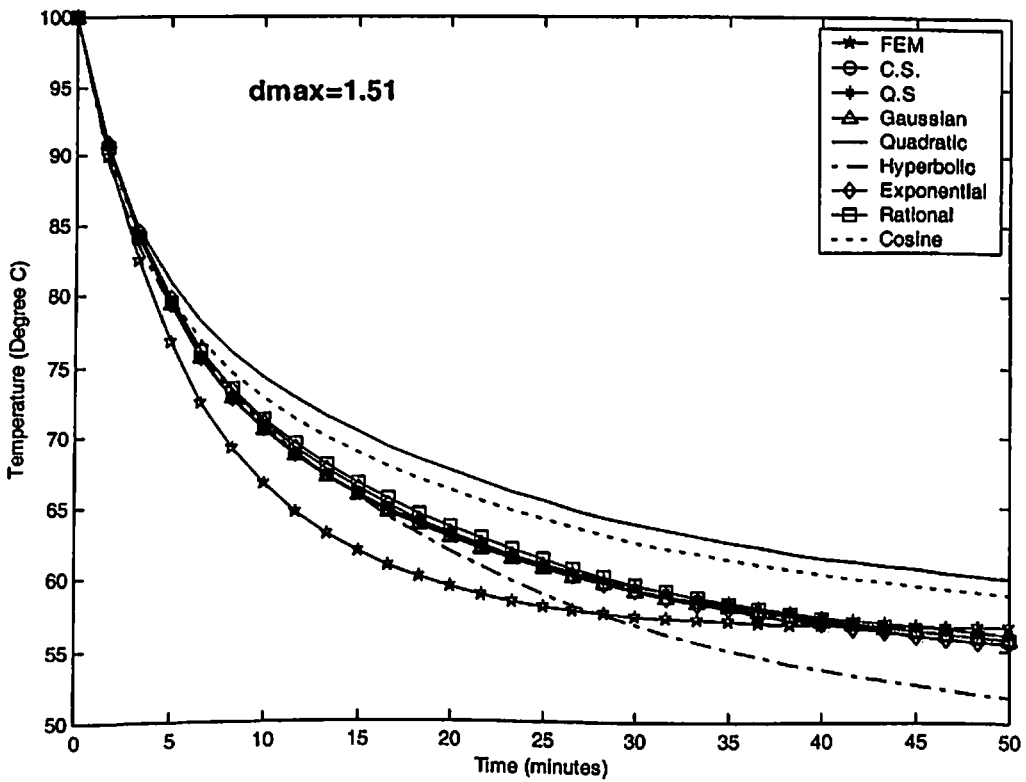
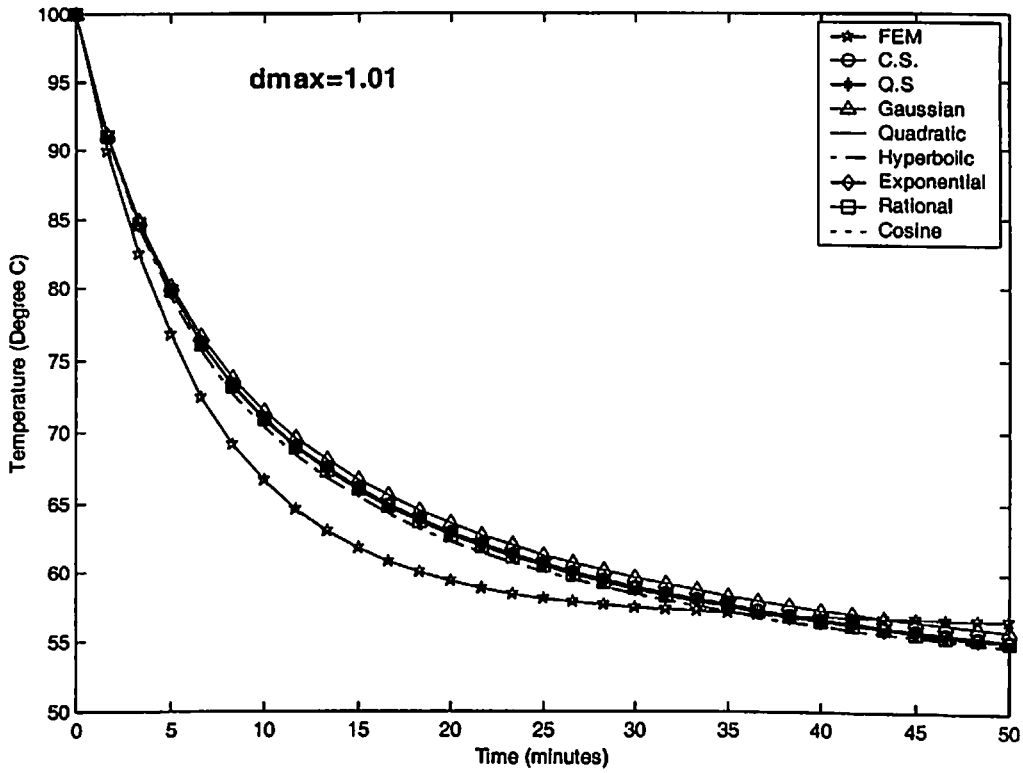


Fig. 6.28 Comparison of EFG results obtained using 72 nodes with FEM at the location ($r = 0.2$ m, $\theta = 0$ m & $z = 0$ m) of the 3-D model shown in Fig. 6.23

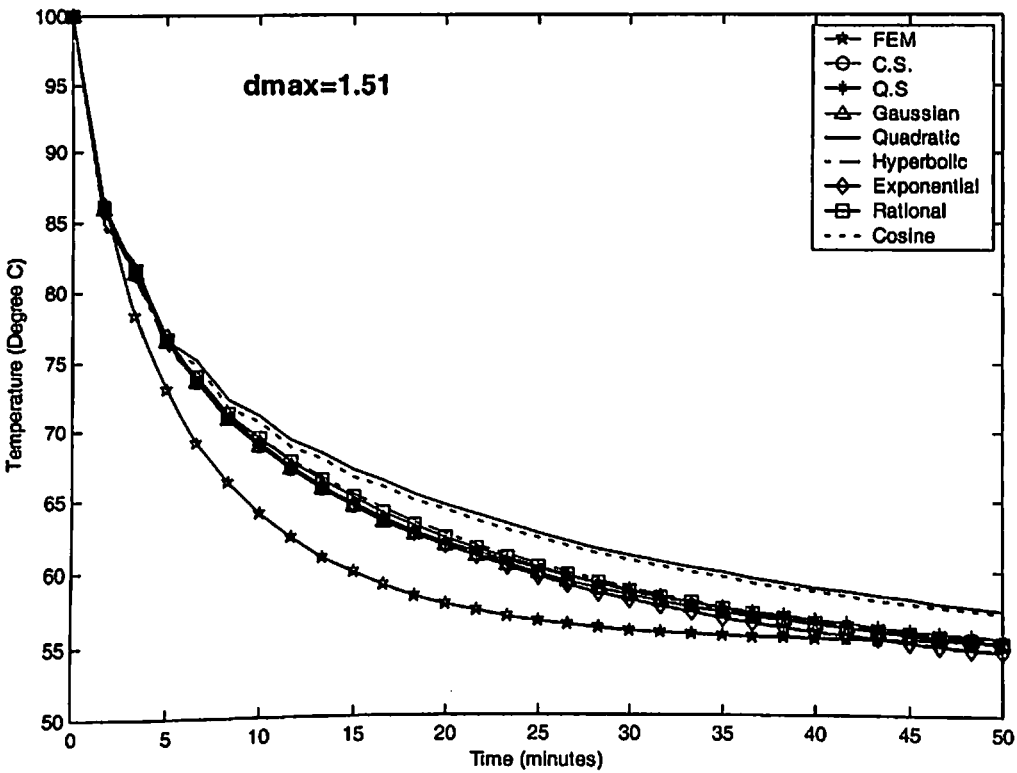
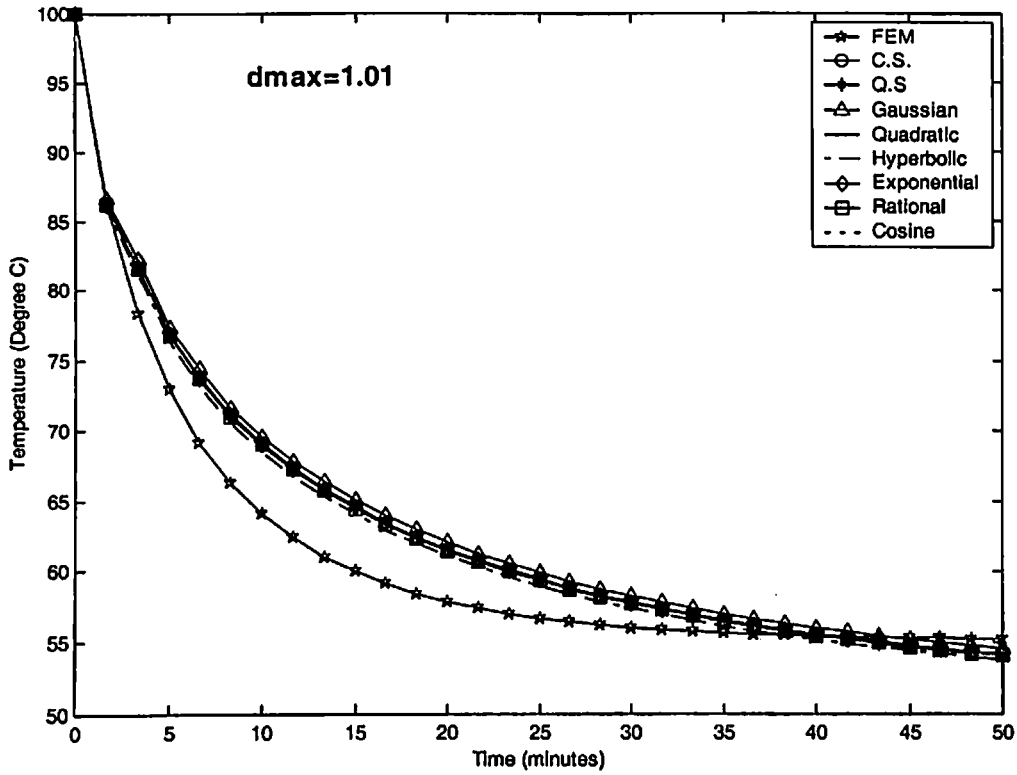


Fig. 6.29 Comparison of EFG results obtained using 216 nodes with FEM at the location ($r = 0.2\text{ m}$, $\theta = 0\text{ m}$ & $z = 0\text{ m}$) of the 3-D model shown in Fig. 6.23

6.10 CONCLUSION

3-D MATLAB codes have been developed to obtain the numerical solution for the different cases presented in this chapter using different EFG weight functions. The results obtained by EFG method are compared with those obtained by FEM (in Case-I analytical method also) at few typical locations. From the numerical analysis carried out in this chapter, it is clear that the EFG method can be successfully used to obtain the numerical solution of 3-D heat transfer problems. A comparative numerical analysis has been carried out to evaluate the performance of different weight functions. It is found that the EFG results obtained using cubicspline, quarticspline, Gaussian, exponential and rational weight functions are in good agreement with those obtained by FEM. From the analysis carried out in this chapter, it is also observed that only cubicspline, quarticspline, Gaussian, exponential and rational weight functions give acceptable results in the range $1.0 < d_{\max} < 1.5$. Out of all weight functions used, the results obtained using exponential weight function are most reliable as compared to other weight functions used because only exponential weight function has minimum variation in the results (temperature values) with the change in the value of scaling parameter.

CHAPTER-7

PARALLEL COMPUTING SOLUTION

7.1 INTRODUCTION

Parallel computation is making rapid inroads in various aspects of scientific and engineering computation. Now a day, there is continual demand for greater computational speed from a computer system that is currently possible. This need of fast computational speed will lead us to a new era of computing on Parallel Random Access Machines (PRAM). With the fast-paced development of processor technology coupled with recent developments in operating system software technology, has made large-scale Multiple-Instruction Multiple-Data (MIMD) machines very much affordable. These machines are based on independent processors with their own local memory. In contrast to writing algorithms for a single processor machine, algorithms for parallel computation involve two critical aspects: efficient data distribution among the processors to keep them as active as possible and minimizing the Inter-Processor Communication (IPC) time for data sharing. Keeping above points in mind, a new algorithm is proposed for the parallelization of the EFG method. The software has been programmed in FORTRAN language using MPI message passing library and executed on MIMD type supercomputing machine PARAM 10000. Three model heat transfer problems have been solved to validate the proposed algorithm. Computational time components (i.e. total time and communication time), speedup and efficiency (See **Appendix** for definition) have been estimated for one-dimensional, two-dimensional and three-dimensional problems. For 8 processors, the speedup & efficiency are obtained to be 2.22 & 27.78% in 1-D for 1100 nodes, 5.44 & 67.95% in 2-D for 1200 nodes and 4.66 & 58.22% for 1320 nodes in 3-D respectively.

7.2 PARALLEL CODE DEVELOPMENT

There are two methods for the parallelization of EFG sequential code. The first method emphasizes on the parallel implementation of the whole sequential code. The second method direct towards the careful analysis of the whole sequential code and then selects the portions wisely where implementing parallel programming will result in reduction of computational cost both in terms of time and complexity. The main drawback with the first method is the increased communication time taken by the processors for mutual transfer of data and also increased complexity. Therefore, a careful analysis of the EFG code has been performed and it has been found that the time required in solving the system of linear equations (i.e. inversion time) increases with the increase in data size (number of nodes) as shown in Table 7.1 & Fig. 7.1 for 1-D, in Table 7.2 & Fig. 7.2 for 2-D and in Table 7.3 & Fig. 7.3 for 3-D, respectively. In other words, the major part of the total computational time is required in solving the system of linear equations. Therefore, parallel code has been developed only for the solution of the system of linear equations, not for the whole EFG sequential code.

Table 7.1 Variation of total time & solution (inversion) time with data size (no. of nodes) for 1-D problem (Chapter 4: Case-III)

Data size (no. of nodes)	Computational time (sec)		$\left(\frac{t_s}{t_t} \times 100\right) \%$
	Total time, t_t	Solution time, t_s (Inversion time)	
101	0.8516	0.5411	65.53
201	6.1343	4.0565	66.13
401	50.3770	34.3117	68.11
601	172.0415	117.3784	68.22
700	281.9550	192.7580	68.36
801	408.9820	279.8802	68.42
951	688.0650	470.9902	68.45

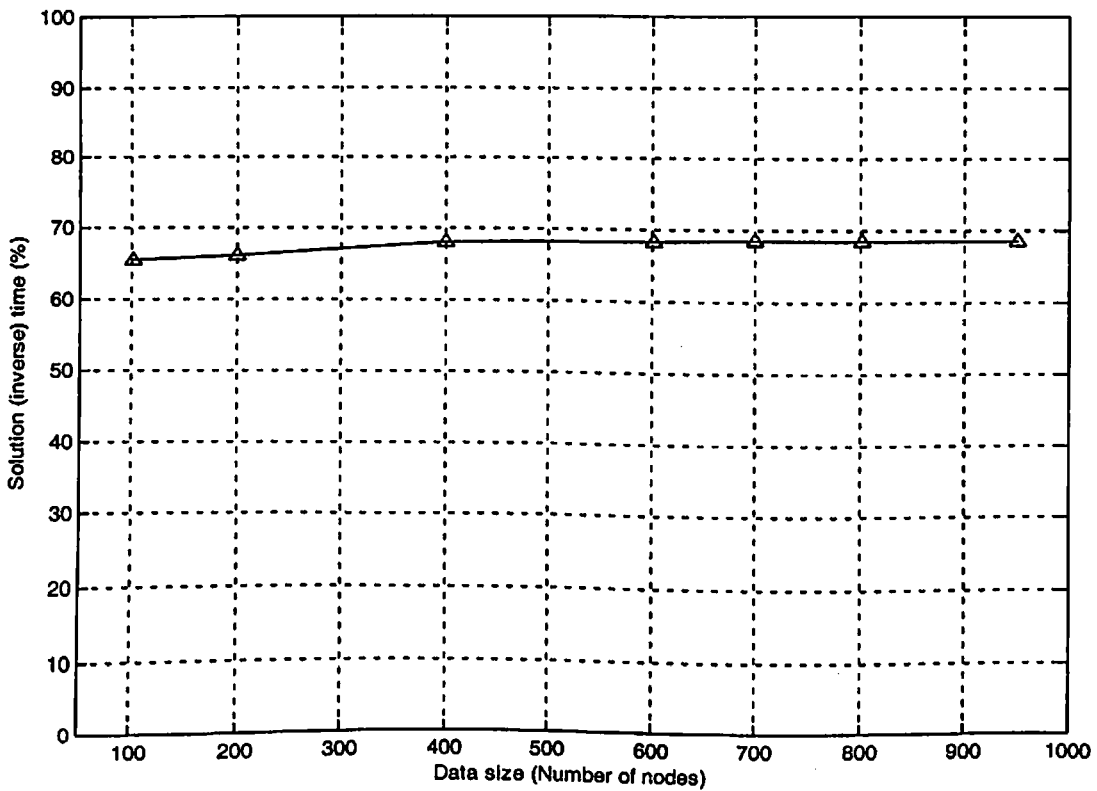


Fig. 7.1 Percentage variation of solution (inverse) time with data size (no. of nodes) for 1-D problem (Chapter 4: Case-III)

Table 7.2 Variation of total time & solution (inversion) time with data size (no. of nodes) for 2-D problem (Chapter 5: Case-I)

Data size (no. of nodes)	Computational time (sec)		$\left(\frac{t_s}{t_t} \times 100\right)\%$
	Total time, t_t	Solution time, t_s (Inverse time)	
81	0.6431	0.3641	56.62
121	1.6158	1.1312	70.00
256	11.3075	9.8999	87.55
441	55.9784	52.740	94.21
676	194.5410	188.2192	96.75
961	598.8565	587.2674	98.06
1200	1179.5400	1161.9026	98.50

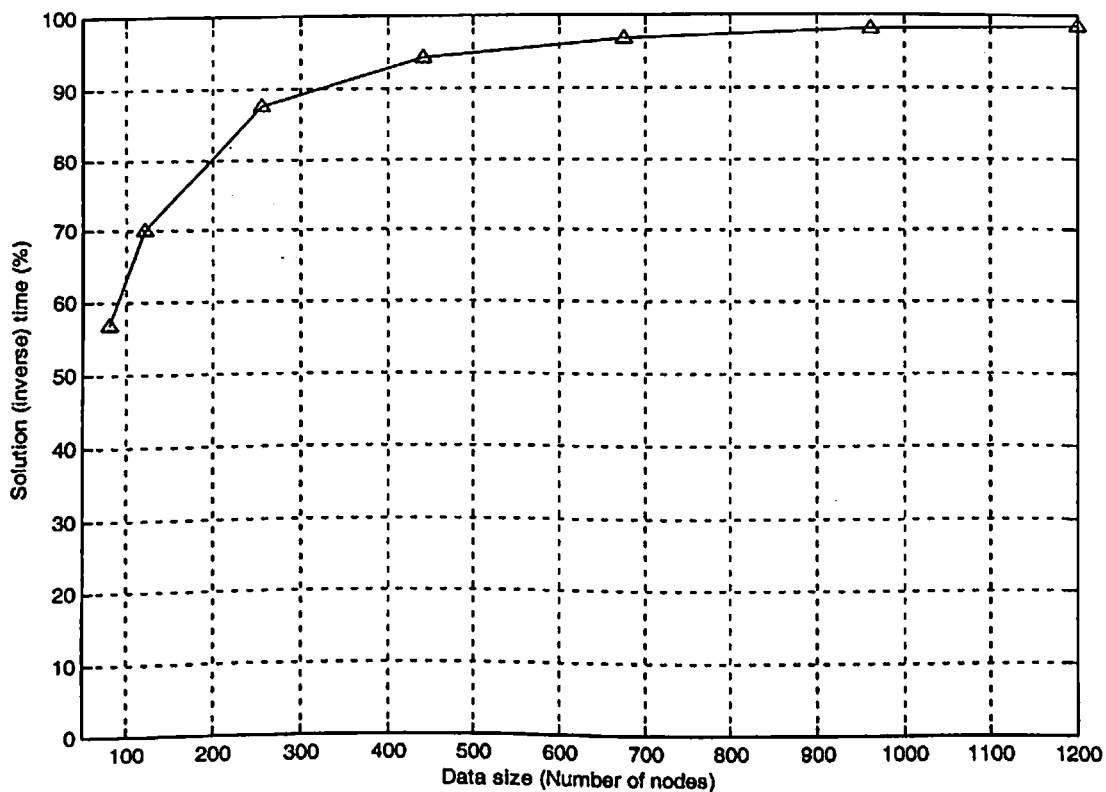


Fig. 7.2 Percentage variation of solution (inverse) time with data size (no. of nodes) for 2-D problem (Chapter 5: Case-I)

Table 7.3 Variation of total time & solution (inversion) time with data size (no. of nodes) for 3-D problem (Chapter 6: Case-I)

Data size (no. of nodes)	Computational time (sec)		$\left(\frac{t_s}{t_t} \times 100\right)\%$
	Total time, t_t	Solution time, t_s (Inversion time)	
125	3.3018	1.6487	49.93
216	11.3304	7.5431	66.57
343	38.2157	30.2130	79.06
512	114.5725	98.6108	86.07
729	308.5035	278.6737	90.33
1000	776.9130	723.1276	93.08
1320	1703.9500	1613.8735	94.71

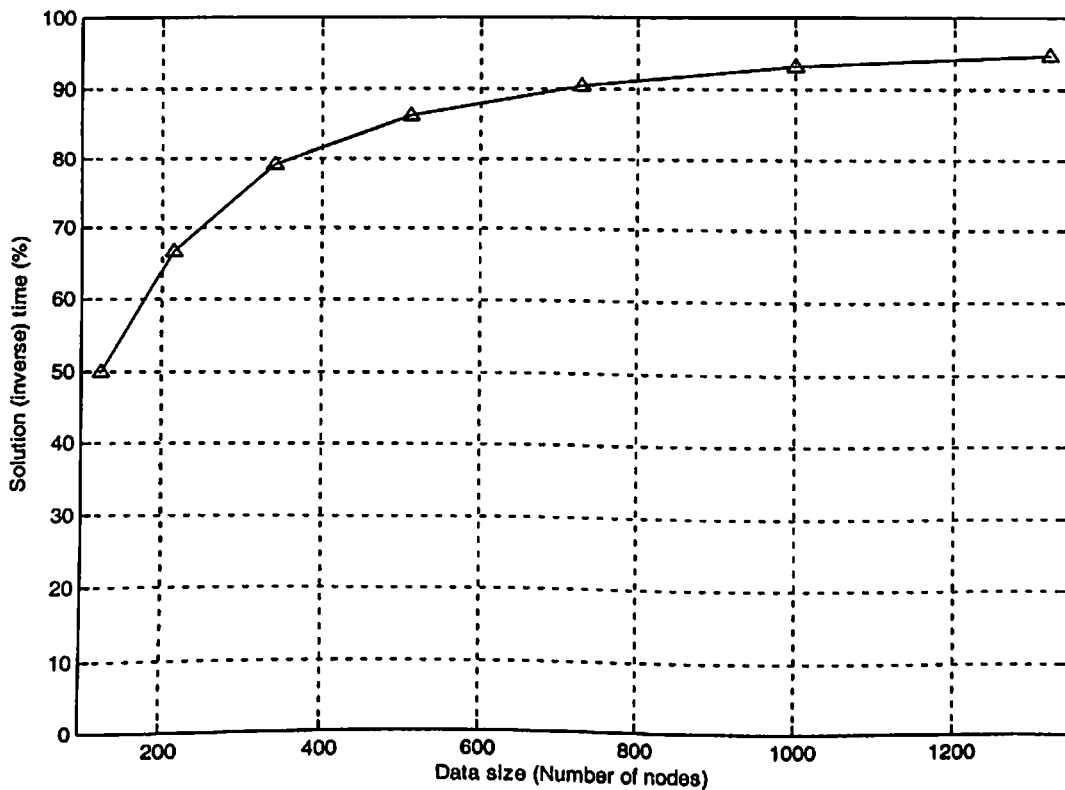


Fig. 7.3 Percentage variation of solution (inverse) time with data size (no. of nodes) for 3-D problem (Chapter 6: Case-I)

7.2.1 Parallel algorithm for the solution of linear equations

Matrix inversion method is one of the common methods adopted for obtaining the solution of the system of linear equations $[A]\{U\} = \{F\}$. In this method, first the inverse of matrix $[A]$ is calculated then the solution is computed using $\{U\} = [A]^{-1}\{F\}$. In this chapter, a parallel algorithm is proposed based on the matrix inversion technique to reduce the computational cost of the EFG method. During implementation of this algorithm on supercomputer (PARAM 10000), first row wise data distribution is carried out. After proper data distribution among the processors, an identity matrix is generated by each processor of size $[A]$. In the process of matrix inversion, row wise operations are carried out. Every non-diagonal element of matrix $[A]$ is converted to zero and every diagonal element of matrix $[A]$ is converted to unity. Whatever operations carried out on matrix $[A]$, the same operations are also carried out on matrix $[I]$. Each processor operates on its own row to achieve less computational time. After finding the inverse of matrix $[A]$, the unknown $[U]$ is calculated by using $\{U\} = [A]^{-1}\{F\}$. The algorithm is given on the next page:

Parallel Algorithm

Global	<i>Numprocs</i>	Number of processors
	\bar{N}	Number of equations
	<i>MyRank</i>	Rank of each processor.
	<i>Rank</i>	Rank of processor holding current row
	$[A]$	Input matrix.
	$\{F\}$	Input column vector
	$[I]$	Inverse matrix of $[A]$
	<i>i</i>	Variable indicating current row
	<i>start</i>	Starting row number for each processor
	<i>end</i>	Ending row number for each processor

```

do i = 0 to Numprocs - 1
    Set start
    Set end
end do
do i = 1 to  $\bar{N}$ 
    Set diagonal elements of  $[A]_i = 1$ 
    Change non-diagonal element of  $[A]_i$ 
    Change elements of matrix  $[I]_i$ 
    do i = 0 to Numprocs - 1
        Find the Rank of the current row
        If (MyRank = Rank) then
            Broadcast current row
        endif
    end do
    do j = start to end
        Change non-diagonal element of  $[A]_{i=0}$ 
        Change elements of matrix  $[I]_i$ 
    end do
end do
do i = start to end
    Compute  $\{U\}_i$ 
end do
do j = 1 to Numprocs - 1
    Send  $\{U\}_i$  to Master Processor
end do

```

7.2.2 Hardware and software employed

The hardware used for numerical solution is a 'PARAM 10000 supercomputer' which has been designed and developed by C-DAC, Pune, India. The PARAM 10000 is 6.4 GF, RISC based distributed memory multiprocessor system and categorized under 'multiple instruction multiple data (MIMD)' type computer. It has total four nodes (three compute nodes and one server node). Each compute node has two UltraSparc II 64-bit RISC CPUs of 400 MHz, 512 MB main memory, two Ultra SCSI HDD of 9.1 GB each, one 10/100 Fast Ethernet Card and Solaris 2.6 while server node has two UltraSparc II 64-bit RISC CPUs of 400 MHz, 1GB of main memory, four Ultra SCSI HDD of 9.1 GB each, one 10/100 Fast Ethernet Card and Solaris 2.6. PARAM 10000 has total 8 processors (each node with two processors), Sun Sparc Compilers (F90 Compiler Version 2.0, F77 Compiler Version 5.0, C Compiler Version 5.0, C++ Compiler Version 5.0) and supports both MPI & PVM message passing environments.

7.3 NUMERICAL RESULTS AND DISCUSSION

A new parallel algorithm has been proposed for the EFG method. The parallel code has been developed in FORTRAN language using MPI message passing library for heat transfer problems. The parallel EFG results have been obtained for three model problems in 1-D, 2-D and 3-D domain to validate the proposed algorithm. The computational time components i.e. (total time and communication time), speedup and efficiency have been executed for the different sets of data size on a network of parallel computer (PARAM 10000).

7.3.1 One-dimensional model problem

The parallel EFG results have been obtained for 1-D model shown in Fig. 4.15 (Chapter 4: Case-III). Table 7.4 shows the variation of total time, communication time, speedup and efficiency with the number of processors for 700 nodes. The variation of total time and communication time with the number of processors is also shown in Fig. 7.4 for same

number of nodes (data size). From Table 7.4 and Fig. 7.4, it is observed that with increase in the number of processors from 1 to 8, total time is decreasing. Fig. 7.5 and Fig. 7.6 show the variation of efficiency and speedup with the number of processors for 700 nodes. For this data size (700 nodes), the speedup and efficiency are obtained to be 2.09 and 26.11% respectively using 8 processors.

Table 7.5 shows the variation of total time, communication time, speedup and efficiency with the number of processors for 951 nodes. The variation of total time and communication time is also presented in Fig. 7.7 for same number of nodes (data size). From Table 7.5 and Fig. 7.7, it can be noted that total time is decreasing with the increase in number of processors 1 to 8. Fig. 7.8 & Fig. 7.9 show the variation of efficiency and speedup respectively with number of processors for 951 nodes. For this data size (951 nodes), the speedup and efficiency are achieved to be 2.21 and 27.62% respectively using 8 processors.

Table 7.6 shows variation of total time, communication time, speedup and efficiency with the number of processors for 1100 nodes. The variation of total time and communication time with the number of processors is also given in Fig. 7.10 for the same number of nodes (data size). From Table 7.6 and Fig. 7.10, it can be noted that with the increase in the number of processors from 1 to 8, total time is decreasing. Fig. 7.11 & Fig. 7.12 show the variation of efficiency and speedup respectively with the number of processors for 1100 nodes. For this data size (1100 nodes), the speedup and efficiency are achieved to be 2.22 and 27.78% respectively using 8 processors.

From the above analysis, it is observed that with the increase in data size (number of nodes), the results are improving both in terms of efficiency and speedup. The contribution of communication time in total computational time is almost negligible. Moreover it is also clear that with the increase in data size (number of nodes), the results are improving with increase in number of processors.

Table 7.4 Variation of total time, communication time, speedup and efficiency with number of processors for 700 nodes

Number of processors	Total time (sec)	Communication time (sec)	Speedup	Efficiency (%)
1	282.1210	0.0000	1.00	100.00
2	190.6980	0.1828	1.48	73.97
3	157.8750	0.2514	1.79	59.57
4	142.5715	0.4078	1.98	49.47
5	137.9845	1.0385	2.04	40.89
6	137.8950	5.8203	2.04	34.10
7	130.7770	2.0245	2.16	30.82
8	135.0520	5.5562	2.09	26.11

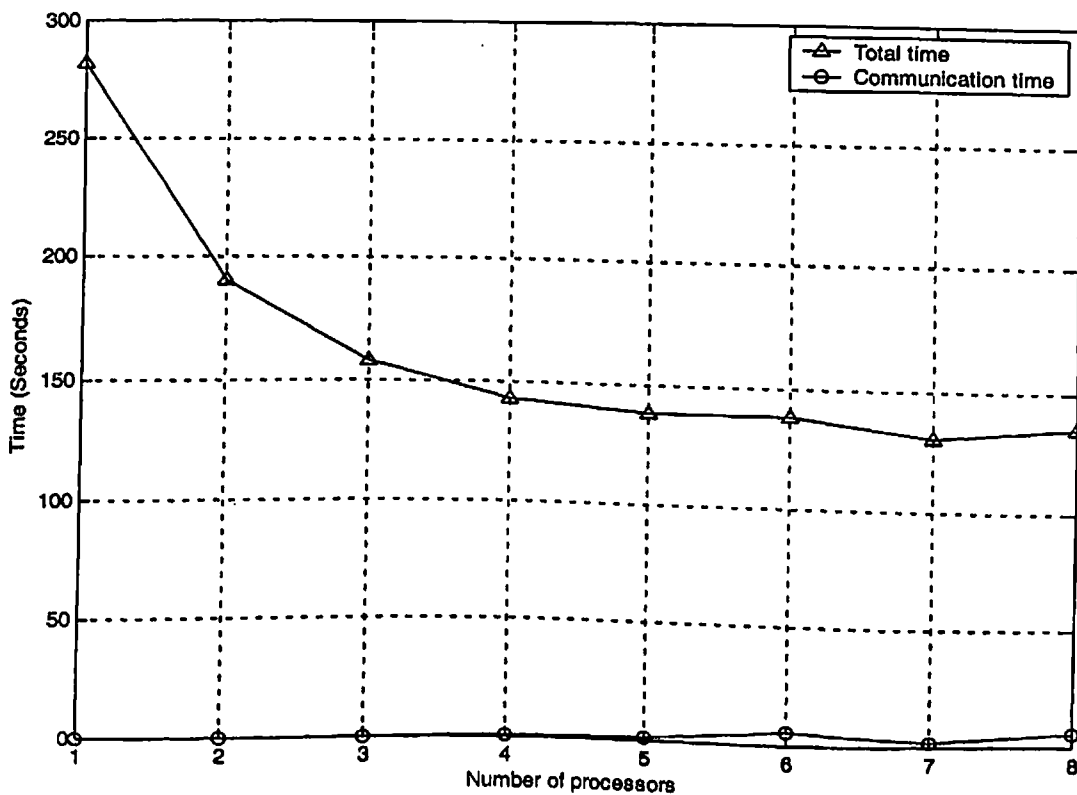


Fig. 7.4 Variation of total time and communication time with number of processors for 700 nodes

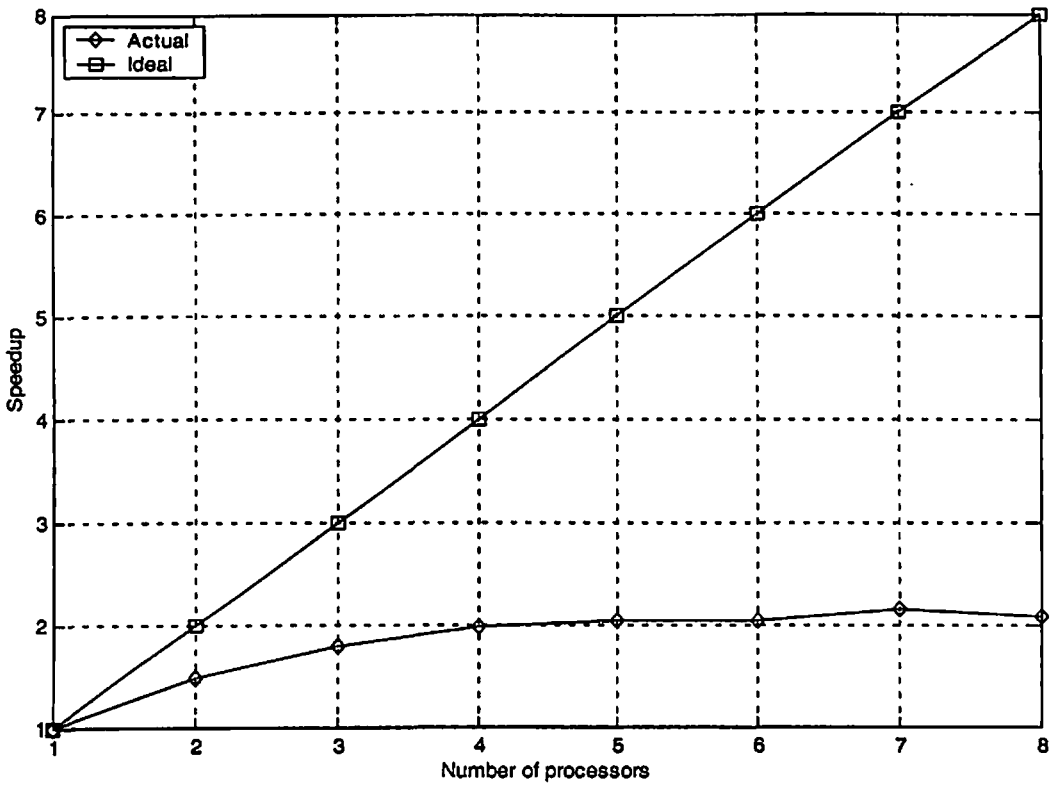


Fig. 7.5 Variation of speedup with number of processors for 700 nodes

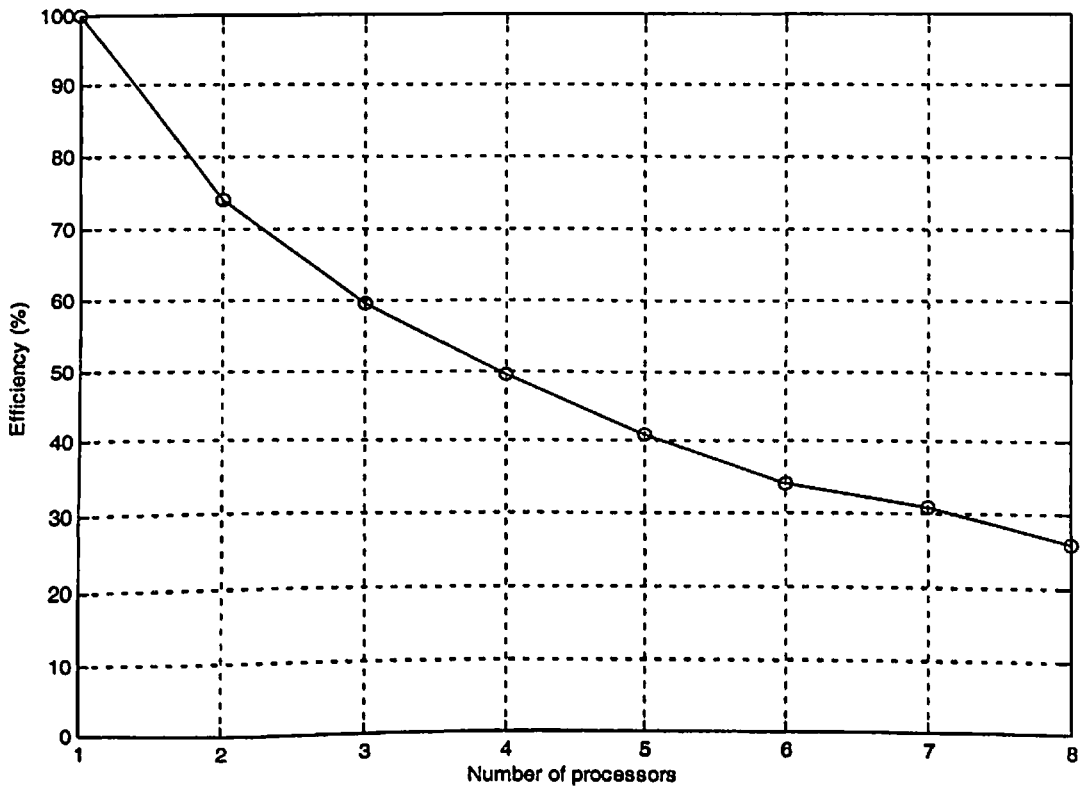


Fig. 7.6 Variation of efficiency with number of processors for 700 nodes

Table 7.5 Variation of total time, communication time, speedup and efficiency with number of processors for 951 nodes

Number of processors	Total time (sec)	Communication time (sec)	Speedup	Efficiency (%)
1	688.0650	0.0000	1.00	100.00
2	459.4145	0.4334	1.50	74.88
3	384.3750	0.2045	1.79	59.67
4	343.3560	0.7479	2.00	50.09
5	329.7055	1.6426	2.09	41.74
6	320.5130	3.6739	2.15	35.78
7	309.2805	2.6484	2.22	31.78
8	311.3995	4.3623	2.21	27.62

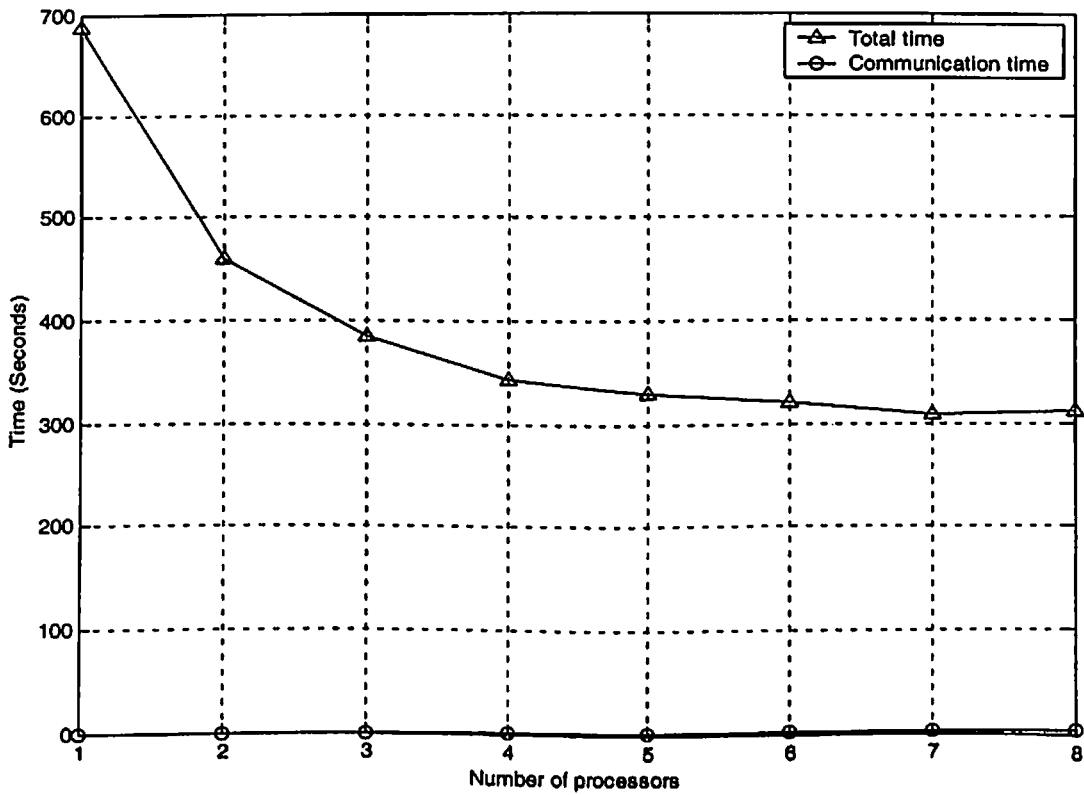


Fig. 7.7 Variation of total time and communication time with number of processors for 951 nodes

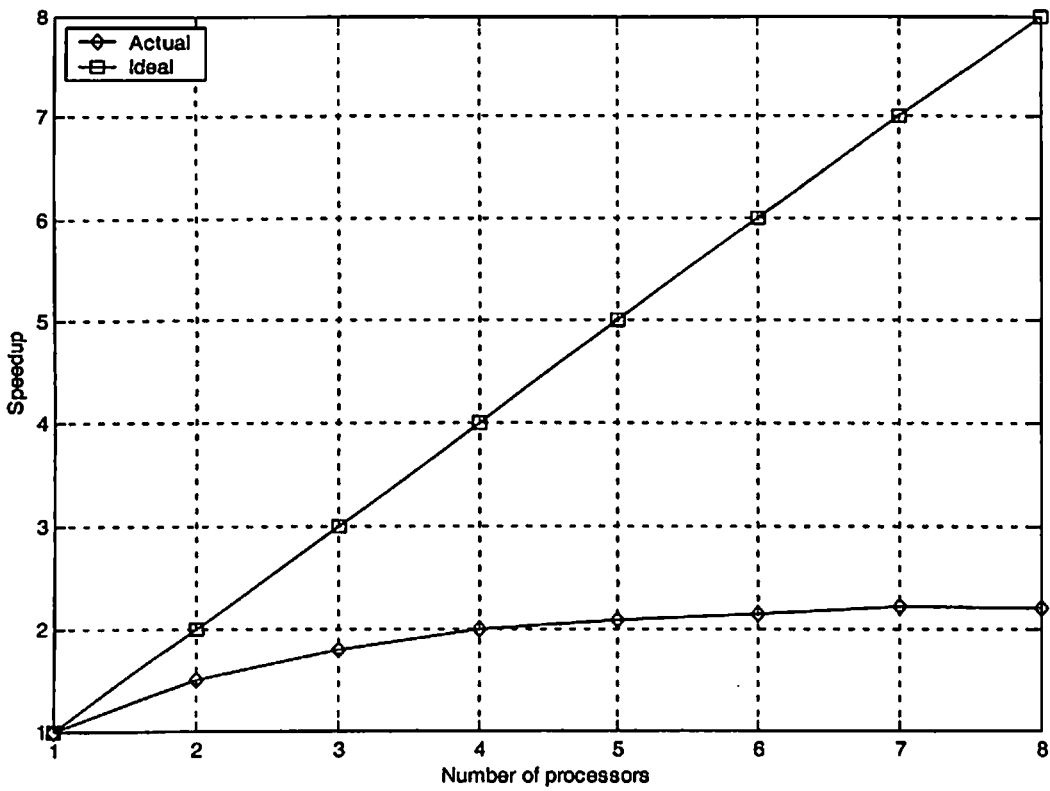


Fig. 7.8 Variation of speedup with number of processors for 951 nodes

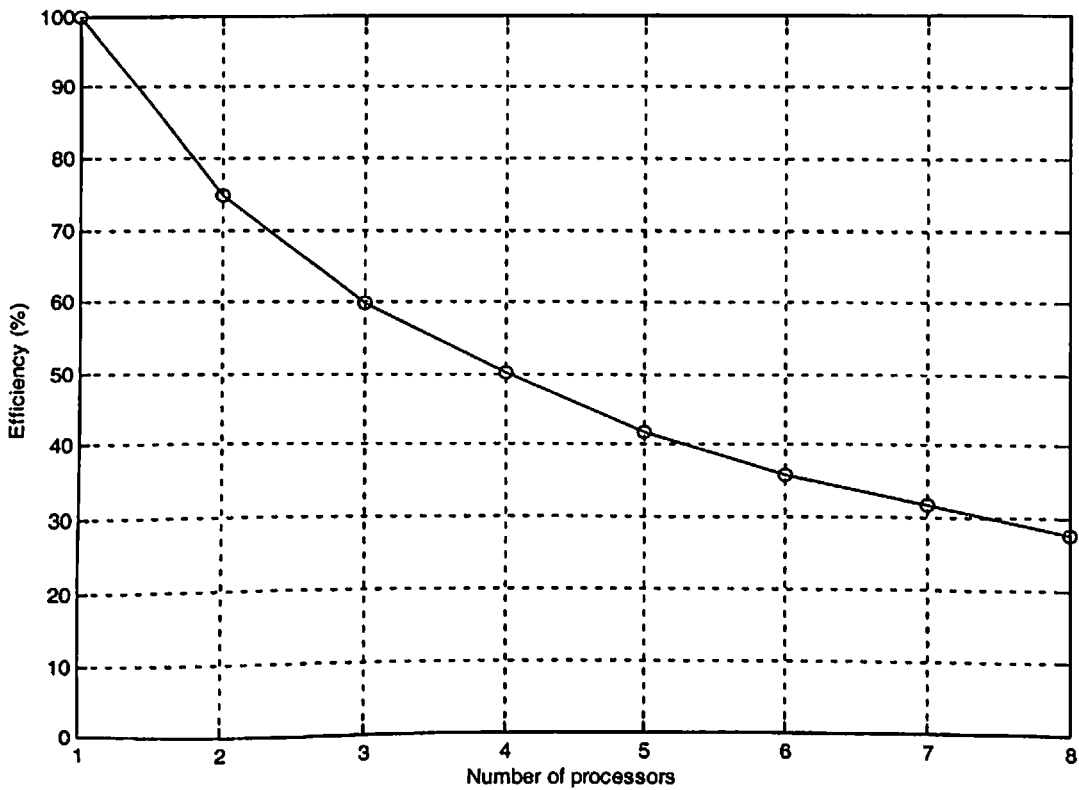


Fig. 7.9 Variation of efficiency with number of processors for 951 nodes

Table 7.6 Variation of total time, communication time, speedup and efficiency with number of processors for 1100 nodes

Number of processors	Total time (sec)	Communication time (sec)	Speedup	Efficiency (%)
1	1102.0100	0.0000	1.00	100.00
2	734.4910	0.1865	1.50	75.02
3	613.3410	0.2221	1.80	59.89
4	550.7370	0.5473	2.00	50.00
5	530.7570	1.4546	2.08	41.52
6	513.6220	7.3639	2.14	35.76
7	494.0510	3.9161	2.23	31.86
8	495.8540	3.0547	2.22	27.78

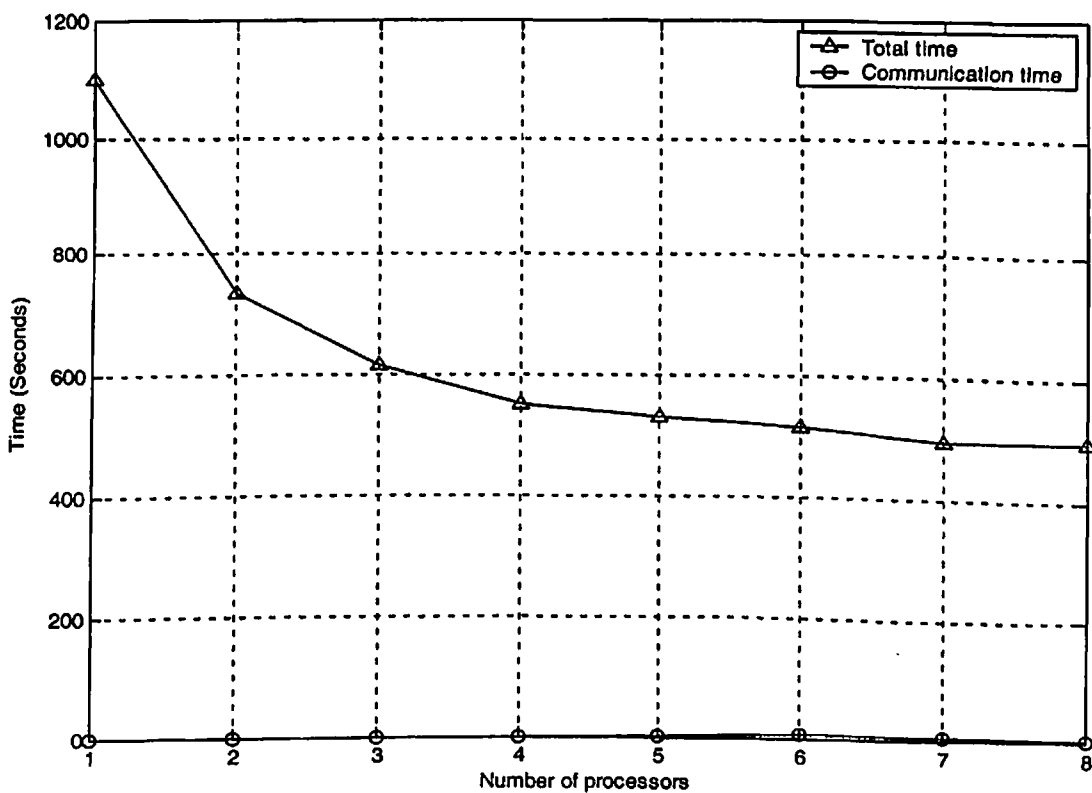


Fig. 7.10 Variation of total time and communication time with number of processors for 1100 nodes

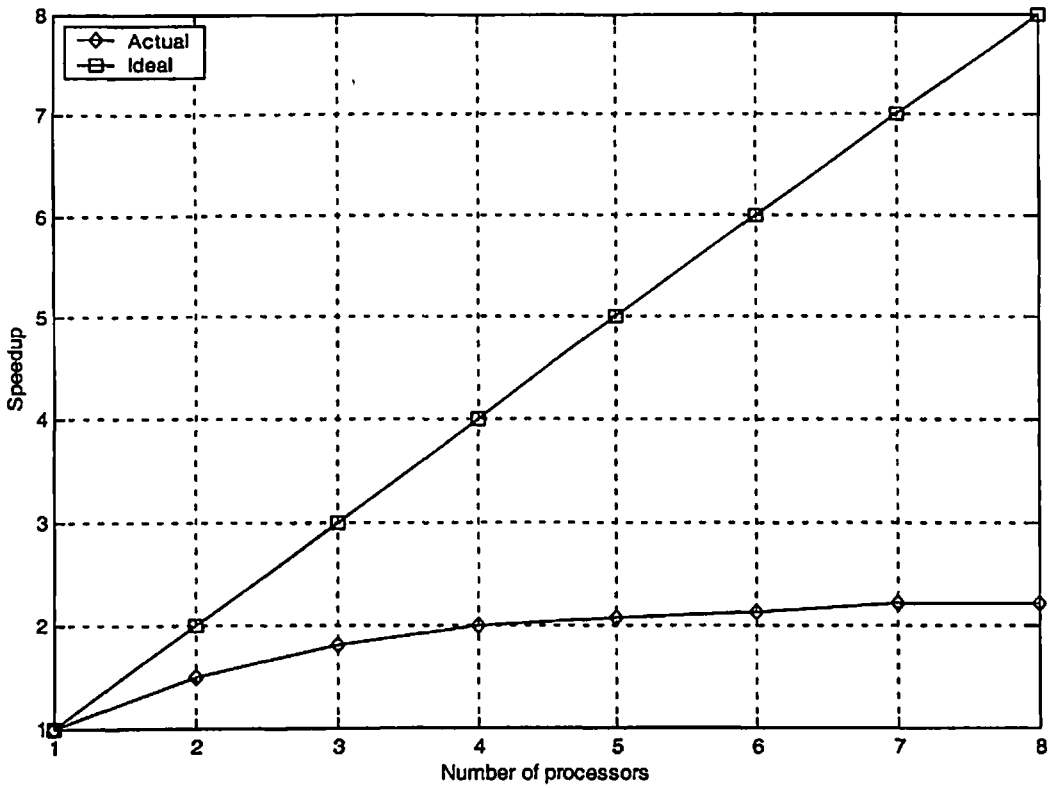


Fig. 7.11 Variation of speedup with number of processors for 1100 nodes

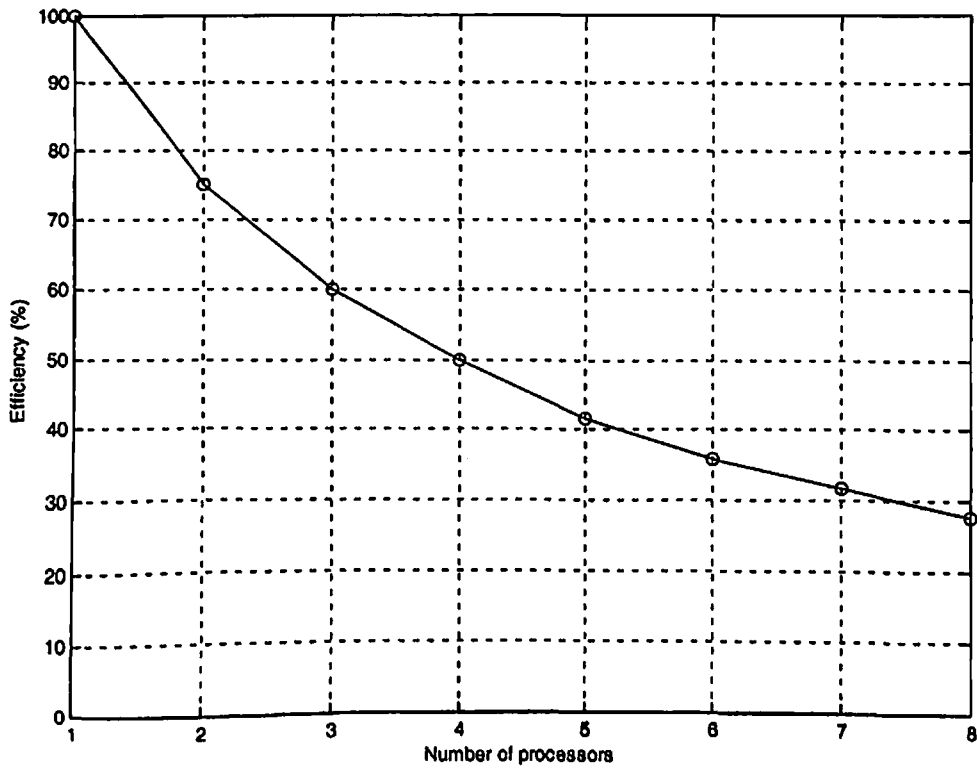


Fig. 7.12 Variation of efficiency with number of processors for 1100 nodes

7.3.2 Two-dimensional model problem

The parallel EFG results have been obtained for 2-D model shown in Fig. 5.1 (Chapter 5: Case-I). Table 7.7 shows the variation of computational time components i.e. (total time and communication), speedup and efficiency with the number of processors for 676 nodes. The variation of total time and communication time with the number of processors is also shown in Fig. 7.13 for same number of nodes (data size). From Table 7.7 and Fig. 7.13, it is observed that with the increase in the number of processors from 1 to 8, total time is decreasing. Fig. 7.14 and Fig. 7.15 show the variation of efficiency and speedup respectively with the number of processors for 676 nodes. For this data size (676 nodes), the speedup and efficiency are found to be 4.23 and 52.83% respectively using 8 processors.

Table 7.8 shows the variation of computational time components, speedup and efficiency with the number of processors for 961 nodes. The variation of computational time components with the number of processors is also presented in Fig. 7.16 for same number of nodes (data size). From Table 7.8 and Fig. 7.16, it can be noted that with the increase in number of processors from 1 to 8, total time decreases. Fig. 7.17 & Fig. 7.18 show the variation of efficiency and speedup respectively with the number of processors for 961 nodes. For this data size (961 nodes), the speedup and efficiency are achieved to be 4.90 and 61.29% respectively using 8 processors.

Table 7.9 shows the variation of total time, communication time, speedup and efficiency with the number of processors for 1200 nodes. The variation of total time and communication time with the number of processors is also shown in Fig. 7.19 for same data size (number of nodes). From Table 7.9 and Fig. 7.19, it can be noted that total time decreases with the increase in number of processors. Fig. 7.20 & Fig. 7.21 show the variation of efficiency and speedup respectively with the number of processors for 1200 nodes. For this data size (1200 nodes), the speedup and efficiency are achieved to be 5.44 and 67.95% respectively using 8 processors.

From the above analysis, it is observed that with increase in data size, the results are improving both in terms of efficiency and speedup. The contribution of communication time to the total time is very less as compared to total computational time. Moreover it is also clear that with the increase in data size (number of nodes), the results are improving with increase in number of processors.

Table 7.7 Variation of total time, communication time, speedup and efficiency with number of processors for 676 nodes

Number of processors	Total time (sec)	Communication time (sec)	Speedup	Efficiency (%)
1	212.2315	0.0000	1.00	100.00
2	111.4260	0.0671	1.90	95.23
3	78.0770	0.1053	2.72	90.61
4	60.6514	0.5706	3.50	87.48
5	55.0408	0.8323	3.85	77.12
6	54.5207	6.0414	3.86	64.41
7	46.3948	1.9330	4.57	65.35
8	50.2148	5.5403	4.23	52.83

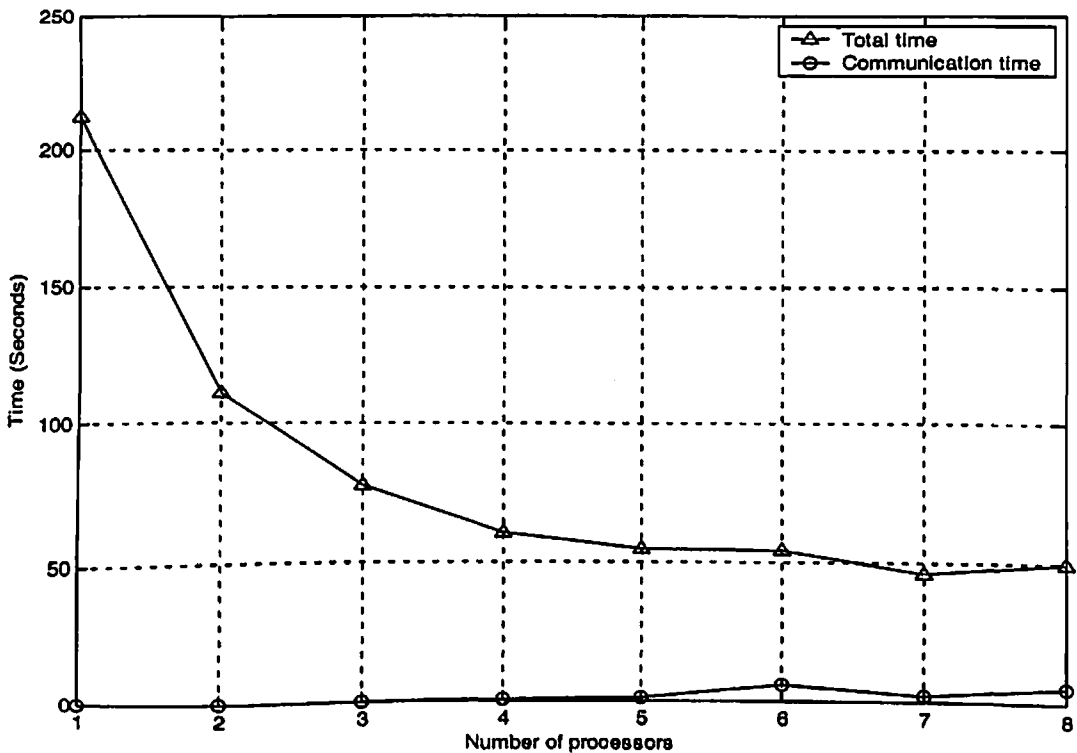


Fig. 7.13 Variation of total time and communication time with number of processors for 676 nodes

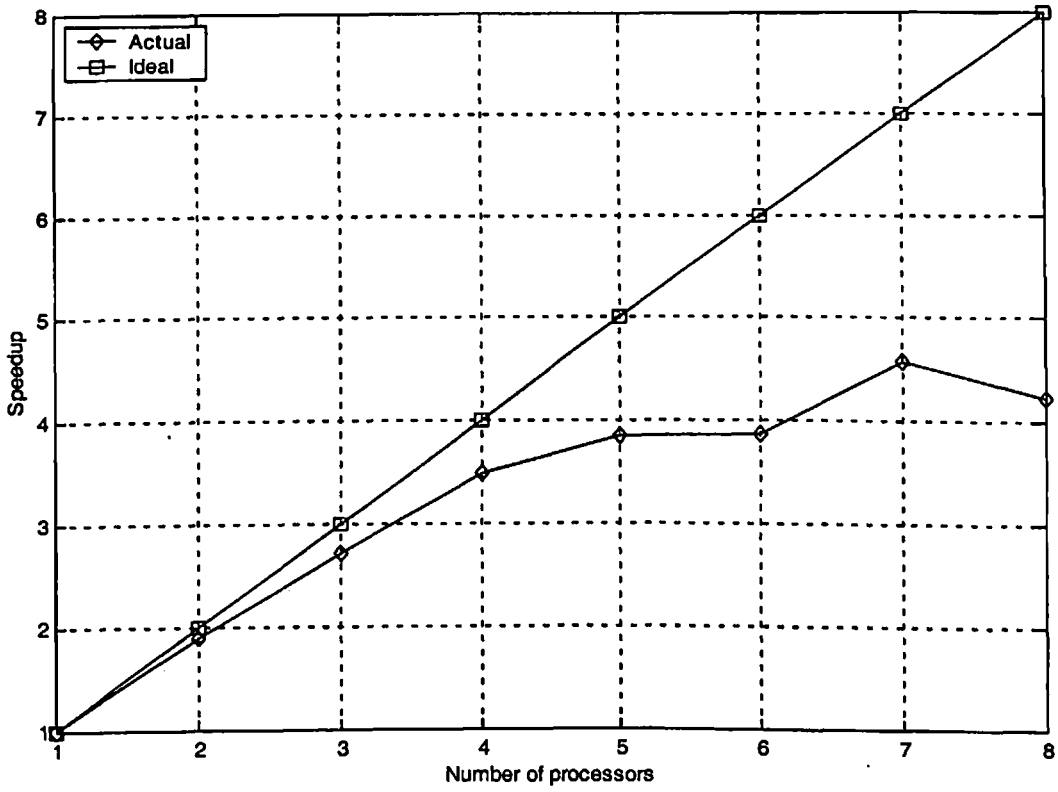


Fig. 7.14 Variation of speedup with number of processors for 676 nodes

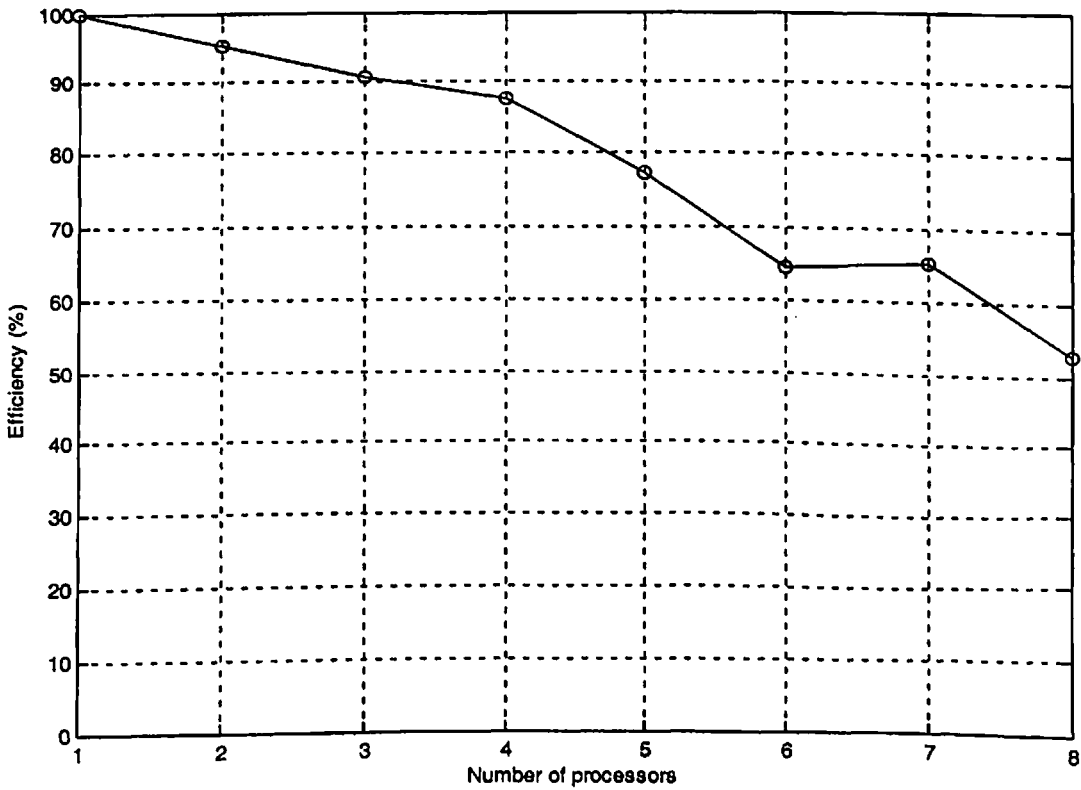


Fig. 7.15 Variation of efficiency with number of processors for 676 nodes

Table 7.8 Variation of total time, communication time, speedup and efficiency with number of processors for 961 nodes

Number of processors	Total time (sec)	Communication time (sec)	Speedup	Efficiency (%)
1	598.8565	0.0000	1.00	100.00
2	310.1355	0.1924	1.93	96.54
3	214.2525	0.2256	2.79	93.13
4	164.6720	0.9013	3.63	90.88
5	141.6955	1.7398	4.21	84.19
6	134.5425	6.8044	4.45	74.15
7	114.9740	3.0855	5.21	74.38
8	122.0950	6.2373	4.90	61.29

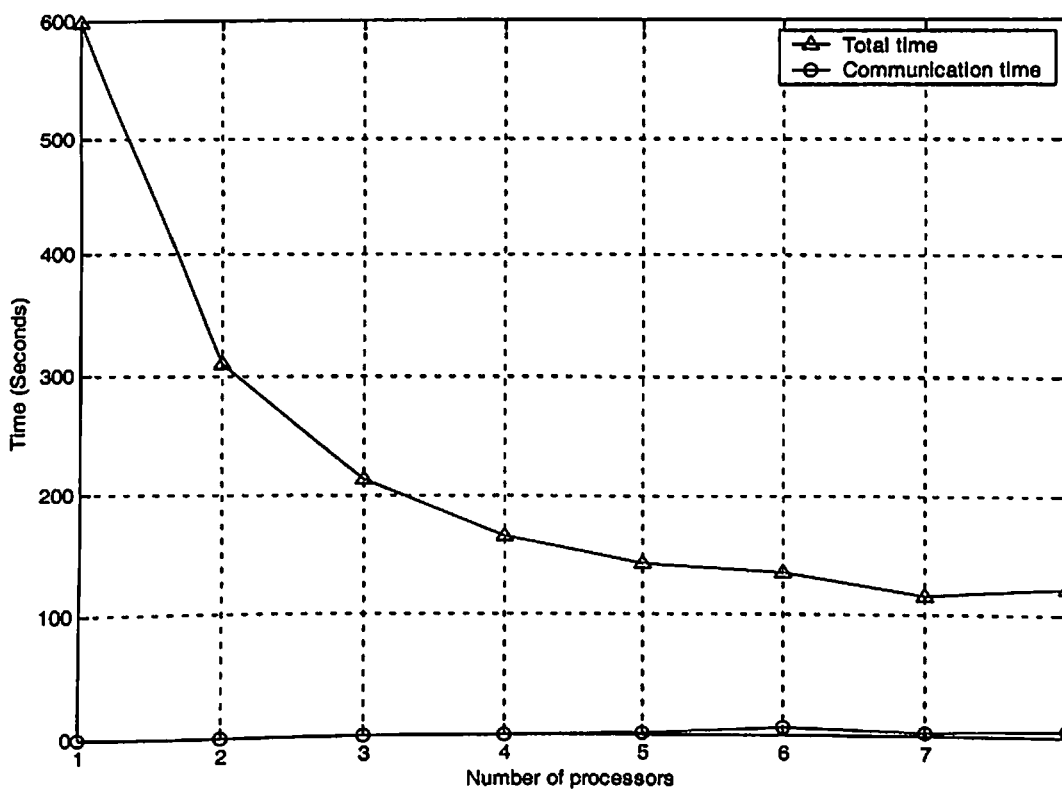


Fig. 7.16 Variation of total time and communication time with number of processors for 961 nodes

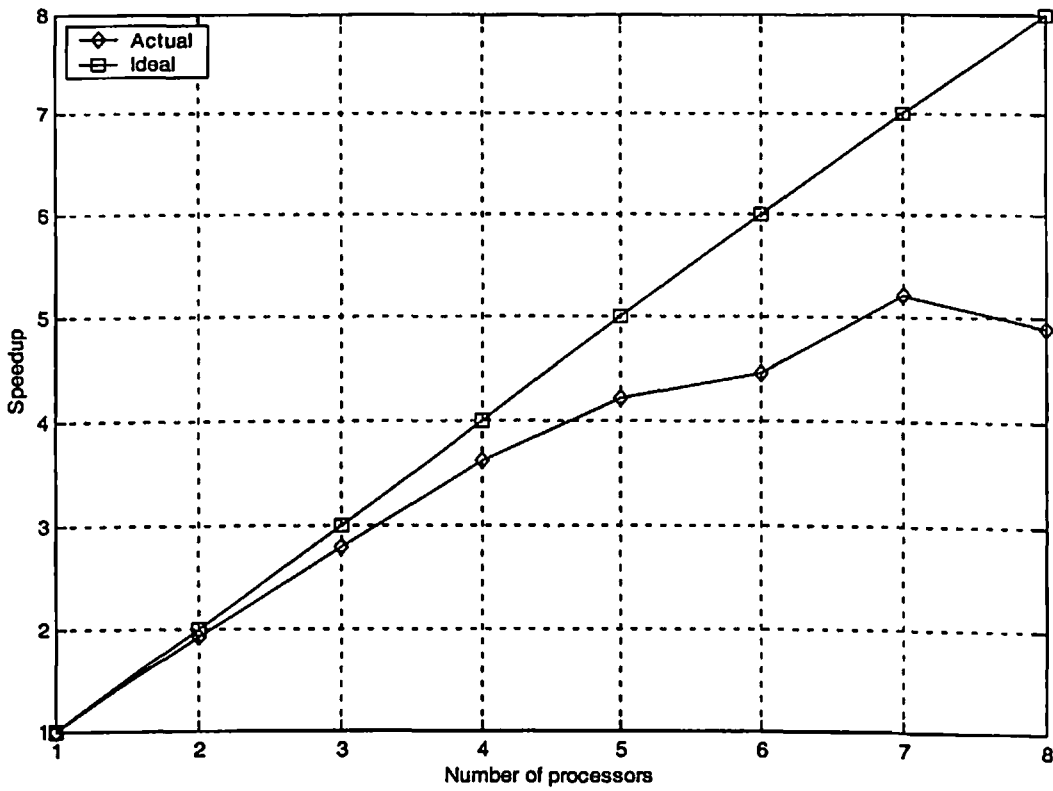


Fig. 7.17 Variation of speedup with number of processors for 961 nodes

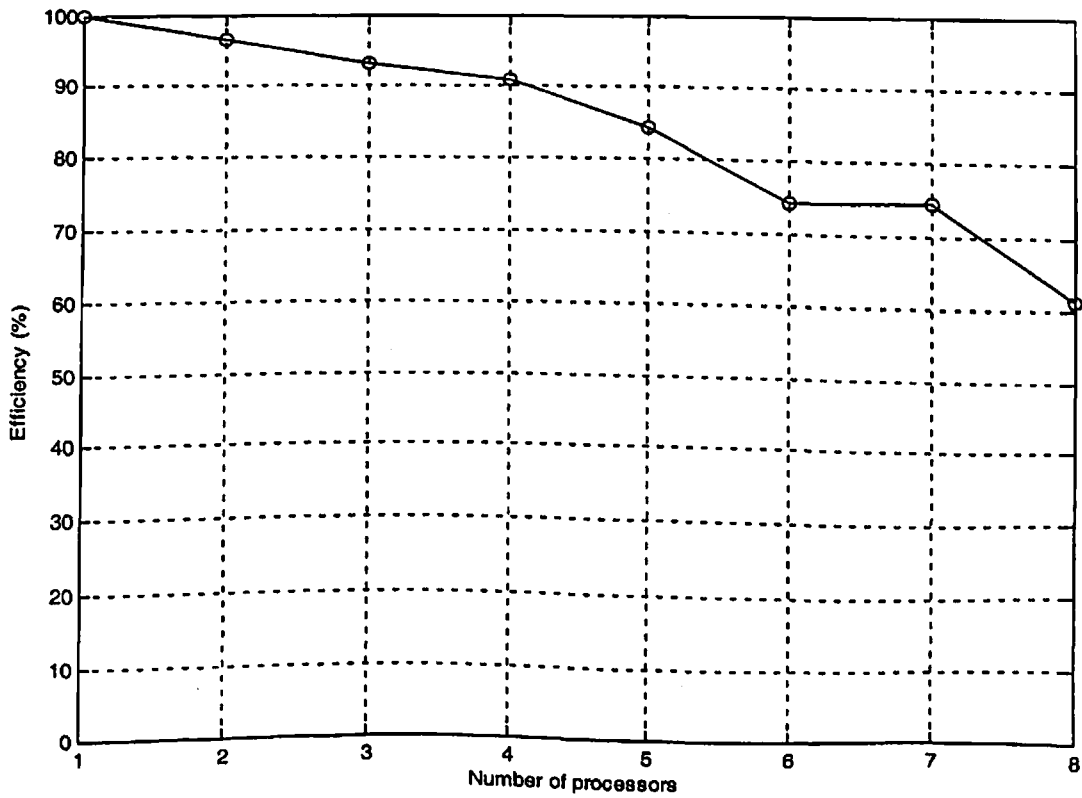


Fig. 7.18 Variation of efficiency with number of processors for 961 nodes

Table 7.9 Variation of total time, communication time, speedup and efficiency with number of processors for 1200 nodes

Number of processors	Total time (sec)	Communication time (sec)	Speedup	Efficiency (%)
1	1179.5400	0.0000	1.00	100.00
2	606.6460	0.2567	1.94	97.22
3	417.6550	0.7822	2.82	94.14
4	320.2650	0.5918	3.68	92.07
5	282.8400	2.6019	4.17	83.41
6	254.3290	4.7861	4.64	77.30
7	222.0310	4.9631	5.31	75.89
8	216.9900	3.8176	5.44	67.95

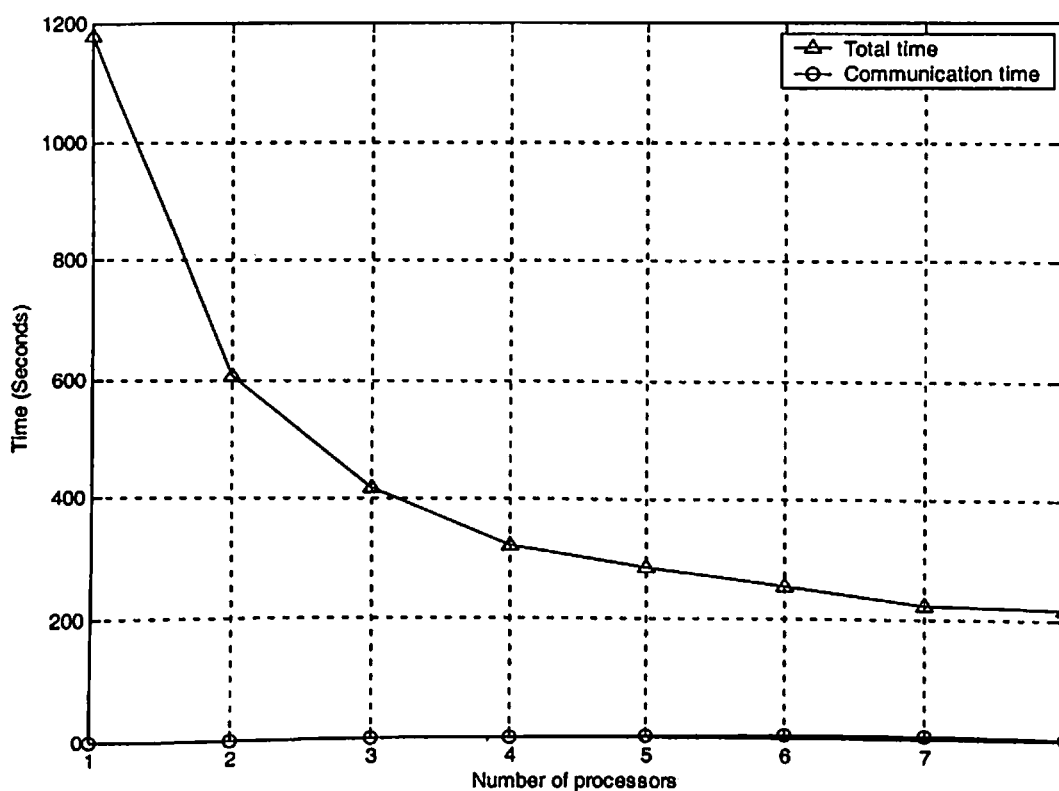


Fig. 7.19 Variation of total time and communication time with number of processors for 1200 nodes

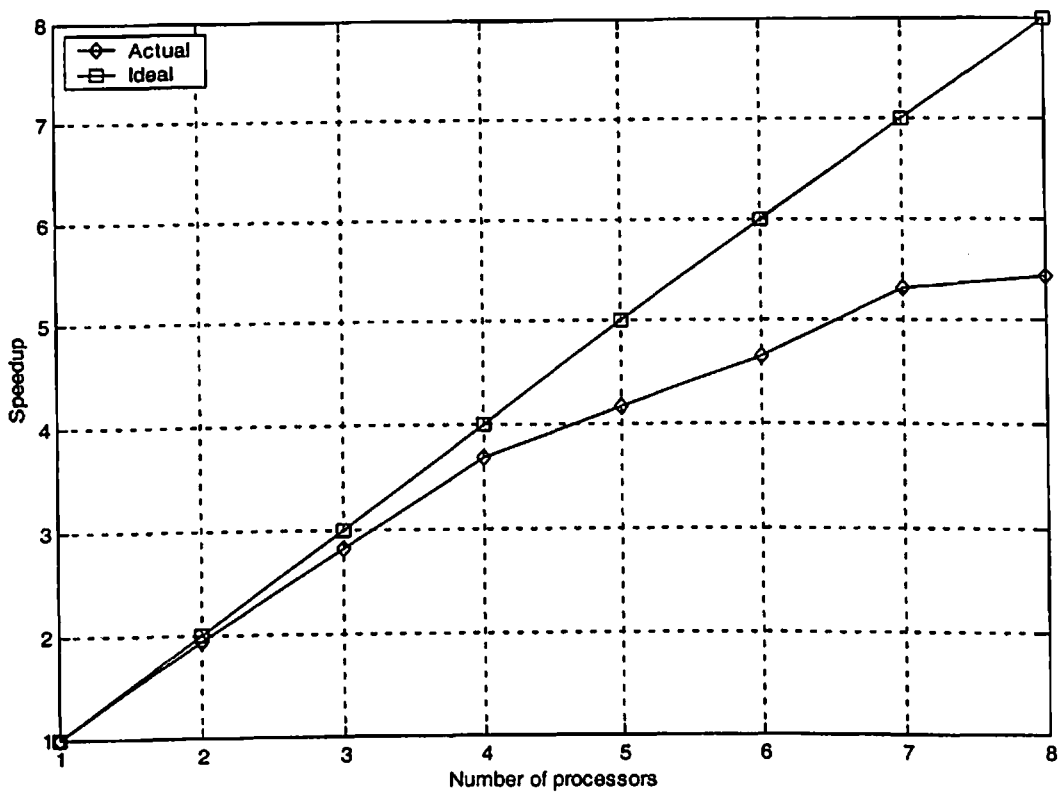


Fig. 7.20 Variation of speedup with number of processors for 1200 nodes

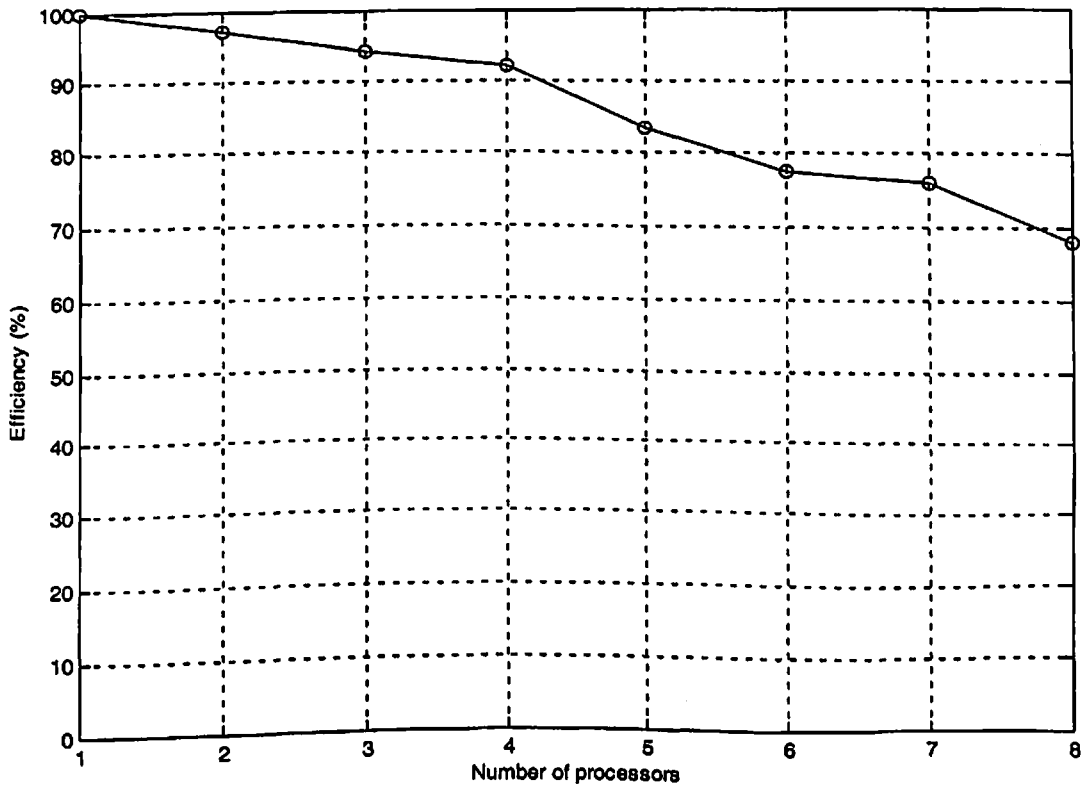


Fig. 7.21 Variation of efficiency with number of processors for 1200 nodes

7.3.3 Three-dimensional model problem

The parallel EFG results have also been obtained for a 3-D heat transfer problem (Chapter 6: Case-I). Table 7.10 shows the variation of total time, communication time, speedup and efficiency with the number of processors for 729 nodes. The variation of total time and communication time with the number of processors is also shown in Fig. 7.22 for same number of nodes (data size). From Table 7.10 and Fig. 7.22, it is observed that total time is decreasing with the increase in the number of processors from 1 to 8. Fig. 7.23 and Fig. 7.24 show the variation of efficiency and speedup respectively with the number of processors for 729 nodes. For this data size (729 nodes), the speedup and efficiency are found to be 3.53 and 44.12% respectively using 8 processors.

Table 7.11 shows the variation of total time, communication time, speedup and efficiency with the number of processors for 1000 nodes. The variation of total time and communication time with the number of processors is also presented in Fig. 7.25 for same number of nodes (data size). From Table 7.11 and Fig. 7.25, it can be noted that with the increase in number of processors from 1 to 8, total time is decreasing. Fig. 7.26 & Fig. 7.27 show the variation of efficiency and speedup respectively with the number of processors for 1000 nodes. For this data size (1000 nodes), the speedup and efficiency are achieved to be 4.14 and 51.73% respectively using 8 processors.

Table 7.12 shows the variation of total time, communication time, speedup and efficiency with the number of processors for 1320 nodes. The variation of computational time components (total time and communication time) with the number of processors is also shown in Fig. 7.28 for the same number of nodes (data size). From Table 7.12 and Fig. 7.28, it can be noted that the total time decreases from processors 1 to 8. Fig. 7.29 & Fig. 7.30 show the variation of efficiency and speedup respectively with the number of processors for 1320 nodes. For this data size (1320 nodes), the speedup and efficiency are achieved to be 4.66 and 58.22% respectively using 8 processors.

From the above analysis, it is observed that with increase in data size, results are improving both in terms of efficiency and speedup. There is very less contribution of communication time in total time. Moreover it is also clear that with the increase in data size (number of nodes); the results are improving with the increase in number of processors.

Table 7.10 Variation of total time, communication time, speedup and efficiency with number of processors for 729 nodes

Number of processors	Total time (sec)	Communication time (sec)	Speedup	Efficiency (%)
1	308.5035	0.0000	1.00	100.00
2	172.4185	0.0660	1.79	89.46
3	129.0555	0.1530	2.39	79.68
4	104.9417	0.3197	2.94	73.49
5	96.3658	1.2153	3.20	64.02
6	93.1113	5.3694	3.31	55.17
7	83.5289	1.8749	3.69	52.76
8	87.4107	5.4367	3.53	44.12

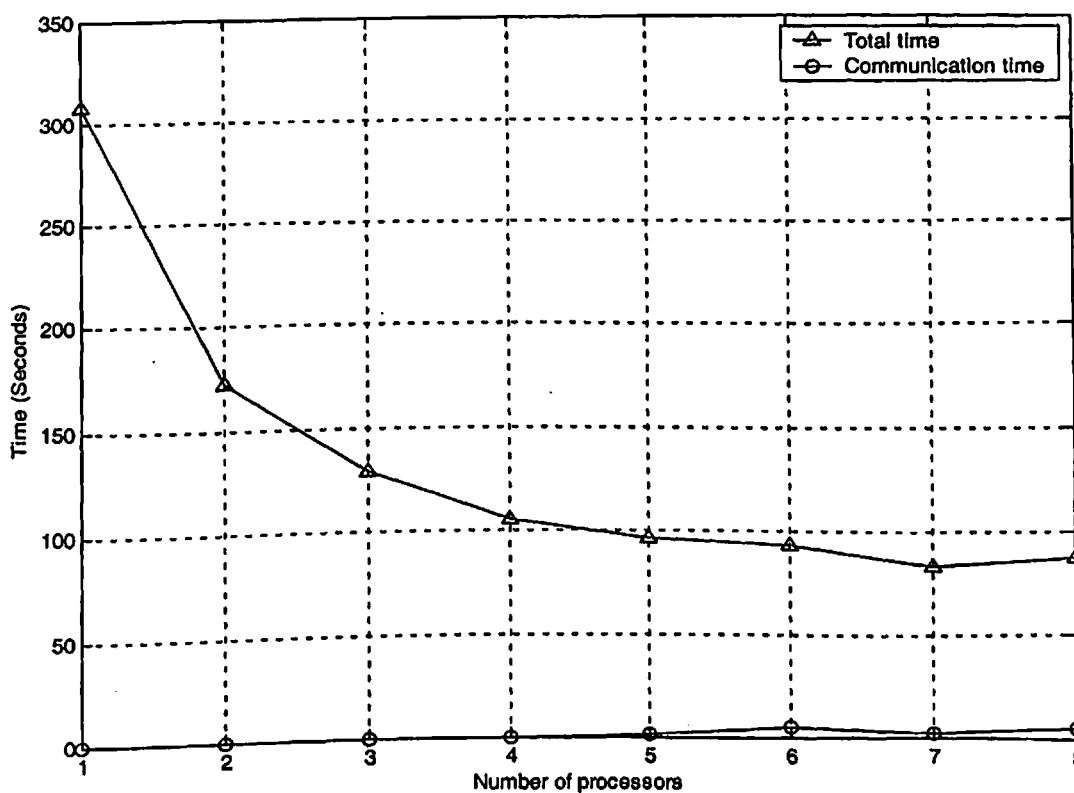


Fig. 7.22 Variation of total time and communication time with number of processors for 729 nodes

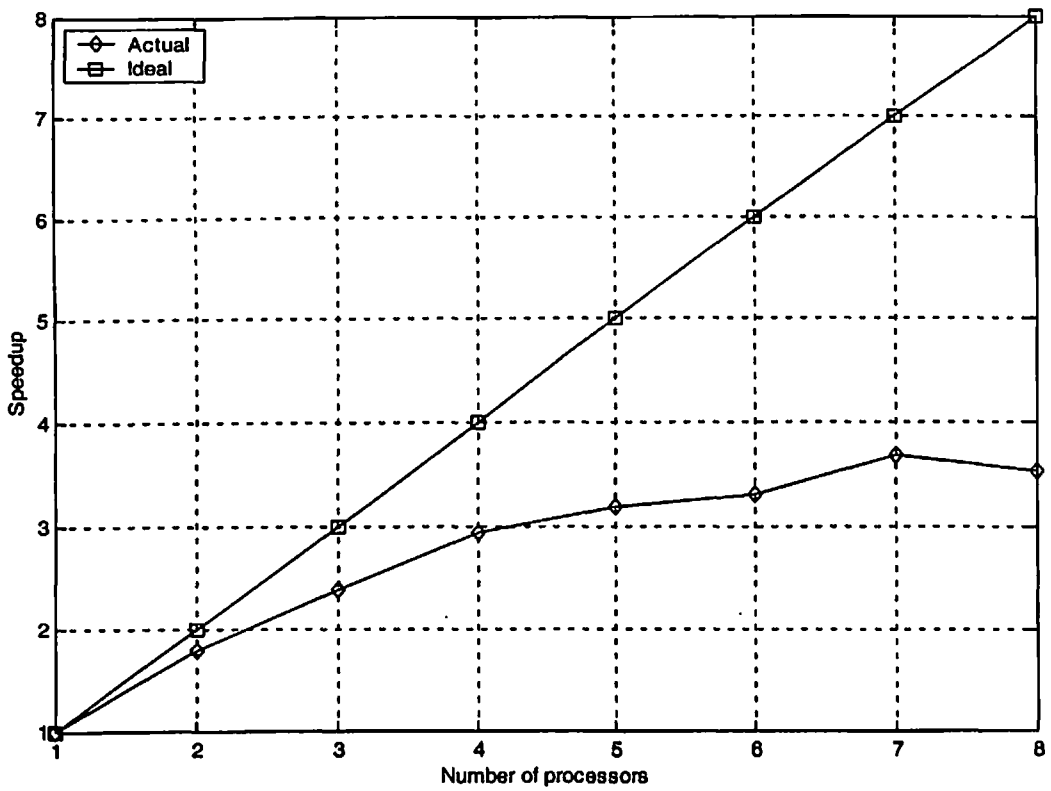


Fig. 7.23 Variation of speedup with number of processors for 729 nodes

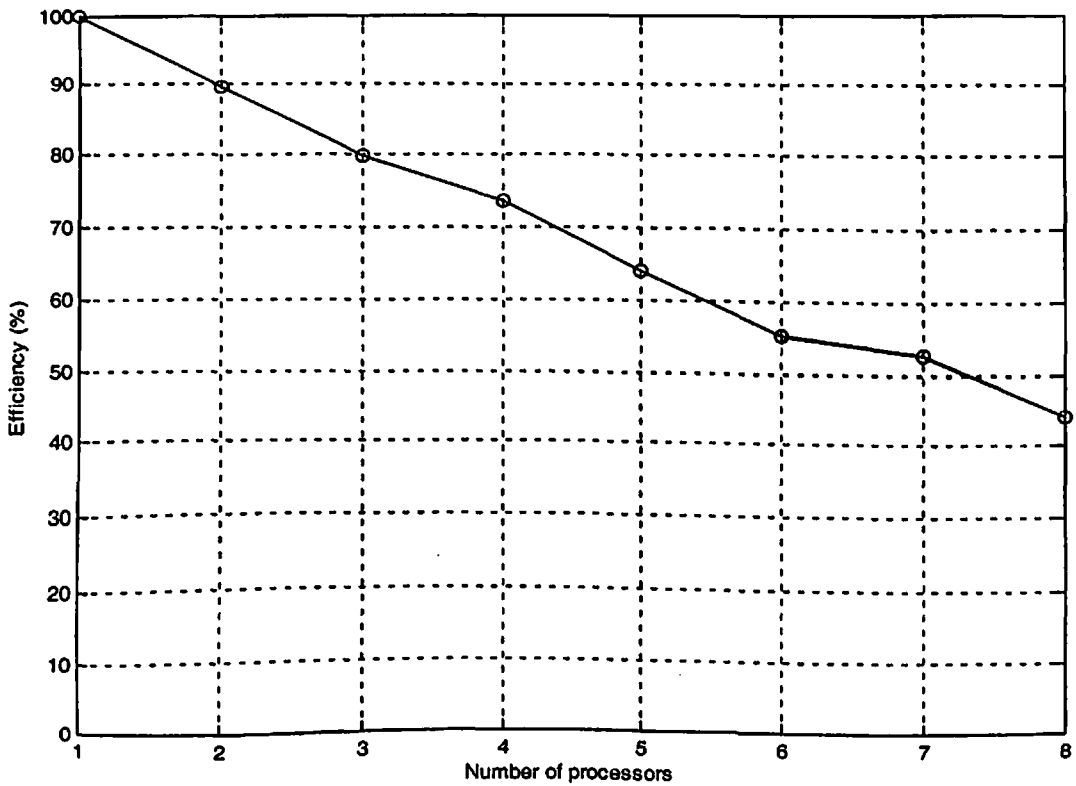


Fig. 7.24 Variation of efficiency with number of processors for 729 nodes

Table 7.11 Variation of total time, communication time, speedup and efficiency with number of processors for 1000 nodes

Number of processors	Total time (sec)	Communication time (sec)	Speedup	Efficiency (%)
1	776.9130	0.0000	1.00	100.00
2	423.4670	0.1054	1.83	91.73
3	311.9410	0.3455	2.49	83.02
4	246.4190	0.2158	3.15	78.82
5	222.2260	1.9002	3.50	69.92
6	203.6020	3.5979	3.81	63.60
7	185.4400	3.9821	4.20	59.96
8	187.7355	8.4302	4.14	51.73

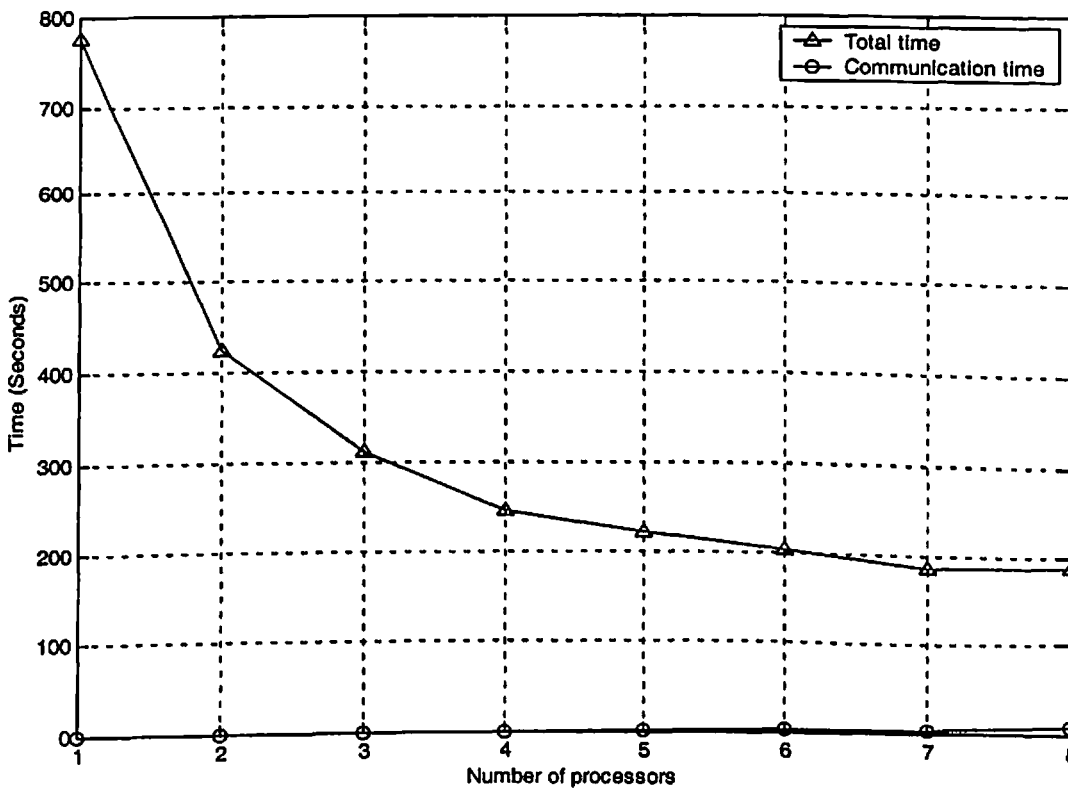


Fig. 7.25 Variation of total time and communication time with number of processors for 1000 nodes

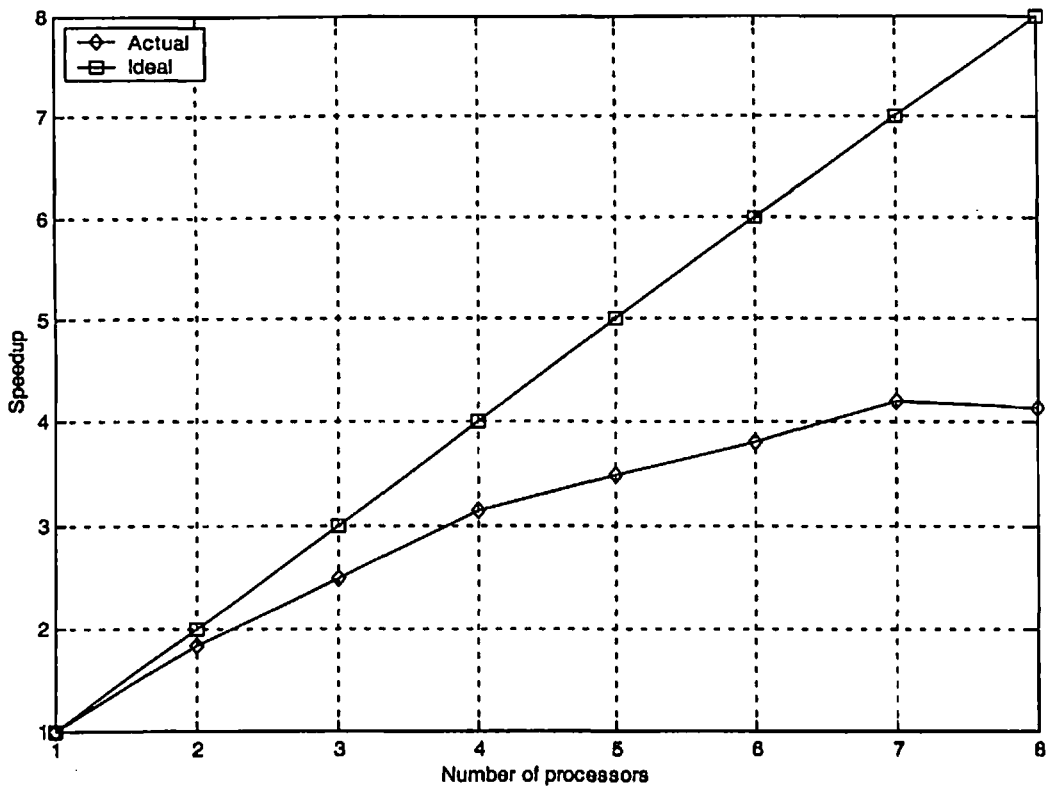


Fig. 7.26 Variation of speedup with number of processors for 1000 nodes

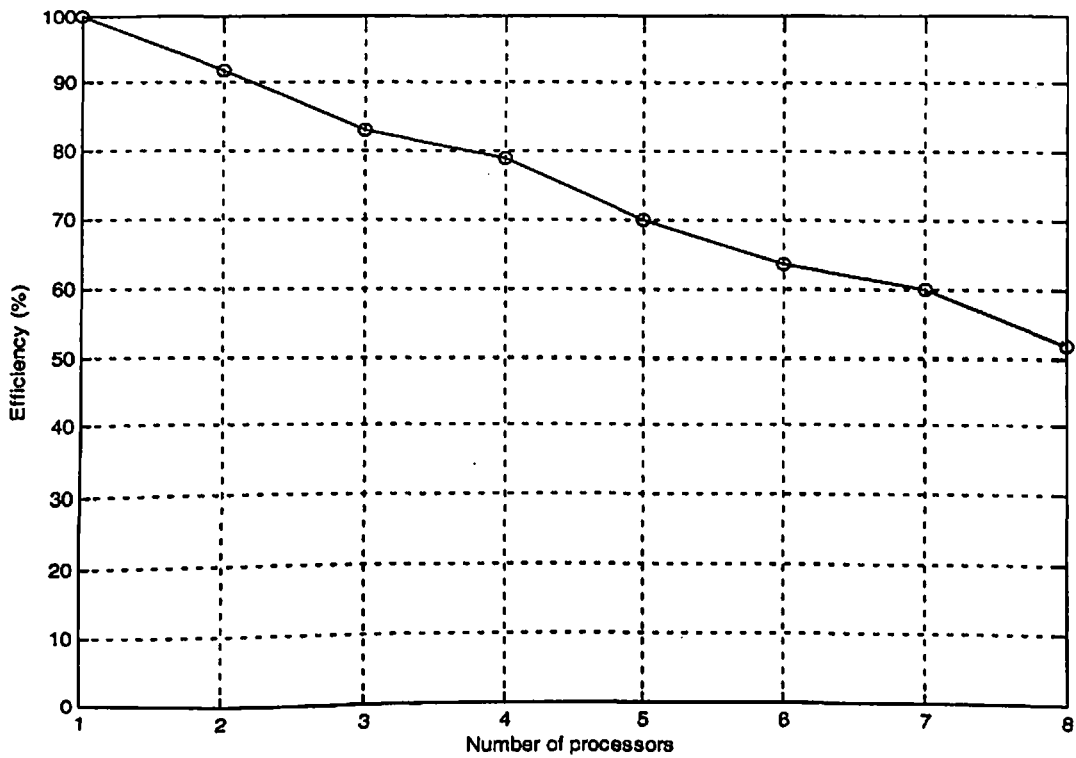


Fig. 7.27 Variation of efficiency with number of processors for 1000 nodes

Table 7.12 Variation of total time, communication time, speedup and efficiency with number of processors for 1320 nodes

Number of processors	Total time (sec)	Communication time (sec)	Speedup	Efficiency (%)
1	1703.9500	0.0000	1.00	100.00
2	910.0000	0.2638	1.87	93.62
3	664.0010	0.5308	2.57	85.54
4	522.8990	0.9960	3.26	81.47
5	455.8030	2.2122	3.74	74.77
6	409.7670	5.0739	4.16	69.30
7	378.7050	5.7916	4.50	64.28
8	365.8310	5.7127	4.66	58.22

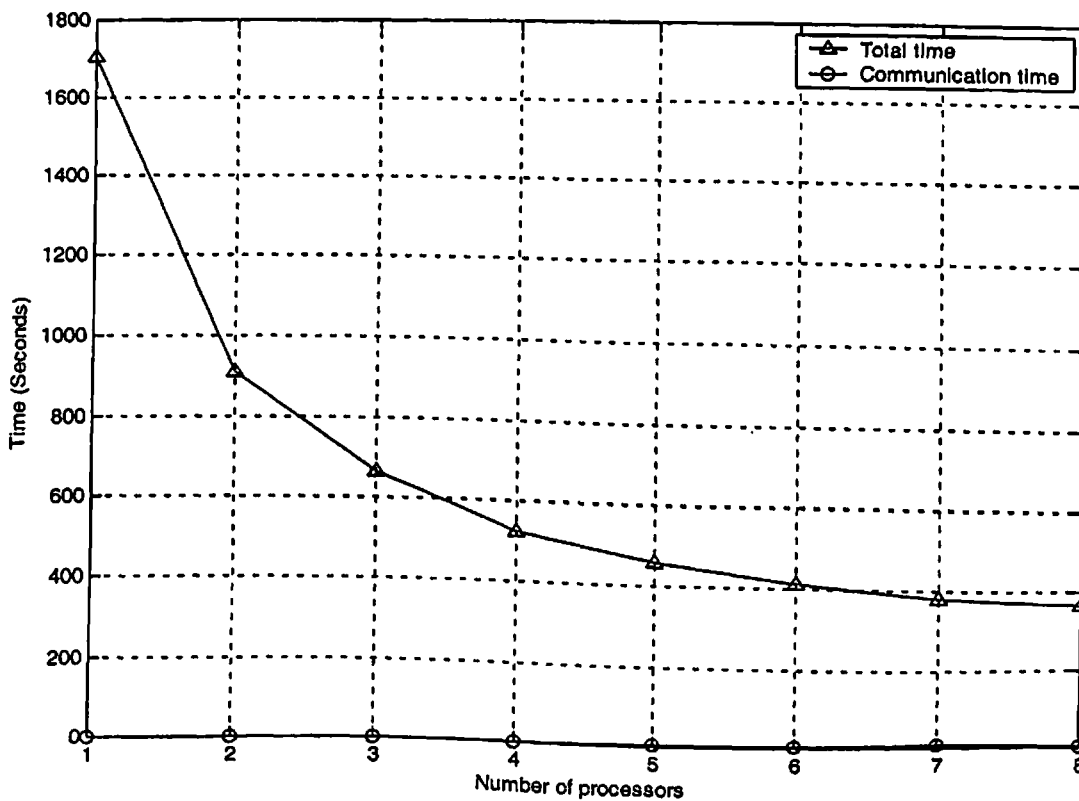


Fig. 7.28 Variation of total time and communication time with number of processors for 1320 nodes

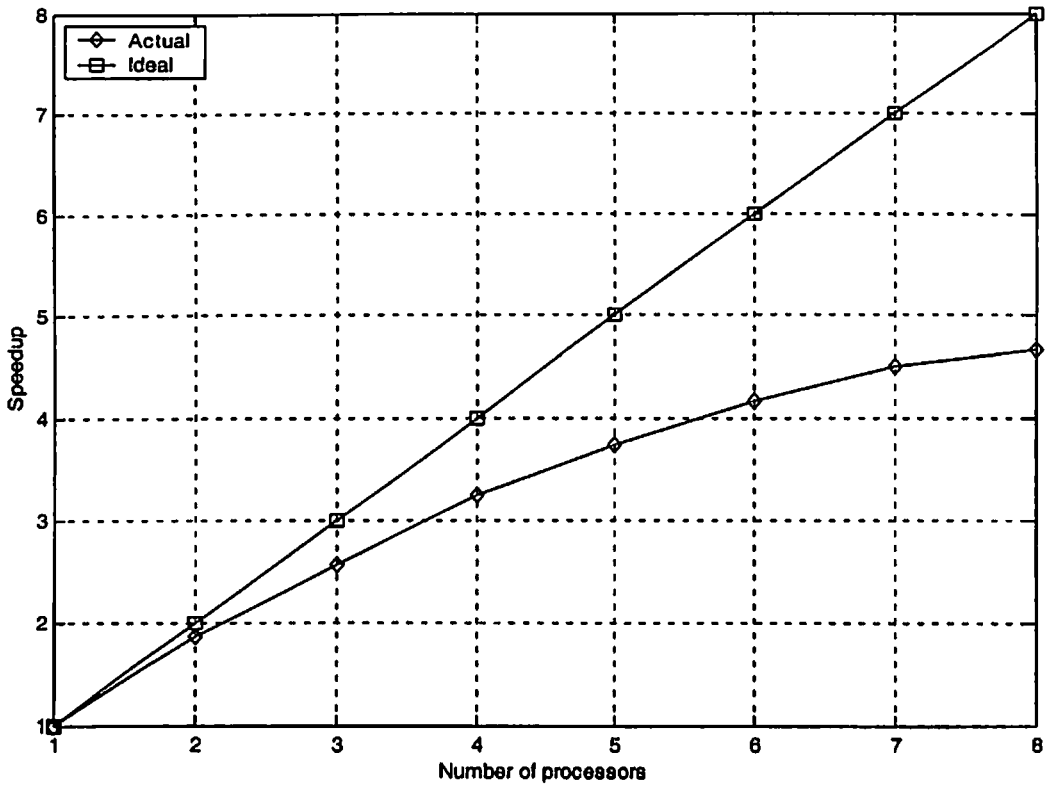


Fig. 7.29 Variation of speedup with number of processors for 1320 nodes

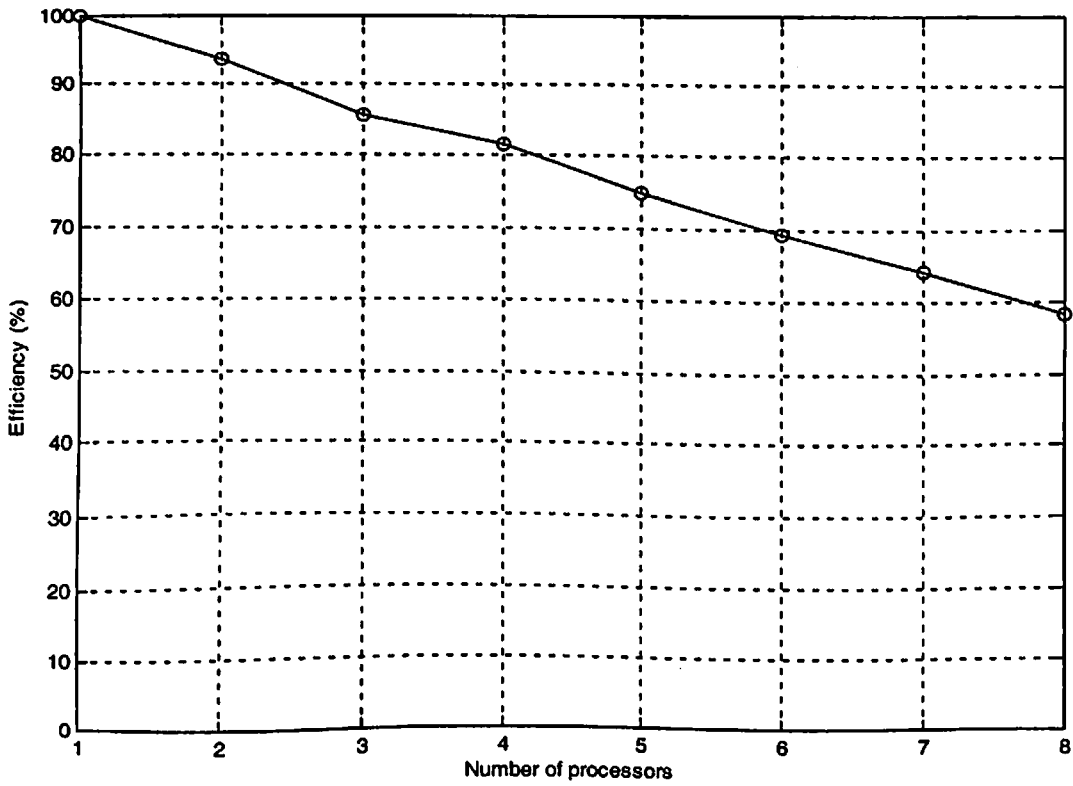


Fig. 7.30 Variation of efficiency with number of processors for 1320 nodes

7.4 CONCLUSION

In this Chapter, a new parallel algorithm has been proposed for the EFG method. The parallel EFG code has been programmed in FORTRAN language using MPI message passing library and executed on a supercomputer (PARAM 10000). The validation of parallel EFG code has been done by solving three model heat transfer problems one each in 1-D, 2-D and 3-D domain. The analysis shows that with increase in data size (i.e. number of nodes), speedup and efficiency both improve. Moreover it is also observed that with the increase in data size, the total time and communication time are improving with the increase in number of processors. The improvement in speedup and efficiency with data size (i.e. number of nodes) for 2-D and 3-D problems is faster than that for 1-D problems. Since, the speedup and efficiency both are improving with the increase in data size (i.e. number of nodes) therefore, by increasing data size further good speedup and efficiency can be achieved easily. From parallel EFG results presented in this chapter, it can be noted that the proposed algorithm is working well for the EFG method. In the proposed methodology (algorithm), instead of collecting data from each processor to the root processor, it can be done in another way such that root processor need not to collect the data from each processor.

CHAPTER-8

CONCLUSION AND FUTURE SCOPE OF WORK

In this thesis, meshless element free Galerkin (EFG) method not only was applied successfully in one-dimensional (1-D), two-dimensional (2-D) and three-dimensional (3-D) heat transfer problems but also the parallel implementation of the EFG code was done successfully.

The MATLAB codes were developed to obtain meshless numerical solution. Four new weight functions namely hyperbolic, exponential, rational and cosine were proposed in this thesis. The numerical results were obtained using existing (cubicspline, quarticspline, Gaussian and quadratic) and proposed EFG weight functions for four cases each in 1-D, 2-D and 3-D problems. It was found that the results obtained using different EFG weight functions are in good agreement with those obtained by finite element method. For CASE-I of 1-D, 2-D and 3-D model problems, analytical results were available and it was noticed that the results obtained by EFG method were found to be more accurate as compared to FEM results.

The effect of scaling parameter (d_{\max}) on EFG results was also discussed in detail. Satisfactory results were found in the range of $1 < d_{\max} < 2.0$ for cubicspline, quarticspline, Gaussian, exponential and rational weight functions in 1-D heat transfer problems. The results obtained using quadratic, hyperbolic and cosine weight functions are not reliable in 1-D heat transfer application. These weight functions showed an abrupt behavior in EFG results for the given range or higher value of d_{\max} . The proposed exponential weight function leads to minimum variation in EFG results. Hence, it is the most reliable for the given range of d_{\max} .

In 2-D and 3-D heat transfer application, it was observed that the scaling parameter gives acceptable results in the range of $1 < d_{\max} < 1.5$ for cubicspline, quarticspline, Gaussian, exponential and rational weight functions. A random change in the values of EFG results was noticed for quadratic, hyperbolic and cosine weight functions in the given range of d_{\max} . Similar to 1-D problems, it was also observed that the results obtained using proposed exponential weight functions are the most reliable for this range of scaling parameter. Among the proposed weight functions, exponential and rational give accurate results for all kind of heat transfer problems. The suitable range of d_{\max} is 1 to 1.5 for 1-D, 2-D and 3-D problems. The proposed exponential weight function was found to be most reliable whereas quadratic, hyperbolic and cosine weight functions are not suitable for heat transfer applications.

A new parallel algorithm was proposed for the EFG method to reduce its computational cost. The parallel code was written in FORTRAN language and executed on network of parallel computer, PARAM 10000. Three model heat transfer problems was solved (one each in 1-D, 2-D and 3-D domains) to validate the proposed parallel algorithm. For 8 processors, the speedup and efficiency are achieved to 2.22 & 27.78% respectively for 1100 nodes in 1-D domain, 5.44 & 67.95% respectively for 1200 nodes in 2-D domain and 4.66 & 58.22% respectively for 1320 nodes in 3-D domain. It was noted that both speedup and efficiency are improving with the increase in data size i.e. number of nodes.

In near future, the EFG method can also be extended to solve geometrically complex three dimensional heat transfer problems. More efficient techniques can be proposed so that the imposing of the essential boundary conditions becomes easier. Moreover, more efficient parallel algorithms can be developed to further reduce the computational cost. The EFG method can also be applied to obtain the numerical solution of fluid flow problems.

REFERENCES

- Aluru, N. R. (1998): A reproducing kernel particle method for meshless analysis of microelectromechanical systems. *Computational Mechanics*, vol. 22, pp. 174-186.
- Atluri, S. N. and Zhu, T. (1998): A new Meshless Local Petrov-Galerkin (MLPG) approach in computational mechanics. *Computational Mechanics*, vol. 22, pp. 117-127.
- Atluri, S. N., Sladek, J., Sladek, V. and T. Zhu (2000): The local boundary integral equation (LBIE) and its meshless implementation for linear elasticity. *Computational Mechanics*, vol. 25, pp. 180-198.
- Atluri, S. N. and Shen, S. (2002): The meshless local Petrov-Galerkin (MLPG) method: A simple & less costly alternative to the finite element and boundary element methods. *Computer Modeling in Engineering and Sciences*, vol. 3(1), pp. 11-51.
- Babuska, I. and Melenk, J. M. (1997): The partition of unity method. *International Journal for Numerical Methods in Engineering*, vol. 40, pp. 727-758.
- Belytschko, T., Lu, Y. Y. and Gu, L. (1994): Element-free Galerkin methods. *International Journal for Numerical Methods in Engineering*, vol. 37, pp. 229-256.
- Belytschko, T. and Tabbara, M. (1996): Dynamic Fracture Using Element-Free Galerkin Methods. *International Journal for Numerical Methods in Engineering*, vol. 39, pp. 923-938.
- Belytschko, T., Organ, D. and Krongauz, Y. (1996a): A coupled finite element-element free Galerkin method. *Computational Mechanics*, vol. 17, pp. 186-195.
- Belytschko, T., Krongauz, Y., Fleming, M., Organ, D. and Liu, W. K. (1996b): Smoothing and accelerated computations in element-free Galerkin method. *Journal of Computational and Applied Mathematics*, vol. 74, pp. 111-126.

- Belytschko, T., Krongauz, Y., Organ, D. J., Fleming, M. and Krysl, P. (1996c): Meshless methods: An overview and recent developments. *Computer Methods in Applied Mechanics in Engineering*, vol. 139, pp. 3-47.
- Belytschko, T., Organ, D. and Gerlach, C. (2000): Element-free Galerkin method for dynamic fracture in concrete. *Computer Methods in Applied Mechanics and Engineering*, vol. 187, pp. 385-399.
- Bouillard, Ph. and Suleau, S. (1998): Element-free Galerkin solutions for Helmholtz problems: formulation and numerical assessment of the pollution effect, *Computer Methods in Applied Mechanics and Engineering*, vol. 162, pp. 317-335.
- Carslaw, H. S. and Jaeger, J. C. (1959): *Conduction of Heat in Solids*, Oxford University Press, London.
- Chen, J. S., Pan, C. and Wu, C. T. (1997): Large deformation analysis of rubber based on a reproducing kernel particle method. *Computational Mechanics*, vol. 19, pp. 211-227.
- Chen, X. L., Liu, G. R. and Lim, S. P. (2003): An element free Galerkin method for the free vibration analysis of composite laminates of complicated shape. *Composite Structures*, vol. 59, pp. 279-289.
- Cho, J. Y. and Atluri, S. N. (2001): Analysis of shear flexible beams using the meshless local Petrov-Galerkin method, based on a locking-free formulation. *Engineering Computations*, vol. 18 (1/2), pp. 215-240.
- Cingoski, V., Miyamoto, N. and Yamashita, H. (1998): Element free Galerkin method for electromagnetic field computations. *IEEE Transactions on Magnetics*, vol. 34 (5), pp. 3236-3239.
- De, S. and Bathe, K. J. (2000): The method of finite spheres. *Computational Mechanics*, vol. 25, pp. 329-345.
- De, S. and Bathe, K. J. (2001a): Towards an efficient meshless computational technique: the method of finite spheres. *Engineering Computations*, vol. 18(1-2), pp. 170-192.

- De, S. and Bathe, K. J. (2001b): The method of finite spheres with improved numerical integration. *Computers and Structures*, vol. 79, pp. 2183-2196.
- Dolbow, J. and Belytschko, T. (1998): An introduction to programming the meshless element free Galerkin method. *Archives in Computational Mechanics*, vol 5 (3), pp. 207-241.
- Du, C. (2000): An element-free Galerkin method for simulation of stationary two-dimensional shallow water flows in rivers. *Computer Methods in Applied Mechanics in Engineering*, vol. 182, pp. 89-107.
- Durate, C. A. and Oden, J. T. (1996): An H - p adaptive method using clouds. *Computer Methods in Applied Mechanics and Engineering*, vol. 139, pp. 237-262.
- Fleming, M., Chu, Y. A., Moran, B. and Belytschko, T. (1997): Enriched element free Galerkin methods for crack tip fields. *International Journal of Numerical Methods in Engineering*, vol. 40, pp. 1483-1504.
- Gavete, L., Falcon, S. and Bellido, J. C. (2000): Dirichlet boundary conditions in element free Galerkin method. *European Congress on Computational Methods in Applied Sciences and Engineering (ECCOMAS-2000)*, Barcelona, 11-14 Sept, 2000.
- Gingold, R. A. and Monaghan, J. J. (1977): Smoothed particle hydrodynamics: Theory and application to non-spherical stars. *Monthly Notices of the Royal Astronomical Society*, vol. 181, pp. 375-389.
- Goozee, R. J. and Jacobs, P. A. (2003): Distributed and shared memory parallelism with a smooth particle hydrodynamics code. *The ANZIAM Journal*, vol. 44, pp. C202-C228.
- Griebel, M. and Schweitzer, M. A. (2002): A particle-partition of unity method-Part IV: Parallelization, *Mesh-Free Methods for Partial Differential Equations (Lecture notes in Computational Science and Engineering)*, vol. 26, pp. 161-192.

- Gu, Y. T. and Liu, G. R. (2001): A local point interpolation method for static and dynamic analysis of thin beams. *Computer Methods in Applied Mechanics in Engineering*, vol. 190, pp. 5515-5528.
- Günther, F., Liu, W. K., Diachin, D. and Christon, M. A. (2000): Multi-scale meshfree parallel computations for viscous, compressible flows, *Computer Methods in Applied Mechanics in Engineering*, vol. 190, pp. 279-303.
- Haitian, Y. and Yan, L. (2003): A combined approach of EFGM and precise algorithm in time domain solving viscoelasticity problems. *International Journal of Solids and Structures*, vol. 40, pp. 701-714.
- Holman J. P. (1989): *Heat Transfer*, Mc Graw-Hill, Singapore, 1989
- Iura, M. and Kanaizuka, J. (2000): Flexible translational joint analysis by meshless method. *International Journal of Solids and Structures*, vol. 37, pp. 5203-5217.
- Jun, S., Liu, W. K. and Belytschko, T. (1998): Explicit reproducing kernel particle methods for large deformation problems. *International Journal for Numerical Methods in Engineering*, vol. 41, pp. 137-166.
- Kamitani, A., Saitoh, A., Ikuno, S. and Yokono, T. (2003): Numerical simulation of shielding current density in HTS by element free Galerkin method. *Physica C*, vol. 392-396, pp. 1118-1123.
- Karim, M. R., Nogami, T. and Wang, J. G. (2002): Analysis of transient response of saturated porous elastic soil under cyclic loading using element-free Galerkin method. *International Journal of Solids and Structures*, vol. 39, pp. 6011-6033.
- Krongauz, Y. V. (1996a): Applications of meshless methods to solid mechanics. Ph.D thesis, Theoretical and Applied Mechanics, Northwestern University, Evanston, IL, USA.
- Krongauz, Y. and Belytschko, T. (1996b): Enforcement of essential boundary conditions in meshless approximations using Finite Elements. *Computer Methods in Applied Mechanics and Engineering*, vol. 131(2), pp. 133-145.

- Krysl, P. and Belytschko, T. (1996a): Analysis of thin plates by the element-free Galerkin method. *Computational Mechanics*, vol. 17, pp. 26-35.
- Krysl, P. and Belytschko, T. (1996b): Analysis of thin shells by the element-free Galerkin method. *International Journal of Solids and Structures*, vol. 33(20-22), pp. 3057-3080.
- Krysl, P. and Belytschko, T. (2001): ESFLIB: A library to compute the element free Galerkin shape functions. *Computer Methods in Applied Mechanics and Engineering*, vol. 190, pp. 2181-2205.
- Lancaster, P. and Salkauskas, K. (1981): Surfaces generated by moving least squares methods. *Mathematics of Computation*, vol. 37, pp. 141-158.
- Lee, S. H. and Yoon, Y. C. (2004): Numerical prediction of crack propagation by an enhanced element-free Galerkin method, *Nuclear Engineering and Design* (in press).
- Li, G. and Belytschko, T. (2001): Element free Galerkin method for contact problems in metal forming analysis. *Engineering Computations*, vol. 18, pp. 62-78.
- Li, G., Ge, J. and Jie, Y. (2003): Free surface seepage based on the element free method. *Mechanics Research communications*, vol. 30, pp. 9-19.
- Liew, K. M., Ren, J. and Kitipornchai, S. (2003): Analysis of the pseudoelastic behavior of a SMA beam by the element-free Galerkin method. *Engineering Analysis with Boundary Elements* (in press).
- Liu, W. K., Jun, S. and Zhang, Y. F. (1995a): Reproducing kernel particle methods. *International Journal for Numerical Methods in Engineering*, vol. 20, pp. 1081-1106.
- Liu, W. K., Jun, S., Li, S., Adee, J. and Belytschko, T. (1995b): Reproducing kernel particle methods for structural dynamics. *International Journal for Numerical Methods in Engineering*, vol. 38, pp. 1655-1679.

- Liu, W. K., Chen, Y., Jun, S., Chen, J. S., Belytschko, T., Pan, C., Uras, R. A. and Chang, C. T. (1996): Overview and applications of the reproducing kernel particle methods. *Archives of Computational Methods in Engineering*, vol. 3, pp. 3-80.
- Liu, G. R. and Gu, Y. T. (2001a): A point interpolation method for two-dimensional solids. *International Journal for Numerical Methods in Engineering*, vol. 50, pp. 937-951.
- Liu, G. R. and Gu, Y. T. (2001b): A local radial point interpolation method (LRPIM) for free vibration analysis of 2-D solids. *Journal of Sound and Vibration*, vol. 246(1), pp. 29-46.
- Liu, L., Liu, G. R. and Tan, V. B. C. (2002a): Element free method for static and free vibration analysis of spatial thin shell structures. *Computer Methods in Applied Mechanics and Engineering*, vol. 191, pp. 5923-5942.
- Liu, G. R., Chen, X. L. and Reddy, J. N. (2002b): Buckling of symmetrically laminated composite plates using the element-free Galerkin method. *International Journal of Structural Stability and Dynamics*, vol. 2(3), pp. 281-294.
- Long, S. and Zhang, Q. (2002): Analysis of thin plates by the local boundary integral equation (LBIE) method. *Engineering Analysis with Boundary Elements*, vol. 26, pp. 707-718.
- Lu, Y. Y., Belytschko, T. and Gu, L. (1994): A new implementation of the element element-free Galerkin method. *Computer Methods in Applied Mechanics and Engineering*, vol. 113, pp. 397-414.
- Lu, Y. Y., Belytschko, T. and Tabbara, M. (1995): Element-free Galerkin method for wave propagation and dynamic fracture. *Computer Methods in Applied Mechanics and Engineering*, vol. 113, pp. 131-153.
- Lucy, L. B. (1977): A numerical approach to the testing of fusion process. *Astronomical Journal*, vol. 88, pp. 1013-1024.

- Marechal, Y., Coulomb, J. L. and Meunier, G. (1993): Use of the diffuse element method for electromagnetic field computations. *IEEE Transactions on Magnetics*, vol. 29(2), pp. 1475-1478.
- Medina, D. F. and Chen, J. K. (2000): Three-dimensional simulations of impact induced damage in composite structures using the parallelized SPH method. *Composites: Part-A*, vol. 31, pp. 853-860.
- Melenk, J. M. and Babuska, I. (1996): The partition of unity finite element method: Basic theory and applications. *Computer Methods in Applied Mechanics in Engineering*, vol. 139, pp. 289-314.
- Monaghan, J. J. (1988): An introduction to SPH. *Computer Physics Communications*, vol. 48, pp. 89-96.
- Monaghan, J. J. (1992): Smoothed particle hydrodynamics. *Annual Review of Astronomy and Astrophysics*, vol. 30, pp. 543-574.
- Mukherjee, Y. X. and Mukherjee, S. (1997): The boundary node method for potential problems. *International Journal for Numerical Methods in Engineering*, vol. 40(5), pp. 797-815.
- Nayroles, B., Touzot, G. and Villon, P. (1992): Generalizing the finite element method: diffuse approximation and diffuse elements. *Computational Mechanics*, vol. 10, pp. 307-318.
- Nayroles B., Touzot, G. and Villon, P. (1994): Using the diffuse approximation for optimizing the location of anti-sound sources. *Journal of Sound and Vibration*, vol. 1, pp. 1-21.
- Onate, E., Perazzo, F. and Miquel, J. (2001): A finite point method for elasticity problems. *Computers and Structures*, vol. 79, pp. 2151-2163.

- Rahman, S. and Rao, B. N. (2001): An element-free Galerkin method for probabilistic mechanics and reliability. *International Journal of Solids and Structures*, vol. 38, pp. 9313-9330.
- Rahman, S. and Rao, B. N. (2002): Probabilistic fracture mechanics by Galerkin meshless methods- part II: reliability analysis. *Computational Mechanics*, vol. 28, pp. 365-374.
- Rao, B. N. and Rahman, S. (2000): An efficient meshless method for fracture analysis of cracks. *Computational Mechanics*, vol. 26, pp. 398-408.
- Rao, B. N. and Rahman, S. (2002): Probabilistic fracture mechanics by Galerkin meshless methods- part I: rates of stress intensity factors. *Computational Mechanics*, vol. 28, pp. 351-364.
- Rao, B. N. and Rahman, S. (2003): Mesh-free analysis of cracks in isotropic functionally graded materials. *Engineering Fracture Mechanics*, vol. 70, pp. 1-27.
- Ren, J., Liew, K. M. and Meguid, S. A. (2002): Modelling and simulation of the superelastic behaviour of shape memory alloys using the element-free Galerkin method. *International Journal of Mechanical Sciences*, vol. 44, pp. 2393-2413.
- Shirazaki, M. and Yagawa, G. (1999): Large-scale parallel flow analysis based on free mesh method: a virtually meshless method. *Computer Methods in Applied Mechanics and Engineering*, vol. 174, pp. 419-431.
- Sibson, R. (1980): A vector identity for the Dirichlet tessellation. *Mathematical Proceedings of the Cambridge Philosophical Society*, vol. 87, pp. 151-155.
- Singh, I. V., Sandeep, K. and Prakash, R. (2002): The element free Galerkin method in three-dimensional steady state heat conduction. *International Journal of Computational Engineering Sciences*, vol. 3(3), pp. 291-303.

- Singh, I. V. and Prakash, R. (2003): The numerical solution of three-dimensional transient heat conduction problems using element free Galerkin method. *International Journal of Heat & Technology* (in Press).
- Singh, I. V., Sandeep, K. and Prakash, R. (2003a): Heat transfer analysis of two-dimensional fins using meshless element-free Galerkin method. *Numerical Heat Transfer: Part A*, vol. 44, pp. 73-84.
- Singh, I. V. and Sandeep, K. and Prakash, R. (2003b): Application of meshless element free Galerkin method in Two-dimensional heat conduction problems. *Computer Assisted Mechanics and Engineering Sciences* (in press).
- Sukumar, N., Moran, B., Black, T. and Belytschko, T. (1997): An element-free Galerkin method for three-dimensional fracture mechanics. *Computational Mechanics*, vol. 20, pp. 170-175.
- Sukumar, N. (1998a): The natural element method in solid mechanics. Ph.D thesis, Theoretical and Applied Mechanics, Northwestern University, Evanston, IL, USA.
- Sukumar, N., Moran, B. and Belytschko, T. (1998b): The natural element method in solid mechanics. *International Journal for Numerical Methods in Engineering*, vol. 43(5), pp. 839-887.
- Ventura, G., Xu, J. X. and Belytschko, T. (2002): A vector level set method and new discontinuity approximations for crack growth by EFG. *International Journal for Numerical Methods in Engineering*, vol. 54 (6), pp. 923-944.
- Xiao, Q. Z. and Dhanasekar, M. (2002): Coupling of FE and EFG using collocation approach. *Advances in Engineering Software*, vol. 33, pp. 507-515.
- Xiao, J. R. and McCarthy, M. A. (2003): Meshless analysis of the obstacle problem for beams by the MLPG method and subdomain variational formulations. *European Journal of Mechanics-A/Solids*, vol. 22, pp. 385-399.

- Xiong, S., Rodrigues, J. M. C. and Martins, P. A. F. (2004): Application of the element free Galerkin method to the simulation of plane strain rolling, *European Journal of Mechanics A/Solids*, vol. 23, pp. 77–93.
- Xuan, L., Zeng, Z., Shanker, B. and Udpa, L. (2001): A Meshless element-free Galerkin method in NDT applications. *28th Annual Review of Progress in Quantitative Nondestructive Evaluation, Maine USA, Published in AIP conference Proceeding.*
- Yagawa, G. and Yamada, T. (1996): Free mesh method, a new meshless finite element method. *Computational Mechanics*, vol. 18, pp. 383-386.
- Yagawa, G. and Furukawa, T. (2000): Recent developments of free mesh method. *International Journal for Numerical Methods in Engineering*, vol. 47, pp. 1419-1443.
- Zhang, J., Yao, Z. and Tanaka, M. (2003): The meshless regular hybrid boundary node method for 2-D linear elasticity. *Engineering Analysis with Boundary Elements*, vol. 27, pp. 259-268.
- Zhang, J. and Yao, Z. (2003): The regular hybrid boundary node method for three-dimensional linear elasticity. *Engineering Analysis with Boundary Elements* (In press)
- Zhu, T., Zhang, J. D. and Atluri, S. N. (1998a): A local boundary integral equation (LBIE) method in computational mechanics and a meshless discretization approach. *Computational Mechanics*, vol. 21, pp. 223-235.
- Zhu, T., Zhang, J. D. and Atluri, S. N. (1998b): A meshless local boundary integral equation (LBIE) method for solving nonlinear problems. *Computational Mechanics*, vol. 22, pp. 174-186.

APPENDIX

1 Computational Time Components

The different components of computational time include real time, system time, user time, CPU time, total time and communication time. Among all these components, emphasis has been given on total time and communication time.

1.1 Total Time

The total time (run time) is the time at which parallel computation starts to the moment at which last processor finishes its execution. The total time is the time measured by the MPI watches built in the program itself.

1.2 Communication Time

The communication time is the time required to transfer the data form one processor to the other processor or processors. As number of processors increase communication time also increases.

2 Performance Matrices

2.1 Speedup Factor

A measure of relative performance between a multiprocessor system and a single processor system is the speedup factor, it is defined as

$$\text{Speedup} = \frac{\text{Total time using one processor (single processor system)}}{\text{Total time using number of processors (multiprocessor system)}}$$

2.2 Efficiency

$$\text{Efficiency} = \frac{\text{Total time using one processor (single processor system)}}{\text{Total time using number of processors} \times \text{number of processors}}$$

LIST OF PUBLICATIONS

International Journal Publications

1. I. V. Singh, K. Sandeep and R. Prakash, The element free Galerkin method in three-dimensional steady state heat conduction, *International Journal of Computational Engineering Sciences*, vol. 3(3), pp.291-303, 2003.
2. I. V. Singh, K. Sandeep and R. Prakash, Heat transfer analysis of two-dimensional fins using meshless element-free Galerkin method, *Numerical Heat Transfer: Part A*, vol. 44, pp.73-84, 2003.
3. I. V. Singh, K. Sandeep and R. Prakash, Meshless EFG method in transient heat conduction problems, *International Journal of Heat & Technology* (in Press).
4. I. V. Singh and R. Prakash, The numerical solution of three-dimensional transient heat conduction problems using element free Galerkin method, *International Journal of Heat & Technology* (in Press).
5. I. V. Singh, K. Sandeep and R. Prakash, Application of meshless element free Galerkin method in two-dimensional heat conduction problems, *Computer Assisted Mechanics and Engineering Sciences* (in press).
6. I. V. Singh, K. Sandeep and R. Prakash, The effect of weight function and scaling parameter on meshless EFG results in heat transfer problems, *International Journal of Heat & Technology* (in Press).

Conferences/Symposium

1. I. V. Singh, K. Sandeep and R. Prakash, The solution of one-dimensional heat transfer problems using meshless element free Galerkin method, *47th Congress of the Indian Society of Theoretical and Applied Mechanics (ISTAM)*, Dec. 23-26, 2002, IIT Guwahati, India.
2. I. V. Singh and R. Prakash, Numerical comparison of meshless solutions in heat transfer problems, *48th Congress of the Indian Society of Theoretical and Applied Mechanics (ISTAM)*, Dec. 18-21, 2003, BIT, MESRA, Ranchi, India.
3. I. V. Singh and R. Prakash, Applications of meshless EFG solutions in heat transfer problems, *17th National Heat and Mass Transfer Conference & 6th ISHMT/ASME Heat and Mass Transfer Conference*, Jan. 5-7, 2004, IGCAR, Kalpakkam, India.
4. I. V. Singh, R. Prakash and Akhilendra Singh, The numerical solution of axisymmetric heat transfer problems using meshless EFG method, *2nd BSME-ASME International Conference on Thermal Engineering*, 2-4 January 2004, Dhaka.